

VOTE 74245

**THE USE OF THERMOPHILIC ORGANISM FOR THE RECOVERY OF
GOLD AND COPPER FROM GRADE ORE**

**(PENGUNAAN ORGANISMA TERMOFILIK UNTUK PEROLEHAN
SEMULA EMAS DAN KUPRUM DARI ARANG GRADE)**

WAN AZLINA AHMAD

**RESEARCH VOTE NO:
74245**

**Fakulti Sains
Universiti Teknologi Malaysia**

2007

PART 5

ABSTRACTS

Applications of Fe(III) Leaching and Biooxidation for the Recovery of Au from Refractory Gold Ores

Mohammad Azri Bunyok

Biooxidation studies were carried out on gold ores isolated from Jugan and Pejiru, Sarawak. The gold and arsenic contents of the Pejiru and Jugan ores are 29.4 ppm, 48.7% and 13.5 ppm and 58.29% respectively. Due to its high concentration of gold, the Pejiru ore was then subjected to biooxidation studies using *L.ferrooxidans*, *A.ferrooxidans*, mesophilic local isolate, *S.thermosulfidioxidans*, *A.brierleyi* and thermophilic local isolates (5B and C cultures). Significant gold recoveries (39.5, 76.09 and 68.16%) were obtained using *L.ferrooxidans*, *S.thermosulfidioxidans* and *A.brierleyi* respectively. Low gold recoveries from other strains used could be due to arsenic toxicity. Fe(III) pretreatment of the ores was carried out to study its effectiveness in dissolution of arsenic from the ores. The optimized parameters for Fe(III) leaching is as follow; 0.2 M Fe₂(SO₄)₃, 45°C, pulp density 10% and a stirring speed of 200 rpm. Indeed higher amounts of gold (73.59, 76.49 and 80.4%) were recovered after biooxidation of Fe(III) leached ore using *L.ferrooxidans* , *S.thermosulfidioxidans* and *A.brierleyi*.

Bioleaching of Sungai Lembing Tin Mine By-Product Using Mesophilic and Thermophilic Bacteria

Abu Bakar Mustaffa@Ramli

Abandoned or disused mines possess an environmental problem because of the possibility of heavy metals present to be leached out into groundwater or natural river system. This issue needs to be addressed because of the toxicity effects that might affect humans. A possible solution is the use of bioleaching technology to treat the low-grade ores, which are normally left idle. For this study, ores from the disused Sungai Lembing mine in Pahang were subjected to ferric leaching and bioleaching using mesophilic and thermophilic bacteria namely *A. ferrooxidans*, *A. thiooxidans*, *L. ferrooxidans* and *S. thermosulfidooxidans* respectively. Optimization of ferric leaching was carried out using $\text{Fe}_2(\text{SO}_4)_3$ and FeCl_3 at concentrations ranging from 0.2 to 1.0 M. The results of the experiment showed that FeCl_3 1M was the best solution for the ferric leached of copper with 86.70% Cu leached. The otherwise, result from bioleaching experiment showed that *A.ferrooxidans* was the highest among the others bacteria with 77.05% Cu was extracted. Parameters optimized during the bioleaching process include Eh, temperature and Cu and Fe solubilization. The copper from the bioleached ores will be recovered using solvent extraction and stripping process.

Recovery of Copper in Printed Circuit Board and Sludge from Semiconductor Industry Using Bioleaching and Chemical Leaching

Nurhayati Deris

With the increasing need of using semiconductor in this millennium, the disposal of printed circuit board has received much attention from the viewpoints of environmental protection and resource utilization. In this research both bioleaching and chemical leaching process for the recovery of copper in printed circuit board sample and sludge sample of the semiconductor solid wastes were attempted. The copper contents of the printed circuit board and sludge sample are 23.17% and 4.89%. In the bioleaching process, mesophilic bacteria; *T.ferrooxidans*, *L.ferrooxidans*, *T.thiooxidans* and moderate thermophilic/thermophilic; *S.thermosulfidioxidans* and *A.brierlyi* were used. Chemical leaching involves the use of oxidizing agents such as ferric chloride, ferric sulphate, acetic acid, sodium thiosulphate and sodium hypochlorite. In bioleaching of the sludge sample, high copper recoveries were obtained using *T.thiooxidans* (5.58%) while for printed circuit board sample high recoveries were obtained using *L.ferrooxidans* (60.84%). Copper in printed circuit board sample and sludge sample were efficiently recovered by ferric chloride leaching (93.30%) and sodium thiosulphate leaching (15.30%) respectively.

Mior Ahmad Khushairi Mohd Zahari

The gold mining industry is an exhaustive process whereby large amounts of ore have to be processed to extract the metal. Also, limitations of the techniques used in gold processing leads to the incomplete recoveries of gold, which normally ends up in the tailings. In this study, biooxidation using mixed cultures consisting of *Thiobacillus thiooxidans* (TT), *Thiobacillus ferrooxidans* (TF), *Leptospirillum ferrooxidans* (LF) and *Caldibacillus ferrivorus* (CF) was carried out in a Continuous Stirred Tank Reactor (CSTR) to recover gold from mines tailings. Biooxidation studies were first conducted using shake flasks, where a mixed culture consisting of TT, TF, LF and CF at a ratio of 3:1:1:3 was found to decrease the percentage of preg-robbing by a factor of 3 compared to the control. Biooxidation was also carried out in a bioreactor using the batch and continuous modes. Results from the batch experiments show that the solubilisation of iron for the 3:1:1:3 (TT: TF: LF: CF) cultures is 0.52 times higher than the 1:1:1:1 (TT: TF: LF: CF) cultures and 1.08 times higher than the control. For the continuous mode, the best iron solubilisation was obtained under the following operating conditions i.e. temperature, 38°C; stirring speed, 350 rpm; pulp density, 15%; bacterial ratio, 3:1:1:3 (TT: TF: LF: CF); pH, 2.00 and 3 days residence time. There was also a great reduction in the heavy metal content of the tailings after biooxidation i.e. 83.02% Fe, 53.09% Cd, 65.00% Cu, 30.16%Pb and 54.72% Zn were solubilised from the tailings. The recovery of gold from the biooxidation process was then carried out using cyanide. The highest gold recovery (>95%) was achieved under the following set of conditions; 30% pulp density, 1000-ppm cyanide and with aeration. However, the amounts of gold recovered after electrorefining process was low i.e. 46.71%.

TABLE OF CONTENTS

CHAPTER	TITLE	PAGE
	TITLE OF PROJECT	
	ACKNOWLEDGEMENT	
	TABLE OF CONTENTS	
	LIST OF TABLES	
	LIST OF FIGURES	
	LIST OF ABBREVIATIONS	
PART 1	ISOLATION OF THERMOPHILIC BACTERIA	1
1.0	Isolation of thermophilic Organisms	1
1.1	Isolation of thermophilic organisms from Hot springs	2
1.1.1	Material and Methods	2
1.1.2	Result and discussion	4
1.2	Solid Medium	5
1.2.1	Material and Methods	5
1.2.2	Result and discussion	6
1.3	Bioleaching Test	6
1.3.1	Material and Methods	6
1.3.2	Result and discussion	7
1.3.2.1	Pyrite biooxidation	7
1.3.2.2	Biooxidation of pyrite using culture C at various pH	9
1.4	Isolation of bacteria from abandoned ore pile	11

1.4.1	Isolation procedure	11
1.4.2	Results and discussion	14
1.5	Solid medium preparation	16
1.5.1	Material and Methods	16
1.5.2	Results and discussion	16
1.6	Bioleaching test	17
1.6.1	Material and Methods	17
1.6.2	Results and discussion	17
	1.6.2.1 Pyrite Oxidation	17
1.6.3	Penjom sulfidic ore oxidation	18
1.6.4	Sungai Lembing copper concentrate Oxidation	20

**PART 2 COLUMN STUDIES ON GOLD ORES AND ITS
CONCENTRATES 22**

2.0	Introduction	22
2.1	World commercial bioleaching plant	22
2.1.1	Refractory gold pretreatment	23
2.1.2	Mineral concentrate	26
2.1.3	Cyanidation	28
2.1.4	Bio-heap leaching of low grade refractory ore	29
2.1.5	Technical consideration for heap Leaching	30
	2.1.5.1 Spraying irrigation	30
	2.1.5.2 Aeration	31
	2.1.5.3 Pad and lining	31
	2.1.5.4 Stacking	33
	2.1.5.5 Climatic factors	34

2.2	Materials and methods	36
2.2.1	Ore and concentrate characterisation	36
2.2.1.1	Chemicals	37
2.2.1.2	Gold ore and concentrated Sample	37
2.2.1.3	Acid digestion	38
2.2.1.4	Carbon and sulphur content	38
2.2.1.5	Size analysis	39
2.2.1.6	Sequential extraction	39
2.2.1.7	Free gold test	39
2.2.1.8	H ₂ SO ₄ treatment	39
2.2.1.9	HCl treatment	40
2.2.1.10	HNO ₃ treatment	40
2.2.1.11	Acid consumption test	40
2.2.1.12	Biological acid producing potential	41
2.2.1.13	Preg-robbing test	41
2.2.2	Column Leaching Test	42
2.2.2.1	Leaching test	42
2.2.2.2	Gold cyanidation	45
2.2.2.3	Column analysis	45
2.3	Results and discussion	46
2.3.1	Elemental analysis	46
2.3.2	Sequential extraction	51
2.3.3	Size analysis	53
2.3.4	Acid consumption test	57
2.3.5	Biological acid producing potential (B.A.P.P)	58
2.3.6	Preg-robbing test	59
2.3.7	Column leaching studies	63
2.3.7.1	pH and E _H profile	63

2.3.7.2	pH profile for sulfur oxidizing related culture	64
2.3.7.3	Iron solubilization behaviour in the column	72
2.7.3.4	Gold extraction using cyanide in the column	77
2.3.7.5	Correlation between solution potential (E_H), Temperature (T), acidity (pH) and iron solubilized [Fe] in the column solution	84
	ATTACHMENT A	90
	ATTACHMENT B	94
PART 3	LEACHING STUDY OF PYRITE USING STIRRED TANK REACTOR (STR) AND THE MODELLING OF LEACHING PROCESS	102
3.0	Foreword	102
3.1	Introduction	102
3.2	Biooxidation using STR	104
3.2.1	Material and Methods	104
3.2.1.1	Mineral used	104
3.2.1.2	Acid digestion of mineral	104
3.2.1.3	Carbon and sulphur determination	104
3.2.1.4	Culture used	105
3.2.1.5	Bioreactor	105
3.2.1.6	Ferrous and ferric determination	108
3.2.1.7	Dissolved oxygen consumption rate	108

3.2.2	Result and discussions	108
3.2.2.1	Elemental analysis	108
3.2.2.2	STR biooxidation of pyrite using different types of culture	112
3.2.2.3	Shrinking particle model for diffusion through liquid film as a limitation step	114
3.2.2.4	Shrinking core model for diffusion through liquid film as a limitation step	115
3.2.2.5	Shrinking core and particle model for chemical reaction on pyrite surface as a limitation step	116
3.2.2.6	Shrinking core model with diffusion of porous inert layer as a limitation step	119
3.2.2.7	Redox potential (E_H) and pH profile for STR biooxidation of pyrite using different types of culture	120
3.2.2.8	Iron solubilization and jarosite formation in the STR biooxidation of pyrite using different types of culture	126
3.2.2.9	Iron speciation in the STR biooxidation of pyrite using different types of culture	130
3.2.2.10	Dissolved oxygen behaviour in the biooxidation of pyrite using different types of culture	137

3.2.3	STR biooxidation of pyrite using SL5B at different pyrite pulp densities.	149
3.2.3.1	Shrinking particle model for diffusion through liquid film as a limitation step	151
3.2.3.2	Shrinking core model for diffusion through liquid film as a limitation step	152
3.2.3.3	Shrinking core and particle model for chemical reaction on pyrite surface as a limitation step	153
3.2.3.4	Shrinking core model with diffusion of porous inert layer as a limitation step	154
3.2.3.5	Iron speciation and jarosite formation in the STR biooxidation at different pyrite pulp densities	156
3.2.3.6	Redox potential (E_H), pH and dissolved oxygen profile for STR biooxidation of pyrite using different types of culture	159
3.2.4	STR bioleaching of different pyrite size using SL5B.	163
3.2.4.1	Disolved oxygen consumption profile, pH, Redox potential (E_H) and Fe^{3+}/Fe^{2+} profile during biooxidation	164
3.2.4.2	Iron speciation in the pyrite and solution.	170
3.2.4.3	Pyrite oxidation rate.	176

3.2.4.4	The dissolution kinetics of pyrite	179
3.2.4.5	Shrinking Particle Model	181
3.2.4.6	Shrinking Core Model	182
3.2.4.7	Shrinking particle model for diffusion through liquid film as a limitation step: Application of model to experimental data	186
3.2.4.8	Shrinking particle and core model for diffusion through chemical reaction as a limitation step: Application of model to experimental data	187
3.2.4.9	Shrinking core model for diffusion through film diffusion as a limitation step: Application of model to experimental data	189
3.2.4.10	Shrinking core model for diffusion through inert product layer as a limitation step: Application of model to experimental data	190
	ATTACHMENT C	192
	ATTACHMENT D	213
	ATTACHMENT E	228
	ATTACHMENT F	236
PART 4	IN SITU APPLICATION	261
4.0	Introduction	261
4.1	Specific Objectives	262
4.2	Collection	263

4.2.1	Suggestion batteries container	266
4.2.2	Financial	268
4.3	Metal determination	269
4.3.1	Physical condition of batteries	269
4.3.2	Metal content	271
4.3.3	Metal content of batteries collected by DBKL	277
4.4	Laboratory test works	278
4.4.1	Column leaching test work	278
4.5	Laboratory test	284
4.5.1	Shake flask test	284
4.6	Laboratory test	297
4.6.1	Stirred tank reactor (STR) test	297
4.7	Case 1: Treatment process conducted by Kualiti Alam Sdn Bhd.	344
4.7.1	Case 2: The BATENUS process	347
4.7.2	Case 3: Recytec process	349
4.7.3	Our proposed batteries recycling process	350
4.7.4	Heat treatment plant	352
	4.7.4.1 Leaching plant	353
	4.7.4.2 Conditions for heap leaching	356
	4.7.4.3 Battery Breaking	360
	4.7.4.4 Battery shredder	360
4.8	Battery Shredding and Emission Control Unit	361
4.8.1	Battery Separating	362
4.9	Cost estimation	363
PART 5	ABSTRACTS	366
PART 6	FINANCIAL REPORT	371

PART 7	LIST OF EQUIPMENTS	372
PART 8	PUBLICATIONS AND AWARDS	373
	APPENDIX	377

ACKNOWLEDGEMENT

And with Allah lies all success and may Allah send prayers and salutations upon our Prophet (sal-Allaahu ‘alayhe wa sallam) and his family and his companions

I would like to acknowledge, firstly the Ministry of Science, Technology and the Environment for the financial support.

My thanks also to Dewan Bandaraya Kuala Lumpur, Kuala Lumpur for the invaluable help rendered. Without their support this project would be only be lab based.

To our collaborator.....

A note of special thanks to the Research Management Centre, UTM.

Last but by no means to Jefri, Azri, Abu Bakar, Nurhayati, Mior, who actually made this work possible.

VOTE 74245

**THE USE OF THERMOPHILIC ORGANISM FOR THE RECOVERY OF
GOLD AND COPPER FROM GRADE ORE**

**(PENGUNAAN ORGANISMA TERMOFILIK UNTUK PEROLEHAN
SEMULA EMAS DAN KUPRUM DARI ARANG GRADE)**

WAN AZLINA AHMAD

**RESEARCH VOTE NO:
74245**

**Fakulti Sains
Universiti Teknologi Malaysia**

2007

ACKNOWLEDGEMENT

The completion of this project would not have been possible without the help of everyone in the Biotechnology Lab, namely Jefri Jaapar, Shahrul Halim Sohor, Mohd Azri Bunyok, Nurhayati Deris and Lai Huat Choi.

The report was made possible by Mohd Saufi Sidek, who persevered with the compilation of this work.

Our sincere thanks to the Research Management Centre, UTM and MOSTI for the financial support.

Last but by no means least, to everyone who have helped make this project a success.

ABSTRACT

The use of thermophilic bacteria organisms in industrial processes is gaining importance due to the many advantages conferred by these organisms. This work reports on the isolation, characterization and application of thermophilic organisms in the recovery of metals from spent dry cell batteries. Column studies were conducted using *Thiobacillus ferrooxidans*, *Leptospirillum ferrooxidans*, *Thiobacillus thiooxidans*, *Sulfobacillus thermosulfodioxidans*, *Acidianus brierleyi* and SL5B. The leaching of roasted batteries using *Thiobacillus thiooxidans* yielded 95% Zn and 12% Mn. Roasting at 200 – 300°C increased yields i.e. 98% using FeCl₃ and 96% using SL5B culture. It was also observed that shredding the battery into the different components is necessary before the bioleaching step. A pilot scale work on bioleaching of batteries was also proposed.

ABSTRAK

Penggunaan organisma termofilik di dalam industri pemrosesan semakin mendapat perhatian disebabkan kelebihan-kelebihan yang diperolehi melalui penggunaan organisma-organisma ini. Kajian ini melaporkan tentang pemencilan, pencirian dan aplikasi organisma termofilik ini di dalam perolehan semula logam dari bateri sel kering terpakai. Kajian turut dijalankan menggunakan *Thiobacillus ferrooxidans*, *Leptospirillum ferrooxidans*, *Thiobacillus thiooxidans*, *Sulfobacillus thermosulfodioxidans*, *Acidianus brierleyi* and SL5B. Kajian larut lesap bagi bateri yang telah dipanaskan pada suhu tinggi menggunakan kultur *Thiobacillus thiooxidans* menghasilkan 95% Zn dan 12% Mn. Pemanasan pada suhu 200 – 300°C meningkatkan lagi peratusan hasil sebanyak 98% menggunakan FeCl₃ dan 96% menggunakan kultur SL5B. Selain itu, pemecahan bateri kepada komponen-komponen berbeza adalah penting sebelum proses larut lesap bio. Kajian larut lesap bio bagi bateri pada skala loji pandu juga dicadangkan di dalam laporan ini.

TABLE OF CONTENTS

CHAPTER	TITLE	PAGE
	TITLE OF PROJECT	i
	ACKNOWLEDGEMENT	ii
	ABSTRACT	iii
	TABLE OF CONTENTS	v
	LIST OF TABLES	viii
	LIST OF FIGURES	x
	LIST OF ABBREVIATIONS	xi
PART 1	ISOLATION OF THERMOPHILIC BACTERIA	1
	1.0 Isolation of thermophilic Organisms	1
	1.1 Isolation of thermophilic organisms from Hot springs	2
	1.1.1 Material and Methods	2
	1.1.2 Result and discussion	3
	1.2 Solid Medium	4
	1.2.1 Material and Methods	4
	1.2.2 Result and discussion	5
	1.3 Bioleaching Test	6
	1.3.1 Material and Methods	6
	1.3.2 Result and discussion	6
	1.3.2.1 Pyrite biooxidation	6
	1.3.2.2 Biooxidation of pyrite using culture C at various pH	8

1.4	Isolation of bacteria from abandoned ore pile	10
1.4.1	Isolation procedure	10
1.4.2	Results and discussion	13
1.5	Solid medium preparation	16
1.5.1	Material and Methods	16
1.5.2	Results and discussion	16
1.6	Bioleaching test	17
1.6.1	Material and Methods	17
1.6.2	Results and discussion	17
	1.6.2.1 Pyrite Oxidation	17
1.6.3	Penjom sulfidic ore oxidation	18
1.6.4	Sungai Lembing copper concentrate oxidation	19

**PART 2 APPLICATION OF THERMOPHILIC BACTERIA:
RECYCLING OF BATTERIES USING
BIOTECHNOLOGY TECHNOLOGY 21**

2.0	Introduction	21
2.1	Objectives of the project	21
2.2	Disposal of house hold batteries	22
	2.2.1 Batteries collection	22
2.3	Metal content	24
2.4	Laboratory test works	27
	2.4.1 Column leaching test work	28
	2.4.2 Shake flask test work	28
	2.4.3 Stirred tank reactor (STR) test work	29
	2.4.4 Metal purification test work	32
2.5	Proposal pilot scale process for batteries recycling	34
	2.5.1 Local technology to treat dry batteries	34

2.5.2	Existing technologies in other countries	37
2.5.3	Proposed Batteries Recycling 1	38
2.5.3.1	Heap of Alkaline and Zn-carbon cell	38
2.5.3.2	Pilot Plant Test Over View	42
2.5.4	Proposed Batteries Recycling 2	43
2.5.4.1	Agitation of Alkaline and Zn-carbon cell	43
2.6	Cost estimation	44
PART 3	PUBLICATIONS AND AWARDS	45
	APPENDIX	48

LIST OF TABLES

TABLES NO	TITLE	PAGE
1.1	Medium for hot spring isolation	3
1.2	Temperature and pH of Pedas hot spring sampling area	3
1.3	Description of colonies obtained on the solid medium	5
1.4	Elemental composition of pyrite	6
1.5	Medium used for isolation from abandoned ore piles	12
1.6	Visual observation of isolates obtained from Ulu Sokor	13
1.7	Microscopic observation of isolates obtained from Ulu Sokor	14
1.8	Visual observation of isolated obtained from Sungai Lembing	14
1.9	Microscopic observation of isolates obtained from Sungai Lembing	15
1.10	Percentages of pyrite oxidation using Ulu Sokor Culture	17
1.11	Percentages of pyrite oxidation using Sungai Lembing Culture	18
1.12	pH change and amount of gold extraction after biooxidation treatment using Ulu Sokor Culture for 3 days.	18
1.13	pH change and amount of gold extraction after	19

	biooxidation treatment using Sungai Lembing Culture for 3 days	
1.14	pH change and amount of iron and copper extraction after 3 days bioleaching using Ulu Sokor Culture	19
1.15	pH change and amount of iron and copper extraction after 3 days bioleaching using Sungai Lembing Culture	20
2.1	Metal content of non rechargeable dry cell (Zn-C and Alkaline batteries).	25
2.2	Metal content of rechargeable dry cell	26
2.3	Metal content of batteries collected by DBKL	27
2.4	Amount of metals extracted from column 1 and 2	28
2.5	Details for every set in stirred tank reactor (STR) leaching process	29
2.6	Purification methods for recovered metal	32

LIST OF FIGURES

FIGURE NO	TITLE	PAGE
1.1	pH profile of bacteria obtained from Pedas Hot spring	7
1.2	Eh profile of bacteria obtained from Pedas Hot spring	7
1.3	[Fe] from pyrite dissolution in the presence of bacteria obtained from Pedas Hot spring	8
1.4	pH profile of pyrite oxidation of culture C at various pH	9
1.5	Eh profile of pyrite oxidation of culture C at various pH	9
1.6	Fe solubilization profile of pyrite oxidation by culture C at various pH	10
2.1	Portion of batteries segregation by size	23
2.2	Portion of batteries segregation by origin of producer	23
2.3	Portion of batteries, segregation by recharge ability	24
2.4	Portion of rechargeable batteries	24
2.5	Portion of non-rechargeable batteries	24
2.6	Cross section of alkaline and zinc carbon batteries	25

LIST OF ABBREVIATIONS

AAS	atomic absorption spectroscopy
DO	dissolved oxygen
DMSZ	<i>Deutsche Sammlung von Mikroorganismen und Zelkulturen GmbH</i>
E _h , E _h	value of SRP (Standard Reduction Potential)
Fig	figure
Hr	hour
kg	kilogram
L	liter
<i>L. ferrooxidans</i>	<i>Leptospirillum ferrooxidans</i>
M	molar
min	minutes
mL	milliliter
mm	millimeter
ppb	part per billion
ppm	part per million
rpm	rotation per minute
<i>T.ferrooxidans</i>	<i>Thiobacillus ferrooxidans</i>
<i>T.thiooxidans</i>	<i>Thiobacillus thiooxidans</i>
µm	micro meter

PART 6

FINANCIAL REPORT

Total IRPA Funding : RM 139,981.00
 Project Start : 4/21/2004
 Project End : 4/20/2007

ITEM	Approved allocation by MOSTI	Expenditure until 30/4/2007	Balance as at 30/4/2007
Temporary & Contract Personnel (J 400)	33,031.00	33,687.48	(656.48)
Travel & Transportation (J 500)	22,750.00	21,483.35	1,266.65
Rentals (J 600)	4,500.00	2,350.00	2,150.00
Research Materials & Supplies (J 700)	16,950.00	16,602.63	347.37
Minor Modifications & Repairs (J 800)	20,250.00	15,403.00	4,847.00
Special Services (J 900)	6,500.00	6,456.10	43.90
Special Equipment & Accessories (J 1000)	36,000.00	35,339.00	661.00
Total	139,981.00	131,321.56	8,659.44

Expenditure Percentage: 93.81%

LIST OF ABBREVIATIONS

AAS	atomic absorption spectroscopy
CSTR	continuous stirred tank reactor
DO	dissolved oxygen
DMSZ	<i>Deutsche Sammlung von Mikroorganismen und Zellkulturen GmbH</i>
Eh, E _h	value of SRP (Standard Reduction Potential)
Fe ²⁺	ferrous ion
Fe ³⁺	ferric ion
FeS ₂	pyrite
Fig	figure
Hr	hour
kg	kilogram
L	liter
<i>L. ferrooxidans</i>	<i>Leptospirillum ferrooxidans</i>
M	molar
min	minutes
mL	milliliter
mm	millimeter
ppb	part per billion
ppm	part per million
rpm	rotation per minute

SEM	scanning electron microscopy
<i>T.ferrooxidans</i>	<i>Thiobacillus ferrooxidans</i>
<i>T.thiooxidans</i>	<i>Thiobacillus thiooxidans</i>
μm	micro meter

PART 7**LIST OF EQUIPMENTS**

Total IRPA Funding : RM 139,981.00
 Project Start : 4/21/2004
 Project End : 4/20/2007

LIST OF J 1000

BIL	ITEM	AMOUNT	SERIAL NO.
1	Spectrophotometer (Genesys 20 (4001-04)	9.965,00	3SSG/6/008
2	Certomat-R	10.920,00	01893
3	Shaker (Orbital) & Clamps	1.990,00	
4	Eppendorf & Eptip Standard	1.188,00	
5	Cable/DSL Router	428,00	76595
6	Hard Disk & 1284 Cable HP	325,00	
7	Magnetic Stirrer / Hotplate	890,00	082603197849
8	Water Still Output 4 Litre	2.890,00	R000100108
9	Single Door Security System	1.600,00	G206080100
10	Document Laminator	1.080,00	2058921
11	Incubator	3.910,00	E406.1007
12	Deskjet Printer	153,00	TH6BG150C5
	TOTAL	35.339,00	

LIST OF FIGURES

FIGURE NO	TITLE	PAGE
1.1	pH profile of bacteria obtained from Pedas Hot spring	7
1.2	Eh profile of bacteria obtained from Pedas Hot spring	7
1.3	[Fe] from pyrite dissolution in the presence of bacteria obtained from Pedas Hot spring	8
1.4	pH profile of pyrite oxidation of culture C at various pH	9
1.5	Eh profile of pyrite oxidation of culture C at various pH	10
1.6	Fe solubilization profile of pyrite oxidation by culture C at various pH	11
2.1	The Youanmi BIOX plant	24
2.2	General overview of a simple floatation process	27
2.3	Heap leaching process diagram	36
2.4	Schematic diagram of the column leaching apparatus	43
2.5	Iron speciation in a gold concentrate	51
2.6	Iron speciation in a gold ore	51
2.7	Gold speciation in a gold concentrate	52
2.8	Gold speciation in a gold ore	52
2.9	Behavior and size distribution of mineral during agglomeration. (Bouffard, 2003)	55
2.10	Thiosulfate mechanism in pyrite oxidation	65
2.11	Polysulfide mechanism in pyrite oxidation	65

2.12	Iron Solubilization profile of collected solution in the column at 70°C	72
2.13	Iron Solubilization profile of collected solution in the column at 45°C	72
2.14	Iron Solubilization profile of collected solution in the column at 30°C	73
2.15	Iron Solubilization profile of collected solution in the column at different temperature	73
2.16	Gold extraction using cyanide in the column	78
2.17	Effect of the mineral porosity on the gold extraction curve in a column. Bartlett [1992]	81
2.18a	SEM image of gold ore before biooxidation. (1000X magnification)	82
2.18b	SEM image of gold concentrate before biooxidation. (1000X magnification)	82
2.18c	SEM image of gold ore after biooxidized using mesophilic culture. (10000 X magnification)	82
2.18d	SEM image of gold ore after biooxidized using moderate thermophilic culture. (15000 X magnification)	82
2.18e	SEM image of gold ore after biooxidized using thermophilic culture. (10000 X magnification)	82
2.18f	SEM image of gold ore after biooxidized using mixture of mesophilic and thermophilic culture. (10000 X magnification)	82
3.1	Diagram of 2L Biostat [®] micro-DCU bioreactor	106
3.2-A	SEM images of ground, fresh pyrite surface. Pyrite was sieve at 75µm (Magnification 3000 X)	110
3.2-B	SEM images of ground, fresh pyrite surface. Pyrite was sieve at 250µm (Magnification 5000 X)	110
3.3-A	SEM photographs of a framboidal pyrite from Germany (Boon et al, 1999) (Magnification 2000 X)	110

3.3-B	SEM photographs of an euhedral pyrite from Prieska, South Africa (Boon et al, 1999) (Magnification 2000 X)	110
3.4-A	Percentages of pyrite solubilize during 24 hours oxidation using different type of culture, TF (30 ⁰ C), ST (45 ⁰ C) and SL5B(70 ⁰ C)	112
3.4-B	Percentages of pyrite solubilize during 24 hours, natural oxidation occurs at different temperature, 30 ⁰ C, 45 ⁰ C and 70 ⁰ C.	112
3.5-A	Percentages of 15 days pyrite solubilization. Oxidation using different type of culture, <i>T. Ferrooxidans</i> (30 ⁰ C), <i>Sb.Thermosulfodooxidans</i> (45 ⁰ C) and SL5B(70 ⁰ C).	117
3.5-B	Percentages of 15 days pyrite solubilization. Natural oxidation occurs at different temperature, 30 ⁰ C, 45 ⁰ C and 70 ⁰ C	117
3.6	pH and E _H profile during bioleaching	122
3.7-A	Sulfur oxidation pathways during natural pyrite oxidation	125
3.7-B	SEM photographs of a pyrite surface after 15 days leaching at 30 ⁰ C, in the absent of culture (Magnification 1000 X)	125
3.8	Iron speciation in a medium solution and in the form of jarosite and iron oxides	126
3.9	SEM photographs of a jarosite attach on a pyrite surface. Precipatation of jarosite during 15 days abiotic leaching at 70 ⁰ C, control, in the absence of culture (Magnification 20 000 X)	130
3.10	SEM photographs of a sulfur on a pyrite surface Precipatation of sulfur during 15 days abiotic leaching at 30 ⁰ C, control, in the absence of culture (Magnification 5000 X)	130
3.11-i	Ratios of [Fe ³⁺] / [Fe ²⁺] in the liquid medium during biooxidation study in STR using different cultures	131
3.11-ii	Ratios of [Fe ²⁺] / [Fe ³⁺] concentration in the liquid medium during biooxidation study in STR at different temperature	131

3.12	Generalized chemiosmotic network for extreme thermoacidophiles under normal growth conditions	132
3.13	The percentages of oxygen partial pressure of solution in a STR abiotik and biotic condition at 70 ⁰ C, 45 ⁰ C and 30 ⁰ C and dissolved oxygen consumption rate during 48 incubation of pyrite free-cell suspension in the presence of <i>SL5B</i>	138
3.14	Polagraphic oxygen electrode	141
3.15	SEM photograph of attachment of SL5B cell on a pyrite surface (Magnification 30 000 X)	145
3.16	SEM photograph of attachment of <i>T. ferrooxidans</i> on a pyrite surface (Magnification 50 000 X)	146
3.17	The model of attachment kinetics of bacteria on pyrite surface	146
3.18	Percentages of pyrite oxidation using SL5B. STR biooxidation conducted at 70 ⁰ C with different liquid medium to pyrite ratios	150
3.19	The composition of solubilized iron in a solution and iron in the form of precipitates in the STR biooxidation using SL5B at pyrite	156
3.20	The concentration of free iron in a form of Fe ²⁺ and Fe ³⁺ during 15 days biooxidation using SL5B	157
3.21	The profiles of pH and E _H of SL5B bioleaching at 1%, 3% and 5% pulp densities	159
3.22	Profile of % pO ₂ of pyrite oxidation using SL5B.	161
3.23	Profile of dissolved oxygen consumption by free-pyrite cell suspension of SL5B	162
3.24	The pH, ln(Fe ³⁺ /Fe ²⁺) and E _H profiles of pyrite oxidation using strain SL5B	165
3.25	The profiles of dissolved oxygen composition rate in a inoculation solution, for the SL5B biooxidation using different size of pyrite	168
3.26	The profiles of Fe ²⁺ and Fe ³⁺ in the sample solution from pyrite biooxidation using SL5B	171

3.27	Profiles of iron composition in solution (solubilized iron) and in the form of jarosite precipitate for the SL5B biooxidation using different size of pyrite	174
3.28	Pyrite oxidation during bioleaching using SL5B at 70°C	176
3.29	Correlation between T_{total} and pyrite size (R) in STR biooxidation using SL5B	178
3.30	Principles of shrinking unreacted core model	180
3.31	Schematic diagram of pyrite under shrinking particle model reaction	181
3.32	Schematic diagram of pyrite under shrinking core model reaction	183
4.1	Box for batteries recycling	266
4.2	Portion of batteries segregation by size	269
4.3	Portion of batteries segregation by origin of producer	269
4.4	Portion of batteries, segregation by recharge ability	270
4.5	Portion of rechargeable batteries	270
4.6	Portion of non-rechargeable batteries	270
4.7	Cross section of alkaline and zinc carbon batteries	272
4.8	Cross section of Ni-Cd and NiMH batteries	276

LIST OF TABLES

TABLES NO	TITLE	PAGE
1.1	Medium for hot spring isolation	3
1.2	Temperature and pH of Pedas hot spring sampling area	4
1.3	Description of colonies obtained on the solid medium	6
1.4	Elemental composition of pyrite	7
1.5	Medium used for isolation from abandoned ore piles	12
1.6	Visual observation of isolates obtained from Ulu Sokor	14
1.7	Microscopic observation of isolates obtained from Ulu Sokor	14
1.8	Visual observation of isolated obtained from Sungai Lembing	15
1.9	Microscopic observation of isolates obtained from Sungai Lembing	15
1.10	Percentages of pyrite oxidation using Ulu Sokor Culture	17
1.11	Percentages of pyrite oxidation using Sungai Lembing Culture	18
1.12	pH change and amount of gold extraction after biooxidation treatment using Ulu Sokor Culture for 3 days.	18
1.13	pH change and amount of gold extraction after biooxidation treatment using Sungai Lembing Culture for 3 days	19

1.14	pH change and amount of iron and copper extraction after 3 days bioleaching using Ulu Sokor Culture	20
1.15	pH change and amount of iron and copper extraction after 3 days bioleaching using Sungai Lembing Culture	20
2.1	The world's commercial gold pre-treatment plants	23
2.2	Column condition and strains used for each column	44
2.3	Elemental analysis of gold concentrate from Penjom Avocet Mine, Lipis Pahang, Malaysia	46
2.4	Elemental analysis of gold ore from a mixture of ore collected from various local gold field	49
2.5	Adsorption behavior of gold in solution to the gold concentrate and ore	59
2.6	Formation of sulfur compound resulting from metal sulfide oxidation	67
2.7	Indirect sulfur compound oxidation mechanisms for metal sulfides	70
2.8	Iron mass balance in the column during 4 months biooxidation	76
2.9	The gold mass balance in the column after 30 days of cyanidation.	83
2.10	The rate equations for microbial oxidation and ferrous-ferric ion behaviour	86
3.1	Parameter used for bioleaching of pyrite using STR	107
3.2	Elemental analysis of pyrite using ICP-MS and Carbon-Sulfur Detector	109
3.3	Iron concentration of pyrite at a different diameter	111
3.4	Time required (t_{total}) for complete pyrite oxidation if the shrinking particle model for diffusion through liquid film as a limitation step	115
3.5	Time required (t_{total}) for complete pyrite oxidation if the shrinking core model for diffusion through liquid film as a limitation step	115

3.6	Time required (t_{total}) for complete pyrite oxidation if the shrinking core model for diffusion through liquid film as a limitation step	116
3.7	Biooxidation stages of SL5B, <i>Sb.thermosulfodoxidan</i> and <i>T. ferrooxidans</i>	118
3.8	The required bioleaching time for pyrite biooxidation using for <i>SL5B</i> , <i>Sb.thermosulfodoxidan</i> and <i>T. ferrooxidans</i> and its control, when product layer diffusion becomes a rate limiting step in leaching reaction	119
3.9	The rate of pyrite formation	127
3.10	pO ₂ reduction in the abiotic STR	142
3.11	The dissolved oxygen consumption rate for pyrite-free suspension cell at the exponential phase	143
3.12	The rate of pyrite oxidation for the irreversible attached bacteria model and chemical oxidation model	151
3.13	Time required (t_{total}) for complete pyrite oxidation if the shrinking particle model for diffusion through liquid film as a limitation step	152
3.14	Time required (t_{total}) for complete pyrite oxidation if the shrinking core model for diffusion through liquid film as a limitation step	152
3.15	Time required (t_{total}) for complete pyrite oxidation if the shrinking core model for diffusion through liquid film as a limitation step	153
3.16	The required bioleaching time for pyrite biooxidation using for <i>SL5B</i> , <i>Sb.thermosulfodoxidan</i> and <i>T. ferrooxidans</i> and its control, when product layer diffusion becomes a rate limiting step in leaching reaction	155
3.17	The decreasing rate rate of initial E _H and Fe ³⁺ /Fe ²⁺ (from t=0 to t=30mnt) for the biooxidation using SL5B strain, containing 75µm, 125 µm and 180 µm of pyrite	167
3.18	The rate of pyrite oxidation for SL5B biooxidation at different pyrite size	177

3.19	The time required for complete pyrite oxidation for diffusion through liquid film as a limitation step	186
3.20	The time required for complete pyrite oxidation for the chemical reaction considered as controlling step	187
3.21	The time required for complete pyrite oxidation for the product diffusion considered as controlling step	189
3.22	The required bioleaching time for pyrite at different particle size, when product layer diffusion becomes a rate limiting step in leaching reaction	190
4.1	Metal content of non rechargeable dry cell (Zn-C and Alkaline batteries).	271
4.2	Zn and Mn content of Zn-C and alkaline batteries dust	271
4.3	Metal content of rechargeable dry cell	274
4.4	Metal content of batteries collected by DBKL (18.36 kg immersed in 50L aqua regia)	277
4.5	Column condition	278
4.6	Leaching condition	279

PART 1

ISOLATION OF THERMOPHILIC BACTERIA

1.0 Isolation of Thermophilic Organisms

The population of microbial community in a habitat is related to their physical and chemical requirements. Acidothermophilic are the second main group among the archaea and is taxonomically very heterogeneous. Various members of the acidothermophilic have been isolated from high temperature and low pH environments. Such prokaryotes may be present in metal and sulfur rich habitats such as hot springs, thermal acidic soil, volcanoes, thermal vents and coal pile drainage. It generally exists as a mixed population and not as pure culture. The enrichment culture technique is the most appropriate isolating technique. This technique involves the use of selective culture medium and a set of incubation condition to inhibit the undesired culture. Repeated agar plate streaking procedure is a frequent method to obtain a pure culture.

The success of enrichment culture technique is dependent on the inoculum source. The most appropriate local habitat of acidothermophilic archaea is a hot spring and abandoned ore pile

The only geothermal resource which exists in Malaysia is hot spring. The thermal spring commonly emerged at low level adjacent to topographic highs. All the local springs are found in Mesozoic sedimentary rocks and located along faults and sheared zones. A smell of H₂S is noted at most springs i.e. Tambun and Pedas Hot Spring. Spring water of sulfur i.e. Balung (Sabah) and Annah Rais (Sarawak) are

acidic and surrounding rocks are coated with sulfur. This is evident of the presence of a metal-sulfur oxidizing bacteria.

Besides hot spring, abandoned ore pile also has a potential for habitats of acidothermophiles archaea. Elevated temperature at the centre of pile during the natural sulfide oxidation promotes the growth of large communities of thermophilic archaea.

1.1 Isolation of thermophilic organisms from Hot springs

1.1.1 Material and Methods

The Pedas Hot Spring area and its vicinity was chosen as the site for bacteria isolation. At each site, 10mL of sample recovered by sterile syringe was transferred to each of the bottles, consisting of 100mL media in a 500mL sterilised Schott bottle. The sampling was conducted in replicates. The bottles were then immediately immersed in hot water to maintain the temperature. All samples were sent to the laboratory within a period of three hours and incubated at 70°C with shaking at 60 rpm in a water shaker. After 24 hours, a sample from each flask was transferred to fresh medium and incubated for a further 3 days at 70°C. The medium used for isolation is shown in Table 1.1.

Table 1.1: Medium for hot spring isolation

Medium	
9K	<p>Solution A 3.00g (NH₄)₂SO₄, 0.50g K₂HO₄.3H₂O, 0.50g MgSO₄. 7H₂O, 0.10g KCl, 700ml distilled-deionised water. pH adjusted to 2.0 using H₂SO₄, autoclaved at 121°C for 15 minutes.</p> <p>Solution B 44.22g FeSO₄.7H₂O, 300ml distilled-deionised water, pH adjusted to 2.0 and sterilised using filtration</p>
9K+Y	Composition similar with 9K either with 1% w/v yeast extract and 20ml of distilled-deionised water water.
TT	0.1g (NH ₄)Cl, 3.0g KH ₂ PO ₄ , 0.1g MgCl ₆ H ₂ O and 0.14g CaCl ₂ H ₂ O, 1L distilled-deionised water water, pH adjusted to 4.2 using H ₂ SO ₄ , autoclaved at 121°C for 15 minutes. 1% sulfur, Sterilised by steaming for 3 hours on each of 3 successive days.
TT+Y	Composition similar with TT either with 1% w/v yeast extract and 20ml of distilled-deionised water water.

1.1.2 Result and discussion

The condition of pool 1 and 2 of Pedas hot spring is shown in Table 1.2.

Table 1.2: Temperature and pH of Pedas hot spring sampling area

	Temperature	pH
Pool 1	52.8	6.45
Pool 2	43.7	5.87

After several inoculations in the respective media, growth was only observed in the 9K+Y medium with water sample from Pool 1 and 2. Growth was observed under the microscope, using hanging drop technique. No growth was observed in the 9K, TT and TT+Y medium.

In a mesophilic system, bacterial growth can be predicted by visual observation, i.e. changing of the medium colour from light green to yellow indicating the oxidation of Fe(II) to Fe(III). The sedimentation of sulfur powder is an indication of sulphur oxidation. However, in a thermophilic system, the change in colour and sedimentation of sulfur powder also observed in a controlled medium, an indication that iron and sulfur are spontaneously oxidized at high temperatures.

The good growth of organism in Pedas hot spring on a 9K+Y medium was shown by the presence of huge amounts of heterophilic iron oxidizer population in the samples.

1.2 Solid Medium

1.2.1 Material and Methods

A non-overlay, ferrous iron-yeast extract medium was used for culturing heterotrophic acidophilic bacteria. This medium was prepared using three different solutions.

Solution I

NH_4SO_4 0.45g/L, KCl 0.05g/L, $\text{MgSO}_4 \cdot 7\text{H}_2\text{O}$ 0.5g, $\text{Ca}(\text{NO}_2)_3$ 0.01 g/L, KH_2PO_4 0.05g and yeast extract 0.2g/L. pH adjusted to 2.5 using H_2SO_4 and autoclaved at 121°C for 20 minutes.

Solution II

A suspension of 4% (w/v) agarose type I, low EEO was melted in the microwave oven for 2 minutes, and then autoclaved at 121°C for 20 minutes.

Solution III

$\text{FeSO}_4 \cdot 7\text{H}_2\text{O}$ (1M) was prepared by adding 4.42g of $\text{FeSO}_4 \cdot 7\text{H}_2\text{O}$ in 30mL distilled water. The pH of the solution was adjusted to 2.0 using H_2SO_4 , the mix was then filtered sterilized.

Solution I and III were cooled prior to mixing it a ratio of 7:3. Solution B was then added to the above mixture at a ratio of 3:1 (A-C:B) and the mixture was poured into sterile Petri dishes.

Culture previously grown in the 9K+Y liquid medium were then streaked onto the solid media plate and the plates were incubated at 70°C .

1.2.2 Result and discussion

After 2 days of incubation at 70⁰C, four distinct colonies were observed on the solid medium. A colony was restreaked onto fresh plates and the same pattern of growth was observed after several transferred on the solids plates. The pattern of each colony is as shown in Table 1.3.

Table 1.3: Description of colonies obtained on the solid medium

Medium	Pool	Named (Remark)	
9K-Y	1	C	Yellow colonies, formation of clear zone around the colony
	1	XC	Yellow colonies
	2	Y	Yellow colonies
	2	W	White colonies

1.3 Bioleaching Test

1.3.1 Material and Methods

The mineral used in this experiment was pyrite (FeS₂) obtained from Peru. The mineral was ground using ball mill in acetone and sieved to 75 µm. The mineral was then washed with HNO₃ (1M) for 1 minute to get rid of any metal oxides. Slurry obtained was then filtered, washed 3 times with DI water and dried using acetone. The treated mineral was stored in the freezer to avoid natural oxidation.

Biooxidation was carried out in 500ml Schott bottle containing 100ml respective medium and treated mineral (1g). The bottle was inoculated with respective culture (20ml) and incubated at 70⁰C with shaking at 60 rpm for 10 days. Aliquots, 10mL were taken every 5 days and check for pH, Eh and metal content.

1.3.2 Result and discussion

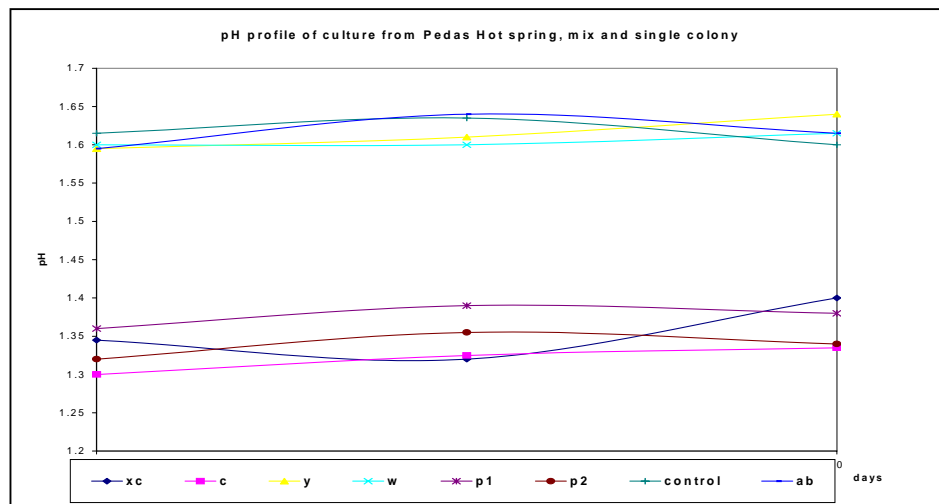
1.3.2.1 Pyrite biooxidation

The main elemental content of pyrite used in this experiment is shown in table 1.4.

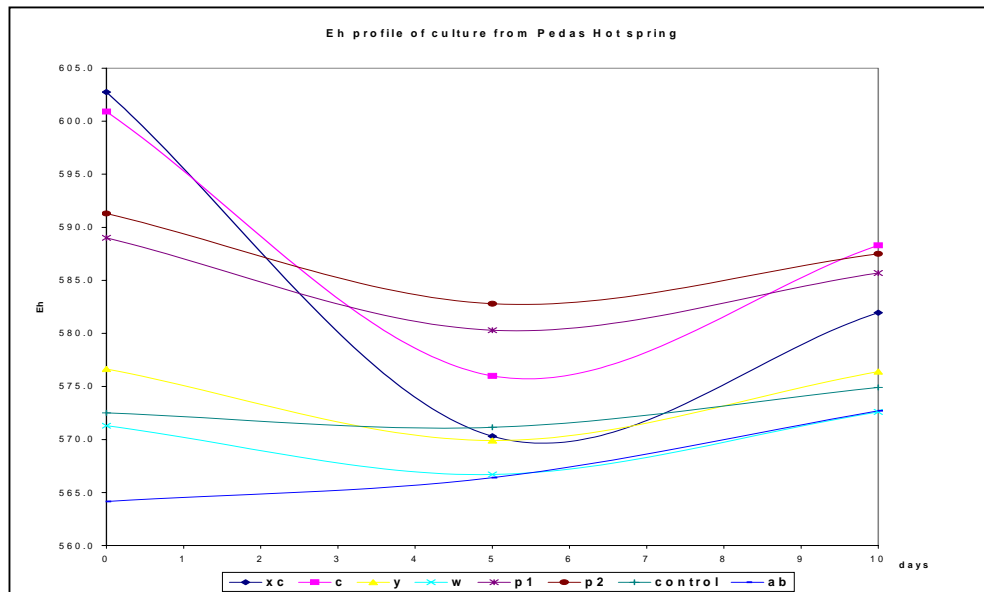
Table 1.4: Elemental composition of pyrite

	S%	C%	Fe%
Pyrite	24.2	0.593	46.28

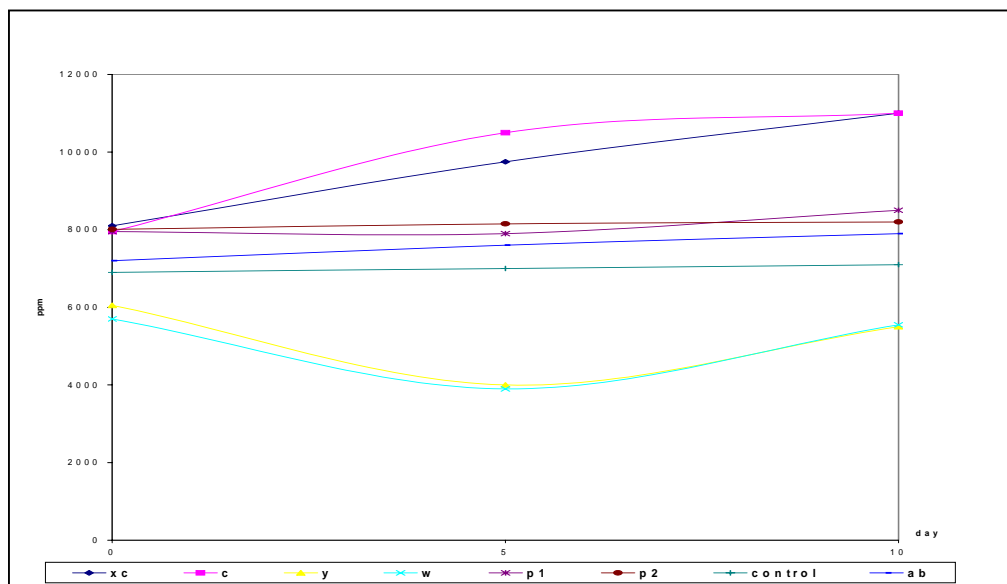
Leaching profile for pyrite oxidation of single and mixed culture of bacteria isolated from Pedas Hot Spring was shown in figures 1.1, 1.2 and 1.3.



Figures 1.1: pH profile of bacteria obtained from Pedas Hot spring



Figures 1.2: Eh profile of bacteria obtained from Pedas Hot spring



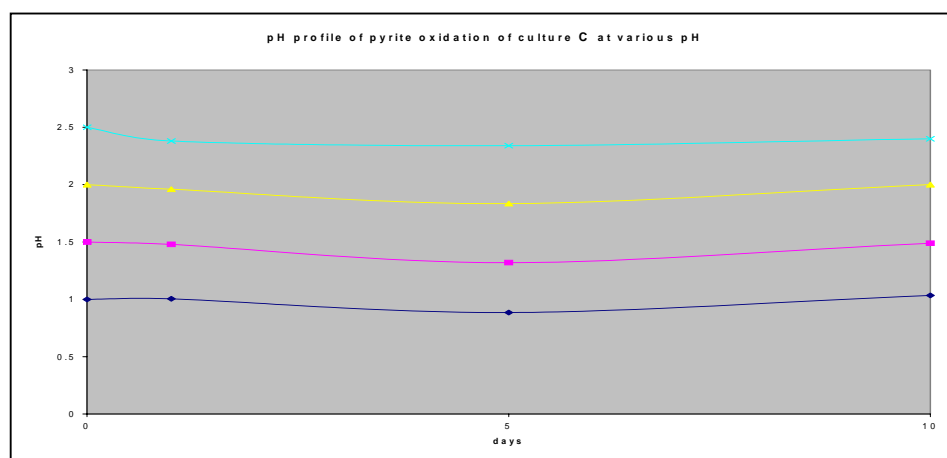
Figures 1.3: [Fe] from pyrite dissolution in the presence of bacteria obtained from Pedas Hot spring

Figures 1.1 showed that the pH decreased from 2.0 to 1.6 for cultures y, w, ab, and control. pH also decreased to 1.35 for cultures xc, c, p1 and p2. The highest Eh values were obtained for cultures c and xc (600 and 603 respectively) after 5 days of incubation. Eh values for both culture decreased to 575 and 570 for culture c and xc. Compared to standard culture of *Acidianus brierleyi* (AB), which acted as control,

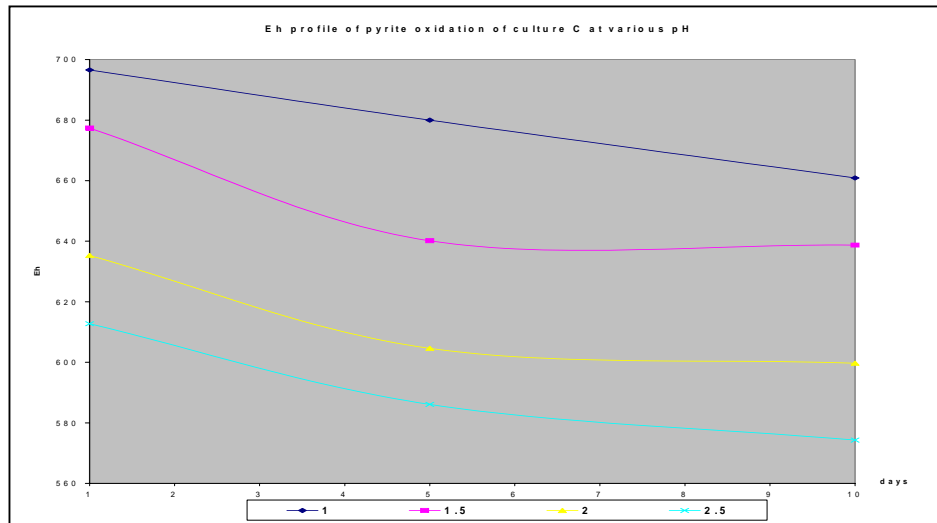
the Eh value was constantly low at 570 mV. High value of initial Eh and low pH value is very important in accelerating pyrite dissolution. It was shown in figure 3.3, the highest [Fe] content in solution was xc and c. However, rate of iron dissolution for c was highest then xc for the first 5 days of inoculation.

1.3.2.2 Biooxidation of pyrite using culture C at various pH

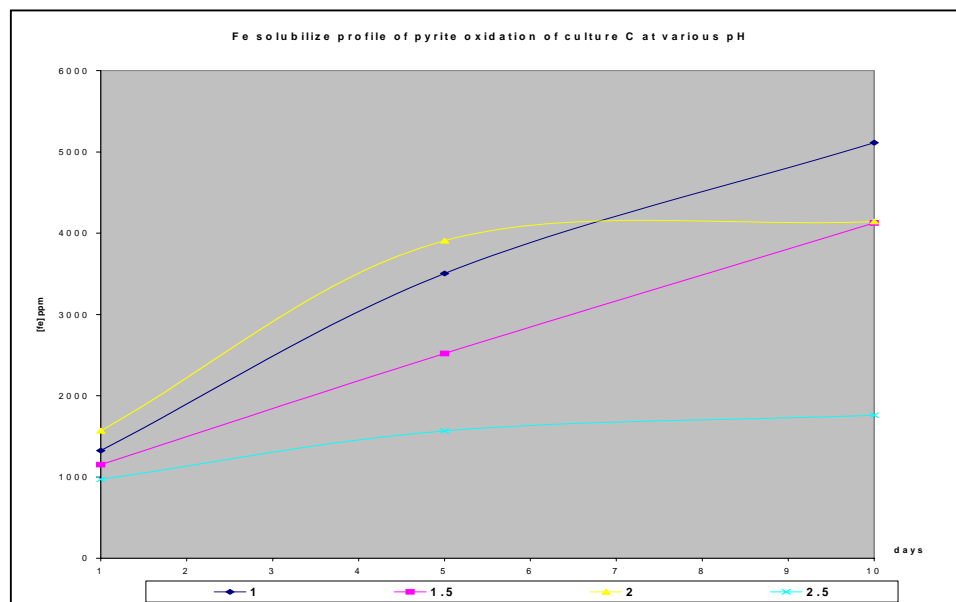
Culture C was then chosen for further experiments to determine the optimum pH for biooxidation of pyrite. The profiles of oxidation at various pH are shown in figures 1.4, 1.5 and 1.6.



Figures 1.4: pH profile of pyrite oxidation of culture C at various pH



Figures 1.5: Eh profile of pyrite oxidation of culture C at various pH



Figures 1.6: Fe solubilization profile of pyrite oxidation by culture C at various pH

The pH profiles for each set of experiment showed a significant trend (Fig 1.1). Every set showed a slight decrease in pH for the first 5 days of inoculation of culture, followed by the increase to the initial pH at day ten. Compared to the pH profile, Eh trends decrease constantly from day 1 to day 10 for every set of experiment (Fig 1.2). Highest iron solubilization was observed when pH of the medium was at 2.0 during the first 5 days of inoculation. A constant iron content was

observed from day 5 to day 10. At low pH i.e. 1.0 and 1.5, iron solubilization constantly increased until day 10. Possibly due to the prevention of jarosite precipitation at low pH (.Nemati *et al*,1998)

1.4 Isolation of bacteria from abandoned ore pile

1.4.1 Isolation procedure

Field sampling was conducted based on *in vitro* culturing method, explained in 1.1.1. Samples were taken from two abandoned ore piles. Descriptions of the sampling site are as follows:

Ulu Sukor

Abandoned heap leaching plant, heap containing 40,000t of sulfidic-carbonaceous gold ores. Samples were taken from a drainage channel emanating from a heap. Temperature and pH of sample taken were 33°C and 4.17 respectively. The plant was left idle without operation for 2 years.

Sg. Lembing

Samples were taken from the slumps around the copper concentrate piles. The concentrate contains chalcopyrite, chalcocite, copper oxide, pyrite and arsenopyrite. The concentrate was left idle due to the strict legal restriction by the Japanese Government on the arsenic limit content in roasting industries. Temperatures and pH of sample were 39°C and 1.97. Bacteria were cultivated aerobically in 13 different media listed in table 1.5

Aerobic culturing was conducted in a 20ml universal bottle, containing a mixture of 5 ml of respective medium and 1ml of sample. The bottle was then immediately immersed in hot water to maintain the temperature. The bottles were kept at 70°C during transportation to the laboratory.

Table 1.5: Medium used for isolation from abandoned ore piles

<p>Medium 1: <i>SULFOLOBUS MEDIUM</i></p> <p>(NH₄)₂SO₄ (1.30), KH₂PO₄ (0.28g), MgSO₄.7 H₂O (0.25 g), CaCl₂.2 H₂O (0.07g), FeCl₃.6 H₂O (0.02 g) MnCl₂.4 H₂O (1.80mg), Na₂B₄O₇.10 H₂O (4.50 mg), ZnSO₄.7 H₂O (0.22 mg), CuCl₂.2 H₂O (0.05 mg), Na₂MoO₄.H₂O (0.03mg), VOSO₄.2 H₂O(0.03mg), CoSO₄ (0.01 mg), Yeast extract (Difco) (1.00g) and Water, freshly distilled (1000ml).Adjust pH to 2.0 with 10 N H₂SO₄</p>
<p>Medium 2:<i>SULFOLOBUS SOLFATARICUS MEDIUM</i></p> <p>Yeast extract (Difco) (1.00g), Casamino acids (Difco)(1.00g), KH₂PO₄ (3.10g), (NH₄)₂SO₄ (2.50g),MgSO₄ x 7 H₂O (0.20 g), CaCl₂ x 2 H₂O (0.25 g), MnCl₂ x 4 H₂O (1.80mg), Na₂B₄O₇ x 10 H₂O (4.50 mg), ZnSO₄ x 7 H₂O (0.22 mg), CuCl₂ x 2 H₂O (0.05mg), Na₂MoO₄ x 2 H₂O (0.03 mg), VOSO₄ x 2 H₂O (0.03 mg), CoSO₄ x 7 H₂O (0.01mg), Distilled water (1000.00 ml).Adjust pH to 4.0 - 4.2 with 10 N H₂SO₄</p>
<p>Medium 3: <i>METALLOSPHAERA MEDIUM</i></p> <p>Use medium 1 either with 0.1% Difco yeast extract, or 0.05% powdered sulfur Sterilize substrates separately: sulfur by steaming for 1 h on three subsequent days.</p>
<p>Medium 4: <i>ACIDIANUS BRIERLEYI MEDIUM</i></p> <p>(NH₄)₂SO₄ (3.00g), K₂HPO₄ x 3 H₂O (0.50 g), MgSO₄ x 7 H₂O (0.50 g),KCl (0.10 g), Ca(NO₃)₂ (0.01 g), Yeast extract (0.20g) ,Sulfur (flowers) (10.00 g), Distilled water (1000.00ml),Adjust pH with 6 N H₂SO₄ to 1.5 - 2.5. Yeast extract (10% w/v in distilled water) is autoclaved separately. Sulfur is sterilized by steaming for 3 hours on each of 3 successive days.</p>
<p>Medium 5: <i>SULFOBACILLUS MEDIUM</i></p> <p><u>Solution A:</u> (NH₄)₂SO₄ (3.00 g), KCl (0.10 g), K₂HPO₄ (0.50 g), MgSO₄ x 7 H₂O (0.50 g), Ca(NO₃)₂ (0.01 g),Distilled water (700.00 ml),Adjust pH to 2.0 - 2.2 with sulfuric acid.</p> <p><u>Solution B:</u> FeSO₄ x 7 H₂O (44.20 g), Distilled water (300.00 ml), H₂SO₄, 10 N (1.00 ml),</p> <p><u>Solution C:</u> Yeast extract (1% w/v in water) (20.00 ml), After autoclaving, combine the three solutions. Medium pH 1.9 - 2.4.</p>
<p>Medium 6: <i>ACIDIMICROBIUM MEDIUM (Heterotrophic)</i></p> <p>MgSO₄ x 7 H₂O (0.5 g), (NH₄)₂SO₄ (0.4 g), K₂HPO₄ (0.2g), KCl (0.1g), Distilled water(1000 ml), Adjust pH to 2.0 with H₂SO₄.To the medium add 10.0 mg/l of FeSO₄ x 7 H₂O. After autoclaving add yeast extract from sterile stock solution to final concentration of 0.25 g/l.</p>
<p>Medium 7: <i>ACIDIMICROBIUM MEDIUM (Autotrophic)</i></p> <p>MgSO₄ x 7 H₂O (0.5g), (NH₄)₂SO₄ (0.4 g), K₂HPO₄ (0.2g), KCl (0.1 g), Distilled water (1000ml), To the medium add 13.9 g/l of FeSO₄ x 7 H₂O and adjust medium pH to 1.7 with H₂SO₄</p>

prior to autoclaving
<p>Medium 8: <i>SULFOBACILLUS DISULFIDOOXIDANS MEDIUM</i></p> <p>(NH₄)₂SO₄ (3.0g), KCl (0.1g), KH₂PO₄ (0.5 g), MgSO₄ x 7 H₂O (0.5g), Ca(NO₃)₂ x 4 H₂O (0.1 g), Yeast extract (0.1g), Distilled water (1000ml), Adjust pH to 2.25 prior to autoclaving. Before use add per liter 10 ml of a filter sterilized 10% (w/v) glutathione solution.</p>
<p>Medium 9: MS-MEDIUM <i>Thiobacillus caldus</i> For DSM 2392</p> <p>(NH₄)₂SO₄ (2.00g), MgSO₄ x 7 H₂O (0.25g), K₂HPO₄ (0.10g), KCl (0.10g), Distilled water (1000. ml),</p> <p>Adjust pH of MS-medium to 2.2 with 4 N H₂SO₄ prior to autoclaving. Before use, add 0.25 ml 40% (w/v) FeSO₄ x 7 H₂O solution (dissolved in 0.2 N H₂SO₄ and filter sterilized or autoclaved under N₂) per 5 ml MS-Medium.</p>
<p>Medium 10: MS-MEDIUM <i>Thiobacillus caldus</i> For DSM 9465</p> <p>(NH₄)₂SO₄ (2.00g), MgSO₄ x 7 H₂O (0.25g), K₂HPO₄ (0.10 g), KCl (0.10g), Distilled water (1000ml),</p> <p>: Adjust pH of MS-medium to 2.2 with 4 N H₂SO₄ prior to autoclaving. Before use, add 0.25 ml 40% (w/v) FeSO₄ x 7 H₂O solution (dissolved in 0.2 N H₂SO₄ and filter sterilized or autoclaved under N₂) per 5 ml MS-Medium.</p>
<p>Medium 11: MS-MEDIUM <i>Thiobacillus caldus</i> DSM 9467</p> <p>(NH₄)₂SO₄ (2.00g), MgSO₄ x 7 H₂O (0.25g), K₂HPO₄ (0.10 g), KCl (0.10g), Distilled water (1000), For: Adjust pH of MS-medium to 3.0 with 2N H₂SO₄ prior to autoclaving. Before use, add 0.2% glucose from filter sterilized 10% w/v stock solution, and 0.01% yeast extract from autoclaved 1% stock solution</p>
<p>Medium 12: 9K</p> <p><u>Solution A:</u> (NH₄)₂SO₄ (3.00g), KCl (0.10g), K₂HPO₄ (0.50g), MgSO₄ x 7 H₂O (0.50g), Distilled water (700ml), Adjust pH to 2.0 - 2.2 with sulfuric acid.</p> <p><u>Solution B:</u> FeSO₄ x 7 H₂O (44.20g), Distilled water (300.00 ml),</p> <p><u>Solution C:</u> Yeast extract (1% w/v in water) (20.00 ml)</p> <p>After autoclaving, combine the three solutions. Medium pH 1.9 - 2.4.</p>
<p>Medium 13: <i>Thiobacillus thiooxidans</i></p> <p>NH₄Cl (0.1g), KH₂PO₄ (3.0g), MgCl₂.6H₂O (0.1g) and CaCl₂.2H₂O (0.14g) in a 1L distilled water, sulfuric acid was added to adjust the pH to 4.2 before sterilising using the autoclave. Sterilised sulphur powder (112⁰C, 10mins) final concentration 5% was added to the solution upon cooling</p>

1.4.2 Results and discussion

The visual and microscopic examination of isolates obtained from Ulu Sokor and Sungai Lembing is shown in Tables 1.6, 1.7, 1.8 and 1.9:

Table 1.6.: Visual observation of isolates obtained from Ulu Sokor

Medium	pH		Eh		Remarks
	initial	final	initial	final	
1	1.89	1.87	625.3	636.1	No colour change
2	4.32	4.11	564.6	589.1	Colourless → brown, black precipitation
3	1.90	1.90	606.3	613.3	No colour change
4	1.93	1.97	618.1	640.7	No colour change, sulphur sediment
5	1.84	1.92	572.3	607.1	Green → light yellow, yellow precipitation
6	1.84	1.83	617.2	629.8	Green → light yellow, white precipitation
7	1.68	1.68	609.8	619.9	Green → colourless, yellow precipitation
8	2.15	2.11	541.3	572.2	No colour change
9	2.14	2.10	590.6	578.9	No colour change, yellow precipitation
10	3.63	3.69	591.4	581.8	No colour change
11	3.09	3.11	609.9	606.1	No colour change
12	1.73	1.72	597.9	613.5	Green → light yellow, yellow precipitation
13	4.02	4.00	417.7	528.5	No colour change

Table 1.7.: Microscopic observation of isolates obtained from Ulu Sokor

Medium	Cell concentration	Cell motility	Colony (Based on motility and shape)	Remarks
1	Low	Low	Mix	
2	Medium	Active	Single	Cell agglomeration
3	Very low	Low	3	
4	-ND-	-	Single	
5	Very low	Active	4	
6	Very high	Active	Single	
7	Very low	Low	Mix	
8	-ND-	-	-	
9	Very low	Low	Single	
10	Very low	Low	Single	
11	-ND-	-	-	
12	Low	Low	Single	Cell attachment on precipitate
13	Low	Active	Single	

Table 1.8.: Visual observation of isolated obtained from Sungai Lembing

Medium	pH		Eh		Remarks
	initial	final	initial	final	
1	2.04	1.93	621.1	638.8	No colour change
2	4.16	4.16	546.6	553.9	Colourless→yellow, yellow precipitation
3	1.94	1.95	614.4	618.8	No colour change
4	1.93	1.95	617.7	624.1	Colourless→cloudy, sulphur sedimentation
5	2.06	1.92	551.4	600.9	Green→light yellow, yellow precipitation
6	1.95	1.95	617.7	623.6	Green→cloudy yellow, white precipitation
7	1.68	1.67	581.6	602.2	Green→light yellow, yellow precipitation
8	2.18	2.17	538.5	561.4	No colour change
9	2.11	2.12	622.6	614.0	No colour change, yellow precipitation
10	2.77	2.49	635.1	624.4	Cloudy, sulphur sedimentation
11	3.03	3.09	588.3	591.2	No colour change
12	1.88	1.95	547.2	593.4	Green→light yellow, yellow precipitation
13	3.82	3.79	409.0	419.8	Cloudy, sulphur sedimentation
<i>Acidianus Brierleyi</i>	1.99	2.00	517.4	541.0	No colour change

Table 1.9.: Microscopic observation of isolates obtained from Sungai Lembing

Medium	Cell concentration	Cell motility	Colony (Based on motility and shape)	Remarks
1	Low	Low	Mix	
2	Low	Low	Mix	Large crystal appears
3	Very low	Very low	Single	
4	Very high	High	2	
5	Very low	Low	2	
6	-ND-	-	-	
7	Medium	Medium	2	
8	Low	Low	Single	
9	High	High	Single	
10	Very high	High	Single	Cell agglomeration
11	High	High	Single	
12	Medium	High	Single	
13	Medium	High	Single	
<i>Acidianus Brierleyi</i>	Medium	Active	Single	

1.5 Solid medium preparation

1.5.1 Material and Methods

Solid medium was prepared according to the ingredients used in liquid medium described in Table 1.5. The medium consists of the following:

- A. 70 mL of liquid medium which is listed in table 1.5. Sulfur powder in the ingredients was replaced with sodium thiosulfate solution.
- B. 30 mL of gelling solution containing 1.67g agarose, sigma type1.
- C. 1mL of sodium thioglycolate solution (1.1g/L)

For aerobic culturing, solutions A and B were mixed and poured into petri plates. The plates were then incubated at 30⁰C overnight to detect any contamination. Cultures from respective liquid media were then transferred using streak-plate and spread-plate techniques and incubated at 70⁰C for 24 hours.

The anaerobic culture isolation was conducted using molten agar technique. Culture (1mL) from respective liquid medium was transferred into sterilized tube test. Molten agar (5mL) containing solutions A, B and C were mixed with respective culture without aeration. It was then allowed to solidify prior to incubation at 70⁰C.

1.5.2 Results and discussion

After 24 hours of incubation, yellow-orange colonies grew on solid medium 5 and 12 for both Ulu Sokor and Sungai Lembing sample. Growth of colonies were not detected on the other plates.

The same observation was also seen in the anaerobic condition. Yellow-orange precipitates were observed at the surface of medium 5 and 12. This is indicates of the successful isolation of obligate aerobic, iron oxidizing organisms.

Work is in progress to purify the colony of other organisms.

1.6 Bioleaching test

1.6.1 Material and Methods

Bioleaching test of mixed culture obtained from Ulu Sokor and Sungai Lembing were conducted as discussed in section 1.3.1.

Biooxidation of ore was carried out in 500ml Schott bottle containing 100ml respective medium and 50g of ore. The bottle were inoculated with respective culture (20ml) and incubated at 70^oC with shaking at 60 rpm for 3 days.

The sulfidic gold ore used in this study was obtained from Penjom-Avecot Gold Mine, Pahang. The ore was first treated with cyanide to eliminate the free gold.

The copper concentrate was obtained from Sungai Lembing Tin Mine, Pahang. The concentrate was washed with tap water at a ratio of 10:1 (water:concentrate) to get rid of any water soluble copper.

1.6.2 Results and discussion

1.6.2.1 Pyrite Oxidation

Ulu Sokor Culture

Table 1.10: Percentages of pyrite oxidation using Ulu Sokor Culture

Medium	1	2	3	4	5	6	7	8	9	10	11	12	13
Fe solubilize (%)	1.55	22.14	22.16	2.62	45.04	9.58	0.00	2.09	5.72	2.79	1.64	7.95	15.06

Sungai Lembing Culture

Table 1.11: Percentages of pyrite oxidation using Sungai Lembing Culture

Medium	1	2	3	4	5	6	7	8	9	10	11	12	13
Fe solubilize (%)	1.43	1.57	6.99	1.06	45.12	15.55	0.38	2.23	8.92	1.67	2.26	16.2	1.22

Percentages of pyrite solubilization using Acidianus Brierleyi: 0.38

1.6.3 Penjom sulfidic ore oxidation

Ulu Sokor Culture

Table 1.12: pH change and amount of gold extraction after biooxidation treatment using Ulu Sokor Culture for 3 days.

Medium	pH		Gold extracted (ppm)
	initial	final	
1	1.87	6.86	3.12
2	4.11	7.47	28.52
3	1.90	7.29	2.87
4	1.97	7.61	9.83
5	1.83	4.25	26.87
6	1.92	6.88	5.23
7	1.68	5.93	1.14
8	2.11	7.84	7.43
9	2.10	7.68	11.41
10	3.69	7.61	3.86
11	3.11	7.62	5.18
12	1.72	4.44	9.54
13	4.00	6.32	3.43

Sungai Lembing Culture

Table 1.13: pH change and amount of gold extraction after biooxidation treatment using Sungai Lembing Culture for 3 days.

Medium	pH		Gold extracted (ppm)
	initial	final	
1	1.93	7.08	6.56
2	4.16	7.59	32.12
3	1.95	7.59	16.13
4	1.95	7.60	10.04
5	1.92	4.40	10.62
6	1.95	7.08	6.43
7	1.67	6.12	5.69
8	2.17	7.81	18.03
9	2.12	7.83	2.84
10	2.49	7.71	4.48
11	3.05	7.37	6.38
12	1.95	4.04	8.93
13	3.79	6.27	2.83

Amount of gold extraction using *Acidianus Brierleyi*: 12.32 ppm (pH: 2.00-7.36)

Amount of gold extraction without biooxidation: 1.44 ppm

1.6.4 Sungai Lembing copper concentrate oxidation

Ulu Sokor Culture

Table 1.14: pH change and amount of iron and copper extraction after 3 days bioleaching using Ulu Sokor Culture.

Medium	pH		Fe solubilize (%)	Copper extracted (%)
	initial	final		
1	1.90	2.03	8.00	0.6
2	2.09	2.10	0	0
3	1.95	2.09	4.10	4.2
4	2.11	2.12	4.31	2.7
5	1.91	1.99	39.34	1.9
6	2.14	1.92	11.45	0.5
7	1.92	2.48	17.69	0.5
8	2.18	2.07	12.98	0.2
9	2.40	2.48	14.52	0.9
10	2.75	2.52	5.92	0.1
11	2.58	2.61	6.46	0
12	1.85	1.96	13.6	0.1
13	1.97	2.16	11.06	0.1

Sungai Lembing Culture

Table 1.15: pH change and amount of iron and copper extraction after 3 days bioleaching using Sungai Lembing Culture.

Medium	pH		Fe solubilize (%)	Copper extracted (%)
	initial	final		
1	2.05	2.08	8.9	2.0
2	2.04	2.12	3.8	1.84
3	2.06	2.13	4.9	3.2
4	2.12	2.08	12.37	3.1
5	1.95	1.97	8.90	5.2
6	2.27	2.32	9.90	4.7
7	1.90	2.09	7.58	0.1
8	2.19	2.20	15.31	4.7
9	2.42	2.10	5.98	0.02
10	2.66	2.01	4.72	0.1
11	2.59	2.69	4.98	0.1
12	1.63	2.06	18.20	1.1
13	2.31	2.26	8.54	0.02

Percentages of copper extraction using *Acidianus Brierleyi*: 0.4% (pH: 2.16-2.19)

The highest pyrite leaching were obtained in a presence of culture in medium 5 (isolated from Sungai Lembing and Ulu Sokor), about 45% of iron was oxidize in medium 5 compared to 0.38% oxidation by culture in *Acidianus brierleyi* medium. Culture from Ulu Sokor in medium 5 also shows the highest amount of iron leaching (39%) for Sungai Lembing concentrate but low amount of copper leaching (1.9%). This shows that the pyrite oxidation was dominating the leaching process and not chalcopyrite. Compared to the culture in medium 5 i.e. Sungai Lembing isolate, highest amount of copper solubilization (5.2%) was occurs at low iron oxidation (8.9%), shows that most of the mineral oxidized were chalcopyrite.

The highest gold extraction was obtained from the ore, which is treated by culture in medium 2, 32.12 ppm for Sungai Lembing isolate and 28.5 ppm for Ulu Sokor isolate. This shows that the bioleaching is very selective on a nature of mineral in the ore, depending on the type of culture used.

PART 1

ISOLATION OF THERMOPHILIC BACTERIA

1.0 Isolation of Thermophilic Organisms

The population of microbial community in a habitat is related to their physical and chemical requirements. Acidothermophilic are the second main group among the archaea and is taxonomically very heterogeneous. Various members of the acidothermophilic have been isolated from high temperature and low pH environments. Such prokaryotes may be present in metal and sulfur rich habitats such as hot springs, thermal acidic soil, volcanoes, thermal vents and coal pile drainage. It generally exists as a mixed population and not as pure culture. The enrichment culture technique is the most appropriate isolating technique. This technique involves the use of selective culture medium and a set of incubation condition to inhibit the undesired culture. Repeated agar plate streaking procedure is a frequent method to obtain a pure culture.

The success of enrichment culture technique is dependent on the inoculum source. The most appropriate local habitat of acidothermophilic archaea is a hot spring and abandoned ore pile.

The only geothermal resource which exists in Malaysia is hot spring. The thermal spring commonly emerged at low level adjacent to topographic highs. All the local springs are found in Mesozoic sedimentary rocks and located along faults and sheared zones. A smell of H₂S was noted at most springs i.e. Tambun and Pedas Hot Spring. Spring water at Balung (Sabah) and Annah Rais (Sarawak) are acidic and the

surrounding rocks are coated with sulfur. This is evident of the presence of a metal-sulfur oxidizing bacteria.

Besides hot spring, abandoned ore pile also has a potential for habitats of acidothermophiles archaea. Elevated temperature at the centre of pile during the natural sulfide oxidation promotes the growth of large communities of thermophilic archaea.

1.1 Isolation of thermophilic organisms from Hot springs

1.1.1 Material and Methods

The Pedas Hot Spring area and its vicinity was chosen as the site for bacteria isolation. At each site, 10mL of sample recovered by sterile syringe was transferred to each of the bottles, consisting of 100mL media in a 500mL sterilised Schott bottle. The sampling was conducted in replicates. The bottles were then immediately immersed in hot water to maintain the temperature. All samples were sent to the laboratory within a period of three hours and incubated at 70^oC with shaking at 60 rpm in a water shaker. After 24 hours, a sample from each flask was transferred to fresh medium and incubated for a further 3 days at 70^oC. The medium used for isolation is shown in Table 1.1.

Table 1.1: Medium for hot spring isolation

Medium	
9K	<p>Solution A 3.00g (NH₄)₂SO₄, 0.50g K₂HO₄.3H₂O, 0.50g MgSO₄. 7H₂O, 0.10g KCl, 700ml distilled-deionised water. pH adjusted to 2.0 using H₂SO₄, autoclaved at 121°C for 15 minutes.</p> <p>Solution B 44.22g FeSO₄.7H₂O, 300ml distilled-deionised water, pH adjusted to 2.0 and sterilised using filtration</p>
9K+Y	Composition similar with 9K either with 1% w/v yeast extract and 20ml of distilled-deionised water water.
TT	0.1g (NH ₄)Cl, 3.0g KH ₂ PO ₄ , 0.1g MgCl ₂ .6H ₂ O and 0.14g CaCl ₂ .2H ₂ O, 1L distilled-deionised water water, pH adjusted to 4.2 using H ₂ SO ₄ , autoclaved at 121°C for 15 minutes. 1% sulfur, Sterilised by steaming for 3 hours on each of 3 successive days.
TT+Y	Composition similar with TT either with 1% w/v yeast extract and 20ml of distilled-deionised water water.

1.1.2 Results and discussion

The condition of pool 1 and 2 of Pedas hot spring is shown in Table 1.2.

Table 1.2: Temperature and pH of Pedas hot spring sampling area

	Temperature	pH
Pool 1	52.8	6.45
Pool 2	43.7	5.87

After several inoculations in the respective media, growth was only observed in the 9K+Y medium with water sample from Pool 1 and 2. Growth was observed under the microscope, using the hanging drop technique. No growth was observed in the 9K, TT and TT+Y medium.

In a mesophilic system, bacterial growth can be predicted by visual observation, i.e. changing of the medium colour from light green to yellow indicating the oxidation of Fe(II) to Fe(III). The sedimentation of sulfur powder is an indication of sulphur oxidation. However, in a thermophilic system, the change in colour and sedimentation of sulfur powder was also observed in a controlled medium, an indication that iron and sulfur was spontaneously oxidized at high temperatures.

The good growth of organism in Pedas hot spring on a 9K+Y medium was shown by the presence of huge amounts of heterophilic iron oxidizer population in the samples.

1.2 Solid Medium

1.2.1 Material and Methods

A non-overlay, ferrous iron-yeast extract medium was used for culturing heterotrophic acidophilic bacteria. This medium was prepared using three different solutions.

Solution I

NH_4SO_4 0.45g/L, KCl 0.05g/L, $\text{MgSO}_4 \cdot 7\text{H}_2\text{O}$ 0.5g, $\text{Ca}(\text{NO}_2)_3$ 0.01 g/L, KH_2PO_4 0.05g and yeast extract 0.2g/L. pH adjusted to 2.5 using H_2SO_4 and autoclaved at 121°C for 20 minutes.

Solution II

A suspension of 4% (w/v) agarose type I, low EEO was melted in the microwave oven for 2 minutes, and then autoclaved at 121°C for 20 minutes.

Solution III

FeSO₄.7H₂O (1M) was prepared by adding 4.42g of FeSO₄.7H₂O in 30mL distilled water. The pH of the solution was adjusted to 2.0 using H₂SO₄, and the mixture was then filtered sterilized.

Solution I and III were cooled prior to mixing it at a ratio of 7:3. Solution B was then added to the above mixture at a ratio of 3:1 (A-C:B) and the mixture was poured into sterile Petri dishes.

Culture previously grown in the 9K+Y liquid medium were then streaked onto the solid media plate and the plates were incubated at 70^oC.

1.2.2 Results and discussion

After 2 days of incubation at 70^oC, four distinct colonies were observed on the solid medium. A colony was restreaked onto fresh plates and the same pattern of growth was observed after several transferred on the solids plates. The pattern of each colony is as shown in Table 1.3.

Table 1.3: Description of colonies obtained on the solid medium

Medium	Pool	Designation	
9K-Y	1	C	Yellow colonies, formation of clear zone around the colony
	1	XC	Yellow colonies
	2	Y	Yellow colonies
	2	W	White colonies

1.3 Bioleaching Test

1.3.1 Material and Methods

The mineral used in this experiment was pyrite (FeS_2) obtained from Peru. The mineral was ground using ball mill in acetone and sieved to 75 μm . The mineral was then washed with HNO_3 (1M) for 1 minute to get rid of any metal oxides. Slurry obtained was then filtered, washed 3 times with DI water and dried using acetone. The treated mineral was stored in the freezer to avoid natural oxidation.

Biooxidation was carried out in 500ml Schott bottle containing 100ml respective medium and treated mineral (1g). The bottle was inoculated with respective culture (20ml) and incubated at 70 $^{\circ}\text{C}$ with shaking at 60 rpm for 10 days. Aliquots, 10mL were taken every 5 days and checked for pH, Eh and metal content.

1.3.2 Result and discussion

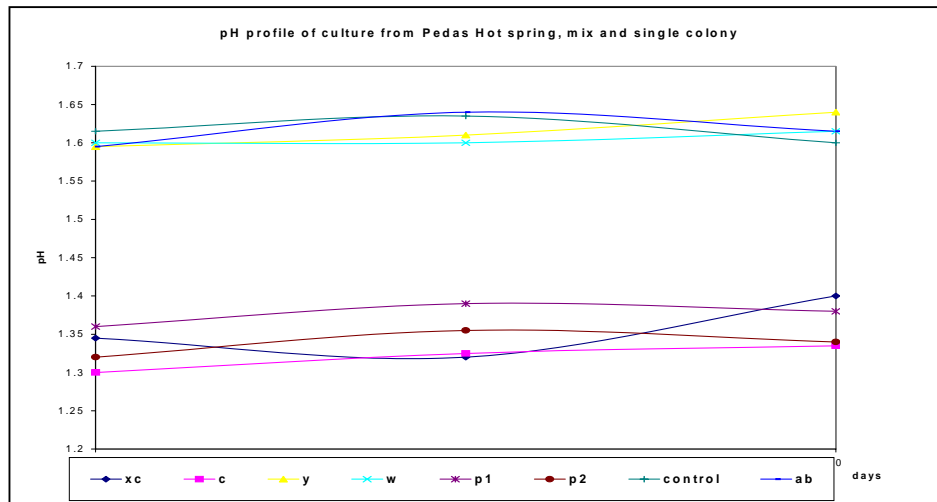
1.3.2.1 Pyrite biooxidation

The main elemental content of pyrite used in this experiment is shown in table 1.4.

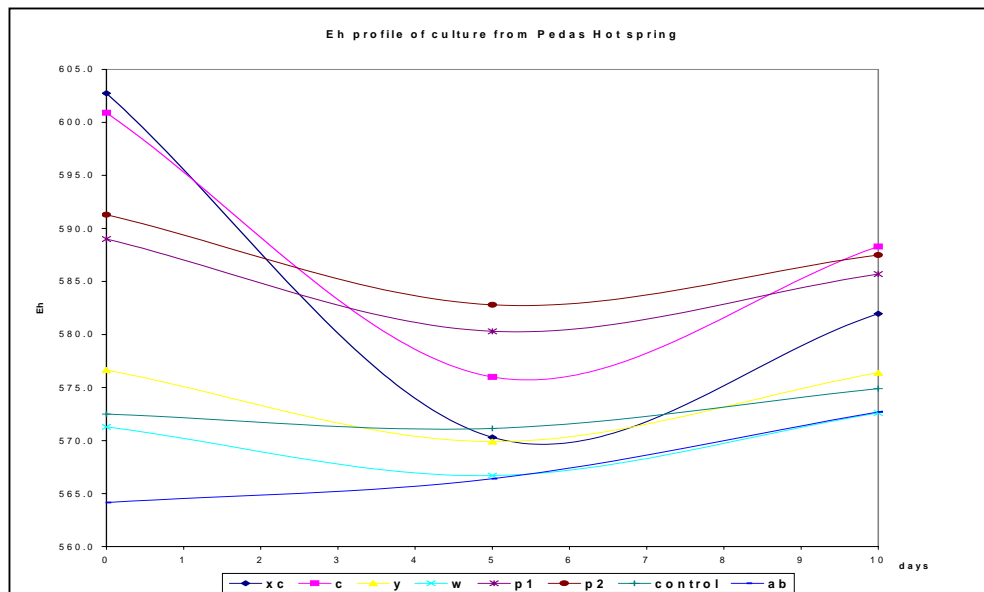
Table 1.4: Elemental composition of pyrite

	S%	C%	Fe%
Pyrite	24.2	0.593	46.28

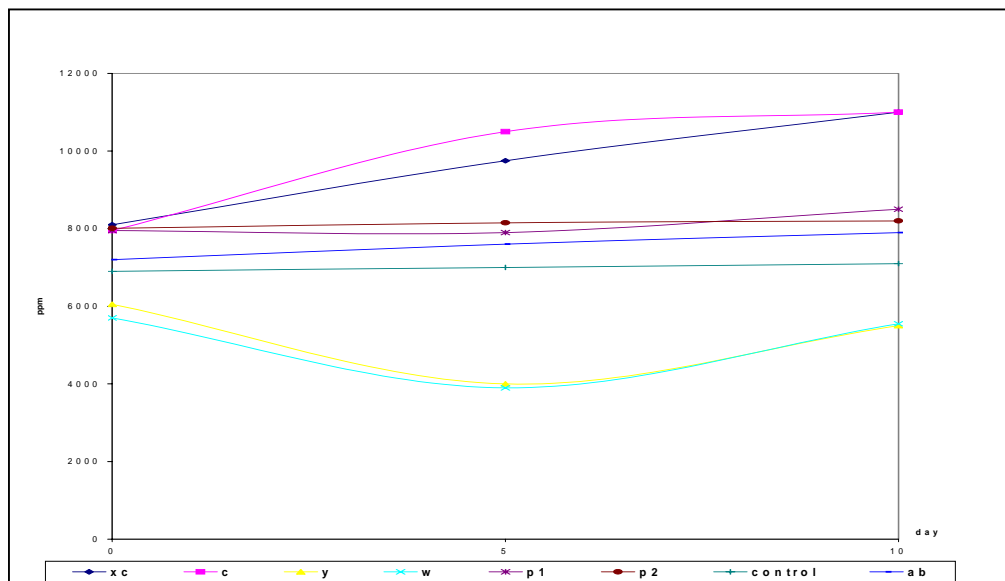
Leaching profile for pyrite oxidation of single and mixed culture of bacteria isolated from Pedas Hot Spring was shown in figures 1.1, 1.2 and 1.3.



Figures 1.1: pH profile of bacteria obtained from Pedas Hot spring



Figures 1.2: Eh profile of bacteria obtained from Pedas Hot spring

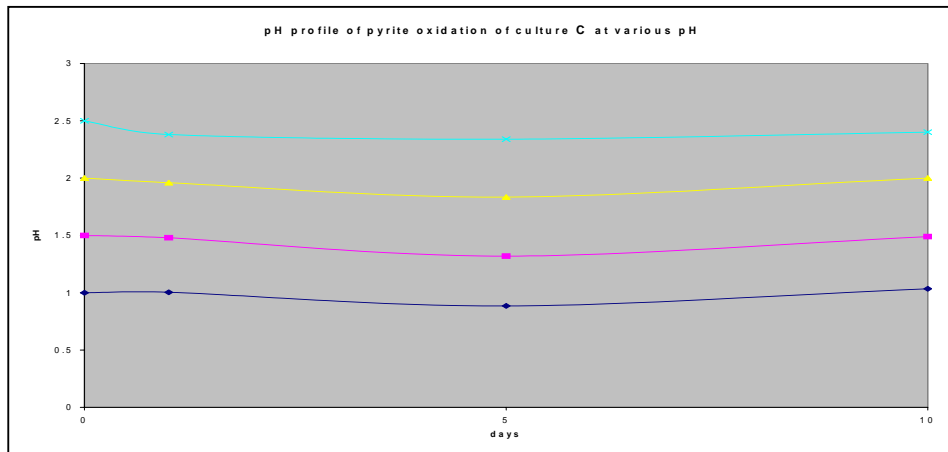


Figures 1.3: [Fe] from pyrite dissolution in the presence of bacteria obtained from Pedas Hot spring

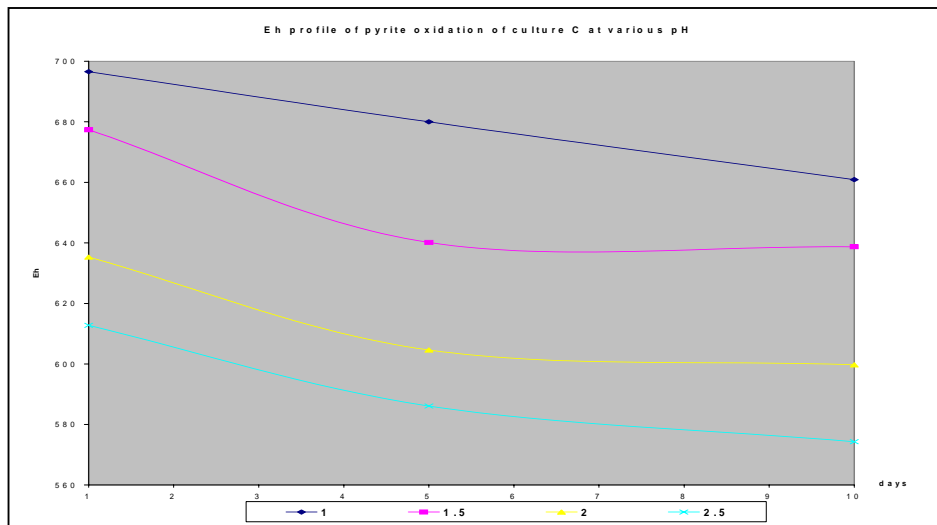
Figures 1.1 showed that the pH decreased from 2.0 to 1.6 for cultures y, w, ab, and control. pH also decreased to 1.35 for cultures xc, c, p1 and p2. The highest Eh values were obtained for cultures c and xc (600 and 603 respectively) after 5 days of incubation. Eh values for both culture decreased to 575 and 570 for culture c and xc. Compared to standard culture of *Acidianus brierleyi* (AB), which acted as control, the Eh value was constantly low at 570 mV. High value of initial Eh and low pH value is very important in accelerating pyrite dissolution. It was shown in figure 1.3, that the highest [Fe] content in solution was xc and c..

1.3.2.2 Biooxidation of pyrite using culture C at various pH

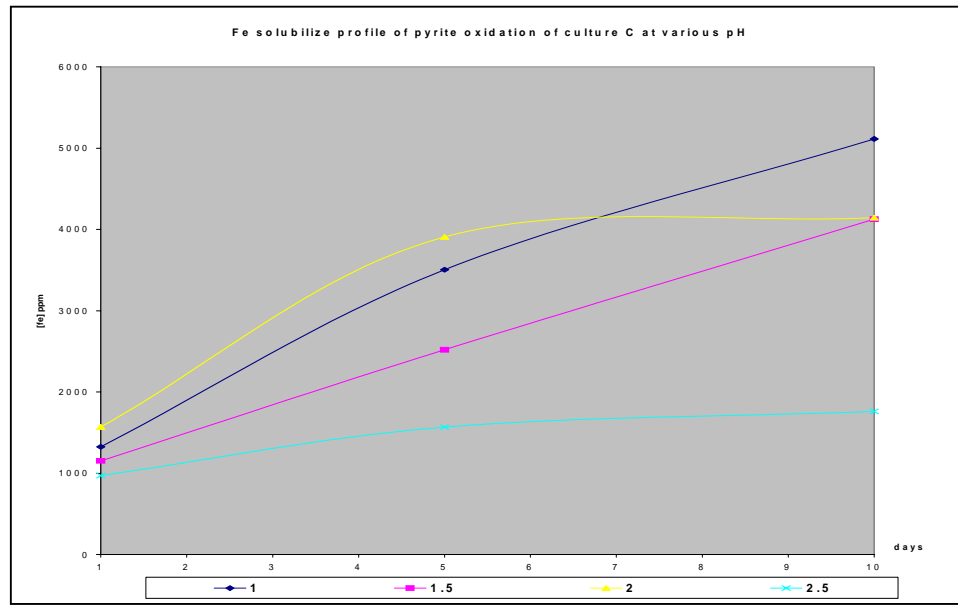
Culture C was then chosen to determine the optimum pH for biooxidation of pyrite. The profiles of oxidation at various pH are shown in figures 1.4, 1.5 and 1.6.



Figures 1.4: pH profile of pyrite oxidation of culture C at various pH



Figures 1.5: Eh profile of pyrite oxidation of culture C at various pH



Figures 1.6: Fe solubilization profile of pyrite oxidation by culture C at various pH

The pH profiles for each set of experiment showed a significant trend (Fig 1.4). Every set showed a slight decrease in pH for the first 5 days of inoculation of culture, followed by the increase to the initial pH at day ten. Compared to the pH profile, Eh trends decrease constantly from day 1 to day 10 for every set of experiment (Fig 1.5). Highest iron solubilization was observed when pH of the medium was at 2.0 during the first 5 days of inoculation. A constant iron content was observed from day 5 to day 10. At low pH i.e. 1.0 and 1.5, iron solubilization constantly increased until day 10. Possibly due to the prevention of jarosite precipitation at low pH (.Nemati *et al*,1998)

1.4 Isolation of bacteria from abandoned ore pile

1.4.1 Isolation procedure

Field sampling was conducted based on *in vitro* culturing method, explained in 1.1.1. Samples were taken from two abandoned ore piles. Descriptions of the sampling site are as follows:

Ulu Sukor

Abandoned heap leaching plant, heap containing 40,000t of sulfidic-carbonaceous gold ores. Samples were taken from a drainage channel emanating from a heap. Temperature and pH of sample taken were 33°C and 4.17 respectively. The plant was left idle without operation for 2 years.

Sg. Lembing

Samples were taken from the slumps around the copper concentrate piles. The concentrate contains chalcopyrite, chalcocite, copper oxide, pyrite and arsenopyrite. The concentrate was left idle due to the strict legal restriction by the Japanese Government on the arsenic limit content in roasting industries. Temperatures and pH of sample were 39°C and 1.97. Bacteria were cultivated aerobically in 13 different media listed in table 1.5

Aerobic culturing was conducted in a 20ml universal bottle, containing a mixture of 5 ml of respective medium and 1ml of sample. The bottle was then immediately immersed in hot water to maintain the temperature. The bottles were kept at 70°C during transportation to the laboratory.

Table 1.5: Medium used for isolation from abandoned ore piles

<p>Medium 1: <i>SULFOLOBUS MEDIUM</i></p> <p>(NH₄)₂SO₄ (1.30), KH₂PO₄ (0.28g), MgSO₄·7 H₂O (0.25 g), CaCl₂·2 H₂O (0.07g), FeCl₃·6 H₂O (0.02 g) MnCl₂·4 H₂O (1.80mg), Na₂B₄O₇·10 H₂O (4.50 mg), ZnSO₄·7 H₂O (0.22 mg), CuCl₂·2 H₂O (0.05 mg), Na₂MoO₄·H₂O (0.03mg), VOSO₄·2 H₂O(0.03mg), CoSO₄ (0.01 mg), Yeast extract (Difco) (1.00g) and Water, freshly distilled (1000ml).Adjust pH to 2.0 with 10 N H₂SO₄</p>
<p>Medium 2:<i>SULFOLOBUS SOLFATARICUS MEDIUM</i></p> <p>Yeast extract (Difco) (1.00g), Casamino acids (Difco)(1.00g), KH₂PO₄ (3.10g), (NH₄)₂ SO₄ (2.50g),MgSO₄ x 7 H₂O (0.20 g), CaCl₂ x 2 H₂O (0.25 g), MnCl₂ x 4 H₂O (1.80mg), Na₂B₄O₇ x 10 H₂O (4.50 mg), ZnSO₄ x 7 H₂O (0.22 mg), CuCl₂ x 2 H₂O (0.05mg), Na₂MoO₄ x 2 H₂O (0.03 mg), VOSO₄ x 2 H₂O (0.03 mg), CoSO₄ x 7 H₂O (0.01mg), Distilled water (1000.00 ml).Adjust pH to 4.0 - 4.2 with 10 N H₂SO₄</p>
<p>Medium 3: <i>METALLOSPHAERA MEDIUM</i></p> <p>Use medium 1 either with 0.1% Difco yeast extract, or 0.05% powdered sulfur Sterilize substrates separately: sulfur by steaming for 1 h on three subsequent days.</p>
<p>Medium 4: <i>ACIDIANUS BRIERLEYI MEDIUM</i></p> <p>(NH₄)₂SO₄ (3.00g), K₂HPO₄ x 3 H₂O (0.50 g), MgSO₄ x 7 H₂O (0.50 g),KCl (0.10 g), Ca(NO₃)₂ (0.01 g), Yeast extract (0.20g),Sulfur (flowers) (10.00 g), Distilled water (1000.00ml),Adjust pH with 6 N H₂SO₄ to 1.5 - 2.5. Yeast extract (10% w/v in distilled water) is autoclaved separately. Sulfur is sterilized by steaming for 3 hours on each of 3 successive days.</p>
<p>Medium 5: <i>SULFOBACILLUS MEDIUM</i></p> <p><u>Solution A:</u> (NH₄)₂SO₄ (3.00 g), KCl (0.10 g), K₂HPO₄ (0.50 g), MgSO₄ x 7 H₂O (0.50 g), Ca(NO₃)₂ (0.01 g),Distilled water (700.00 ml),Adjust pH to 2.0 - 2.2 with sulfuric acid.</p> <p><u>Solution B:</u> FeSO₄ x 7 H₂O (44.20 g), Distilled water (300.00 ml), H₂SO₄, 10 N (1.00 ml),</p> <p><u>Solution C:</u> Yeast extract (1% w/v in water) (20.00 ml), After autoclaving, combine the three solutions. Medium pH 1.9 - 2.4.</p>
<p>Medium 6: <i>ACIDIMICROBIUM MEDIUM (Heterotrophic)</i></p> <p>MgSO₄ x 7 H₂O (0.5 g), (NH₄)₂SO₄ (0.4 g), K₂HPO₄ (0.2g), KCl (0.1g), Distilled water(1000 ml), Adjust pH to 2.0 with H₂SO₄.To the medium add 10.0 mg/l of FeSO₄ x 7 H₂O. After autoclaving add yeast extract from sterile stock solution to final concentration of 0.25 g/l.</p>
<p>Medium 7: <i>ACIDIMICROBIUM MEDIUM (Autotrophic)</i></p> <p>MgSO₄ x 7 H₂O (0.5g), (NH₄)₂SO₄ (0.4 g), K₂HPO₄ (0.2g), KCl (0.1 g), Distilled water (1000ml), To the medium add 13.9 g/l of FeSO₄ x 7 H₂O and adjust medium pH to 1.7 with H₂SO₄ prior to autoclaving</p>
<p>Medium 8: <i>SULFOBACILLUS DISULFIDOOXIDANS MEDIUM</i></p> <p>(NH₄)₂SO₄ (3.0g), KCl (0.1g), KH₂PO₄ (0.5 g), MgSO₄ x 7 H₂O (0.5g), Ca(NO₃)₂ x 4 H₂O (0.1 g),Yeast extract (0.1g), Distilled water (1000ml),Adjust pH to 2.25 prior to autoclaving. Before use add per liter 10 ml of a filter sterilized 10% (w/v) glutathione solution.</p>
<p>Medium 9: MS-MEDIUM <i>Thiobacillus caldus</i> For DSM 2392</p> <p>(NH₄)₂SO₄ (2.00g), MgSO₄ x 7 H₂O (0.25g), K₂HPO₄ (0.10g), KCl (0.10g), Distilled water (1000. ml), Adjust pH of MS-medium to 2.2 with 4 N H₂SO₄ prior to autoclaving. Before use, add 0.25 ml 40% (w/v) FeSO₄ x 7 H₂O solution (dissolved in 0.2 N H₂SO₄ and filter sterilized or autoclaved under N₂) per 5 ml MS-Medium.</p>

<p>Medium 10: MS-MEDIUM <i>Thiobacillus caldus</i> For DSM 9465 $(\text{NH}_4)_2\text{SO}_4$ (2.00g), $\text{MgSO}_4 \times 7 \text{H}_2\text{O}$ (0.25g), K_2HPO_4 (0.10 g), KCl (0.10g), Distilled water (1000ml), : Adjust pH of MS-medium to 2.2 with 4 N H_2SO_4 prior to autoclaving. Before use, add 0.25 ml 40% (w/v) $\text{FeSO}_4 \times 7 \text{H}_2\text{O}$ solution (dissolved in 0.2 N H_2SO_4 and filter sterilized or autoclaved under N_2) per 5 ml MS-Medium.</p>
<p>Medium 11: MS-MEDIUM <i>Thiobacillus caldus</i> DSM 9467 $(\text{NH}_4)_2\text{SO}_4$ (2.00g), $\text{MgSO}_4 \times 7 \text{H}_2\text{O}$ (0.25g), K_2HPO_4 (0.10 g), KCl (0.10g), Distilled water (1000),For: Adjust pH of MS-medium to 3.0 with 2N H_2SO_4 prior to autoclaving. Before use, add 0.2% glucose from filter sterilized 10% w/v stock solution, and 0.01% yeast extract from autoclaved 1% stock solution</p>
<p>Medium 12: 9K <u>Solution A:</u> $(\text{NH}_4)_2\text{SO}_4$ (3.00g), KCl (0.10g), K_2HPO_4 (0.50g), $\text{MgSO}_4 \times 7 \text{H}_2\text{O}$ (0.50g), Distilled water (700ml), Adjust pH to 2.0 - 2.2 with sulfuric acid. <u>Solution B:</u> $\text{FeSO}_4 \times 7 \text{H}_2\text{O}$ (44.20g), Distilled water (300.00 ml), <u>Solution C:</u> Yeast extract (1% w/v in water) (20.00 ml) After autoclaving, combine the three solutions. Medium pH 1.9 - 2.4.</p>
<p>Medium 13: <i>Thiobacillus thiooxidans</i> NH_4Cl (0.1g), KH_2PO_4 (3.0g), $\text{MgCl}_2 \cdot 6\text{H}_2\text{O}$ (0.1g) and $\text{CaCl}_2 \cdot 2\text{H}_2\text{O}$ (0.14g) in a 1L distilled water, sulfuric acid was added to adjust the pH to 4.2 before sterilising using the autoclave. Sterilised sulphur powder (112°C, 10mins) final concentration 5% was added to the solution upon cooling</p>

1.4.2 Results and discussion

The visual and microscopic examination of isolates obtained from Ulu Sokor and Sungai Lembing is shown in Tables 1.6, 1.7, 1.8 and 1.9:

Table 1.6.: Visual observation of isolates obtained from Ulu Sokor

Medium	pH		Eh		Remarks
	initial	final	initial	final	
1	1.89	1.87	625.3	636.1	No colour change
2	4.32	4.11	564.6	589.1	Colourless → brown, black precipitation
3	1.90	1.90	606.3	613.3	No colour change
4	1.93	1.97	618.1	640.7	No colour change, sulphur sediment
5	1.84	1.92	572.3	607.1	Green → light yellow, yellow precipitation
6	1.84	1.83	617.2	629.8	Green → light yellow, white precipitation
7	1.68	1.68	609.8	619.9	Green → colourless, yellow precipitation
8	2.15	2.11	541.3	572.2	No colour change
9	2.14	2.10	590.6	578.9	No colour change, yellow precipitation
10	3.63	3.69	591.4	581.8	No colour change
11	3.09	3.11	609.9	606.1	No colour change
12	1.73	1.72	597.9	613.5	Green → light yellow, yellow precipitation
13	4.02	4.00	417.7	528.5	No colour change

Table 1.7.: Microscopic observation of isolates obtained from Ulu Sokor

Medium	Cell concentration	Cell motility	Colony (Based on motility and shape)	Remarks
1	Low	Low	Mix	
2	Medium	Active	Single	Cell agglomeration
3	Very low	Low	3	
4	-ND-	-	Single	
5	Very low	Active	4	
6	Very high	Active	Single	
7	Very low	Low	Mix	
8	-ND-	-	-	
9	Very low	Low	Single	
10	Very low	Low	Single	
11	-ND-	-	-	
12	Low	Low	Single	Cell attachment on precipitate
13	Low	Active	Single	

Table 1.8.: Visual observation of isolated obtained from Sungai Lembing

Medium	pH		Eh		Remarks
	initial	final	initial	final	
1	2.04	1.93	621.1	638.8	No colour change
2	4.16	4.16	546.6	553.9	Colourless → yellow, yellow precipitation
3	1.94	1.95	614.4	618.8	No colour change
4	1.93	1.95	617.7	624.1	Colourless → cloudy, sulphur sedimentation
5	2.06	1.92	551.4	600.9	Green → light yellow, yellow precipitation
6	1.95	1.95	617.7	623.6	Green → cloudy yellow, white precipitation
7	1.68	1.67	581.6	602.2	Green → light yellow, yellow precipitation
8	2.18	2.17	538.5	561.4	No colour change
9	2.11	2.12	622.6	614.0	No colour change, yellow precipitation
10	2.77	2.49	635.1	624.4	Cloudy, sulphur sedimentation
11	3.03	3.09	588.3	591.2	No colour change
12	1.88	1.95	547.2	593.4	Green → light yellow, yellow precipitation
13	3.82	3.79	409.0	419.8	Cloudy, sulphur sedimentation
<i>Acidianus brierleyi</i>	1.99	2.00	517.4	541.0	No colour change

Table 1.9.: Microscopic observation of isolates obtained from Sungai Lembing

Medium	Cell concentration	Cell motility	Colony (Based on motility and shape)	Remarks
1	Low	Low	Mix	
2	Low	Low	Mix	Large crystal appears
3	Very low	Very low	Single	
4	Very high	High	2	
5	Very low	Low	2	
6	-ND-	-	-	
7	Medium	Medium	2	
8	Low	Low	Single	
9	High	High	Single	
10	Very high	High	Single	Cell agglomeration
11	High	High	Single	
12	Medium	High	Single	
13	Medium	High	Single	
<i>Acidianus brierleyi</i>	Medium	Active	Single	

1.5 Solid medium preparation

1.5.1 Material and Methods

Solid medium was prepared according to the ingredients used in liquid medium described in Table 1.5. The medium consists of the following:

- A. 70 mL of liquid medium which is listed in table 1.5. Sulfur powder in the ingredients was replaced with sodium thiosulfate solution.
- B. 30 mL of gelling solution containing 1.67g agarose, sigma type1.
- C. 1mL of sodium thioglycolate solution (1.1g/L)

For aerobic culturing, solutions A and B were mixed and poured into petri plates. The plates were then incubated at 30⁰C overnight to detect any contamination. Cultures from respective liquid media were then transferred using streak-plate and spread-plate techniques and incubated at 70⁰C for 24 hours.

The anaerobic culture isolation was conducted using molten agar technique. Culture (1mL) from respective liquid medium was transferred into sterilized tube test. Molten agar (5mL) containing solutions A, B and C were mixed with respective culture without aeration. It was then allowed to solidify prior to incubation at 70⁰C.

1.5.2 Results and discussion

After 24 hours of incubation, yellow-orange colonies grew on solid medium 5 and 12 for both Ulu Sokor and Sungai Lembing sample. Growth of colonies were not detected on the other plates.

The same observation was also seen in the anaerobic condition. Yellow-orange precipitates were observed at the surface of medium 5 and 12. This indicates the successful isolation of obligate aerobic, iron oxidizing organisms.

1.6 Bioleaching test

1.6.1 Material and Methods

Bioleaching test of mixed culture obtained from Ulu Sokor and Sungai Lembing were conducted as discussed in section 1.3.1.

Biooxidation of ore was carried out in 500ml Schott bottle containing 100ml respective medium and 50g of ore. The bottle were inoculated with respective culture (20ml) and incubated at 70^oC with shaking at 60 rpm for 3 days.

The sulfidic gold ore used in this study was obtained from Penjom-Avecot Gold Mine, Pahang. The ore was first treated with cyanide to eliminate the free gold.

The copper concentrate was obtained from Sungai Lembing Tin Mine, Pahang. The concentrate was washed with tap water at a ratio of 10:1 (water:concentrate) to get rid of any water soluble copper.

1.6.2 Results and discussion

1.6.2.1 Pyrite Oxidation

Ulu Sokor Culture

Table 1.10: Percentages of pyrite oxidation using Ulu Sokor Culture

Medium	1	2	3	4	5	6	7	8	9	10	11	12	13
Fe solubilize (%)	1.55	22.14	22.16	2.62	45.04	9.58	0.00	2.09	5.72	2.79	1.64	7.95	15.06

Sungai Lembing Culture

Table 1.11: Percentages of pyrite oxidation using Sungai Lembing Culture

Medium	1	2	3	4	5	6	7	8	9	10	11	12	13
Fe solubilize (%)	1.43	1.57	6.99	1.06	45.12	15.55	0.38	2.23	8.92	1.67	2.26	16.2	1.22

Percentages of pyrite solubilization using *Acidianus brierleyi*: 0.38

1.6.3 Penjom sulfidic ore oxidation

Ulu Sokor Culture

Table 1.12: pH change and amount of gold extraction after biooxidation treatment using Ulu Sokor Culture for 3 days.

Medium	pH		Gold extracted (ppm)
	initial	final	
1	1.87	6.86	3.12
2	4.11	7.47	28.52
3	1.90	7.29	2.87
4	1.97	7.61	9.83
5	1.83	4.25	26.87
6	1.92	6.88	5.23
7	1.68	5.93	1.14
8	2.11	7.84	7.43
9	2.10	7.68	11.41
10	3.69	7.61	3.86
11	3.11	7.62	5.18
12	1.72	4.44	9.54
13	4.00	6.32	3.43

Sungai Lembing Culture

Table 1.13: pH change and amount of gold extraction after biooxidation treatment using Sungai Lembing Culture for 3 days.

Medium	pH		Gold extracted (ppm)
	initial	final	
1	1.93	7.08	6.56
2	4.16	7.59	32.12
3	1.95	7.59	16.13
4	1.95	7.60	10.04
5	1.92	4.40	10.62
6	1.95	7.08	6.43
7	1.67	6.12	5.69
8	2.17	7.81	18.03
9	2.12	7.83	2.84
10	2.49	7.71	4.48
11	3.05	7.37	6.38
12	1.95	4.04	8.93
13	3.79	6.27	2.83

Amount of gold extraction using *Acidianus brierleyi*: 12.32 ppm (pH: 2.00-7.36)

Amount of gold extraction without biooxidation: 1.44 ppm

1.6.4 Sungai Lembing copper concentrate oxidation

Ulu Sokor Culture

Table 1.14: pH change and amount of iron and copper extraction after 3 days bioleaching using Ulu Sokor Culture.

Medium	pH		Fe solubilize (%)	Copper extracted (%)
	initial	final		
1	1.90	2.03	8.00	0.6
2	2.09	2.10	0	0
3	1.95	2.09	4.10	4.2
4	2.11	2.12	4.31	2.7
5	1.91	1.99	39.34	1.9
6	2.14	1.92	11.45	0.5
7	1.92	2.48	17.69	0.5
8	2.18	2.07	12.98	0.2
9	2.40	2.48	14.52	0.9
10	2.75	2.52	5.92	0.1
11	2.58	2.61	6.46	0
12	1.85	1.96	13.6	0.1
13	1.97	2.16	11.06	0.1

Sungai Lembing Culture

Table 1.15: pH change and amount of iron and copper extraction after 3 days bioleaching using Sungai Lembing Culture.

Medium	pH		Fe solubilize (%)	Copper extracted (%)
	initial	final		
1	2.05	2.08	8.9	2.0
2	2.04	2.12	3.8	1.84
3	2.06	2.13	4.9	3.2
4	2.12	2.08	12.37	3.1
5	1.95	1.97	8.90	5.2
6	2.27	2.32	9.90	4.7
7	1.90	2.09	7.58	0.1
8	2.19	2.20	15.31	4.7
9	2.42	2.10	5.98	0.02
10	2.66	2.01	4.72	0.1
11	2.59	2.69	4.98	0.1
12	1.63	2.06	18.20	1.1
13	2.31	2.26	8.54	0.02

Percentages of copper extraction using *Acidianus brierleyi*: 0.4% (pH: 2.16-2.19)

The highest pyrite leaching were obtained in a presence of culture in medium 5 (isolated from Sungai Lembing and Ulu Sokor), about 45% of iron was oxidized in medium 5 compared to 0.38% oxidation by culture in *Acidianus brierleyi* medium. Culture from Ulu Sokor in medium 5 also showed the highest amount of iron leaching (39%) for Sungai Lembing concentrate but low amount of copper leaching (1.9%). This shows that the pyrite oxidation was dominating the leaching process and not chalcopyrite. Compared to the culture in medium 5 i.e. Sungai Lembing isolate, highest amount of copper solubilization (5.2%) occurred at low iron oxidation (8.9%), suggesting that most of the mineral oxidized was chalcopyrite.

The highest gold extraction was obtained from the ore, which is treated by culture in medium 2, 32.12 ppm for Sungai Lembing isolate and 28.5 ppm for Ulu Sokor isolate. This shows that bioleaching is very selective on the nature of mineral in the ore, and is dependent on the types of culture used.

PART 2

Column studies on gold ores and its concentrates

2.0 Introduction

This chapter will discuss on the feasibility studies of the gold ores and its concentrates in the biooxidation process in a column. However, before the test can be carried out, it is important to characterize the type of ore and whether microorganisms can be used to treat the ore. Some basic tests have been conducted to characterize the ore which will be used in the bioleaching process

2.1 World commercial bioleaching plant

Bioleaching would best be performed in reactors. For commercial bioleaching application of biohydrometallurgy, a continuous stirred tank reactor, CSTR, appears to be as the first choice. The use of reactors would allow a good control of the pertinent variables, resulting in a better performance in metal extraction (Avecedo, 2000). The processes use mesophilic or moderate thermophilic mixed cultures at approximately 40–50°C. Since 1999, Billiton and Mintek/Bactech, two companies involved in the development of bioleaching processes in agitated tanks, have been publishing results concerning continuous bioleaching testwork on chalcopyrite concentrates with thermophilic bacteria (Dew et al., 1999; Miller et al., 1999; Gericke and Pinches, 1999; Gericke et al., 2001).

2.1.1 Refractory gold pretreatment

There are several plants were been commissioned for biooxidation pretreatment of sulphidic-refractory gold concentrates. These plants were used to extract gold from pyrite and arsenopyrite minerals which lock the gold values. For gold bioleaching, stirred tank reactors were being used to process flotation concentrates, although a few use heaps for low-grade ores and tailings. The commercial gold pre-treatment were shown in Table 2.1

Table 2.1: The world's commercial gold pre-treatment plants.

Plant	Years in operation	Size (tonnes/day)
Fairview, South Africa	1986, 1991–Present	35
Sao Bento, Brazil	1990–Present	150
Harbour Lights, Australia	1992–1994	40
Wiluna, Australia	1993–Present	115
Ashanti, Ghana	1994–Present	1000
Youanmi, Australia	1994–1998	120
Tamboraque, Peru	1999–Present	60

These plants used moderate thermophilic bacteria to pretreat the gold ores.

The Youanmi plant used the BacTech Australia technology, which uses a moderately thermophilic bacterial culture similar to *Sulfobacillus thermosulfidooxidans*. The biooxidation were carried out at temperatures between 45°C and 55°C (6a). The other six plants use the BIOX[®] process, which is a mixed culture of *Thiobacillus* and *Leptospirillum* operating at 40°C to about 45°C (7a). Figure 2.3 shows the Youanmi BIOX plant situated at Western Australia.

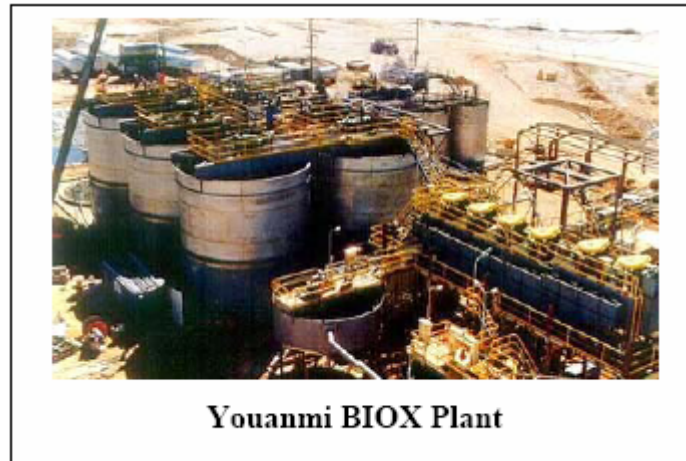


Figure 2.1: The Youanmi BIOX plant

The commercial metal industries are facing an increasing number of problems nowadays including pollution and others. Therefore, there is a need to find a simple and a cheap process to resolve the problem faced by the industries. Biohydrometallurgical processes are the best answer to all the problems arising from the typical pyrometallurgical processes. It is a solution for extracting metals from low grade after the depletion of high grade ores.

In the fields of biohydrometallurgy, bioreactor can be classified by the method of agitation and the mode of continuous phase i.e. liquid or gas phase. Bioreactor operation can be done by mechanical agitation or by air sparging using external pump. The typical bioreactors used in biohydrometallurgy are mechanically agitated bioreactor and air lift bioreactor. Other types of reactors that have been studied for their application in biomining are the percolation column, the Pachuca tank, the air-lift column, and some special designs such as rotary reactors (Barrette and Couillard, 1993 and Rossi, 1999).

Gold deposit, can be classified into free milling ores and refractory ores. Free milling ores exist in the form of gold nugget at an alluvial deposit and a native gold element in a host rock (reef gold). Gravity separation and direct cyanidation are the best processes for extracting gold from this type of ores. Refractory gold ore is one in which the gold is found in association with sulphides and carbonaceous material. Low

recoveries of gold was observed upon cyanidation due to the gold being locked up by sulphide minerals such as pyrite and arsenopyrite and also due to adsorption of solubilized gold by carbonaceous materials in the ore.(Brierley and Hill, 1993).

The ores associated with biooxidation is usually known as sulphide ores, which can be categorized into 4 major groups as follows; porphyry deposits, where by sulphide and other minerals are scattered uniformly and the grade maybe low but it is important for large scale with low capital cost. Secondly, massive sulphide deposits with higher metal concentration, oxide ore originates from upper portion and sulphide ore from lower portion. Third, native ores occurring unadulterated in nature. Fourth, the mixed ores, where usually ores being accompanied with other metal in nature such as copper, nickel, zinc, lead and platinum. These ores have been mined for gold but at the same time the other metals are sold as by product (Gasparini, 1993).

In Malaysia, gold is mainly found in the states of Kelantan, Terengganu, Sarawak and the Central Belt in Semenanjung Malaysia. However, gold production in Malaysia has decreased due to the closure of mines as a result of exhaustion of good grade ores.

2.1.2 Mineral concentrate

Direct gold extraction from low-grade refractory ores is not an economical process as excessive amounts of cyanide have to be used which then leads to environmental problems. Instead of pre-treatment process, i.e: biooxidation and roasting, the ores are usually concentrated using froth floatation process. The purpose of this technique is to provide a small volume of material for extraction process (King, 1997).

Flotation process is a widely utilised technique for mineral processing and is based on the principle of the different minerals having different wetting characteristics. These processes generally separate the copper sulphide from other minerals such as copper oxide and other metals. This process was carried out with the help of reagents termed as depressants and activators. The depressants and activators are reagents that will reduce and increase the tendency of mineral to float respectively (Walter, 1996). Selective collectors and specific conditions are used to achieve higher recovery of metal. The collectors enhance the mineral to bind with the bubble from the air sparged. Generally, a copper sulphide collector containing hydrocarbon radical is attached to a polar group, which plays an important role in binding with copper sulphide surface.

Usually the floatation process takes place in the floatation cell or column which contains ore slurry that needs to be concentrated. Air is sparged through the cell causing hydrophobic particles to stick to the bubble and float (Arbiter et.al, 1995). Then the floating particles consisting of the Cu are collected, whereas the unfloat particles are transferred to another floatation cell, the conditions of which have been modified to get the desired byproduct. An overview of the floatation process is shown in figure 2.1. (Arbiter et.al, 1995).

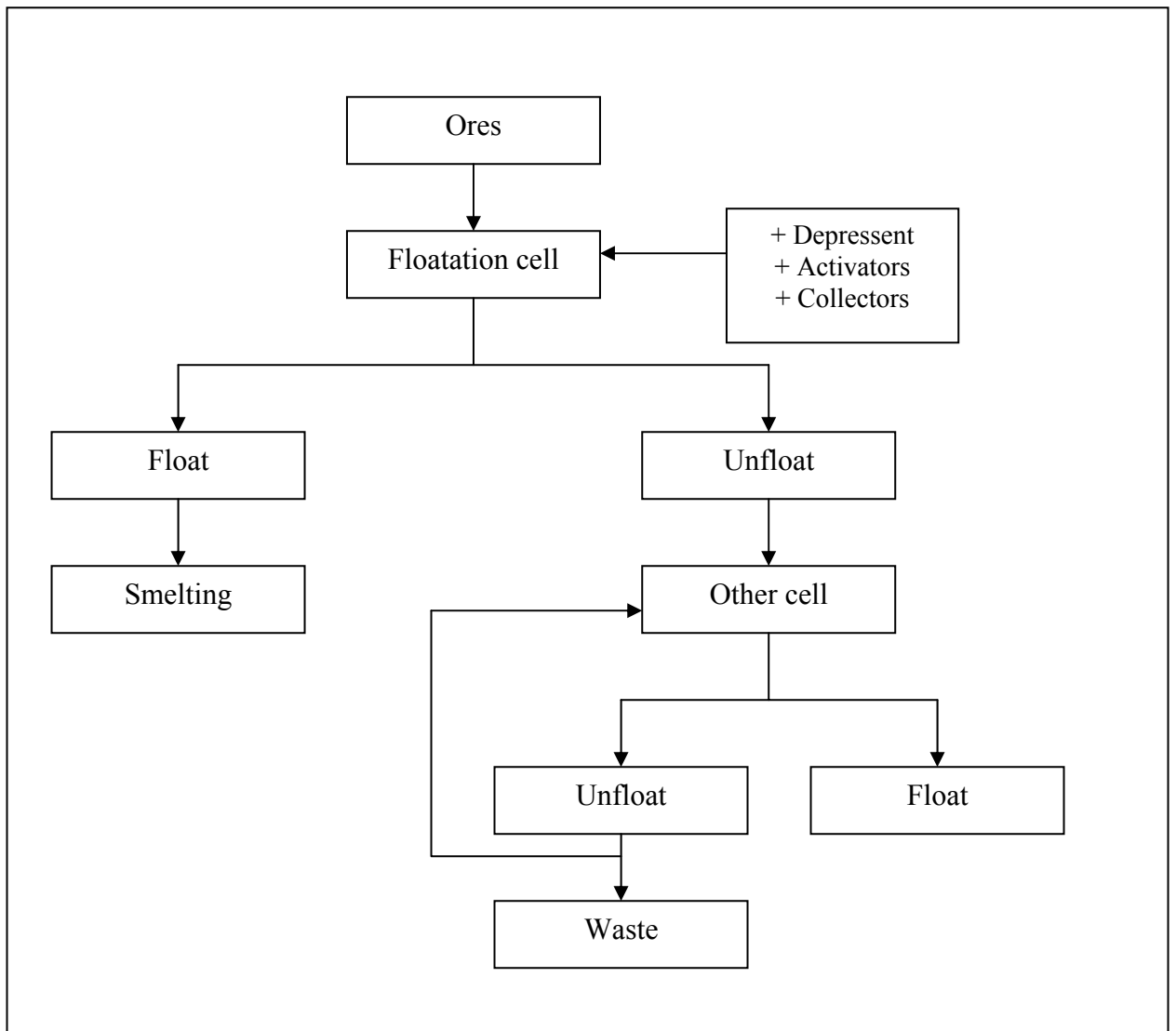


Figure 2.2: General overview of a simple flotation process

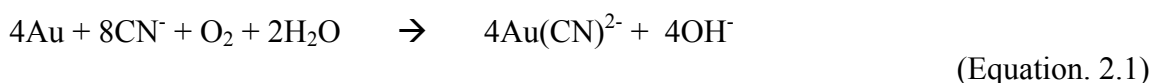
2.1.3 Cyanidation

Chemical extraction refers to the separation of desired metal and compound from finely ground ore by dissolution. As gold does not dissolve directly in acidic condition, there is a need to complex the gold to form a more soluble gold-complex ion. Some lixiviant solutions which have been used include cyanide, thiourea and thiosulphate (Jefri, 2002).

Direct cyanidation technique is used for mustard gold which is finely disseminated in the host rock of which gravity separation method had not been successful in extracting the gold. As a lixiviant solution, cyanide complexes with the gold and will leach out gold from the ore. There are two types of direct cyanidation; flooded and static beds. (*Institut Penyelidikan Galian Malaysia*, 1988).

McArthur and Forest patented the basic process of cyanidation in 1887. Among the earlier established mine, which utilised cyanidation in its operation, are Crown Mine, New Zealand (1889) and the Bau Mine, Sarawak (1899). This technique has been a dominant method for gold dissolution (Ubal dini *et al*, 1996) until the present day.

Au (1) forms a strong cationic complex with cyanide in an alkaline solution with oxygen as the oxidising agent (Equation. 2.1).



This can be considered as a very effective and viable process because of the high amounts of gold obtained even at low concentrations of cyanide. Overall recovery of free milling ore is around 97% (Kettle, 1982).

2.1.4 Bio-heap leaching of low grade refractory ore

Bio-heap leaching is synonymous to heap leaching, the only difference being the incorporation of bacteria for bio-heap. The bio-heap process has been applied in the Mt. Leyshon Mine in Queensland, Australia at a capacity of 1370tonne/day with an ore grade of 1.73ppm since 1992. In 1995 this operation was also commissioned in Newmont-Carlin Mine, Nevada, USA. The process capacity is 10,000tonnes/day with an ore grade of 1ppm

The advantages of this process are the low energy and chemical reagent consumption and investment cost. It is also a clean process, which does not pollute the environment and economical exploitation of low-grade deposits. Bio-heap leaching is an alternative to the stirred tank reactor, roaster and autoclave which low-grade ore process cannot support because of the cost. It has been suggested that bio-heap leaching is an alternative process in developing countries (Brierley, 1997).

To fully utilize the potential of bacterial oxidation, several experimental techniques will be evaluated. The shake flask and stirred tank reactor techniques can be used to simulate a commercial continuous tank reactor process. However, due to the differences in conditions; i.e. size of ore, proper aeration and mixing of slurry. The results obtained from those studies cannot be applied to large scale heap leaching. (Rossi, 1990).

In a percolating leaching system; i.e. heap and dump, the ore was inadequately prepared and solid liquid contact was not efficient. The oxygen and carbon dioxide transfer may be low or even non-existent whilst the temperature could vary considerably between different zones of heaps. Hence, the behavior of a heap will be much more complex and for these reasons, experiments were carried out in a column (Monuz *et al*, 1995) which provides fairly accurate conditions for heap leaching.

The column apparatus is quite simple, the ore was packed in the column where solution was sprayed at the top of the column and the metal laden solution collected at the bottom. Various parameters for example, the size range of suitable ore, height of the dump or heap, biooxidation and leaching profiles and flow of liquid can be studied before applying to a large scale heap. The use of columns also avoid the failure of more expensive semi-commercial pilot scale testing using several hundred or thousand tonnes of ore.

2.1.5 Technical consideration for heap leaching

Heap leaching is a relatively simple process where a low-grade ore is stacked on leach pad. There are significant amounts of technical information on heap leaching (Readett and Miller, 1997). However, most information is theoretically based, with reference to commercial experiences.

There are many critical factors to be considered when selecting the type of heap leach operation; these factors include material characteristics, height, leach cycle, production level, project life, economic viability and site topography. Overlooking any of the critical factors can affect the overall leaching performance. It is important to ensure that the ore is properly stacked. Failure to do so might affect solution spraying in general and the whole leaching process in particular.

2.1.5.1 Spraying irrigation

It is really important to ensure that heap is kept wet and well drained. Solution distribution over the heap surface can affect the rate of gold recovery which can be carried out using sprayer or dripper.

Drip irrigation system does not only minimize evaporation, but also prevent freezing up in frigid climates and allow minimum impact force on a heap surface. However, based on pilot plant experiences, it was very difficult to ensure a good solution distribution. Furthermore, cost for dripper piping system is higher than spraying system.

Rainbird sprinkler and wobbler sprinkler is commonly used in irrigation systems. It covers a large area and can be installed quickly. Sprinkler provides the best solution for surface distribution and increases the DO by air diffusion. Disadvantages of the sprinkler include rapid evaporation due to exposure to wind friction and cyanide degradation due to exposure to ultra violet rays.

2.1.5.2 Aeration

Biooxidation and thiosulphate leaching require a rich oxygen supply for the biochemical and chemical reactions. Large amounts of air as a source of oxygen must be provided via the bottom of the heap or in the collecting pond.

2.1.5.3 Pad and lining

Heap base must be constructed with minimal earth works, utilising the natural topography as much as possible. Pad area is cut and filled as required and trimmed to achieve the desired slope of 0.5 to 1°. Nevertheless, some earth works such as bund wall, interior drainage ditches and leak detection drain are inevitable. Pad must be layered using clay or sand. The complete pad is carefully inspected before a plastic liner is installed.

The chemicals used in the process can affect the pad and liner material. If a toxic reagent i.e. cyanide is used, HDPE geomembrane (0.5mm thickness) covered with geotextile is suggested (Readett and Miller, 1997). Cyanide leakage detector must be placed under the pad to avoid contamination. However, if a non-toxic reagent i.e. thiosulphate is used, a thin PVC liner is sufficient. A layer of clay (30cm) can be used as an alternative for the plastic liner. Selection of liner can have a big impact on the capital cost of a heap leaching project.

Generally, the pad used in heap leaching construction can be divided into 2 types that is permanent pad and reusable pad (Martin, 1998). Permanent pad allows ore to be stacked in a multiple lift of heap. Meanwhile, ore is stacked on one lift in a reusable pad, leached, reclaimed and then replaced with a new one. Permanent pad is a common and widely accepted type of pad.

Reusable pad is usually applied on a biooxidation heap plant, in which the ore is handled many times. Double handling of the ore provides a good metallurgical control but producing it might be uneconomical. However, in many cases, it is actually less expensive to handle ore twice rather than to elevate it and pump the solution to higher lifts on a permanent pad (Martin, 1998).

Permanent pad is a simple process but it is more difficult to monitor the solution through the heap because of the stacking height. Recovered metal can be precipitated if the condition is not correctly balanced. However, intermediate liner or clay can be placed on the existing heap to reduce the amount of solution that might seep through the old heap.

2.1.5.4 Stacking

Stacking of ore in a heap can be achieved using truck dumping, excavator loading and conveyor stacking. Selection of the method of stacking is dependant on the actual project duration and the amounts of material to be stacked. Ore must be stacked properly in the heap to ensure the overall efficiency of the heap.

Excavator loading allows the ore to be placed uncompacted but it is slow, heap height is restricted by the loader lift capacity which is about 3m. In a commercial operation, excavator is not used for ore stacking.

Truck dumping is considered as a standard method in the mining industry. It is a fairly straight forward method, for ores which do not require crushing. It is the best method for a cost sensitive project in terms of contract hauling, low fuel and labour cost, whether it is purchased, leased or hired. Its manoeuvrability allows ore to be stacked on an extreme or irregular pad shape (Martin, 1998)

However, ground pressure impact by truck dumping can lead to compaction and reduced heap permeability. The truck is not efficient to climb a slope of more than 8° inclination due to the increased haul times, fuel consumption and maintenance of truck. A track can be prepared during stacking to reduce the heap slope.

Conveyor loading is commonly used in combination with agglomerator and crusher. There must be sufficient ore deposit to recover the capital investment of a conveyor. It is commonly employed on a project which is sensitive to heap permeability, i.e. ore used is clayey or heap is too high, compaction could damage the overall process.

2.1.5.5 Climatic factors

The major reason for the lack of commercial interest of heap leaching in a tropical country is because of the rainy season. In Malaysia, the rainy season starts from October till February.

A slight amount of rain is good for the heap leaching operation; it increases the heap moisture, subsequently decreasing evaporation. However, long periods of heavy rain can cause problems on a heap leaching process. High impact of rain water on a heap surface leads to a reduced heap porosity and permeability. Channeling of the solution may occur in the heap. Excess solution volume in the heap can cause heap flooding and damaging the heap structure. Pregnant solution can be diluted during the rainy season which will result in low gold recovery.

However, some measures to counter the rainy season have been suggested. Canvas or plastic sheet may be used to cover the heap. The canvas should be placed 2m from the surface to allow spraying. However, strong wind can blow the canvas. Workers must recover the canvas immediately, a dangerous task during the rainy season and especially when cyanide is being used.

The other alternative is by placing the canvas on the heap surface. Although dripper may be applied, it is still very difficult to control the solution distribution. Pyrite oxidation releases heat and heat build up during biooxidation leads to jarosite precipitation which will inhibit bacterial activities.

Another point worth considering is to agglomerate the ore with cyanide and lime. Heap can then be left during the rainy season. The rain water can solubilize the cyanide and extract the gold. The idea sounds practical but it is difficult to control cyanide concentration. It may be higher during the initial stages but can be lower towards the end of the process. The discharge solution may contain concentrated cyanide and gold. Agglomeration is quite costly to implement.

To overcome problems faced during the rainy season, a new heap set up is proposed, as shown in figure 2.3. When rainfall starts, the pump (P1) will be automatically turned off. The rainwater could be diluting the cyanide and when the cyanide concentration falls below 200ppm (minimum concentration to extract gold), the valve (V1) controlling the pregnant pond closes automatically and the solution is then by-passed into the overflow pond. A level regulator is used to control valves (V2 and V3). If the overflow pond is full, the controller automatically opens V2, close V3 and vice versa. The diluted cyanide solution then flows into the discharge pond. Water in the overflow pond can be recirculated, while cyanide must be degraded using biological and chemical treatment before being released to the environment. There is no need to cover the discharge pond as the rain water can dilute the cyanide, whereas direct sunlight can degrade the cyanide. The discharge pond is too large and too expensive to cover. However periodic sampling must be carried out to check the cyanide discharge level (must be lower than 0.1ppm). (Environmental Quality Act, 1974)

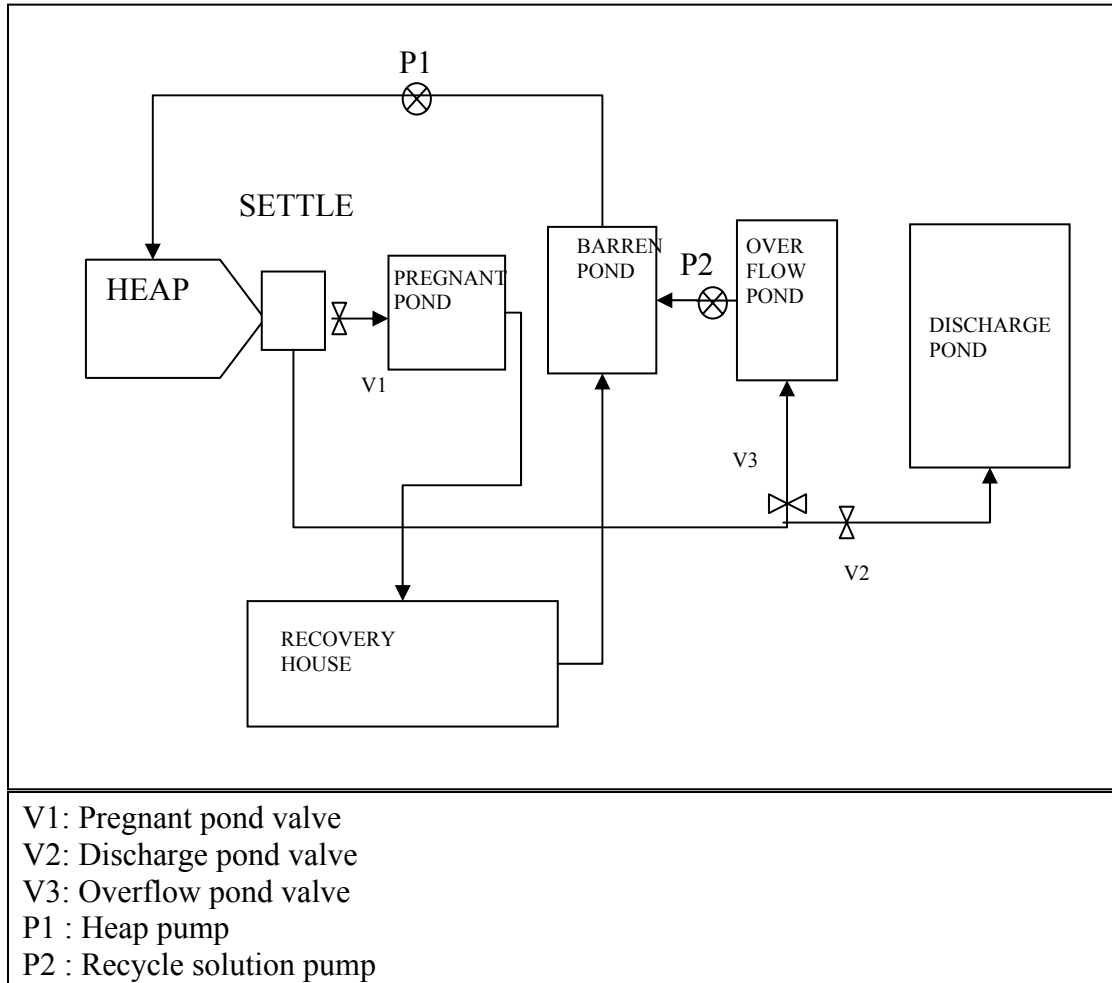


Figure 2.3: Heap leaching process diagram

Column studies on gold ores and its concentrates

2.2 Materials and methods

2.2.1 Ore and concentrate characterisation

The characterisation of the ore was carried out as follows: elemental analysis using AAS and fire assay (Malaysia Mining Co. Laboratory), sulphur and carbon determination using carbon and sulphur determination (Leco HF-400, Antara Steel Pte. Ltd., Pasir Gudang). The refractory characteristic of the ore was carried out using

sequential extraction methods). Acid consumption test and Biological acid producing potential was carried out to assess the suitability of ore for biooxidation.

2.2.1.1 Chemicals

All experiments were carried out using analytical grade chemicals and all glassware used was soaked in 10% HNO₃ overnight, washed with tap water and rinsed with distilled deionized water.

2.2.1.2 Gold ore and concentrated sample

The gold concentrate used throughout this chapter was obtained from the Penjom-Avocet Gold Mine, Sungai Lembing, Pahang, Malaysia. The ore was ground using industrial ball miller to liberate the mineral particle. Froth flotation process for separating sulfide from gangue in the ore bodies was carried out using surfactants and wetting agents. The reagent was to achieve a hydrophobic surface condition on the sulfide particle. The separation of a binary solids mixture may be accomplished by the selective attachment of hydrophobic solid particles to air bubbles. The unattached hydrophobic solid particles remain in the water. The difference in the density between the air bubbles and water provides buoyancy that preferentially lifts the hydrophobic solids particles to the surface where they remain entrained in a froth which can be drained off. The gold in the concentrate was then extracted using alkaline cyanide solution. (2% NaCN, NaOH used to adjust pH to 10). The tailing from this process was then collected and tagged as a sample of gold concentrated in this work.

The sample of gold concentrate used was washed using 10:1 ratio of tap water:sample in order to remove the NaCN and neutralized the pH. The sample then dried at 80°C overnight.

Ore samples were obtained from various local gold mines i.e: Penjom-Avocet Gold Mine, Pahang; Lubuk Mandi Gold Mine, Terengganu; Raub-Australia Gold Mine, Pahang; and Buffalo Reef, Pahang. The ores were crushed using jaw-impact crusher to a size of 0.5mm to 5mm. The ores were then mixed before use in the column study.

The gold ore and concentrate sample was ground using fine-impact mill grinder and sampling was carried out using the coning and quartering technique.(International Atomic Energy Agency, 1990).

2.2.1.3 Acid digestion

Dried and finely ground ore, 25g was roasted at 600°C for 2 hours. Aqua regia (100mL) consisting of a mixture of concentrated HCl : HNO₃ at a ratio of 3:1 was then added to the dried ore. The slurry was heated gently for 1.5hrs at 70-80°C. Upon cooling, the slurry was transferred into a 250mL volumetric flask. The volume was then made up to the mark and an additional 4mL of water was added to replace the undissolved ore. Under this condition, all the metal was assumed to dissolve in the solution. The sample was analysed using AAS. For gold analysis, 20mL of the solution was extracted with 5mL DIBK (Diisobutyl ketone) to avoid any interference from iron and to concentrate the gold.

2.2.1.4 Carbon and sulphur content

Dried method analysis was conducted at Antara Steel Sdn Bhd, Pasir Gudang Johor Malaysia for carbon and sulphur determination while samples for fire assay were conducted at Malaysia Mining Co. Laboratory, Batu Caves, Selangor.

2.2.1.5 Size analysis

Dried gold concentrate was sieved using standard sieve size 75 μ m, 106 μ m, 125 μ m, 180 μ m, 250 μ m, 500 μ m, 1mm, 2mm and 4mm respectively. The ore in each sieve was weighed to determine the size distribution.

2.2.1.6 Sequential extraction

The purpose of this test is to assess the association of gold in the host minerals i.e. either as free gold, unextracted gold, gold associated with iron oxide or pyrite.

2.2.1.7 Free gold test

Finely ground and sieved ore 10% (200g) was mixed with 2.0L of water in a 10L Schott bottle. Lime was added to the mixture to maintain the pH between 10 and 11.5. Then, NaCN (2.0g) was added to the mixture and placed in a bottle, and rolled for 24 hrs at 50rpm. Finally, the mixture was filtered and the filtrate was assayed using AAS.

2.2.1.8 H₂SO₄ treatment

Finely dried residue from the free gold test was mixed with 2.0L of H₂SO₄ (1.0M) and the mixture was heated gently for 1.5hrs at 70-80°C. Upon cooling, the slurry was then filtered and the residue was washed with 2.0L water. The mixture was again filtered and the gold content was determined using the procedure outlined in 2.2.1.7

2.2.1.9 HCl treatment

Finely dried residue from the free gold test was mixed with 2.0L of HCl (20%) and the mixture was then stirred for 4 hrs at ambient temperature in the orbital shaker. The mixture was then filtered and the residue was washed with 2L water. The mixture was again filtered and the gold content was determined following the procedure outlined in 2.2.1.7

2.2.1.10 HNO₃ treatment

The residue from the HCl treatment was mixed with 2.0L HNO₃ (30%) and the mixture was then stirred for 4 hrs at 80°C. Again, the gold content was determined following the procedure outlined in 2.2.1.7. The final residue was then digested as described in 2.2.1.3.

2.2.1.11 Acid consumption test

Slurry containing 10g of ore and 100mL water was stirred for 15 min, and the pH was then recorded. H₂SO₄, 5M was added to the slurry in order to adjust the pH to 3.5. Acid was added every 30 min to maintain the pH at 3.5. After 4 hrs and when the increase in pH was below 0.1 units, the experiment was terminated (Bruynesteyn and Duncan, 1979).

2.2.1.12 Biological acid producing potential

The pulverized ore was dried overnight before adding to the basal salt medium (30g ore in 70mL basal salt). The pH of the mixture was adjusted to 2.5 using sulphuric acid. The flasks were then placed in the orbital shaker at 200rpm, 30⁰C for 4 hrs.

Following this, a fresh culture of bacteria (10%v/v) was inoculated aseptically. Pure cultures of *T. ferrooxidans* *Sb. thermosulfodooxidans* and *A. brierleyi* were used in this test. The flasks were then returned to the orbital shaker, and shaken at 200rpm, 30⁰C for 4 hrs.

For the first 3 days, the pH of the mixture was monitored daily to ensure that it remained below 2.5. When the pH reached 2.5 and remained constant, it was further monitored until there was no drop in pH value. Then half of the initial ore's weight (15g) was added into the flasks and the flasks were shaken. The pH value was then monitored and the experiment was terminated when the pH remained below 3.5 (Brierley, 1997).

2.2.1.13 Preg-robbing test

Dried tailings, 200g was mixed with 500mL water to achieve 40% pulp density in a 2L bottle. Soluble gold, 5 ppm was added to the slurry and pH adjustment to 10 – 11.5 was made using lime. NaCN, 0.05g was added to the mixture and the bottle was rolled at 50 rpm for 24 hours. Slurry was then filtered and the gold content in the filtrate was determined using AAS.

2.2.2 Column Leaching Test

2.2.2.1 Leaching test

Biooxidation experiments were conducted in 8 columns. The plastic columns measured 1.5m in height and 12.0cm in internal diameter. A HDPE support plate with multiple 3mm holes was placed at the bottom of each column. Each column was packed with approximately 25kg of gold concentrate and 50kg of gold ore. The mixture of gold ore and concentrate were agglomerated with 5% w/w of respective cultures. Agglomeration was conducted in a 2L roller bottle for an hour in order to ensure better attachment of gold concentrate on the ore surface. Sand at a height of 15 cm was packed at the bottom of the column to enable uniform dispersion of air in the columns. It was then packed with 25kg agglomerated ore, added with 5cm sand and the procedure repeated twice. Finally, 15 cm sand was placed on the top of the column to ensure even flow of lixiviant solution (figure 2.4.). The column was then tightly using PVC cover to prevent solution lost via evaporation. The column was fed with the bacterial solution (24 hours growth using bioreactor) using a peristaltic pump at a rate of 50ml/min. The solution was applied to the surface of the column using a 4 point drip irrigation systems. The leach solution was passed through the ore sample by gravity and re-circulated through a side loop with a peristaltic pump. The pregnant solution was collected using 10L plastic container. The solution level was maintained at a sufficient height by provide a freshly cultured medium into container.

In order to control the column temperature, the columns was placed in a 1m x 0.5m x 1.7m steel box, which was covered by 2cm fibrous insulation material. Each box was supported by 2 units of high temperature fan and heater with temperature controller (figure 2.4). For the column at ambient temperature, the column was covered by 2cm fibrous insulation material to prevent heat loss via column surface. The pregnant solution was sampled and analyzed to determine metal concentrations, pH and E_H .

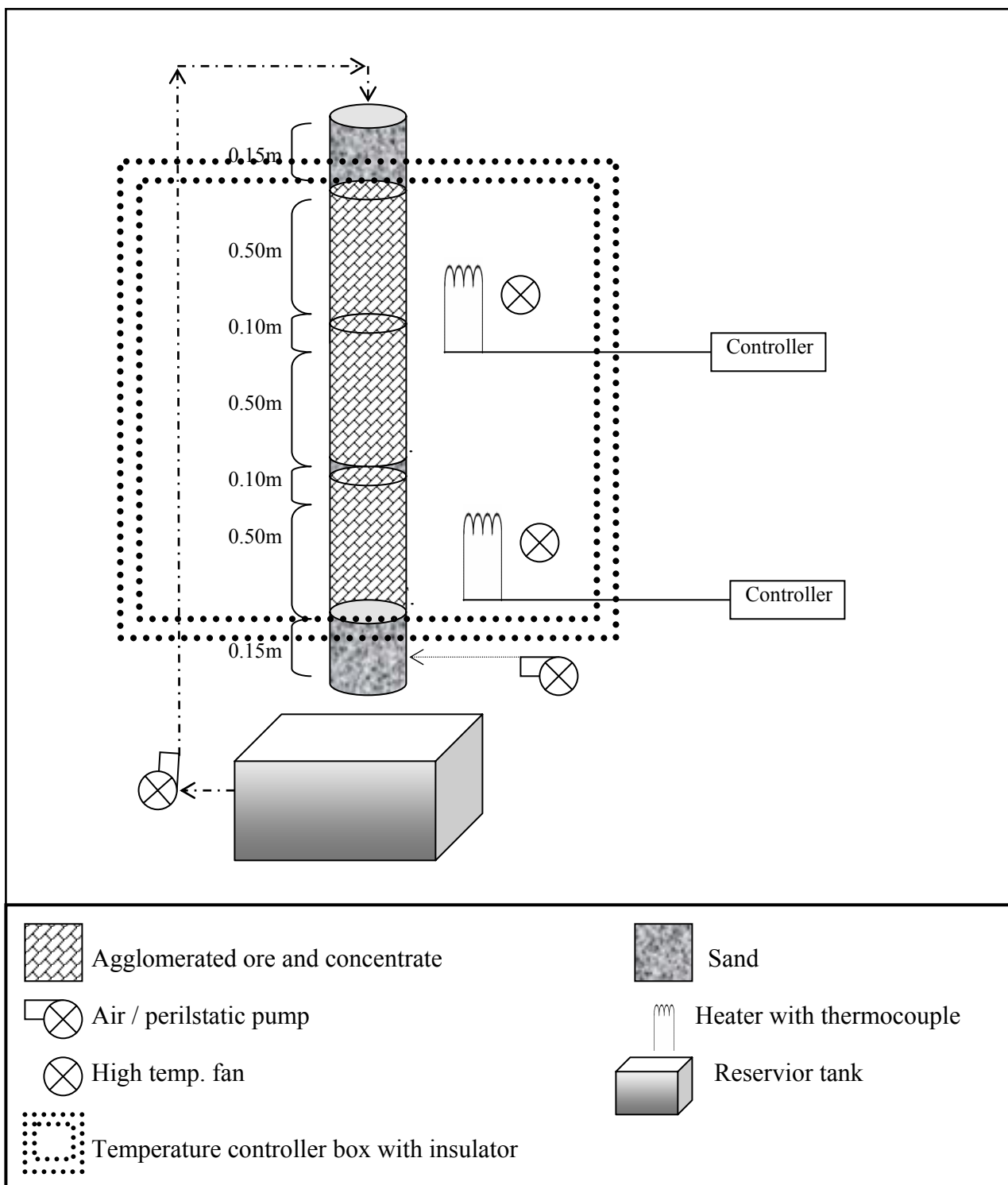


Figure. 2.4: Schematic diagram of the column leaching apparatus

The column test was conducted using different type of bacterial strains and at the temperatures suitable for the optimum growth of the strains. The column was first biooxidized using the sulfur oxidizing strains followed by the iron oxidizing strains (table 2.2).

Table 2.2. Column condition and strains used for each column.

Column \ Time (Days)	Day 1 st – Day 40 th	Day 45 st - Day 60 th	Day 70 st - Day 120 th
A (THERMOPHILIC TEST)	Culture: <i>A. brierleyi</i> Medium: <i>A. brierleyi</i> medium Temperature: 70°C	Culture: SL5B Medium: <i>Sb thermosulfidioxidans</i> medium Temperature: 70°C	
B (THERMOPHILIC CONTROL)	Culture: - nil- Medium: <i>A. brierleyi</i> medium Temperature: 70°C	Culture: - nil- Medium: <i>Sb thermosulfidioxidans</i> medium Temperature: 70°C	
C (MOD. THERMO. TEST)	Culture: <i>T. caldus</i> Medium: <i>T. caldus</i> medium Temperature: 45°C	Culture: <i>Sb thermosulfidioxidans</i> Medium: <i>Sb thermosulfidioxidans</i> medium Temperature: 45°C	
D (MOD. THERMO. CONTROL)	Culture: - nil- Medium: <i>T. caldus</i> medium Temperature: 45°C	Culture: - nil- Medium: <i>Sb thermosulfidioxidans</i> medium Temperature: 45°C	
E (MESOPHILIC TEST)	Culture: <i>T.thiooxidans</i> Medium: <i>T.thiooxidans</i> medium Temperature: ambient temperature	Culture: <i>T. ferrooxidans</i> , <i>L. ferrooxidans</i> Medium: 9K medium Temperature: ambient temperature	
F (MESOPHILIC CONTROL)	Culture: - nil- Medium: <i>T.thiooxidans</i> medium Temperature: ambient temperature	Culture: - nil- Medium: 9K medium Temperature: ambient temperature	
G (VARIABLE TEMP. TEST)	Culture: : <i>Thiobacillus thiooxidans</i> <i>T. ferrooxidans</i> and <i>L. ferrooxidans</i> Medium: 9K medium Temperature: ambient temperature	Culture: , <i>T. caldus</i> and <i>Sb thermosulfidioxidans</i> Medium: <i>Sb.T.</i> medium Temperature: 45°C	Culture: <i>A. brierleyi</i> and SL5B Medium: <i>Sb.T.</i> medium Temperature: 70°C
H (VARIABLE TEMP. CONTROL)	Culture:- nil- Medium: 9K medium Temperature: ambient temperature	Culture: - nil- Medium: <i>Sb.T.</i> medium Temperature: 45°C	Culture: - nil- Medium: <i>Sb.T.</i> medium Temperature: 70°C
* Columns were shutting down at days 20-25 th , 40-45 th , 60-70 th , 90-100 th and 120 th for sampling and re-condition of columns.			

2.2.2.2 Gold cyanidation

After the biooxidation process, the columns were sprayed with distilled water overnight until the collected solution becomes clear. Lime solution (CaOH, 1% w/v) was applied on the column in order to maintain the pH of solution to more than 10 for subsequent cyanide leaching.

The columns were then sprayed with a gold-lixiviant solution containing 400ppm of NaCN. The pH of the solution was maintained at 9-11 using lime. The concentration of gold extracted in cyanide solution was analyzed every 3 days using AAS. At the end of test, the agglomerates were dried, sieved and weighed to determine the weight lost.

2.2.2.3 Column analysis

During the off irrigation period, days i.e: 20-25, 40-45, 60-70, 90-100 and 120. The agglomerated ore sample (approximated 1000g) was carefully taken out from each section of the column [Top (0m-0.5m), middle (0.5m-1.0m) and bottom (1.0m-1.5m)]. Sample from each column section, approximately 2.5g was transferred into 25mL of its respective medium (table 2.2). The slurry was shaken for 48hrs, at its respective temperature. The free ore-suspended solution then transferred into fresh medium. The culture was incubated for 48hrs before inoculation into oxygen-saturated fresh medium. The dissolve oxygen consumption was monitored periodically for 48 hrs. The activity of the bacterial cultured was also monitored under the microscope.

The ore and concentrate were dried and separated using ordinary kitchen sieve. The ore was then pulverized to a size of 75 μ m. Pulverized ore and concentrate (each 100g) was then added with 1L of distilled water containing 400ppm of NaCN at a pH of 10 – 11.5 in 2L bottles separately. The bottles were placed on a roller at 50rpm for 24hrs. The residue was then treated with 1.0L of H₂SO₄ (1.0M) and the mixture was

heated gently for 1.5hrs at 70-80°C. Upon cooling, the slurry was then filtered and the residue was washed with 2.0L water. The mixture was again filtered and the cyanide gold leaching was determined using the procedure outlined section 2.2.1.7 (free gold determination). The sample was then subsequently treated with 2.0L of HCl (20%), stirred for 4 hrs at ambient temperature in the orbital shaker and with 2.0L HNO₃ (30%), stirred for 4 hrs at 80°C. The residual sample was acid digested as described in section 2.2.1.3. The gold and iron content from each sequent steps were analyzed using the Atomic Adsorption Spectrometer.

2.3 Results and discussion

2.3.1 Elemental analysis

The elemental analysis of the gold concentrate used in this study is shown in table 2.3

Table 2.3: Elemental analysis of gold concentrate from Penjom Avocet Mine, Lipis Pahang, Malaysia

Gold concentrate	
Gold, Au	140.694 ppm (mg/l)
Iron, Fe	34.089 %
Sulfur, S	27.450 %
Carbon, C	0.042 %
Zinc, Zn	0.590 %
Silver, Ag	0.608 %
Aluminum, Al	179.900 ppm (mg/kg)
Manganese, Mn	24.838 ppm (mg/kg)
Copper, Cu	8.248 ppm (mg/kg)
Arsenic, As	3.461 ppm

	((mg/kg)
Nikel, Ni	0.101 ppm (mg/kg)
Cadmium, Cd	0.424 ppm (mg/kg)
Chromium, Cr	4.55 ppm (mg/kg)
Cobalt, Co	0.586 ppm (mg/kg)
Lead, Pb	0.129 ppm (mg/kg)

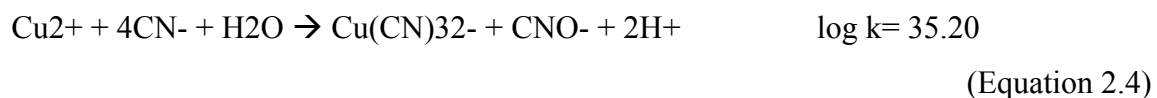
From the results obtained, it was clearly shown that the penjom gold concentrate contains a substantial amount of gold (120.694ppm), silver (0.608 %) and Zinc (0.590 %). The concentrate also contains high amounts of iron (34.089%). Due to the high amounts of sulfur (27.45 %) and low carbon content (0.042 %), the concentrate is suspected to be a sulfidic refractory mineral. High amounts of iron and other metals in the gold concentrate can affect the cyanidation process used in gold recovery in which the metals will compete with gold to form complexes with cyanide which can contribute to high cyanide consumption for gold recovery. It has been reported that Fe^{3+} and Fe^{2+} have a greater tendency to form complexes with cyanide compared to Au. The following reaction shows the strengths of the various ions in forming complexes with cyanide (Zhang et-al, 1997).

Gold-cyanide complexes



Other complexes





Cyanide also forms complexes with other metals including nickel and zinc to form $(\text{NiCN})_4^{2-}$ and $\text{Zn}(\text{CN})_4^{2-}$ and also with silver to form $\text{Ag}(\text{CN})_4^{3-}$. The formation of these complexes will decrease free cyanide availability in the slurry to leach the gold hence increasing cyanide consumption and eventually affecting, gold recovery.

Instead of valuable metals such as gold, zinc and copper, the concentrate contains a high amount of toxic metal i.e: arsenic (3.461ppm) and chromium (4.55 ppm) The high metal content in the concentrate can be toxic to the bacteria, thus affecting the bioleaching process. *T.ferrooxidans*, believed to be the dominant bacteria in metal sulphide solubilization has been reported to be affected by high metal content. The tolerance level of *T.ferrooxidans* grown in Fe^{2+} ion towards other metal ion is as follows; 0.4 g Cr^{3+}/l , 10 g Cu^{2+}/l , 10 g Cd^{2+}/l , 30 g Zn^{2+}/l and 30 g Ni^{2+}/l (Cabrera et al, 2005). The tolerance level of *T. ferrooxidans* towards As ion was $1.4 \times 10^2 \mu\text{M}$ (Shafnaz Shahir,1998). Hallberg (1996) also reported a lower metal tolerance level on a thermophilic biooxidation related bacteria, The IC_{50} for *S. acidocaldarius* strain BC (iron oxidizing extremely thermophile) was found to be approximately 0.5 mM for both arsenite and arsenate. For *T.caldus* strain which is an iron oxidizing moderate thermophile), the IC_{50} was 8.5 mM and 74 mM for arsenite and arsenate respectively.

The thermophilic strains such as *Sulfolobus* and *Acidianus* spp are sensitive to metal concentration as they lack a rigid peptidoglycan cell wall. Further the fluidity of cellular membrane increases with temperature. A combination of these factors

contributes to sensitivity to high metal concentrations in the leaching systems. (Nemati and Harrison, 2000)

However, it is believed that continuous subculturing of bacteria at higher metal concentrations can produce a high metal tolerant strain which is better suited for the bioleaching process (Natarajan et.al. 1997). Escobar,2000 has reported that the the maximum arsenic concentration on a adapted culture *Sulfolobus* BC was 370 mg/l in the bacterial leaching solution and 420 mg/l in the ferric solution..

Besides the metal content, the effects of chemicals used in preparation of mineral concentrates for example flotation utilizing collectors (xanthates, thiocarbamic,acid esters, and aliphatic and aromatic dithiophosphates) to the bacterial activity should be considered. Frother Flotanol C-7 for example decreased the chalcopyrite leaching rate by *S. metallicus*. and the potassium ethyl xanthate is the most toxic flotation chemical to *T. ferrooxidans* (Tuovinen, 1978). This is probably due to inhibition of oxygen transfer during bioleaching (Dopson, 2006 and Okibe and Johnson, 2002).

The elemental content of various mixture of ore, is shown in table 2.4.

Table 2.4: Elemental analysis of gold ore from a mixture of ore collected from various local gold field.

Gold ore	
Gold, Au	5.748 ppm ((mg/kg)
Iron, Fe	7.622 %
Sulfur, S	6.087 %
Carbon, C	4.777 %
Zinc, Zn	25.867 ppm (mg/kg)
Silver, Ag	48.250 ppm (mg/kg)
Aluminum, Al	129.600 ppm (mg/kg)
Manganese, Mn	1.373 ppm (mg/kg)
Copper, Cu	50.653 ppm

	(mg/kg)
Arsenic, As	0.6743 ppm (mg/kg)
Nikel, Ni	3.541 ppm (mg/kg)
Cadmium, Cd	191.467 ppm (mg/kg)
Chromium, Cr	1.8437 ppm (mg/kg)
Cobalt, Co	29.857 ppm (mg/kg)
Lead, Pb	306.767 ppm (mg/kg)

From the data presented, it was shown that the gold ore contains a substantial amount of gold (5.748 ppm). The ore can be classified as moderate grade. It is important to note that the ore grade varies from mine to mine, depending on gold price and operation cost. Newmont Mining Co. for example defined low grade ore as one containing 1.0 to 3.0ppm gold (Brierley, 2000b Personal communication).

It was also observed that the concentrations of other metals in the ore were greatly lower compared to the gold concentrate (table 2.3.). The ore contained 48.25 mg/kg silver, 50.65 mg/kg copper, 129.6 mg/kg Al and 29.9 mg/kg cobalt. At these levels, the metal are not worthy for recovery. However, low metal content in the ore bodies is advantages to the cyanidation process.

It is important to note, that the froth flotation process is able to increase the gold concentration 24.5 times higher compared to the original ore. This is due to the ability of froth chemical to concentrate iron sulfide mineral from the ore bodies. The flotation process also increased the concentration of other valuable metals which is naturally associated with sulfides i.e Zn (19.2 times folds), Ag (120 times fold) Al (3.7 fold) and Mn (18.1 fold). The concentration of arsenic also increased 5.13 times due to the presence of Arsenopyrite (FeAsS) in the ore body.

2.3.2 Sequential extraction

Sequential extraction method using different leaching agents was carried out to elucidate the speciation of iron in the minerals used (Brierley, 2000b Personal communication). Figures 2.5 and 2.6 show the percentages of iron in a different species. Treatment with H_2SO_4 was conducted to determine the concentration of iron in the form of jarosite and HCl to determine the dolomite, while HNO_3 treatment was conducted to determine the concentration of iron in the form of pyrite and sulphide mineral (Brierley, 2000b Personal communication).

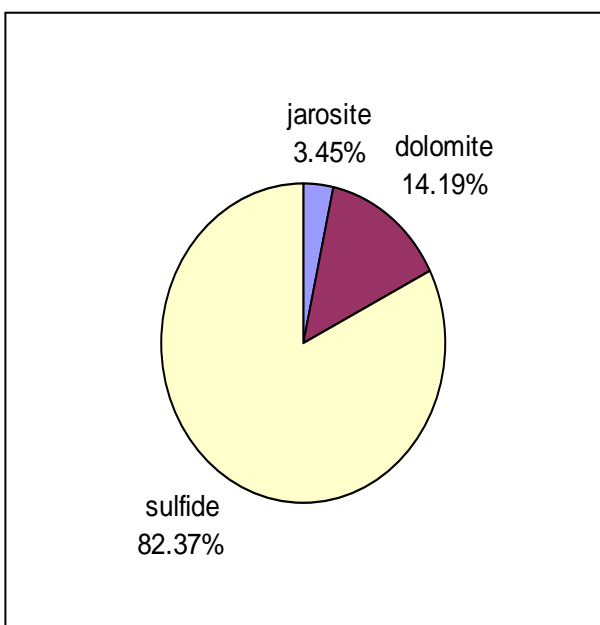


Figure 2.5: Iron speciation in a gold concentrate

■ Iron in the form of jarosites
■ Iron in the form of dolomite
■ Iron in the form of sulfide mineral

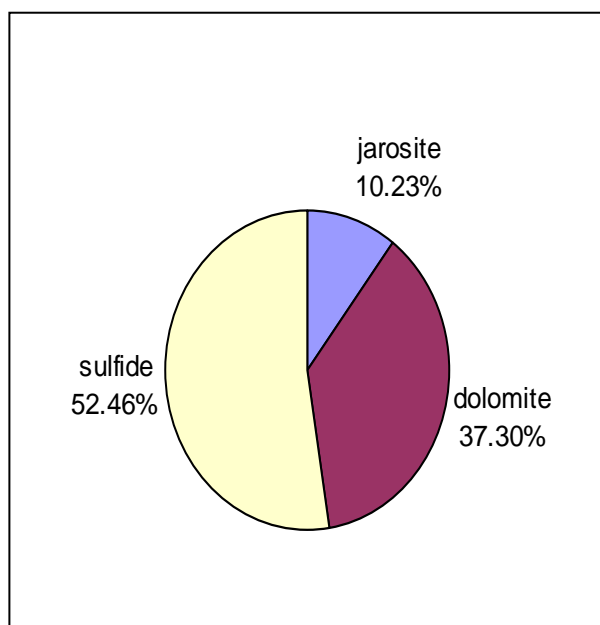


Figure 2.6: Iron speciation in a gold ore

■ Iron in the form of jarosites
■ Iron in the form of dolomite
■ Iron in the form of sulfide mineral

From the results obtained, it was observed that the iron in both mineral is mostly present as a sulfide mineral. The concentration of sulfide mineral i.e: pyrite, sphalerite and arsenopyrite increased to 82.37% from 52.46% using froth flotation process.

However, the iron in the form of dolomite and jarosite was reduced drastically from 37.30% and 10.23% to 14.19% and 3.45% respectively.

During the sequential leaching test, the extraction using cyanide roller bottle test was conducted at each level to elucidate the association of gold with the different iron minerals (Brierley, 2000 Personal communication). Figures 2.7 and 2.8 shows the distribution of gold particles in the concentrate and ore based on the sequential extraction test carried out.

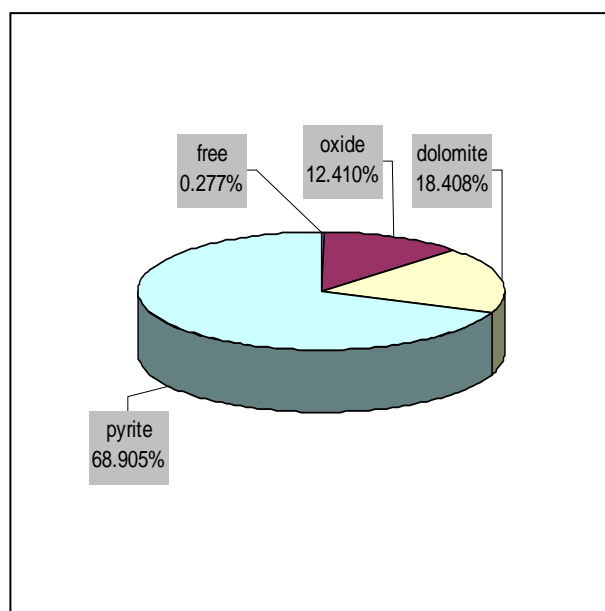


Figure 2.7: Gold speciation in a gold concentrate

- Free gold
- Gold locked in a jarosite or iron oxide precipitate
- Gold locked in a dolomite mineral
- Gold locked in a sulfide mineral

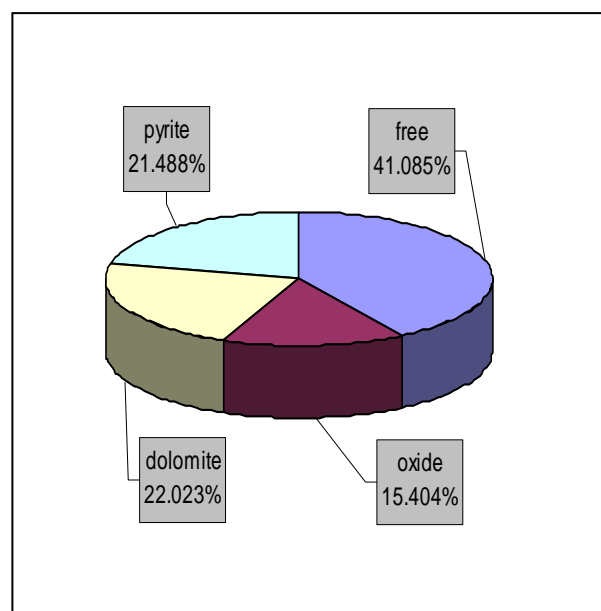


Figure 2.8: Gold speciation in a gold ore

- Free gold
- Gold locked in a jarosite or iron oxide precipitate
- Gold locked in a dolomite mineral
- Gold locked in a sulfide mineral

The results show that the concentrate contains only 0.277% free gold using direct cyanidation. This also implies that 99.7% of the gold is unextractable. For the gold ore (figure 2.8) only 58.9% of the gold is unextractable. The ore and concentrate is

considered as highly refractory because of the free gold content is less than 80% (Brierley, 2000b personal communication).

After treatment with HNO_3 , further 68.9% and 21.5% gold in the concentrate and ore respectively, were obtained upon extraction with cyanide indicating that the gold was physically trapped in sulphide mineral such as pyrite and chalcopyrite (Brierley, 2000b Personal communication). Biooxidation may be required to break up the sulphide in order to render gold amenable to the subsequent cyanide leaching.

2.3.3 Size analysis

Particle size analysis is very important for the leaching optimization study. Figures A-1 and A-2 shows the size distribution of gold concentrate and ore used for columns study. Based on size distribution analysis used dry sieved method, average size (based on 80% of accumulated size distribution) the ore and concentrate size is 1.63mm and 169 μm respectively. The size is nearly suitable for tank leaching (concentrate) and heap operation (ore). As suggested by Sia Hok Kiang, 2000. Personal communication and (Brierley, 1997) the suitable size for tank biooxidation and heap leaching was 75 μm and 8mm respectively. The correlation between mineral size distribution with rate of bioleaching is due to the, enzymatic (direct) and Fe^{3+} abiotic (indirect) reaction, occurring on the particle. Hence, the rate of bioleaching should increase with decrease particle size of the ore since the smaller the particles, the larger the surface area per unit weight. Indeed it is well documented that the highest solubilization rates were achieved for pyrite, chalcopyrite and sphalerite at the smallest particle size fraction i.e 25 μm (Rossi, 1990).

However, grinding operation the ore to such size is a very expensive operation. Optimum biooxidation operation should be based on a compromise between grinding cost and profit deriving from recovery rates. In this case, ultra fine grinding of mineral

ore will produce an increase in surface dislocation densities on the mineral surface and therefore greater instability of the crystal structure which will deactivate the bacterial activity (Rossi, 1990).

The first-order deactivation rate of bacterial cells was found to increase with decreasing particle size down to a certain size of 63 μm to 45 μm (Deveci, 2004). The action of solid particles on the cells will cause damage to bacterial cells and therefore results in the loss of viability of bacterial cells. The attrition of bacterial cells is also effected depending upon the impeller type, solids concentration, and intensity of agitation. It was suggested (Deveci, 2004) that exposure of microorganisms in general to shear environments could result in the lysis of cells, the inhibition of growth or product synthesis, the denaturation of extracellular proteins, the change in morphology, or the thickening of the cell wall. In bioleaching processes, the shear conditions have been postulated to affect the bacterial cells that are in contact with sulphide minerals or in solution (i.e., unattached). This leads possibly to the disruption of bacterial cells, the inhibition of the attachment of bacteria to sulphide minerals, or the detachment of the cells from the mineral surface (Rossi, 2001). Nemati et al. (2000) did not observed any thermophiles activity, namely *Sulfolobus metallicus* in the presence of fine pyrite particles at 25 μm and 3% w/v solids density despite a general trend of increase in oxidation rate with decreasing particle size. The researcher concluded that the fine particles caused damage to the bacterial cells resulting in loss of oxidizing activity.

Compared to tank leaching, the heap bioleaching required a coarser mineral size to achieve optimal condition. Reaction on a coarser ore bodies is very slow, which explains why not much effort has been focused on the kinetics of heap bioleaching. Heap leaching is usually simulated in columns charged with ore where leaching solution percolates from the top. At steady state conditions, metal leaching has been described as being pore-diffusion controlled by a reacted porous zone surrounding a region of unreacted ore, similar to shrinking core kinetics. However, the shrinking core equation does not apply at the initial stages of bioleaching (Lizama, 2004). Peralta (1997) gave a good explanation why particle size is an important physical factor that affects the bio-

heap process. Coarse-grained mining wastes allow greater oxygen advection and hence active acid and ferric generation bacteria can occur to a greater depth in a body heap than fine-grained ore. In coarse metal mine rock dumps, air convection is promoted by wind action, barometric pressure changes, and internal heap heating from the exothermic oxidation reactions. Under these conditions, active bacteria may occur throughout the dump rather than being limited to the surface zone, as in fine-grained ore.

With this assessment, it may be more advantageous not to have very fine grain particles in the heap during leaching. Problems related to fine particle in the heap are decrepitation, flooding, channeling, slumping and compaction. However, in order to determine the behavior of the fine ore concentrate, the concentrate was agglomerated onto gold ore using the iron or ferric producing bacteria as agglomerating agent. Agglomeration will be able to increase particle size in the ore, particle permeability and promote a better leachate and air distribution inside heap (Geobiotic Inc, 2002).

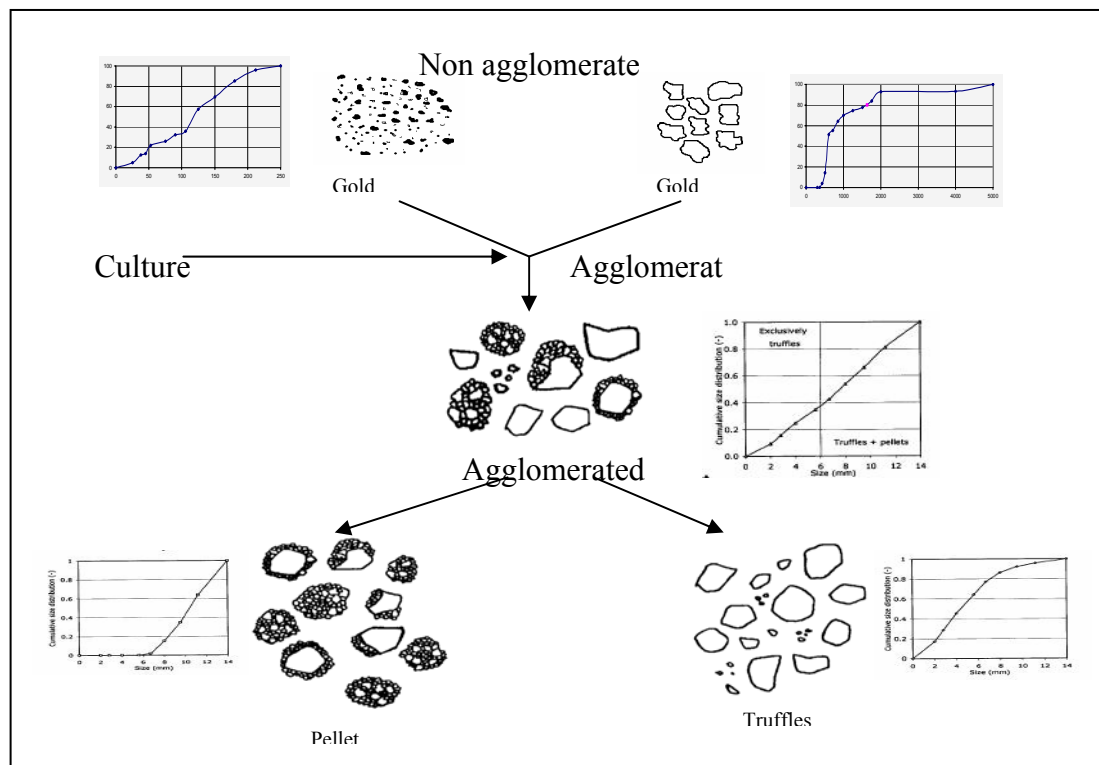


Figure 2.9: Behavior and size distribution of mineral during agglomeration. (Bouffard, 2003)

It was reported that the agglomerates prepared by mixing crushed ore particles with any liquid may belong to either one of two types: truffles or pellets as shown in figure 2.9 (Bouffard, 2003). Truffles are simply dusty, crushed ore particles with very little porosity. The chemical and diffusion controlled modeling approaches may fall short with the present pyritic ore sample. Indeed, even among particles of the same size, pyrite occurred as disseminated micron-size grains, as disks or plates sandwiched between gangue minerals, as veins, and filling open spaces. The latter three types of mineralization were noted for the most part in the coarsest fractions and be classified into three groups i.e. no visible grains, visible grains, and disks.

The usual assumption of homogeneous distribution of monosize grains is invalid in this context. Furthermore, modeling the leaching of any of the observed types of liberated pyrite occurrences using, for instance, shrinking-plate or -cylinder models, entails proper characterization of grain geometries using more sophisticated techniques than the naked eye.

Observed variations in pyrite grade, shape, and size distributions between ore particle of different sizes calls for a simpler strategy to model any diffusion and reaction phenomena taking place simultaneously within ore particles. A more generalized topological function is written as:

$$g(1 - X) = (1 - X)\phi \quad \text{Eq. 2.7}$$

where Φ may vary over the course of the leach, taking values greater than or equal to 2/3. The parameter Φ should, in principle, be evaluated for each particle size. A collection of particles will instead be modeled as a single-size class. The parameter Φ is not strictly speaking the weighted average of the individually-measured Φ parameters of fine, medium, and coarse particles in a particular assemblage, but rather fits the overall oxidation profile as obtained from leaching different size particles altogether in the same vessel.

Pellets are relatively spherical, more porous aggregates comprised of several ore particles held together in close proximity by the agglomerating fluid. The complete saturation of the pellet pores excludes air. All agglomerates smaller than 6 mm consisted exclusively of truffles. In contrast to truffles that see the same reagent concentrations on their external surfaces, the ore particles in pellets bathe in a stagnant solution saturating the pellet pores. Reagents must therefore first diffuse through the pellet pores before accessing reactive mineral grains on the external surfaces of the ore particles, and/or further diffusing into the minuscule pores of the same ore particles to reach embedded grains. The truffle model must therefore be altered to reflect these successive phenomena. A comprehensive pellet leaching model would consider both the oxidation kinetics of ore particles forming pellets and the physical arrangement of ore particles of different sizes within pellets of identical or variable sizes.

However, considering the contentious reliability and reproducibility of the method employed to evaluate the proportion of truffles and pellets, it is extremely doubtful, if not impossible, to obtain statistically representative figures to represent any variations of particle size distribution between pellets of identical and different sizes. For this reason, pellets of any size will be assumed to contain the same distribution of ore particles throughout their entire volume, i.e.: fine, medium, and coarse particles are homogeneously distributed within the pellet volume. Furthermore, due to the size of supported mineral (gold ore) is entirely below 5mm (fig 2.10) the agglomerated particle can be considered as pellet.

2.3.4 Acid consumption test

Result of the acid consumption test is shown in Table A-1 and A-2 . The acid consumption value of the ore was much lower than that for the concentrate i.e 1.42mL and 0.412 mL of H₂SO₄ respectively. The value is quite high compared to that reported by Menon and Dave, 1993, where the acid consumption is 0.08mL concentrated H₂SO₄

per gram ore. It must be noted that low pH is an important factor for the proliferation of acidophilic bacteria, thus high acid consumption would retard or arrest the reaction by withdrawing sulphuric acid present (Brierley and Luinstra, 1993). In order to maintain low pH, some external acid sources may be required, which will eventually increase the cost. However, for the concentrate used in this experiment, washing with distilled water was carried out order eliminate to the alkaline content from the previous cyanidation process.

2.3.5 Biological acid producing potential (B.A.P.P)

Biological acid producing potential test was conducted to determine the ability of bacterial consortium used in the bioleaching study to generate H_2SO_4 from the sulphide minerals in order to maintain low pH, which is the optimum condition for bioleaching process using acidophilic bacteria. Most literature cited gave evidence of ferrous ion bacterial oxidation occurring around pH 3.5 (Mervane and Vargas, 2000). Thus, an increase in pH will cause a decrease in iron oxidation by bacteria thus affecting bioleaching rate. Figures A-3 and A-4 shows the pH profile for Biological acid producing potential test on gold concentrate and gold ore respectively using *T. ferrooxidans*, *Sb. Thermosulfodooxidans* and *A. Brierleyi*.

From figure A-3 it can be concluded that the pH increased to pH 3.9 for *T. ferrooxidans*, 4.12 for *Sb. Thermosulfodooxidans* and 3.44 for *A. Brierleyi* on day 3 upon addition of gold concentrate and bacteria. The pH then slightly decreased below 2.5 on day 6 (*A. Brierleyi*), day 8 (*T. ferrooxidans*) and day 10 (*Sb. Thermosulfodooxidans*). When the pH reached 2.5 and remained constant, there will be no more drop in the pH value. Then half of the initial ore's weight (15g) was added to increase the concentration of mineral. During the ramp-up increased in mineral concentration, the pH was drastically increased to pH 3.23-4.13. A different profile was observed in the BAPP test on gold ore using *T. ferrooxidans*, *Sb. Thermosulfodooxidans*

and *A. Brierleyi* (fig A-4). The overall pH was low which might be related to the low acid consumption by the ore.

2.3.6. Preg-robbing test

Gold losses during processing is a major problem throughout the gold mining industry and can lead to significant amounts of gold found in the tailings. One of the ways by which these gold losses take place is known as preg-robbing, whereby constituents of the ore adsorb the aurocyanide complex ($\text{Au}(\text{CN})_2^-$) from solution. During the processing of preg-robbing carbonaceous ores, a significant fraction of the gold present in the ore is not adsorbed by the commercial activated carbon. It has been presumed that gold was adsorbed onto the naturally occurring fine-grained organic carbon present in the ore, and is subsequently discarded with the ore tailings, since this fine grained carbon is not retained by screening (Schmitz, 2001). From the preg-robbing test, the tendency of gold concentrate and ore to adsorb gold from the gold-cyanide solution will be determined. In the preg-robbing test, a percent preg-robbing value is obtained by measuring the change in solution of gold concentration after contacting a gold-cyanide solution with a known mass of ore in batch. However, the ability of the preg-robbing test to predict the preg-robbing behavior of the ore during CIL processing is limited, since no commercial activated carbon is added during the test. Table 2.5 shows the adsorption behavior of gold in solution of the gold concentrate and ore.

Table 2.5: Adsorption behavior of gold in solution to the gold concentrate and ore.

Mineral	[Au] _{initial} , ppm	[Au] _{final} , ppm	[Au] _{adsorb} , ppm	% Au adsorb
Gold concentrate	5.023	4.928	0.095	1.89
Gold ore	5.034	3.299	1.735	34.47

From the preg-robbing test, 34.47% of gold in the form of gold-cyanide complex was adsorbed by the original gold ore compared to the 1.89% for concentrated mineral. The

value is considered high compared to the value reported by Goodwall, 2005. The preg robbing value for the ore from Barrick Goldstrike Mines, one of the most famous gold mines known for its ore preg robbing behaviour was 27.97%. The most common and well documented cause of preg-robbing is carbonaceous matter present in the ore. High carbon content in the Penjom gold ore 4.77% is the main contributor of high preg robbing value compared to the its concentrate at 0.042%. The carbonaceous components can be in the form of wood chips, organic carbon and elemental carbon (Tan et al, 2005). It can also in the form of heavy hydrocarbons, organic acids or natural carbon. Of this material, native carbon is the most important species for preg-robbing.

This carbonaceous ore has kerogen as the principal preg-robbing component. Stated that carbonaceous matter locks up a proportion of gold in the ore and also adsorbs gold from the pregnant solution. As example, for ore from the Carlin trend, Nevada that the preg-robbing characteristics were inversely correlated to the Lc (002) crystallite dimension of pyrite and directly related to the d-spacing of the carbonaceous material. (Rees, 2000). This type of carbonaceous preg-robbing may be inhibited by the addition of diesel or kerosene to leaching circuit of a plant. However this procedure is generally not recommended due to the inhibition of gold cyanide adsorption onto activated carbon in the presence of organic impurities. (Tan et al, 2005).

The other causes of preg-robbing are the minerals themselves, predominantly either sulphides or silicates. Goodwall, 2005 suggested that preg-robbing mechanisms can be divided into two types. Reversible (Type I) preg-robbing occurs by simple ion exchange of the large aurocyanide anion. This type of preg-robbing is common to some extent in most ores, but in most cases is reversible in the presence of activated carbon or by washing. Irreversible (Type II) preg-robbing is considered so because of the long time or unusually severe conditions required to redissolve the gold.

Type I preg-robbing provides few problems in modern CIP/CIL circuits if the activity of the ore constituents is less than that of activated carbon, however, constituents with a greater activity will compete strongly for adsorption of the aurocyanide

complex. It has been shown for a number of ores, most notably those from Carlin, Nevada that native carbon will compete with activated carbon in this way (Schmitz et al., 2001) The adsorption of gold onto native carbon is thought to follow much the same mechanism as the adsorption to activated carbon in a CIP/CIL circuit and although the number of active sites is smaller, it has been demonstrated that the adsorption kinetics are up to 4 times faster for native carbon. For sulphide ores (Rees and Van Deventer, 2000) suggested that preg-robbing was cyanide concentration dependent. In the presence of free cyanide it was shown that preg-robbing was unlikely to occur and any that did occur was easily reversed by the addition of activated carbon.

Irreversible (Type II) preg-robbing involves precipitation of the gold complex and can occur by a number of separate mechanisms. The first mechanism (Type IIa) involves a lack of available cyanide causing the aurocyanide complex to be stripped of one radical and the resulting auromonocyanide radical to form long chains, which are only vulnerable to attack from the tips making redissolution possible but very slow. A similar mechanism was presented by Rees and van Deventer (2000) who showed that aurocyanide was reduced to the surface of chalcopyrite in a cyanide deficient environment. The second mechanism for irreversible preg-robbing (Type IIb) is a co-precipitation of gold with metal cyanides.

Rees and van Deventer (2000) demonstrated clear cyanide concentration dependence for preg-robbing on pyrite and chalcopyrite with very strong adsorption of gold in cyanide deficient solutions. Chalcopyrite and pyrite were shown to be very strongly preg-robbing. A mechanism was proposed where the gold was reduced at the chalcopyrite surface, along with the oxidation of chalcopyrite to form copper- cyanide complexes in solution. The effect of contaminant carbonaceous coatings on preg-robbing behaviour of minerals has been neglected in the literature. Ibrado and Fuerstenau, 1995 reported that the carbonaceous coating could be selective on mineral surfaces. Both carbon and sulphide surfaces are hydrophobic to some extent. It is expected that carbon could preferentially coat on sulphide surfaces over other hydrophilic gangue mineral

surfaces. Sulphides have been demonstrated to be preg-robbing via chemical and physical adsorption, or gold reduction at the sulphide surfaces. (Vergouw, et al 1998)

Pyrrhotite and alumina were also found to adsorb gold. A mechanism was proposed where dicyanoaurate (I) was reduced at the pyrrhotite surface, with the sulphide ion of the pyrrhotite being oxidised to elemental sulphur. Afterwards, Adams et al. (1996) undertook a study on the preg-robbing behaviour of minerals. It was indicated by Mossbauer spectroscopy that gold cyanide was reduced at the surfaces of chalcopyrite and arsenopyrite, with metallic gold accumulating at defect sites on the mineral surfaces.

Silicate minerals, especially clays have also been proposed as potential preg-robbars. It has been suggested that the positively charged edge surfaces of clay particles could attract negatively charged colloidal gold (Cook et al 1989.). The negative colloidal gold particles attached to positive kaolinite edges, although this was in acid solution and adsorption would be greatly reduced in an alkaline environment. However the effect of silicate preg-robbing is usually neglected.

For the ore containing double refractory behavior, i.e contains both sulfides and carbonaceous matter; Amankwah et al 2005 have suggested a two-stage bacterial pretreatment process. The first stage, deals with sulfide oxidizing bacteria i.e: *Thiobacillus ferrooxidans*, *Thiobacillus thiooxidans* and *Leptospirillum ferrooxidans* in order to decompose the sulfide matrix to release gold particles. Unfortunately, carbonaceous materials are not oxidized by this pretreatment step and continue to serve as preg-robbars in the subsequent gold leaching process. Biooxidizing the carbonaceous material with an actinomycete, i.e; *Streptomyces setonii*, to degrade the carbon material is carried out in the second stage in order to enhance gold recovery.

2.3.7 Column leaching studies

In this the leach behaviour of agglomerated ore and ore concentrate system and gold leaching using various organism i.e: mesophilic (30 °C), moderately thermophilic (45 °C) and extremely thermophilic (70 °C) was carried out. The investigation was subsequently taken further to elucidate the interplay between the microbes and the various mineral phases present in the concentrate and ore.

The present work evolved from a series of tests conducted using the agglomerated ore (Geocoat technique), whereby a concentrate is coated onto inert or low-grade support rock and subsequently subjected to heap bioleaching (Harvey et al, 2002). The commercial advantage of this approach over tank bioleaching is based on lower capital and operating costs associated with heap leaching. As a scientific tool it offers the ability to study heap leaching with highly exposed mineral surfaces and the ability to customize mineral compositions in the heap. A previous study by the Harvey et al, 2002 has allowed the determination of heat generation associated with bioleaching of a pyrite concentrate and thus established that the process is feasible in principle, i.e. the energy necessary to operate a thermophilic heap bioleach can be provided entirely by the heat of reaction.

2.3.7.1 pH and E_H profile

The results of the single temperature experiments in terms of pH and solution potential (in mV vs. Ag/AgCl) in the column effluent are summarized in Fig, B-5 (Test) and Fig, B-6 (Control) at ambient temperature, Fig, B-3 (Test) and Fig, B-4 (Control) at 45 °C, and Fig, B-1 (Test) and Fig, B-2 at 70 °C (available in attachment B). In a real heap situation, thermophilic conditions would have to be attained by gradually heating from ambient. To achieve this, the heap would have to be condition with mesophiles, which gradually give way to moderate thermophiles, which eventually give way to the

extreme thermophiles. Heat generation would be entirely due to sulfide mineral oxidation.

In laboratory columns the self-heating effect cannot be harnessed, as heat is rapidly lost through the column walls, even if well insulated. Therefore, an experiment was conducted to study leaching under conditions of gradually increasing temperatures through external heating. In this study, the temperature in columns 7 and 8 was raised from 30 °C to 45 °C level over a 40-day period and 45 °C to the 70 °C level over a 20-day period. This profile has been established from an analysis of the heat generation potential of the mineral in the fixed temperature experiments and subsequent modeling of heat profiles in a typical heap. This method has been presented by the Dixon and Peterson, 2002 in a similar study on a different material. The experiment consisted of two columns (7 and 8) run under identical conditions. The mesophilic, moderately thermophilic, and extremely thermophilic consortia were introduced in the test column (column 7) during the ramp-up phase at days 40 and 60. The pH and solution potential (in mV vs. Ag/AgCl) indicated in Fig. B-7 and B-8 (attachment B).

2.3.7.2 pH profile for sulfur oxidizing related culture

The sulfur oxidizing related culture was pumped into the column for the first 15 days of biooxidation. The culture namely *T. Thiooxidans* (mesophile), *T. Caldus* (moderate thermophile) and *A. brierleyi* (extreme thermophile) was used in this test. Studies on pyrite degradation were mostly indicated that metal sulfides are only degradable by an oxidizing attack, i.e. by Fe^{3+} . However, pyrite was also degraded via acidification of leach biotopes and a formation of acid rock drainage. (Schippers and W. Sand, 1999 and Dutrizac and MacDonald, 1974).

According to pyrite molecular orbital considerations, Fe (III). hexahydrate ions cleave the chemical bonding between the iron and the disulfide in the pyrite lattice, after

the disulfide group has been oxidized to a thiosulfate group. As a consequence, thiosulfate and Fe (II). Hexahydrate ions occur as dissolution products. The thiosulfate is then oxidized via tetrathionate, disulfane-monosulfonic acid, and trithionate to mainly sulfate in a cyclic mechanism by *T. thiooxidans*, *A. Calvus* and *A. Brierleyi*. Besides that, minor amounts of elemental sulfur and pentathionate occur as by-products (Schippers et al, 1996). Thiosulfate and polysulfide mechanism become a key compound in the oxidation of the sulfur moiety of pyrite and the mechanisms were shown in figure 2.10 and 2.11.

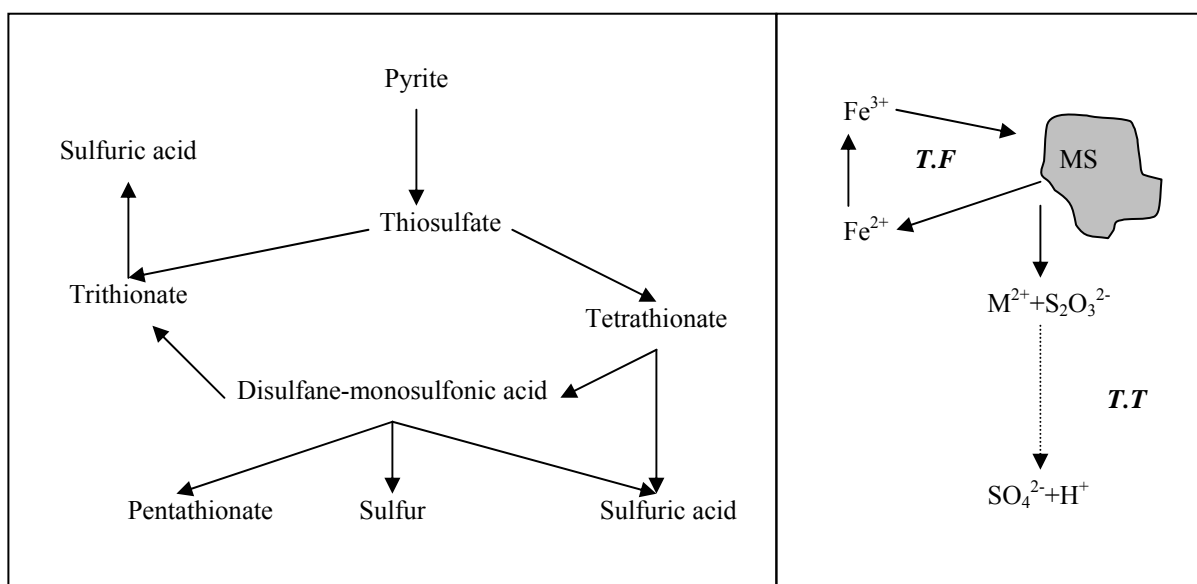


Figure 2.10: Thiosulfate mechanism in pyrite oxidation

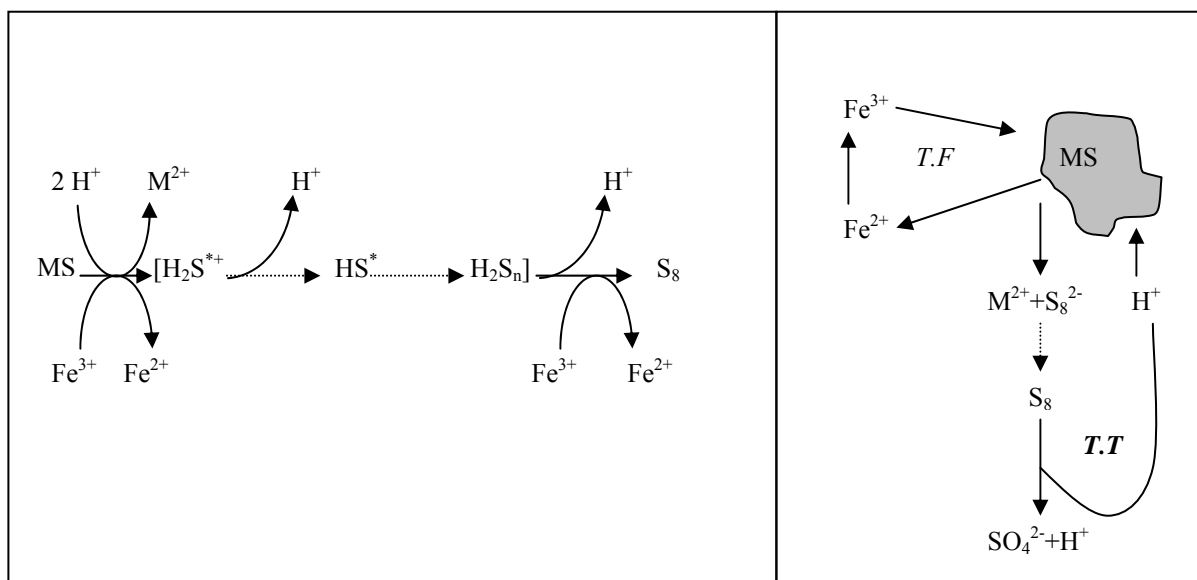


Figure 2.11: Polysulfide mechanism in pyrite oxidation

In thiosulfate mechanism, all reactions occur on a purely chemical basis. However, sulfur compound oxidizing enzymes, like the tetrathionate hydrolase of culture may be involved.

The thiosulfate mechanism is mainly occurs for chemical pyrite oxidation at higher pH (near to neutral pH), i.e: in carbonate ore and pyrite containing mine waste. At higher pH, the chemical pyrite oxidation rate is about 10 times higher than the one under very acidic conditions (Hackl and Jones, 1997 and Schippers, et al 1995). Thiosulfate, trithionate, and tetrathionate are the main products of pyrite oxidation in carbonate buffered solutions. These substances are suitable substrates for moderately acidophilic, sulfur compound oxidizing bacteria. These bacteria live from the “energy gap” between the incomplete chemical oxidation of the sulfur moiety of pyrite at nearly neutral pH values and its complete oxidation to sulfuric acid. In addition, by acid production the pH is lowered, allowing acidophilic iron oxidizing leaching bacteria, like *T. ferrooxidans*, to grow and to oxidize pyrite (Fowler, Holmes and Crundwell, 1999).

It still needs to be elucidated, to what extent these enzymes catalyze the reactions in competition with chemistry. This would allow to manipulate the flux of intermediary sulfur compounds, the accumulation of elemental sulfur in bioleaching and coal desulphurization processes could be prevented or sulfate formation in bioleaching plants could be enhanced. Six metal sulfides differing in crystal and electronic structure in a pyrite were develop a unique structure. Based on molecular orbital and valence bond theories, the pyrite are be degraded by an oxidizing and proton attack. This process will produce a several sulfur compound. The formation of sulfur compounds in the course of ferric ion mediated chemical oxidation (10mM FeCl₃, pH 1.9 and 28°C) of metal sulfides i.e: Pyrite, Sphalerite, Chalcopyrite, Galena and Hauerite was reported in table 4.6 (Schippers and Sand,1999)

Table 2.6: Formation of sulfur compound resulting from metal sulfide oxidation.

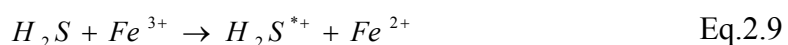
	S ₈ (%)	SO ₄ ²⁻ (%)	S ₄ O ₆ ²⁻ (%)	S ₃ O ₆ ²⁻ (%)
Pyrite (FeS ₂)	16.1	81.7	1.3	0.9
Hauerite(MnS ₂)	93.6	3.7	1.2	1.5
Sphalerite (ZnS)	94.9	4.8	0.1	0.2
Chalcopyrite (CuFeS ₂)	92.2	7.3	0.3	0.2
Galena (PbS)	99.9	0.1	0.0	0.0

The oxidation products of pyrite consisted of up to 82% of sulfate, 16% of elemental sulfur and to 2% of polythionates. This result is caused by a polysulfides mechanism as key intermediate. Due to their principal solubility in acid, the first reaction is assumed to be:

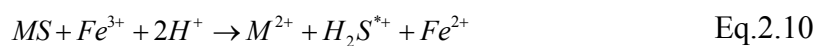


In contrast to pyrite oxidation, in other sulfides the MS bonding is cleaved, before the sulfidic sulfur is oxidized. The kinetics of this reaction is dependent on the solubility product of the respective metal sulfide.

In the oxidation mechanism of aqueous sulfide, the H₂S is subjected to a one electron oxidation by a Fe³⁺:



Instead of that, the cation radical H₂S^{*+} may also directly be formed by an attack of Fe³⁺ on a metal sulfide:



By dissociation of the strong acid H₂S^{*+} the radical HS^{*} occurs:



Two of these radicals may react to a disulfide ion:



The disulfide ion can further be oxidized by HS* radical:

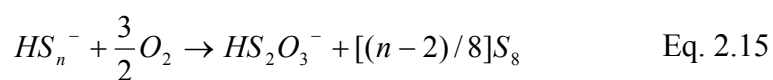


Tetrasulfide can occur by dimerization of two HS* or trisulfide by reaction of HS* with HS* radicals. Chain elongation of the polysulfides may proceed by analogous reactions. In acidic solutions, polysulfides decompose, liberating rings of elemental sulfur, mainly S₈ (99%)

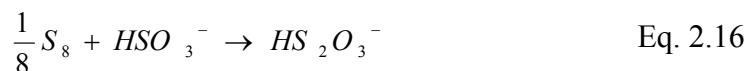


This mechanism does not necessarily function only in the presence of Fe³⁺ ions. An electron transfer from a semiconductor metal sulfide to an O₂ molecule is also possible. The O₂ molecule is reduced via a superoxide radical and a peroxide molecule to water. However, Fe³⁺ ions are generally much more efficient in extracting electrons from a metal sulfide lattice than O₂.

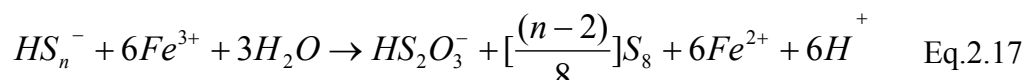
The reactions in equation 2.14 inherently explain the formation of elemental sulfur as the main sulfur compound. Minor amounts of sulfate and polythionates are products of thiosulfate reactions. Thiosulfate may arise by a side reaction:



or be formed in the following one:



However, under anaerobic conditions only minor amounts of sulfate and polythionates were formed. Formation of polythionates was elucidated in equation 2.17 where the Fe^{3+} become an oxidizing agent:



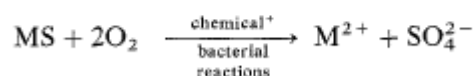
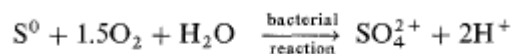
Thiosulfate and polythionates play a key role in the sulfur pathways in sulfide degradation. However, these compounds play only a side role in the polysulfide mechanism. The complex mechanism is simplified in the figures 2.10. In any case, the main end-product is elemental sulfur. The latter is biologically oxidized to sulfuric acid. This explains the ability of sulfur oxidizing bacteria i.e; *T. thiooxidans*, *T. Caldus* and *A. Brierleyi* to leach some metal sulfides. Two indirect oxidation mechanisms for metal sulfides via sulfur compound pathways exist, which are summarized in table 2.7.

Table 2.7: Indirect sulfur compound oxidation mechanisms for metal sulfides

Thiosulfate mechanism (FeS , MoS , and WS).	$FeS_2 + 6Fe^{3+} + H_2O \rightarrow S_2O_3^{2-} + 7Fe^{2+} + 6H^+$
	$S_2O_3^{2-} + 8Fe^{3+} + 5H_2O \rightarrow 2SO_4^{2-} + 8Fe^{2+} + 10H^+$
Polysulfide mechanism (ZnS, CuFeS , PbS)	$MS + Fe^{3+} + H^+ \rightarrow M^{2+} + 0.5H_2S_n + Fe^{2+} (n \geq 2)$
	$0.5H_2S_n + Fe^{3+} \rightarrow 0.125S_8 + Fe^{2+} + H^+$
	$0.125S_8 + 1.5O_2 + H_2O \rightarrow SO_4^{2-} + 2H^+$

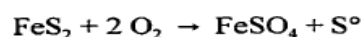
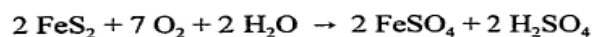
In the column with sulfur oxidizing related bacteria (first 40 days of biooxidation). The initial discharged solution pH were akin (around pH 1.9) between the test column and control column for the column at a 45°C and 70°C. However, the pH was slightly higher for the column at ambient temperature i.e pH 2.73 for column with

T.Thiooxidans and pH 4.26 for control at 30°C. From the results obtained, the column with sulfur oxidizing culture (*T.Thiooxidans*, *T.Caldus* and *A.Brierleyi*) were remain low due to the bacterial was oxidize sulfur in the solution and pyrite via the reaction 4.xx to produce sulfuric acid.(Sand et al,1995)



Eq 2.18

However, for the control column at elevated temperature, the pH was low due to the spontaneous oxidation of metal sulfide at high temperature as mention by Hu Long, 2000.



Eq 2.19

As example, for column with thermophile, the pH profile for control and test is identical; the pH was started at around 1.9 and then constantly decreased at the rate of 0.01 pH/hr. For the test column, the presence of *A. Brierleyi* was persuading the mineral oxidation of inorganic sulfur compound to achieve its optimum condition at pH 1.5 (Konishi et al, 1997) via equation 2.18. However, the pH trend for control column was powered by equation 2.19. Due to the both reaction did not associate with Fe³⁺-Fe²⁺ system, the pH and E_H affiliation in the column was shown in equation 4.20 (Rossi,1990)where,.

$$E_H = [-0.01rH_2] + k_{H_2} pH$$

Eq 2.20

Referring to the figure B-3 and B-4, the pH verses E_H for column solution at 70°C, the rate constant k_{H_2} for column contained *A. Brierleyi* was 76.96 pH/mV and 69.21 pH/mV for the control. The finding was contradict with the reported by Bunyok (2003) and Sjahrir (2000), where the k_{H_2} value was negative (E_H value were decreased with increased in pH value).

In experiment column 3 (biotic, fig B-5) and 4 (abiotic, fig B-6) using moderate thermophiles at moderate temperature (45 °C), the pH value for the test column (3) proceeded at rates similar to those observed in column 4 (control) for the first 25 days. The pH for column containing *T.Caldus* were increased at the rate of 0.0217 pH value /day before constantly dropped at 0.0316 pH value /day at the day 25th to day 40th . However, for the control column (column 4) the pH value was steadily increased at the rate of 0.0098 pH value /day from day 0 to 40th. The correlation between pH and E_H in the column at 45°C were shown in table B-7 and B-8. The k_{H_2} value for column 3 (biotic, *T. caldus*) and column 4 (abiotic, control) was at -67.83 pH/mV and -38.09 pH/mV respectively.

In the mesophile experiment (Fig B-9: Column 5 and Fig. B-10: Column 6). The initial discharged solution pH were slightly increased at the rate of 0.0395 pH value/day (Day 0- 15) for the column containing *T. Thiooxidans* and 0.0453 pH value/day (day 0- 12) for control column. The pH solution then subsequently decreased from pH 3.25 to 2.16 for test and ph 4.75 to 3.65 for control. The initial solution potential was identical between biotic and abiotic column. The initial solution potential value level at 622 mV (vs. Ag/ AgCl) and decreased to 550 mV after 40 days biooxidation. The correlation between pH and E_H of column solution was shown in fig FigG-11: Column 5 and Fig.G-12: Column 6. The k_{H_2} value for column 5 (biotic, *T. Thiooxidans*) and column 4 (abiotic, control) was at 76.96 pH/mV and 69.21 pH/mV respectively.

2.3.7.2 Iron solubilization behaviour in the column

The results of the single temperature experiments in terms of iron solubilization in the column effluent are summarized in figure 2.14 at ambient temperature, figure 2.13 at 45 °C and figure 2.12 at 70°C. Furthermore, figure 2.15 show the iron solubilization profile.

In the column leaching study under conditions of gradually increasing temperatures through external heating at the ramp-up phase at days 40 (45°C) and 60 (70°C).

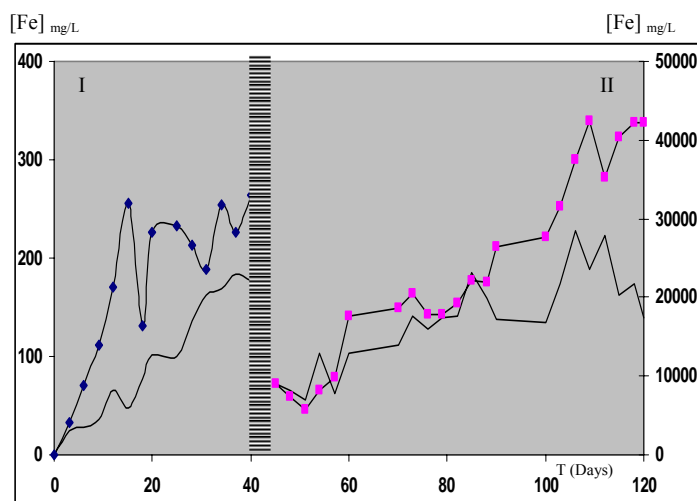


Figure 2.12 : Iron Solubilization profile of collected solution in the column at 70°C.

I: Fe free lixiviant (*A. Brierleyi* Medium)
 II: Fe containing lixiviant (*Sb. Thermosulfodooxidans* medium)
 --■-- Test
 ----- Control

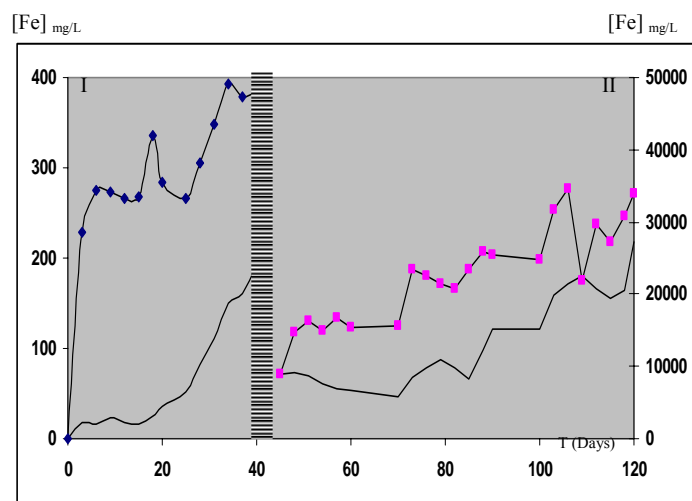


Figure 2.13 : Iron Solubilization profile of collected solution in the column at 45°C.

I: Fe free lixiviant (*A. Calvus* Medium)
 II: Fe containing lixiviant (*Sb. Thermosulfodooxidans* medium)
 --■-- Test
 ----- Control

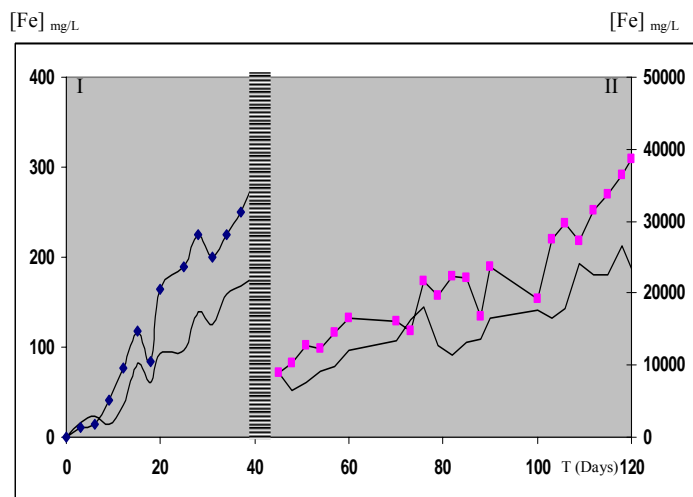


Figure 2.14 : Iron Solubilization profile of collected solution in the column at 30°C.

I: Fe free lixiviant (*T. Thiooxidans* Medium)
 II: Fe containing lixiviant (9K medium)
 --■— Test
 ----- Control

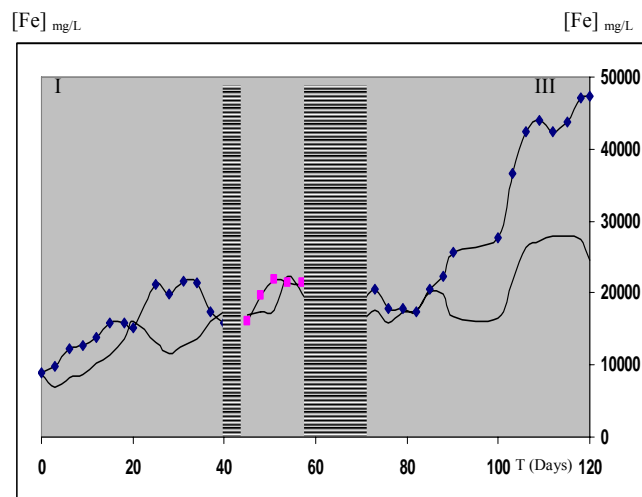


Figure 2.15 : Iron Solubilization profile of collected solution in the column at different temperature

I: Column at 30°C, 9K medium
 II: Column at 45°C, *Sb. Thermosulfodooxidans* medium
 III: Column at 70°C, *Sb. Thermosulfodooxidans* medium
 --■— Test
 ----- Control

From the results obtained, it was observed that the entire test column showed a higher iron solubilization compared to their control at respective temperature. For the single temperature column test, with the presence of *T. Caldus* (Fig 2.13-I), the overall amount of iron solubilization was 3.5 times fold higher than control. It followed by *Sb. Thermosulfodooxidans* (Fig 2.13-II), *T. Thiooxidans* (Fig 2.16-I), *A. Brierleyi* (Fig 2.12-I), isolate SL5B (Fig 2.12) and mixture of *T. Ferrooxidans* and *L. Ferrooxidans* at (Fig 2.14-II) at the 71.4%, 68.7%, 58.5%, 40.7% and 38.1% higher in iron solubilized concentration compared to its control respectively.

The highest iron soluble was observed in a column at 70°C (Fig 2.14) with a 4.23% $\text{kg}_{[\text{Fe}]}/\text{L}$, which is 25% and 10% higher than column at 45°C and 25°C. From the iron solubilization profiles, the trend line of the iron solubilization versus time is shown as follows;

Column at temperature 70°C. Iron free lixiviant:

$$T = 0.0492 [\text{Fe}]^{1.1527} \quad R^2 = 0.82 \quad \text{In the presence of } A. \text{ Brierleyi}$$

$$T = 0.209 [\text{Fe}] \quad R^2 = 0.96 \quad \text{Control}$$

Column at temperature 45°C. Iron free lixiviant:

$$T = 0.1958 [\text{Fe}] \quad R^2 = 0.75 \quad \text{In the presence of } T. \text{ Caldus}$$

$$T = 12.051 \ln [\text{Fe}] - 24.651 \quad R^2 = 0.91 \quad \text{Control}$$

Column at temperature 25°C. Iron free lixiviant:

$$T = 0.1268 [\text{Fe}] \quad R^2 = 0.95 \quad \text{In the presence of } T. \text{ Thiooxidans}$$

$$T = 0.2013 [\text{Fe}] \quad R^2 = 0.95 \quad \text{Control}$$

Column at temperature 70°C. Iron containing lixiviant:

$$T = 0.7359 [\text{Fe}]^{0.4736} \quad R^2 = 0.93 \quad \text{In the presence of Strain SL5B}$$

$$T = 0.0032 [\text{Fe}] \quad R^2 = 0.74 \quad \text{Control}$$

Column at temperature 45°C. Iron containing lixiviant:

$$T = 0.0175 [\text{Fe}]^{0.844} \quad R^2 = 0.83 \quad \text{In the presence of } Sb. \text{ Thermosulfodooxidans}$$

$$T = 45.99 \ln [\text{Fe}] - 348.63 \quad R^2 = 0.78 \quad \text{Control}$$

Column at temperature 25°C. Iron containing lixiviant:

$$T = 0.0027 [\text{Fe}] \quad R^2 = 0.88 \quad \text{In the presence of } L. \text{ ferooxidans and } T. \text{ Ferooxidans.}$$

$$T = 0.0039 [\text{Fe}] \quad R^2 = 0.84 \quad \text{Control}$$

From the trend line equation, it was observed that the temperature have a significant effect on the iron solubilization behaviour in the column, as an example, The iron solubilised in the 25°C column (test and control) is increased linearly to the time. ($T \propto f [\text{Fe}]$). And for the biotic column at 70°C, the iron solubilization were increased exponential with time ($T \propto f [\text{Fe}]^x$).

In the column leaching study under conditions of gradually increasing temperatures through external heating, the final iron solubilization in the biotic column was 11.8% higher compared to abiotic column. At the first stage of leaching at 25°C, the iron solubilised were increased exponential with time at the rate of $T = 1.0774 e^{1.6919[\text{Fe}]}$ for test and $T = 1.2657 e^{2.1193[\text{Fe}]}$ for control (Fig 2.15-I). However, under condition of 45°C (Fig 2.15-II), the iron solubilized were relatively similar in the biotic and abiotic column. An interesting point to note is that iron solubilised rate was drastically increased when a biotic column temperature was ramp up to 70°C. The iron solubilization rate was at 677 ppm_{Fe}/ day for the column containing SL5B compared to 244 ppm_{Fe}/ day for control column (Fig 2.15-III).

The iron content in the column (gold ore and gold concentrate) has been determined gradually at the day 40th, 60th and 120th. The iron mass balance in the column was shown in the table 2.8.

Table 2.8: Iron mass balance in the column during 4 months biooxidation

Column	COL 1	COL 2	COL 3	COL 4	COL 5	COL 6	COL 7	COL 8
	Test 70°C	Control 70°C	Test 45°C	Control 45°C	Test 30°C	Control 30°C	Test Ramp up temp	Control Ramp up temp
[Fe] _{mg/L, T=0}	167570	164741	168731	164677	168346	165027	167533	165080
[Fe] _{mg/L, T=40}	153758	162577	151233	164495	152608	165095	160073	163007
[Fe] _{mg/L, T=60}	-	-	-	-	-	-	146820	161371
[Fe] _{mg/L T=120}	130888	159814	135479	159788	136619	161608	121809	157503
% Loss,[Fe] _{T=40}	8.243	1.314	10.370	0.110	9.348	0.000	4.453	1.256
% Loss,[Fe] _{T=60}	-	-	-	-	-	-	12.364	2.247
% Loss,[Fe] _{T=120}	21.891	2.990	19.707	2.968	18.846	2.072	27.293	4.590
* [Fe] _{mg/L, T=40} for column 1,2,3,4,5 and6: Iron concentration during biooxidation test using iron free medium [Fe] _{mg/L T=120} for column 1,2,3,4,5 and 6: Iron concentration during biooxidation test using iron containing medium [Fe] _{mg/L, T=40} for column 7 and 8: Iron concentration during biooxidation test at 30°C [Fe] _{mg/L, T=60} for column 7 and 8: Iron concentration during biooxidation test at 45°C [Fe] _{mg/L, T=120} for column 7 and 8: Iron concentration during biooxidation test at 70°C								

From the results obtained, it was observed that the highest percentages of iron solubilized was observed in the column 7 (column with 3 stages temperature condition) at 27.3% of iron was solubilized after 120 days biooxidation. The value is 24.7%, 38.5% and 44.8% higher compared to the iron solubilization in the column at fix temperature of 70°C, 45°C and 25°C respectively. This result indicates that, the mixed of mesophilic and thermophilic (moderate and extreme) culture is capable of the effective biooxidation of gold ore and concentrate.

From the results also, it was interesting to note that the percentage of iron solubilization is very low for the each control column, especially for the experiments with iron free lixiviant i.e: 0.11% for column at 45°C, 1.3% for column at 70°C and no iron lost detected in column at 25°C . However for the control column with iron based lixiviant, the percentages of iron solubilized were slightly increased to the 2.07%, 2.97% and 2.99% for the abiotic column at 70°C, 45°C and 25°C respectively.

However, with the addition of biooxidation related culture, the iron solubilization of pyrite in the gold ore and gold concentrate were increased radically, ranging from 2.5 to 90 times fold compared to control, as an example, the iron lost in the column packed was 93.2 times higher with the presence of *T. Caldus*, 8.0 times higher for *T. Ferrooxidans* and *L. ferrooxidans*, 6.32 times for SL5B, 5.6 times for *Sb. Thermosulfodooxidans* and 5.27 times higher for *A. Brierleyi*. For the column with a ramp up temperature condition, the presence of mixture mesophilic culture (*L. Ferrooxidans*, *T. Ferrooxidans* and *L. ferrooxidans*) was capable to increase the iron solubilization 2.5 times higher than its control, 4.5 times higher for the moderate thermophilic culture (*T. Caldus* and *Sb. Thermosulfodooxidans*) and 4.9 higher for the extreme thermophilic culture (*A. Brierleyi* and isolate SL5B).

2.7.3.3 Gold extraction using cyanide in the column

Cyanidation process has been conducted on the biooxidized ore and concentrate in the column. The columns were rinsed with tap water and the pH was increased to pH 10 before the cyanide solution (200ppm NaCN) sprayed in the column to extract the gold from the ore.

Figure 2.16-a, b, c and d shows the gold concentration in a pregnant solution during the cyanidation process. . From the results obtained, it was observed that the iron solubilization behaviour, pH and EH during biooxidation pre-treatment process have a significant effect on the rate of gold recovery in column.

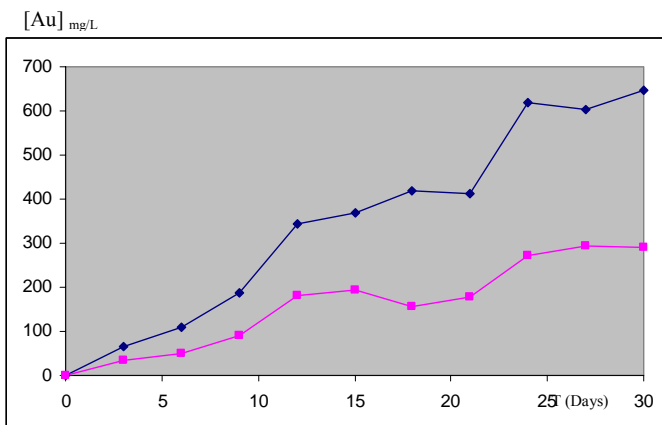


Figure 2.16-a: Gold extraction using cyanidation after 4months column bioleaching at 70⁰C.

◆ test column
■ control column

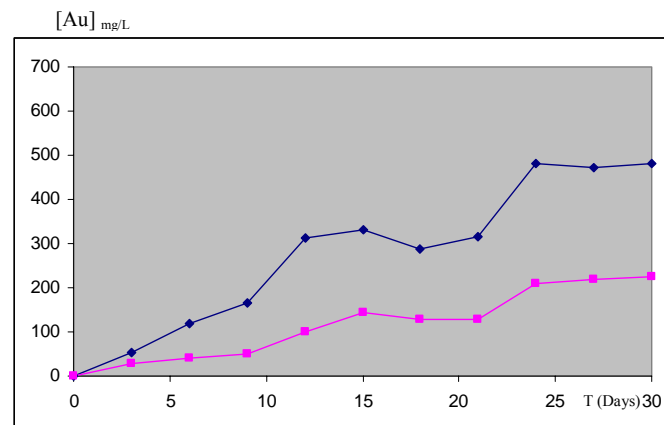


Figure 2.16-b: Gold extraction using cyanidation after 4months column bioleaching at 45⁰C.

◆ test column
■ control column

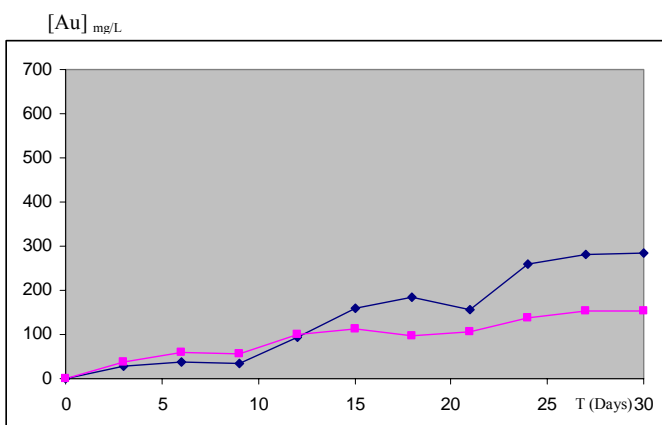


Figure 2.16-c: Gold extraction using cyanidation after 4months column bioleaching at 30⁰C.

◆ test column
■ control column

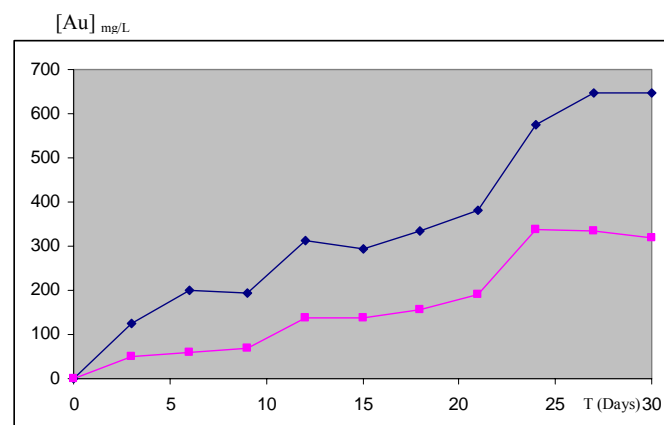
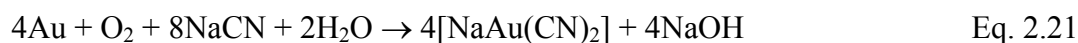


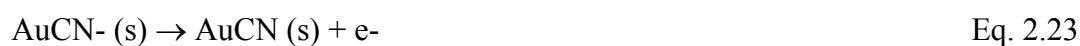
Figure 2.16-d: Gold extraction using cyanidation after 4months column sequential bioleaching at 30⁰C , 45⁰C and 70⁰C.

◆ test column
■ control column

Cyanidation has been the main process used for the production of gold since 1890, during its 110-year history, cyanidation of gold ore has evolved into a safe, efficient and predictable technology (Gasparrini, 1993). In cyanidation, the gold in ore is dissolved by treating it with a very dilute cyanide solution in the presence of lime and oxygen from the air (Kettle, 1982). The stoichiometry by which this reaction occurs is known as the Elsner (1846) equation:



In this process, the pH of the slurry is adjusted around 10 to 11.5 with hydrated lime, and cyanide is added to solubilize the gold. Oxygen is dispersed through the column by air pump. In cyanidation reaction, an electrochemical process takes place, in which the anodic reaction is gold oxidation while the cathodic reaction is oxygen reduction (Jeffrey and Breuer, 2000; Wadsworth, 2000; Fleming, 1992; Kondos, et al. 1995b). The overall stoichiometry for the dissolution of gold is shown in Eq. 2.21, while the important steps during anodic reactions are as follows:



where in the above equations refers to surface adsorbed species and AuCN is the neutral species adsorbed on the surface. The cathodic reaction is shown as follows:



In cyanidation, air provides the oxygen that is necessary to oxidize gold from the metallic state, in which it occurs in nature, to the gold (I) state. (Fleming, 1992).

From the results obtained, it was observed that higher percentages of gold recovery were achieved at biooxidized column compared to the control experiments. As an example, the rate of gold extraction for ramp-up temperature biooxidation column was at 219.9mgAu/days compared to the 110.4 mg_{Au}/days for the abiotic column (fig 2.16-d). The value shows the gold extraction rate was increased about 99.16% for multi stages biooxidation column. The similar observation is also obtained in another set of column i.e; 129.7% rate of gold extraction was increased using mesophilic culture (fig 2.16-c), 118.8% for extremely thermophile (fig 2.16-a) and 65.7% using moderate

thermophile (fig 2.16-c). This result indicates that the selection of suitable operating condition is very important to improve the biooxidation efficiencies, which subsequently contribute to increase the gold recovery.

It is like to note that the final concentration of gold in a cyanide solution was comparable between the column treated with thermophilic culture and column with ramp-up temperature at the 646.7 mg_{Au}/L and 647.0 mg_{Au}/L. However, the final concentration of gold in a cyanide solution using those culture were found higher compared to experiment using moderate thermophile and mesophile i.e. 34.5% and 126.2%, respectively.

This result was expected as higher amount of Fe solubilised observed earlier in the biooxidation experiments. From this results also, it revealed that there appeared to be definite relationship between the amounts of gold recovered with percentage of iron solubilization. Higher recovery of gold in both tests probably due to maximum iron solubilization observed earlier in biooxidation experiments using isolate SL5B and *A. Brierleyi* for column A and mixture of mesophilic and thermophilic culture for column G. Solubilization of pyrite in the ore and concentrate leads to the increased of porosity in the particle in the column and exposed the transports considers the cyanidation reaction in a bed of uniformly sized spherical porous mineral particles, through which the leaching solution trickles. The leaching agents diffuse into the porous particles to react with the grains of metallic gold. The effective wetting of the particles is correlated with an apparent effective diffusivity for the different type of mineral within the partially wetted particles. Sanchez-Chacon and Lapidus (1997) reported that the controlling phenomenon in the gold extraction rate in a column is the diffusion of the gold cyanide complex out of the mineral particles. For this reason, parameters such as mineral porosity, particle radius, leaching solution flow rate, gold grain size, the concentration of reagents and the heap height will effect the gold extraction rate.

The effect of mineral porosity acquires special importance in the gold extraction rate. Decreasing this parameter increases the resistance to internal mass transport. The

reduction in the diffusion rate of reactants and products within the particle increases leaching time considerably. Bartlett [1992] reports a porosity range effects of 0.02 and 0.08 for typical minerals processed by heap leaching in figure 2.17.

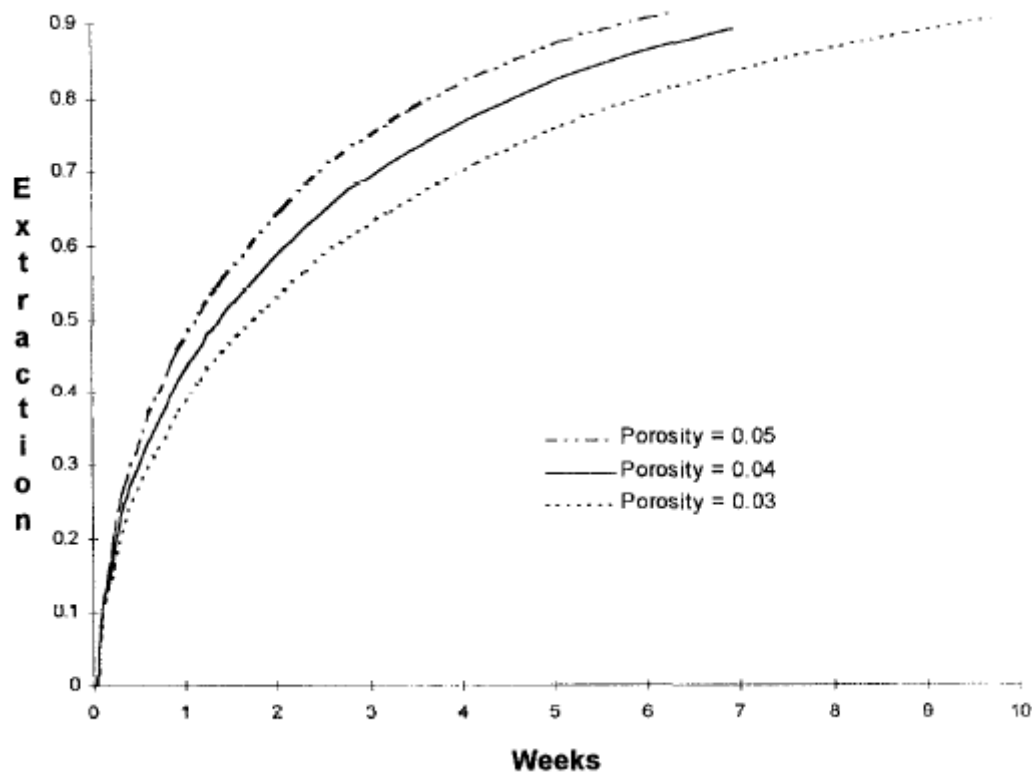


Fig 2.17: Effect of the mineral porosity on the gold extraction curve in a column. Bartlett [1992]

As a consequence of this last finding, it is not surprising to find that heap leaching is normally enhanced by bacterial oxidation. These treatments have the virtue of opening up the pores, by dissolving acid leachable material, thereby increasing the porosity of the mineral as shown in figure 2.18. It is like to note, that the particle surface in the column is become more porous after biooxidation process, especially the ore oxidized with thermophile and the ore from a column with ramp-up temperature condition.

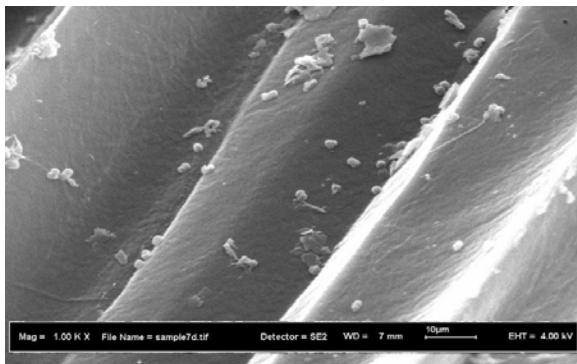


Fig 2.18a: SEM image of gold ore before biooxidation. (1000X magnification)

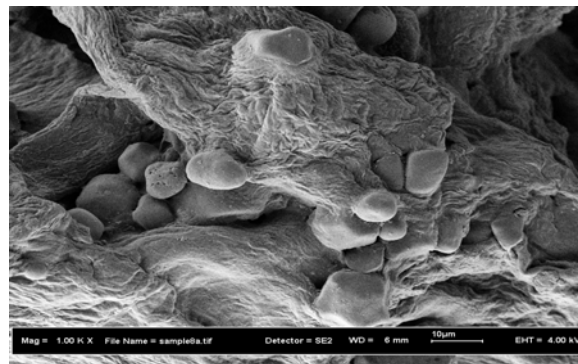


Fig 2.18b: SEM image of gold concentrate before biooxidation. (1000X magnification)

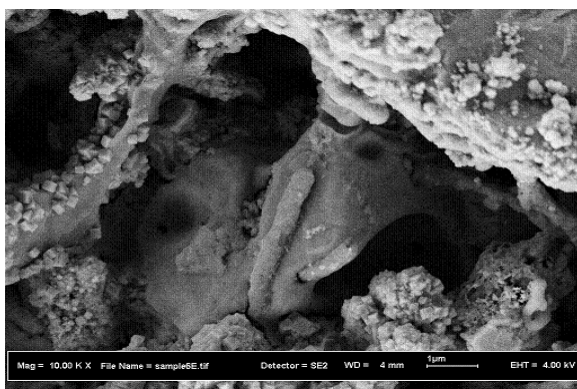


Fig 2.18c: SEM image of gold ore after biooxidized using mesophilic culture. (10000 X magnification)

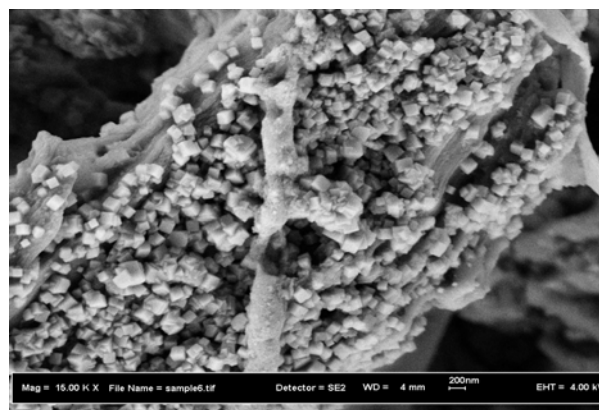


Fig 2.18d: SEM image of gold ore after biooxidized using moderate thermophilic culture. (15000 X magnification)

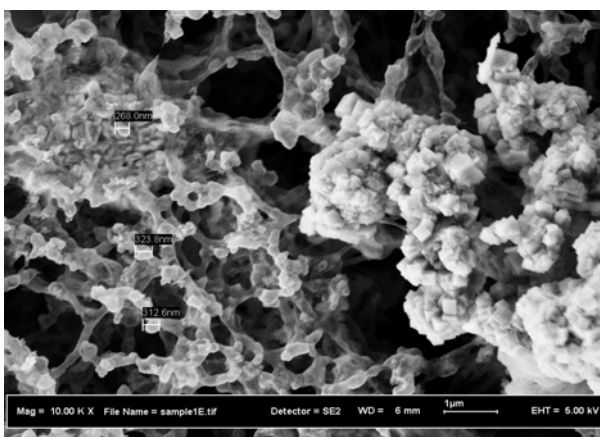


Fig 2.18e: SEM image of gold ore after biooxidized using thermophilic culture. (10000 X magnification)

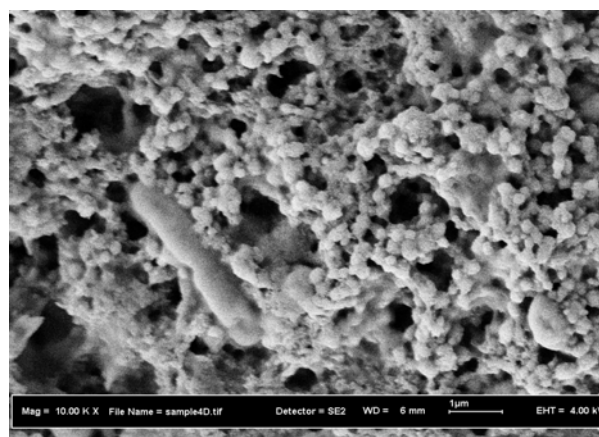


Fig 2.18f: SEM image of gold ore after biooxidized using mixture of mesophilic and thermophilic culture. (10000 X magnification)

The gold content analysis on the column residual after cyanidation process shows the amount of gold loss in the mineral is significant with the gold extraction in the cyanide solution. The gold mass balance in the column after 30 days of cyanidation is shown in table 2.9.

Table 2.9: The gold mass balance in the column after 30 days of cyanidation.

Column test								
	COL 1 70 ⁰ C		COL 3 45 ⁰ C		COL 5 30 ⁰ C		COL 7 Sequential leaching	
	Initial	Final	Initial	Final	Initial	Final	Initial	Final
[Au] _{mg/L, solid}	129.635	43.408	129.523	65.416	129.614	91.494	129.569	43.475
[Au] _{mg/L, liquid}	0.0	646.7	0.0	480.8	0.0	285.9	0.0	645.7
% gold extraction	66.515		49.495		29.410		66.446	
Column control								
	COL 2 70 ⁰ C		COL 4 45 ⁰ C		COL 6 30 ⁰ C		COL 8 Sequential leaching	
	Initial	Final	Initial	Final	Initial	Final	Initial	Final
[Au] _{mg/L, solid}	129.643	90.837	129.638	99.651	129.640	109.166	129.635	87.189
[Au] _{mg/L, liquid}	0.0	291.1	0.0	224.9	0.0	153.6	0.0	318.4
% gold extraction	29.933		23.131		15.792		32.743	

From the results obtained, it was observed that the highest percentages of gold extracted was observed in the column 1 (column with thermophile biooxidation) and column 7 (column with 3 stages temperature condition) at 66.5% and 66.4% of gold was extracted after 30 days cyanidation. The value is 1.22 and 1.03 times fold compared to its control experiments. This result indicates that, the amount of iron solubilization will effect the amount of gold cyanidation ore and concentrate. As an example, the increased in iron solubilization at 18.9% (Table 2.8; column 1 and 2) using extreme thermophilic culture resulting an increased in gold solubilization at 36.58% (Table 2.9; column 1 and 2).

2.3.7.4 Correlation between solution potential (E_H), Temperature (T) , Acidity (pH) and iron solubilized [Fe] in the column solution

Modeling of heap bioleaching is complex as it has to incorporate a large number of phenomena, such as solution, gas and heat transport, multi-mineral kinetics, bacterial kinetics and diffusion effects. Previous studies have shown that there is clear evidence that heap bioleaching can be rate-limited by the microbial oxidation step in solutions with a composition of heap. Modeling of these effects remains strictly empirical, however, as none of the existing rate equations have been confirmed to be valid under such extreme conditions. [Ojuma et al, 2006].

Rate equations have been applied to tank bioleach systems, which usually operate under controlled conditions near the optimum. Heap bioleach systems, on the other hand, often operate far from optimum conditions with respect to temperature, pH, solution potential, flow condition and oxygen supply, at the same time. The kinetics of such sub-optimal systems is still poorly understood. This study will be directed towards the development of a comprehensive rate equation useful for describing the kinetics of heap bioleaching over a wide range of conditions.

The reaction between ore and ferric iron in acid solution was investigated by monitoring the redox potential of a leachate solution during leaching test. The redox potential measures the tendency for a solution to either gain or lose electrons when it is subject to change by introduction of a new species. A solution with a higher redox potential will have a tendency to gain electrons from new species (i.e. oxidize them) and a solution with a lower redox potential will have a tendency to lose electrons to new species (i.e. reduce them).

If it assumed that the ferric/ferrous exchange current density at the surface of a leaching particle is large enough to make the effect of the corrosion current, the surface potential of the particle can be considered equal to the redox potential of the solution at the surface [Eaton et al 2005]. A measurement of the solution redox potential can be

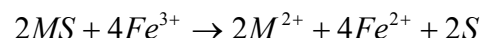
related to the ratio of free ferric to free ferrous iron in an iron solution via the Nernst equation (Eq. 2.22).

$$E_H = E^0 + \frac{RT}{zF} \ln \frac{[Fe^{3+}]}{[Fe^{2+}]}$$

Eq. 2.27

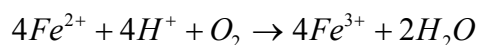
Although measurement of the redox potential in aqueous samples is relatively straightforward, many factors limit its interpretation; such as irreversible reactions, slow electrode kinetics, non-equilibrium, presence of multiple redox couples, electrode poisoning, small exchange currents and inert redox couples [ABB instrument, 1999]. In this study platinum electrodes filled with 3M KCl combined with an Ag/AgCl electrode solutions were used as a reference.

Although the stoichiometry of the overall reaction will vary according to the particular metal sulphide being bioleached, a typical reaction for a metal sulphide (MS) as follows:



Eq. 2.28

The ferrous-iron is then re-oxidized to the ferric form by microbial action:



Eq.2.29

It is the kinetics of this reaction and the subsequent biomass synthesis and maintenance including initial rate studies investigations in batch and continuous culture and investigations using iso-potential devices. The data has been fitted with modified Monod or Michaelis equations or to models derived from chemiosmotic theory or electrochemical analogies. There is little information on the effects of dissolved oxygen,

carbon dioxide, metal cations and anions. The effects of temperature and pH have largely been limited to conditions near the optimum or to those used in tank bioleaching operations. The rate equations for microbial oxidation, ferrous-ferric ion (E_H) behaviour will be review in table 2.10 (Boon, 1999). Some of the models have been developed from the simple equation for specific growth rate based on substrate utilization via a Michaelis–Menten mechanism, which corresponds to a basic Monod type model

Table 2.10: The rate equations for microbial oxidation and ferrous-ferric ion behaviour

Model	
$\mu = \frac{r_x}{c_x} = \frac{\mu_{\max}[Fe^{2+}]}{Y_{SX}K_m + [Fe^{2+}]} *$	A specific growth rate based on substrate utilization via a Michaelis–Menten mechanism and corresponds to a basic Monod type model.
$\mu = \frac{\mu_{\max}[Fe^{2+}]}{K_m + [Fe^{2+}]}$	
$\mu = \frac{\mu_{\max}[Fe^{2+}]}{[Fe^{2+}] + K_m \left(1 + \frac{[Fe^{3+}]}{K_i}\right)} *$	The effects of ferric inhibition on microbial growth take into consideration
$\mu = \frac{\mu_{\max}([Fe^{3+}] - [Fe^{2+}]_t)}{K_m + ([Fe^{2+}] - [Fe^{2+}]_t)} *$	Inclusion of threshold values, that no growth will occur at low ferrous concentrations
$\mu = \frac{\mu_{\max}[Fe^{2+}]}{[Fe^{2+}] + K_s(1 + K_i[Fe^{3+}])}$	
$\mu = \frac{\mu_{\max}[Fe^{2+}]}{[Fe^{2+}] + K_s + [Fe^{3+}] \frac{K_s}{K_i} + \frac{([Fe^{2+}])^2}{K_{s,i}}}$	
$-r_{O_2} = \frac{k_3[X][Fe^{2+}]}{[Fe^{2+}] + K_m \left(1 + \frac{[X]}{[K_i]} + \frac{[Fe^{3+}]}{K_{i_f}} + \frac{[X][Fe^{3+}]}{\alpha K_{i_f} K_{i_f}}\right)}$	A model based on the fundamental chemiosmotic theory of the electron and

$-r_{Fe^{2+}} = a_1 \left(\frac{\rho_{O_2}}{k_B + \rho_{O_2}} \right) \left(\frac{[Fe^{2+}]}{[Fe^{2+}] + K_{Fe^{2+}} \left(1 + \frac{[Fe^{3+}]}{K'} \right)} \right)$	<p>proton transport mechanism of culture. In recognizing that this mechanism serves as the energy generator for the entire cell's metabolic activity, the ferrous oxidation process is modeled analogous to an electrochemical fuel cell.</p>
$-r_{Fe^{2+}} = k \left(\frac{[Fe^{2+}]}{[H^+]} \right)^{0.5} \left(\frac{\rho_{O_2}}{K_B + \rho_{O_2}} \right)^{0.5} *$	
$q_{Fe^{2+}} = \frac{q_{Fe^{2+}}^{\max}}{1 + K_{Fe^{2+}} \frac{[Fe^{3+}]}{[Fe^{2+}]}} *$	<p>A simplified version of ferric inhibited growth model, expressed in terms of specific ferrous utilization rate.</p>
$\frac{d[Fe^{2+}]}{dt} = \frac{K_o e^{-\frac{E_a}{RT}} [X] [Fe^{2+}]}{\left(1 + \frac{[Fe^{3+}]}{K_i} \right) (K_m + [Fe^{2+}])}$	
$q_{O_2} = \frac{q_{O_2}^{\max}}{1 + \frac{K_s}{[Fe^{2+}] - [Fe^{2+}]_l} + \frac{K_s}{K_i} \left(\frac{[Fe^{3+}]}{[Fe^{2+}] - [Fe^{2+}]_l} \right)}$	<p>Combination of the ferric inhibition model and threshold approach, expressed in terms of ferrous utilization rate.</p>
$q_{Fe^{2+}} = \frac{K_1^* \exp \left[\frac{nF}{2RT} (E^m - E_H^0) \right] \left\{ 1 - \exp \left[\frac{nF}{RT} (E^m - E) \right] \right\}}{1 + \frac{K_2^*}{[Fe^{2+}]} + K_3^* \exp \left[\frac{nF}{RT} (E_H - E_H^0) \right]}$	<p>A model derived from a combining electrochemical theory with Michaelis-Menten dynamics for the ferrous-ferric oxidation reaction.</p>

Changes in pH have not been found to have a significant effect on either the growth or the iron oxidation kinetics of iron oxidizing microbes a narrow range around their optimum pH. Breed and Hansford (1999) have modelled the effect of pH by letting constant K increase linearly with increasing pH within the range studied (1.1–1.7) with no significant effect on the maximum specific ferrous iron and oxygen utilization rates in this range. The relation between Michaelis Menten based models and pH were shown as followed:

The Michaelis Menten based models equations are formulated in terms of ferrous utilisation. This approach acknowledges the correlation between ferrous oxidation rate, microbial growth and maintenance via the Pirt equation (Boon, 1999)

$$q_{Fe^{2+}}^{\max} = \frac{\mu^{\max}}{Y_{Fe^{2+}}^{\max}} + m_{Fe^{2+}}$$

Eq. 2.30

From that model, Breed and Hansford (1999) was suggested a simple model to predict a variation in the specific ferrous-iron utilization rate (Eq. 2.31) and bacterial specific oxygen utilization rate (Eq. 2.32) with changes in the ferric/ferrous-iron ratio (Eh) and different pH values.

$$q_{Fe^{2+}}(predicted) = \frac{15.53}{(0.0048pH - 0.0043) \frac{[Fe^{3+}]}{[Fe^{2+}]}}$$

Eq. 2.31

And

$$q_{O_2}(predicted) = \frac{3.85}{(0.0043pH - 0.0037) \frac{[Fe^{3+}]}{[Fe^{2+}]}}$$

Eq. 2.32

Where the $K_{Fe^{2+}}, K_{O_2} = f(pH)$

Although the resistance of iron oxidizing microbes to low pH as been attributed to the composition of the cell wall, at very low pH the cell might require more energy to maintain the proton gradient, since the cell cytoplasm must be maintained at or near neutral values. Thus cell maintenance will be at the expense of cell growth. Inhibition at high pH, on the other hand, could be explained by the fact that protons are required as a substrate in reaction, and also by the fact that the proton gradient is the driving force for the synthesis of ATP.

Microorganisms are classified in terms of the temperature range in which they survive, with optimum temperatures in the 30–40 °C range for mesophiles, around 50 °C

for moderately thermophiles and above 65 °C for extreme thermophiles. At temperatures below the optimum the microbes become inactive, and they become rapidly destroyed at temperatures above it. The models proposed by Hinshelwood and Ratkowsky are most commonly used to show the dependency of bacterial growth on temperature. (Ojumu et al, 2006).

Hinshelwood model:

$$\mu_{\max} = K_1 e^{\frac{E_0}{RT}} - K_2 e^{\frac{E_0}{RT}}$$

Eq. 2.33

Ratkowsky model

$$\mu_{\max} = b(T - T_{\min}) \{1 - e^{c(T - T_{\max})}\}$$

Eq. 2.34

where K_1 , K_2 , b and c are constants; T_{\min} and T_{\max} are the minimum and maximum growth temperatures. In both cases a dependence of the maximum specific growth rate on temperatures is proposed. Optimum and maximum growth temperatures are usually close, as was shown by Nemati and Webb, and Breed and Hansford, (1999) also showed the dependence of maximum specific substrate utilization rate on temperature, and included an Arrhenius term in their respective kinetic models. The optimum temperature has also been reported to be pH dependent, decreasing with decreasing pH.

ATTACHMENT A

Data for Ore and concentrate characterization (Chapter 2.3)

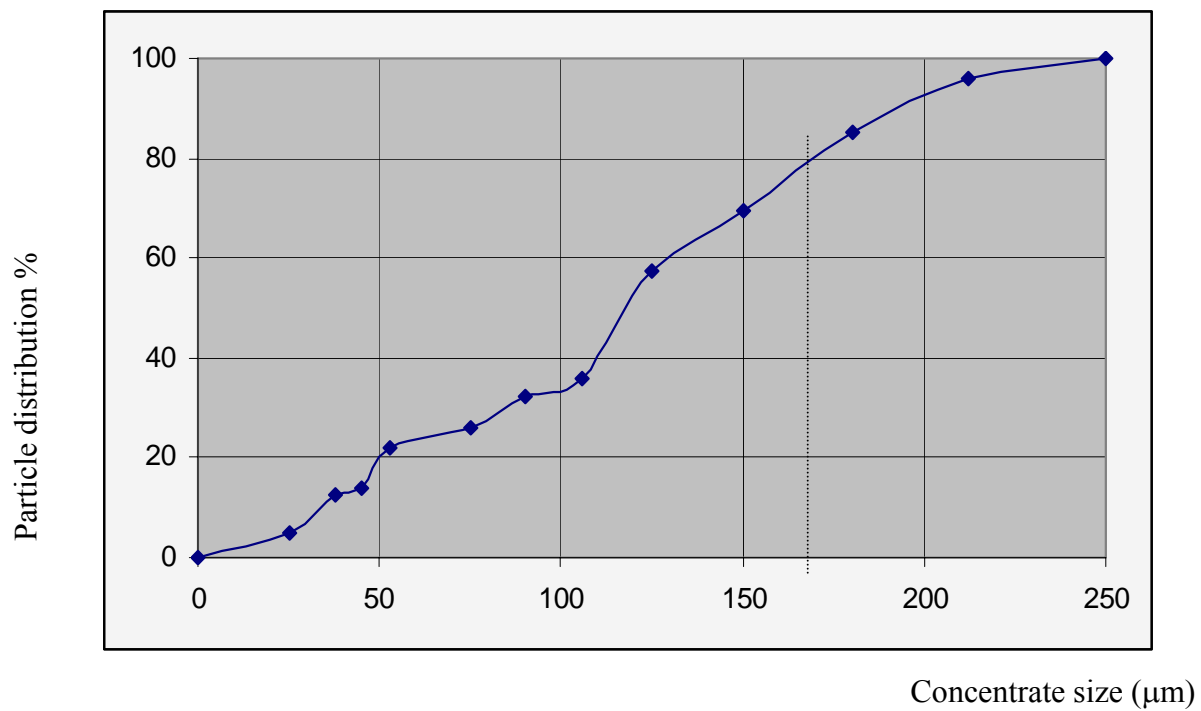


Figure A-1: Size distribution for gold concentrate

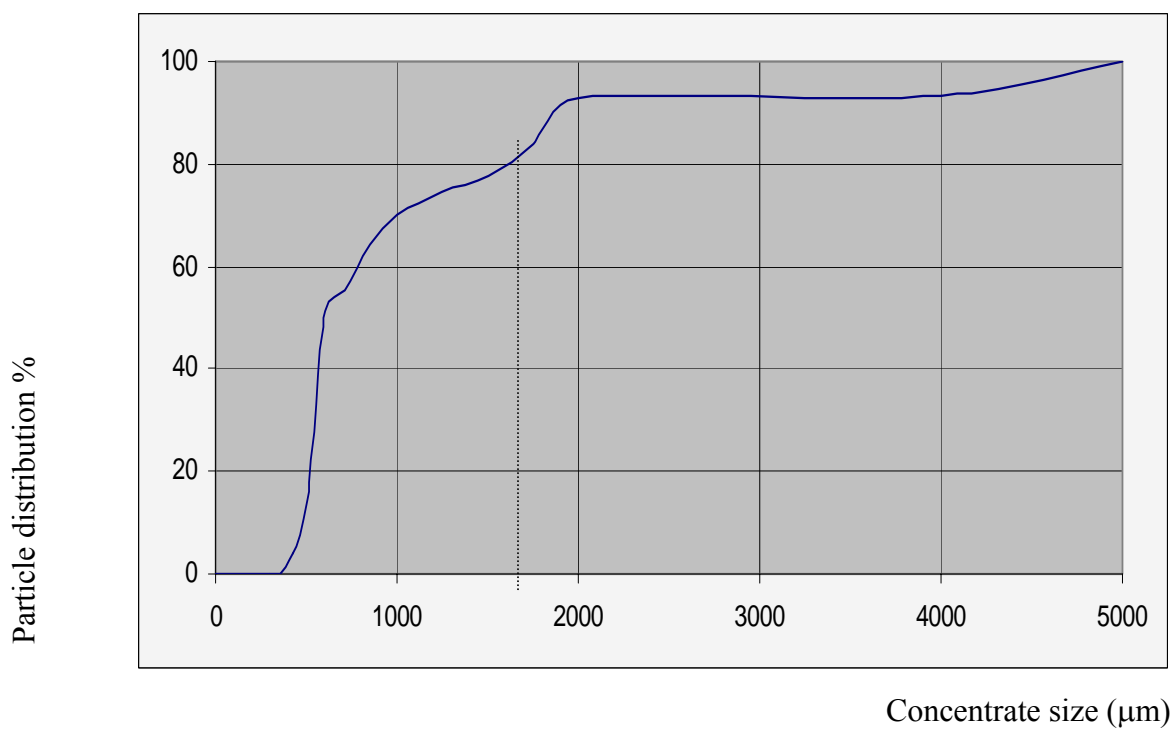


Figure A-2: Size distribution for gold ore

Table A-1: Acid consumption test for gold concentrate

Time (min)	H ₂ SO ₄ ,5M(ml)	pH
15 min	3.24	4.42
45 min	0.06	3.56
1 hrs 15 min	0.08	3.53
1 hrs 45 min	0.12	3.58
2 hrs 15 min	0.22	3.58
2 hrs 45 min	0.21	3.62
3 hrs 15 min	0.10	3.71
3 hrs 45 min	0.04	3.53
4 hrs 15 min	0.02	3.52
4 hrs 45 min	0.03	3.52
Total	4.12 ml	
Acid consumption for gold concentrate		0.412 ml _{(5M,H₂SO₄)/g_{ore}}

Table A-2: Acid consumption test for gold ore

Time (min)	H ₂ SO ₄ ,5M(ml)	pH
15 min	0.33	3.52
45 min	0.12	3.51
1 hrs 15 min	0.14	3.54
1 hrs 45 min	0.1	3.52
2 hrs 15 min	0.13	3.53
2 hrs 45 min	-	3.50
3 hrs 15 min	0.05	3.51
3 hrs 45 min	0.08	3.53
4 hrs 15 min	0.08	3.51
4 hrs 45 min	0.32	3.62
5 hrs 15 min	0.03	3.51
5 hrs 45 min	0.04	3.52
Total	1.42	
Acid consumption for gold concentrate		0.142 ml _{(5M,H₂SO₄)/g_{ore}}

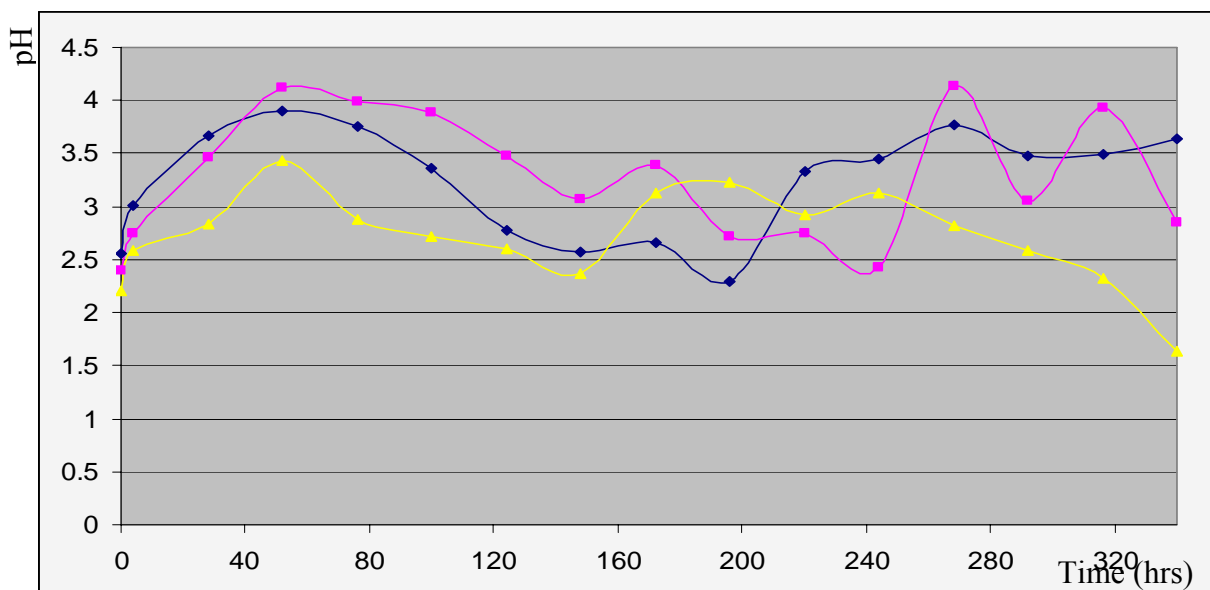


Figure A-3 : pH profile for Biological acid producing potential test on gold concentrate using ■ *T. ferrooxidans*, ■ *Sb. Thermosulfodooxidans* and ■ *A. Brierleyi*

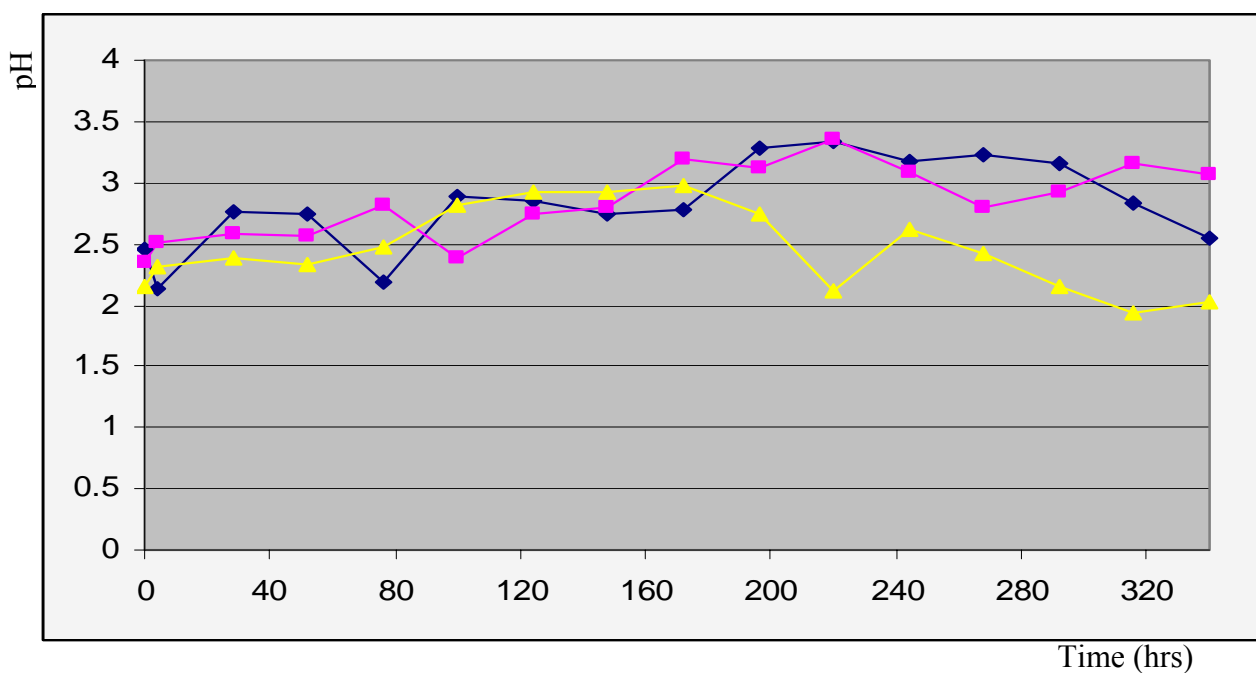


Figure A-4 : pH profile for Biological acid producing potential test on gold ore using ■ *T. ferrooxidans*, ■ *Sb. Thermosulfodooxidans* and ■ *A. Brierleyi*

ATTACHMENT B

pH and EH profile for column (Chapter 2.3.7.1)

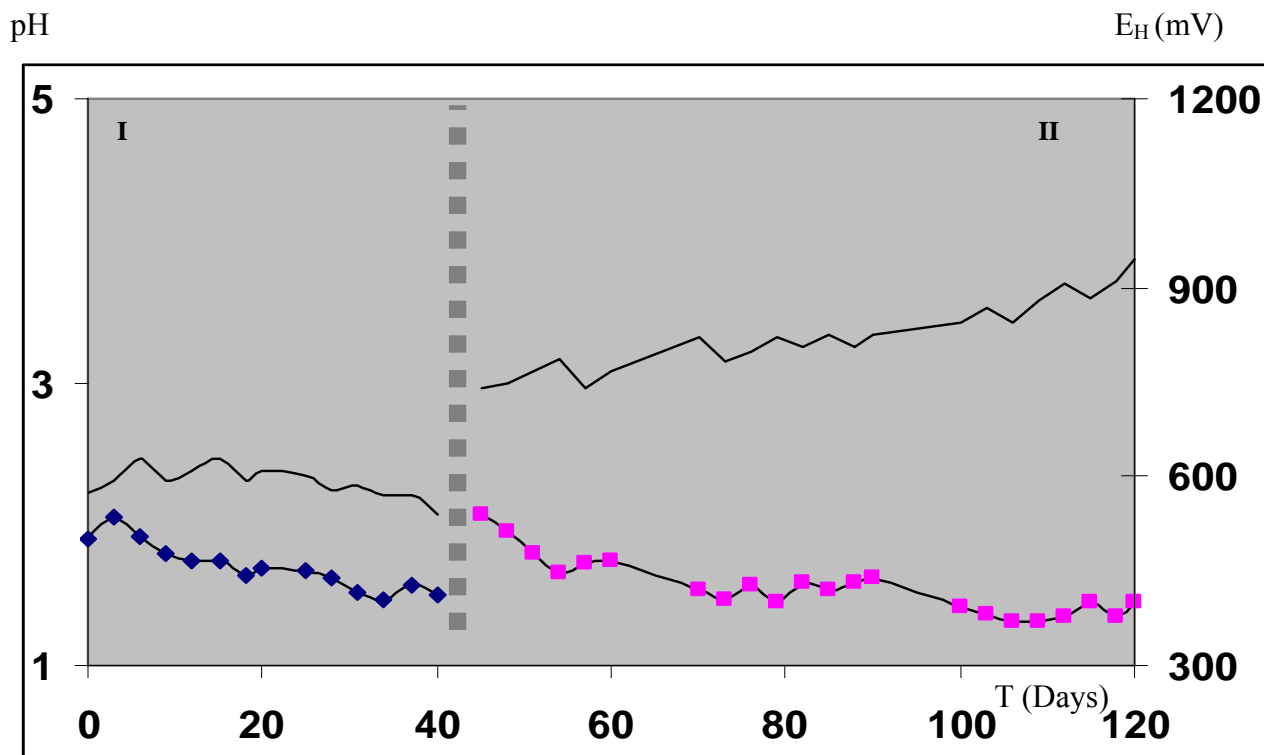


Figure B-1 : E_H (----) and pH (---■) profile of lixiviant solution in the column (test) at 70°C.

I: Fe free lixiviant (*A. Brierleyi* Medium)

II: Fe containing lixiviant (*Sb. Thermosulfodooxidans* medium)

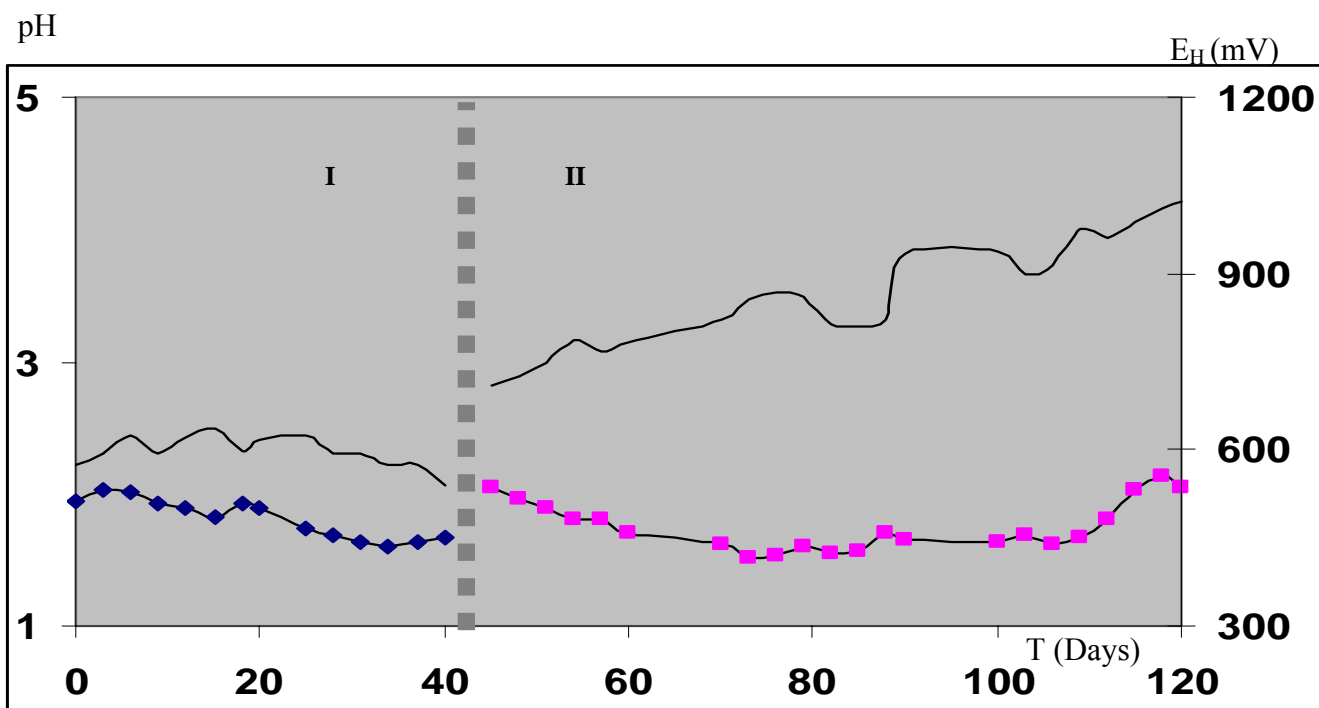


Figure B-2 : E_H (----) and pH (--■-) profile of lixiviant solution in the column (control) at 70°C.

I: Fe free lixiviant (*A. Brierleyi* Medium)

II: Fe containing lixiviant (*Sb. Thermosulfodooxidans* medium)

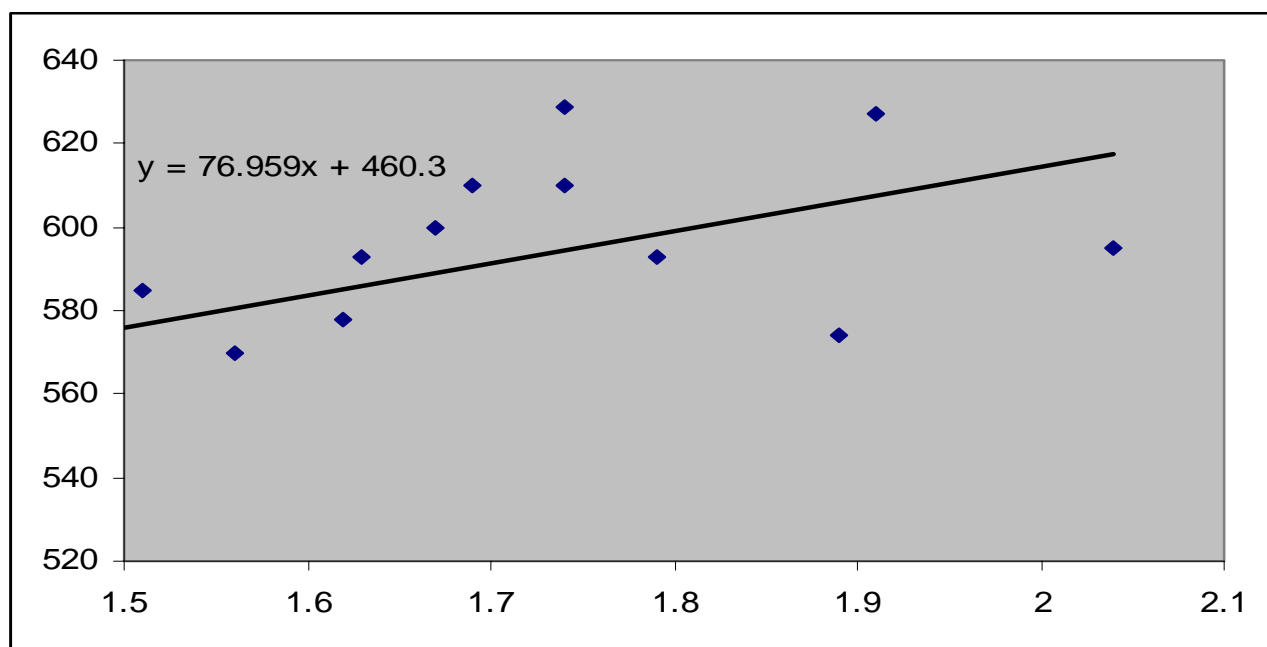


Figure B-3 : E_H vs pH for the column at 70°C. using *A. Brierleyi*

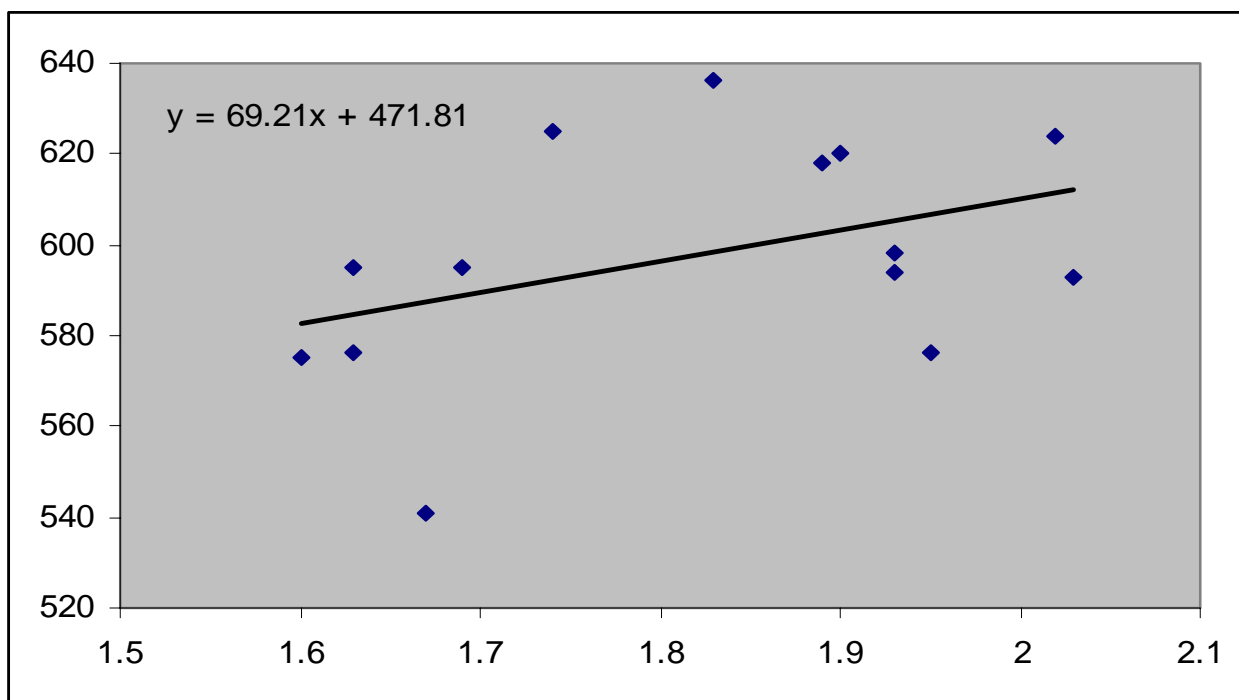


Figure B-4 : E_H vs pH for the control column at 70°C. using *A. Brierleyi* medium

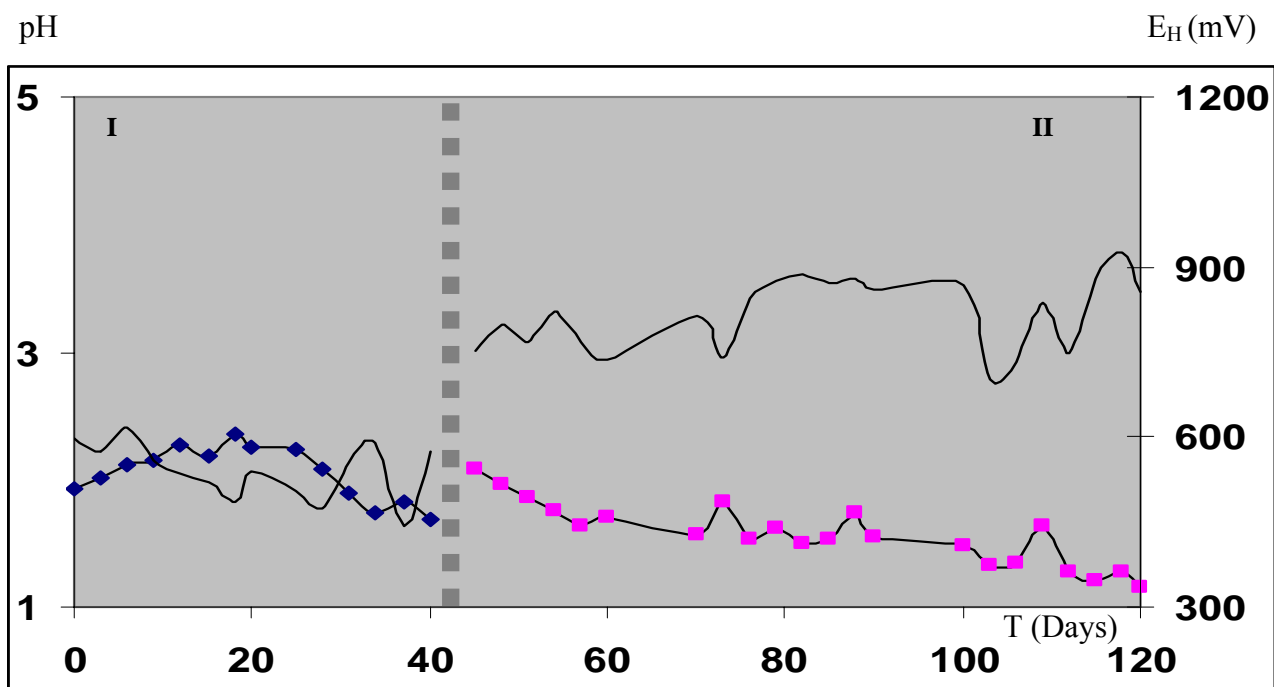


Figure B-5 : E_H (----) and pH (--■-) profile of lixiviant solution in the column (test) at 45°C.

I: Fe free lixiviant (*T. Caldus* Medium)

II: Fe containing lixiviant (*Sb. Thermosulfodooxidans* medium)

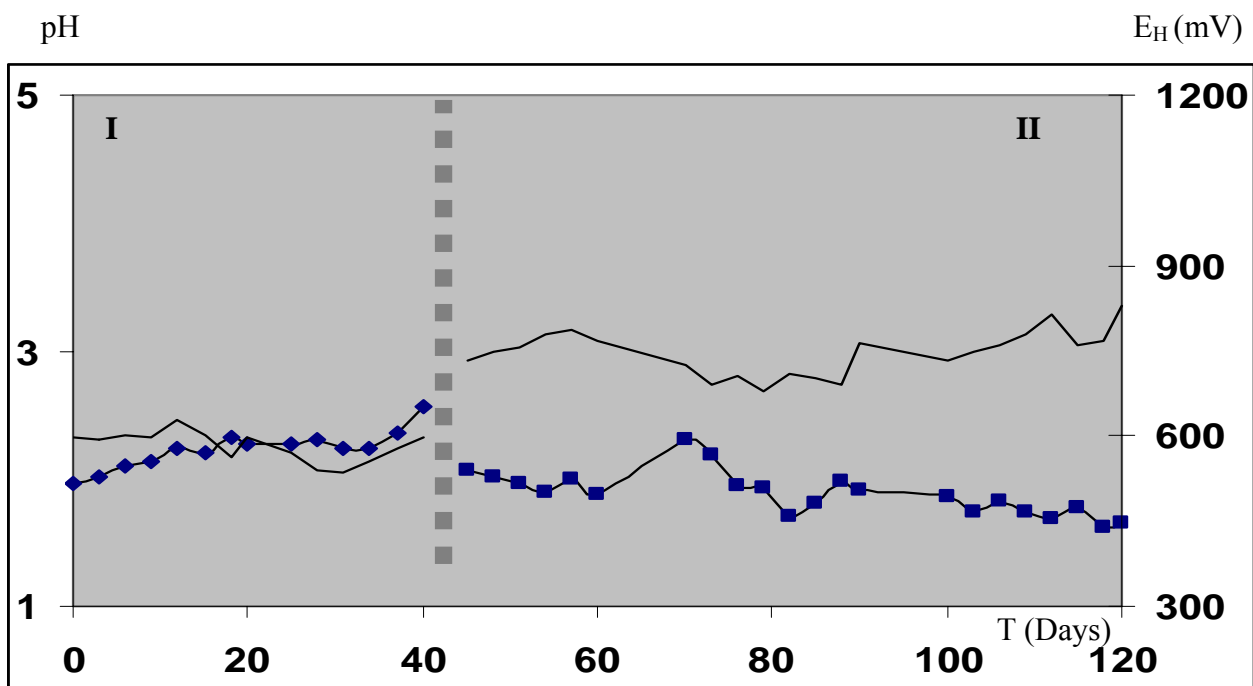


Figure B-6 : E_H (----) and pH (--■-) profile of lixiviant solution in the column (control) at 45°C.

I: Fe free lixiviant (*T. Caldus* Medium)

II: Fe containing lixiviant (*Sb. Thermosulfodooxidans* medium)

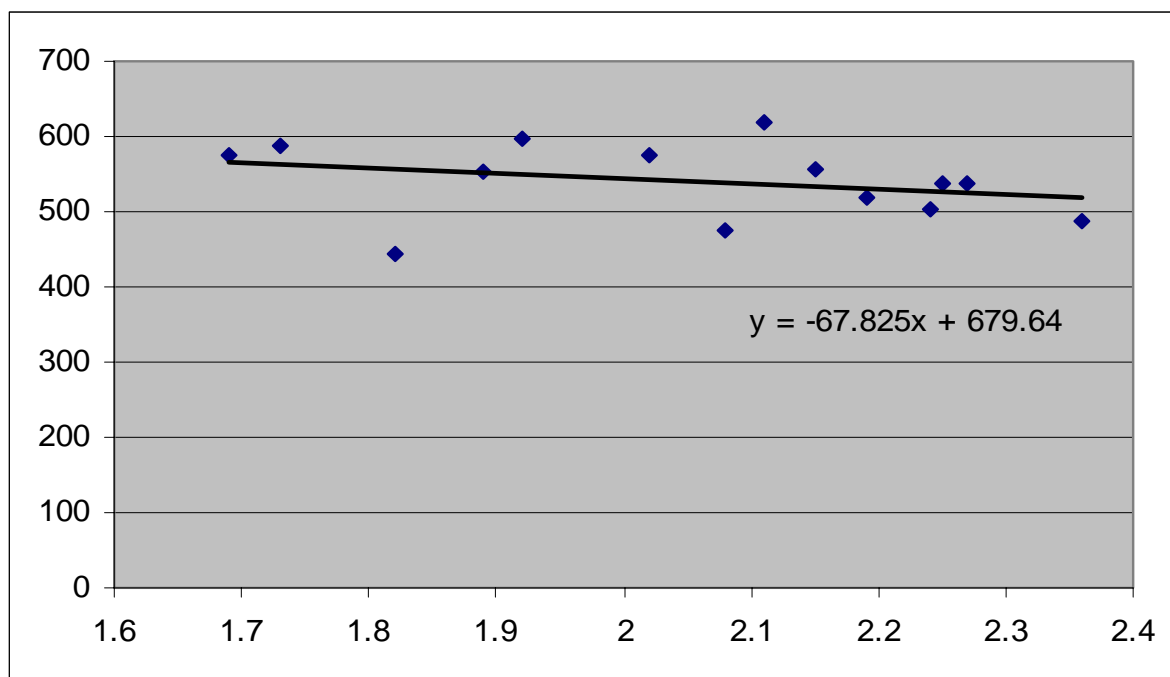


Figure B-7: E_H vs pH for the column at 45°C. using *T. Caldus*

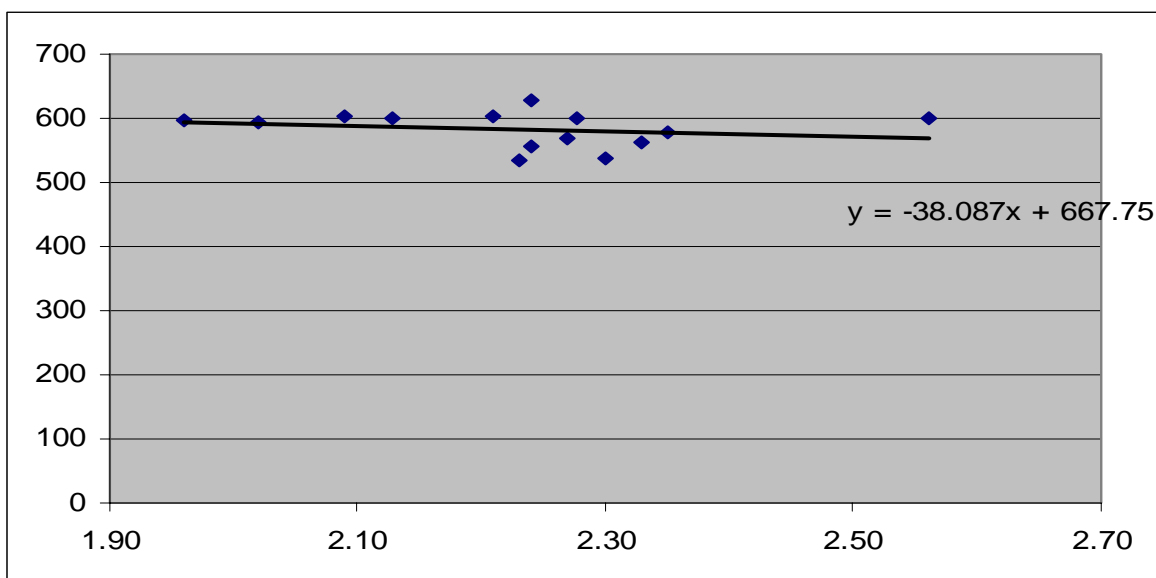


Figure B-8: E_H vs pH for the control column at 45°C. using *T. Caldus* medium

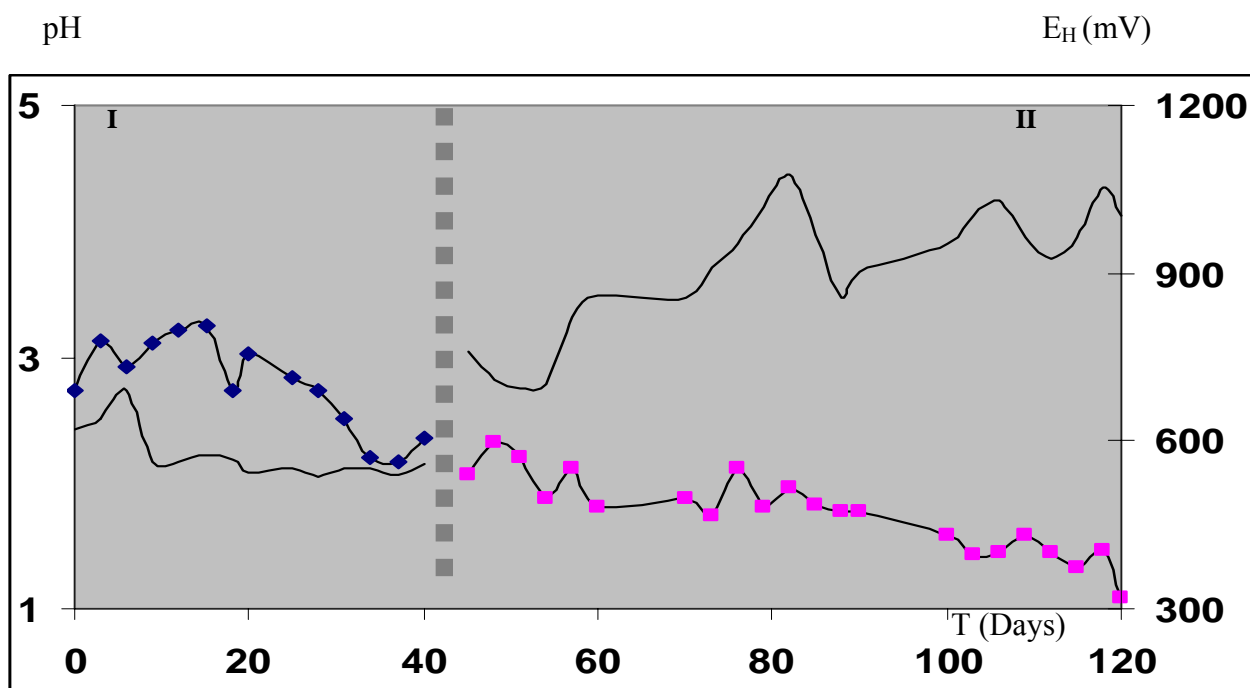


Figure B-9: E_H (----) and pH (--■-) profile of lixiviant solution in the column (test) at 30°C.

I: Fe free lixiviant (*T. Thiooxidans* Medium)

II: Fe containing lixiviant (9K medium)

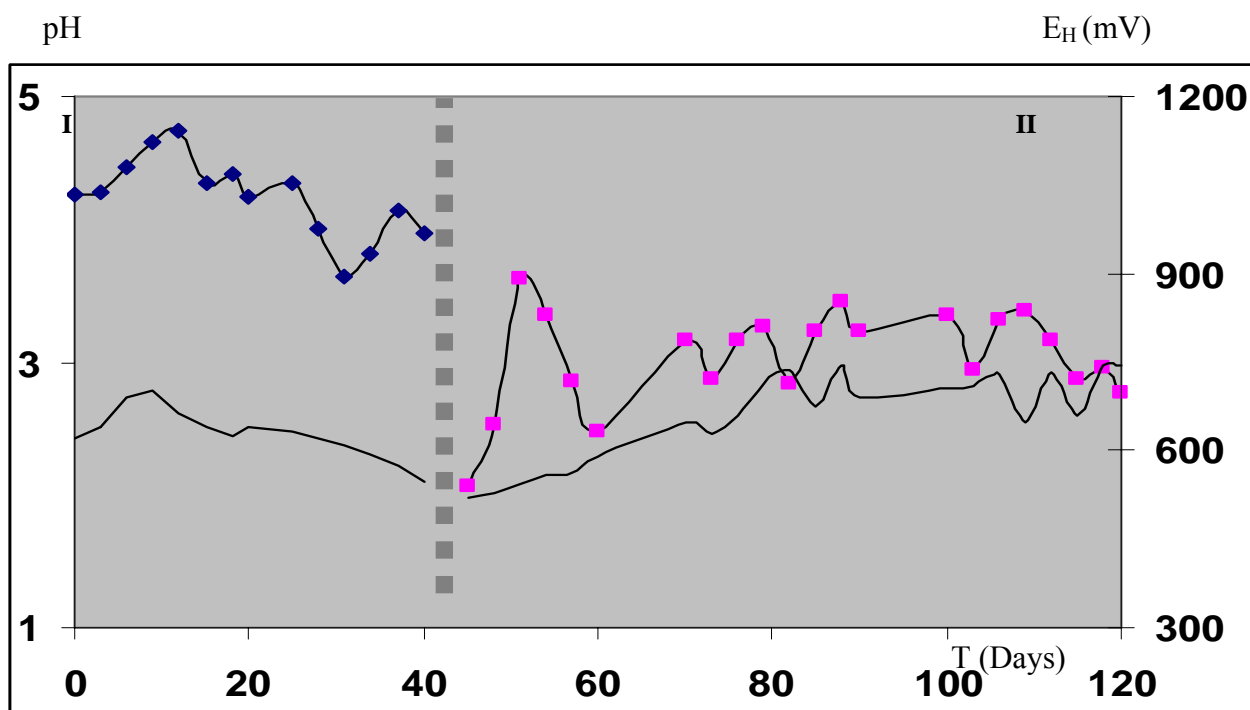


Figure B-10 : E_H (----) and pH (--■-) profile of lixiviant solution in the column (control) at 30°C.

I: Fe free lixiviant (*T. Thiooxidans* Medium)
 II: Fe containing lixiviant (9K medium)

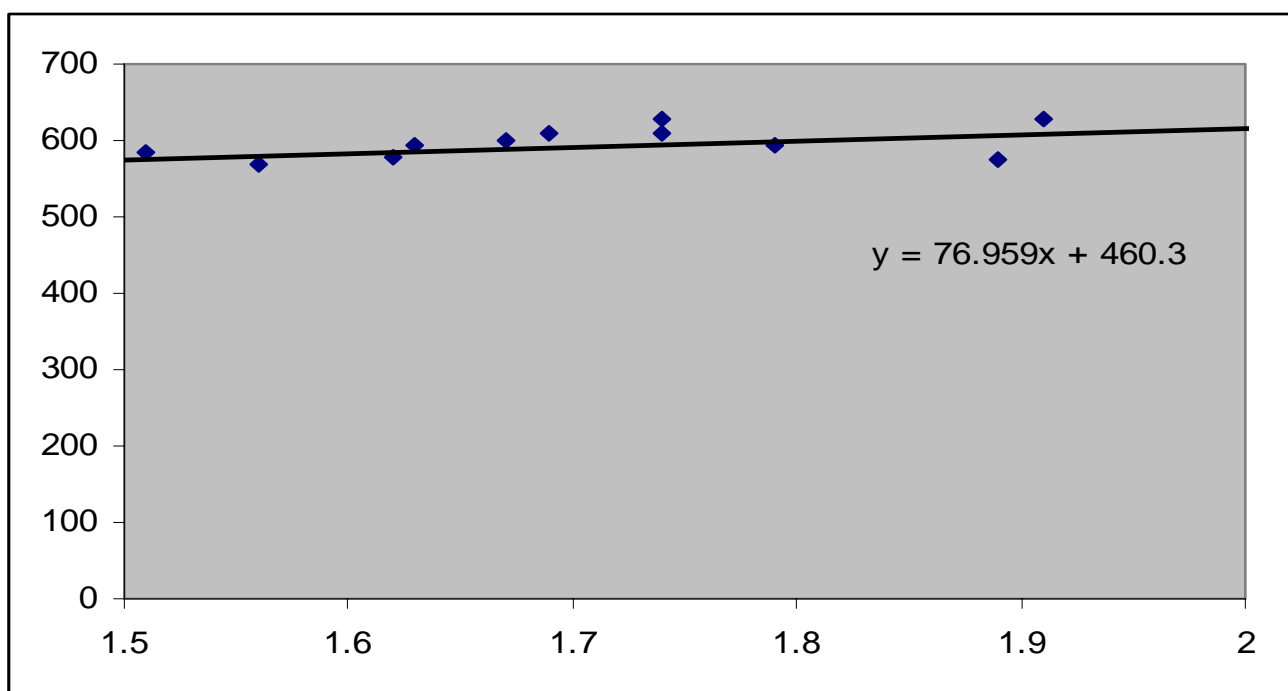


Figure B-11 : E_H vs pH for the column at 30°C. using *T. Thiooxidans*

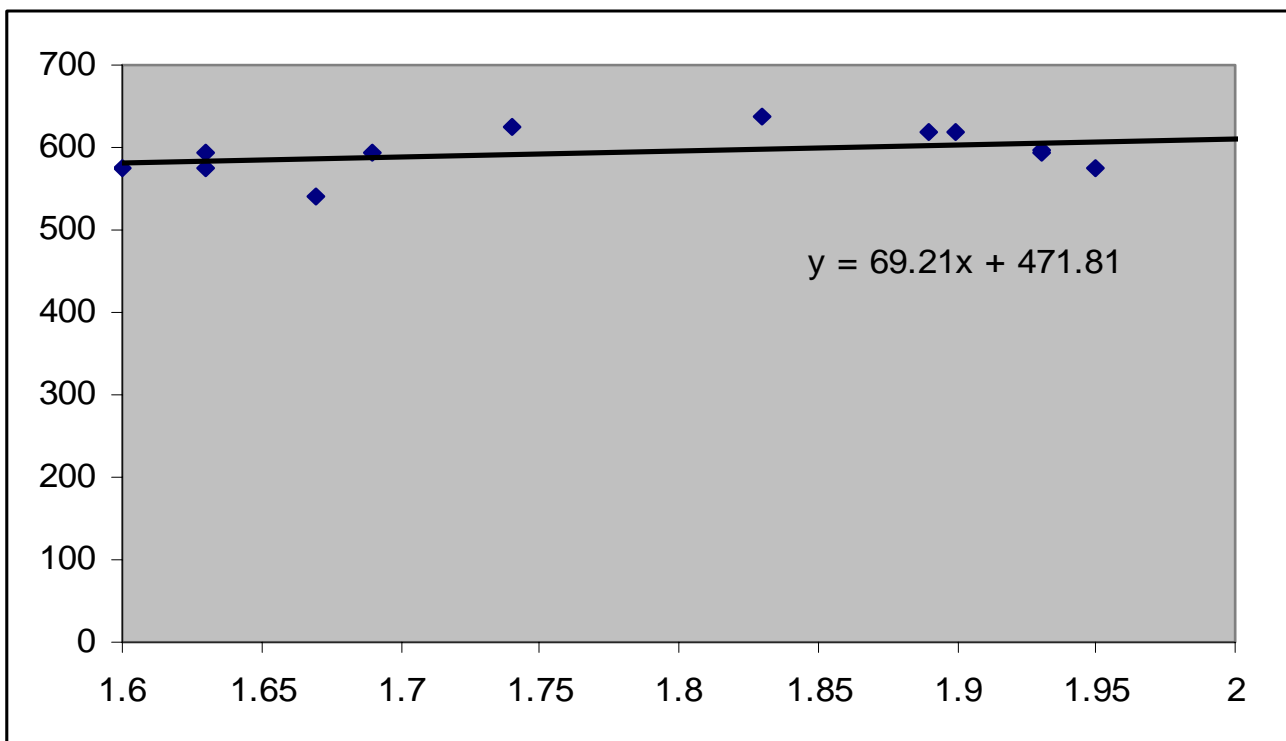


Figure B-12 : E_H vs pH for the control column at 40°C. using *T. Thiooxidans* medium

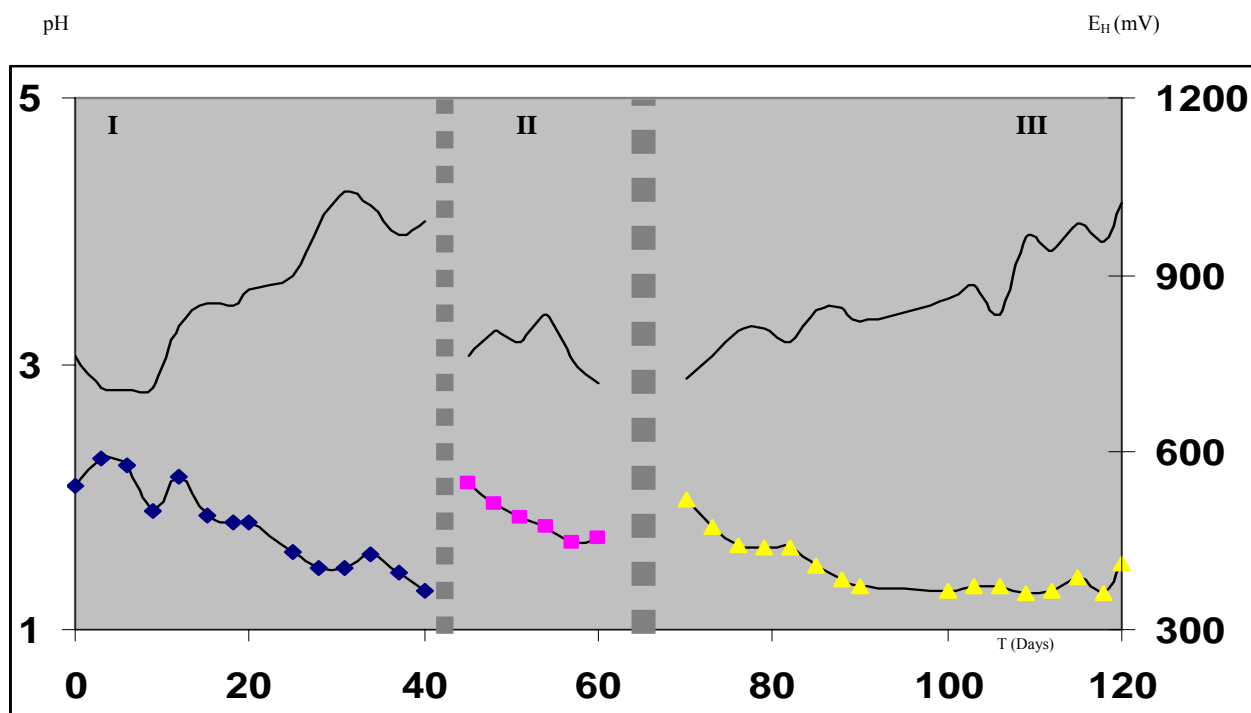


Figure B-7 : E_H (----) and pH (--■-) profile of lixiviant solution in the sequential leaching column (test), 30°C, 45°C and 70°C

I: Leaching at 30°C, (9K medium)
 II: Leaching at 45°C, (*Sb. Thermosulfodooxidans* medium)
 III: Leaching at 45°C, (*Sb. Thermosulfodooxidans* medium)

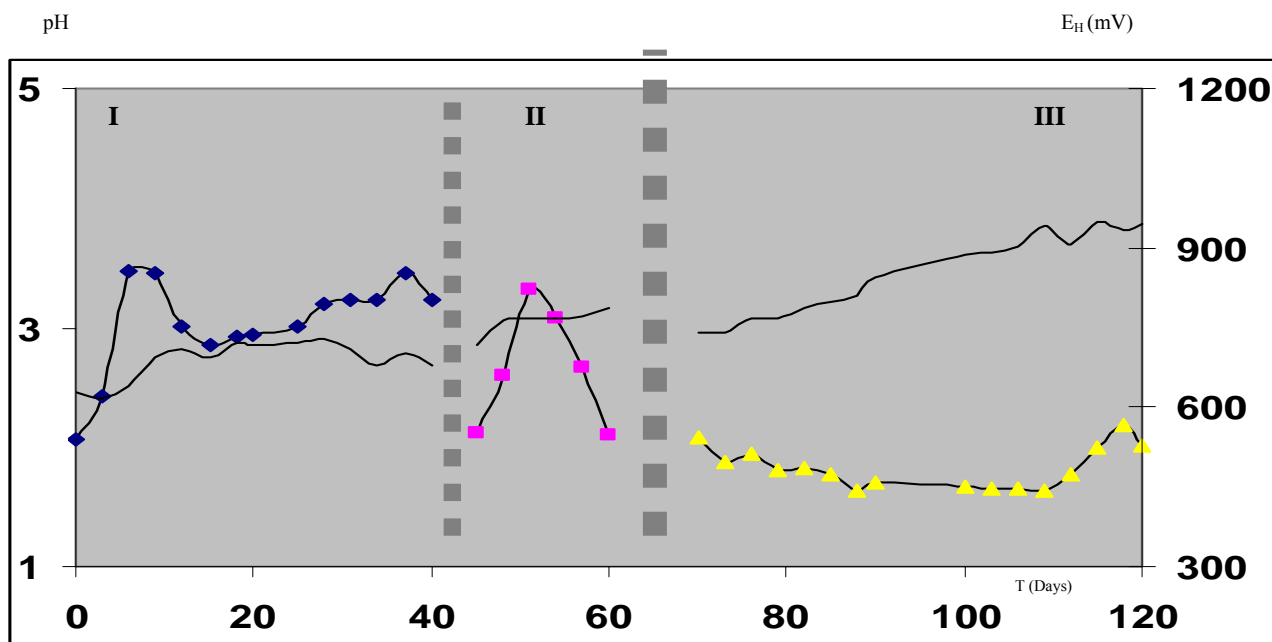


Figure B-8-b : E_H (----) and pH (---■---) profile of lixiviant solution in the sequential leaching column (control), 30°C, 45°C and 70°C

I: Leaching at 30°C, (9K medium)

II: Leaching at 45°C, (*Sb. Thermosulfodooxidans* medium)

III: Leaching at 45°C, (*Sb. Thermosulfodooxidans* medium)

PART 2

APPLICATION OF THERMOPHILIC BACTERIA: RECYCLING OF BATTERIES USING BIOTECHNOLOGY TECHNOLOGY

2.0 Introduction

Demand for batteries will increase as the usage of portable electronic devices i.e. laptop computers, telecommunications equipment and cordless tools are more rapid nowadays as it is one of the main parts for these electronic gadgets.

Based on the total number of batteries manufactured, non rechargeable batteries have the largest amount amongst the other type of batteries, which is 78.72%. Briefly, battery consists of several components such as metallic and plastic contents. Non rechargeable batteries have low prices and short lifetime of usage if compared to rechargeable batteries. Non rechargeable batteries are commonly disposed by the public without caring the consequences of their action.

The fate of batteries is an important and timely issue, primarily because of the toxic and hazardous materials that are used.

2.1 Objectives of the project

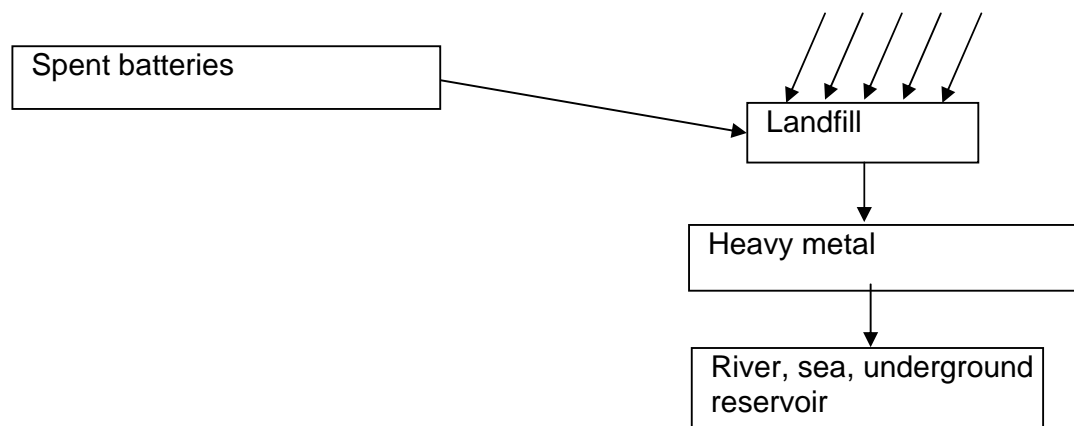
- Protection of the environment according to the precautionary principle.
- Optimum use of resources
- Solving disposal problems
- Economically acceptable waste management

- Socially acceptable waste management

2.2 Disposal of house hold batteries

House hold batteries or spent batteries usually are disposed off in landfill, which lead to hazardous leachate and not environmental friendly. Certain landfill had to be closed and is now a contaminated site which requires continuous monitoring and remediation.

The flow of spent batteries is shown in the figure below:



2.2.1 Batteries collection

From 158 kg of batteries received from DBKL, the batteries were mixed well and divided into 4 portions. The batteries were then sorted by their physical condition i.e: size, origin and type. (Fig. 2.1)

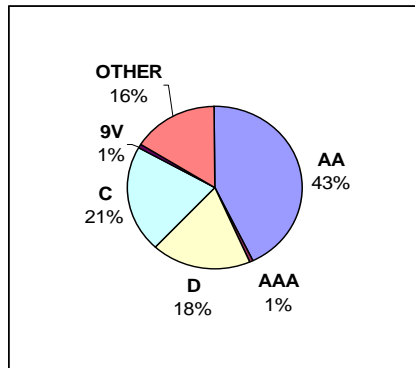


Figure 2.1: Portion of batteries segregation by size

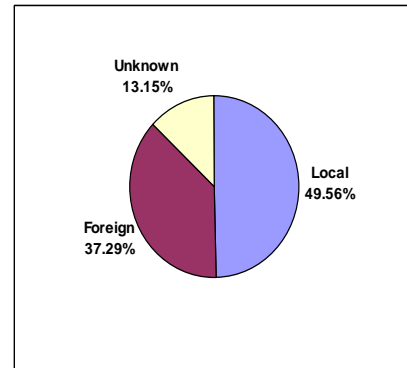


Figure 2.2: Portion of batteries segregation by origin of producer

The largest portion of collected batteries were those of AA size (27.76 kg), followed by D (11.96kg) and C (13.76kg). Most portable devices require AA, C or D batteries, which accounts for the largest percentage of batteries used for general household purposes. i.e: AA (Clock, toys and walkman), D (Radio and torchlight) and C (torchlight). Button cell, mobile phone batteries and 6V type batteries (16.14%) constitute those grouped under miscellaneous

It is interesting to note that 37.29% of the total batteries collected was imported (mostly from China), compared to 49.56% which was produced locally. Large portion of imported batteries found inside our waste stream is due to its cheap prices, short life time and is usually sold together with equipment, especially toys. The cheap imported type batteries have a high tendency to leak and might have a high Hg and Pb content.

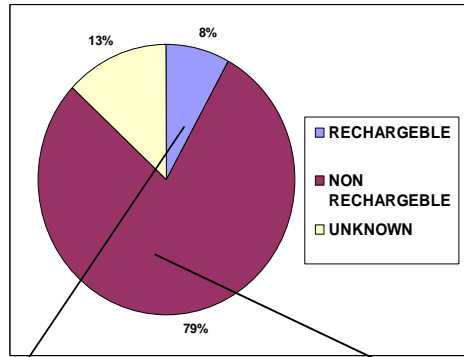


Figure 2.3: Portion of batteries, segregation by recharge ability

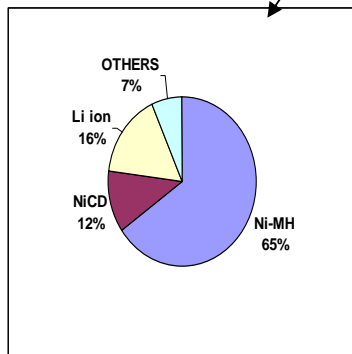


Figure 2.4: Portion of rechargeable batteries

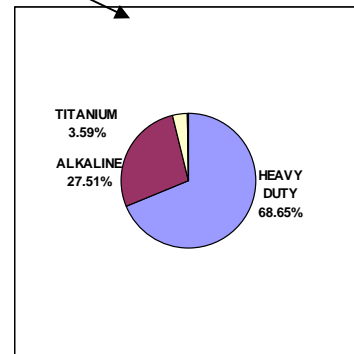


Figure 2.5: Portion of non-rechargeable batteries

From the batteries collected, 79% was the non rechargeable type, 13% rechargeable and 8% of unknown type. More non rechargeable batteries have been collected compared to the rechargeable batteries. Low prices and short lifetime contribute to the large consumption of non rechargeable batteries.

2.3 Metal content

The metal composition differs considerably depending on the battery type, thus some batteries are potentially more hazardous than others. Changing the trend of batteries consumption will affect the efficiency of metal recovery. As an example, for the Ni–Cd batteries, cadmium, mercury and lead are very toxic metals commonly found in these batteries.

A) Metal content of non rechargeable dry cell (Zn-C and Alkaline batteries).

Table 2.1: Metal content of non rechargeable dry cell (Zn-C and Alkaline batteries).

Element	Zn-C (entire batteries)	Zn-C (Dry powder)	Alkaline (entire batteries)	Alkaline (dry powder)
Mn (%)	27.065	33.023	29.025	38.596
Zn (%)	5.023	7.0568	12.4862	19.85634
Fe (%)	2.184	0.021245	1.9658	0.001453
As (ppm)	3.425	-	2.159	-
Cd (ppm)	12.47	-	4.253	-
Co (ppm)	26.14	-	84.25	-
Cr (ppm)	23.45	-	29.48	-
Cu (ppm)	5.124	-	2.814	-
Hg (ppm)	-	0.002356	-	0.04598
Ni (ppm)	52.34	69.85	85.23	102.35
Pb (ppm)	23.92	1.5625	49.87	65.68

The metal composition of zinc-carbon and alkaline batteries is quite similar. These batteries contain basically manganese, zinc and iron as main metallic species. The outer layer of batteries comprises mainly of iron (Fe). Steel casing can be separated easily using a magnetic separator. Other heavy metals Cu, Ni, Cr, As, Cd, Co, Hg and Pb are found in trace amounts. Low levels of mercury have been detected at 0.002 ppm and 0.04ppm from the Zn-C and alkaline batteries respectively, even though have been labeled as no mercury added.

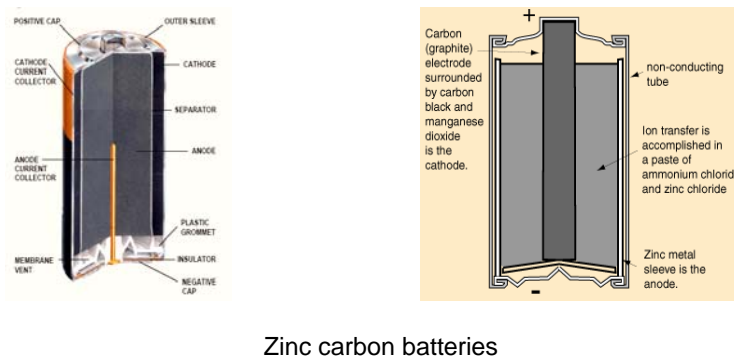
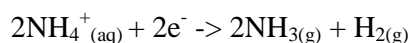
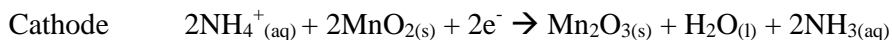
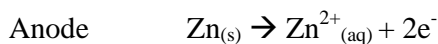


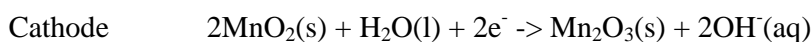
Figure 2.6: Cross section of alkaline and zinc carbon batteries

The chemical reaction involved in zinc-carbon and alkaline-manganese batteries is as follows:

Zinc-carbon



Alkaline-manganese



B) Metal content of Rechargeable batteries

Table 2.2: Metal content of Rechargeable batteries

Element	Ni Cd	Ni MH	Li ion
As (ppm)	1.025	1.5234	3.1402
Cd (%)	17.953	-	-
Co (%)	0.617	3.569	15.756
Cr (ppm)	22.018	21.052	37.156
Cu (ppm)	64.248	59.482	6897.42
Hg (ppm)	0.2631	0.01186	0.00952
Mn (%)	0.086	1.482	12.729
Ni (%)	19.127	35.876	9.256
Pb (ppm)	263.5	1.048	0.9235
Fe (%)	29.354	22.485	6.152
Zn (%)	0.04356	0.5725	-
Al (%)	0.053	0.6235	5.689
Li (%)	-	-	4.315
La	-	2.458	-
V	-	-	13.248

Compared to disposable batteries, the metal content of rechargeable batteries is more varied. Metal content of Ni Cd, NiMH and Li ion batteries is slightly higher at 67.3%, 67.1% and 74.0% respectively, compared to 43.5 % for alkaline batteries.

Nickel metal hydride (NiMH) batteries represent one of the fastest growing sectors in the battery market. Amongst the many uses include cordless power tools, personal stereos, portable telephones, lap-top computers, shavers, motorised toys with a life of 4-5 years. NiMH batteries are a more environmental friendly alternative to NiCd and tend to have a longer life. Energy storage capacity of Lithium ion (Li-Ion) batteries are reported to be greater than NiCd and NiMH batteries.

C) Metal content in collected batteries by DBKL

Table 2.3: Metal content in collected batteries by DBKL

Element	Content
As (ppm)	5.0236
Cd (%)	0.3835
Co (%)	2.1356
Cr (ppm)	26.139
Cu (ppm)	242.47
Hg (ppm)	7.0235
Mn (%)	22.842
Ni (%)	5.1454
Pb (ppm)	31.534
Fe (%)	5.2996
Zn (%)	6.0357
Al (%)	0.2777
Li	0.1517
La	0.3020
V	0.4658

The batteries were found to contain 22.84% Mn, 6.04% Zn and 5.3% Fe 5.15 % Ni and 0.38% Al. The quantity of these metals are worthy for recycling.

2.4 Laboratory Test Work

For this project, laboratory based experiments were carried out first before the implementation of large scale recycling process. The laboratory based experiments consist of column leaching test, shake flask test, stirred tank reactor (STR) test and

metal purification test. Every parts of the experiment are simplified as described below:

2.4.1 Column leaching test work

- 2 identical column unit, simulation heap leaching
- Duration 1 year, multi stages and total: 330 kg each batteries leaching, locally produced.
- Low leaching rate.
- Batteries were not broken
- Difficult for lixiviant solution to access into batteries core

Important findings

- Amount of metal extracted from each column is shown in table 4.

Table 2.4: Amount of metals extracted from column 1 and 2.

METAL	Column 1	Column 2
Zn	43%	51%
Mn	38%	36%
Fe	73%	65%

2.4.2 Shake flask test work

Set 1: Shaken, not broken,

Set 2: Unshaken, broken

Set 3: Shaken, broken

Batteries AA used: Zn-C batteries, alkaline batteries, Ni-Cd rechargeable batteries, Li-rechargeable batteries

Set 4: Shaken, broken and inner part dismantling

Set 5: Shaken, broken, inner part dismantling and roasted

Set 6: Combination of chemical leaching and bioleaching **test**

Batteries AA used: Zn-C batteries

Culture used:

- *Thiobacillus ferrooxidans*
- *Leptospirillum ferrooxidans*
- *Thiobacillus thiooxidans*
- *SulfobacillusThermosulfodioxidans*
- *Acidianus Brierleyi*
- *SL5B*

Chemicals used:

- Hydrochloric acid
- Sulfuric acid
- Ferric chloride
- Ferric sulphate
- Sodium thiosulphate
- Sodium hypochlorite

2.4.3 Stirred tank reactor (STR) test work

Set of various experiments have been set up in testing the leaching process in stirred tank reactor. Details for every set of test are described in table 2.5.

Table 2.5: Details for every set in stirred tank reactor (STR) leaching process.

SET	TYPE OF LEACHING	CONDITION
1	H ₂ SO ₄ leaching	1: Variable: H ₂ SO ₄ concentration 2: Variable: Temperatures 3: Variable: Pulp densities 4: Variable: Duration

2	HCl leaching	1: Variable: HCl concentration 2: Variable: Temperatures 3: Variable: Pulp densities 4: Variable: Duration
3	Ammonium carbonate leaching	1: Variable: Ammonium carbonate concentration 2: Variable: Temperatures 3: Variable: Pulp densities 4: Variable: Duration
4	<i>Thiobacillus thiooxidans</i> leaching	1: Variable: Pulp densities 2: Variable: Duration
5	<i>Acidianus Brierleyi</i> leaching	1: Variable : Pulp densities 2: Variable : Duration
6	Fe ₃ (SO ₄) ₂ leaching	1: Variable : Fe ₃ (SO ₄) ₂ concentration 2: Variable : Temperatures 3: Variable : Pulp densities 4: Variable : Duration
7	Fe ₃ Cl leaching	1: Variable : Fe ₃ Cl concentration 2: Variable : Temperatures 3: Variable : Pulp densities 4: Variable : Duration
8	Mix culture of <i>Thiobacillus ferrooxidans</i> (TF) and <i>Leptospirillum ferrooxidans</i> (LF) at ratio: 1:1 leaching	1: Variable : Pulp densities 2: Variable : Duration
9	SL5B leaching	1: Variable : Pulp densities 2: Variable : Duration
10	Roasted, H ₂ SO ₄ leaching	1: Variable : H ₂ SO ₄ concentration 2: Variable : Temperatures 3: Variable : Pulp densities 4: Variable : Duration
11	Roasted, HCl leaching	1: Variable : HCl concentration 2: Variable : Temperatures 3: Variable : Pulp densities 4: Variable : Duration
12	Roasted, Fe ₃ (SO ₄) ₂ leaching	1: Variable : Fe ₃ (SO ₄) ₂ concentration

		2: Variable : Temperatures 3: Variable : Pulp densities 4: Variable : Duration
13	Roasted, FeCl ₃ leaching	1: Variable : FeCl ₃ concentration 2: Variable : Temperatures 3: Variable : Pulp densities 4: Variable : Duration
14	Roasted, <i>Thiobacillus thiooxidans</i> leaching	1: Variable : Pulp densities 2: Variable : Duration
15	Roasted, <i>Acidianus Brierleyi</i> leaching	1: Variable : Pulp densities 2: Variable : Duration
16	Roasted, Mix culture of <i>Thiobacillus ferrooxidans</i> (TF) and <i>Leptospirillum ferrooxidans</i> (LF) at ratio: 1:1 leaching	1: Variable : Pulp densities 2: Variable : Duration
17	Roasted, SL5B leaching	1: Variable : Pulp densities 2: Variable : Duration

Important findings

- Leaching capacity on original batteries is very limited
- Breaking and shaking will increase the leaching capacity
- Roasting at lower temperature 200 – 350°C increased yields to nearly 100%, i.e: 98% using FeCl₃ and 96% using SL5B culture. However, Li-ion batteries must be removed before roasting or it will explode.
- Leaching on roasted batteries using *Thiobacillus thiooxidans* - selective process. 95% Zn and 12% Mn
- Leaching on unroasted batteries using (NH₄)₂CO₃ is highly selective process. 95% Zn and >1% Mn.
- Formation of jarosites is very aggressive, especially for alkaline and rechargeable batteries- can retard the process and disturb the heap leaching process
- Leachate solution is very corrosive, even for stainless steel.
- For column leaching, rate of metal leaching at the bottom of column is much higher than top of column.
- The overall optimum pulp densities for STR at 20%.

2.4.4 Metal purification test work

Purification of metal recovered is done after the leaching process. Details for the purification method are described in table 2.6.

Table 2.6: Purification methods for recovered metal.

SET	TYPE OF PURIFICATION	CONDITION
1	Precipitation, pH adjustment	1. Solution from column test H_2SO_4 2. Solution from column test $Fe_2(SO_4)_3$ 3. Solution from column test HCl 4. Solution from column test $FeCl_3$
2	Precipitation, Different temperature	1. Solution from column test $Fe_2(SO_4)_3$ 2. Solution from column test $FeCl_3$
3	Solvent extraction: Mixture of 5-dodecylsalicylaldoxime and tridecanol in a high flash-point hydro-carbon diluent	Stripping using: 1M Sulfuric acid 1. Solution from batteries digestion 2. Solution from column test HCl 3. Solution from column test $FeCl_3$ 4. Solution from column test H_2SO_4 5. Solution from column test $Fe_2(SO_4)_3$
4	Solvent extraction: Mixture of 5-dodecylsalicylaldoxime and 2-hydroxy-5-nonyl-acetophenone oxime in a high flash point kerosene	Stripping using: 1M Sulfuric acid 1. Solution from batteries digestion 2. Solution from column test HCl 3. Solution from column test $FeCl_3$ 4. Solution from column test H_2SO_4 5. Solution from column test $Fe_2(SO_4)_3$

5	Solvent extraction: Mixture of 5-dodecylsalicylaldoxime and tridecanol in a high flash-point hydro-carbon diluent	Variable: Solution/Solvent ratio 1. Solution from batteries digestion 2. Solution from column test FeCl ₃ Solution from column test Fe ₂ (SO ₄) ₃
6	Solvent extraction: Mixture of 5-dodecylsalicylaldoxime and 2-hydroxy-5-nonyl-acetophenone oxime in a high flash point kerosene	Variable: Solution/Solvent ratio 1. Solution from batteries digestion 2. Solution from column test FeCl ₃ 3. Solution from column test Fe ₂ (SO ₄) ₃

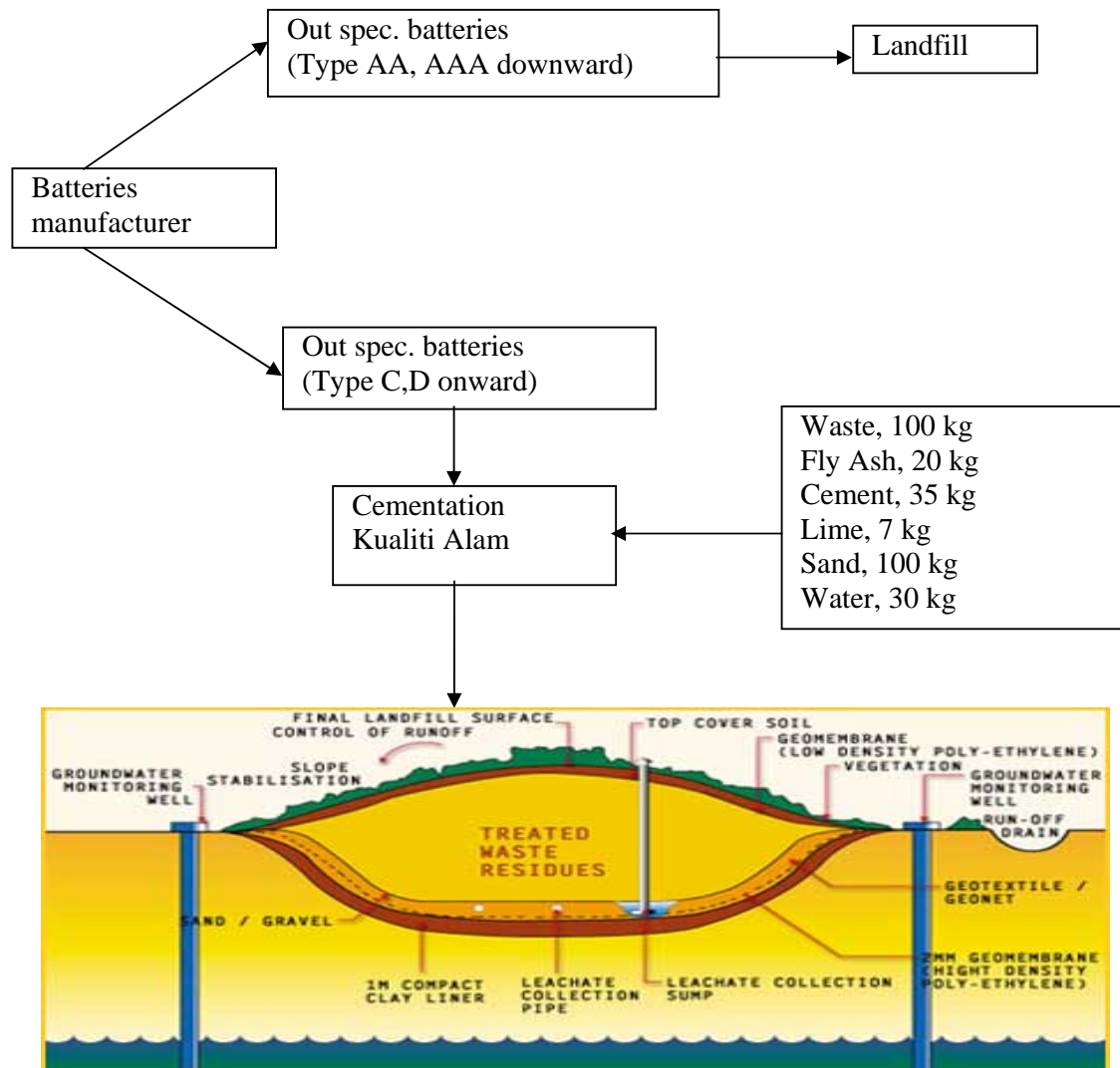
Important findings

- Zn can be recovered via precipitation at different pH.
Examples - H₂SO₄: pH 6-7 and HCl: pH 9.
Difficult on iron based leachate solution.
- Purification via precipitation at different temperature is difficult.
- Zn can be purified using mixture of 5-dodecylsalicylaldoxime and tridecanol in a high flash-point hydro-carbon diluents in Chloride based leachate at ratios 2:1
- Mn can be extracted using mixture of 5-dodecylsalicylaldoxime and 2-hydroxy-5-nonyl-acetophenone oxime in a high flash point kerosene

2.5 Proposal pilot scale process for batteries recycling

2.5.1 Local technology to treat dry batteries

1. Cementation and secured landfill



Cementation is prescribed for the treatment of dry cell batteries and other miscellaneous wastes which could not be properly and safely treated by existing treatment facilities. Cement and sand are the main materials used to encapsulate and cement hazardous and toxic contaminants in the wastes and prevent them from leaching into the environment. The cost for cementation and disposal at a secured landfill is RM 900 per tonne of dry cell batteries.

A number of companies have been sending their wastes for these two treatment methods since 1997. Dry cell type C onwards and button cell have been classified as scheduled waste for batteries manufacturers, while AA and AAA batteries is permitted to landfill.

In the cementation plant, metal containing wastes, which do not fulfill the criteria for disposal directly into the Secure Landfill, are treated. Such wastes are typically metal hydroxide sludge containing heavy metals such as lead, arsenic, nickel, zinc and chromium. During the cementation process the heavy metals become insoluble and the wastes therefore can safely be disposed off in the Secure Landfill. Fly ash from the Incinerator Plant and sludge from the PCT Plant are also treated at the cementation plant.

At the cementation plant, waste is loaded into waste bunkers, where it will be mixed with other similar waste. It is then loaded into the waste hopper before being transferred to the mixer by screw conveyors. In the mixer, waste is carefully mixed with consumables such as cement, lime and water. The system is able to handle waste that contains foreign materials such as stones, wood and scrap iron

After treatment, the waste will appear as a concrete mixture. The mixture is disposed off to the secure landfill for the final curing over a few days. The objective of the whole process is to fix all the heavy metals in the inorganic solid waste into a concrete/silica matrix for long-term disposal in the secure landfill. As a result, hazardous heavy metals will not leach out to the environment.

The Secure Landfill is the final destination for the cemented batteries. The landfill site is some 80 acres in area to accommodate the construction of 8 secure landfill cells with a total volume of 2.5 million cubic meters. As it is a permanent

waste disposal facility, all waste materials have to meet the strict Landfill Acceptance Criteria as provided for under the Department of Environment Secure Landfill Licensing Conditions. Only inorganic solid waste that meets all parameters of the Landfill Acceptance Criteria is eligible for direct landfill disposal. Otherwise, the waste will have to be treated at either the solidification or incineration plant.

The secure landfill is designed to prevent seepage of leachate into ground water with a double membrane comprising a one-meter thick compacted clay liner and a 2 mm thick High Density Poly-Ethylene geo-membrane. Above the HDPE membrane is a drainage system made up of a 0.4-meter thick layer of crushed rocks. Rainwater, which percolates from the top of the landfill, is called leachate and it is channeled to the leachate collection sump found within each landfill cell

Waste can be disposed off in the landfill in drums, polypropylene bags, in bulk or in cemented form. Radioactive, infectious and explosive wastes are not treated or disposed off at this Waste Management Centre. The records, including the consignment note numbers, amount and location are kept at the landfill office. Internal waste, such as slag from the incineration plant and solidified materials from the solidification plant are sent to the landfill for final disposal. Other internal waste such as incineration ash and physical/chemical treatment plant slurry, are treated at the solidification plant prior to disposal.

The Leachate Treatment Plant (LTP) is capable of treating leachate from secure and rubber sludge landfills, internal wastewater generated from plant operations as well as the first ten-minute flush of rainwater run-off. The Leachate Treatment Plant is a requirement under Kualiti Alam's Environmental Management Programme.

- Cementation is a simple method to treat batteries, preventing it from natural leaching.
- Low cost, low explosion and leakage risk during process.
- No metals can be recovered

2.5.2 Existing technologies in other countries

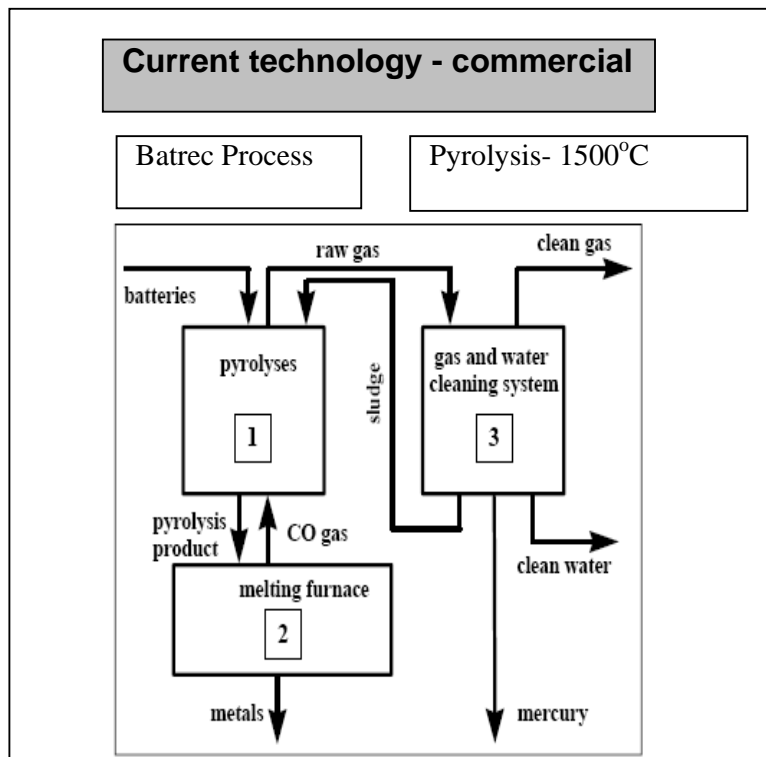
Switzerland: Recytec process (1994)

Batrec (3000 tons/yr)

Germany: Batenus process (7500 tons/yr)

USA: 2300tons/yr nickel–cadmium, nickel–iron and nickel–metal hydride batteries

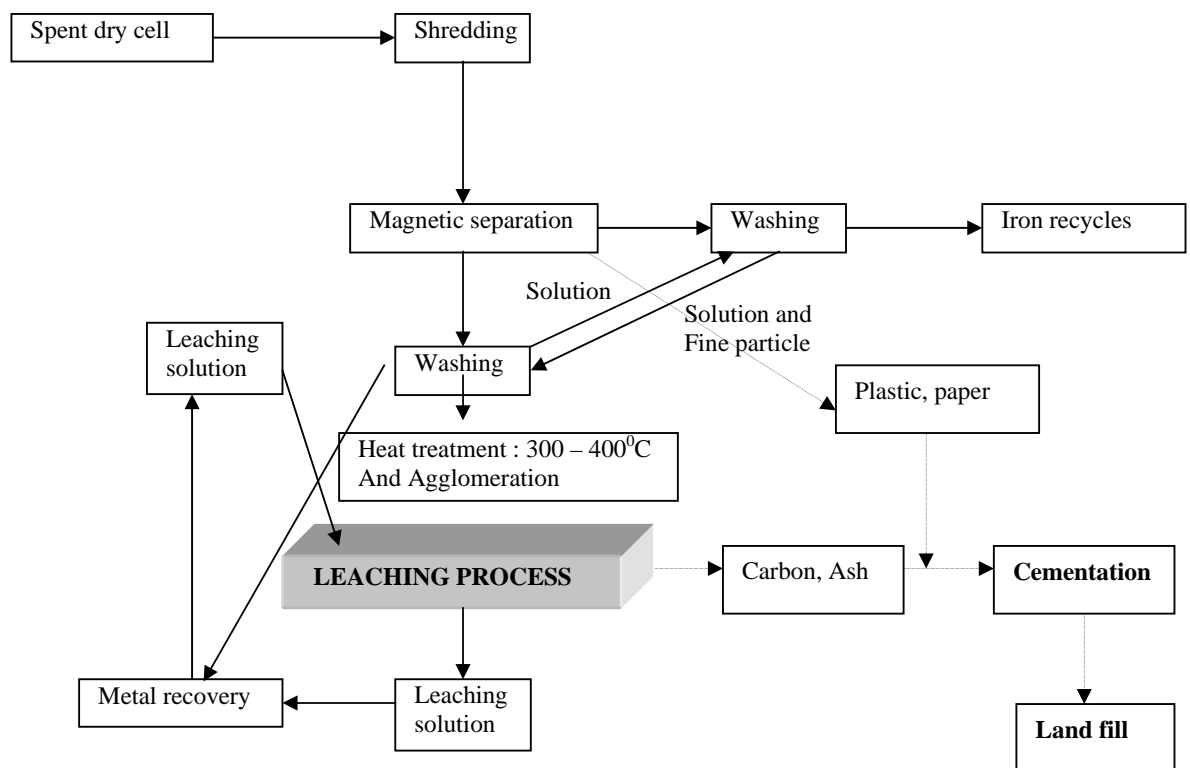
Example of one the battery treatment system applied in other countries:



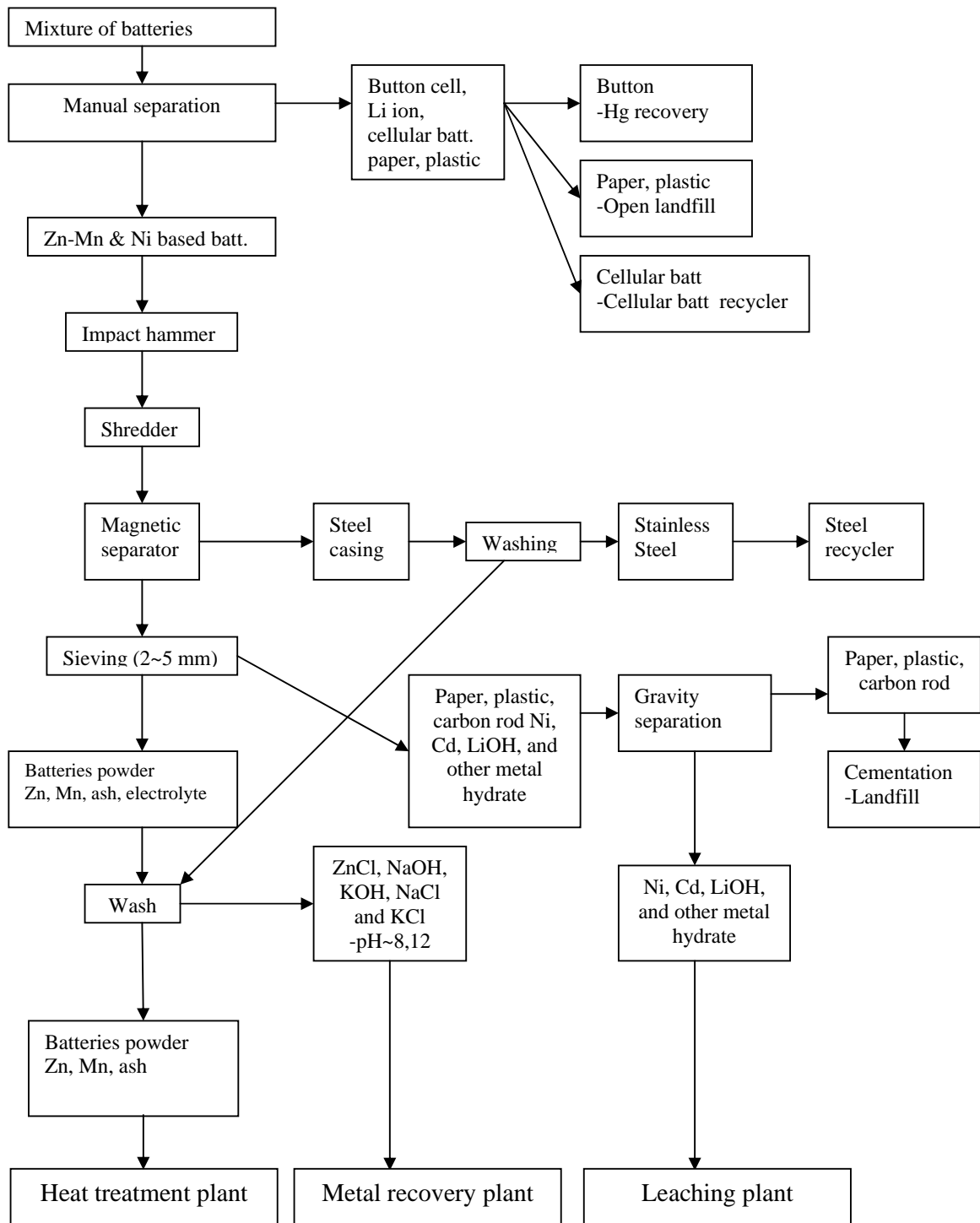
2.5.3 Proposed Batteries Recycling 1

2.5.3.1 Heap of Alkaline and Zn-carbon cell

The components of the process are magnetic separation, washing using water, heat pre-treatment, bioleaching process, metal recovery, regeneration of leaching solution and cementation.

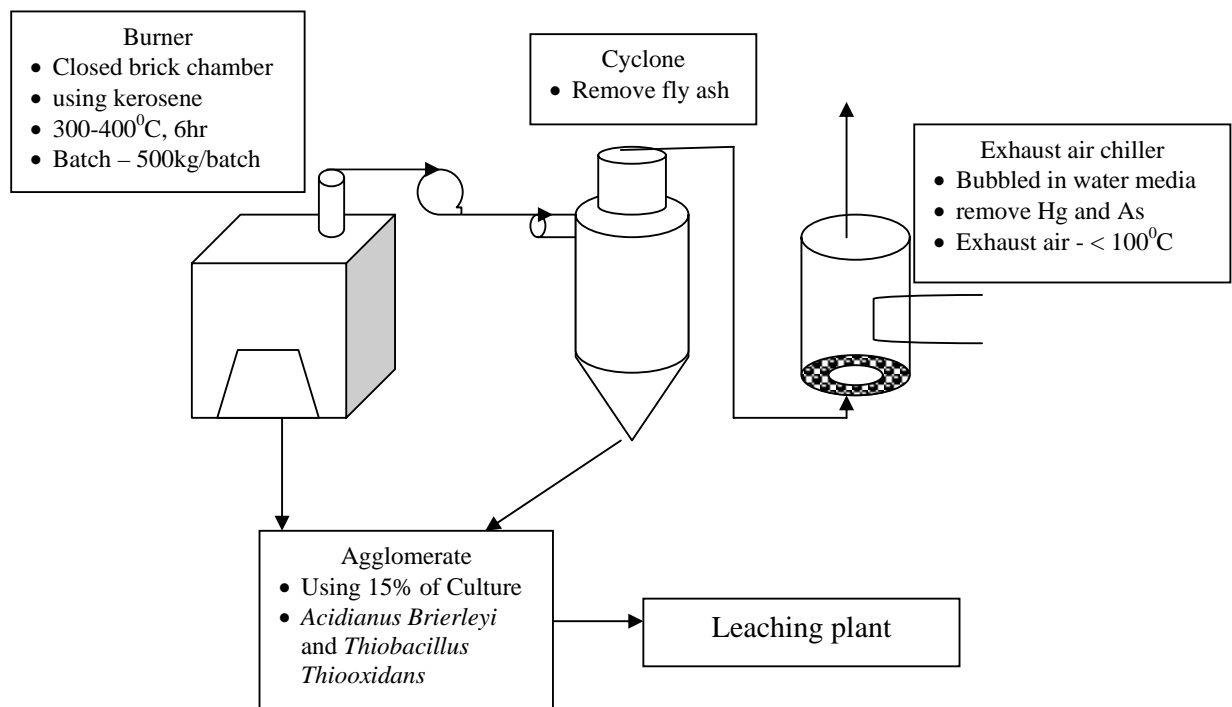


Part 1: Mechanical separation



The first mechanical operation is sieving out the button cells, paper and plastic. Those cells are sent to a mercury recovery company. The batteries are shredded. At the shredder exit, a magnet removes scrap iron. After washing, this scrap is sold to a scrap dealer. Paper, plastics and nonferrous metals are separated from the battery contents with the aid of sieves. A further separation yields a paper/plastics portion and a nonferrous scrap portion using gravity separator. The battery powder is then subjected to the heat treatment plant and hydrometallurgical unit.

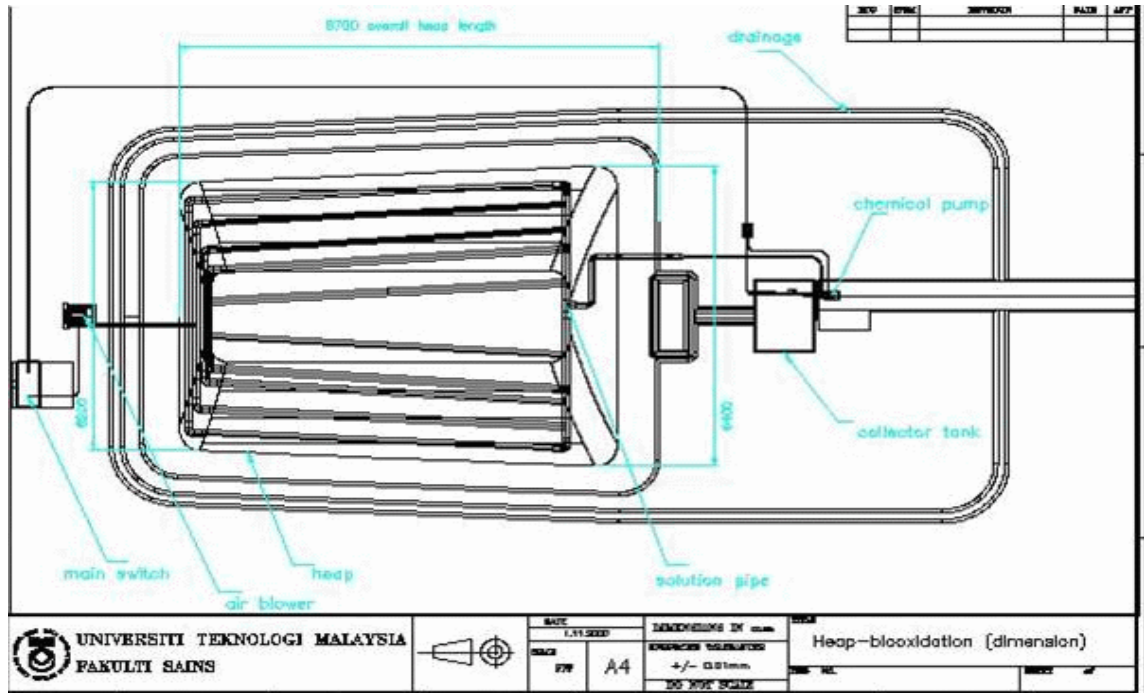
Part 2: Heat Treatment Plant



Part 3: Heap Leaching

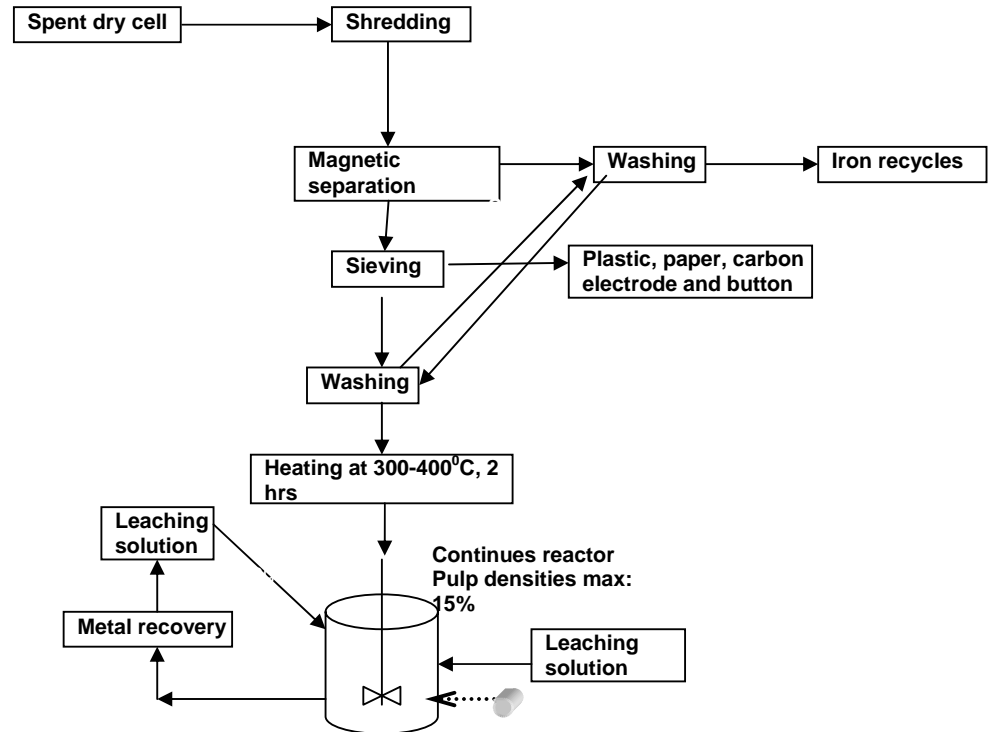
Material and equipment	Description
Heap content	<ul style="list-style-type: none"> - 100 tonnes of roasted-non rechargeable batteries powder - Agglomerate with 15% culture - Fully covered with roof - Safety leakage protection system
Pad and liner	<ul style="list-style-type: none"> - Area: 10m x 5m at 2m height - Pad slope: 0.5⁰-1.0⁰ - Liner type: 0.2mm HDPE pad / layering with sand - Pond: Pregnant pond Overflow pond Settlement pond Biooxidation tank Chemical storage tank
Spraying irrigation	<ul style="list-style-type: none"> - Sprayer: Rain bird garden spray with radius of spraying 1m - Rate of irrigation – 36.3 m³/hour - Drainage: total leakage system with a improved drainage system
Leaching media	<ul style="list-style-type: none"> - Biological leaching Mixed culture of mesophilic and thermophilic

2.5.3.2 Pilot Plant Test Over View



2.5.4 Proposed Batteries Recycling 2

2.5.4.1 Agitation of Alkaline and Zn-carbon cell



Advantages

1. Higher extraction rate- compared to latest technologies.
2. Low chemical consumption
3. Environmentally friendly than high smelting- SO₂ emission.
4. Less landscape damage as the bacteria grow naturally and can be recycled.
5. Smelting produced great amounts of sludge, which is concentrated with heavy metals.
6. Simpler and cheaper operating plant.

2.6 Cost estimation

- Setting up of the pilot scale based on the test of metal recovery from 100 t spent dry cell.
- The cost is not inclusive of manpower, chemical analysis, transportation and travelling

Operation	Estimated Costs (RM)
Battery Breaking and Separating	33 500
Pre-leaching: Tank leaching & Zn recovery	67 200
Roaster	23 000
Leaching: Heap leaching & Mn recovery	71 600
Total	195 000

PART 3

Leaching Study of Pyrite Using Stirred Tank Reactor (STR) and The Modelling of leaching process

3.0 Foreword

This chapter will discuss on the biooxidation of pure mineral i.e.: pyrite and chalcopyrite. Biooxidation test will be carried out using stirred tank reactor (STR). In this chapter, operating condition, which affect the biooxidation behaviour including bacterial type, particle size, pH, temperature, residence time and agitation will be optimised. Parameters including DO, pH, Eh, iron and copper profiles will be assessed to determine the biooxidation process. The study on the kinetic aspect of the leaching process and the modelling of the leaching process are also included in this part.

3.1 Introduction

Basically there are two types of bioreactor, which are the batch reactor and the continuous reactor. Batch process reactors are simplest type of reactor i.e. shake flask, agitated tanks or vessel. In this mode, the process reactor is filled with medium and the reaction is allowed to process. When the reaction has finished, the contents are emptied for another process. The reactor will be shut down, cleaned, refilled, reinoculated and then the reaction process will start again. Batch reactors are usually used for small scale operation, for testing new processes and for processes that are difficult to convert to

continuous operation (Fogler, 1992 and Mior, 2001). While for the continuous process reactors, fresh media is continuously added and reactor fluid is continuously removed. As a result, the material being process continuously receives fresh medium and products and waste products and materials are continuously removed for processing. The reactor can thus operated for a long periods of time without having to be shut down. Continuous process reactors can be many times more productive than batch reactors. This is partly due to the fact that the reactor does not have to be shut down as regularly and also due to the fact that the growth rate of the bacteria in the reactor can easily be controlled and optimized. In addition, cells can also be immobilized in continuous reactors, to prevent their removal and thus further increase the productivity of these reactors.

In general term, bioreactor can be defined as any systems that have boundaries and where biochemical reaction took place. It also can be described as the system or process can be controlled. In term of biohydrometallurgy, bioreactor ca be classified by the method of agitation and the mode of continuous phase was carried out i.e. liquid or gas phase. Bioreactor operation can be done by mechanically agitation or by air sparging using external pump. The typical bioreactors used in biohydrometallurgy are mechanically agitated bioreactor or stirred tank bioreactor and air lift bioreactor. Other types of reactors that have been studied for their application in biomining are the percolation column, the Paschua tank, the air-lift column and some special designs such as rotary reactors (Atkins and Pooley, 1983; Atkins et. al. 1986; Nikolov et. al. 1986; Acevedo et. al. 1988; Barrette and Couillard 1993; Loi et. al. 1995; Herrera et. al. 1997; Acevedo et. al. 1999 Canaleset et. al. 1999; Nedeltchev et. al. 1999; Rossi 1999)

3.2 Biooxidation using STR

3.2.1 Material and Methods

3.2.1.1 Mineral used

The mineral used in this experiment was pyrite (FeS_2) obtained from Peru. The pyrite was ground using ball mill in acetone or ordinary blender and sieved. The mineral was then soaked with H_2SO_4 (1M) at 70°C for 1 minute to get rid of any metal oxides. Slurry obtained was then filtered, washed 3 times with distilled-deionized water at a ratio 1:10 (pyrite: DI water) and dried using acetone. The treated mineral was stored in the freezer to avoid natural oxidation.

3.2.1.2 Acid digestion of mineral

Acid digestion test was carried out to determine the composition of base metals in the sample. The dried and ground mineral (pyrite and chalcopyrite), 1.0g were roasted in the furnace at 600°C for 1.5 hrs and the sample was mixed with 100mL aqua regia ($\text{HCl}:\text{HNO}_3$) 3:1 ratio. The mixture was then heated at $80\text{-}90^\circ\text{C}$ for 2 hrs. During this time, it was assumed that all the base metal remained soluble. Upon cooling, the slurry was then transferred into a 250mL volumetric flask. The volume was then made up to the mark using distilled deionised water (DDW). The sample was then analysed using ICP-MS and AAS to determine the base metal concentration in the sample.

3.2.1.3 Carbon and sulphur determination

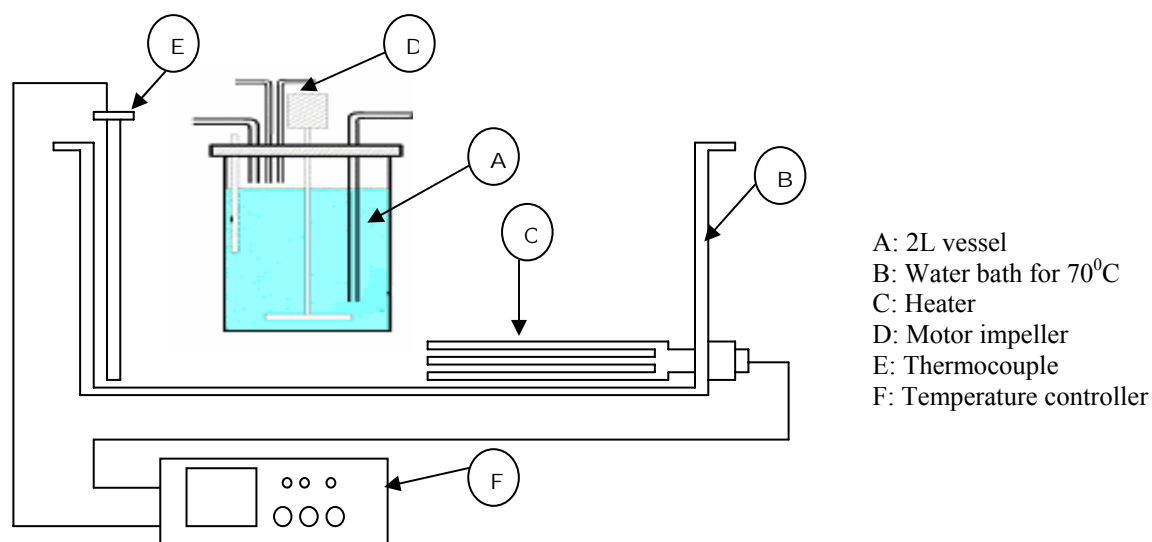
This test was carried out at Antara Steel Sdn. Bhd., Pasir Gudang, Johor Bahru using a carbon and sulphur dcterminator (Leco HF-400).

3.2.1.4 Culture used

The bacteria used in this study are standard strains of *Sulfobacillus thermosulfodoxidans* (*Sb.T*) obtained from the German culture Collection (DSMZ), grown in *Sulfobacillus* medium at 45⁰C. Mesophilic culture, *T. ferrooxidans* (*T.F*) previously isolated from a local gold mine were grown aerobically in the 9K medium and 30⁰C (Shafinaz Shahir,1998) while, locally isolated thermophilic culture, SL5B was grown in *Sulfobacillus* medium at 70⁰C. Initial cultures were incubated aerobically at respective temperature using 2.0L shake flasks. Each flask contained 200L of culture. The strain was then transferred to the 2.0L fermentor and grown at 350rpm with continuous air sparging at 25L/min for 24 hours.

3.2.1.5 Bioreactor

A 2.5L of fermentor Biostat[®] A, B. Braun with 2L operating volume as shown in figure 3.4 was used in this study. The tank reactor used to perform the continuous biooxidation tests was a round-bottomed glass jar, 30 cm in height and 25 cm in diameter. The reactor was equipped with two six-blade turbine impellers each 5 cm diameter (liquid stirrer), an air sparger, a pH controller, DO probe and a reflux condenser. Thermoregulator has been design using water bath to increase the maximum operating temperature to 70⁰C. Figures 3.1 show a fermentor operation diagram.



Figures 3.1: Diagram of 2L Biostat[®] micro-DCU bioreactor

The biooxidation study of pure mineral was run in a batch mode. Pure mineral (pyrite), 10g was added into 2.0L culture that grown in 3.2.3. Sample (10mL) were taken periodically from the start of the experiment till day 15. Sterilized distilled water at pH 2 (adjusted using H₂SO₄) was added into the reactor before sampling to replenish the condensate, maintaining the volume of slurry at 2.0L. Air and sample point were sprayed with ethanol (96%) to minimize contamination. Stirring speed was increased to 600rpm during sampling to ensure sample homogeneity.

Solution portion of sample was taken for KMnO₄ titration, in order to determine ferrous and ferric content. The pH and E_H of slurry was then taken before the slurry was filtered. Iron content in the filtrated was determined using AAS. The residue was then washed with 50mL distilled water and left to dry. HNO₃ (1M) 25mL was added to the dry residue for a minute to get rid of oxides and jarosite. The mixture was filtered and iron content in the filtrate was determined using AAS.

The acid washed residue was soaked with distilled water and dried. It was digested using 10mL aqua regia, (HCl : HNO₃ at the ratio 3:1). The slurry was heated

gently using water bath for 1.5hrs at 70°C. Upon cooling, the slurry was transferred into a 25mL volumetric flask. The sample was analysed using AAS

The parameter used for bioleaching of pyrite using stirred tank reactor is shown table 3.1:

Table 3.1: Parameter used for bioleaching of pyrite using STR

	Temp	Culture	Medium	Mineral size	Pulp densities
SET 1: TEMPERATURE					
Condition 1	70 ⁰ C	SL 5 B	ST medium	75 µm	1%
Condition 2	70 ⁰ C	Aseptic	ST medium	75 µm	1%
Condition 3	45 ⁰ C	ST	ST medium	75 µm	1%
Condition 4	45 ⁰ C	Aseptic	ST medium	75 µm	1%
Condition 5	30 ⁰ C	TF	9K	75 µm	1%
Condition 6	30 ⁰ C	Aseptic	9K	75 µm	1%
SET 1: SIZE					
Condition 1	70 ⁰ C	SL 5 B	ST medium	75 µm	1%
Condition 2 (pyrite only)	70 ⁰ C	SL 5 B	ST medium	125 µm	1%
Condition 3	70 ⁰ C	SL 5 B	ST medium	180 µm	1%
Condition 4 (pyrite only)	70 ⁰ C	SL 5 B	ST medium	250 µm	1%
Condition 5	70 ⁰ C	SL 5 B	ST medium	500 µm	1%
SET 1: PULP DENSITIES					
Condition 1	70 ⁰ C	SL 5 B	ST medium	75 µm	1%
Condition 2	70 ⁰ C	SL 5 B	ST medium	75 µm	3%
Condition 3	70 ⁰ C	SL 5 B	ST medium	75 µm	5%

3.2.1.6 Ferrous and ferric determination

Concentration of ferrous iron was determined by titrating with 0.001M potassium permanganate (KMnO_4) in the presence of ferroin indicator. To assess the concentration of total iron, ferric iron was reduced to ferrous iron using stannous chloride as reducing agent, followed by titration with 0.001M potassium permanganate (KMnO_4). The ferric iron concentration was then determined by subtracting the ferrous iron concentration from the total iron concentration. The end point was indicated by a change of color from orange to pale blue (Sjahrir, 2000).

3.2.1.7 Dissolved oxygen consumption rate.

The sample from stirred tank reactor was taken aseptically and filtrated using aseptic filter paper. The pyrite and its precipitated were considered separate from medium, but not the bacteria. The solution (2ml) then transferred into oxygen-saturated fresh medium (20ml) in 250 shake flasks. Sterile silicone oil (2ml) was added into inoculums to prevent any oxygen transfer between air and the solution. The culture was incubated at respective temperature and shaken at 150rpm. Sample from inoculums was taken at hrs 0, 24 and 48 using sterile syringe and the dissolved oxygen reading was recorded. The dissolved oxygen consumption rate was then determined to represent the presence of bacteria in the stirred tank reactor.

3.2.2 Result and discussions

3.2.2.1 Elemental analysis

Elemental analysis of the pyrite is shown in table 3.2. From the analysis, it was noted that the pyrite contained the significant heavy metals as the pyrite used by

previous researchers (Boon, 1996 and May et al 1997). It was also observed that the pyrite contains high concentrations of metals i.e: 44.36% iron, 0.08% silver, 0.06% aluminum and 0.04% Manganese. Copper, zinc, nickel and cobalt is found as trace elements. Pyrite also contains 46.28% sulfur and 0.06% carbon. It was also observed that the sample does not contain arsenic, which is generally associated with natural pyrite (Nemati and Harrison, 2000 and Jacques et. al., 2005).

Ratio of iron content over sulfur (Fe:S) is 0.9585, which is significant with a stoichiometry of FeS_2 at a 0.875 (ratio of Fe: 2S). A higher iron proportion might be due to the iron interference from the steel ball used for grinding the pyrite.

Table 3.2: Elemental analysis of pyrite using ICP-MS and Carbon-Sulfur Detector

Pyrite	Elemental content
Iron (Fe)	44.36 %
Sulfur (S)	46.28 %
Copper (Cu)	72.75 mg/L
Zinc (Zn)	62.75 mg/L
Nikel (Ni)	27.25 mg/L
Cobalt (Co)	90.50 mg/L
Silver(Ag)	0.0792 %
Aluminum (Al)	0.0594 %
Manganese (Mn)	0.0420 %
Carbon (C)	0.0593 %

Figures 3.2 (A and B) shows the SEM images of fresh pyrite surface. Pyrite was ground and sieve for 250 μm and 75 μm .

From the SEM micrograph of the 75 μm pyrite (fig.3.2-A), very fine particles was seen on the pyrite surface. The presence of very fine particle on a pyrite surface will retard the bacterial activity during bioleaching. Nemati, Lowenadler and Harrison (2000) have reported that decreasing the particle size to a diameter of 6.4 micron did not improve the rate of bioleaching. The presence of the fine particles apparently damaged the structure of the cells and, after a short period of operation, a dramatic decrease in

concentration of the cells was observed. This implies that the reduction of particle size below a critical level could increase the extent of the particle-particle collision and impose severe attrition on the cells. However, intensive agitation, aeration and attrition, which are usually associated with a tank bioleaching system, can adversely influence the activity of the cells.

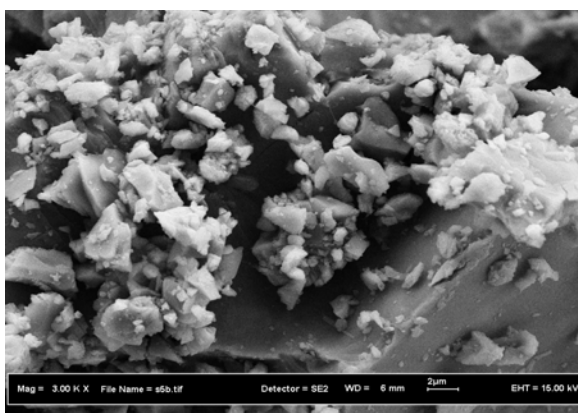


Figure 3.2-A: SEM images of ground, fresh pyrite surface. Pyrite was sieve at 75µm (Magnification 3000 X)

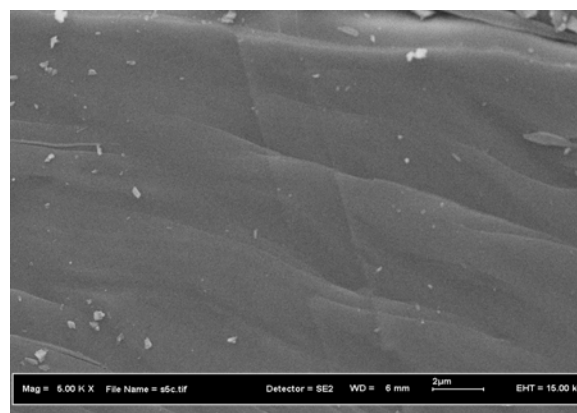


Figure 3.2-B: SEM images of ground, fresh pyrite surface. Pyrite was sieve at 250µm (Magnification 5000 X)

According to SEM images in figure 3.2-A, sample of pyrite has a highly crystalline surface structure. Sample can be classified as framboidal pyrite. The surface structure is comparable with SEM images from Boon et al. 1999 (figure 3.3A and B)

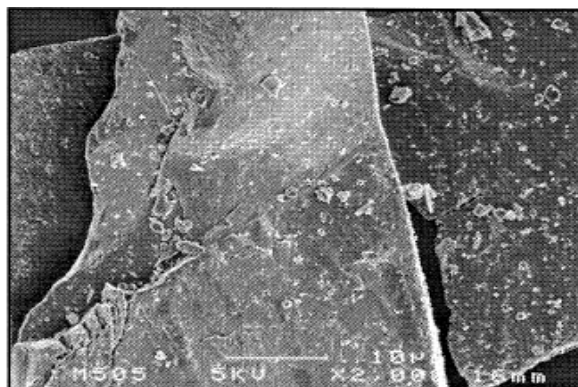


Figure 3.3-A: SEM photographs of a framboidal pyrite from Germany (Boon et al, 1999) (Magnification 2000 X)



Figure 3.3-B: SEM photographs of an euhedral pyrite from Prieska, South Africa (Boon et al, 1999) (Magnification 2000 X)

The German, framboidal pyrite has a granular and irregular surface structure, which is probably more chemically reactive than the highly crystalline surface structure of euhedral, Prieska pyrite. Some bioleaching-related culture i.e: *T. ferrooxidans* was not able to oxidise euhedral pyrite. It was reported that the maximum chemical oxidation rate of the framboidal pyrite, $v_{\text{FeS}_2, \text{max}(\text{framboidal})} = 0.017 \text{ h}^{-1}$, which is 2.5 times larger than $v_{\text{FeS}_2, \text{max}(\text{euhedral})}$ and the value of $B_{\text{framboidal}} = 200$, which is a factor of 10 smaller than B_{euhedral} . (Boon et al. 1999)

Where;

B: Kinetic constant in chemical pyrite oxidation

$v_{\text{FeS}_2, \text{max}}$; maximum chemical oxidation rate of the framboidal pyrite

That makes the sample used (Pyrite from Peru, euhedral pyrite) is more refractory than pyrite used by other workers.

Iron content analysis of the pyrite using AAS at a different fraction of size was determined individually and shown in table 3.3:

Table 3.3: Iron concentration of pyrite at a different diameter

Size	75 μm	106 μm	180 μm	250 μm	500 μm
Fe (%)	42.36	40.78	39.67	41.97	36.86

Iron content analysis show that the Fe concentration of pyrite is ranges from 42.36% to 36.86% for pyrite size from 75 μm to 500 μm . This descending trend in the iron concentration with regards to increasing size is due to the larger particles of pyrite containing a high amount of silica. (Nemati et al, 2000). Grindability index for silica sand at 35 HGI (Hardgrove grindability index) is higher than pyrite, at 13HGI

3.2.2.2 STR biooxidation of pyrite using different types of culture

Manipulation of thermophilic acidophiles in bioleaching processes has also been reported to enhance the dissolution of finely ground mineral sulphide in stirred tank reactors (Sampson and Philips, 2001; Sandstrom and Petersson, 1997; Norris *et al*, 2000) and in bioheap processes (Brierley, 1999). A comparison of mesophilic, moderately thermophilic and thermophilic acidophiles bacteria on pyrite oxidation was used in this test. Bacterial leaching of pyrite using different types of culture was conducted using 2L Biostat[®] bioreactor. Stirred tank reactor contains isolate SL5B, *Sb. thermosulfodooxidans* and *T. ferrooxidans* in the respective media and. 1% Peru, euhedral pyrite (D= 75 μ m). Control set of experiments were conducted at 70°C, 45°C and 30°C

Figure 3.4A shows a percentage pyrite oxidation using different types of culture namely *T. ferrooxidans* (mesophilic), *Sb. thermosulfodooxidans* (moderate thermophilic) and isolate SL5B(thermophilic). Figures 3.4B shows natural oxidation of pyrite at sterile condition. The experiment was using respective medium at 70°C, 45°C and 30°C.

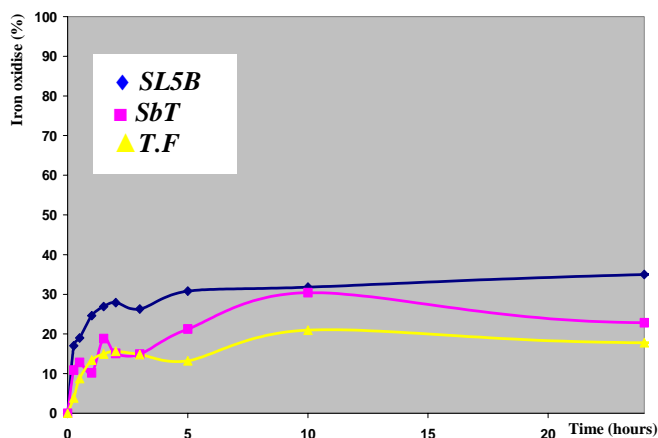


Figure 3.4A: Percentages of pyrite solubilize during 24 hours oxidation using different type of culture, TF (30°C), ST (45°C) and SL5B(70°C).

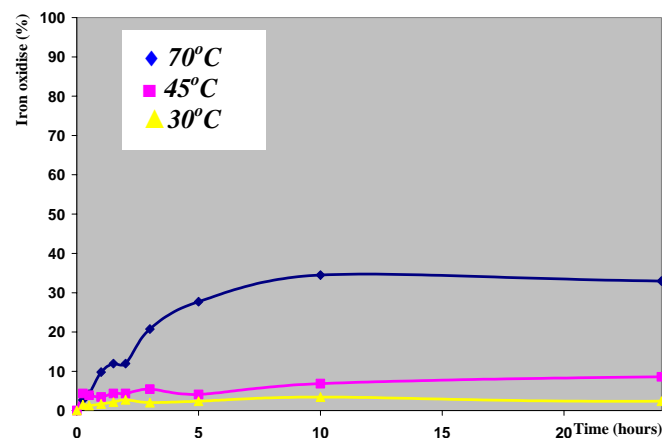


Figure 3.4B: Percentages of pyrite solubilize during 24 hours, natural oxidation occurs at different temperature, 30°C, 45°C and 70°C. Systems were run without a present of culture

The pyrite oxidation capacity was determined using the following equation:

$$\text{Pyrite oxidation \%} = \frac{[\text{Fe}_{\text{py residue, initial}}] - [\text{Fe}_{\text{py residue, test}}]}{[\text{Fe}_{\text{py residue, initial}}]} \quad \text{Eq. 3.1}$$

$[\text{Fe}_{\text{py residue, initial}}]$: iron content in non- biooxidized pyrite after treat with 1M H_2SO_4

$[\text{Fe}_{\text{py residue, test}}]$: : iron content in biooxidized pyrite after treat with 1M H_2SO_4

Solid-liquid contact between Fe^{3+} and pyrite surface was maximized at the initial stages of biooxidation (first 24hrs after addition of pyrite), before iron and sulfur precipitation and porous product layer become a rate limiting step. Percentages of the iron dissolution increased drastically during first 2 hours of biooxidation using entire culture (Figure 3.2A). After 5 hours oxidation, 26.9%, 18.8% and 14.9% pyrite were oxidized by SL5B, *Sb.Thermosulfodooxidans* and *T. Ferrooxidans* respectively.

The pyrite oxidation trend during 5hour to 24hours of bioleaching indicated that the bioleaching capacity of thermophilic bacteria (SL5B) is quite similar compared with control at 70°C . However, the solubilization rate of *Sb.Thermosulfodooxidans* and *T. Ferrooxidans* are obviously high compared with its control at 30°C and 45°C . These results were consistent with the reports (Kandemir, 1985 and Sand et al., 2001).

Regarding to Kandemir, 1985 and Sand et al., 2001, the efficiency of leaching was directly related to the Fe^{3+} and H^+ concentrations in solution. All of sulphides have valence bands formed by atomic orbitals from both metallic and sulphur atoms. The result is that these sulphides can be attacked not only by Fe^{3+} but also by protons (Ruitenberg *et al.*, 1999 and May *et al.*, 1997). The control experiment at 30°C has a low Fe^{3+} concentration; however, sulphuric acid will provide protons to the medium for the mineral hydrolysis. (Battaglia-Brunet et al., 1998 and Bosecker, 1997)

Experiment at 70°C indicated a higher percentage of Fe^{3+} ions as shown in figure 3.13 (for abiatic and biotic leaching). Higher temperature would promote the formation of ferric iron even at low solution pH value. (Holliday and Richmond, 1990). Figure 3.5

shows that the initial pyrite dissolution via ferric oxidation (control 70⁰C) is 10.02 times higher compared to acid leaching (control at 30⁰C).

The findings also indicated the high leaching capacity of Fe³⁺ is limited until the 5th hour (figure 3.13-biooxidation with SL5B and control at 70⁰C). The rate of pyrite oxidation is presumably zero during 5 to 24 hours for control at 70⁰C and SL5B. Compared with the system dominated by acid leaching i.e: Control at 45⁰C and 30⁰C (due to the low Fe³⁺/Fe²⁺ reading at figure 3.13), the pyrite oxidation rate were steadily occur at the rate 0.1667 and 0.0984 (ppm Fe /hour) respectively until the 24 hours. Its might be due to the high tendency of jarosite formation in the high temperature and high concentration of Fe³⁺, where the biooxidation process was retard by diffusion of product layer as a limiting step.

Due to the formation of jarosite was minimal for the initial stages of biooxidation (first 24 hours). The rate of solubilization of pyrite for the can be expressed into shrinking core and particle model with the film diffusion and chemical reaction considered as a limiting step.

3.2.2.3 Shrinking particle model for diffusion through liquid film as a limitation step

From the figure D2-D7 (attachment D), where $1-(1-X_B)^{2/3}$ vs leaching time (Shrinking particle model for diffusion through liquid film as a limitation step), the time required for complete pyrite oxidation for each set of biooxidation experiment can be predicted and it shown in table 3.4.

Table 3.4: Time required (t_{total}) for complete pyrite oxidation if the shrinking particle model for diffusion through liquid film as a limitation step

Culture	$1-(1-X_B)^{2/3}$ vs t	T_{total}	Regression coefficient (R^2)
SL5B	$t = 0.0298x + 0.1014$	30.15	0.5161
Control (70°C)	$t = 0.0386x + 0.0127$	25.58	0.9681
<i>Sb. Thermosulfodooxidans</i>	$t = 0.0048x + 0.0857$	190.48	0.3781
Control (45°C)	$t = 0.0016x + 0.0228$	610.75	0.6394
<i>T. Ferrooxidans</i>	$t = 0.0033x + 0.0689$	282.15	0.3136
Control (30°C)	$t = 0.0004x + 0.0113$	2471.75	0.2113

3.2.2.4 Shrinking core model for diffusion through liquid film as a limitation step

From the figure D2-D7 (attachment D), where X_B vs leaching time (Shrinking core model for diffusion through liquid film as a limitation step), the time required for complete pyrite oxidation for each set of biooxidation experiment can be predicted and it shown in table 3.5.

Table 3.5: Time required (t_{total}) for complete pyrite oxidation if the shrinking core model for diffusion through liquid film as a limitation step

Culture	X_B vs t	T_{total}	Regression coefficient (R^2)
SL5B	$t = 0.0416x + 0.1467$	20.51	0.5018
Control (70°C)	$t = 0.0549x + 0.0203$	17.85	0.9638
<i>Sb. Thermosulfodooxidans</i>	$t = 0.0048x + 0.0857$	190.48	0.3746
Control (45°C)	$t = 0.0024x + 0.034$	402.50	0.6342
<i>T. Ferrooxidans</i>	$t = 0.0048x + 0.1009$	187.31	0.3093
Control (30°C)	$t = 0.0006x + 0.0168$	1638.67	0.2111

3.2.2.5 Shrinking core and particle model for chemical reaction on pyrite surface as a limitation step

The time required for complete pyrite oxidation for each set of biooxidation experiment can be predicted and it shown in table 3.6 (figure D2-D7: attachment D).

Table 3.6: Time required (t_{total}) for complete pyrite oxidation if the shrinking core model for diffusion through liquid film as a limitation step

Culture	$1-(1-X_B)^{1/3}$ vs t	T_{total}	Regression coefficient (R^2)
SL5B	$t = 0.016x + 0.0526$	59.21	0.5305
Control (70°C)	$t = 0.0204x + 0.0059$	48.73	0.9720
<i>Sb.Thermosulfodooxidans</i>	$t = 0.0026x + 0.0441$	367.66	0.3781
Control (45°C)	$t = 0.0008x + 0.0115$	1235.63	0.6446
<i>T. Ferrooxidans</i>	$t = 0.0017x + 0.0353$	567.47	0.3179
Control (30°C)	$t = 0.0002x + 0.0056$	4972.00	0.2115

From tables 3.4, 3.5 and 3.6, it is clearly shows that the addition of *T. ferrooxidans* and *Sb.thermosulfodooxidans* will accelerate the biooxidation process to around 8.7 times fold and 3.0 times fold respectively. However, for the biooxidation process at 70°C, the system without culture showed the higher initial biooxidation rate compared to with the present of SL5B.

Compared to table 3.2, figure 3.5 shows the pyrite solubilization profiles carried out for 15 days. Figure 3.5-A shows the pyrite oxidation profiles in the presence of SL5B, *Sb.thermosulfodooxidans* and *T. ferrooxidans*, while, figure 3.5-B shows the pyrite oxidation profiles minus the presence of culture at 30°C, 45°C and 70°C.

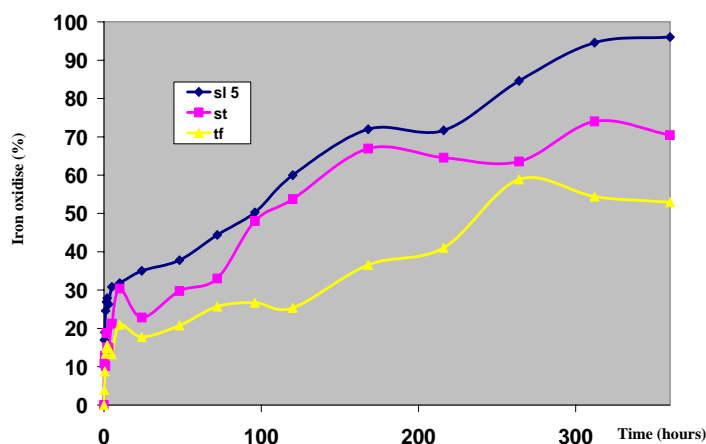


Figure 3.5-A: Percentages of 15 days pyrite solubilization. Oxidation using different type of culture, *T. Ferrooxidans* (30⁰C), *Sb. Thermosulfodooxidans* (45⁰C) and SL5B(70⁰C).

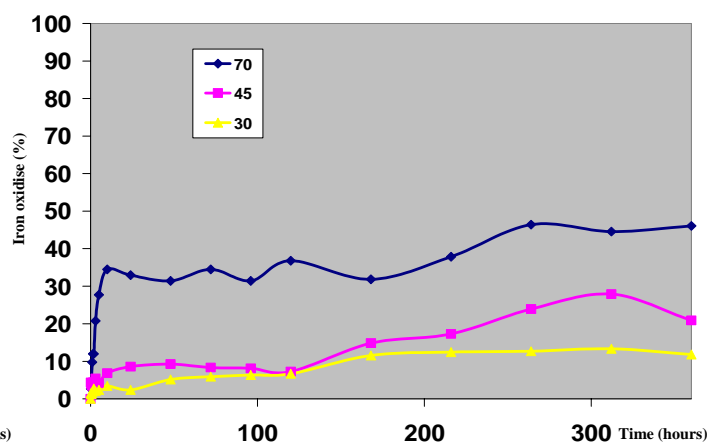


Figure 3.5-B: Percentages of 15 days pyrite solubilization. Natural oxidation occurs at different temperature, 30⁰C, 45⁰C and 70⁰C. Systems were run without a present of culture

It was interesting to note that pyrite bioleaching in the presence of SL5B resulted in 96.05% iron oxidation. Also, the biooxidation rate using SL5B was 1.36 and 1.81 times higher compared to the biooxidation rate in the presence of *Sb.thermosulfodooxidans* and *T. ferrooxidans* respectively

It was also observed from fig 3.5-A that biooxidation of pyrite was enhanced in the presence of the thermophilic bacteria *SL5B* as compared to the mesophilic, *T. ferrooxidans*. This could be due to greater dissolution of sulphide mineral at elevated temperature. This was consistent with the reports for the improved dissolution kinetics of sulphides by extremely thermophilic bacteria (Dew et al., 1999; Konishi et al., 1998; Witne and Phillips, 2001). Also, the ability of the thermophilic culture *SL5B* to maintain low pH and high Eh values (figures 3.6-I_(test) and figures 3.6-II_(control)) could become important for the biooxidation process so that the formation of potentially deleterious precipitates could be minimized (figures 3.7-I_(test) and figures 3.7-II_(control)). These results were consistent with that reported by Arslan and Arslan, 2003; Dutrizac, 1983; Konishi et al., 1998a and Welham et al., 2000)

In general, bioleaching process can be divided into three stages. An initial stage with extensive Fe^{3+} attack to the pyritic surface, which liberates Fe^{2+} . The presence of high concentration of Fe^{2+} in solution, causes an increase in the concentration of free cells, which uses Fe^{2+} as an energy source. A small amount of bacteria is found attached to the pyritic phase. This stage is of major importance in order to obtain high dissolution rates. In second stage a balance between free and attached cells is reached, giving rise to a cooperative mechanism. In this case, the attached cells attack the pyrite phase of the mineral generating Fe^{2+} . This in turn is oxidized by the free cells in solution, regenerating the oxidizing agent (Fe^{3+}) for the indirect bioleaching of the mineral. The third stage involved extensive bacterial attachment to the pyritic phase. Pyrite surface is then saturated by the attached cells. Free cell slightly diminishes due to the saturation of the Fe^{3+} in solution (González et. al.1999 and Norris *et al*, 2000).

Referring to the pyrite solubilization trends (fig 3.6A), Trends of jarosite formation and ferric-ferrous trend (figures D-8 to D-13, Attachment D) and dissolved oxygen trends (figures D-14 to D-16, Attachment D). The leaching stages of *SL5B*, *Sb.thermosulfodoxidan* and *T. ferrooxidans* can be summarized in table 3.7:

Table 3.7: Biooxidation stages of SL5B, *Sb.thermosulfodoxidan* and *T. ferrooxidans*

Culture		SL5B	<i>Sb.T</i>	<i>T. F</i>
1 st stage	Times (hrs)	0-2	0-10	0-10
	Solubilization rate: ($\%_{\text{Fe}_{\text{sol}}}/\text{hr}$) (0-2 nd hrs)	17.787	10.281	9.5787
2 nd stage	Times (hrs)	2-168	24-168	24-120
	Solubilization rate: ($\%_{\text{Fe}_{\text{sol}}}/\text{hr}$) (24 th -120 th hrs)	0.2604	0.3336	0.087
3 rd stage	Times (hrs)	216-360	216-360	168-360
	Solubilization rate: ($\%_{\text{Fe}_{\text{sol}}}/\text{hr}$) (216 th – 360 hrs)	0.1731	0.0587	0.065

From table 3.7 it was observed that the highest solubilization rate of pyrite has been obtained at an initial stage of biooxidation (Fe^{3+} attack). Solubilization rate for the first 2 hrs oxidation are as follows; 17.79 ($\%_{\text{Fe sol}}/\text{hr}$), 10.28 ($\%_{\text{Fe sol}}/\text{hr}$) and 9.58 ($\%_{\text{Fe sol}}/\text{hr}$) for SL5B, *Sb.thermosulfodoxidan* and *T. Ferrooxidans* respectively. The lowest iron solubilization rate was observed when the bacterial attachment to a pyrite surface was maximum (3rd stage). Iron solubilization rate during the 216th to 316th hours was at 0.1731 ($\%_{\text{Fe sol}}/\text{hr}$), 0.059 ($\%_{\text{Fe sol}}/\text{hr}$) and 0.065 ($\%_{\text{Fe sol}}/\text{hr}$) for SL5B, *Sb.thermosulfodoxidan* and *T. ferrooxidans*. This rate was 10 fold lower than that observed during the first stage, which assumes that pyrite solubilization rate was controlled by diffusion of reactant (Fe^{3+}) through permeable layer of pyrite oxidation product around the particle.

3.2.2.6 Shrinking core model with diffusion of porous inert layer as a limitation step

The iron oxidation behaviour for the 360 hrs can be simplified and elaborated into a shrinking core model with the film diffusion with product layer considered as the controlling step as shown in equation C-51 (attachment C). From figures D-17 to D-19, the reaction model and required reaction time (T_{total}) can be predicted in table 3.8.

Table 3.8: The required bioleaching time for pyrite biooxidation using for SL5B, *Sb.thermosulfodoxidan* and *T. ferrooxidans* and its control, when product layer diffusion becomes a rate limiting step in leaching reaction:

Initial pyrite size (r)	$1-3(1-X_B)^{2/3}+2(1-X_B)$ vs t	T_{total}	Regression coefficient (R^2)
SL5B	$t=0.0018XB-0.0034$	557.4 hrs	0.95
70°C	$t=0.0002XB+0.0159$	4920.5 hrs	0.78
<i>Sb.thermosulfodoxidan</i>	$t=0.0008XB+0.0104$	1237.0 hrs	0.93
45°C	$t=0.00006XB-0.0002$	16670.0 hrs	0.81
<i>T. ferrooxidans</i>	$t=0.0004+0.0016$	2496.0 hrs	0.88
30°C	$t=0.00002+0.0001$	49995.0 hrs	0.90

From table 3.8, it was clear that the regression coefficient for shrinking core model with the product layer diffusion as controlling step is definitely high compared to the shrinking core and particle model with the film diffusion and chemical reaction as controlling step. i.e : (R^2) were at 0.95, 0.93 and 0.88 (shrinking core model with the product layer diffusion) compared to 0.5,0.4 and 0.3 (shrinking core and particle model with the film diffusion and chemical reaction as controlling step, Table 3.5 and 3.6) for biooxidation using *SL5B*, *Sb.thermosulfodoxidan* and *T. ferrooxidans* respectively. Its show that the product layer diffusion is become dominant to the pyrite oxidation process in STR. However, it is like to note that the time required for complete oxidation of pyrite is highly increased if the product layer diffusion become a rate limiting step, as an example, the t_{total} were increased 9.4, 3.4 and 4.4 times fold higher compared to the chemical reaction as limiting step (Table 3.6) for the STR biooxidation using *SL5B*, *Sb.thermosulfodoxidan* and *T. ferrooxidans* respectively.

3.2.2.7 Redox potential (E_H) and pH profile for STR biooxidation of pyrite using different types of culture

Figures 3.6 (I-VI) shows the pH and E_H profile during bioleaching. TetraCon[®] combined electrode with WTW multi lab P4 meter was used to monitor solution pH. The electrode was standardized using 1 point calibration using pH-2 (di- Sodium hydrogen phosphate/potassium dihydrogen phosphate/orto-phosphoric acid) buffer solution. Solution redox potential was determined using WTW-SenTix ORP electrode. The electrode was filled with 3M KCl solution. The thermodynamic relation of the potential E_H to the composition of the solution is generally known as the Nernst equation (Stumm and Morgan, 1996) (Eq 3.2):

$$E_H = E_H^0 + \frac{2.303.R.T}{n.F} \log \frac{\prod_i \{ox\}^{n_i}}{\prod_i \{red\}^{n_i}} \quad \text{Eq. 3.2}$$

The redox potential measures the tendency for a solution to either gain or lose electrons when it is subject to change by introduction of a new species. A solution with a higher redox potential will have a tendency to gain electrons from new species (i.e. oxidize them) and a solution with a lower redox potential will have a tendency to lose electrons to new species (i.e. reduce them).

If it is assumed that the ferric/ferrous exchange current density at the surface of a leaching particle is large enough to make the effect of the corrosion current, the surface potential of the particle can be considered equal to the redox potential of the solution at the surface. (Eaton, 1995) .A measurement of the solution redox potential can be related to the ratio of free ferric to free ferrous iron in an iron solution via the Nernst equation (Eq. 3.2).

$$E = E^{\circ} + \frac{RT}{zF} \ln \frac{[\text{Fe}^{3+}]}{[\text{Fe}^{2+}]} \quad \text{Eq. 3.2}$$

Although measurement of the redox potential in aqueous samples is relatively straightforward, many factors limit its interpretation, such as irreversible reactions, slow electrode kinetics, non-equilibrium, presence of multiple redox couples, electrode poisoning, small exchange currents and inert redox couples. (ABB Instrumentation, 1999)

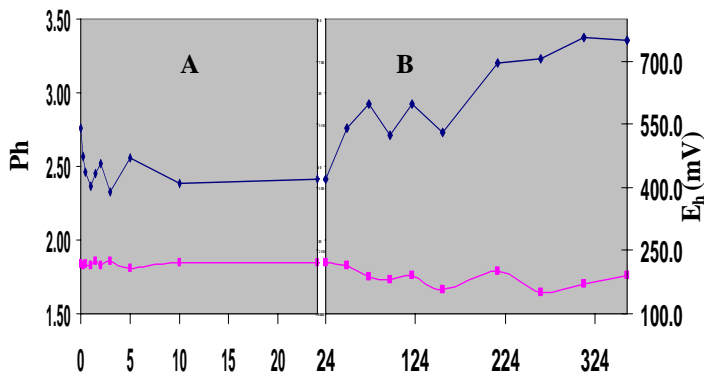


Figure 3.6-I: pH \blacksquare and E_h \blacklozenge profile during biooxidation study in STR using SL5B at 70°C.

A: Profile for first 24 hours of biooxidation

B: Profiles for day 1 to day 15 of biooxidation

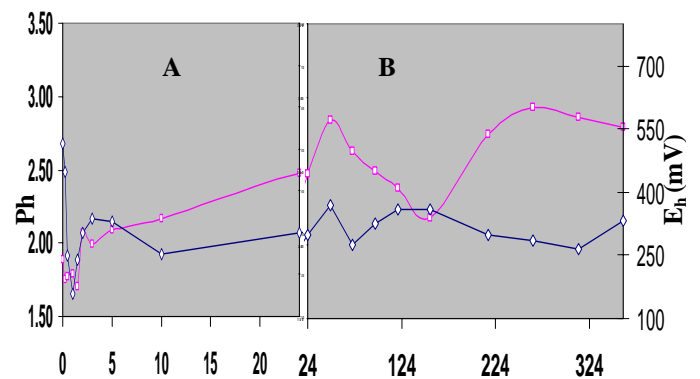


Figure 3.6-II: pH \blacksquare and E_h \blacklozenge profile during natural oxidation in STR using *Sb.Thermosulfidooxidans* medium at 70°C. Sterile condition

A: Profile for first 24 hours of oxidation

B: Profiles for day 1 to day 15 of oxidation

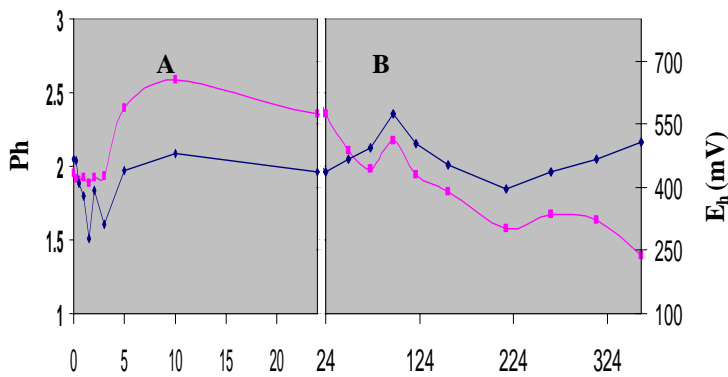


Figure 3.6-III: pH \blacksquare and E_h \blacklozenge profile during biooxidation study in STR using *S.Thermosulfidooxidans* at 45°C.

A: Profile for first 24 hours of biooxidation

B: Profiles for day 1 to day 15 of biooxidation

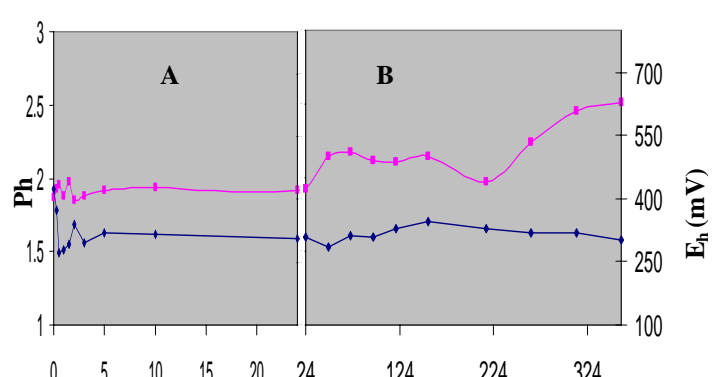


Figure 3.6-IV: pH \blacksquare and E_h \blacklozenge profile during natural oxidation in STR using *Sb.Thermosulfidooxidans* medium at 45°C. Sterile condition

A: Profile for first 24 hours of oxidation

B: Profiles for day 1 to day 15 of oxidation

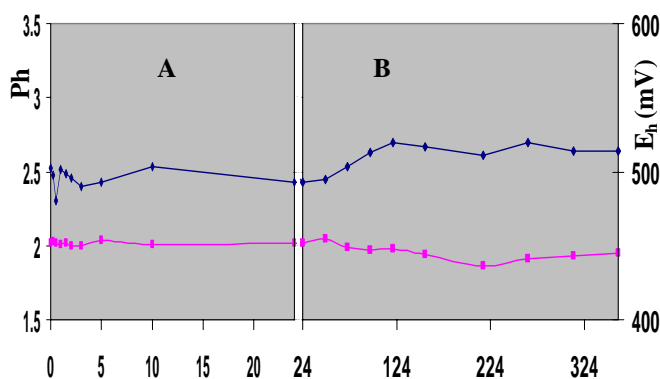


Figure 3.6-V: pH \blacksquare and E_h \blacklozenge profile during biooxidation study in STR using *T. Ferrooxidans* at 30°C.

A: Profile for first 24 hours of biooxidation

B: Profiles for day 1 to day 15 of biooxidation

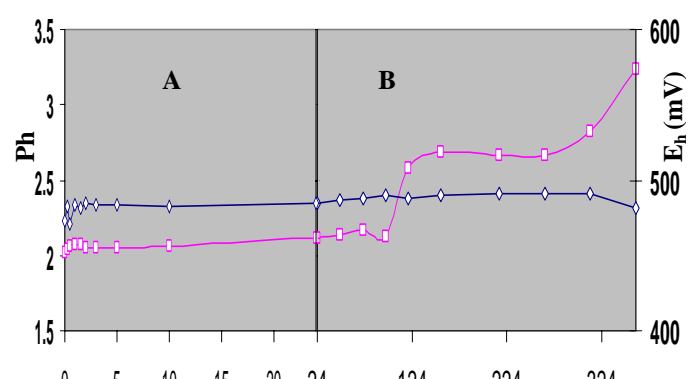


Figure 3.6-VI: pH \blacksquare and E_h \blacklozenge profile during natural oxidation in STR using 9K medium at 30°C. Sterile condition

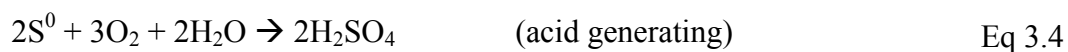
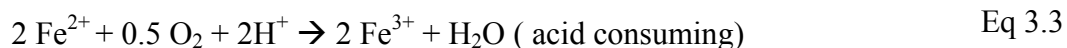
A: Profile for first 24 hours of oxidation

B: Profiles for day 1 to day 15 of oxidation

From figures 3.4 it was shown that SL5B, *Sb.thermosulfodoxidan* and *T. ferrooxidans* was able to maintain the low pH and high E_H of solution compared to its control. It can be clearly seen that the pH profiles for the test experiment (containing culture) remained below pH 2.0 (except for the first 24 hrs for *S.thermosulfodoxidans*). However, overall ph of SL5B i.e; 1.64 -1.86 was lower as compared to the overall pH of *T.ferrooxidans* which was between 1.91 to 2.04.

It is interesting to note that the initial E_H value decreased drastically at a magnitude of 129.46 mV/hrs (0-1st hrs of culture SL5B), 124.49 mV/hrs (0-1.5th hrs of *Sb.thermosulfodoxidan*), 45.4 mV/hrs (0-0.5th hrs of *T. ferrooxidans*), 377.05 mV/hrs (0- 1st hrs of control at 70⁰C), 301.59 mV/hrs (0-0.5th hrs of control at 45⁰C) and 3.0 mV/hrs (0-0.5th hrs of control at 30⁰C). At this zone, there was extensive attack of Fe^{3+} ion on the pyrite surface, producing Fe^{2+} , leading to the decrease in Fe^{3+} / Fe^{2+} ratios.

During the biooxidation process, Fe^2 is oxidized $^+$ to Fe^{3+} (Equation 3.3) and S^0 to SO_4^{2-} (Equation 3.4) in acidic sulphate medium (Harrison 1982).

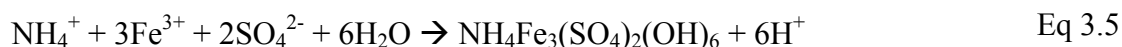


By regenerating ferric iron, the bacteria is able to maintain a high redox potential in bioleaching systems. The existence of an indirect mechanism implies that the bacterial and chemical sub-processes can be characterised separately, allowing for the independent optimisation of bacterial growth and metabolism and mineral oxidation kinetics.

The pH trend for the control set (without culture) were remains increased from pH 1.89 to pH 2.93 (control at 70⁰C), pH 1.87 to pH 2.51 (control at 45⁰C) and pH 2.02 to pH 3.24 (control at 30⁰C). For the elevated temperature condition (control at 70⁰C

and 45⁰C) the increasing of pH is relative to the formation of jarosite and iron oxide (Table D-2 and D-4, attachment D).

The similar finding was also reported by Arslan and Arslan, 2003; Dutrizac, 1983; Konishi et al., 1998; Welham et al., 2000. A high temperature would promote the precipitation of ferric iron even at low solution pH values. The formation of jarosite is a crystallization and acid consuming reaction, shown by the following stiochiometry (Equation 3.5, Elgesma *et al*, 1990). :



However, for the control at 30⁰C, the Fe³⁺ concentration in the solution is very low and the tendency of jarosite formation is very low. High pH trend for control at 30⁰C might be due to the formation of sulfur during the leaching. Elemental sulfur formation is favoured in a high acidity and low temperature solution, its become stable end product. Therefore, the oxidation of pyrite at 30⁰C is not reaching final sulfur oxidation state like sulfate(Bo Hu 2002). It will resulting a fluctuations in the pH value as shown in figure 3.7-IV.

The pyrite solubilization of control at 30⁰C (figure 3.7-IV) takes place in the absence of ferric iron. The the pyrite solubilization probably proceeds via the acid attack. Kandemir, 1985 and Sand et al., 2001, have reported that oxidation of mineral sulphate by the acid attack, results in the formation of polythionates. Kandemir (1985) also reported that, in the absence of ferric iron, the overall oxidation of mineral sulphate is controlled by the removal of sulphur deposited on the mineral surface via sulfur oxidation pathways . And the oxidation of pyrite via sulfur oxidation pathways is a slow reaction. Sulfur oxidation pathways during pyrite dissolution are shown in figure 3.7A (Bo Hu 2002). Figure 3.7B shows the formation of sulfur on the pyrite surface after natural leaching (without culture) using 9K medium at 30⁰C for 15 days.

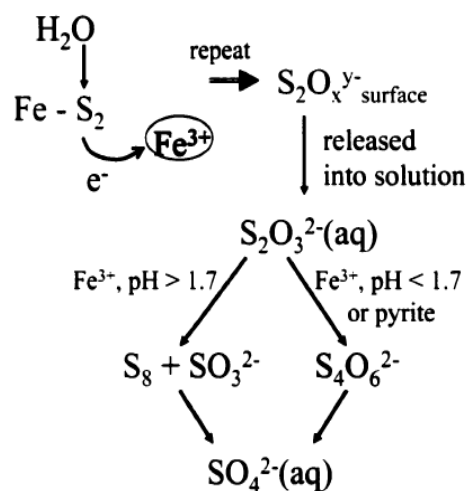


Figure 3.7A: Sulfur oxidation pathways during natural pyrite oxidation

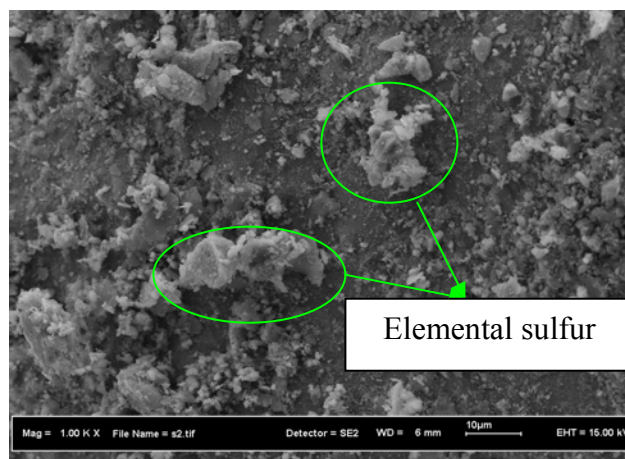


Figure 3.7B: SEM photographs of a pyrite surface after 15 days leaching at 30°C, in the absent of culture (Magnification 1000 X)

3.2.2.8 Iron solubilization and jarosite formation in the STR biooxidation of pyrite using different types of culture

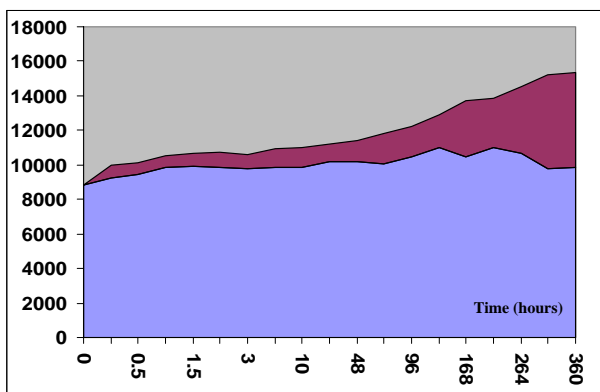


Figure 3.8-I: Concentration of iron present in medium ■ and jarosite ■ after 15 days biooxidation using SL5B at 70°C.

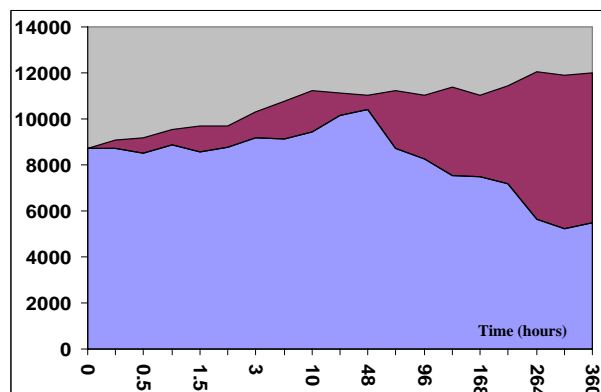


Figure 3.8-II: Concentration of iron present in medium ■ and jarosite ■ after 15 days leaching using *S. termosulfidoxidans* medium at 70°C. Acted as control test (sterile condition)

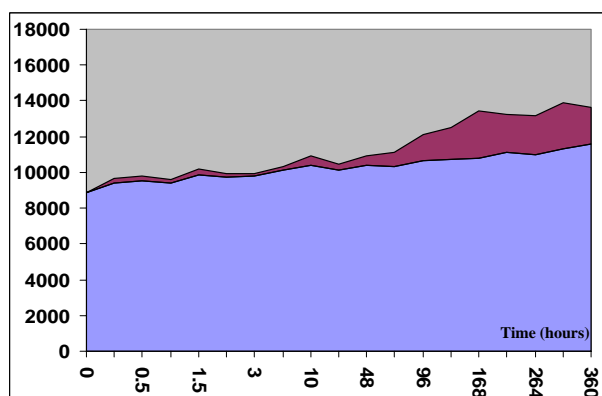


Figure 3.8-III: Concentration of iron present in medium ■ and jarosite ■ after 15 days biooxidation using *S. termosulfidoxidans* at 45°C.

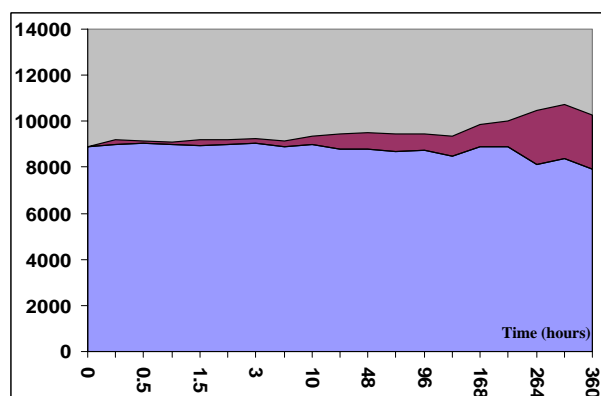


Figure 3.8-IV: Concentration of iron present in medium ■ and jarosite ■ after 15 days leaching using *S. termosulfidoxidans* medium at 45°C, Acted as control test (sterile condition)

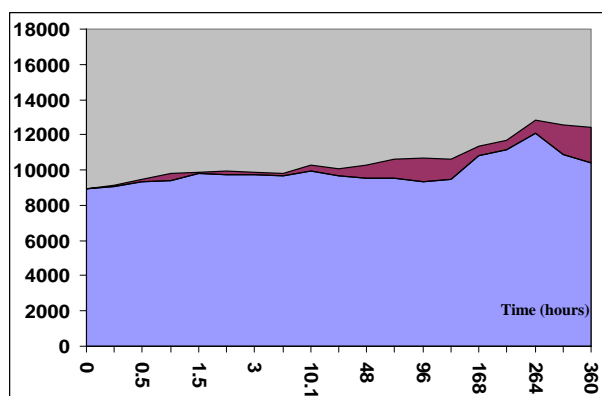


Figure 3.8-V: Concentration of iron present in medium ■ and jarosite ■ after 15 days biooxidation using *T. ferrooxidans* at 45°C.

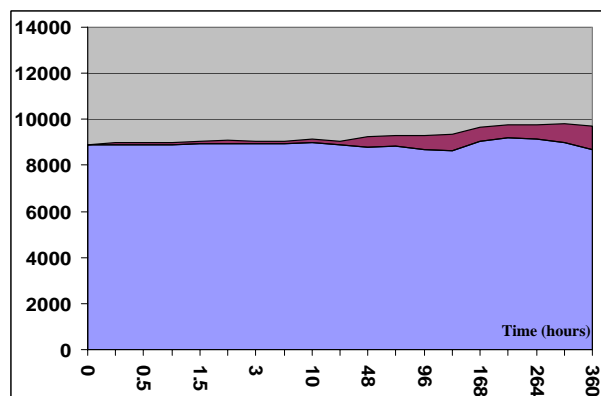


Figure 3.8-VI: Concentration of iron present in medium ■ and jarosite ■ after 15 days leaching using 9K at 30°C, Acted as control test (sterile condition)

Figures 3.8 I-VI shows the iron speciation in a medium solution and in the form of jarosite and iron oxides. Based on experiments in figures 3.8 I to VI, formation of iron hydroxide precipitation is related to the temperature of process. Highest rate of precipitation was observed at 70°C (Figure 3.8 I and II). The overall rate of precipitation is at 21.38 ppm_{Fe} / hrs for control (Table D-2, attachment D) at 70°C and 16.15 ppm_{Fe} / hrs for SL5B (Table D-1, attachment D). Iron precipitation during 15 days pyrite biooxidation using SL5B is 1.83 and 3.4 times fold higher than using *Sb.thermosulfodoxidans* and *T.ferrooxidans* respectively (Table D-3 and D-5, attachment D).

Jarosite formation in control experiment at 70°C is found to take 2.97 and 7.19 times fold higher than control experiment at 45°C and 30°C respectively. The overall iron precipitation rate can be expressed in table 3.9:

Table 3.9: The rate of pyrite formation

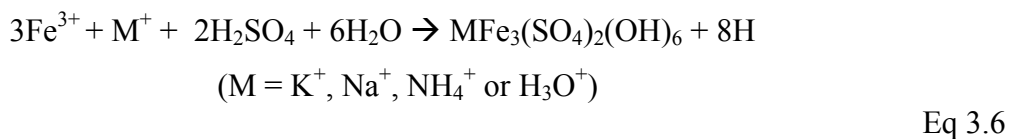
	$d[Fe_{\text{precipitation, ppm}}] / dt_{hr}$	Regression coefficient
SL5B	$d[Fe] / dt = 13.001t + 745.41$	0.96
Control at 70°C	$d[Fe] / dt = 17.49 t + 921.09$	0.93
<i>S. Thermosulfodoxidans</i>	$d[Fe] / dt = 7.2032 t + 358.19$	0.82
Control at 45°C	$d[Fe] / dt = 6.2737 t + 218.34$	0.93
<i>T. Ferrooxidans</i>	$d[Fe] / dt = 3.9155 t + 290.63$	0.64
Control at 30°C	$d[Fe] / dt = 2.2809 t + 164.45$	0.80

Another factor which influences the formation of jarosite is pH, Fe³⁺/Fe²⁺ ratios, pulp densities, Fe concentration and the presence of alkaline cation i.e: K⁺, Na⁺, NH₄⁺ or H₃O⁺. The extensive precipitation of jarosite presumably affects the overall pyrite leaching. The formation of jarosites occurs via free ferric ion precipitates, which leads to the decrease in the concentration of ferric ion in solution (fig 3.8-II), reduce Eh value and increased pH value (fig 3.6-II and IV). Precipitation of jarosite leads to

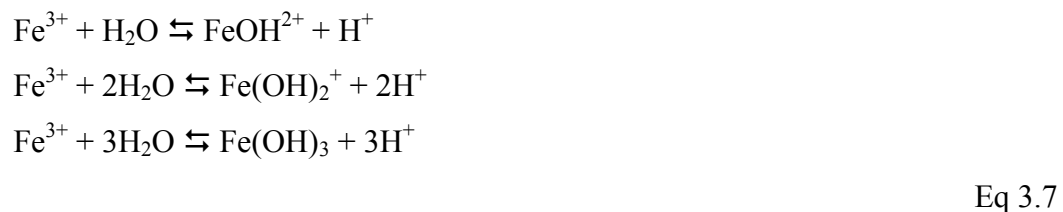
agglomeration and crystallization, which will form a protective layer on the mineral surface, thus retarding the continued dissolution of pyrite. (Elgersma *et al.*,1993).

Instead of a maintaining low pH value by SL5B, it has the potential to prevent massive formation of jarosite and iron oxides at elevated temperature (fig 3.8-I compare to 3.8-II) which is another key factor for the successful near-complete oxidation of euhydrated pyrite (96.05%). In this state, high concentrations of Fe³⁺ ion is in the free form in solution which leads to the increase in E_H value, which the best possible leaching condition.

However, the bioleaching behaviour of *S. thermosulfidooxidans* is slightly different with SL5B. Even at high pH value (pH~2.5) and elevated temperature (fig 3.6-III A), the amount jarosite precipitation is minimized (fig. 3.8-III and 3.8- IV). Jarosite was precipitated after the 48th hour. In the following periods, the pH value decreased from pH 2.11 to pH 1.39, probably as a result of excessive consumption of alkaline cation (K⁺, Na⁺, NH₄⁺ and H₃O⁺) due to the precipitation. The stoichiometry of jarosite formation is show in equation 3.6 (Nemati *et al.*, 1998)



Instead of jarosite precipitation, the hydrolysis of ferric iron is a acid producing reaction, thus reducing the pH, and tends to stabilise the low pH. The ferric iron hydrolysed in aqueous solution is shown as follows (Nemati *et al.*, 1998):



However, the precipitation behaviour for the control at 70°C was very different when pH increased (fig 3.6-II and 3.6- IV) with increased jarosite formation. (fig 3.8-II and 3.8-IV). Jarosite formation reactions would also contribute to the acid consumption as shown in equation 3.6.

Another factor which affects the jarosite formation behaviour is presence of K^+ , NH_4^+ , and Na^+ in solution. The behaviour of K^+ and Na^+ during the precipitation of iron was in accordance with the relative stability of K-jarosite over Na-jarosite, as suggested by Dutrizac (1983), who reported that participation of alkali ions in the jarosite structure would be in the order of $K^+ > NH_4^+ > Na^+$.

Dutrizac (1983) reported the minimum concentrations of Fe^{3+} , K^+ , and Na^+ in solution to be 0.001 M, 0.02 M, and 0.05 M respectively, for the precipitation of jarosites presumably at high temperatures. Despite the relatively low operating temperature the precipitation of K-jarosite was observed to occur from solutions containing 4.2 mM K^+ and 12 mM Na^+ .

Fig 3.9 shows the formation of jarosite on a pyrite surface after abiotic leaching at 70°C (control) compared with sulfur attachment on pyrite surface (Figure 3.10), abiotic leaching at 30°C. Jarosite is in the crystallized and agglomerated form, and have a high tendency to attach on a mineral surface.

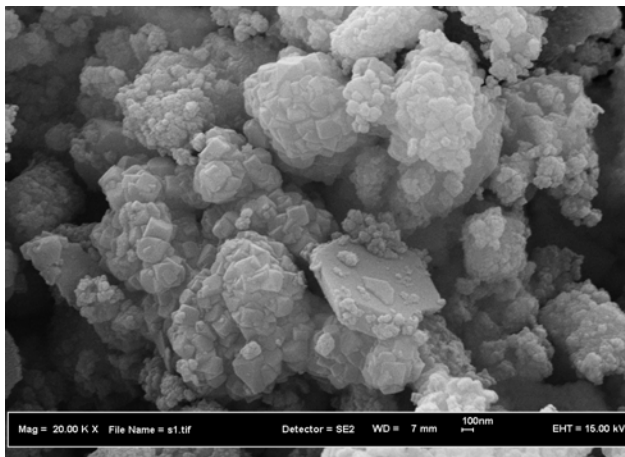


Figure 3.9: SEM photographs of a jarosite attach on a pyrite surface. Precipitation of jarosite during 15 days abiotic leaching at 70°C, control, in the absence of culture (Magnification 20 000 X)

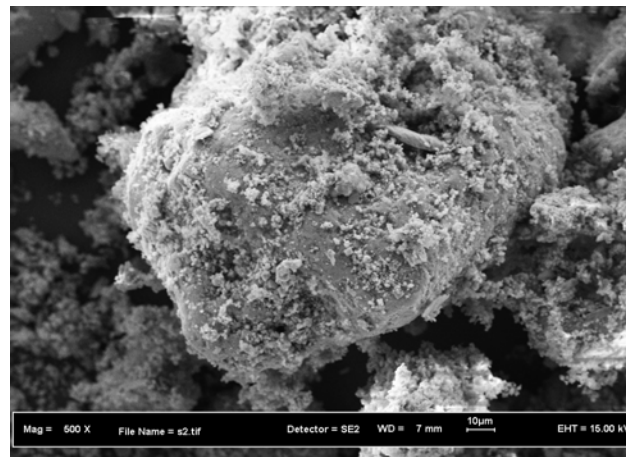


Figure 3.10: SEM photographs of a sulfur on a pyrite surface Precipitation of sulfur during 15 days abiotic leaching at 30°C, control, in the absence of culture (Magnification 5000 X)

3.2.2.9 Iron speciation in the STR biooxidation of pyrite using different types of culture

From figures D-20 until D-25 (the speciation of free iron in a form of (ferrous ion) Fe^{2+} and (ferric ion) Fe^{3+} , determined using KMnO_4 titration (Sjahrir, 2001), the ratio of Fe^{3+} to Fe^{2+} in a medium during 15 days leaching, (within and without the present of culture) is present in table 3.7 (I: Bioleaching, II: control)

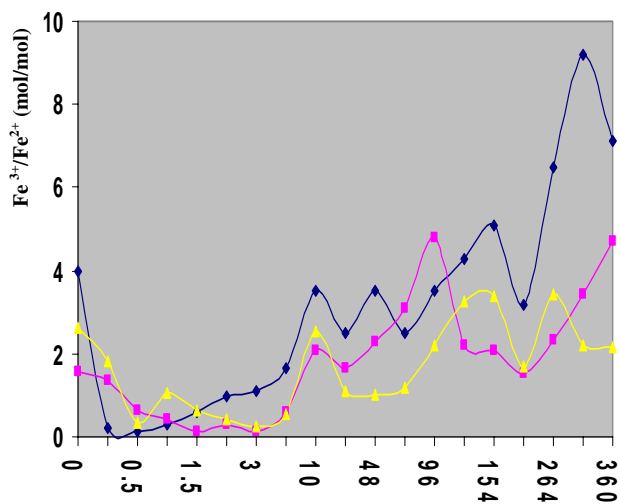


Figure 3.11-I: Ratios of $[\text{Fe}^{3+}] / [\text{Fe}^{2+}]$ in the liquid medium during biooxidation study in STR using ■ *SL5B*, ■ *S. Thermosulfodoxidans* and ■ *T. ferrooxidans*

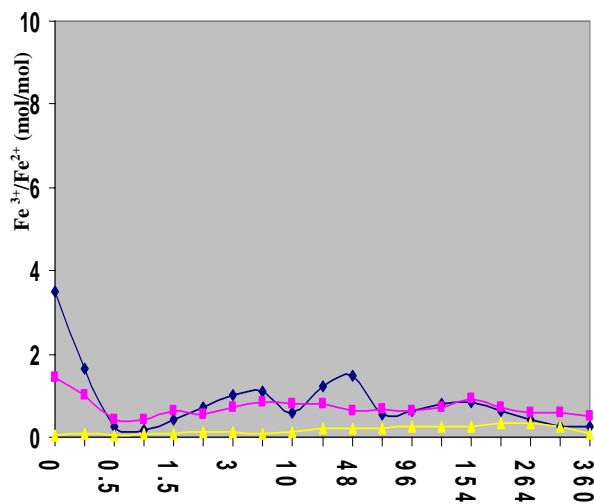


Figure 3.11-II: Ratios of $[\text{Fe}^{2+}] / [\text{Fe}^{3+}]$ concentration in the liquid medium during biooxidation study in STR at ■ 70°C, ■ 45°C and ■ 30°C

Results from figures D-20 to D-25 show that the Fe^{3+} concentration in solution is higher in the present of culture (figures D-20, D-22, D-24) compared to the control (figures D-21, D-23 and D-25). The highest amount of Fe^{3+} in a solution was obtained in the present of SL5B compared to *Sb. Thermosulfodoxidans* and *T. ferrooxidans*. Iron dissolution rate and final extraction (fig. 3.5A) show a direct relationship with the Fe^{3+} concentration in solution (figures D-20 to D-25). It was more rapid with the thermophilic microorganisms than with the mesophilic microorganisms. Thermophiles also yielded a final Fe^{3+} concentration and dissolution extraction (96%: fig 3.7) higher than mesophiles due in part to the catalytic effect of the higher temperature used in the process (Boogerd et al., 1991). These results confirm that indirect bioleaching has a larger contribution to the dissolution mechanism of this mineral. This is in agreement with previous studies (Basaran and Tuovinen, 1987; Zeng et al., 1986; McKibben and Barnes, 1986; Kawakami et al., 1988; Boogerd et al., 1991; Mandl et al., 1999).

According to Huber et al., 1989, an extremely thermoacidophilic culture grows optimally at 70°C and at pH 2.0. This organism grows chemolithotrophically by oxidizing reduced iron and sulfur species (fig 3.7) through a membrane-bound transport system which coordinates electron and proton fluxes to produce ATP (Cobley and Cox, 1983; Lübben and Schäfer, 1989; Schäfer et al., 1990)

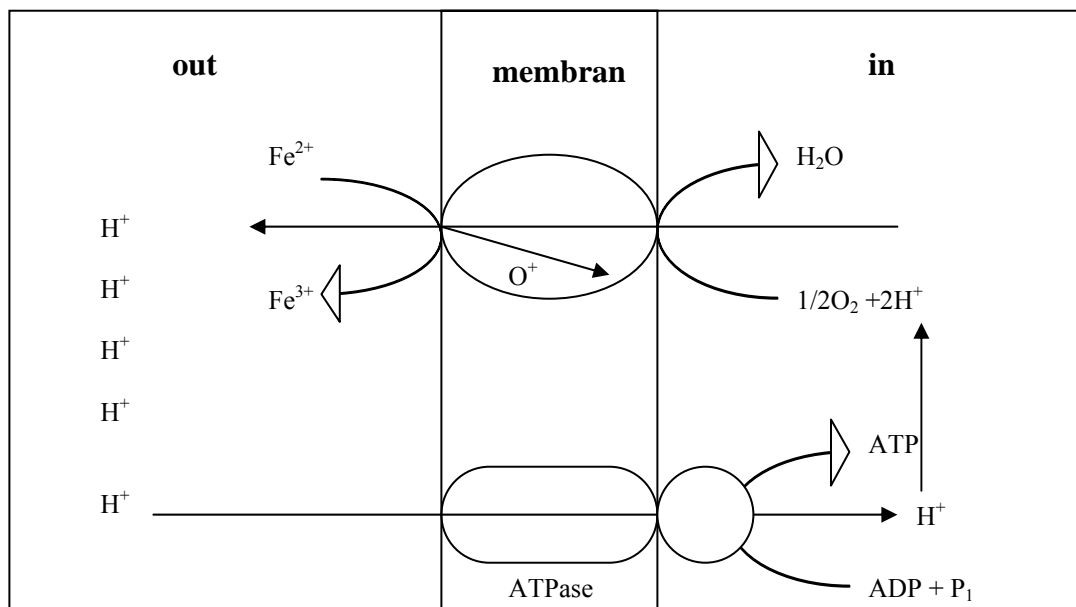


Figure 3.12: Generalized chemiosmotic network for extreme thermoacidophiles under normal growth conditions. This model (modified from Cobley and Cox, 1983) couples the generation of proton-motive force to the phosphorylation of ADP and Fe^{2+} oxidation. Outside protons are translocated to inside the cell via an ATPase channel and pumped out through the electron transport chain (ETC). The electrons released from Fe^{2+} oxidation are consumed by oxygen which acts as a terminal electron acceptor.

Studies of thermal stress in extreme thermoacidophiles have shown that either a small set of proteins or a single protein induced by heat shock has been associated with their prolonged survival at supraoptimal temperatures (Guagliardi et al., 1994; Han et al., 1997; Kagawa et al., 1995; Knapp et al., 1994; Peeples and Kelly, 1995; Trent et al.,

1990; Waldmann et al., 1995). A significant transmembrane pH gradient must be maintained across the cell membrane which, in fact, is required for chemiosmosis and subsequent electron translocation via iron turnover (Cobley and Cox, 1983). If this energy network were to be disrupted partially or entirely by chemical or thermal stress, one possible result is excess accumulation of protons intracellularly and a drop in internal pH (Peeples and Kelly, 1995). To survive, thermoacidophiles would need to reestablish the proton gradient, possibly through higher iron or sulfur oxidation rates, to generate ATP to compensate for the additional bioenergetic burden. The adaptation or metabolic response of extreme thermoacidophiles to certain bioenergetic challenges i.e., heat shock or respiratory uncouplers could be exploited to increase biooxidation rates (Chae J. Han, Robert M. Kelly, 1997).

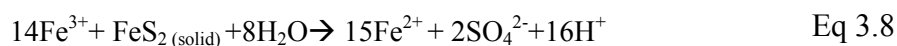
Referring to figures D-21, D-23 and D-25, the concentration of Fe^{2+} ion in a solution is highly dependent on temperature. Almost the entire Fe ion is in the form of Fe^{2+} in the control at 30°C compared to control at 45°C and 70°C . The tendency of ferric ion formation will be increased at temperature and abiotic condition

The ratio of $[\text{Fe}^{3+}]$ to $[\text{Fe}^{2+}]$ is related to E_{H} value i.e: high $[\text{Fe}^{3+}] / [\text{Fe}^{2+}]$ ratio leads to the high E_{H} value. However, the correlation does not follow the theoretical $[\text{Fe}^{3+}] / [\text{Fe}^{2+}] - E_{\text{H}}$ correlation in a Nernst equation (Eq: 3.2, section 3.3.2.7) due to reasons discussed earlier.

Results from figures 3.11 shows that the initial ratio ($T=0$) of $[\text{Fe}^{3+}] / [\text{Fe}^{2+}]$ is much dependant on temperature of reactor (Except for *T.ferrooxidans*). The initial ratio ($T=0$) of $\text{Fe}^{3+} / \text{Fe}^{2+}$ was around 4.0 $[\text{Fe}^{3+}] / [\text{Fe}^{2+}]$ at 70°C (SL5B and control), 1.5 $[\text{Fe}^{3+}] / [\text{Fe}^{2+}]$ at 45°C (*Sb. Termosulfodoxidans* and control) and 0.05 $[\text{Fe}^{3+}] / [\text{Fe}^{2+}]$ at 30°C . The initial $[\text{Fe}^{3+}] / [\text{Fe}^{2+}]$ ratio for *T.ferrooxidans* is 2.64 $[\text{Fe}^{3+}] / [\text{Fe}^{2+}]$. The results also shows that the initial $[\text{Fe}^{3+}] / [\text{Fe}^{2+}]$ ratio in liquid medium at elevated temperature (70 and 45°C) is similar either, in the presence and absence of culture. However, in the presence of SL5B and *Sb. Termosulfodoxidans*, the $[\text{Fe}^{3+}] / [\text{Fe}^{2+}]$ ratio was 14% and 9% higher compared to its control. The initial $[\text{Fe}^{3+}] / [\text{Fe}^{2+}]$ ratio for *T.ferrooxidans* is 53.5

fold times higher compared to its control (at 30⁰C). This indicates that the *T.ferrooxidans* has a great capability to oxidize ferrous ion in its medium (figure D-24).

During the initial stages of leaching, all the systems show a drastic reduction in $[Fe^{3+}]/[Fe^{2+}]$ ratios. The highest $[Fe^{3+}]/[Fe^{2+}]$ reduction was obtained in *SL5B* bioleaching, at $7.78 \frac{[Fe^{3+}]}{[Fe^{2+}]} hr^{-1}$, followed by $6.51 \frac{[Fe^{3+}]}{[Fe^{2+}]} hr^{-1}$ for control at 70⁰C, $4.63 \frac{[Fe^{3+}]}{[Fe^{2+}]} hr^{-1}$ for *T.ferrooxidans*, $2.02 \frac{[Fe^{3+}]}{[Fe^{2+}]} hr^{-1}$ for control at 45⁰C and $1.82 \frac{[Fe^{3+}]}{[Fe^{2+}]} hr^{-1}$ for *Sb.Termosulfodoxidans*. No $[Fe^{3+}]/[Fe^{2+}]$ reduction was observed in a control at 30⁰C. During this phase, pyrite surface oxidized via Fe^{3+} attack as shown in equation 3.8: (Shrihari et al, 1995)

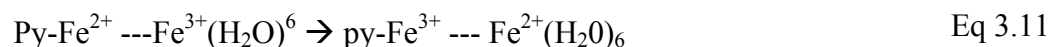


It is possible to suggest that the Fe^{3+} reaction with pyrite (indirect leaching) is so fast that most of it is reduced to Fe^{2+} , even in the presence of iron oxidizing microorganism (Nordstrom and Alpers 1998). It was observed that chemical pyrite oxidation rate per unit of surface area approaches a maximum at the start of the experiment i.e: minimum value of formation of sulfur and jarosite, polymers block by attaching cells and Fe^{3+} consumed at the surface. (Boon and Heijnen, 1998; Boon et al., 1999 and Katrina et al 1998). It can be suggested that the mass transfer rate of ferric iron from the bulk-phase to the pyrite surface does not become rate-limiting at the initial stage of bioleaching (M. Boon and J.J. Heijnen, 2001).

Oxidation of pyrite via ferric ion oxidation is an electrochemical process. This process is further complicated by the fact that the oxidation of pyrite must require up to seven elementary steps, depending on how elementary steps are defined. Furthermore, the minerals are semiconductors and the reactions are electrochemical in nature. (Brown and Jurinak, 1989). This reaction is a cathodic reaction, which is associated with many oxidants that can accept electrons from iron sulfide minerals, including NO^{3+} , Cl_2 , and H_2O_2 , but the most important ones in nature are O_2 and Fe^{3+} . These react with pyrite based on the reactions 3.9 and 3.10:



Cathodic reaction becomes the rate-determining step for the overall sulfide mineral oxidation. Brown and Jurinak (1989) and Williamson and Rimstidt (1994) showed that the pyrite oxidation rate depends on the concentration of Fe^{3+} or O_2 . Studies of the interaction of the pyrite surface with O_2 and H_2O conducted under ultrahigh vacuum conditions using scanning tunneling microscopy, along with ultraviolet photoelectron spectroscopy by Rosso et al., (1999), indicated that the surfaces exposed to O_2 show oxidative consumption of low-binding-energy electrons occupying dangling bond surface states localized on surface Fe atoms. When O_2 is combined with H_2O , there is a more aggressive oxidation of the surface, with discrete oxidation patches, where reacted surface Fe sites have lost surface state density to the sorbed species. Thus, for pyrite, the activated complex might involve the transfer of an electron to a hydrated Fe^{3+} adsorbed from solution from Fe^{2+} in the mineral surface.



The Fe^{2+} is then released back to the solution, and an electron moves from an anodic site to reduce the Fe^{3+} back to Fe^{2+} (Lowson, (1982). Fenton-type mechanism has been employed for the reduction of O_2 at the surface of oxidizing pyrite. Firstly, O_2 adsorbs at the Fe^{2+} site, and this is followed by the transfer of an electron from this site to the O_2 :



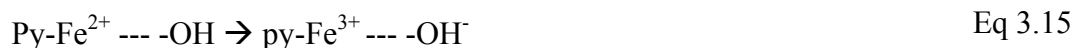
Then, a hydrogen ion reacts with the oxygen to produce HO_2 , and concurrently, an electron moves from an anodic site to reduce the Fe^{3+} back to Fe^{2+} . This allows another electron to be transferred to the oxygen.



An additional hydrogen reacts with this peroxide group to produce H_2O_2 , and concurrently, an electron moves from an anodic site to reduce the Fe^{3+} back to Fe^{2+} . The transfer of a third electron from the Fe^{2+} to the peroxide converts one of the oxygen atoms to a hydroxide ion that is released to the solution and the other to a -OH radical:



The Fe^{3+} is again recycled to Fe^{2+} by the transfer of another electron from the anodic site, and this electron moves to the -OH radical to convert it to OH^- , which is released to the solution:



Then, a final electron moves from an anodic site to reduce the Fe^{3+} back to Fe^{2+} , leaving the site the same as it was in the beginning of the process, even though four electrons were transferred through. (Braga and Connick, 1982, Craig, Vokes and Solberg, 1998, Doyle and Mirza, 1996, Holmes and Crundwell, 2000 and Williamson and Rimstidt, 1993)

According to figure 3.11-I and II, extremely low $[\text{Fe}^{3+}]/[\text{Fe}^{2+}]$ ratios value were observed in these experiments (0.25th hrs for SL5B, 0.5th hrs for *Sb. Thermofulfoxidans*, control at 70 and 45^oC and 1.5th hr for *T. ferroxidans*). At these points, Fe^{2+} accumulated on the mineral surface, produces a diffusion barrier to attack of the mineral by Fe^{3+} (Cabral and Ignatiadis, 1999) and stops the dissolution process (Figure 3.6A). This phenomenon has also been observed by other researchers who attributed the pyrite oxidation rate by Fe^{3+} to the competitive chemisorption of ferrous

and ferric ions at the mineral surface (Zeng et al., 1986; Kawakami et al., 1988; Boogerd et al., 1991).

It is also interesting to note, that after the stated points, the $[\text{Fe}^{3+}]/[\text{Fe}^{2+}]$ ratios increased constantly in the presence of culture. The increasing rate of $[\text{Fe}^{3+}]/[\text{Fe}^{2+}]$ ratios during these phase were at $0.0184^{[\text{Fe}^{3+}]/[\text{Fe}^{2+}]} \text{ hr}^{-1}$ for SL5B, $0.0082^{[\text{Fe}^{3+}]/[\text{Fe}^{2+}]} \text{ hr}^{-1}$ for *Sb. Thermosulfodoxidans* and $0.0054^{[\text{Fe}^{3+}]/[\text{Fe}^{2+}]} \text{ hr}^{-1}$ for *T. ferrooxidans*. However, the $[\text{Fe}^{3+}]/[\text{Fe}^{2+}]$ ratios remained low for the control set (Figure 3.12-II). The formation rate of $[\text{Fe}^{3+}]/[\text{Fe}^{2+}]$ ratios is nearly zero. The trend of $[\text{Fe}^{3+}]/[\text{Fe}^{2+}]$ ratios for control is slightly different. The low value of $[\text{Fe}^{3+}]/[\text{Fe}^{2+}]$ for control at 30°C due to ferrous ion maintaining its form at this temperature. At 70°C however, the precipitation of ferric ion is become dominating factor.

3.2.2.10 Dissolved oxygen behaviour in the biooxidation of pyrite using different types of culture

Figures 3.13- I ,II and III shows the percentages of oxygen partial pressure of solution in a STR abiotik and biotic condition at 70°C , 45°C and 30°C and dissolved oxygen consumption rate during 48 incubation of pyrite free-cell suspension in the presence of SL5B (fig 3.13-I) *Sb.thermosulfudoxidans* (fig 3.13-II) and *T.ferrooxidans*(3.13-III). Dissolved oxygen consumption rate for pyrite free-cell suspension is determine to verify amount of cells in the liquid medium, where the solids in the leaching sample were sediment (removing all solid particles but not the cells) and the liquid part obtained was used as the inoculum in freshly prepared medium.

The mineral dissolution process is also related to the cell growth since it establishes a higher or a lower Fe^{3+} regeneration capacity by microorganisms. (Jones and Kelly, 1983; Lizama and Suzuki, 1989; Curutchet et al., 1992; Nyakor et al., 1996) However, the studies of cell densities in correlation with bioleaching process is intricate. Ordinary methods using direct colony-forming unit (CFU) and turbidity determination

looks impracticable due to the formation of color during leaching, disturbance from pyrite, jarosite and sulfur particle and inability of iron oxidizer related bacteria to grow on solid medium.

The oxidation of iron–sulphide minerals results in the consumption of both oxygen and carbon dioxide (Harahuc et al., 2000), approximately equal amounts of total Fe being released per organism, at 4.3×10^{27} mmol Fe/ cell·day. (May et al, 1997). It is because of the ease of measurement of dissolved oxygen and the importance of this essential compound to determining the behavior of cell growth, a vast database of scientific literature has been produced regarding its effect on microbial kinetics (Peeples and Kelly, 1993 and Breed et al., 1999) Several investigations have successfully made use of respirometry methods to evaluate the activity of iron- and sulphide-oxidizing microbial activities (Sampson and Blake, 1999 and Harahuc et al., 2000). Boon (1996) introduced the combination of dynamic biological oxygen monitor (BOM) test and on-line vent-gas analysis as an indication of culture growth behavior.

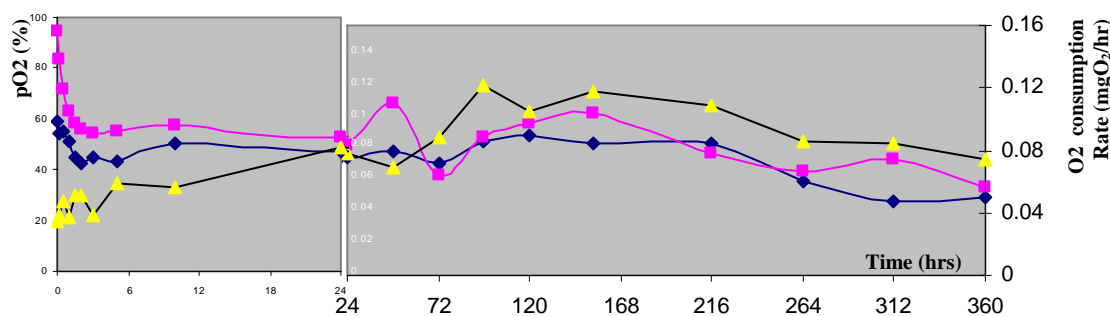


Figure 3.13-I: pO₂ profile in STR using ■ SL5B and ■ control at 70°C. Dissolved oxygen consumption rate ■ for 48 hrs inoculation from STR solution containing SL5B.

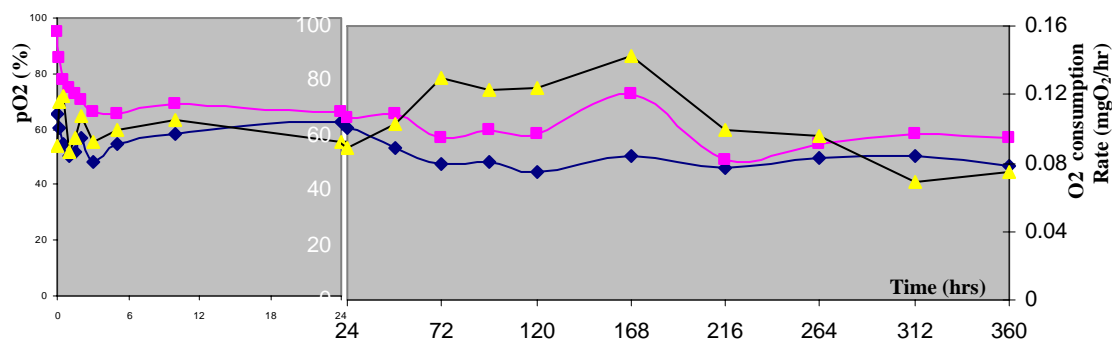


Figure 3.13-II: pO₂ profile in STR using ■ *S. Themorsulfodooxidans* and ■ control at 70°C. Dissolved oxygen consumption rate ■ for 48 hrs inoculation from STR solution containing *S. Themorsulfodooxidans*.

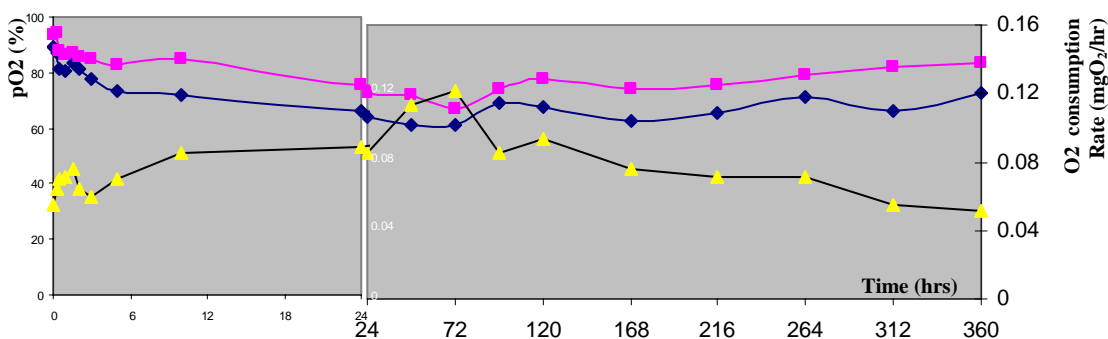


Figure 3.13-III: pO₂ profile in STR using ■ *T. ferroxidans* and ■ control at 70°C. Dissolved oxygen consumption rate ■ for 48 hrs inoculation from STR solution containing *T. ferroxidans*.

The solubility of oxygen (DO) is affected by temperature and by the partial pressure (pO₂) of oxygen over the water. Oxygen in water obeys Henry's law. The solubility is roughly proportional to the partial pressure of oxygen in the air (*Standard Methods for the Examination of Water and Wastewater*, 1965):

$$p_{O_2} = K_{O_2} x_{O_2} \quad \text{Eq 3.16}$$

where p_{O_2} : partial pressure of oxygen (Torr)
 x_{O_2} : mole fraction of oxygen in oxygen-saturated water
 K_{O_2} : is the Henry's law constant for oxygen in water ($3.30 \times 10^7 \text{ K/Torr}_{298 \text{ K}}$)

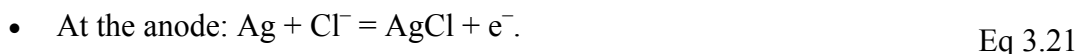
Higher air pressure means higher partial pressure of oxygen, Many empirical equations are available to accurately estimate oxygen solubility as a function of temperature, pressure, and humidity. The following empirical equations that give the saturated dissolved O₂ concentration (DO) in mg O₂/L water (Atkins,, 1998)

$$t < 30^{\circ}\text{C} \quad \text{DO} = \frac{(P - p_{\text{O}_2}) \times 0.678}{35 + t} \quad \text{Eq 3.17}$$

$$t > 30^{\circ}\text{C} \quad \text{DO} = \frac{(P - p_{\text{O}_2}) \times 0.827}{49 + t} \quad \text{Eq 3.18}$$

where p_{O_2} : partial pressure of oxygen (torr)
 P: baromatic pressure (torr)
 T: temperature ($^{\circ}\text{C}$)

During the experiment, the polarographic oxygen electrode has been used to measure the oxygen partial pressure in a medium in STR. A platinum cathode and a silver/silver chloride anode in a sodium chloride electrolyte solution, and a voltage of 700 mV is applied . The following reactions occur.



Electrons are taken up at the cathode and the current generated is proportional to oxygen tension. A membrane separates the electrode from medium, preventing deposition of protein but allowing the oxygen tension in the medium to equilibrate with the electrolyte solution. The electrode is calibrated at a constant temperature of 30 $^{\circ}\text{C}$. Two point calibration using air saturated distilled water and distilled water with zeroing gel. The solution indicated a 100% pO₂ and 0% pO₂ respectively. The value is equals to 7.6 mgO₂/L and 0 mgO₂/L. (Mohd Zahari, 2002) Figure 3.15 shows the polagraphic oxygen electrode.

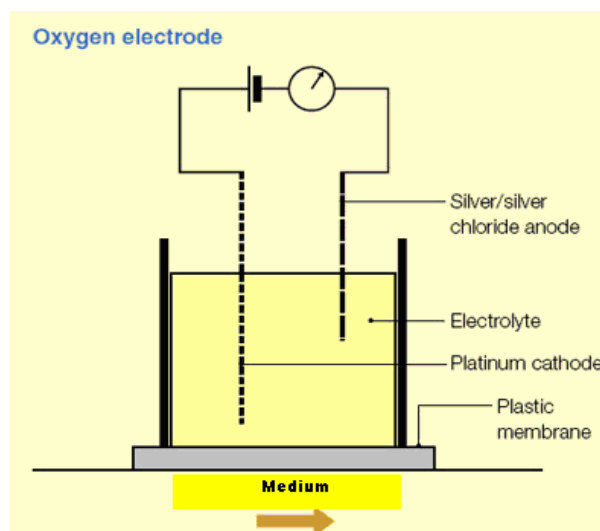
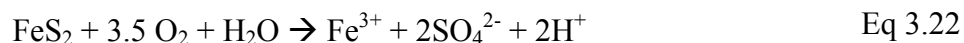


Figure 3.14: Polargraphic oxygen electrode.

Results from figures 3.13 (I, II and III) show, in general, the value of pO_2 percentages in a bioleaching process is particularly higher compared to its respective control. It is due to the higher oxygen (dissolved) consumption via bacterial respiratory and oxidation reaction than air bubbled-liquid oxygen transfers. Highest pO_2 reduction was obtained in the SL5B at $0.046\% pO_2/hr$, followed by *Sb. Thermosulfodoxidans* at $0.020\% pO_2/hr$ and increment of pO_2 in *T.ferrooxidans* at $0.018\% pO_2/hr$.

The lower pO_2 values indicated higher bacterial concentration in a solution. The cell grows autotrophically and obtains energy from the oxidation of ferrous iron and elemental or reduced sulfur compounds, using DO as the electron acceptor under oxidizing conditions (Colmer and Hinkle (1947) Keller and Murr (1982) Southam and Beveridge (1992) and Ledin and Pedersen (1996)). The reaction involved in biologically dissolved oxygen consumption is shown in equations 3.22 and 3.23:



and



The direct mechanism (Eq 3.22) occurs with bacterial cells attached to the pyrite surface, where the cells use dissolved oxygen as the electron acceptor and biologically oxidize sulfur or iron by an enzyme system. In the indirect mechanism (Eq 3.23) the cells oxidize soluble ferrous iron to ferric iron which chemically degrades pyrite (Brock and Gustafson (1976), Ehrlich (1981), Edwards et al (1999) and Yu et al. (2001))

Another important point to note is a reduction of pO_2 for the control set. Decreasing behavior for control set, which can be expressed in table 3.10:

Table 3.10: pO_2 reduction in the abiotic STR

For control at 70 ⁰ C:	$d[DO (\%pO_2)]/dt = 13.04T_{(hrs)}^2 - 44.33 T_{(hrs)} + 93.403$
For control at 45 ⁰ C:	$d[DO (\%pO_2)]/dt = 2.5983 T_{(hrs)}^2 - 18.559 T_{(hrs)} + 94.7$
For control at 30 ⁰ C:	$d[DO (\%pO_2)]/dt = -63.2 T_{(hrs)}^2 + 20.2 T_{(hrs)} + 93.3$

Large magnitudes of dissolved oxygen have been diminished from control solution at a elevated temperature, due to the low solubility of oxygen at high temperature. The oxygen slips into "pockets" that exist in the loose hydrogen-bonded network of water molecules without forcing them apart. The oxygen is then caged by water molecules, which weakly pin it in place. The dissolution is exothermic overall, so cooling shifts the equilibrium towards the dissolved form of oxygen.

Figures 3.13 (I,II and III) is also shows the rate of dissolved oxygen consumption of fresh inoculum of *SL5B*, *Sb. Thermosulfodooxidans* and *T. ferroxidans* for 48 hrs. Pyrite-free inoculum was taken from STR. The dissolved oxygen consumption rate from pyrite-free inoculums will provided useful information on a cell concentration in a STR. Stoichiometric relation between the bacterial growth rate on

substrate and oxygen consumption has been developed by Boon (1996) is shown in equation 3.24:

$$-r_{O_2} = r_x / Y_{ox}^{max} + m_{O_2} C_x \quad \text{Eq 3.24}$$

Where r_{O_2} : O_2 consumption rate (mol O_2 /L/hr)
 C_x : Biomass concentration (Cmol/L)
 m_{O_2} : Maintenance coefficient of O_2 (mol O_2 / C-mol/s)
 Y_{ox}^{max} : Maximum yield coefficient per mol per oxygen (C-mol/ mol O_2)
 r_x : substrate consumption rate

Dissolved oxygen consumption rate for pyrite-free suspension cell can be easily divided into 3 phase; exponential phase, stationary phase and death phase. The exponential phase for the *SL5B*, *Sb thermosulfodoxidans* and *T.ferrooxidans* can be expressed in table 3.11:

Table 3.11: The dissolved oxygen consumption rate for pyrite-free suspension cell at the exponential phase

<i>SL5B</i> T=0 to T= 96hrs	$d[r_{D O \text{ mg/LO}_2 \text{ hr}^{-2}}]/dt = 0.0418e^{0.0114T \text{ hrs}}$ ($R^2 = 0.7934$)
<i>Sb.thermosulfodoxidans</i> T=0 to T= 72hrs	$d[r_{D O \text{ mg/LO}_2 \text{ hr}^{-2}}]/dt = 0.0905e^{0.004 T \text{ hrs}}$ ($R^2 = 0.608$)
<i>T.ferrooxidans</i> T=0 to T= 48hrs	$d[r_{D O \text{ mg/LO}_2 \text{ hr}^{-2}}]/dt = 0.0622e^{0.013 T \text{ hrs}}$ ($R^2 = 0.7879$)

$d[r_{D O \text{ mg/LO}_2 \text{ hr}^{-2}}]/dt$: dissolved oxygen consumption rate

During this phase, the cell was enormously generated at a leaching medium. Singer and Stumm (1970) reported that the presence of ferrous ion, oxygen, pyrite surface and acidic condition will support the bacterial growth. The presence of iron-oxidizing bacteria accelerated the oxidation of ferrous iron by a factor larger than 10^6 compared to abiotic conditions. The rate of pyrite dissolution in the enrichment non surface-attaching culture is reported to the approximately five times higher than the corresponding control. (Katarina et al).

The several kinetic studies on non microbial pyrite oxidation under oxic conditions successfully addressed the dependence of abiotic pyritic oxidation on DO concentration, ferric iron concentration and pH (Olson,(1991)McKibben and Barnes, (1986); Nicholson, (1994); Williamson and Rimstidt, (1994). The rate laws of pyrite oxidation have been expressed as follows:

$$R = 10^{-8.19} \frac{[\text{O}_2]^{0.50}}{[\text{H}^+]^{0.11}} \quad [\text{molm}^{-2} \text{ s}^{-1}] \quad \text{Eq 3.25}$$

And
$$R = 10^{-8.58} \frac{[\text{Fe}^{3+}]^{0.30}}{[\text{Fe}^{2+}]^{0.47}[\text{H}^+]^{0.32}} \quad [\text{molm}^{-2} \text{ s}^{-1}] \quad \text{Eq 3.26}$$

The dissolved oxygen consumption remains high during the stationary stage. Rates of dissolved oxygen consumption ($-r_{\text{DO}_2}$) was at $-r_{\text{DO}_2} = 0.113$ [$\text{mg O}_2\text{L}^{-1}\text{hr}^{-1}$] for SL5B (hr 96th till hr 216th, fig 3.15-I), $-r_{\text{DO}_2} = 0.130$ [$\text{mg O}_2\text{L}^{-1}\text{hr}^{-1}$] for *Sb. thermosulfodoxidans* (hr 72nd till hr 168th, fig 3.15-II) and $-r_{\text{DO}_2} = 0.117$ [$\text{mg O}_2\text{L}^{-1}\text{hr}^{-1}$] for *T.ferrooxidans* (hr 48th till hr 72nd, fig 3.15-III). During this phase, the cell concentration in a medium was maximal. The concentration of Fe^{2+} and transfer availability of atmospheric CO_2 in the medium became a limitation factor for bacterial growth (Katarina et al,)

The dissolved oxygen consumption rate ($-r_{\text{DO}_2}$) value for the death phase of cell in solution was performed at the end of test. The rate of dissolved oxygen consumption ($-r_{\text{DO}_2}$) were found to decreased after hr 216th (SL5B), hr 168th (*Sb. Thermosulfodoxidans*) and 72nd (*T.ferrooxidans*) . The rate of decline was identical for SL5B, *Sb. Thermosulfodoxidans* and *T.ferrooxidans* at 0.0002 [$\text{mg O}_2\text{L}^{-1}\text{hr}^{-2}$]. However, the *T.ferrooxidans* achieved a death period quicker then SL5B and *Sb. Thermosulfodoxidans*. (Jones and Kelly (1983), Lizama and Suzuki (1989); Curutchet et al.(1992) and Nyakor et al.(1996) were reported that the diminishing of mesophile cell is due to the inhibition of the enzymatic path of Fe^{2+} oxidation in the presence of high Fe^{3+} concentrations.

Comparison between % of pO_2 reading in STR and dissolved oxygen consumption rate ($-r_{DO_2}$) (figure 3.14-I,II,III), demonstrates the tendency of cell to adhere on the pyrite surface during the final phase of bioleaching test. Even at low dissolved oxygen consumption rate ($-r_{DO_2}$), the amount of pO_2 in a STR (which is containing SL5B and *Sb. Thermosulfodoxidans*) is found decreased. In the death phase for the SL5B (216hrs onward) and *Sb. Thermosulfodoxidans* (168hrs onwards), the reducing of pO_2 in the STR is dominated by the cell which is attach to mineral surface. In this experiments, the thermophiles cell attachment kinetics was greater compared to mesophiles. The finding is dissimilar with reported by Clark and Norris (1996) and Nemati and Harrison (1999)

A number of studies have reported the ability of the bioleaching microorganisms to adhere to mineral surfaces (Konishi et al. (1990), Dziurla et al. (1992) and Ohmura et al. (1993). A relationship thus exists between attachment and mineral dissolution rates. In the direct mechanism, bacterial attachment to the mineral surface takes place first, followed by enzymatic oxidation by electron transport from the reduced mineral. Shrihari et al. (1995), Dziurla et al. 1997 and Savic et al. (1999).

Scanning Electron Microscopy (SEM) of cell attachment to pyrite after 15 days biooxidation by SL5B and *T. ferrooxidans* is shown in figure 3.16 and 3.17 respectively. The distribution of SL5B on a pyrite surface is even as compared to agglomeration of *T.ferrooxidans*, on pyrite surface, mostly found in a pitting corrosion caused by bacteria.

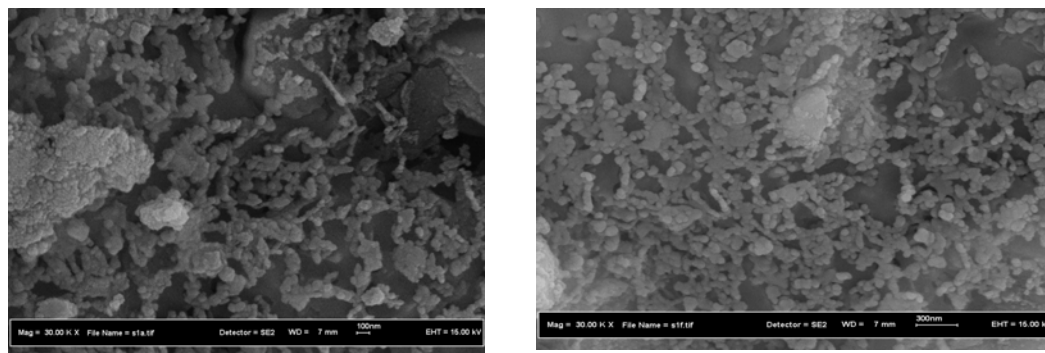


Figure 3.15: SEM photograph of attachment of SL5B cell on a pyrite surface (Magnification 30 000 X)

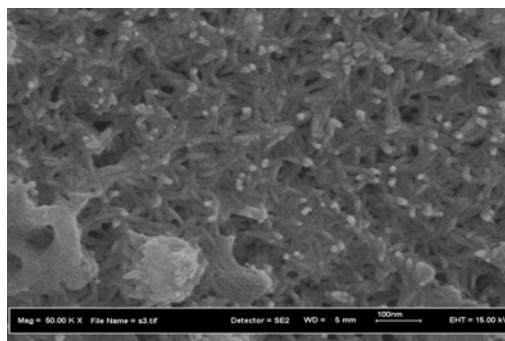


Figure 3.16: SEM photograph of attachment of *T. ferrooxidans* on a pyrite surface (Magnification 50 000 X)

The attachment kinetics was evaluated from the common bacterial adhesion model. This model assumes that bacterial adsorption follows a second-order irreversible kinetics with respect to the concentration of bacteria and substrate surface area in the system (figure 3.16). The model comprises two stages: an initial stage of reversible adhesion followed by an irreversible attachment. This can be represented in equation 3.27:

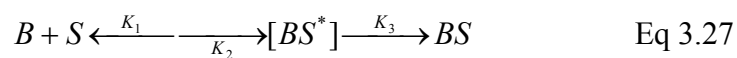


Figure 3.17: The model of attachment kinetics of bacteria on pyrite surface.

According to this model, the initial interaction between bacteria (B) and surface sites (S) involves the formation of a metastable complex ([BS]*), where the bacteria are held at a finite distance from the surface by a balance of repulsion and attraction forces. Once formed, the complex may dissociate reversibly, regenerating a free cell and surface site. Alternatively, the bacteria may expend metabolic energy for the production of biopolymers necessary to establish a permanent bacterium-surface site association (BS). However, the equation that describes the bacterial attachment phenomenon to metal sulfides is:

$$K_{at} = \frac{1}{1/a A_0 - X_{bo}} \ln \left[\frac{X_{bo} (1/a A_0 - X_{bs})}{1/a A_0 (X_{bo} - X_{bs})} \right] \quad \text{Eq 3.28}$$

K_a , is the attachment rate constant (ml/Cell.h);
 A_0 , is the concentration of surface adsorption sites (cm²/cm³);
 a , is the projected area per bacteria (cm²/Cell);
 X_{bo} , is the initial concentration of free bacteria (Cell/ml);
 X_{bs} , is the concentration of attached bacteria on the solid surface (Cell/ml);
 t , is the time (h).

The attachment of acidophilic bacteria to mineral surfaces has been an area of much research. The interaction of the cell with the surface is dependent on a number of physical and biochemical parameters. Other studies have reported that the bacteria attach to the mineral surface by a variety of methods i.e: via adsorption (Takakuwa *et al*, 1979), protein binding receptors (Sakamoto *et al*, (1989), Ohmura *et al*, (1996) and Ohmura and Blake, (1997), via chemical attachment (Schaeffer, (1963), via hydrophobic interactions (Loosdrecht van *et al*(1987), attachment by means of pili (Weiss, (1973) and the secretion of a slime layer (Golovacheva, 1979).

The parameters such as incubation time, agitation (Murthy and Natarajan (1992) particle size and pulp density (Shirhari *et al*, (1995), are important to the overall attachment and it has also been suggested that the actual attachment mechanism is based on specific and non-specific interactions of the system (Busscher and Weerkamp (1987). The interactions of the microorganism and mineral are shown to change the surface chemistry of the cell as well as that of the pyrite which it had interacted (Devasia *et al*,

(1993). Electrostatic, hydrophobic and specific protein interactions have all been investigated with respect to the attachment mechanism. The surface of a microbial cell is charged due to the presence of different functional groups; carboxyl (-COOH), amino (-NH₂) and hydroxyl (-OH) groups which are found in the cell wall material (Barrett *et al.*, 1993). Blake *et al.* (1994) showed that electrostatic interactions were only qualitatively involved in the attachment of *Thiobacillus ferrooxidans* to pyrite and sulfur. Devasia *et al.* (1993) found significant shifts in the isoelectric points of sulfur, pyrite and chalcopyrite after they had been in contact with cell. Similarly, hydrophobic interactions as measured through the contact angle have been shown to influence the cell attachment with hydrophobic cells having a greater adherence than hydrophilic cells (Loosdrecht van *et al.* (1987), while the effect of electrostatic interactions was shown to increase with decreasing hydrophobicity.

The hydrophobic interaction is due to the specific protein apo-rusticyanin acting as a receptor for the initial attachment (Ohmura and Blake 1997, Sasaki *et al.*, 1999). Apo-rusticyanin can be considered as an iron atom surrounded by four amino acid ligands and is located on the cell surface. The attachment of the strain was shown to be very dependent on the growth conditions (Loosdrecht van *et al.*, (1987), Ohmura and Blake (1999), the protein form (Sasaki *et al.*, (1999), the addition of ferrous iron which caused a high percentage of the bacteria to detach from the pyrite surface (Ohmura and Blake, (1999).

Sb. thermosulfidoxidans, a moderately thermophilic bacteria which grows autotrophically at 45°C was found to attach to pyrite with the formation of a slime layer. The cell produced abundant quantities of the slime, particularly in the area adjacent to the mineral (Golovacheva, 1979). A slime layer is a polysaccharide layer secreted from the cell which is often a zone of diffuse, unorganised material and is often easily removed (Prescott *et al.*, (1996). Golovacheva (1979) suggested that a cellular chemoreceptor was a participant in the adhesion process of *Sb.thermosulfidoxidans*. Weiss (1973) suggested the attachment of *Sulfolobus* to a mineral surface was by means of clusters of pili or a well-developed glycolyx. Also, Murr and Berry (1976) found the

tenacious attachment (to pyrite or chalcopyrite) of an extremely thermophilic bacteria, similar to *Sulfolobus acidocaldarius* using scanning electron microscopy, provided strong support for the direct mechanism of the bacterial oxidation of sulfide minerals. Larrson et al. (1993) found that the attachment of *Acidianus brierleyi* to pyrite was important to the growth of the culture and the amount of pyrite dissolution.

3.2.3 STR biooxidation of pyrite using SL5B at different pyrite pulp densities.

The objectives of the present work is to study the effect of mineral pulp density on the activity of *SL5B* and its ability to oxidize sulfide minerals and also to verify the maximum mineral concentration tolerated by thermophilic strain (*SL5B*) in a stirred tank bioreactor. In the presence of solids, the kinematics viscosity of the fluid tends to increase with the addition and increasing the concentration of solids. As a consequence, the smallest eddy size tends to increase significantly tempering further the likelihood of the potentially detrimental interactions between the cells and turbulent eddies in the presence of solids. (Deveci, 2001). The damage to bacterial cells would be compounded by increase in pulp density. In addition, Cherry and Papoutsakis (1986) postulated that there are actually three potential mechanisms lead to the bacterial damage at higher pulp densities namely: interactions with the turbulent eddies, particle–particle collisions, collisions between the particles and cells and reactor walls and impeller blades in particular, whereby the damage to microorganisms cells may occur. However, the size of the extreme thermophiles is most likely to be too small compared with the smallest eddy size generated in bioleaching operations suggesting the minimal hydrodynamic shear effects on the cells. (Clark and Norris, 1996; Nemati and Harrison, 2000; Gericke et al., 2001; d_Hugues et al., 2002). Figure 3.18 shows the percentages of pyrite oxidation using *SL5B* using stirred tank reactor for 15 days.

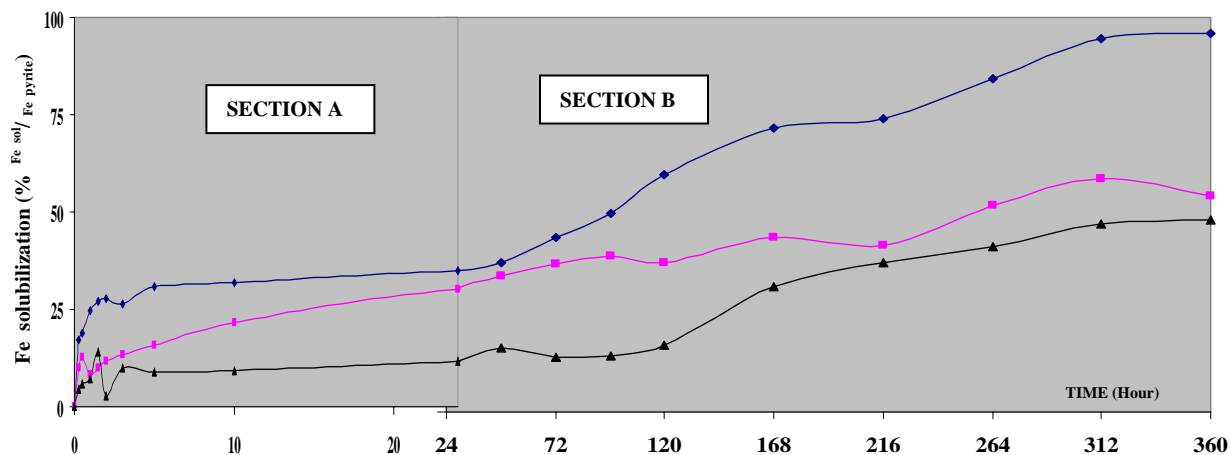


Figure 3.18: Percentages of pyrite oxidation using SL5B. STR biooxidation conducted at 70°C with different liquid medium to pyrite ratios: 1% (◆), 3% (■) and 5% (▲); Section A: 0 to 24hrs of biooxidation, Section B: 24hrs to 360hrs of biooxidation.

The results show that the ability of the thermophile SL5B to oxidize pyrite in a conventional stirred tank bioreactor is dependent on the mineral pulp density. The final pyrite oxidation was reduced 43.1% and 49.3% when pyrite concentration was increased to 3% and 5% compare to 1% pyrite ratio. The finding is different from that reported by Nemati and Harrison (2000) and Devenci (2002), where pyrite oxidation was affected at pulp densities greater than 10%. However the finding is in agreement with Acevedo et al (2004).

During the first 24 hrs oxidation (section 1, figure 3.18), the initial part of the curves with a sharper slope (0-5 hrs for 1% pyrite, 0-1hrs for 3% pyrite and 0-1.5hrs for 5% pyrite) represents the oxidation of pyrite due to catalytic activity of growing cells, whereas the second part (5-24 hrs for 1% pyrite, 1-24hrs for 3% pyrite and 3-24hrs for 5% pyrite) with a smaller slope represents the activity of a non-growing population of the cells (Nemati and Harrison, 2000). Boon (1996) is also proposed two sub-process mechanisms in the initial pyrite bioleaching i.e: 1) irreversible attached bacteria on the mineral surface specifically interact with sulfur moiety of the mineral and 2) pyrite is chemically oxidized to generate ferrous iron and sulfur, in this stages all bacteria and ferric ion has a full access to substrate. The first model was found 10 to 20 times larger

than second model, calculated using pyrite oxidation kinetic model. Irreversible cell attachment required 50% to 100% of pyrite surface recovered with mono layer attached bacteria with specific rate at $\mu \approx 0.1 \text{h}^{-1}$ (Boon, 1996)

Table 3.12: The rate of pyrite oxidation for the irreversible attached bacteria model and chemical oxidation model.

	Model 1. Irreversible attached bacteria		Model 2. Chemical oxidation model	
Pulp densities	Time	Oxidation rate	Time	Oxidation rate
1%	0-5 hrs	$d[X_{(\%, \text{Fe pyrite})}]/dt = 17.79 \text{ x}$	5-24 hrs	$d[X_{(\%, \text{Fe pyrite})}]/dt = 0.22 \text{ x} + 29.64$
3%	0-1 hrs	$d[X_{(\%, \text{Fe pyrite})}]/dt = 12.99 \text{ x}$	1-24 hrs	$d[X_{(\%, \text{Fe pyrite})}]/dt = 0.90 \text{ x} + 9.79$
5%	0 -1.5 hrs	$d[X_{(\%, \text{Fe pyrite})}]/dt = 9.10 \text{ x}$	1.5-24 hrs	$d[X_{(\%, \text{Fe pyrite})}]/dt = 0.13 \text{ x} + 8.49$

From table 3.12, the rate of pyrite oxidation for irreversible bacteria attachment was decreased with increased in pulp densities i.e the rate of pyrite oxidation rate was at $17.79 \text{ } \%_{\text{Fe}}/\text{hr}$ for 1% pyrite, $0.0736 \text{ } \%_{\text{Fe}}/\text{hr}$ for 3% pyrite and $0.1291 \text{ } \%_{\text{Fe}}/\text{hr}$ for 5 % pyrite. As mention before, the rate of oxidation at model 2 (Table 3.16) was 81, 14 and 70 times lower compared to model 1 (Table 3.12) for 1%, 3% and 5% pyrite respectively.

During the initial stages of pyrite oxidation deals with all bacteria and ferric ion has a full access to substrate. The rate of solubilization of pyrite for the initial stages of biooxidation can be expressed into shrinking core and particle model with the film diffusion and chemical reaction considered as a limiting step.

3.2.3.1 Shrinking particle model for diffusion through liquid film as a limitation step

From the figure E1-E3 (attachment E), where $1-(1-X_B)^{2/3}$ vs leaching time (Shrinking particle model for diffusion through liquid film as a limitation step), the

time required for complete pyrite oxidation for each set of biooxidation experiment can be predicted and it shown in table 3.13.

Table 3.13: Time required (t_{total}) for complete pyrite oxidation if the shrinking particle model for diffusion through liquid film as a limitation step

Culture	$1-(1-X_B)^{2/3}$ vs t	T_{total}	Regression coefficient (R^2)
SL5B, 1% pyrite	$t = 0.008x + 0.2016$	99.8 hrs	0.35
SL5B, 3% pyrite	$t = 0.0098 + 0.087$	93.2 hrs	0.80
SL5B, 5% pyrite	$t = 0.0028x + 0.0612$	335.3 hrs	0.23

3.2.3.2 Shrinking core model for diffusion through liquid film as a limitation step

From the figure E1-E3 (attachment E) where X_B vs leaching time (Shrinking core model for diffusion through liquid film as a limitation step), the time required for complete pyrite oxidation for each set of biooxidation experiment can be predicted and it shown in table 3.14.

Table 3.14: Time required (t_{total}) for complete pyrite oxidation if the shrinking core model for diffusion through liquid film as a limitation step.

Culture	X_B vs t	T_{total}	Regression coefficient (R^2)
SL5B, 1% pyrite	$t = 0.0058x + 0.1405$	148.2 hrs	0.39
SL5B, 3% pyrite	$t = 0.0070x + 0.0587$	134.5 hrs	0.82
SL5B, 5% pyrite	$t = 0.0019x + 0.0414$	504.5 hrs	0.23

3.2.3.3 Shrinking core and particle model for chemical reaction on pyrite surface as a limitation step

The time required for complete pyrite oxidation for each set of biooxidation experiment can be predicted and it shown in table 3.15 (fig D2-D7: attachment D).

Table 3.15: Time required (t_{total}) for complete pyrite oxidation if the shrinking core model for diffusion through liquid film as a limitation step

Culture	$1-(1-X_B)^{1/3}$ vs t	T_{total}	Regression coefficient (R^2)
SL5B, 1% pyrite	$t = 0.0032x + 0.0735$	289.5 hrs	0.38
SL5B, 3% pyrite	$t = 0.0037x + 0.0297$	262.2 hrs	0.84
SL5B, 5% pyrite	$t = 0.0010x + 0.021$	979.0 hrs	0.23

From tables 3.13, 3.14 and 3.15, it is clearly shows that the increasing of pyrite pulp densities to 3% will accelerate the initial biooxidation process (formation of inert products is negligible) to 6.65%, 9.26% and 9.42% when the diffusion through liquid film for shrinking core and shrinking particle, and chemical reaction considered as limitation step respectively. However, increasing of pyrite to 5% the time required for complete oxidation was increased around 3.4 times higher for the shrinking core and particle model with the liquid film diffusion and chemical reaction become a limitation step.

After 24 hr of bioxidation, the pyrite solubilization steadily increased at a rate of 0.1902 %_{Fe}/hr . 0.0736 %_{Fe}/hr and 0.1291 %_{Fe}/hr for 1%, 3% and 5% pulp densities of pyrite. The reduction in the bioleaching rate can be due to the fact that at higher concentrations of solids, friction between particles increases, and may consequently cause some mechanical damage to the cell (Deveci, 2002 and Chong et al 2002). Extremely thermophilic archae such as Sulfolobus and Acidianus lack a rigid peptidoglycan cell wall (Michel and Neugebauer, 1980, Konig and Stetter, 1986 and Konig,1988).Also, the fluidity of cellular membrane increases with temperature (Kelly and Deming, 1988). A combination of these factors results in a potential for archae to be sensitive to shearing effect. The effect is due to the hydrodynamic interactions between moving particles,

which leads to shearing effects on immobilized microorganisms from the surface of sulfide particles (Karamanev et al, 2001). However, the effect of particle shearing on the leaching rate has not been measured quantitatively. The effect will be applied by the addition of solid particles. The addition of particles creates a significant shear stress in liquid media (Soljanto et al.1980). It is worth noting that the overall effect depends on the relative importance of each of the following mechanisms i.e: The surface of the added particles is used by microorganisms to form a biofilm. This accelerates bioreaction because the number of microorganisms in the biofilm is extremely high. The increase in the production of ferric ions will also increase the rate of oxidation of pyrite (Crundwell, 1996, Loi et al., 1993, and Karamanev and Nikolov, 1988). The addition of particles creates a significant shear stress in liquid media. This probably affects negatively the microbial growth and, therefore, the bioreaction rate; when oxygen was dissolved by air sparging, the addition of fine particles decreases the rate of oxygen transfer from gas bubbles to liquid. In the case of the oxygen-transfer controlled process, this will reduce the overall rate of biooxidation. (Bailey and Hansford, 1993; Neale and Pinches, 1994; Van Weert et al., 1995). However, each of these mechanisms is affected differently by the nature of solid particles: size, density, surface characteristics, and chemical composition.

3.2.3.4 Shrinking core model with diffusion of porous inert layer as a limitation step

As mentioned at 3.2.2.4, the iron oxidation behaviour for the 360 hrs can be simplify and elaborate into shrinking core model with the film diffusion with product layer considered as controlling step as shown in equation C-51 (attachment C). From figure E-4 (attachment E), the reaction model and required reaction time (T_{total}) can be predicted in table 3.16:

Table 3.16: The required bioleaching time for pyrite biooxidation using for *SL5B*, *Sb.thermosulfodoxidan* and *T. ferrooxidans* and its control, when product layer diffusion becomes a rate limiting step in leaching reaction:

Initial pyrite size (r)	$1-3(1-X_B)^{2/3}+2(1-X_B)$ vs t	T _{total}	Regression coefficient (R ²)
SL5B, 1% pyrite	t=0.0019XB-0.0032	528.0 hrs	0.96
SL5B, 3% pyrite	t=0.0004XB+0.0102	2474.5 hrs	0.93
SL5B, 5% pyrite	t=0.0003XB+0.0026	3324.7 hrs	0.94

From table 3.16, it was clear that the regression coefficient for shrinking core model with the product layer diffusion as controlling step is definitely high compared to the shrinking core and particle model with the film diffusion and chemical reaction as controlling step. i.e : (R²) were at 0.96, 0.93 and 0.94 (shrinking core model with the product layer diffusion) compared to 0.35, 0.80 and 0.23 (shrinking core and particle model with the film diffusion and chemical reaction as controlling step, Table 3.14 and 3.15) for biooxidation using 1%, 3% and 5% of pyrite respectively. It shows that the product layer diffusion is become dominant to the pyrite oxidation process in STR at pyrite pulp densities 1 to 5%. The required time for complete oxidation for the pyrite oxidation with the product layer diffusion as controlling step is related to the pulp densities, increasing of pyrite to 3% and 5% were increased the T_{total} to 4.69 and 6.30 times higher respectively.

3.2.3.5 Iron speciation and jarosite formation in the STR biooxidation at different pyrite pulp densities

Fig 3.19 shows the composition of solubilized iron in a solution and iron in the form of precipitates in the STR biooxidation using SL5B at pyrite.

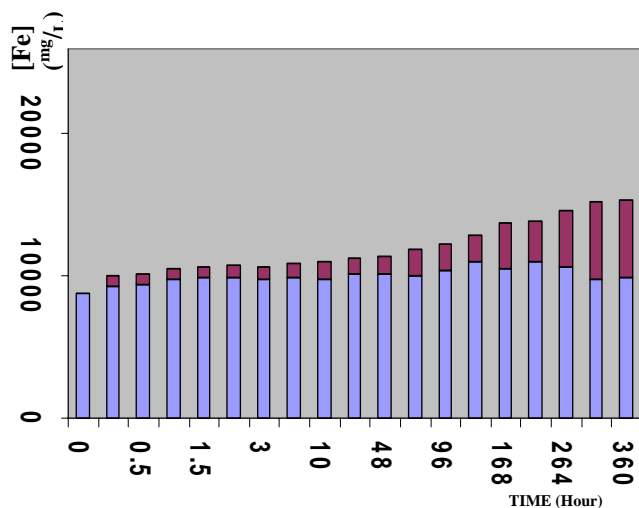


Figure 3.19.A: Profiles of free-iron (■) and iron-jarosites (■). 1% Pyrite concentration

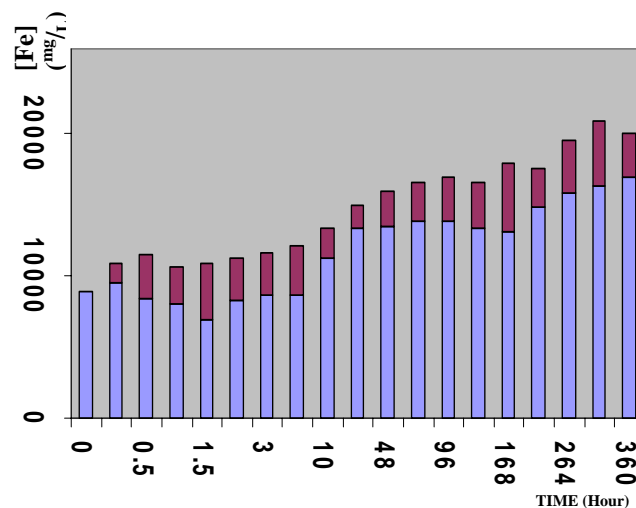


Figure 3.19.B: Profiles of free-iron (■) and iron-jarosites (■). 3% Pyrite concentration

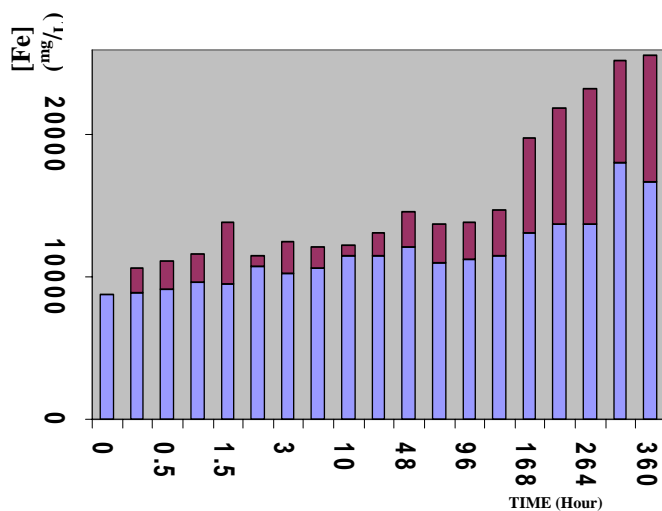


Figure 3.19.C: Profiles of free-iron (■) and iron-jarosites (■). 5% Pyrite concentration

Even at low percentages of pyrite oxidation, the actual iron oxidized at 5% pyrite concentration is 158% and 51% higher compared to 1% and 3% pulp densities. The overall rate of iron oxidation is at 53.81 ppm Fe/hr , 41.41 ppm Fe/hr and 22.375 ppm Fe/hr for

5%, 3% and 1% pulp densities respectively. The other interesting point is a rapid formation rate of jarosite was observed at 96th to 360th hrs for 5% pulp densities. At this moments, the DO consumption rate by freely suspension culture (fig 3.20), pH (fig 3.21), E_H (fig 3.21) and Fe^{3+}/Fe^{2+} ratios (fig 3.20) were found reduced drastically. The formation of precipitates of the jarosite-type are accelerated by the physiological stress imposed by the high mineral concentration at high temperature environment, which is caused the diminishing of free suspended culture, (Elgersma et. al, 1993 and Johnson et al, 1999 and Shrihari,1993).

Figures 3.20 show the concentration of free iron in a form of Fe^{2+} and Fe^{3+} during 15 days biooxidation using SL5B.

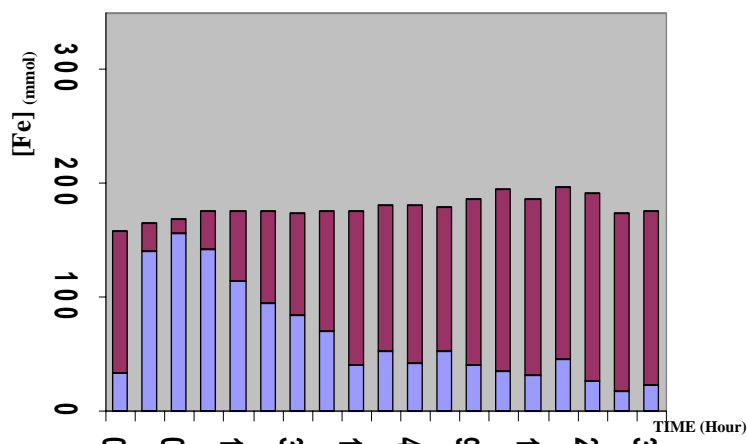


Figure 3.20.A: Profiles of Fe^{2+} (■) and Fe^{3+} (■). At 1% pyrite concentration

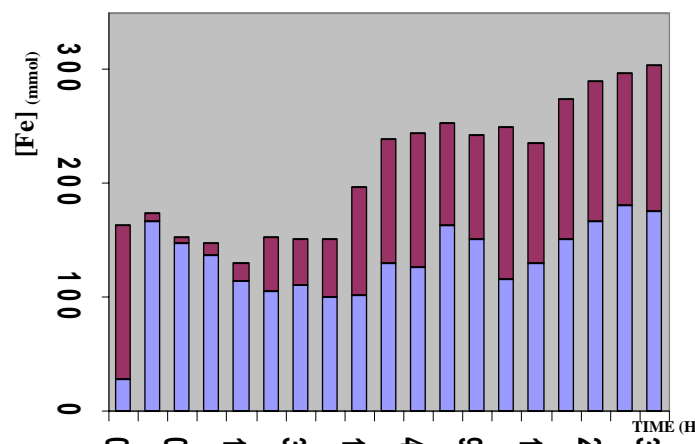


Figure 3.20.B: Profiles of Fe^{2+} (■) and Fe^{3+} (■). At 3% pyrite concentration

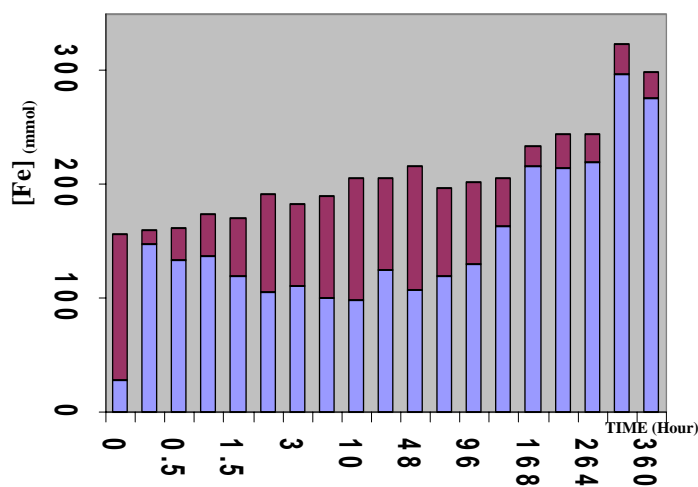


Figure 3.20.C: Profiles of Fe^{2+} (■) and Fe^{3+} (■). At 5% pyrite concentration

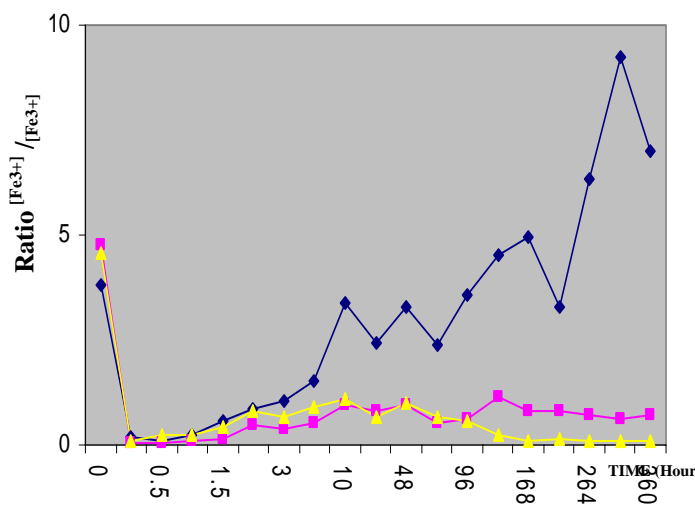


Figure 3.20.D: Profiles of Fe^{3+}/Fe^{2+} ratios for 1% (◆), 3% (■) and 5% (▲) concentration pyrite /medium

The ferric ion concentration was reduced immediately after addition of pyrite. At a high temperature (70°C), reduction of Fe³⁺ was found at 401.4 mol/hr (1% pyrite), 517.5 mol/hr (3% pyrite) and 466.4 mol/hr (5% pyrite). High rate of Fe²⁺ generation during the early process was due to the direct attack of Fe³⁺ on reactive sites at the pyrite (Boon, 1996). The Fe³⁺ production then steadily increased during biooxidation with 1% and 3% pyrite. The rate of Fe³⁺ production for 1% pyrite was at 11.242 [Fe³⁺]_{mol}/hr for 0.5 hr to 10 hr and decreased to 0.082 [Fe³⁺]_{mol}/hr for subsequent hours; for 3% pyrite, the rate was slightly low, at 8.874 [Fe³⁺]_{mol}/hr and 0.072 [Fe³⁺]_{mol}/hr. Compared with 5% pyrite, the Fe³⁺ production was negative after 48 hours biooxidation. For the first 10 hrs, the Fe³⁺ production increased exponentially at 26.87 hr⁻¹. The Fe³⁺ however, diminished exponential at a rate of 41.93 hr⁻¹ after 48 hour of biooxidation. The production of Fe³⁺ in a solution is highly related to the amount of freely suspended culture in the systems (fig 3.22). Fig 3.20-D shows the impact of pyrite concentration on the ratios of (Fe³⁺/Fe²⁺). Low pyrite concentration leads to the higher [Fe³⁺]:[Fe²⁺] ratios. As an example, the average [Fe³⁺]:[Fe²⁺] ratio were at 3.04, 0.57 and 0.45 for biooxidation with 1%, 3% and 5% pyrite respectively. High [Fe³⁺]:[Fe²⁺] ratio at the end of biooxidation with 1% pyrite is a important factor for superior performance in the pyrite solubilization rate.

3.2.3.6 Redox potential (E_H), pH and dissolved oxygen profile for STR biooxidation of pyrite using different types of culture

The profiles of pH and E_H of SL5B bioleaching at 1%, 3% and 5% pulp densities is shown in figures 3.21 A-C.

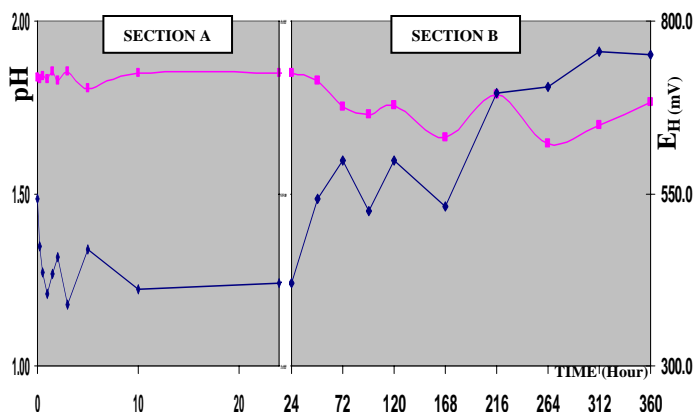


Figure 3.21.A: pH and EH profiles for biooxidation using 1% pyrite

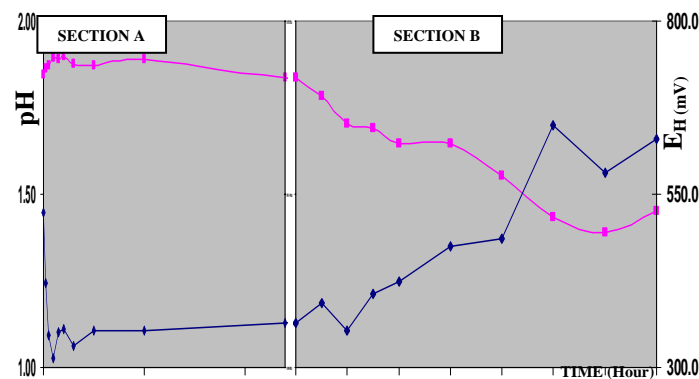


Figure 3.21.B: pH and EH profiles for biooxidation using 1% pyrite

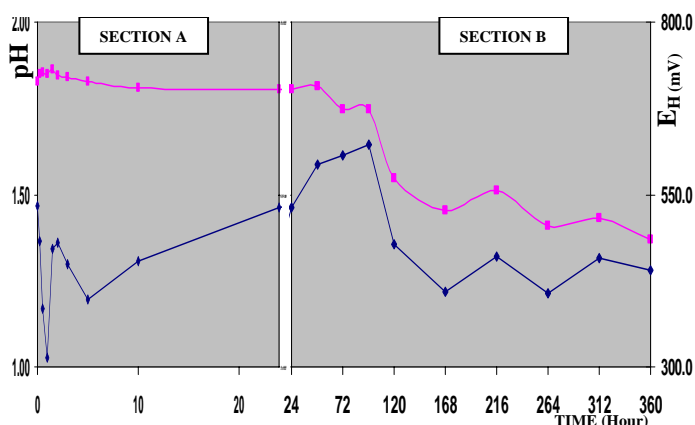
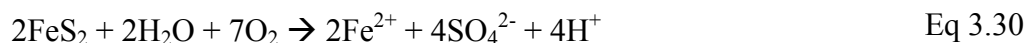


Figure 3.21.C: pH and EH profiles for biooxidation using 1% pyrite

Figure 3.21: pH (■) and E_H (◆) profiles of pyrite oxidation using SL5B. STR biooxidation conducted at 70°C with different ratios of medium: pyrite: 1%(A), 3%(B) and 5%(C); Section A: First 24th hrs of biooxidation, Section B: Subsequent biooxidation at hr 24th to hr 360th.

The pH value for first 24th hrs bioleaching were found significantly similar for the concentration of pyrite at 1%, 3% and 5%. The pH then steadily decreased at a rate of 0.0004 pH unit/h_{hrs}, 0.0014 pH unit/h_{hrs} and 0.0015 pH unit/h_{hrs} for leaching at 1%, 3% and 5% pulp densities of pyrite. The immediate reduction in Eh value was observed during the first hour upon pyrite addition. The initial E_H decreased at a rate of 129.46 mV ORP/h_{hrs}, 201.13 mV ORP/h_{hrs} and 225.65 mV ORP/h_{hrs} for 1%, 3% and 5% pulp densities respectively.

The possibilities of initial E_H reduction is due to the bulk formation of ferrous ion in solution, as shown in pyrite anodic oxidation reactions: (Holmes and Crundell, 1999)



The Eh value showed a constant increase from 1st hr to the 96th hr. its might be due to the formation of ferric ion via bacterial oxidation in the system, as shown in the following equation:



The overall rate of E_H increased was at a 1.6178 $\text{mV ORP}/\text{hrs}$, 0.582 $\text{mV ORP}/\text{hrs}$ and 2.4076 $\text{mV ORP}/\text{hrs}$ for 1%, 3% and 5% pulp densities respectively. The ferrous and ferric ions are cycled between the pyrite oxidation reaction and ferrous ion oxidation reaction. The overall reaction generates acid, which results in decreasing pH values as shown in figures 3.24.

The E_H -pH trends in the experiments involving 1% and 3% pyrite were quite similar. Where, decreasing pH values leads to increasing E_H value. Similar findings were reported by Bunyok, 2004 and Shahjir 2001. This is an ideal condition in bioleaching; where the iron and sulfur in the pyrite were completely oxidize to the ferric ion and acid sulfuric.

However, the trends of E_H -pH bioleaching in the presence of 5% mineral contrasted with that achieved with pulp densities of 1% and 3%. Initially a short lag phase in pH decreased was observed from 0 to 96 hrs. This was followed by a sharp decrease in pH value. During this phase, the E_H value ranged from 622mV to 441mV. Rapid pyrite oxidation at low E_H and pH value is most likely due to the presence of partially oxidised ions of sulphur, such as $\text{S}_2\text{O}_4^{2-}$:-, SO_2^- , which are the intermediate products released into liquid by the cells attached to solids (Asai, 1992)..These

intermediate ions are known to inhibit oxidation of Fe^{2+} and can also form the substrate for the cells in the liquid (Asai, 1992), thus explaining their survival. While this mechanism has been shown to be operative in the case of the leaching of sulphur (Shrihari, 1993), it could also be operating in the present case. When a lesser quantity of solid substrate is available, the alternate substrate may not be present in sufficient quantity and the bacteria in the liquid phase may have to use the Fe^{3+} present in the liquid (Asai, 1992).

Figure 3.22 show the dissolved oxygen in the STR during the SL5B biooxidation using 1%, 3% and 5% of pyrite. The free pyrite solution from the STR then inoculated in the 25L shake flasks. The dissolved oxygen consumption after 48hrs of inoculation is then shown in figure 3.24. Dissolved oxygen level in reactor (fig 3.22) will indicate the amount of active culture in theSTR, while the 48hrs oxygen consumption rate of inoculum will indicate a freely suspended culture in the solution. The method is a modification from off-gas Clark cell methods by Boon (1996)

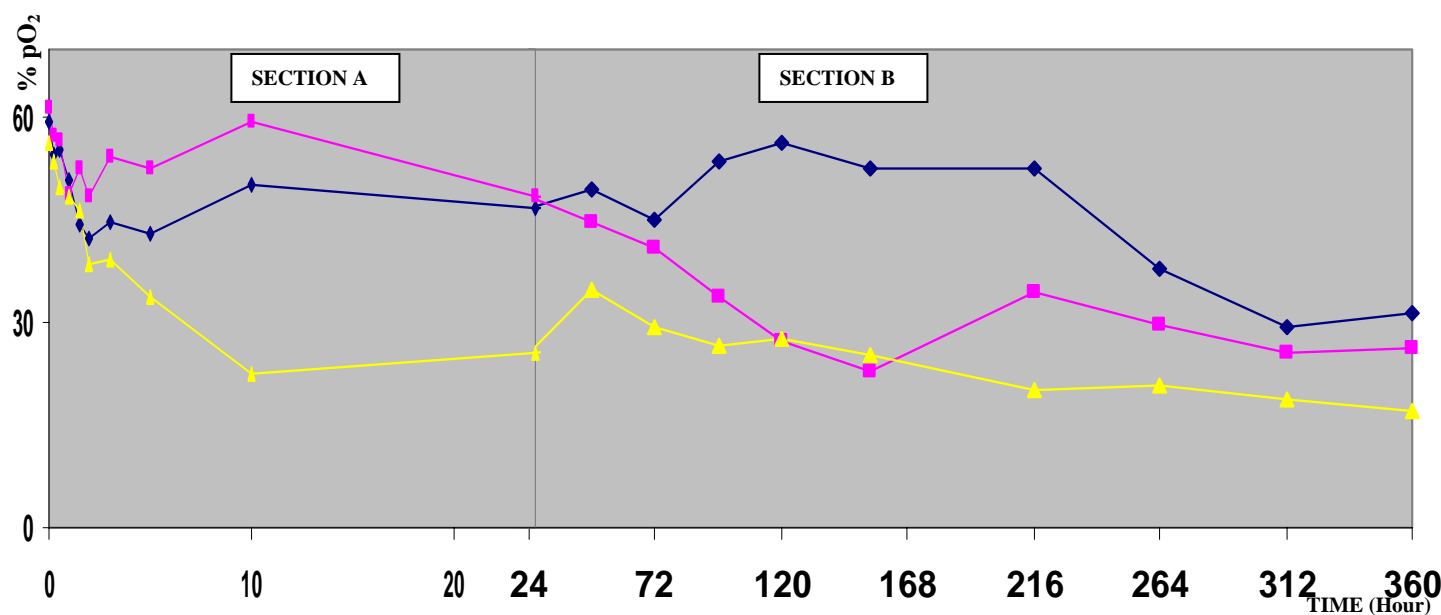


Figure 3.22: Profile of %pO₂ of pyrite oxidation using SL5B. STR biooxidation conducted at 70⁰C with different pyrite concentration: 1% (◆), 3% (■) and 5%(▲);
 Section A: First 24 hrs of biooxidation,
 Section B: Biooxidation at 24 to 360 hr.

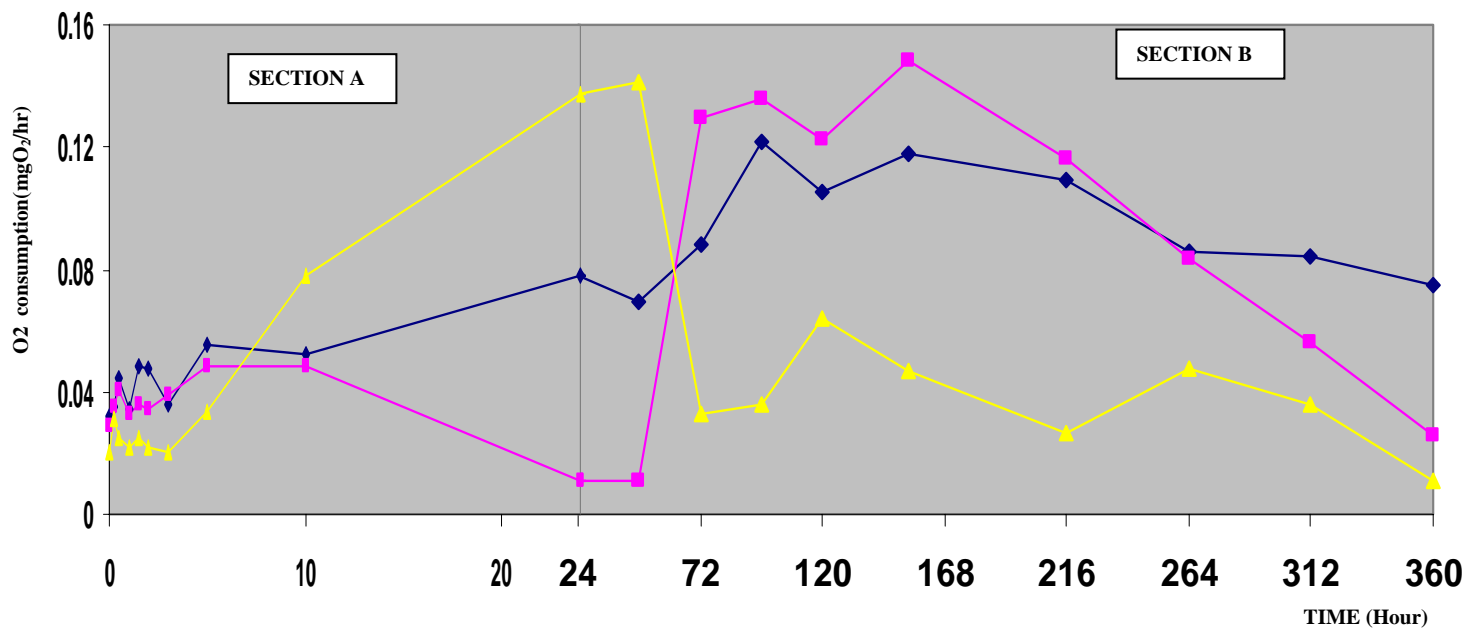


Figure 3.23: Profile of dissolved oxygen consumption by free-pyrite cell suspension of SL5B . Cell from STR biooxidation conducted at 70°C with pyrite concentration : 1% (◆), 3% (■) and 5%(▲); inoculated in a fresh medium for 48 hrs; Section A: First 24 hrs of biooxidation, Section B: Biooxidation at 24 to 360 hr.

A higher dissolved oxygen concentration was observed in the reactor containing lower concentration of pyrite. The average oxygen partial pressure (%pO₂) in a STR were 46.76%, 42.47% and 32.14% in the medium containing 1%, 3% and 5% of pyrite respectively. During biooxidation processes, the pulp density affected the oxygen and carbon dioxide transfer between gas and liquid phase. At high pyrite concentration, more force from impeller agitation and bubble flow are consumed to meet the demand of solids suspension.

The dissolved oxygen level was found to decrease after addition of pyrite: for the biooxidation containing 1% and 3% pyrite, the %pO₂ level decreased at a rate of 8.41 %pO₂/hr and 5.87%pO₂/hr for the first 2 hrs. For the biooxidation with 5% pyrite, the %pO₂ reduced constantly until the 10 hrs, at a rate of 3.16 %pO₂/hr. This might be due to the hydrodynamic shear forces effect in the reactor and a rapid increase in bacterial population. However, the dissolved oxygen consumption rate by free-pyrite cell

suspension shows no increment during the first 2hrs of bioleaching for the entire test. During this period, the bacteria has a high tendency to attach on the pyrite surface.

For the experiment with 1% pyrite, the dissolved oxygen consumption rate by freely suspended cell increased considerably until the 154th hr at a rate of 5.0×10^4 mgO₂/hr², followed by a decrease in DO consumption at a rate of 2.0×10^4 mgO₂/hr². Compared to the system with 3% pyrite, the DO consumption rate remains constant at 0.033 mgO₂/hr² until 48 hours of biooxidation. The DO consumption rate then suddenly increased at 72 hrs and followed by a plateau region between 72 hrs to 154th hrs, indicating the stationary phase of microbial growth. A decreased in dissolved oxygen consumption rate at 6.0×10^4 mgO₂/hr², representing the dead phase of culture at the end of the biooxidation stages i.e; hrs 154th to hrs 360th.

3.2.4 STR bioleaching of different pyrite size using SL5B.

The rate of biooxidation of refractory gold concentrates is influenced by several operational factors. It is recognized that increasing pulp densities and decreasing particle sizes have a positive effect in the volumetric rate of biooxidation, as both situations result in an increase in surface area. Nevertheless, it has also been noted that the interaction among these factors together with a variety of associated phenomena such as mechanical damage, metabolic stress and inhibitory concentrations of ferric ion, can limit this positive effect and even result in declining leaching rates (Bailey and Hansford 1993, Kandler & Konig 1998, Sleytr and Beveridge 1999 d'Hugues et al. 2001; Sissing and Harrison 2003).

On the other hand, decreasing particle size can reduce the leaching rate, probably because of difficulties in cell attachment when the diameters of particles and cells become of similar magnitude. It is also likely that the rate of collision between particles increases as particle size diminishes and that the physicochemical properties of the suspension are altered (Howard and Crundwell 1999; Nemati et al. 2000; Harrison et al.

2003). The objective of this work was to determine the optimal values of particle size that maximize the volumetric rate of solubilization of iron from a pyrite when using the thermophilic culture SL5B in STR.

3.2.4.1 Dissolved oxygen consumption profile, pH, Redox potential (E_H) and Fe^{3+}/Fe^{2+} profile during biooxidation

Figure 3.24 shows the pH, $\ln(Fe^{3+}/Fe^{2+})$ and E_H profiles of pyrite oxidation using strain SL5B. STR biooxidation conducted at 70°C with different size of pyrite: 75µm (3.30-A), 125 µm (3.30-B) 180 µm (3.30-C), 250 µm (3.30-D) and 500 µm (3.30-E). These parameters develop a suitability of the environment to microbial life. It's very convenient ways of characterizing the viability of certain species (Lundgren and Dean, 1979).

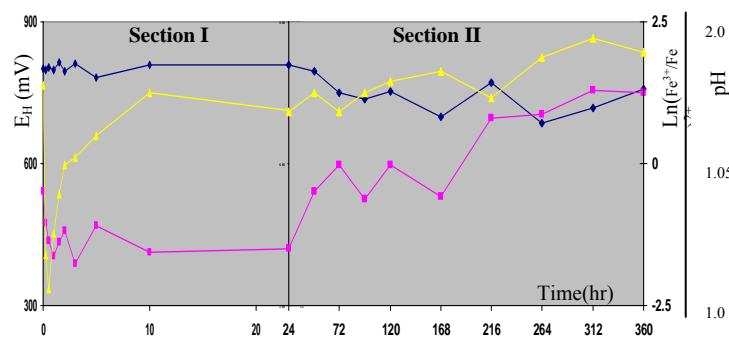


Figure 3.24-A: pH (◆), $\ln(\text{Fe}^{3+}/\text{Fe}^{2+})$ (▲) and E_H (■) profiles of pyrite at size $75\mu\text{m}$

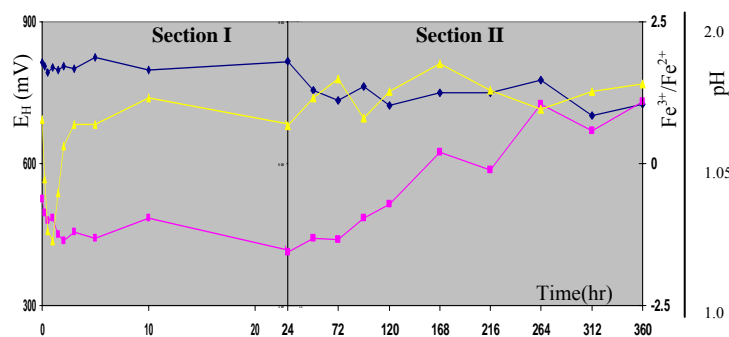


Figure 3.24-B: pH (◆), $\ln(\text{Fe}^{3+}/\text{Fe}^{2+})$ (▲) and E_H (■) profiles of pyrite at size $125\mu\text{m}$

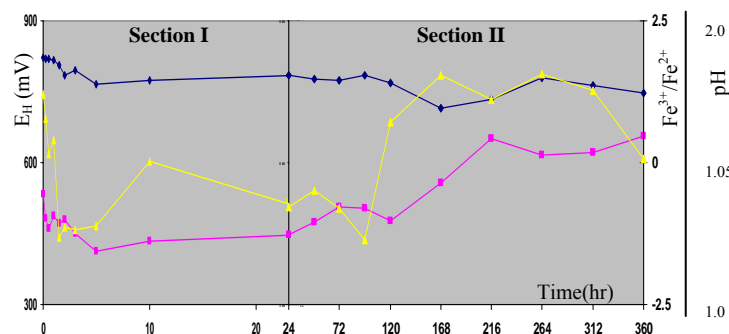


Figure 3.24-C: pH (◆), $\ln(\text{Fe}^{3+}/\text{Fe}^{2+})$ (▲) and E_H (■) profiles of pyrite at size $180\mu\text{m}$

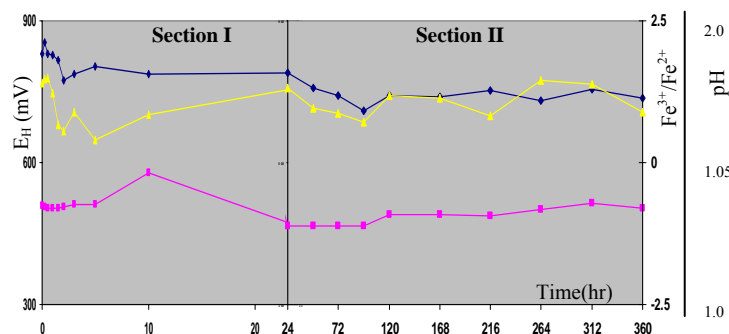


Figure 3.24-D: pH (◆), $\ln(\text{Fe}^{3+}/\text{Fe}^{2+})$ (▲) and E_H (■) profiles of pyrite at size $250\mu\text{m}$

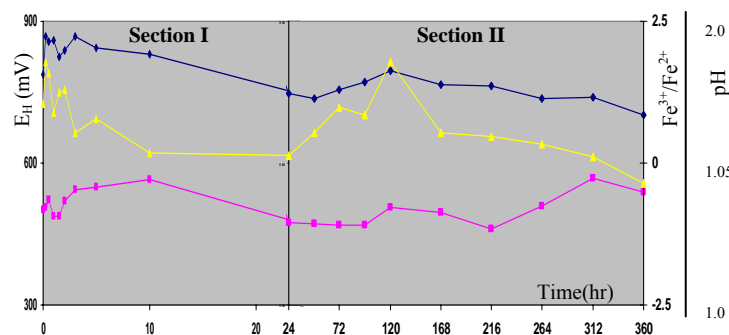


Figure 3.24-E: pH (◆), $\ln(\text{Fe}^{3+}/\text{Fe}^{2+})$ (▲) and E_H (■) profiles of pyrite at size $500\mu\text{m}$

The pH, ratios of Fe^{3+}/Fe^{2+} and E_H value is very dependent to each other, and become a limiting parameters in the biooxidation process (Boon, 1996). It is also become indicator in the performance of the biooxidation process. The correlation between the following parameter is shown in equation 3.32, 3.33 and 3.34 (Rossi, 1990):

$$E_H = 0.771 + 0.059 \log \frac{[Fe^{3+}]}{[Fe^{2+}]} \quad \text{Eq 3.32}$$

The pH and Eh value is express from electrochemistry study, where the relationship between hydrogen partial pressure, hydrogen ion and redox potential is shown in equation 3.33 and 3.34 (Rossi, 1990).

$$E_H = -\frac{0.059}{2} \log P_{H_2} - 0.059 pH \quad \text{Eq 3.33}$$

Where

$$rH_2 = \frac{E_H}{0.020} + 2pH \quad \text{Eq 3.34}$$

The pH trends for biooxidation with 75 μ m, 125 μ m and 180 μ m remains constant at average pH 1.85 for the initial phase of biooxidation (for the first day of biooxidation). Compared to the larger particle, 250 μ m and 500 μ m pyrite, the pH were sudden increased (hour 0 to 15th mnt) after addition of pyrite. The pH rate increased was higher with 500 μ m pyrite, at 0.53 pH/hr compared to the 0.15 pH/hr for 250 μ m pyrite. Its might be due to the the larger particles of pyrite containing a high amount of silica and carbonates (Nemati et al, 2000). The pH then sharply decreased at the rate of 0.05 and 0.07 pH/hr for 500 μ m and 250 μ m pyrite.

It is like to stress that amount of pH reduction for the first day of biooxidation (from mnt 15th to hours 24th) were highly influence by the size of pyrite. The average pH

reduced were at 0.0005 pH/hr, 0.0008 pH/hr, 0.0026 pH/hr, 0.002 pH/hr 8 and 0.0063 pH/hr for 75 μ m, 125 μ m, 180 μ m, 250 μ m and 500 μ m of pyrite respectively.

Compared with the E_H and Fe^{3+}/Fe^{2+} trend, The value for the finer particle of pyrite was drastically decreased after addition of pyrite (from $t=0$ to $t=30$ mnts) . The higher drop rate of the E_H and Fe^{3+}/Fe^{2+} value were observed in a biooxidation process containing finer particle of pyrite. The decreasing rate rate of initial E_H and Fe^{3+}/Fe^{2+} is shown as follows (table 3.17). In contrast with fine partile, the E_H and Fe^{3+}/Fe^{2+} value for coarse particle 500 μ m shows a little increased after addition of pyrite.

Table 3.17: The decreasing rate rate of initial E_H and Fe^{3+}/Fe^{2+} (from $t=0$ to $t=30$ mnt) for the biooxidation using SL5B strain, containing 75 μ m, 125 μ m and 180 μ m of pyrite.

75 μ m	$dE_H/dt = -210.6$ mV/hr	$\ln [Fe^{3+}]/[Fe^{2+}]/dt = -7.147$ hr ⁻¹
125 μ m	$dE_H/dt = -88.8$ mV/hr	$\ln [Fe^{3+}]/[Fe^{2+}]/dt = -3.932$ hr ⁻¹
180 μ m	$dE_H/dt = -147.6$ mV/hr	$\ln [Fe^{3+}]/[Fe^{2+}]/dt = -2.124$ hr ⁻¹
250 μ m	$dE_H/dt = -9.4$ mV/hr	$\ln [Fe^{3+}]/[Fe^{2+}]/dt = 0.175$ hr ⁻¹
500 μ m	$dE_H/dt = 39.0$ mV/hr	$\ln [Fe^{3+}]/[Fe^{2+}]/dt = 1.055$ hr ⁻¹

From the results, the initial E_H and Fe^{3+}/Fe^{2+} is highly dependent on a pyrite size, finer pyrite size or higher pyrite surface area leads to the higher rate of initial E_H and Fe^{3+}/Fe^{2+} reduction. During the first hour of oxidation, the surface pyrite oxidation by ferric ions was dominating the process. However, due to the limitation in pyrite

surface area in larger particle i.e: 500 μm , its become a limiting factor on the ferric surface reaction.

Contrastive with pH trends, the overall E_H values were considered increased during biooxidation process for the 75 μm , 125 μm and 180 μm . It is follows by the increasing in the ratios of $\text{Fe}^{3+}/\text{Fe}^{2+}$ value. The identical observation is also reported by Sjahrir (2000) and Bunyok (2004). Synonym with the pH trend observation, the rate of increasing in E_H value were inspired by particle size. The finer particle size leads to the superior increased in overall E_H value. The average E_H raised were at 0.852, 0.823 and 0.573 mV/hr for 75 μm , 125 μm and 180 μm of pyrite respectively. However, for biooxidation with 250 μm and 500 μm of pyrite, the E_H value considerably constant at the low value (at average of 495mV and 503mV for 250 μm and 500 μm) until the end of experiments.

Liquid solution from the biooxidation process was taken from the STR and inoculum in the 250ml shake flasks. Sterilized silicon oil was then added into flasks to avoid oxygen transfer into inoculum. The dissolved oxygen consumption for 48 hour incubation were recorded. Figures 3.25 shows the profiles of dissolved oxygen composition rate in a inoculation solution, for the SL5B biooxidation using different size of pyrite.

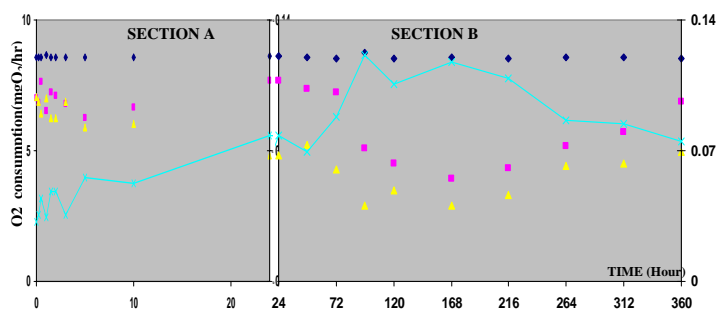


Figure 3.25-A: Profile of DO consumption rate by free-pyrite cell suspension of SL5B. Pyrite size: 75 μm .

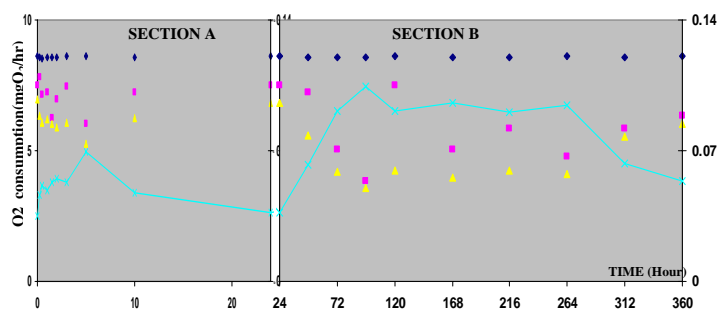


Figure 3.25-B: Profile of DO consumption rate by free-pyrite cell suspension of SL5B Pyrite size: 125 μm .

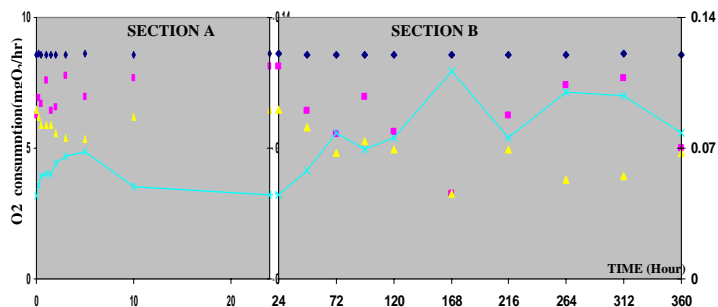


Figure 3.25-C: Profile of DO consumption rate by free-pyrite cell suspension of SL5B Pyrite size: 180 μm .

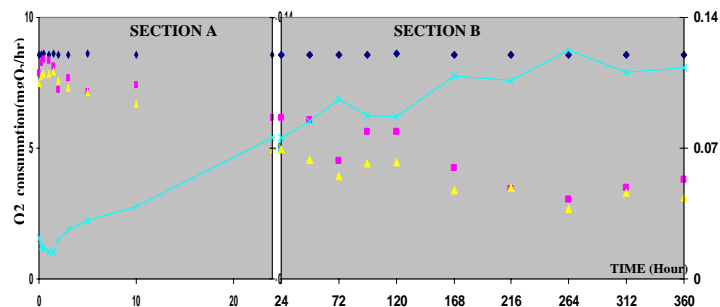


Figure 3.25-D: Profile of DO consumption rate by free-pyrite cell suspension of SL5B Pyrite size: 250 μm .

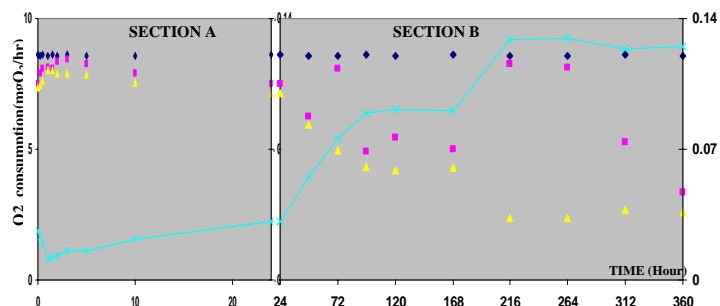


Figure 3.25-E: Profile of DO consumption rate by free-pyrite cell suspension of SL5B Pyrite size: 500 μm .

Figure 3.25: Profile of Dissolved oxygen consumption by free-pyrite cell suspension of SL5B . Cell from STR biooxidation conducted at 70⁰C with different size of pyrite: 75 μm (A), 125 μm (B), 180 μm (C), 250 μm (D) and 500 μm (E). Inoculated in a fresh medium for 48 hrs; \blacklozenge :initial DO reading for inoculate, \blacksquare :DO reading after 24 hrs inoculate, \blacktriangle :DO reading after 48 hrs inoculate and $-x-$: DO consumption rate during 48 hrs inoculation. Section A: First 24th hrs of biooxidation, Section B: Subsequent biooxidation at hr 24th to hr 360th.

The trends in microbial growth and bioleaching observed with finer size fractions (75 μm , 125 μm and 180 μm) were similar to one another but contrasted with the experiment in the presence of pyrite with a larger diameter of 250 μm and 500 μm . The initial period of experiments coincided with a short lag phase in microbial growth, which was more pronounced in the presence of larger particles (Figs. 3.25 D and E). The microbial growth was reducing hastily after addition of 250 μm and 500 μm pyrite. The rate of 48 hours freely pyrite suspended DO consumption were reduce at 0.011 mgO_2/hr^2 for 500 μm of pyrite and 0.005 mgO_2/hr^2 for 250 μm of pyrite for the first 1.5 hrs of reaction. This was followed by the exponential phase of growth (from hrs 1.5th to hrs

72nd for 250 μm of pyrite and from hrs 1.5th to hrs 216th for 500 μm of pyrite) . During that phase, the DO consumption were increased at the rate of 0.0011 mgO_2/hr^2 for 250 μm of pyrite and 0.0005 mgO_2/hr^2 for 500 μm of pyrite.

Compared with the fine pyrite particles (75 μm , 125 μm and 180 μm), the microbial growth were found increased until hrs 96th for 75 μm and 125 μm pyrite and hrs 168th for 180 μm of pyrite. During these phase, the rate of microbial growth were dependent to pyrite size. The finer of pyrite will increased the initial growth rate, i.e: 0.0008 mgO_2/hr^2 , 0.0005 mgO_2/hr^2 and 0.0003 mgO_2/hr^2 for 75, 125 and 180 μm of pyrite respectively.

It is like to stress that the death phase have been observed at the end of experiment, in fermenter containing a fine particle of pyrite. The death phase have been started at hrs 216th, 264th and 312th for 75, 125 and 180 μm of pyrite respectively. Its shows that the culture reached the death phase earlier in a system containing finer particle.

The possible reason is a the extremely thermophilic culture such as *Sulfolobus* and *Acidianus spp.* lack a rigid peptidoglycan cell wall .Further, the fluidity of the cellular membrane increases with temperature (Kelly and Deming,1988). A combination of these factors results in a potential for culture to be sensitive to shear. Decreasing the particle size of the mineral adversely influenced the activity of the cells. The presence of fine particles apparently damaged the structure of the cells.

3.2.4.2 Iron speciation in the pyrite and solution.

Speciation of Fe ion in the acidic solution consist of ferrous [Fe^{2+}] and ferric [Fe^{3+}]ion. The concentration of each species was determined using titration method. Figures 3.26 shows the profiles of Fe^{2+} and Fe^{3+} in the sample solution from pyrite

biooxidation using SL5B. The test were conducted on a different size of pyrite at 75 μm , 125 μm , 180 μm , 250 μm and 500 μm .

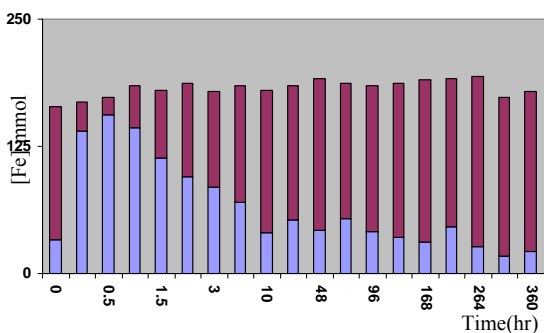


Figure 3.26-A: Fe²⁺ (■) and Fe³⁺ (■) profiles of pyrite at size 75 μm

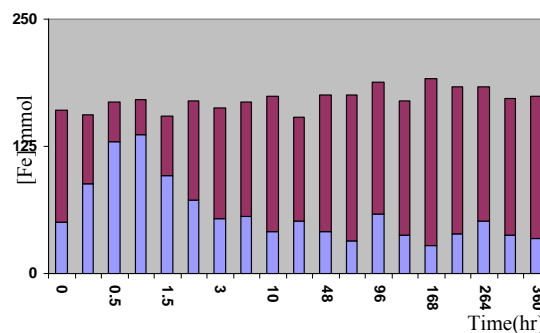


Figure 3.26-B: Fe²⁺ (■) and Fe³⁺ (■) profiles of pyrite at size 125 μm

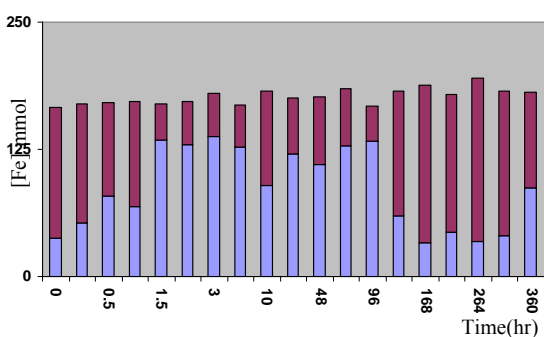


Figure 3.26-C: Fe²⁺ (■) and Fe³⁺ (■) profiles of pyrite at size 180 μm

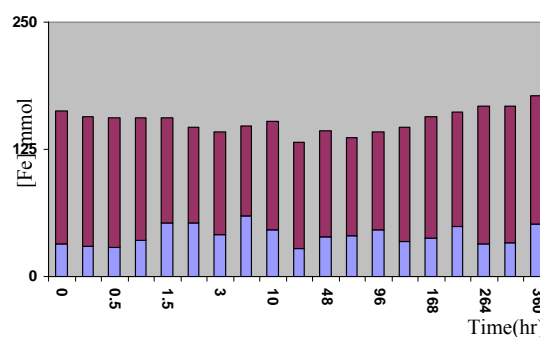


Figure 3.26-D: Fe²⁺ (■) and Fe³⁺ (■) profiles of pyrite at size 250 μm

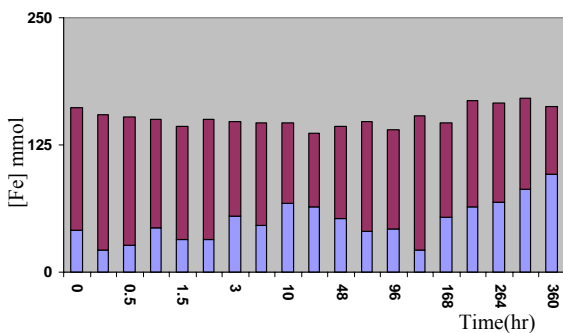


Figure 3.26-E: Fe²⁺ (■) and Fe³⁺ (■) profiles of pyrite at size 500 μm

Figure 3.26: Fe²⁺ (■) and Fe³⁺ (■) profiles of pyrite oxidation using SL5B. STR biooxidation conducted at 70⁰C with different size of pyrite: 75 μm (A), 125 μm (B) 180 μm (C), 250 μm (D) and 500 μm (E);

Results from 3.26 shows the similarity in the profile of Fe^{2+} and Fe^{3+} for the biooxidation using $75\mu\text{m}$, $125\mu\text{m}$ and $180\mu\text{m}$. The Fe^{2+} concentration is found increased dramatically over a short period. The concentration of Fe^{2+} was peak at the value around 140mM several hours after biooxidation. However the rate of increasing in Fe^{2+} concentration is found dependent on the size of pyrite. The initial Fe^{2+} concentration was increased at the rate of 247.2mM/hr , 84.1mM/hr and 35.3mM/hr for biooxidation using $75\mu\text{m}$, $125\mu\text{m}$ and $180\mu\text{m}$ of pyrite respectively. It's due to the initial oxidation deal with a Fe^{3+} oxidation on a pyrite surface. (Boon, 1999). Hence the reactions occurring on the surface of particle, rate of reaction should be increased with decreasing particle size of pyrite since the smaller particles, the larger the surface area per unit weight. It is shown in equation 3.34 and 3.35, by combining the equation, relation between mineral surface area (S) and particle radius (R) is shown in equation 3.36:

$$S=4\pi r^2 \quad \text{Eq 3.34}$$

$$N_A = \rho \frac{4}{3} \pi r^3 \quad \text{Eq 3.35}$$

$$\frac{1}{r_A} = S_A \quad \text{Eq 3.36}$$

where

ρ is the molar density, mol/vol, and

r is the radius of the particle as a function of time.

For the biooxidation containing $75\mu\text{m}$ and $125\mu\text{m}$ of pyrite, the Fe^{2+} concentration was then found decreased as well as increasing of Fe^{3+} concentration for the subsequent hours. The rate of Fe^{3+} formation is found higher in a system containing $75\mu\text{m}$ of pyrite, at 18.1mM compared to the 13.1mM for $125\mu\text{m}$ pyrite. During this period,

formation of Fe^{3+} ion in solution is due to oxidation of Fe^{2+} in solution by strain SL5B.

The steady state condition for Fe^{3+} and Fe^{2+} concentration have been observed at hours 1.5th to hours 96th for the biooxidation with 180 μm pyrite, the Fe^{2+} concentration was stagnant at a value around 130mM. During this phase, pyrite oxidation via Fe^{3+} attack on pyrite surface and bacterial oxidation on Fe^{2+} ion is considered in equilibrium.

It is interesting to note that the concentration of ferrous iron for the for the biooxidation using 75 μm , 125 μm and 180 μm decreased as the pyrite exhausted or 30% oxidize and, at the termination of the experiment, all the soluble iron was considered in the ferric state. With larger particles (250 μm and 500 μm), however, high concentration of the dissolved iron was in the Fe^{3+} state, even at the early stage of biooxidation. The similar observation also reported by Nemati et al (2000). In addition, the initial redox potential of the solution in the presence of larger particles was higher than that observed when smaller particles were used. This seems to occur because the oxidation of pyrite either biologically or chemically is slower than the regeneration of ferric iron by the cells with bigger particles of mineral and, as a result, part of the released iron remains in the Fe^{3+} form. The depletion of surface area in the larger pyrite particle (250 μm and 500 μm) became a limitation to the Fe^{3+} and bacterial to attach on the pyrite surface.

Instead of iron solubilized in the biooxidation process, there is also has a high tendency to reprecipitate in the form of jarosite. The formation of jarosite in the STR can be determined using sequential leaching using sulfuric acid. Figures 3.27 shows the profiles of iron composition in solution (solubilized iron) and in the form of jarosite precipitate for the SL5B biooxidation using different size of pyrite.

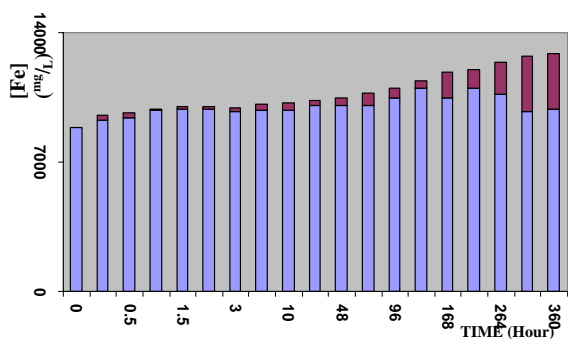


Figure 3.27.A: Profiles of iron solubilized (■) and iron-jarositic (■). Pyrite size: 75µm

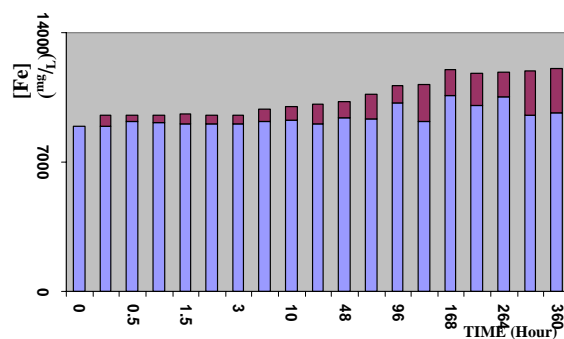


Figure 3.27.B: Profiles of iron solubilized (■) and iron-jarositic (■). Pyrite size: 125µm

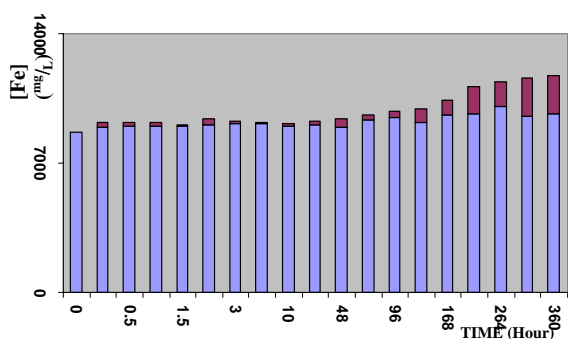


Figure 3.27.C: Profiles of iron solubilized (■) and iron-jarositic (■). Pyrite size: 180µm

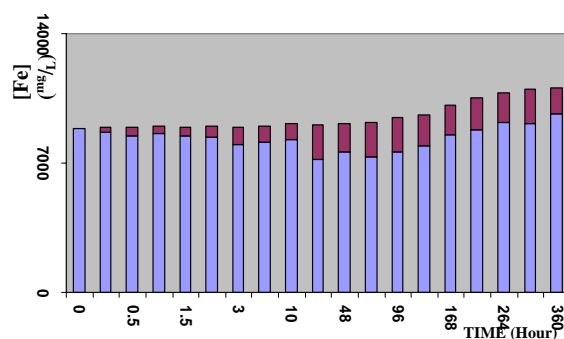


Figure 3.27.D: Profiles of iron solubilized (■) and iron-jarositic (■). Pyrite size: 250µm

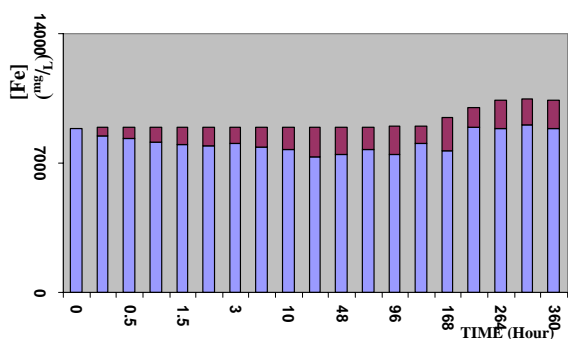


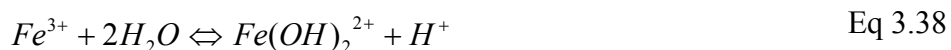
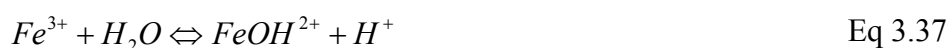
Figure 3.27.E: Profiles of iron solubilized (■) and iron-jarositic (■). Pyrite size: 500µm

Figure 3.27: Profiles of iron solubilized (■) and iron-jarositic (■) of pyrite oxidation using SL5B. STR biooxidation conducted at 70°C with different pyrite size: 75µm (A), 125 µm(B), 180 µm(C), 250 µm(D) and 500 µm(E)
X-axis: Time (hour) is not in the scale

The profile of jarosite formation is fluctuate in a each test. However, the final jarosite formation in test containing fine pyrite is higher compared to the system contain coarser pyrite. As an example, the jarosite concentration in a reactor containing 75 µm

pyrite were 2 times higher compared to jarosite concentration in a 250 μm and 500 μm . That might be due to the higher concentration of Fe^{3+} ion and pH value of the solution containing 75 μm pyrite.

It is quite visible that the pH and E_H of the system has effect on the extent of the oxidation and hydrolysis reaction. Since there is consumption of hydrogen ions, the pH of the liquid media were increased. However, this pH increase is counteracted by the hydrolysis of ferric iron as shown in equations 3.37, 3.38 and 3.39:



Furthermore, there is a reaction in competition with the hydrolysis reaction giving products of basic ferric hydroxysulphates with the formula $\text{MFe}_3(\text{SO}_4)_2(\text{OH})_6$ where $\text{M} = \text{K}^+, \text{Na}^+, \text{NH}_4^+, \text{Ag}^+$ or H_3O^+ (Jensen and Webb, 1995). These hydroxysulphate precipitates are known as jarosites. The following is the formula for jarosite precipitation (Eq 3.40):



Since the 9K medium contains a high concentration of NH_4 ions, the jarosites produced were ammoniojarosites with the formula $\text{NH}_4\text{Fe}_3(\text{SO}_4)_2(\text{OH})_6$. Jarosite formation has negative effects on many applications that require the use of biooxidation culture, especially in the process of biological gas desulphurization. Some of the effects include the diminishment of ferric iron used as the absorbent for hydrogen disulfide, blockage of pumps, valves, pipes, etc., and the creation of kinetic barriers due to the small diffusion of reactants and products through the precipitation zone (Jensen and Webb, 1995).

3.2.4.3 Pyrite oxidation rate.

Figure 3.28 shows a pyrite oxidation during bioleaching using SL5B at 70°C

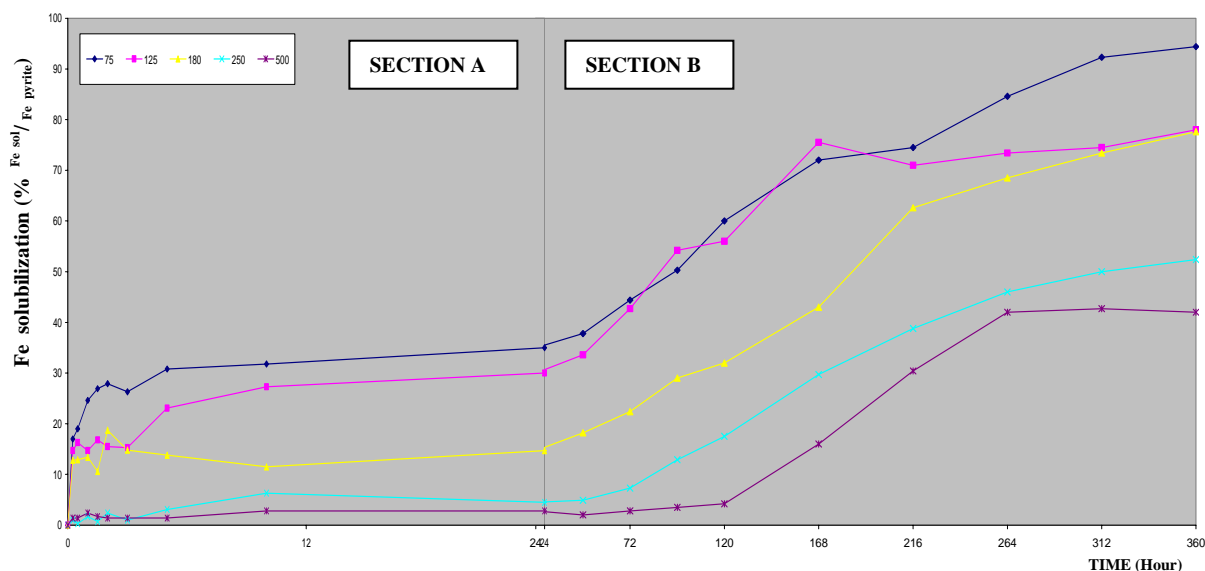


Figure 3.28: Percentages of pyrite oxidation using SL5B. STR biooxidation conducted at 70°C with different size of pyrite: 75μm (◆), 125μm (■) and 180μm (▲), 250μm (⊗) and 500μm (×); Section A: First 24th hrs of biooxidation, Section B: Subsequent biooxidation at hr 24th to hr 360th.

Result from figure 3.28 shows that the particle size of pyrite can influence the performance of biooxidation using SL5B. The highest pyrite oxidation (94.4%) was obtained using 75μm pyrite, followed by 78% for 125 and 180μm, 52% for 250μm and 42% for 500 μm pyrite. The initial oxidation of pyrite (first 5th hours) were exponential increased to achieve 28%, 17% and 14% for 75μm, 125μm and 180μm of pyrite respectively. The pyrite oxidation then increased linearly till the end of the experiment. The oxidation rate for system containing 75μm, 125μm and 180μm of pyrite were at 0.19%_{Fe/hr}, 0.16%_{Fe/hr} and 0.20%_{Fe/hr} to achieve 94.4%, 78.0% and 77.6% oxidation of pyrite correspondingly

For the coarser pyrite size, a lag phase of pyrite oxidation was observed at the initial stages. However, the lag phase for reactor containing 250 μm of pyrite (72 hrs) is

shorter than that containing 500 μm pyrite (120hrs). During this period, the pyrite was slightly oxidized at a rate of 0.12% Fe/hr and 0.04 % Fe/hr for 250 μm and 500 μm . The exponential phase of the 250 μm pyrite oxidation was observed at 0.21% Fe/hr between 72 to 360 hour. For the 500 μm pyrite, oxidation was at 0.23% Fe/hr between 120 to 264 hour. The stationary phase of pyrite oxidation was observed at the end of the experiment (264 to 360 hr) using 500 μm pyrite. This descending trend was obvious in experiments using larger particles of pyrite, initially containing a high amount of silica. This suggests that the lack of an energy source is not the only contributing factor to cell death. The freely suspended biomass also undergoes rapid attrition in the presence of silica under conditions of non growth. This is in agreement with the finding of Scholtz et al. 1997

From the results in figure 3.27, there exists a relationship between bioleaching rate and particle size of pyrite. A decrease in the pyrite size leads to an increase bioleaching rates. In other words, a reduction in particle size and, thus, an increase in the surface area per unit mass of pyrite, improved mass transfer and accelerated the bioleaching of pyrite. The overall oxidation rate for SL5B at respective pyrite size is shown in table 3.18

Table 3.18: The rate of pyrite oxidation for SL5B biooxidation at different pyrite size

Pyrite size	Oxidation rate	T _{total}
75 μm	$\text{Ox } (\%, \text{ Fe pyrite}) = -0.0004 T_{\text{hrs}}^2 + 0.3551 T_{\text{hrs}} + 22.04$	396 hours
125 μm	$\text{Ox } (\%, \text{ Fe pyrite}) = 2 \times 10^{-6} \times T_{\text{hrs}}^3 - 0.0018 T_{\text{hrs}}^2 + 0.5616 T_{\text{hrs}} + 14.288$	517 hours
180 μm	$\text{Ox } (\%, \text{ Fe pyrite}) = -3 \times 10^{-10} T_{\text{hrs}}^4 - 2 \times 10^{-06} T_{\text{hrs}}^3 + 0.0011 T_{\text{hrs}}^2 + 0.0774 T_{\text{hrs}} + 11.85$	462 hours
250 μm	$\text{Ox } (\%, \text{ Fe pyrite}) = -3 \times 10^{-05} T_{\text{hrs}}^2 + 0.1665 T_{\text{hrs}} + 0.5539$	680 hours
500 μm	$\text{Ox } (\%, \text{ Fe pyrite}) = 0.1273 T_{\text{hrs}} - 0.7623$	791 hours

Table 3.18 shows that the smaller pyrite size enhances biooxidation rates. As an example, the reduction of size from 500 μm to 75 μm will reduce the T_{total} (predict

complete oxidation) by a factor of 2.0. The correlation between T_{total} and particle size (R) is shown in figure 3.29

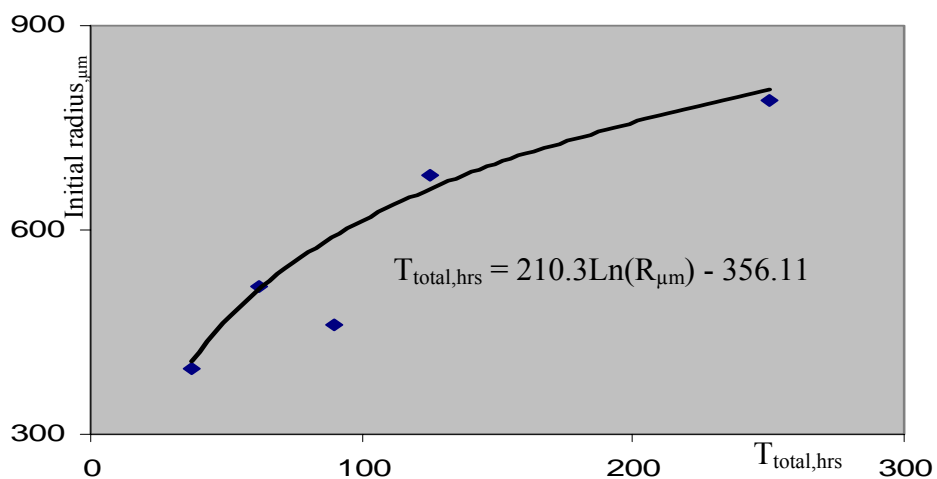


Figure 3.29: Correlation between T_{total} and pyrite size (R) in STR biooxidation using SL5B

A similar trend of pyrite oxidation using different sizes of pyrite was also reported by Kargi and Robinson (1985). It was reported that the removal of pyrite from coal using *S. acidocaldarius* was improved by a factor of 2.1 when the particle size was decreased from 270 micron to 48 micron. The decrease of the particle size from a mean diameter of 202 micron (size fraction: 150 ± 180 micron) to a mean diameter of 42.5 micron (size fraction: 25 ± 45 micron) also has the capability to increase the bioleaching rate from $0.05 \text{ kg m}^3 \text{ h}^{-1}$ to $0.098 \text{ kg m}^3 \text{ h}^{-1}$. (Lindstrom et al. 1993)

It is important to note that information concerning the particle size effects in bioleaching of minerals by mesophiles such as *T. ferrooxidans* is well documented (Torma et al. 1972, Blancarte-Zurita et al. 1986, Hansford and Chapman 1992). However, in the case of thermophilic organisms, this effect is not completely understood. Thus, the mathematical modelling of fluid–solid systems is normally used to interpret experimental results and to gain insight into the reaction mechanisms. It is also useful in the design of liquid–solid reactors by quantifying rate parameters. (Levenspiel, 1999).

3.2.4.4 The dissolution kinetics of pyrite

The dissolution kinetics of pyrite using thermophilic culture may depend on four major effects i.e: the reaction kinetics and, specifically, the dependence of the dissolution rates on the concentration of fluid reactants; transport effects and mass transfer limitations; the structural properties of particles expressed by the particle distribution function (Crundwell and Bryson,1992) and the mechanical and dissolution effects leading to particle fragmentation and break-up induced either by the mechanical stirring or by the dissolution kinetics itself (Edwards et al 1990 and Chai et al 1991). The latter two effects depend on the polydispersity of the mixture and influence the dynamics of the particle distribution function during the process.

The decomposition of pyrite follows the unreacted core model and may be controlled by zero-order surface reaction, gas film/product layer diffusion or a combination of these mechanisms, depending on the reaction conditions. (Guilin Hu et al, 2005). However, inward diffusion of oxygen due to the pore-blocking effect by the formation of ferric oxide and product intermediate will interfere with the model.

The major models that have been developed for non-catalytic fluid–solid reactions are the shrinking core, shrinking particle, homogeneous and grain models. The shrinking core model is applicable to an initially non-porous particle, which reacts with a reagent leaving a reacted layer around the unreacted core. The shrinking particle model is similar to the shrinking core model except that no product layer is left around the unreacted core. The homogeneous model is applicable to a solid with a homogeneous distribution of pores, while the grain model is applicable to a solid consisting of individual dense grains compacted together. Among these models, the shrinking core model has been widely used in the area of hydrometallurgy to model leaching systems (Philip et al 2004, Szekely et al. (1976) and Levenspiel (1999)). The shrinking core model was first developed by Yagi and Kunii (1955). In the establishment of the shrinking core model, the solid reactant is considered to be non-porous and is initially surrounded by a fluid film through which mass transfer occurs between the solid particle

and the bulk of the fluid (shown in figure 3.30). As the reaction proceeds, a pyrite layer forms around the unreacted core. (Szekely et al. 1976 and Levenspiel, 1999).

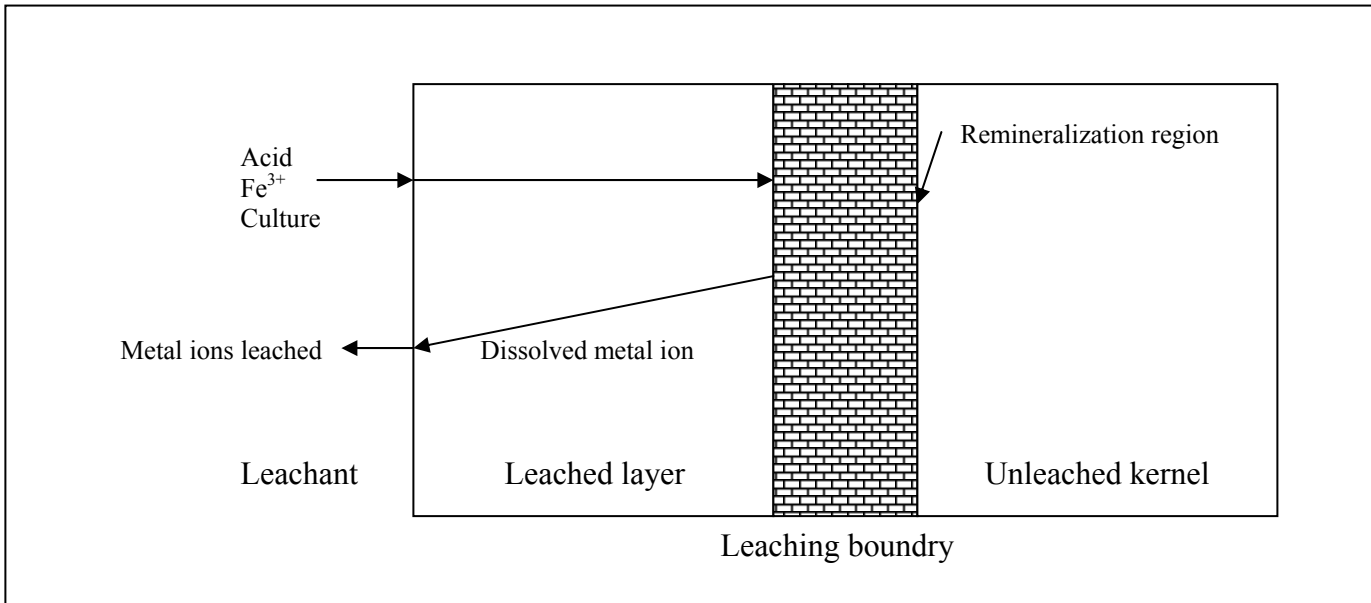
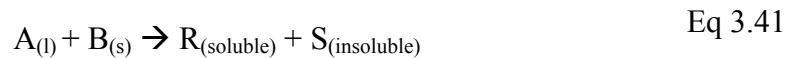


Figure 3.30: Principles of shrinking unreacted core model (Baker and Bishop, 1997)

In leaching models, a liquid contact a solid, reacts with it, and transforms it into products shown in equation 3.41 and 3.42:



Where

A: Fe^{3+} or acid

B: Pyrite

C: Fe^{2+} and SO_4^{2-}

D: Jarosite, iron oxide, sulfur and its intermediate

3.2.4.5 Shrinking Particle Model

The major difference between the shrinking particle model and the shrinking core model is that in the former case, there is no inert layer formed figure 2.31. Schematic diagram of a particle undergoing the shrinking particle form of reaction

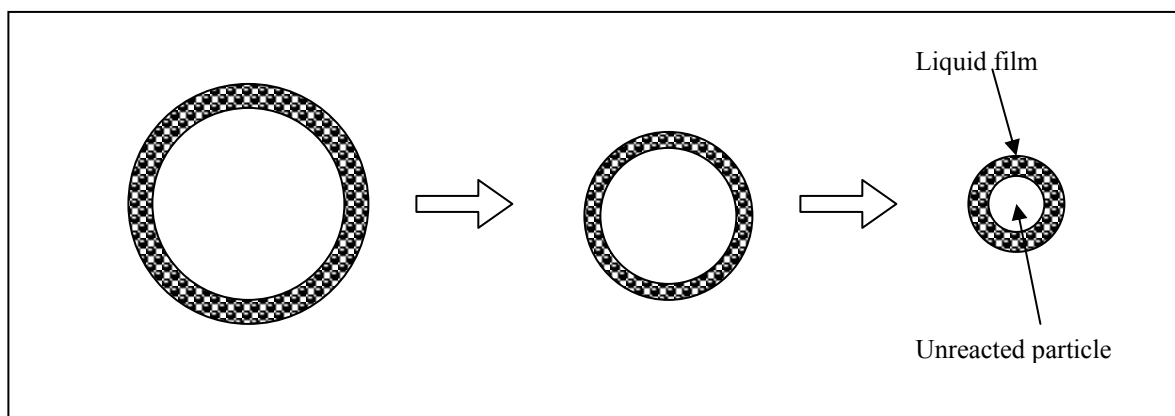


Figure 3.31: Schematic diagram of pyrite under shrinking particle model reaction

During shrinking particle and shrinking core reaction, the following processes can occur: (1) Diffusion of reactant A from bulk solution through film surrounding the solid particle to the surface of the solid.; (2) Diffusion of reactant A through the blanket of ash to the surface of the unreacted core.; (3) Reaction of reactant A with the solid at the solid surface.;(4) Diffusion of products through the ash back to the exterior surface of the solid and (5) Diffusion of products through the liquid film back into the main body of fluid.

Due to the back-reaction kinetics are rarely important in hydrometallurgical leaching reactions kinetics, only the first three steps is included in the development of the model. This however, might not be the case in all leaching reactions. It is possible that diffusion of products through the ash or the liquid film could be the controlling process. If all products were solid, step 4 and 5 will be insignificant. The

slowest step controls the overall process. The case for which either of steps 1 to 3 may be controlling is considered below.

Shrinking particle model for diffusion through liquid film as a limitation step (The model was derived at attachment A: Shrinking core and particle model). Shrinking particle model for diffusion through liquid film as a limitation step for small particles

$$1 - (1 - X_B)^{2/3} = k_3 t \quad \text{Eq 3.43}$$

Shrinking particle model for diffusion through liquid film as a limitation step for large particles

$$1 - (1 - X_B)^{1/2} = k_4 t \quad \text{Eq 3.44}$$

k_3 and k_4 are constants which depends on the fluid properties and particles size.

Shrinking particle model for diffusion surface chemical reaction as a limitation step

$$1 - (1 - X_B)^{1/3} = k_r t \quad \text{Eq 3.45}$$

3.2.4.6 Shrinking Core Model

The shrinking core model is similar to the shrinking particle model. In the shrinking core model, the solid reactant is considered to be non-porous and is initially surrounded by a fluid film through which mass transfer occurs between the solid particle and the bulk of the fluid (Figure 3.32). The shrinking core model was first developed by

Yagi and Kunii (1955). Detailed treatment has also been done by Wen (1968), Szekely *et al.* (1976), Ramachandran and Doraiswamy (1982), and Missen *et al.* (1999).

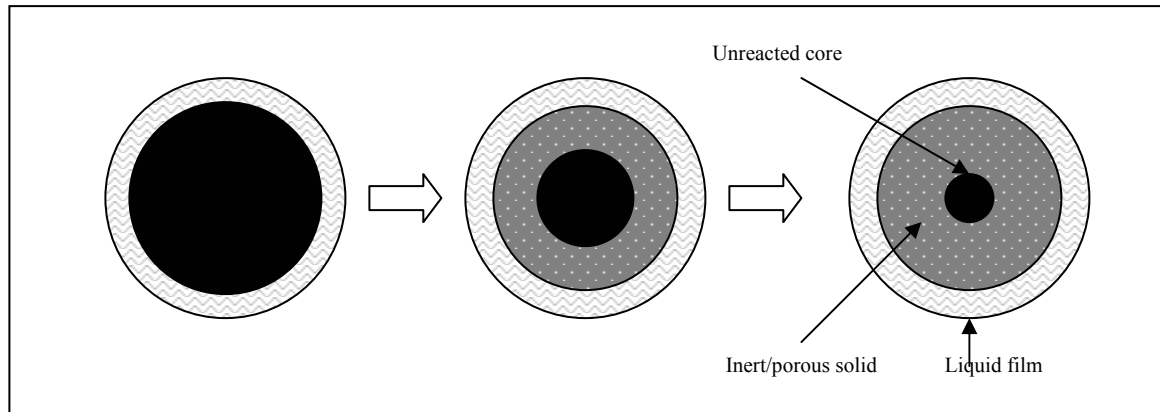


Figure 3.32: Schematic diagram of pyrite under shrinking core model reaction

Pyrite oxidation rate behavior for diffusion through liquid film as a limitation step

$$\frac{dN_A}{S_{ex} dt} = -k_1(C_{Ab} - C_{As}) \quad \text{Eq 3.46}$$

Where

N_A = moles of A in solution

C_{Ab} = concentration of Fe^{3+} in bulk fluid (mol/m^3)

C_{As} = concentration of Fe^{3+} in surface solid (mol/m^3)

k_1 = mass transfer coefficient between fluid and particle ms^{-1}

t = time second

S_{ex} = external surface area of solid m^2

R = radius of solids m

Shrinking core model for diffusion through liquid film as a limited step (The model was derived at attachment C: Shrinking core and particle model)

$$X_B = k_m t \quad \text{Eq 3.47}$$

$$k_m = \frac{3bk_1 C_{Ab}}{\rho R} \quad \text{Eq 3.48}$$

Where

ρ = molar density of B in solid mol/m³

B = mol of pyrite consumed per mol Fe³⁺ reacted

X_B = fraction of pyrite oxidized

Pyrite oxidation rate behavior for diffusion through inert layer as a limitation step

$$\frac{dN_A}{dt} = -4\pi r^2 D_e \frac{dC_A}{dr} \quad \text{Eq 3.49}$$

Shrinking core model for diffusion through inert layer as a limited step (The model was derived at attachment 1: Shrinking core and particle model)

$$1 - 3(1 - X_B)^{2/3} + 2(1 - X_B) = k_d t \quad \text{Eq 3.50}$$

and

$$k_d = \frac{6bD_e C_{Ab}}{\rho R^2} \quad \text{Eq 3.51}$$

D_e : effective diffusion coefficient of A through inert layer m²s⁻¹

R : radial distance from centre of solid, m

k_d : reaction constant rate

Pyrite oxidation rate behavior surface chemical reaction controls

$$\frac{dN_A}{S_{ex} dt} = -k_2(C_{Ab}^n - C_{As}) \quad \text{Eq 3.52}$$

Shrinking core model for surface chemical reaction as a limited step (The model was derived at attachment 1: Shrinking core and particle model)

$$1 - (1 - X_B)^{1/3} = k_r t \quad \text{Eq 3.53}$$

and

$$k_d = \frac{bk_2 C_{Ab}^n}{\rho R} \quad \text{Eq 3.54}$$

n = order of reaction with respect to Fe^{3+}
 k_2 = reaction rate constant, $\text{mol}^{(1-n)}\text{m}^{(3n-2)}\text{s}^{-1}$

Instead of model stated, Nona and Liddell (2005) was also suggested four shrinking core models were fit to the other condition of experimental data i.e:

Spherical particles under heterogeneous chemical reaction as the controlling step:

$$t \propto 1 - (1 - X_B)^{1/3} \quad \frac{1}{t_{total}} = \frac{bk_r C_b}{R\rho} \propto \frac{1}{R} \quad \text{Eq 3.55}$$

Spherical particles under product layer diffusion as the controlling step:

$$t \propto 3 - 2X_B - 3[1 - X_B]^{2/3} \quad \frac{1}{t_{total}} = \frac{6bDC_b}{R^2 \rho} \propto \frac{1}{R^2} \quad \text{Eq 3.56}$$

Cylindrical particles under heterogeneous chemical reaction as the controlling step:

$$t \propto 1 - (1 - X_B)^{\frac{1}{2}} \qquad \frac{1}{t_{total}} \propto \frac{1}{R} \qquad \text{Eq 3.57}$$

Cylindrical particles under product layer diffusion as the controlling step:

$$t \propto X_B + (1 - X_B) \ln(1 - X_B) \qquad \frac{1}{t_{total}} \propto \frac{1}{R^2} \qquad \text{Eq 3.58}$$

3.2.4.7 Shrinking particle model for diffusion through liquid film as a limitation step: Application of model to experimental data

The shrinking particle model behavior of pyrite was determined using STR biooxidation with culture SL5B at different size, and the particle was considered as a sphere shape. From the figure $1-(1-X_B)^{2/3}$ vs leaching time (Shrinking particle model for diffusion through liquid film as a limitation step), the time required for complete pyrite oxidation can be predicted and it shown in table 3.19.

Table 3.19: the time required for complete pyrite oxidation for diffusion through liquid film as a limitation step

Initial pyrite size (r)	$1-(1-X_B)^{2/3}$ vs t	T_{total}	Regression coefficient (R^2)
75 μm	$t = 0.0021x - 0.0102$	481.05	0.99
125 μm	$t = 0.0017x + 0.1406$	505.53	0.87
180 μm	$t = 0.0016x + 0.0695$	581.56	0.97
250 μm	$t = 0.0012x + 0.0029$	830.92	0.98
500 μm	$t = 0.0009x - 0.0069$	1118.78	0.91

The relationship between required reaction time (t_{total}) and initial pyrite size (R) is shown in figure 3.19,

$$\frac{1}{t_{total}} = \frac{2bDC_b}{\rho R^2} \propto \frac{1}{R^2} \quad \text{Eq 3.59}$$

based on the integration between equation 3.60 and 3.61.

$$\frac{1}{t_{total}} = \frac{5.6182}{R^2} + 0.0012 \quad \text{Eq 3.60}$$

Based on equation 3.60, the required leaching time for a pyrite bioleaching at certain particle size can be predicted, if diffusion through liquid film become a limiting step.

3.2.4.8 Shrinking particle and core model for diffusion through chemical reaction as a limitation step: Application of model to experimental data

For the pyrite dissolution model with the chemical reaction considered as controlling step, the equation for shrinking particle model and the shrinking core model is similar. Table 3.20 show the shrinking particle behavior of pyrite during STR biooxidation using SL5B at different pyrite size.

Table 3.20: The time required for complete pyrite oxidation for the chemical reaction considered as controlling step

Initial pyrite size (r)	$1-(1-X_B)^{1/3}$ vs t	T_{total}	Regression coefficient (R^2)
75 μm	$t = 0.0013x - 0.0132$	779.38	0.97
125 μm	$t = 0.0011x + 0.0724$	843.27	0.90
180 μm	$t = 0.0010x + 0.0316$	968.40	0.97
250 μm	$t = 0.0006x + 0.00006$	1666.58	0.98
500 μm	$t = 0.0005x - 0.0044$	2008.80	0.91

The relationship between required reaction time (t_{total}) and initial pyrite size (R) is shown in 3.20, based on the equation 3.61,

$$\frac{1}{t_{total}} = \frac{bk_r C_b}{\rho R} \propto \frac{1}{R} \quad \text{Eq 3.61}$$

Therefore is the relation between $1/t_{total}$ and $1/R$ for the pyrite dissolution with the chemical reaction considered as controlling step, for the shrinking particle model and the shrinking core model

$$\frac{1}{t_{total}} = \frac{0.0717}{R} + 0.0004 \quad \text{Eq 3.62}$$

Table 3.20 shows the low regression coefficient was obtained for $1/t_{total}$ vs $1/R$ or $1/R^2$ for the shrinking particle model. For the model with chemical reaction considered as controlling step, the regression coefficient is a 0.7198. For the liquid film diffusion as a limitation step the regression coefficient was at 0.6013.

It is importance to note, that the biooxidation is a very complex process, which is dealing with precipitation (jarosite and sulfur) and formation of intermediate mineral (dolomite and iron sulfide). The precipitate is found has a high tendency to attach on a particle surface and intermediate mineral will develop a porous layer in the pyrite particle. Which is forming a porous layer between liquid medium and pyrite surface as shown in shown in fig.F-32 till F-34 (attachment F). Thus, the shrinking core model will be practically viable for this experiment.

3.2.4.9 Shrinking core model for diffusion through film diffusion as a limitation step: Application of model to experimental data

Table 3.21 show the shrinking core behavior of pyrite during STR biooxidation using SL5B at different size, with the film diffusion with product layer considered as controlling step and the particle was in a sphere shape.

Table 3.21: The time required for complete pyrite oxidation for the product diffusion considered as controlling step

Initial pyrite size (r)	X _B vs t	T _{total}	Regression coefficient (R ²)
75 μm	t = 0.0022x + 0.2479	341.86	0.92
125 μm	t = 0.002x + 0.2036	398.20	0.85
180 μm	t = 0.002x + 0.1101	444.95	0.97
250 μm	t = 0.0016x + 0.0077	620.19	0.98
500 μm	t = 0.0013x - 0.0076	775.08	0.91

The relationship between required reaction time (t_{total}) and initial pyrite size (R) is shown in Table 3.21, based on the equation 3.63

$$\frac{1}{t_{total}} = \frac{3bk_m C_b}{\rho R} \alpha \frac{1}{R} \quad \text{Eq 3.63}$$

Therefore is the relation between 1/t_{total} and 1/R for the pyrite dissolution with the chemical reaction considered as controlling step, for the shrinking particle model and the shrinking core model

$$\frac{1}{t_{total}} = \frac{0.1438}{R} + 0.0012 \quad \text{Eq 3.64}$$

3.2.4.10 Shrinking core model for diffusion through inert product layer as a limitation step: Application of model to experimental data

Table 3.22 show the shrinking particle behavior of pyrite during STR biooxidation using SL5B at different size, with the product layer diffusion considered as controlling step and the particle was in a sphere shape

Table 3.22: The required bioleaching time for pyrite at different particle size, when product layer diffusion becomes a rate limiting step in leaching reaction:

Initial pyrite size (r)	$1-3(1-X_B)^{2/3}+2(1-X_B)$ vs t	T_{total}	Regression coefficient (R^2)
75 μm	$t = 0.0017x + 0.0012$	587.53	0.97
125 μm	$t = 0.001x + 0.0147$	985.30	0.93
180 μm	$t = 0.0009x + 0.0116$	1124.00	0.93
250 μm	$t = 0.0003x + 0.0068$	3356.00	0.93
500 μm	$t = 0.0002x - 0.0054$	5027.00	0.85

The required leaching time for pyrite with product layer diffusion as controlling step is much higher compared with direct chemical reaction. Increasing of pyrite size from 75 μm to 500 μm will increased the reaction time to 8.5 times folds.

By integrating equation 3.61 and 3.62 with required leaching times, the relationship between required reaction time (t_{total}) and initial pyrite size (R) have been postulated and presented in table 3.22 and equation 3.65:

$$\frac{1}{t_{total}} = \frac{6bkC_b}{\rho R^2} \alpha \frac{1}{R^2} \quad \text{Eq 3.65}$$

If the product layer diffusion becomes a rate controlling step in the bioleaching, the required leaching time for a pyrite bioleaching at certain particle size can be predicted by equation 3.66.

$$\frac{1}{t_{total}} = \frac{8.1014}{R^2} + 0.0003$$

Eq 3.66

ATTACHMENT C

MODELING AND KINETIC OF FLUID-SOLID REACTION

C. Shrinking particle model and Shrinking core model

Leaching reactions are heterogeneous reactions involving a solid and an aqueous solution containing the leaching agent. The solid in contact with water forms a stagnant saturated solution at the surface (boundary layer). When a reagent chosen to attack is incorporated into the water, it diffuses through the boundary layer to the surface of the solid where the chemical reaction takes place. The nature of the process varies, depending on the rate of the reaction at the boundary between the liquid and the solid. If it is fast, then the rate is primarily controlled by diffusion of the added reagent species and the process becomes a diffusion controlled process. However, if the reaction is slow, then it becomes a chemical reaction controlled process. Mixed control situations also do occur when both rates are comparable. A diffusion controlled process is characterized by being slightly dependent on temperature while a chemically controlled process is strongly dependent on temperature. The activation energy of diffusion controlled process is characterized as being 4 to 12 kJ/mole, while for a chemically controlled process, it is usually > 40 kJ/mole. An intermediate controlled process has an activation energy 20-35 kJ/mole (Habashi, 1980). Many models have been developed to describe fluid-solid reactions. These include the shrinking/unreacted core model, shrinking particle model, homogeneous model and grain model (Levenspiel, 1999).

C.1 Shrinking particle model

Shrinking particle model applied on a situation which no product layer forms. For example, when the leaching pyrite in an autoclave at 160°C (Wadsworth, 1969),

the reacting particle shrinks during reaction, and finally disappears. This process is illustrated in Figure A-1. In this situation, the film diffusion and/or surface chemical reaction become the rate controlling step.

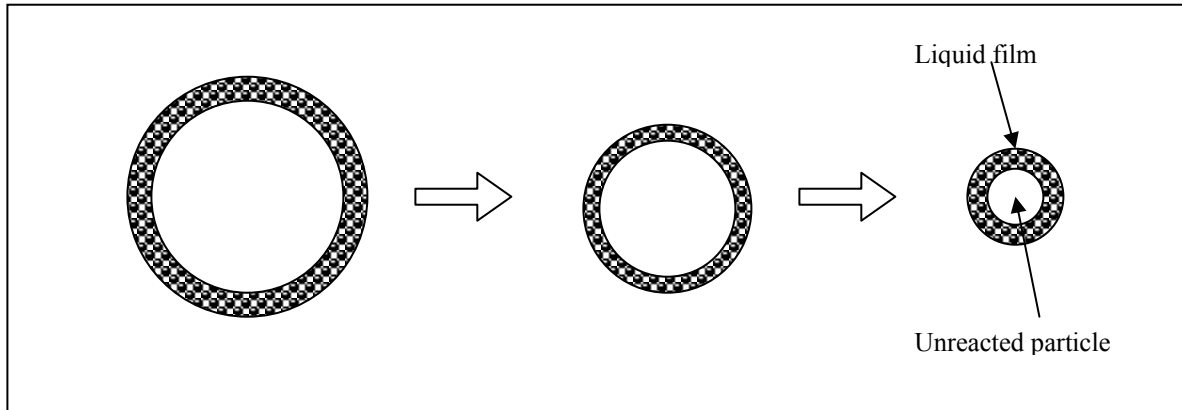


Figure C.1: Schematic diagram of pyrite solution under shrinking particle model reaction

C.1.1 Shrinking Particle Model with film diffusion as control step

In this situation, the concentration of Fe^{3+} will be uniform up to

$$r = r_c + \delta \quad \text{Eq. C-1}$$

where

Fe^{3+} approaches zero at $r = r_c$.

δ : Diffusion boundary layer thickness.

Figure C.2 describe the shrinking particle model with film diffusion as step control pictorially.

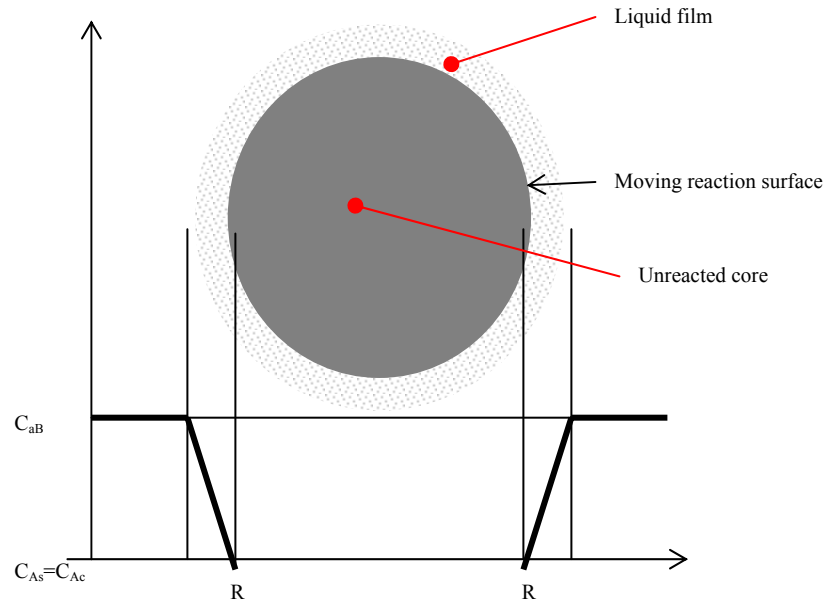


Figure C.2: Shrinking particle reaction when diffusion through liquid film is the controlling step

The rate of pyrite solubilization described as equation C-2.

$$-\frac{1}{S} \frac{dN_b}{dt} = -\frac{1}{S} \frac{dN_A}{dt} \quad \text{Eq. C-2}$$

where

S is the surface area of the particle, as defined in equation

$$S = 4\pi r^2 \quad \text{Eq. C-3}$$

where

r is the particle radius at time = t .

$$-\frac{1}{4\pi r^2} \frac{dN_A}{dt} = k_m C_b \quad \text{Eq. C-4}$$

therefore

$$-\frac{1}{4\pi r^2} \frac{dN_B}{dt} = bk_m C_b \quad \text{Eq. C-5}$$

By substituting Eq. C-6

$$bdN_A = dN_b = 4\rho\pi r^2 \quad \text{Eq. C-6}$$

Into equation C-5,

$$-\rho \frac{dr}{dt} = bk_m C_b \quad \text{Eq. C-7}$$

By integrating equation C-7,

$$\left(\frac{bk_m C_b}{R\rho} \right) t = 1 - \frac{r}{R} \quad \text{Eq. C-8}$$

Because

$$\frac{r}{R} = (1 - X_B)^{\frac{1}{3}} \quad \text{Eq. C-9}$$

By substituting C-8 to C-9,

$$\frac{bk_m C_b}{\rho R} (t) = 1 - (1 - X_B)^{\frac{1}{3}} \quad \text{Eq. C-10}$$

If

$$\frac{1}{t_{total}} = \frac{bk_m C_b}{\rho R} \quad \text{Eq. C-11}$$

Therefore

$$\frac{t}{t_{total}} = 1 - (1 - X_B)^{\frac{1}{3}} \quad \text{Eq. C-12}$$

If the particle size is very small

$$k_m = \frac{D}{R} \quad \text{q1} \quad \text{Eq. C-13}$$

where D is the molecular diffusion coefficient,

$$-\rho \frac{dr}{dt} = b \frac{D}{r} C_b \quad \text{q2} \quad \text{Eq. C-14}$$

Therefore

$$\frac{t}{t_{total}} = 1 - (1 - X_B)^{\frac{2}{3}} \quad \text{q3} \quad \text{Eq. C-15}$$

Where

$$\frac{1}{t_{total}} = \frac{bDC_b}{\rho R^2} \quad \text{q 4} \quad \text{Eq. C-16}$$

C.1.2. Shrinking particle model with the diffusion through chemical reaction is the rate controlling step,

The leaching behavior is when the diffusion through chemical reaction is the rate controlling step is represent in a figure C.3:

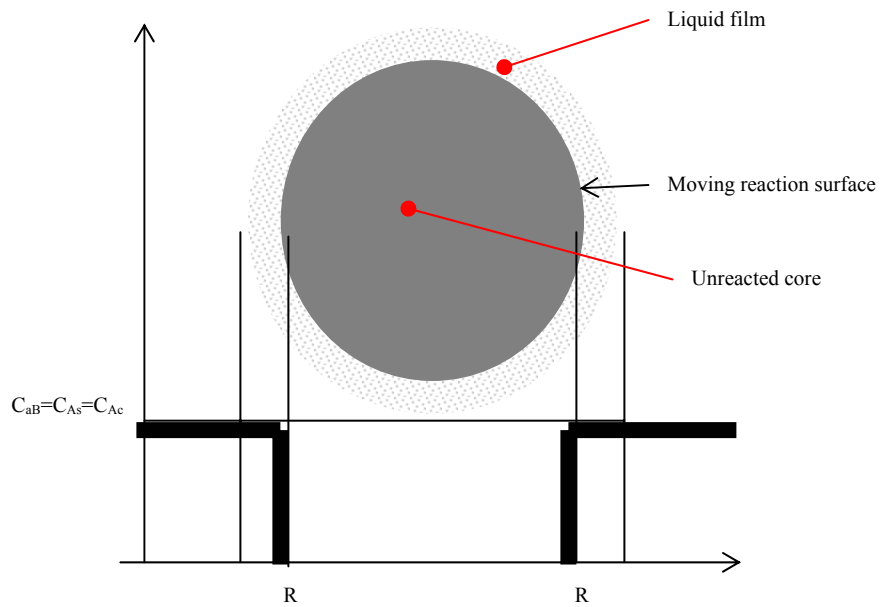


Figure C.3: Shrinking particle reaction when diffusion through chemical reaction is the controlling step

Assuming the reaction is first order and irreversible, and k_r is the first order rate constant.

At steady state,

$$-\frac{1}{4\pi r^2} \frac{dN_B}{dt} = -\frac{b}{4\pi r^2} \frac{dN_A}{dt} = bk_r C_A \quad \text{Eq: C-17}$$

And considering

$$\frac{bk_r C_B(t)}{\rho R} = 1 - \left(\frac{r}{R}\right) \quad \text{Eq: C-18}$$

and

$$\left(\frac{r}{R}\right) = (1 - X_B)^{\frac{1}{3}} \quad \text{Eq: C-19}$$

Substituting Eq C-20

$$dNB = 4\rho\pi r^2 dr \quad \text{Eq: C-20}$$

into the equation C-17 And integrating with equation C-18 and C-19, Therefore :

$$\frac{bk_r C_B}{\rho R} = \left(\frac{1}{t_{total}} \right) \quad \text{Eq: C-21}$$

Then equation C-21 And integrating with equation A-19:

$$\frac{t}{t_{total}} = 1 - (1 - X_B)^{\frac{1}{3}} \quad \text{Eq: C-22}$$

C.2. Shrinking core model

The shrinking core model is widely used to model liquid–solid reactions such as the leaching of metals from minerals. The major models that have been developed for non-catalytic fluid–solid reactions are the shrinking core, shrinking particle, homogeneous and grain models. The shrinking core model is applicable to an initially non-porous particle, which reacts with a reagent leaving a reacted layer around the unreacted core. The shrinking particle model is similar to the shrinking core model except that no product layer is left around the unreacted core. The homogeneous model is applicable to a solid with a homogeneous distribution of pores, while the grain model is applicable to a solid consisting of individual dense grains compacted together. Among these models, the shrinking core model has been widely used in the area of hydrometallurgy to model leaching systems (Philip et al 2004, Szekely et al. (1976) and Levenspiel (1999)). The shrinking core model was first developed by Yagi and Kunii (1955). In the establishment of the shrinking core model, the solid reactant is considered to be non-porous and is initially surrounded by a fluid film through which mass transfer occurs between the solid particle and the bulk of the fluid (shown in figure C-4). As the reaction proceeds, an pyrite layer forms around the unreacted core. (Szekely et al. 1976 and Levenspiel, 1999).

Solid particles remain unchanged in size during reaction when it contains large amounts of unleachable materials at such leaching conditions. The unleachable materials form a porous product layer surrounding the particle by the reaction A-23,

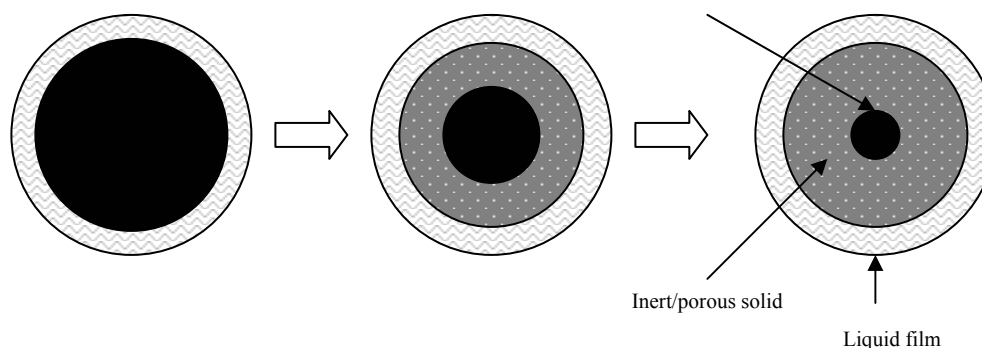
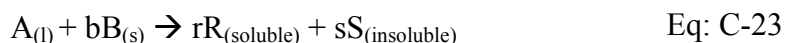


Figure C.4: Schematic diagram of pyrite under shrinking core model reaction



Where

A: Fe^{3+} or acid

B: Pyrite

C: Fe^{2+} and SO_4^{2-}

D: Jarosite, iron oxide, sulfur and its intermediate

Shrinking core model occurs in many practical situations, selective leaching of solids occurs first at the outer skin of the particle. The zone of reaction then moves into the solid, and may leave behind completely converted material and inert solid. The insoluble product generated from the leaching reaction forms a permeable layer through which ions must diffuse in and out. For example, leaching of pyrite in ferric sulfide solution produces sulfur, jarosite, iron sulfite and dolomite through which ferric ions can diffuse, so the leaching reaction can proceed further. The net result may be an unreacted shrinking core with a solid non-reacted diffusion layer surrounding it, as illustrated in figures C.5.

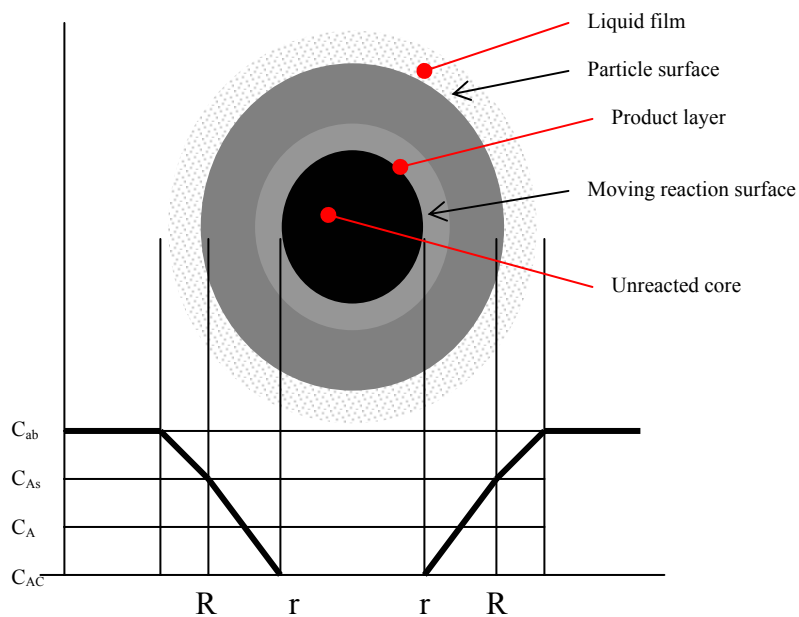


Figure C.5: Shrinking core reaction. Reactant A concentration for the reaction:



for a unchanged particle size and a solid non-reacted diffusion layer surrounded

C.2.1. Shrinking core model with film diffusion as step control

Figure C.6 represents the profile in a leaching system when the film diffusion of the reactant A is the limiting step.

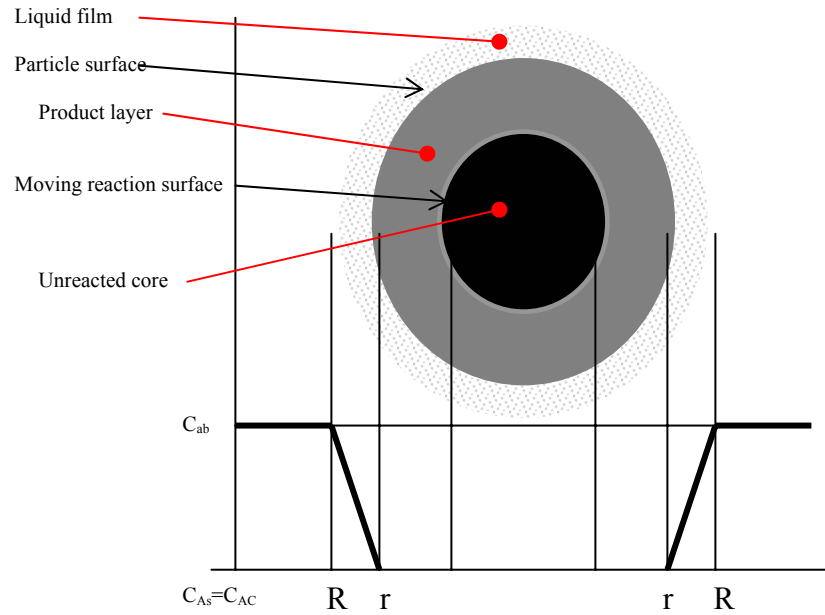


Figure C.6: Reaction condition of pyrite when diffusion through the liquid film is the limiting step

The concentration of A (Fe^{3+} and SO_4^{2-}) will be considered uniform up to $r = R + \delta$ and approaches zero at $r = R$. Here, δ is the diffusion boundary layer thickness. If the pyrite particle is considered to be a sphere, the surface area of the particle may be represented by the equation C-24

$$S=4\pi r^2 \quad \text{Eq: C-24}$$

The reaction rate of pyrite (B) can be described in equation C-25:

$$-\frac{1}{S} \frac{1}{b} \frac{dN_B}{dt} = \frac{1}{S} \frac{dN_A}{dt} \quad \text{Eq: C-25}$$

where

S is the surface area of the pyrite particle

b is the stoichiometric coefficient.

N_B and N_A are the total amount of reactant A (Fe^{3+} and SO_4^{2-}) and B (pyrite) in the reaction system

R is the particle radius during leaching

More complicated geometric shapes may be treated graphically by calculating the change in area with the fraction reacted. The negative sign in the equation C-25 implies that N_A the total amount of reactant A (Fe^{3+} and SO_4^{2-}), is decreasing with time. The reaction rate of A can be described by the equation C-26,

$$-\frac{1}{S} \frac{dN_A}{dt} = k_m (C_b - C_s) \quad \text{Eq: C-26}$$

where

k_m is a diffusion coefficient,

C_B and C_s are the Fe^{3+} and H_2SO_4 concentration in the bulk solution and at the pyrite surface

If film diffusion is the rate controlling step, then, $C_s=0$. Therefore,

$$-\frac{1}{S} \frac{dN_A}{dt} = k_m C_b \quad \text{Eq: C-27}$$

The N_A relationship holds at any given time:

$$N_A = \rho \frac{4}{3} \pi r^3 \quad \text{Eq: C-28}$$

where

ρ is the molar density, mol/vol

r is the radius of the particle as a function of time.

By differentiating equation C-28;

$$dN_A = \rho \frac{4}{3} \pi r^3 dr \quad \text{Eq: C-29}$$

Combining equation C-24, C-27 and C-29 gives the equation Eq C-30:

$$-\frac{1}{S} \frac{dN_B}{dt} = -\frac{\rho r^2}{R^2} \frac{dr}{dt} = bk_m C_b \quad \text{Eq: C-30}$$

By integrating equation C-30

$$\left(\frac{3bk_m C_b}{R\rho} \right) t = \left[1 - \left(\frac{r}{R} \right)^3 \right] \quad \text{Eq: C-31}$$

The equation A-31 gives the time required for a reaction to proceed from a particle radius of R to r. Also note that

$$X_B = \left[1 - \left(\frac{r}{R} \right)^3 \right] \quad \text{Eq: C-32}$$

where X_B is the fractional conversion of pyrite. Therefore

$$\frac{3bk_m C_B}{\rho R} (t) = X_B \quad \text{Eq: C-33}$$

If defining $t=t_{total}$ when $X_B=1$, then

$$\frac{1}{t_{total}} = \frac{3bk_m C_B}{\rho R} \quad \text{Eq: C-34}$$

By substituting equation C-33 into C-34,

$$\frac{t}{t_{total}} = X_B \quad \text{Eq: C-35}$$

C.2.2. Shrinking core model with heterogeneous chemical reaction is the controlling step

When the heterogeneous chemical reaction is the controlling step, the concentration of reactant (Fe^{3+} and H_2SO_4) at the unreacted core surface is the same as that of the bulk solution. Figure C.7 illustrates the concentration gradient with particles for this situation.

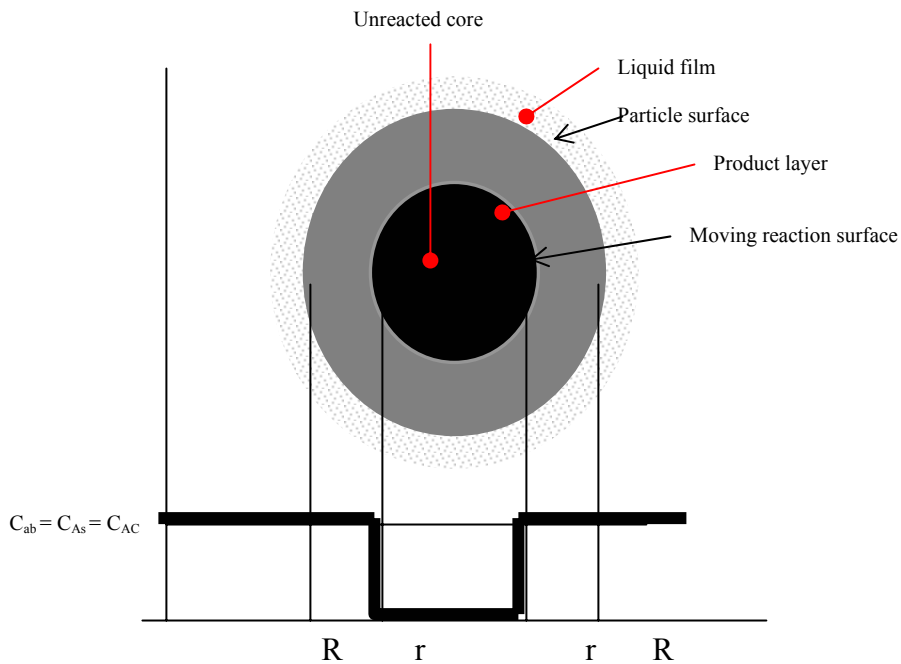


Figure C.7: Pyrite reaction shrinking core diagram when the heterogeneous chemical reaction becomes a limiting step

Assuming the heterogeneous reaction is first order and irreversible, and k_r is the first order rate constant. At steady state,

$$-\frac{1}{4\pi r^2} \frac{dN_B}{dt} = -\frac{b}{4\pi r^2} \frac{dN_A}{dt} = bk_r C_A$$

Eq: C-36

And considering

$$\frac{bk_r C_B}{\rho R}(t) = 1 - \left(\frac{r}{R}\right) \quad \text{Eq: C-37}$$

and

$$\left(\frac{r}{R}\right) = (1 - X_B)^{\frac{1}{3}} \quad \text{Eq: C-38}$$

Substituting Eq: C-39

$$dNB = 4\rho\pi r^2 dr \quad \text{Eq: C-39}$$

into the equation C-36:

$$\frac{bk_r C_B}{\rho R} = \left(\frac{1}{t_{total}}\right) \quad \text{Eq: C-40}$$

Then equation C-40 integrating with equation C-37:

$$\frac{t}{t_{total}} = 1 - (1 - X_B)^{\frac{1}{3}} \quad \text{Eq: C-41}$$

C.2.3. Shrinking core model with product layer diffusion control become a limiting step

The model is applicable when the reactant diffusion through the product layer is limiting, the concentration of the reactant A is uniform up to r equal to R and approaches zero at the unreacted core surface $r = r_s$. At steady state, this situation can be described in figure C.8.

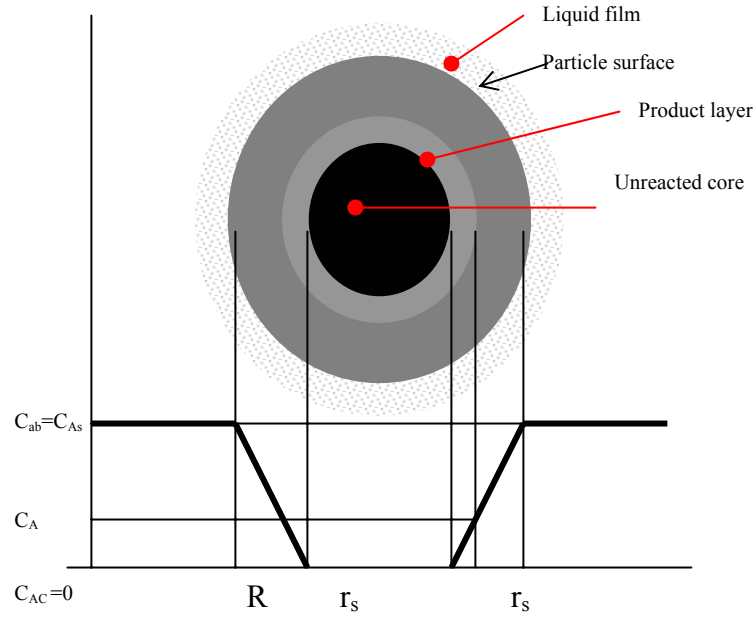


Figure C8: Pyrite reaction, shrinking core diagram when the product layer diffusion become a limiting step

$$-\frac{dN_A}{dt} = -4\pi r^2 \left[-D_s \frac{dC_A}{dr} \right] \quad \text{Eq: C-42}$$

where

D_s is the effective diffusivity

By integrating equation C-42:

$$-\frac{dN_A}{dt} \int_R^r \frac{dr}{r^2} = -4\pi D_s \int_{C_B}^{C_s=0} dC_B \quad \text{Eq: C-43}$$

$$-\frac{dN_A}{dt} \left[\frac{1}{R} - \frac{1}{r} \right] = -4\pi D_s C_B \quad \text{Eq: C-44}$$

Replacing $b dN_A = dN_B = 4\pi r^2 dr$, therefore,

$$-\frac{4\pi r^2}{b} \frac{dr}{dt} \left[\frac{1}{R} - \frac{1}{r} \right] = 4\pi D_s C_B \quad \text{Eq: C-45}$$

$$\rho \int_R^r r^2 \left[\frac{1}{R} - \frac{1}{r} \right] dr = bD_s C_B \int_0^t dt \quad \text{Eq: C-46}$$

Therefore

$$\left(\frac{6bD_s C_B}{\rho R^2} \right) t = 1 - 3 \left[\frac{r}{R} \right]^2 + 2 \left[\frac{r}{R} \right]^3 \quad \text{Eq: C-47}$$

By integrating equation C-47 with C-49:

$$X_B = \left[1 - \left(\frac{r}{R} \right)^3 \right] \quad \text{Eq: C-48}$$

$$\frac{r}{R} = (1 - X_B)^{1/3} \quad \text{Eq: C-49}$$

$$\frac{6bD_s C_B}{\rho R^2} = \left(\frac{1}{t_{total}} \right) \quad \text{Eq: C-50}$$

Substituting equation C-50 in C-47 gives C-51

$$\frac{t}{t_{total}} = 3 - 2X_B - 3[1 - X_B]^{2/3} \quad \text{Eq: C-51}$$

C.3. Homogeneous Model

This model applies to the case when the initial solid particle is porous. In this case, the reaction between the fluid and the solid reactant may be viewed as occurring

homogeneously throughout the solid to produce a gradual variation in solid reactant concentration in all parts of the particle (see Figure 2.S). The solid is considered as an ensemble of small lumps of reactants distributed uniformly throughout the solid phase (Doraiswamy and Sharma, 1984; Wen, 1968). Figure 2.5. Variation of solid reactant concentration with time for the homogeneous model (Levenspiel,1999).

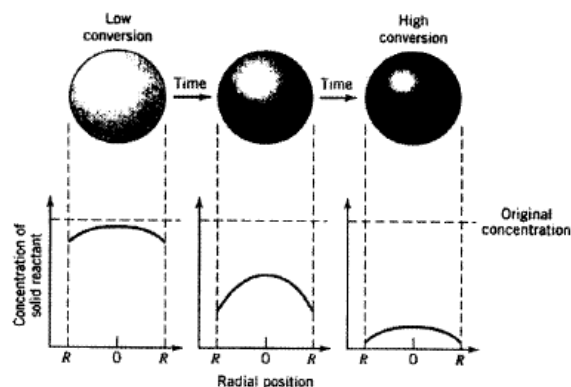


Figure 2.5. Variation of solid reactant concentration with time for the homogeneous model (Levenspiel, 1999).

(i) When Diffusion of A Through Solid is Rate Controlling

In this case

$$\frac{\theta_v}{\theta_v^*} = 1 - 3(1 - X_B)^{2/3} + 2(1 - X_B)$$

where θ_v is a dimensionless time and $\theta_v^* \propto R^2$

(ii) When Chemical Reaction is Rate Controlling

In this case,

$$\frac{\theta_v}{\theta_v^*} = X_B$$

where $\theta_v^* \propto R^0$ (independent of R)

C.4. The Uniform Pore Model

This model was derived by Peterson (1951). The model assumes that the solid contains uniform, open and completely wetted cylindrical pores. The physical size of the porous solid does not change but the consumption of the solid phase will lead to progressive enlargement of the pores, till the whole structure collapses. When diffusion through the pores is rapid and hence offers little resistance, the concentration of the reactant is uniform throughout the particle and the conversion of the solid under the chemical reaction controlled regime is given by

$$X_B = \frac{\varepsilon_0}{1 - \varepsilon_0} \left[\left(1 + \frac{t}{\tau_c} \right)^2 \left(\frac{G - 1 - t/\tau_c}{G - 1} \right) - 1 \right]$$

where, ε_0 is the initial porosity of the solid particle, G is the positive root of

$$\frac{4}{27} \varepsilon_0 G^3 - G + 1 = 0$$

τ_c is the time for the pore radius to become twice the initial value and is given by

$$\tau_c = \frac{r_p \rho_B}{bk^n C_A^n}$$

where r_p is the initial radius of the pore and k is the surface chemical reaction rate constant.

C.5. The Random Pore Model

The model assumes that the solid particle contains overlapping sets of randomly distributed cylindrical pores. The size of each cylindrical pore is different and the pore size follows a specific distribution function. For a chemically controlled reaction, Bhatia and Perlmutter (1980) derived the following relationship between time and conversion,

$$\frac{dX_B}{dt} = \frac{k^n C_A^n (1 - X_B) [1 - \psi \ln(1 - X_B)]^{1/2}}{(1 - \epsilon_o)}$$

where, $\psi = \frac{4\pi L_o (1 - \epsilon_o)}{S_o^2}$

L_o is the initial characteristic length of the pore (m/m³), S_o is the initial reaction surface area per unit volume (m²/m³). For ash layer diffusion controlled process, the equation derived was more complicated and is reported in Bhatia and Perlmutter (1981).

C.6. Grain Model

In this model, the solid particle is visualized as pellets consisting of individual dense grains compacted together. Each grain reacts individually following the shrinking core model (Figure 2.6). The derivation of the model is similar to the case of the SCM, and the details is given by Szekely et al. (1976) and Doraiswamy and Sharma (1984).

(i) When Chemical Reaction is Rate Controlling

In this case, the concentration within the pellet is uniform and all the grains are exposed to the same fluid concentration. The time-conversion relationship is given by,

$$t^* = 1 - (1 - X_B)^{1/3}$$

$$\text{where, } t^* = \frac{bC_{Ab}k''t}{\rho_B R_{Go}}$$

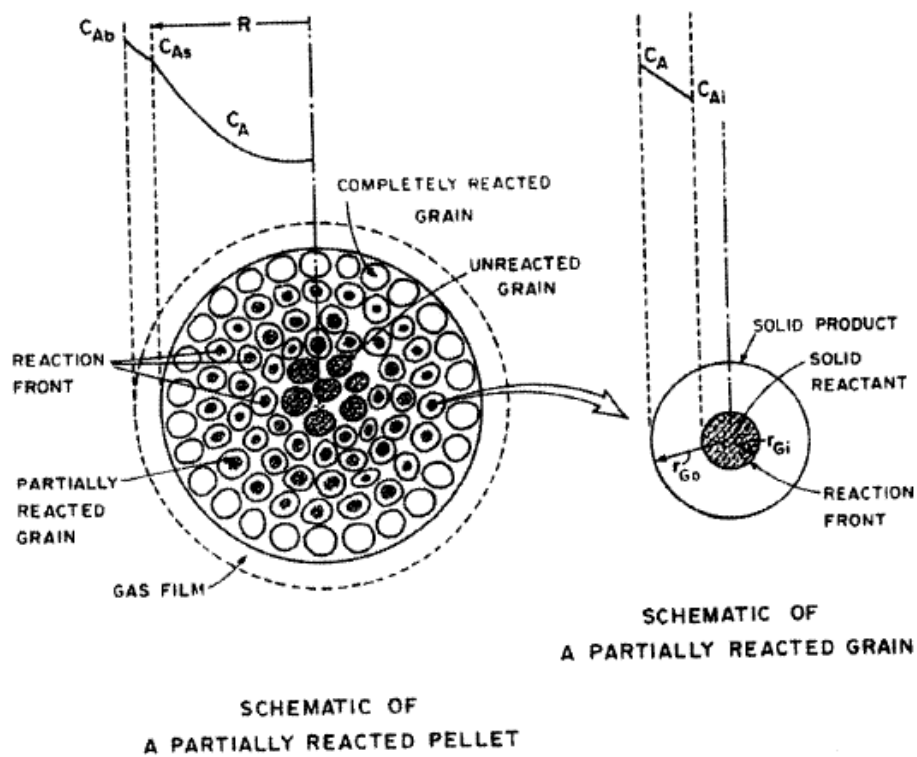
R_{Go} is the initial radius of a grain in the pellet

(ii) When Pore Diffusion is Rate Controlling

In this case, a sharp demarcation can be observed between the reacted and unreacted portions of the pellet and the behavior is similar to that of the SCM. the conversion-time relationship is,

$$\frac{18t^*}{\phi^2} = 1 - 3(1 - X_B)^{2/3} + 2(1 - X_B)$$

$$\text{where, } \phi = R \left[\frac{3(1 - \varepsilon_o)k''}{D_e R_{Go}} \right]^{1/2}$$



ATTACHMENT D

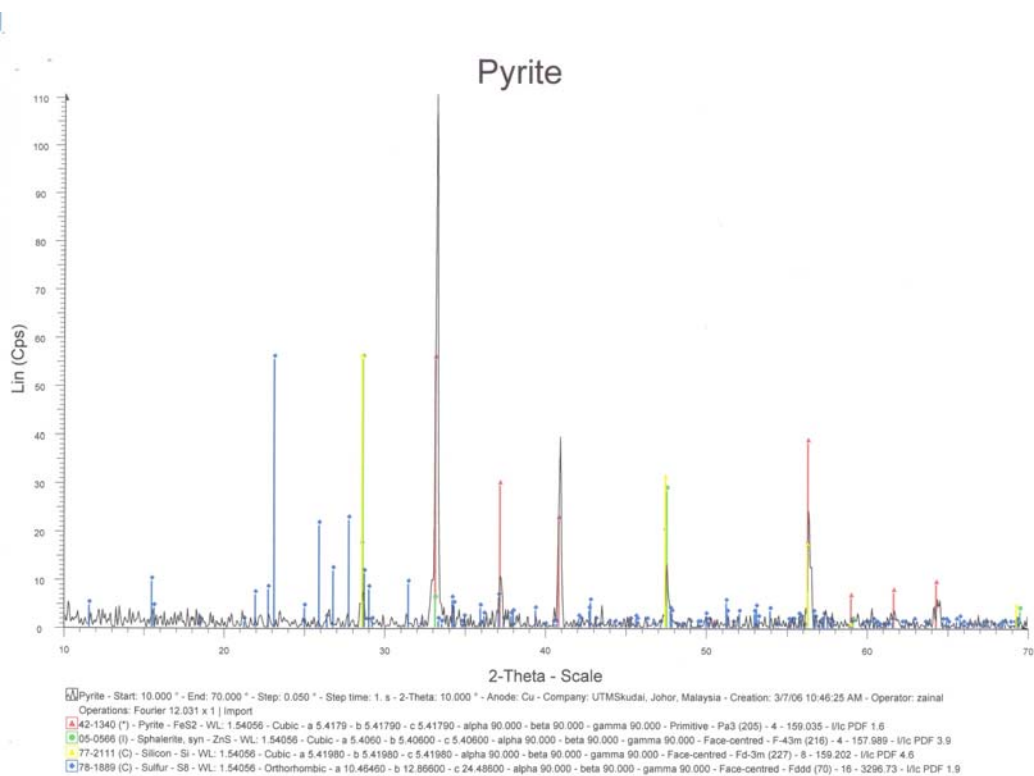


Figure D-1: XRD analysis of pyrite surface

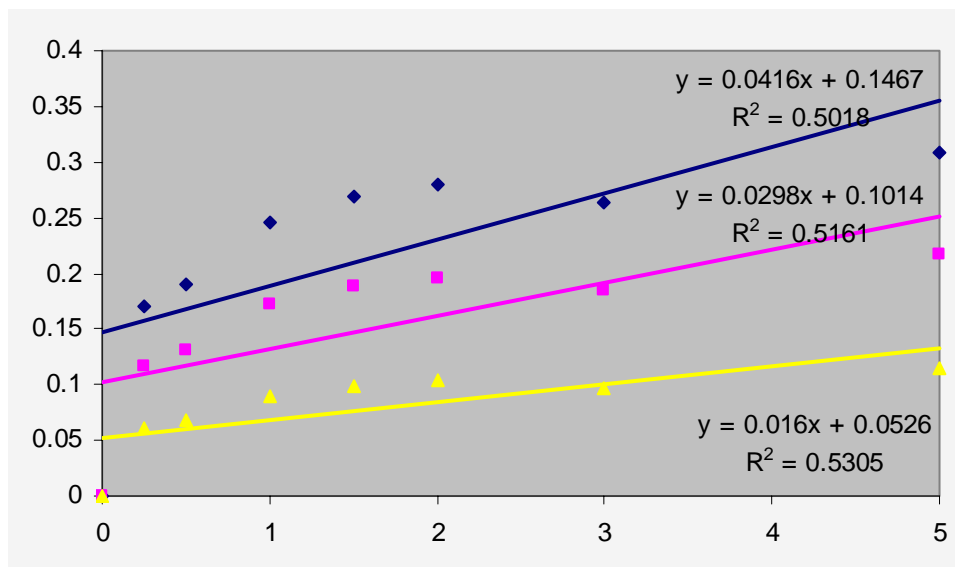


Fig D-2: Shrinking particle and core model for biooxidation of pyrite using SL5B on a 75 μm pyrite.

- Shrinking particle model with film diffusion as limiting step
- Shrinking particle/core model with chemical reaction as limiting step
- Shrinking core model with film diffusion as limiting step

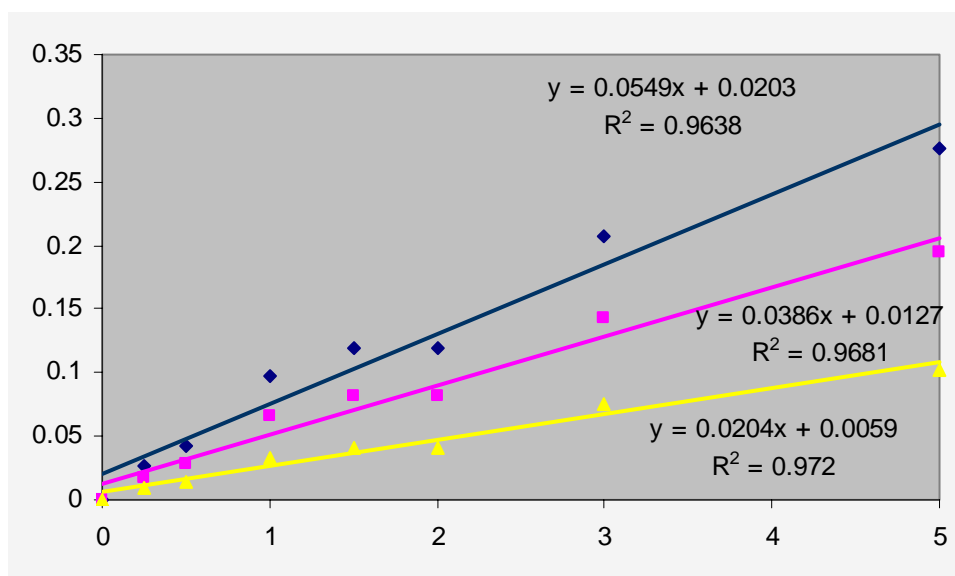


Fig D-3: Shrinking particle and core model for pyrite oxidation at 70°C as control experiment.

- Shrinking particle model with film diffusion as limiting step
- Shrinking particle/core model with chemical reaction as limiting step
- Shrinking core model with film diffusion as limiting step

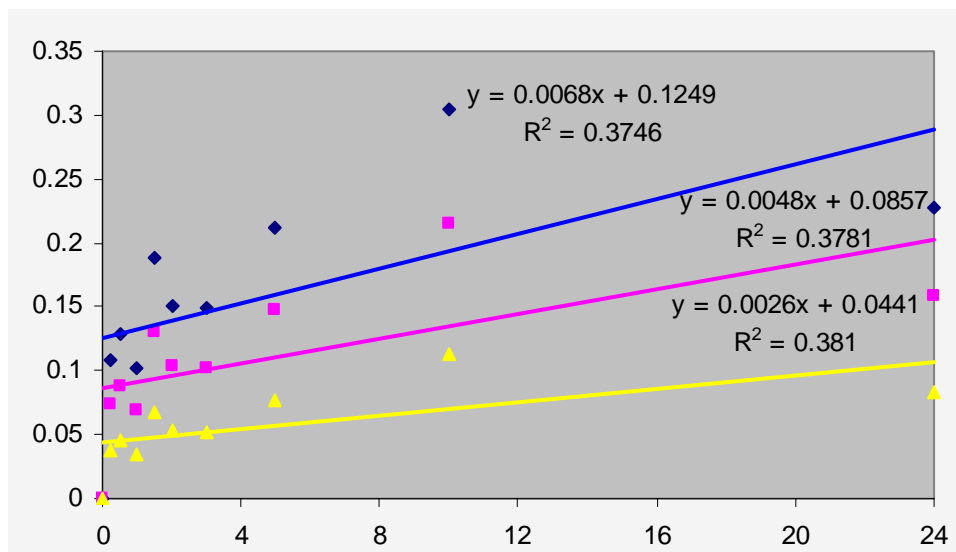


Fig D-4: Shrinking particle and core model for biooxidation of pyrite using *Sb. thermosulfidooxidans* on a 75 μm pyrite.

- Shrinking particle model with film diffusion as limiting step
- Shrinking particle/core model with chemical reaction as limiting step
- Shrinking core model with film diffusion as limiting step

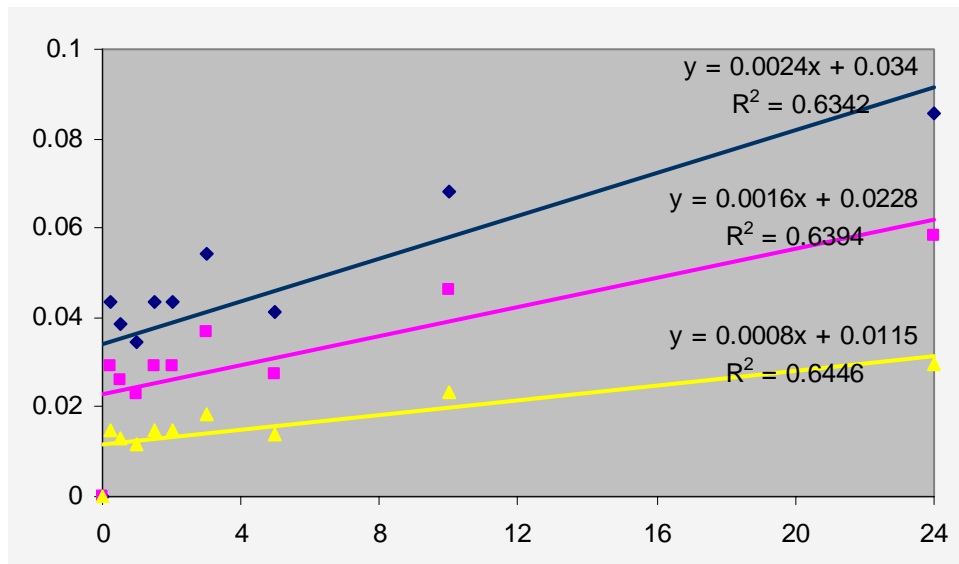


Fig D-5: Shrinking particle and core model for pyrite oxidation at 45°C as control experiment.

- Shrinking particle model with film diffusion as limiting step
- Shrinking particle/core model with chemical reaction as limiting step
- Shrinking core model with film diffusion as limiting step

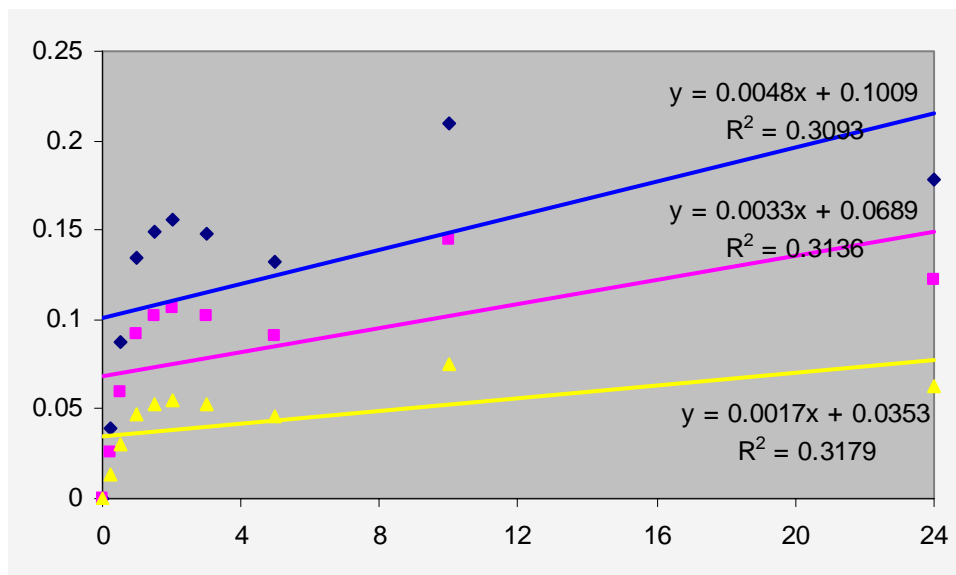


Fig D-6: Shrinking particle and core model for biooxidation of pyrite using *T. ferrooxidans* on a 75 µm pyrite.

- Shrinking particle model with film diffusion as limiting step
- Shrinking particle/core model with chemical reaction as limiting step
- Shrinking core model with film diffusion as limiting step

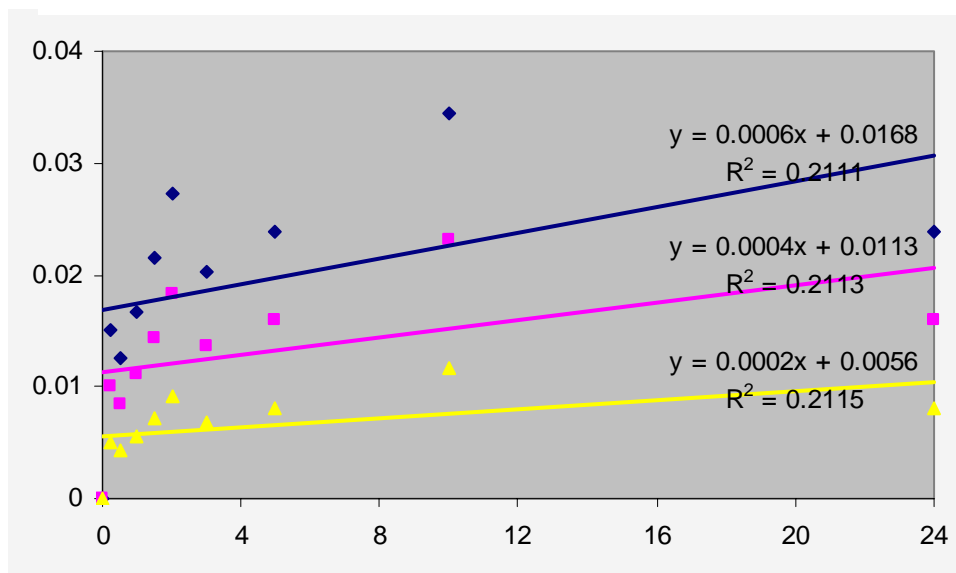


Fig B-7: Shrinking particle and core model for pyrite oxidation at 30°C as control experiment.

- Shrinking particle model with film diffusion as limiting step
- Shrinking particle/core model with chemical reaction as limiting step
- Shrinking core model with film diffusion as limiting step

Table D-1: Iron speciation during biooxidation using *SL5B*

Time	Solubilized iron in medium (mg/L)	Iron in the form of jarosite (mg/L)	Total oxidized iron (mg/L)	[Fe ²⁺] (mL _{KMnO4})	[Fe ³⁺] (mL _{KMnO4})
0	8834.5	0	8834.5	8.175	32.7
0.25	9246.2	740.7	9986.9	35.1	7.1
0.5	9408.2	714.3	10122.5	39.075	4.325
1	9815.1	687	10502.1	35.7	10.45
1.5	9892	765.7	10657.7	28.475	16.6
2	9877.8	847.9	10725.7	23.675	22.95
3	9762.8	854.5	10617.3	21.275	23.55
5	9846	1076.1	10922.1	17.425	28.6
10	9836.5	1153.6	10990.1	10	35
24	10156	1050.9	11206.9	13.225	32.925
48	10189	1207.5	11396.5	10.575	37.25
72	10045	1798.38	11843.38	13.35	33.275
96	10456	1787.7	12243.7	10.225	35.925
120	10982	1918.82	12900.82	8.9	37.975
168	10476	3238.14	13714.14	7.825	39.775
216	11015	2865.66	13880.66	11.5	36.45
264	10698	3870.22	14568.22	6.5	42.05
312	9752.2	5491.9	15244.1	4.25	39.025
360	9852.3	5491.8	15344.1	5.5	39.2

Table D-2: Iron speciation during control oxidation at 70°C

	Solubilized iron in medium (mg/L)	Iron in the form of jarosite (mg/L)	Total oxidized iron (mg/L)	[Fe ²⁺] (mL _{KMnO4})	[Fe ³⁺] (mL _{KMnO4})
0	8721.8	0	8721.8	15.625	24.275
0.25	8740.2	335	9075.2	18.125	24.725
0.5	8520.6	654.6	9175.2	26.725	17.225
1	8890.6	664.6	9555.2	29.85	12.35
1.5	8570.5	1132.7	9703.2	39.15	5.225
2	8760.9	942.3	9703.2	34.6	9.575
3	9200.8	1098.4	10299.2	38.275	5.125
5	9130.4	1640.8	10771.2	29.05	16.8
10	9440.1	1791.1	11231.2	15.2	31.625
24	10156.6	970.6	11127.2	17	28.1
48	10400.5	622.7	11023.2	14.375	32.625
72	8710.6	2520.6	11231.2	11.35	35.275
96	8240.5	2782.7	11023.2	8.3	39.7
120	7560.6	3826.6	11387.2	14.9	33.1
168	7490.4	3560.8	11051.2	15.95	33
216	7200.6	4258.6	11459.2	20.1	30.625
264	5640.4	6398.8	12039.2	14.975	34.625
312	5250.6	6664.6	11915.2	11.3	38.825
360	5510.6	6504.6	12015.2	9.15	43.2

Table D-3: Iron speciation during biooxidation using *Sb. thermosulfidoxidans*

Time	Solubilized iron in medium (mg/L)	Iron in the form of jarosite (mg/L)	Total oxidized iron (mg/L)	[Fe ²⁺] (mL _{KMnO4})	[Fe ³⁺] (mL _{KMnO4})
0	8892.4	0	8892.4	11.375	30
0.25	9380.3	248.9	9629.2	14.875	26.85
0.5	9530.2	231.4	9761.6	32.2	10.4
1	9390.9	191.5	9582.4	20.9	21.85
1.5	9892.5	273.9	10166.4	27.7	17.65
2	9720.3	194.1	9914.4	31.6	13
3	9762.8	139.6	9902.4	36.15	9.25
5	10108	222.4	10330.4	29.05	15.4
10	10394	556.4	10950.4	13.1	33.25
24	10105	333.4	10438.4	21.35	23.2
48	10396	510.4	10906.4	22.15	22.85
72	10303	827.4	11130.4	18.95	22.7
96	10624	1518.4	12142.4	13.1	29.1
120	10742	1788.4	12530.4	10.05	32.8
168	10792	2630.4	13422.4	11.25	37.9
216	11118	2144.4	13262.4	18.65	31.9
264	10995	2199.4	13194.4	12.5	42.9
312	11296	2606.4	13902.4	15.1	33
360	11563	2099.4	13662.4	14.9	32.25

Table D-4: Iron speciation during control oxidation at 45°C

Time	Solubilized iron in medium (mg/L)	Iron in the form of jarosite (mg/L)	Total oxidized iron (mg/L)	[Fe ²⁺] (mL _{KMnO4})	[Fe ³⁺] (mL _{KMnO4})
0	8893.7	0	8893.7	8.625	30.3
0.25	9000.6	179.4	9180	14.7	24.3
0.5	9030.5	117.5	9148	30.225	7.825
1	8970.4	149.6	9120	33.625	6.05
1.5	8920.6	259.4	9180	27	11.25
2	8970.2	209.8	9180	23	16.1
3	9060.5	191.5	9252	20.275	20.8
5	8890.6	273.4	9164	19.6	21.15
10	9000.2	343.8	9344	26.7	15.425
24	8800.4	659.6	9460	20.275	25.125
48	8800.4	703.6	9504	18.575	27.725
72	8690.6	753.4	9444	25	13.875
96	8750.4	677.6	9428	22.8	13.975
120	8490.9	881.1	9372	18.75	15
168	8880.7	991.3	9872	18	15.45
216	8880.4	1155.6	10036	19.425	12.675
264	8100.3	2371.7	10472	17.9	7.3
312	8400.1	2335.9	10736	19	4.45
360	7910.4	2361.6	10272	19.6	5

Table D-5: Iron speciation during biooxidation using *T. ferrooxidans*

Time	Solubilized iron in medium (mg/L)	Iron in the form of jarosite (mg/L)	Total oxidized iron (mg/L)	[Fe ²⁺] (mL _{KMnO4})	[Fe ³⁺] (mL _{KMnO4})
0	8910.7	0	8910.7	16.35	23.35
0.25	9040.2	115	9155.2	20.175	20.825
0.5	9350.6	132.6	9483.2	28.65	11.9
1	9390.2	405	9795.2	28	12.325
1.5	9792.6	87.4	9880	24.625	15.925
2	9720.2	223	9943.2	26	14.55
3	9762.8	128.4	9891.2	24	16.75
5	9680.5	102.7	9783.2	21.875	18.125
10	9960.5	342.7	10303.2	22.625	17.925
24	9690.6	400.6	10091.2	22.15	17.55
48	9510.3	780.9	10291.2	23.775	15.075
72	9560.6	1062.6	10623.2	23.775	16.225
96	9330.4	1360.8	10691.2	24	15
120	9441.3	1157.9	10599.2	22	16.2
168	10796	559.2	11355.2	21.225	19.325
216	11116	539.2	11655.2	23	16.7
264	12075	780.2	12855.2	22.7	13.45
312	10873	1682.2	12555.2	23.55	13.8
360	10415	2040.2	12455.2	23.55	12.1

Table D-6: Iron speciation during control oxidation at 30°C

Time	Solubilized iron in medium (mg/L)	Iron in the form of jarosite (mg/L)	Total oxidized iron (mg/L)	[Fe ²⁺] (mL _{KMnO4})	[Fe ³⁺] (mL _{KMnO4})
0	8900.6	0	8900.6	38	1.9
0.25	8906.6	87.8	8994.4	37.875	2.8
0.5	8908.6	69.8	8978.4	36.8	2.325
1	8906.6	99.8	9006.4	36.5	3.85
1.5	8925.6	112.8	9038.4	37	3.675
2	8940.6	137.8	9078.4	37	4
3	8930.5	99.9	9030.4	36.175	4.175
5	8940.4	114	9054.4	36.8	3.725
10	9000.6	125.8	9126.4	36.8	4.2
24	8900.6	153.8	9054.4	33.4	6.8
48	8800.5	441.9	9242.4	32.175	7.425
72	8830.9	463.5	9294.4	32.775	6.825
96	8670.4	652	9322.4	31.075	7.925
120	8610.6	735.8	9346.4	31.4	7.6
168	9060.5	617.9	9678.4	32.475	8.825
216	9200.4	538	9738.4	31	10.45
264	9170.6	583.8	9754.4	30.625	10.975
312	9011.6	786.8	9798.4	32.775	8.35
360	8670.6	1023.8	9694.4	35.725	3.7

Table D-7: Dissolved oxygen reading for STR biooxidation at 70°C

STR of pyrite at 70°C					
Time (hrs)	<i>SL5b</i>				Control DO in STR (%pO)
	DO in STR (%pO)	DO from free suspended pyrite inoculums			
		0 hr	24 hr	48 hr	
0	59.4	8.57	7.03	7.04	94.7
0.25	54.6	8.57	6.85	6.87	83.3
0.5	55.3	8.56	7.65	6.43	71.5
1	50.8	8.68	6.54	7.02	62.6
1.5	44.5	8.56	7.25	6.24	58.5
2	42.4	8.56	7.09	6.26	55.7
3	44.9	8.57	6.77	6.86	54.5
5	43.1	8.55	6.25	5.88	54.9
10	50.2	8.56	6.65	6.04	57.7
24	46.9	8.6	7.69	4.84	52.4
48	49.6	8.56	7.36	5.24	68.5
72	45.2	8.53	7.24	4.29	40.2
96	53.5	8.74	5.11	2.91	54.9
120	56.4	8.52	4.51	3.46	60.5
154	52.7	8.57	3.92	2.91	64.6
216	52.7	8.54	4.34	3.31	48.8
264	37.9	8.55	5.16	4.42	41.5
312	29.5	8.57	5.71	4.51	46.6
360	31.5	8.54	6.87	4.95	35.4

Table D-8: Dissolved oxygen reading for STR biooxidation at 45°C

STR of pyrite at 45°C					
Time (hrs)	Sb. thermosulfodoxidans				Control DO in STR (%pO)
	DO in STR (%pO)	DO from free suspended pyrite inoculums			
		0 hr	24 hr	48 hr	
0	65.2	8.51	5.34	4.35	94.7
0.25	60.7	8.54	3.66	3.16	85.4
0.5	54.8	8.52	4.55	2.97	77.5
1	50.5	8.51	4.95	4.51	74.5
1.5	51.7	8.53	3.66	4.15	72.8
2	56.9	8.55	4.85	3.61	70.8
3	48.5	8.51	5.14	4.25	66.5
5	54.8	8.55	4.24	3.98	65.2
10	58	8.56	3.51	3.71	69.1
24	62.7	8.51	4.45	4.24	66.5
48	55.7	8.55	4.74	3.64	68.2
72	49.4	8.52	3.66	2.27	58.8
96	50.4	8.54	4.25	2.64	62.2
120	46.8	8.59	3.86	2.63	60.5
168	52.7	8.5	2.81	1.68	75.5
216	48.4	8.56	4.36	3.77	50.8
264	51.5	8.53	4.05	3.96	56.6
312	52.7	8.54	5.27	5.24	60.4
360	49.2	8.54	4.72	4.96	59.1

Table D-9: Dissolved oxygen reading for STR biooxidation at 30°C

STR of pyrite at 30°C					
Time (hrs)	<i>T. ferrooxidans</i>				Control DO in STR (%pO)
	DO in STR (%pO)	DO from free suspended pyrite inoculums			
		0 hr	24 hr	48 hr	
0	89.3	8.53	6.52	6.03	93.3
0.25	87.1	8.49	5.61	5.54	94.4
0.5	81.6	8.52	5.88	5.34	87.6
1	80.4	8.53	6.08	5.29	86.2
1.5	83.5	8.52	6.25	5.04	87.1
2	81.6	8.53	5.44	5.64	85.4
3	77.4	8.56	6.08	5.84	84.7
5	73.7	8.53	6.28	5.34	82.6
10	71.8	8.54	5.64	4.60	84.9
24	66.5	8.52	5.04	4.45	75.3
48	63.8	8.51	4.35	3.07	74.3
72	63.4	8.55	3.91	2.72	69.7
96	71.8	8.53	5.74	4.45	76.4
120	70.4	8.51	5.25	4.01	80.4
168	65.2	8.49	5.29	4.85	76.4
216	68.2	8.55	5.93	5.14	77.9
264	73.7	8.51	6.33	5.09	81.5
312	68.7	8.54	5.88	5.88	84.8
360	75.3	8.52	6.03	6.03	86

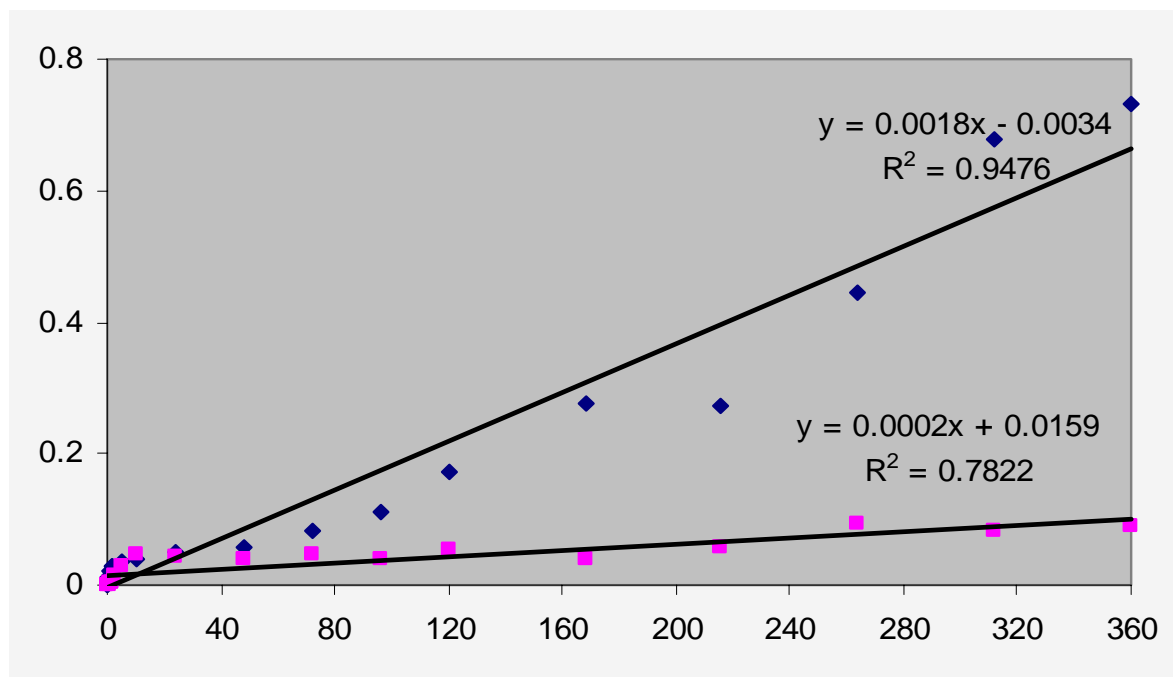


Fig D-8: Shrinking core model with porous product diffusion as limiting step for pyrite oxidation at 70°C.

■ STR biooxidation using SL5B

■ Control at 70°C

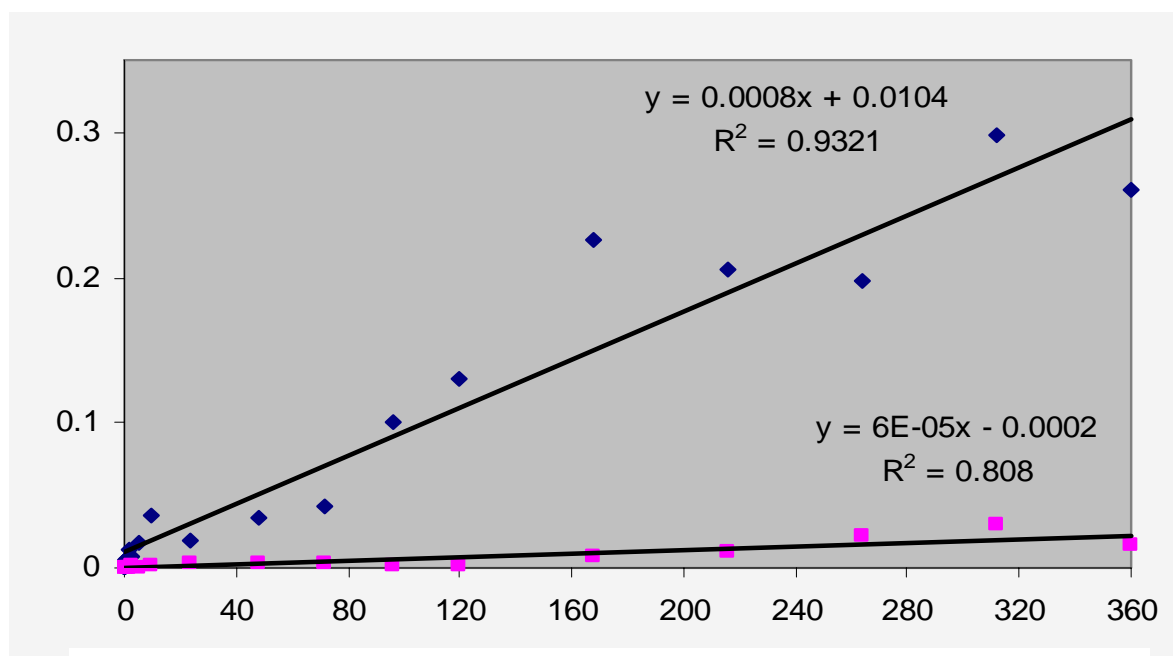


Fig D-9: Shrinking core model with porous product diffusion as limiting step for pyrite oxidation at 45°C.

■ STR biooxidation using *Sb. thermosulfodooxidans*

■ Control at 45°C

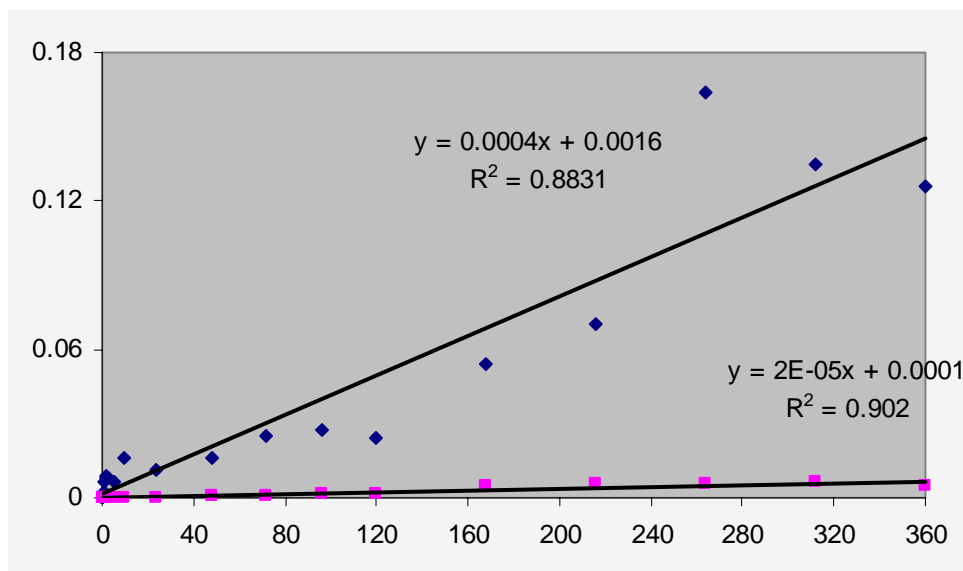


Fig D-10: Shrinking core model with porous product diffusion as limiting step for pyrite oxidation at 30°C.

■ STR biooxidation using *T.ferrooxidans*
■ Control at 30°C

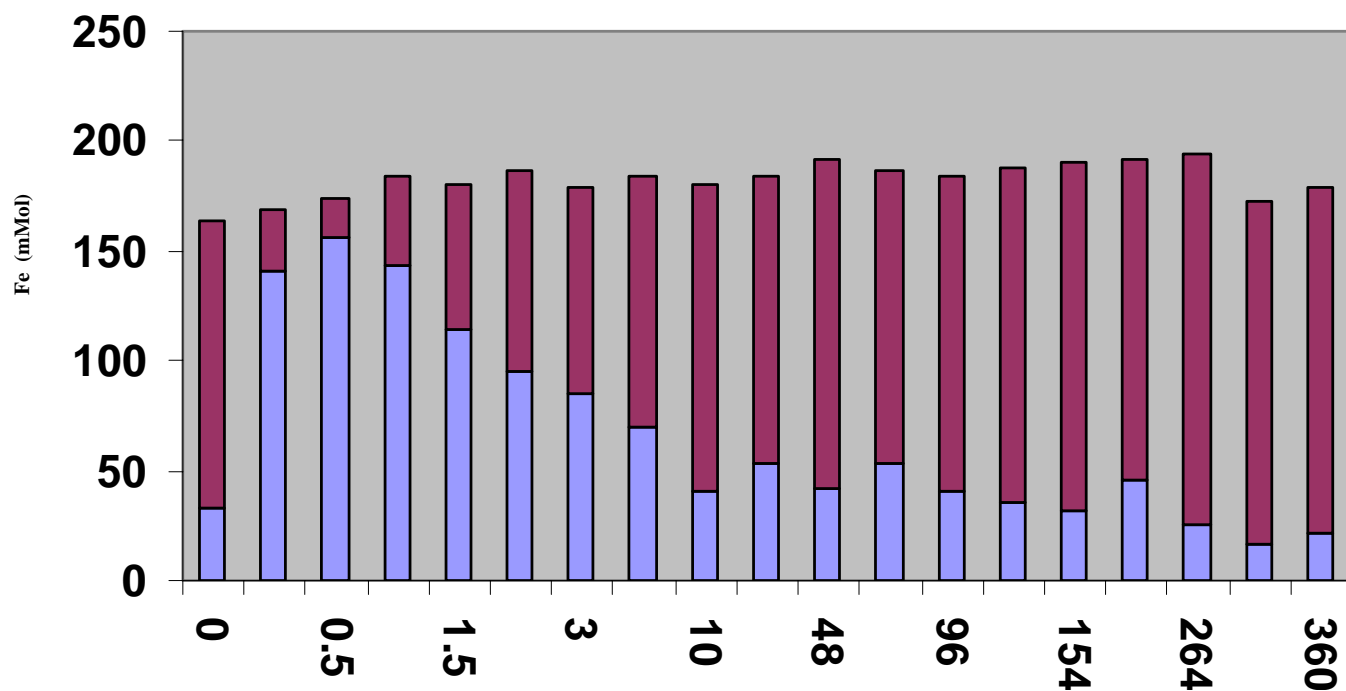


Figure D11: Fe²⁺ and Fe³⁺ concentration in the liquid medium during biooxidation using *SL5B* at 70°C.

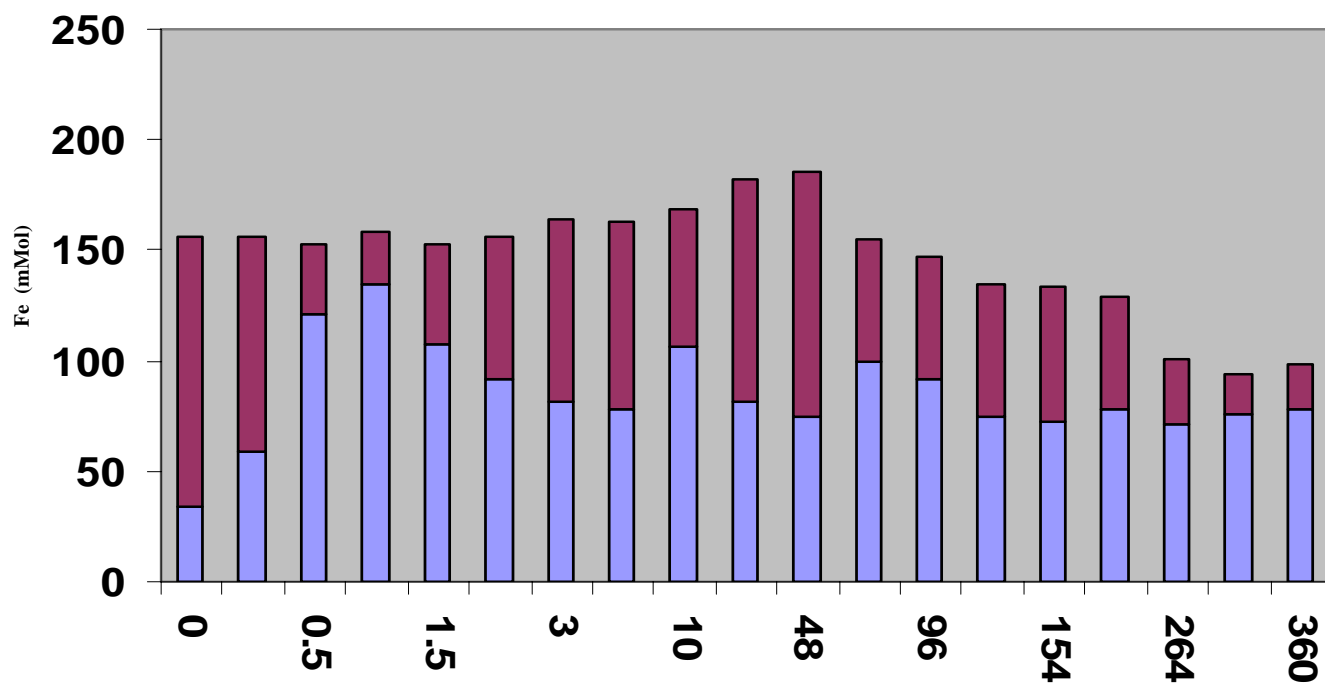


Figure D12: Fe²⁺ and Fe³⁺ concentration in the liquid medium for the control at 70°C.

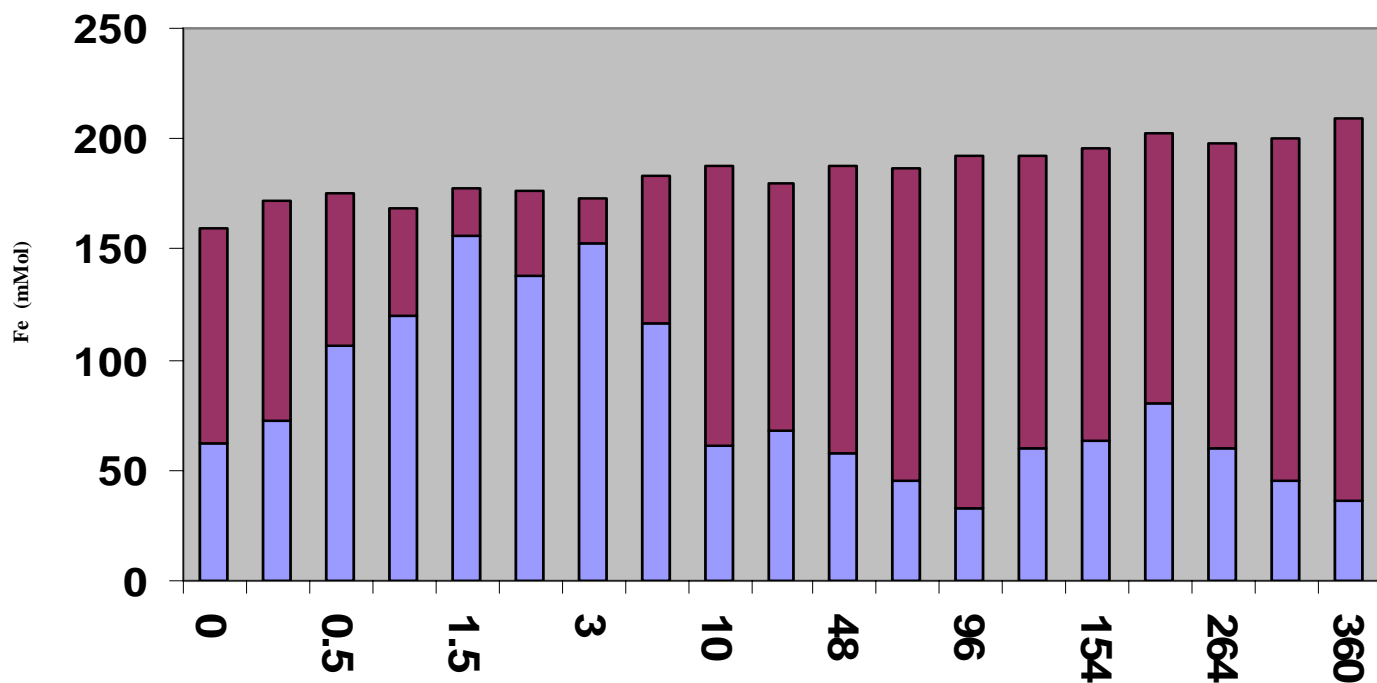


Figure D13: Fe²⁺ and Fe³⁺ concentration in the liquid medium using *S. Themorsulfodooxidans* at 45°C.

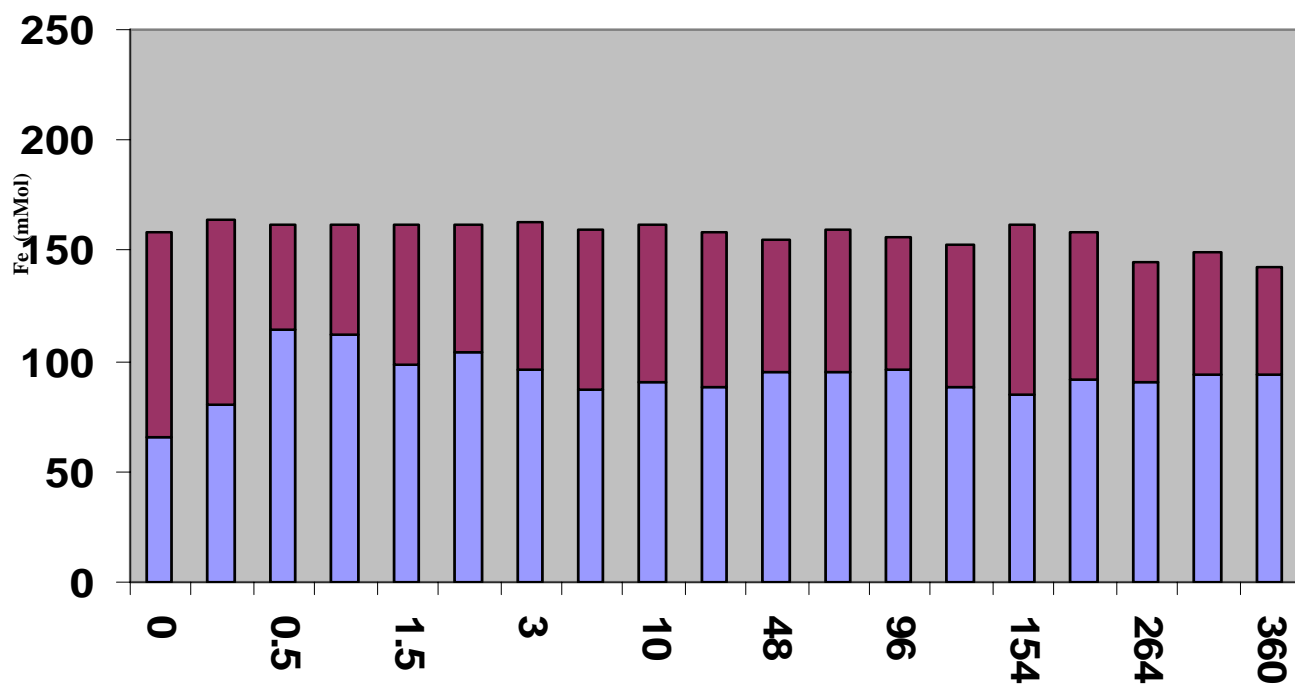


Figure D-14: Fe²⁺ and Fe³⁺ concentration in the liquid medium for the control at 45°C.

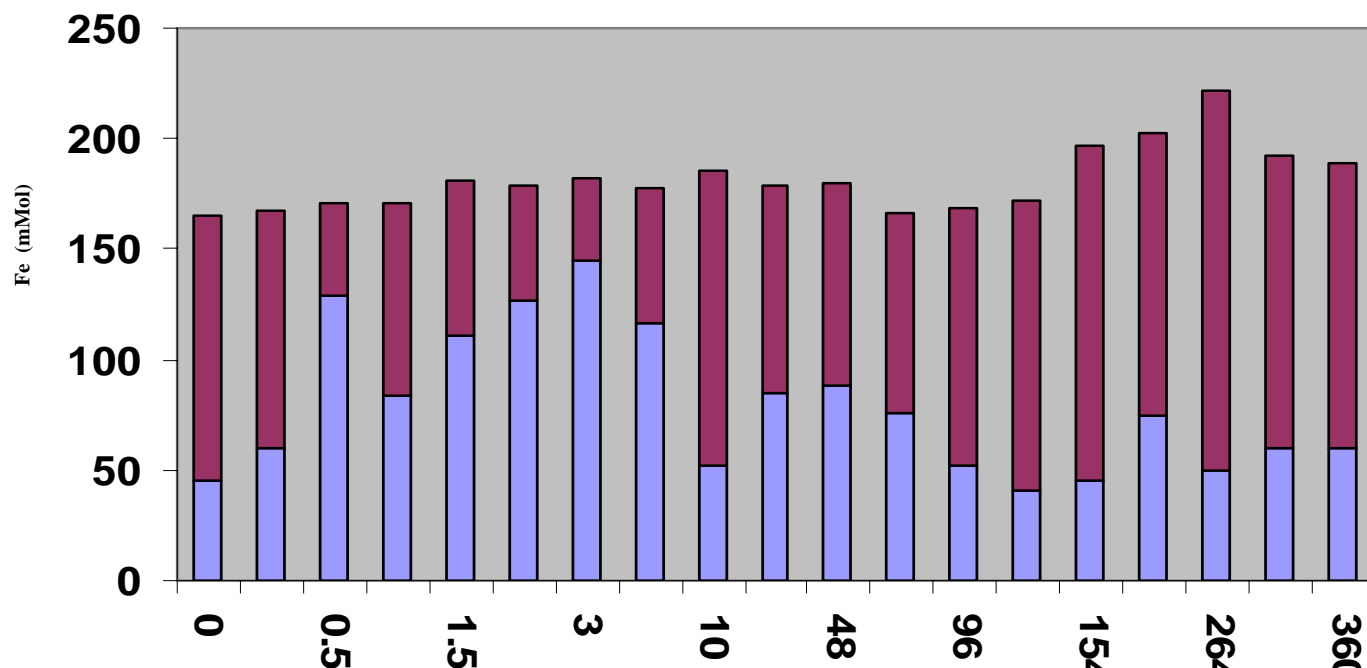


Figure D-15: Fe²⁺ and Fe³⁺ concentration in the liquid medium during biooxidation using *T. Ferrooxidans* at 30°C..

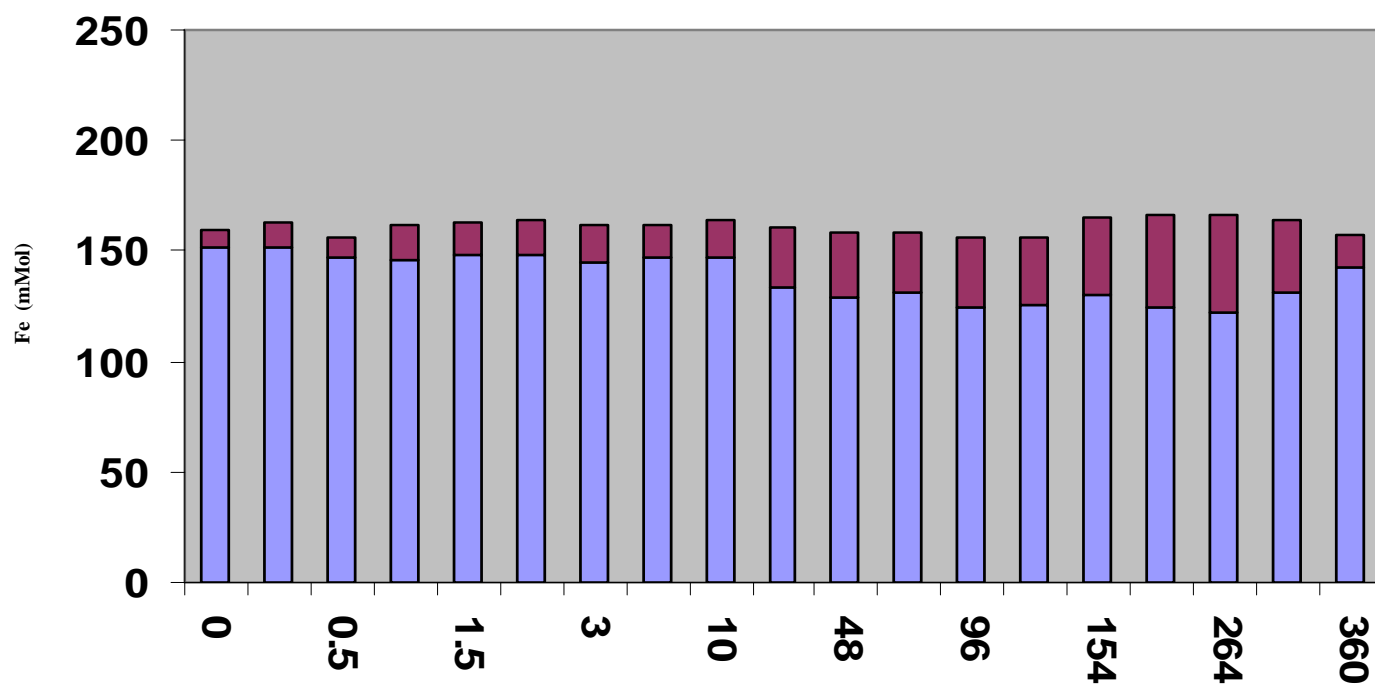


Figure D-16: Fe²⁺ and Fe³⁺ concentration in the liquid medium during for control at 30°C.

ATTACHMENT E

Data for Stirred Tank Reactor of pyrite using SL5B, using different medium to pyrite ratios

Shrinking particle model

Shrinking particle behavior of pyrite, with the film diffusion considered as controlling step

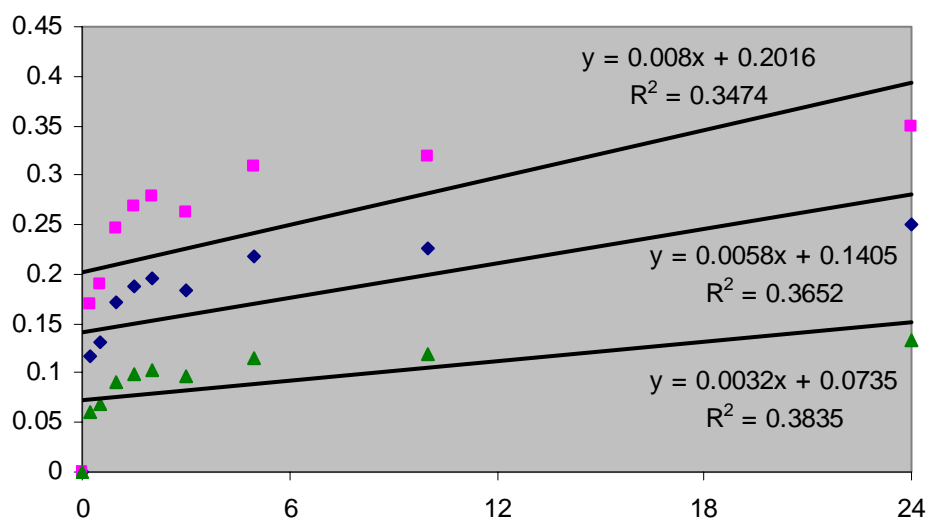


Fig E-1 : Shrinking particle and core model for initial biooxidation of pyrite using SL5B with 1% pyrite.

- Shrinking particle model with film diffusion as limiting step
- Shrinking particle/core model with chemical reaction as limiting step
- Shrinking core model with film diffusion as limiting step

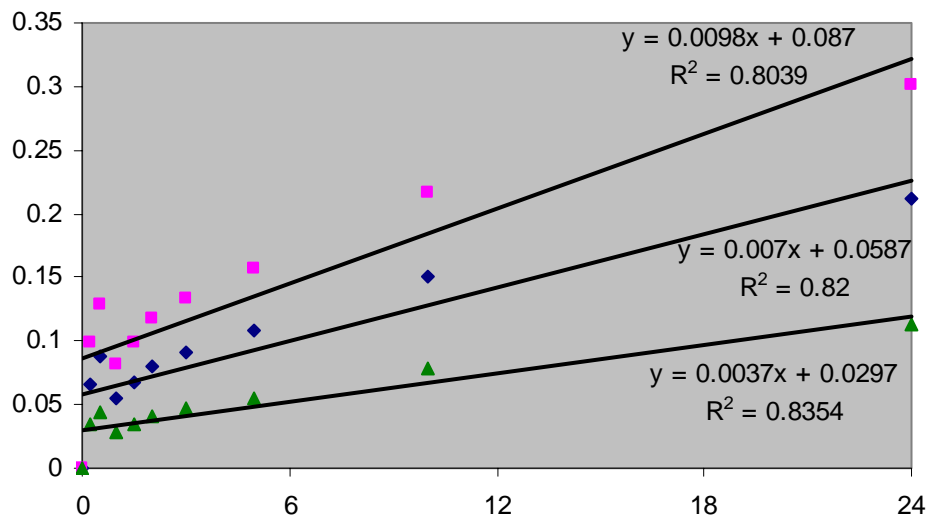


Fig E-2 : Shrinking particle and core model for initial biooxidation of pyrite using SL5B with 3% pyrite.

- Shrinking particle model with film diffusion as limiting step
- ◆ Shrinking particle/core model with chemical reaction as limiting step
- ▲ Shrinking core model with film diffusion as limiting step

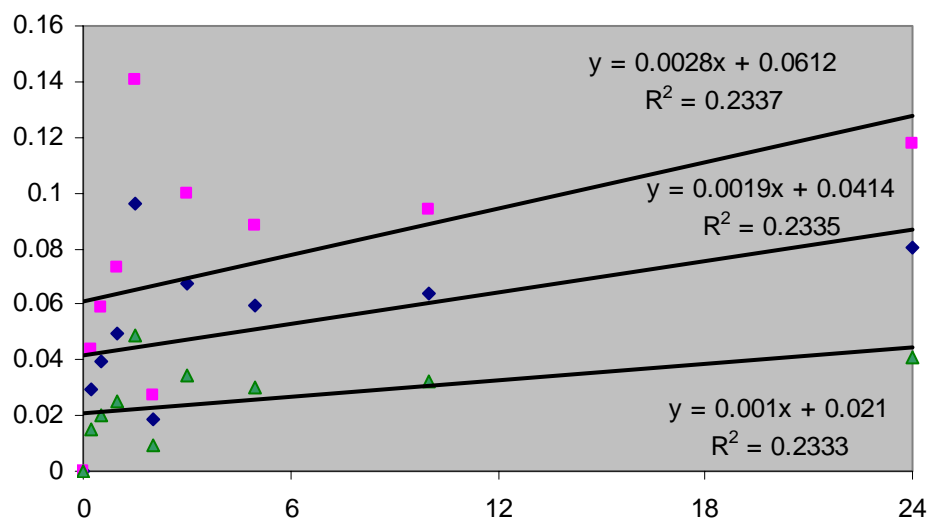


Fig E-3 : Shrinking particle and core model for initial biooxidation of pyrite using SL5B with 5% pyrite.

- Shrinking particle model with film diffusion as limiting step
- ◆ Shrinking particle/core model with chemical reaction as limiting step
- ▲ Shrinking core model with film diffusion as limiting step

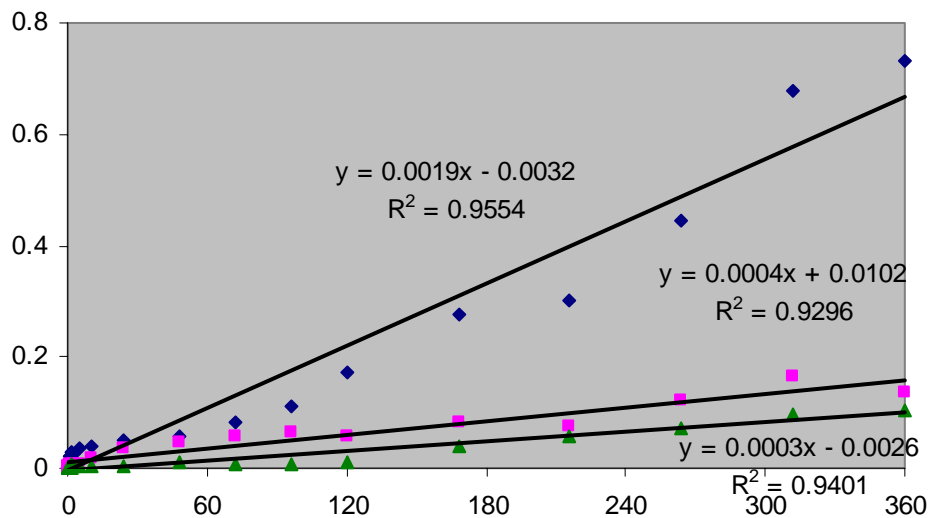


Fig E-4 : Shrinking core model with porous product diffusion as limiting step for pyrite oxidation at 1%, 3% and 5% pyrite densities.

- STR biooxidation using SL5B, 1% pyrite densities
- STR biooxidation using SL5B, 3% pyrite densities
- STR biooxidation using SL5B, 5% pyrite densities

Table E-1 : Iron speciation for biooxidation on 1% pyrite

Time	Solubilized iron in medium (mg/L)	Iron in the form of jarosite (mg/L)	[Fe ²⁺] (mL _{KMnO4})	[Fe ³⁺] (mL _{KMnO4})
0	8834.5	0	32.7	157.8
0.25	9246.2	740.7	140.4	165.1
0.5	9408.2	714.3	156.3	168.0
1	9815.1	687.0	142.8	175.3
1.5	9892.0	765.7	113.9	176.6
2	9877.8	847.9	94.7	176.4
3	9762.8	854.5	85.1	174.3
5	9846.0	1076.1	69.7	175.0
10	9836.5	1153.6	40.0	175.5
24	10156.0	1050.9	52.9	180.4
48	10189.0	1207.5	42.3	180.4
72	10045.0	1798.4	53.4	179.3
96	10456.0	1787.7	40.9	186.6
120	10982.0	1918.8	35.6	196.1
168	10476.0	3238.1	31.3	187.0
216	11015.0	2865.7	46.0	196.6
264	10698.0	3870.2	26.0	190.9
312	9752.2	5491.9	17.0	174.1
360	9852.3	5491.8	22.0	175.9

Table E-2 : Iron speciation for biooxidation on 3% pyrite

Time	Solubilized iron in medium (mg/L)	Iron in the form of jarosite (mg/L)	[Fe ²⁺] (mL _{KMnO4})	[Fe ³⁺] (mL _{KMnO4})
0	8927.4	0	28.4	164.0
0.25	9589.2	1335.1	167.7	174.0
0.5	8363.8	3164.1	147.0	153.0
1	8073.8	2515.7	138.0	148.0
1.5	6928.2	3997.3	114.0	130.0
2	8336.6	2982.5	105.0	153.0
3	8683.0	2938.5	110.0	152.0
5	8636.2	3485.7	100.0	152.0
10	11236.6	2086.5	102.0	197.0
24	13425.0	1605.7	131.0	240.0
48	13485.0	2448.1	126.0	245.0
72	13815.0	2751.7	164.0	253.0
96	13873.0	3050.1	152.0	243.0
120	13393.0	3209.7	116.0	250.0
168	13183.0	4738.1	130.0	236.0
216	14873.0	2650.8	152.0	274.0

Table E-3 : Iron speciation for biooxidation on 5% pyrite

Time	Solubilized iron in medium (mg/L)	Iron in the form of jarosite (mg/L)	[Fe ²⁺] (mL KMnO ₄)	[Fe ³⁺] (mL KMnO ₄)
0	8797.6	0	28.2	157.1
0.25	8918.6	1685.2	147.0	159.3
0.5	9105.6	1996.2	133.0	162.6
1	9705.4	1894.2	138.0	173.3
1.5	9505.2	4360.4	120.0	169.7
2	10768.6	723.4	105.0	192.3
3	10247.8	2237.8	110.0	183.0
5	10656.6	1445.7	100.0	190.3
10	11507.6	784.9	98.0	205.5
24	11516.8	1588.8	124.0	205.7
48	12078.8	2532.8	107.0	215.7
72	11076.8	2712.8	119.0	197.8
96	11307.8	2581.8	130.0	201.9
120	11505.8	3279.8	164.0	205.5
168	13076.8	6754.8	216.0	233.5
216	13706.4	8159.2	214.0	244.8
264	13700.6	9591	220.0	244.7
312	18077.6	7132.5	297.0	322.8
360	16769.4	8836.2	276.0	299.5

Table E-4 : Dissolved oxygen reading for STR biooxidation with 1% pyrite

Time (hrs)	DO in STR (%pO)	DO from free suspended pyrite inoculums		
		0 hr	24 hr	48 hr
0	59.4	8.57	7.03	7.04
0.25	54.6	8.57	6.85	6.87
0.5	55.3	8.56	7.65	6.43
1	50.8	8.68	6.54	7.02
1.5	44.5	8.56	7.25	6.24
2	42.4	8.56	7.09	6.26
3	44.9	8.57	6.77	6.86
5	43.1	8.55	6.25	5.88
10	50.2	8.56	6.65	6.04
24	46.9	8.6	7.69	4.84
48	49.6	8.56	7.36	5.24
72	45.2	8.53	7.24	4.29
96	53.5	8.74	5.11	2.91
120	56.4	8.52	4.51	3.46
154	52.7	8.57	3.92	2.91
216	52.7	8.54	4.34	3.31
264	37.9	8.55	5.16	4.42
312	29.5	8.57	5.71	4.51
360	31.5	8.54	6.87	4.95

Table E-5 : Dissolved oxygen reading for STR biooxidation with 3% pyrite

Time (hrs)	DO in STR (%pO)	DO from free suspended pyrite inoculums		
		0 hr	24 hr	48 hr
0	61.4	8.34	6.72	6.96
0.25	57.5	8.54	7.56	6.86
0.5	56.6	8.54	7.82	6.6
1	48.8	8.49	7.23	6.93
1.5	52.5	8.34	7.05	6.63
2	48.5	8.61	7.46	6.95
3	54.2	8.51	7.43	6.65
5	52.5	8.34	6.03	6.01
10	59.4	8.59	6.65	6.27
24	48.4	8.57	6.87	3.25
48	44.8	8.59	8.02	8.05
72	41.1	8.58	5.14	2.35
96	33.8	8.58	5.01	2.05
120	27.3	8.63	3.97	2.75
154	22.8	8.61	5.16	1.48
216	34.5	8.63	3.87	3.05
264	29.7	8.55	4.95	4.55
312	25.6	8.59	6.6	5.88
360	26.4	8.57	7.75	7.35

Table E-6 : Dissolved oxygen reading for STR biooxidation with 5 % pyrite

Time (hrs)	DO in STR (%pO)	DO from free suspended pyrite inoculums		
		0 hr	24 hr	48 hr
0	56.4	8.59	7.15	7.61
0.25	53.7	8.52	7.35	7.02
0.5	49.7	8.57	7.76	7.38
1	48.5	8.52	7.65	7.47
1.5	46.4	8.52	7.26	7.32
2	38.5	8.56	7.65	7.48
3	39.1	8.56	7.99	7.59
5	33.8	8.57	6.82	6.97
10	22.7	8.57	6.88	4.84
24	25.5	8.63	3.24	2.05
48	34.9	8.78	5.75	2.01
72	29.3	8.59	7.53	7.01
96	26.5	8.34	7.15	6.61
120	27.7	8.34	7.84	5.26
154	25.2	8.34	6.97	6.08
216	20.3	8.59	7.25	7.31
264	20.9	8.35	7.84	6.05
312	18.8	8.35	7.12	6.61
360	17.1	8.57	8.08	8.06

ATTACHMENT F

Reading for Stirred Tank Reactor of pyrite using SL5B, using different size of pyrite size

Table F-1: pH value for STR test at different pyrite size

Pyrite size (μm) Time (Hr)	75	125	180	250	500
0	1.84	1.86	1.87	1.89	1.81
0.25	1.83	1.85	1.87	1.92	1.95
0.5	1.84	1.82	1.87	1.88	1.93
1	1.83	1.84	1.86	1.88	1.93
1.5	1.86	1.83	1.85	1.86	1.88
2	1.83	1.84	1.81	1.79	1.90
3	1.85	1.83	1.83	1.81	1.95
5	1.80	1.88	1.78	1.84	1.91
10	1.85	1.83	1.79	1.81	1.88
24	1.85	1.86	1.81	1.82	1.74
48	1.83	1.76	1.80	1.76	1.73
72	1.75	1.72	1.79	1.74	1.76
96	1.73	1.77	1.81	1.68	1.79
120	1.76	1.70	1.78	1.74	1.83
168	1.66	1.75	1.69	1.73	1.78
216	1.79	1.75	1.72	1.76	1.77
264	1.64	1.80	1.80	1.72	1.73
312	1.70	1.67	1.77	1.76	1.73
360	1.76	1.71	1.75	1.73	1.67

Table F-2: Eh value for STR test at different pyrite size

Pyrite size (μm)					
Time (Hr)	75	125	180	250	500
0	541.2	523.7	533.8	508.2	502.1
0.25	473.3	495.5	482.6	505.5	506.2
0.5	435.9	479.3	460.0	503.5	521.6
1	404.4	486.1	487.3	502.8	488.0
1.5	434.2	450.0	470.5	504.1	486.6
2	458.0	436.8	480.0	506.2	518.4
3	389.1	455.5	449.6	510.8	544.8
5	470.0	441.0	412.9	512.5	549.1
10	411.2	485.3	434.2	578.8	564.4
24	420.0	412.2	446.1	465.0	474.4
48	542.2	443.3	475.0	465.0	471.7
72	597.5	440.0	507.4	465.0	470.0
96	525.2	485.0	503.1	465.0	470.0
120	596.7	514.2	476.7	490.0	507.5
168	530.6	623.1	556.7	490.9	496.2
216	695.4	586.2	651.1	487.6	460.0
264	704.7	726.0	617.1	501.5	509.5
312	755.8	669.0	622.2	514.7	567.0
360	750.7	731.9	656.2	504.8	537.2

Table F-3: $\ln \text{Fe}^{3+}/\text{Fe}^{2+}$ value for STR test at different pyrite size

Pyrite size (μm)					
Time (Hr)	75	125	180	250	500
0	1.3863	0.7917	1.2144	1.4064	1.0545
0.25	-1.5981	-0.2761	0.7919	1.4643	1.7940
0.5	-2.2011	-1.1742	0.1523	1.4939	1.5821
1	-1.2285	-1.3573	0.4006	1.2221	0.8858
1.5	-0.5396	-0.5033	-1.3143	0.6587	1.2474
2	-0.0311	0.3083	-1.1299	0.5650	1.3041
3	0.1016	0.6916	-1.1896	0.8869	0.5253
5	0.4955	0.7020	-1.1065	0.4083	0.7795
10	1.2528	1.1641	0.0220	0.8567	0.1689
24	0.9121	0.6737	-0.7802	1.3122	0.1261
48	1.2592	1.1716	-0.4958	0.9658	0.5273
72	0.9133	1.4971	-0.8090	0.8755	0.9933
96	1.2566	0.8046	-1.3640	0.7250	0.8473
120	1.4509	1.2657	0.7097	1.1802	1.7872
168	1.6259	1.7622	1.5469	1.1327	0.5331
216	1.1536	1.3002	1.1211	0.8232	0.4727
264	1.8671	0.9531	1.5550	1.4432	0.3385
312	2.2173	1.2806	1.2669	1.3863	0.1065
360	1.9639	1.4000	0.0774	0.8874	-0.3567

Table F-4: Dissolved oxygen value for the free pyrite-anaerobic inoculation from STR sample at 75 μ m pyrite

Time of sample taken form STR	Inoculums duration			$d[O_2]/dt$	Regression coefficient
	0	24	48		
0	8.57	7.03	7.04	0.0319	0.7451
0.25	8.57	6.85	6.87	0.0354	0.7412
0.5	8.56	7.65	6.43	0.0431	0.993
1	8.68	6.54	7.02	0.0354	0.5463
1.5	8.56	7.25	6.24	0.0469	0.9945
2	8.56	7.09	6.26	0.0492	0.9748
3	8.57	6.77	6.86	0.0346	0.7106
5	8.55	6.25	5.88	0.0554	0.8517
10	8.56	6.65	6.04	0.0531	0.9185
24	8.6	7.69	4.84	0.0792	0.9185
48	8.56	7.36	5.24	0.0715	0.975
72	8.53	7.24	4.29	0.0892	0.9514
96	8.74	5.11	2.91	0.0983	0.9803
120	8.52	4.51	3.46	0.1054	0.8976
168	8.57	3.92	2.91	0.1192	0.8788
216	8.54	4.34	3.31	0.1108	8.0117
264	8.55	5.16	4.42	0.088	0.9472
312	8.57	5.71	4.51	0.0862	0.9472
360	8.54	6.87	4.95	0.0708	0.9984

Table F-5: Dissolved oxygen value for the free pyrite-anaerobic inoculation from STR sample at 125 μm pyrite

Time of sample taken form STR	Inoculums duration			$d[O_2]/dt$	Regression coefficient
	0	24	48		
0	8.63	7.52	6.95	0.0369	0.9667
0.25	8.56	7.8	6.34	0.0456	0.9679
0.5	8.53	7.15	6.06	0.0513	0.9954
1	8.56	7.25	6.21	0.0488	0.9956
1.5	8.58	6.24	6.02	0.052	0.8139
2	8.56	6.95	5.91	0.0556	0.9848
3	8.61	7.46	6.07	0.0513	0.997
5	8.61	6.03	5.27	0.0694	0.9099
10	8.56	7.24	6.27	0.0469	0.9923
24	8.63	7.52	6.85	0.0356	0.98
48	8.59	7.23	5.6	0.0619	0.9973
72	8.56	5.06	4.18	0.0912	0.8934
96	8.58	3.84	3.57	0.1063	0.7903
120	8.63	7.52	4.25	0.0925	0.925
168	8.56	5.06	3.98	0.0956	0.9149
216	8.59	5.85	4.23	0.092	0.9785
264	8.63	4.78	4.11	0.0944	0.8584
312	8.56	5.83	5.52	0.0688	0.8256
360	8.61	6.32	6.02	0.0525	0.8356

Table F-6: Dissolved oxygen value for the free pyrite-anaerobic inoculation from STR sample at 180 μm pyrite

Time of sample taken form STR	Inoculums duration			$d[O_2]/dt$	Regression coefficient
	0	24	48		
0	8.58	6.23	6.47	0.0425	0.6691
0.25	8.61	6.92	6.2	0.05	0.9488
0.5	8.56	6.71	5.91	0.055	0.9503
1	8.58	7.6	5.89	0.0569	0.9749
1.5	8.58	6.43	5.89	0.0569	0.8956
2	8.56	6.55	5.6	0.0625	0.959
3	8.56	7.77	5.42	0.0656	0.924
5	8.63	6.96	5.35	0.0669	0.9999
10	8.58	7.68	6.2	0.05	0.9806
24	8.62	8.13	6.47	0.0425	0.9096
48	8.57	6.43	5.8	0.0594	0.9119
72	8.56	5.54	4.82	0.0775	0.888
96	8.59	6.96	5.26	0.07	0.9999
120	8.56	5.63	4.94	0.0744	0.8868
168	8.59	3.25	3.25	0.1	0.75
216	8.56	6.27	4.94	0.0775	0.9771
264	8.59	7.4	3.8	0.1	0.9222
312	8.63	7.68	3.93	0.0975	0.8942
360	8.56	5.02	4.8	0.0781	0.7937

Table F-7: Dissolved oxygen value for the free pyrite-anaerobic inoculation from STR sample at 250 μm pyrite

Time of sample taken form STR	Inoculums duration			$d[O_2]/dt$	Regression coefficient
	0	24	48		
0	8.56	7.86	7.5	0.0219	0.9668
0.25	8.59	8.26	7.75	0.0175	0.9848
0.5	8.61	8.39	7.85	0.016	0.9428
1	8.56	8.36	7.86	0.015	0.9423
1.5	8.62	8.13	7.94	0.0144	0.9423
2	8.56	7.23	7.58	0.0213	0.5092
3	8.58	7.68	7.31	0.0269	0.9464
5	8.63	7.14	7.14	0.0313	0.75
10	8.56	7.4	6.71	0.036	0.9789
24	8.56	6.15	4.94	0.075	0.9647
48	8.59	6.07	4.55	0.0844	0.98
72	8.56	4.5	3.94	0.0975	0.8394
96	8.57	5.61	4.41	0.0863	0.945
120	8.63	5.63	4.46	0.0856	0.9397
168	8.57	4.26	3.38	0.1088	0.8753
216	8.59	3.45	3.48	0.1056	0.7456
264	8.56	3.05	2.69	0.1194	0.7958
312	8.57	3.5	3.29	0.1106	0.7828
360	8.56	3.78	3.13	0.1169	0.8383

Table F-8: Dissolved oxygen value for the free pyrite-anaerobic inoculation from STR sample at 500 μm pyrite

Time of sample taken form STR	Inoculums duration			$d[O_2]/dt$	Regression coefficient
	0	24	48		
0	8.63	7.5	7.37	0.0256	0.8265
0.25	8.58	7.88	7.46	0.0231	0.9796
0.5	8.6	8.08	7.64	0.02	0.998
1	8.56	8.12	8.02	0.012	0.8833
1.5	8.6	8.08	8.05	0.01	0.795
2	8.56	8.36	7.92	0.0125	0.9552
3	8.61	8.43	7.88	0.015	0.9192
5	8.59	8.26	7.85	0.0156	0.9963
10	8.58	7.88	7.54	0.0219	0.9627
24	8.63	7.5	7.14	0.03	0.9183
48	8.59	6.25	5.94	0.0556	0.8364
72	8.57	8.08	4.96	0.0769	0.8471
96	8.63	4.91	4.33	0.0894	0.8491
120	8.56	5.45	4.18	0.09	0.9444
168	8.63	5	4.29	0.0906	0.8689
216	8.58	8.26	2.37	0.1231	0.9997
264	8.56	8.12	2.35	0.125	0.8029
312	8.63	5.26	2.68	0.124	0.9942
360	8.59	3.35	2.61	0.1263	0.8423

Shrinking particle model

Shrinking particle behavior of pyrite, with the film diffusion considered as controlling step.

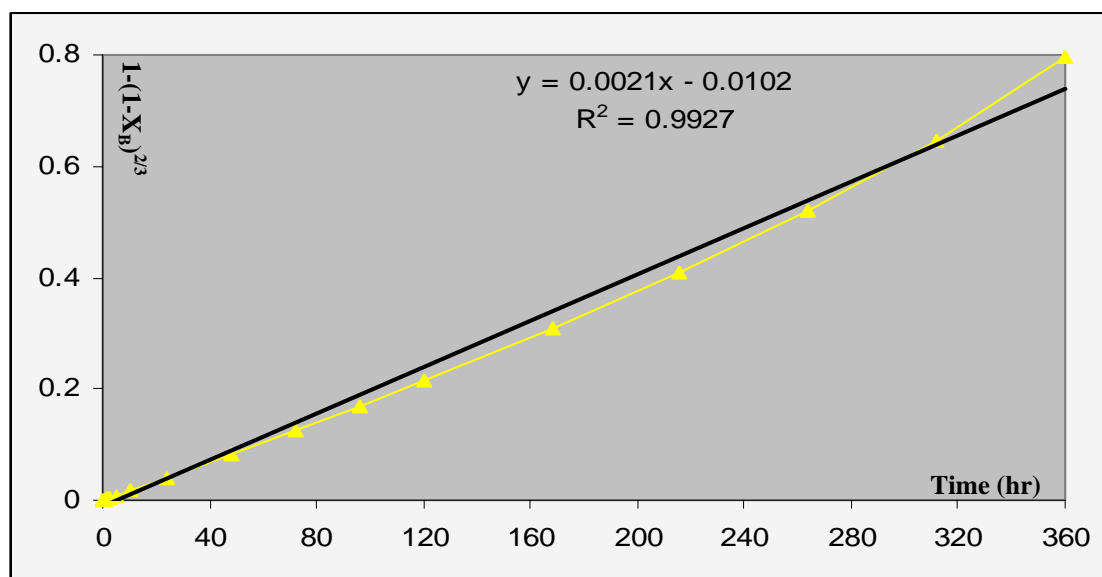


Fig F-1 : Shrinking particle behavior for film diffusion considered as controlling step ($1-(1-X_B)^{2/3}$) on a 75 μm pyrite.

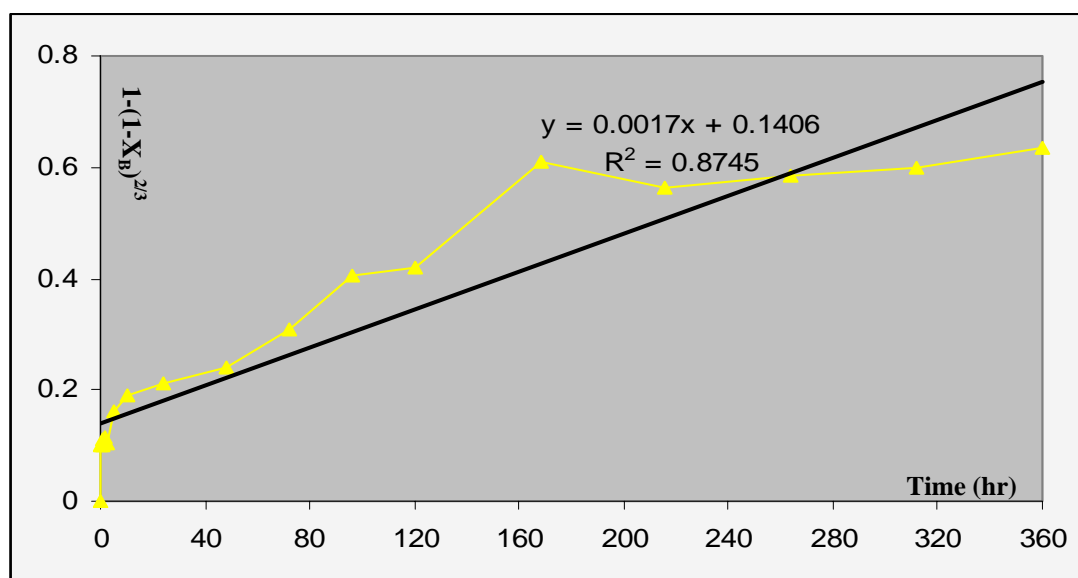


Fig F-2 : Shrinking particle behavior for film diffusion considered as controlling step ($1-(1-X_B)^{2/3}$) on a 125 μm pyrite.

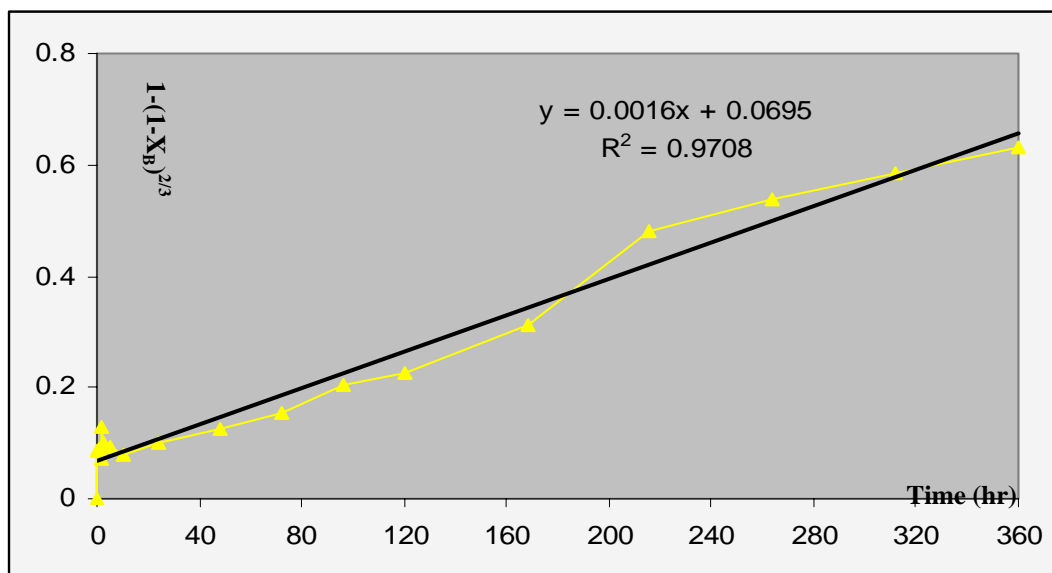


Fig F-3 : Shrinking particle behavior for film diffusion considered as controlling step ($1-(1-X_B)^{2/3}$) on a 180 μm pyrite.

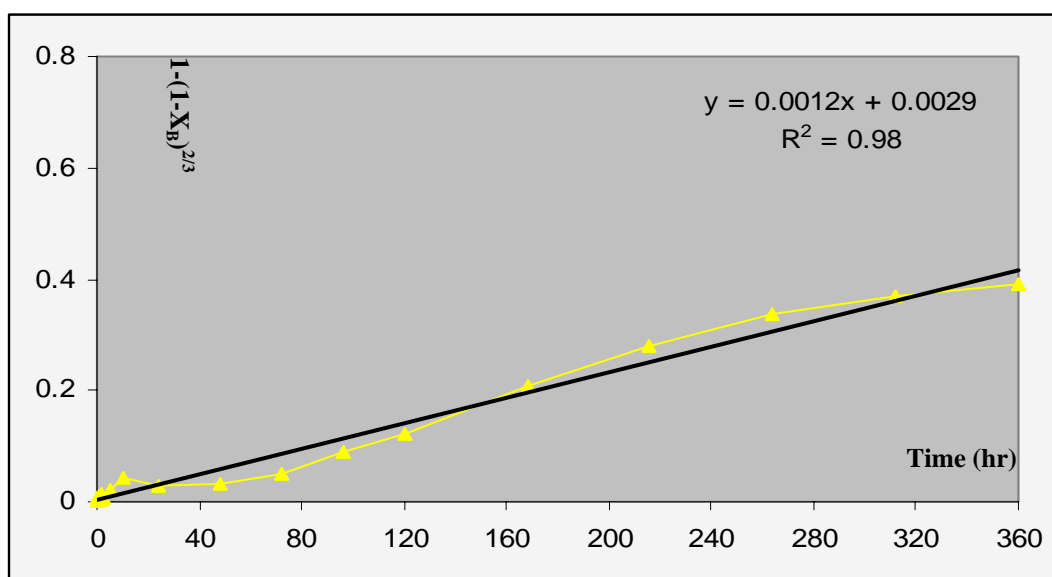


Fig F-4 : Shrinking particle behavior for film diffusion considered as controlling step ($1-(1-X_B)^{2/3}$) on a 250 μm pyrite.

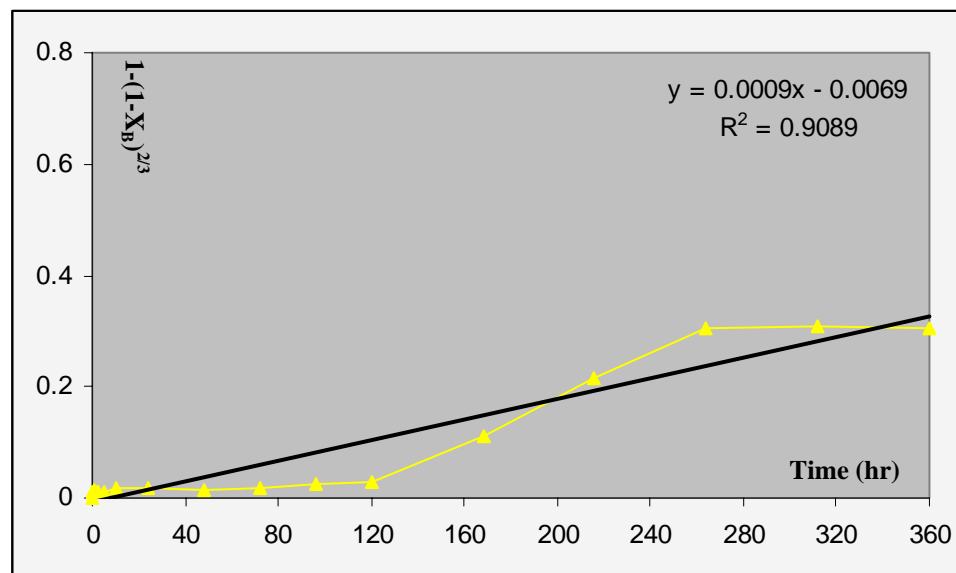


Fig F-5 : Shrinking particle behavior for film diffusion considered as controlling step ($1-(1-X_B)^{2/3}$) on a 500 μm pyrite.

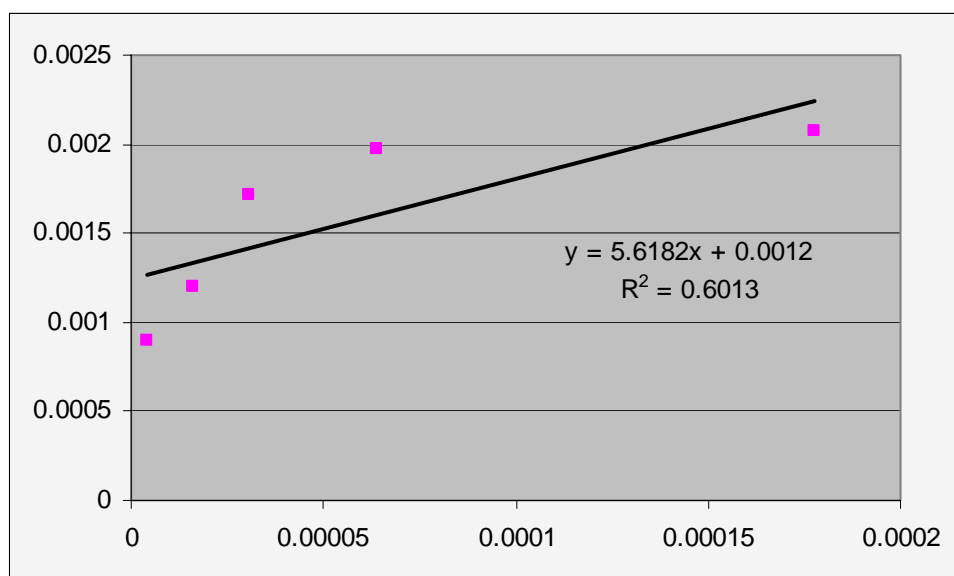


Fig F-6 : relation of required leaching time (t_{total}) and initial particle size for Shrinking particle model for film diffusion considered as controlling step

Shrinking particle behavior of pyrite, with the film diffusion considered as controlling step for the large particle

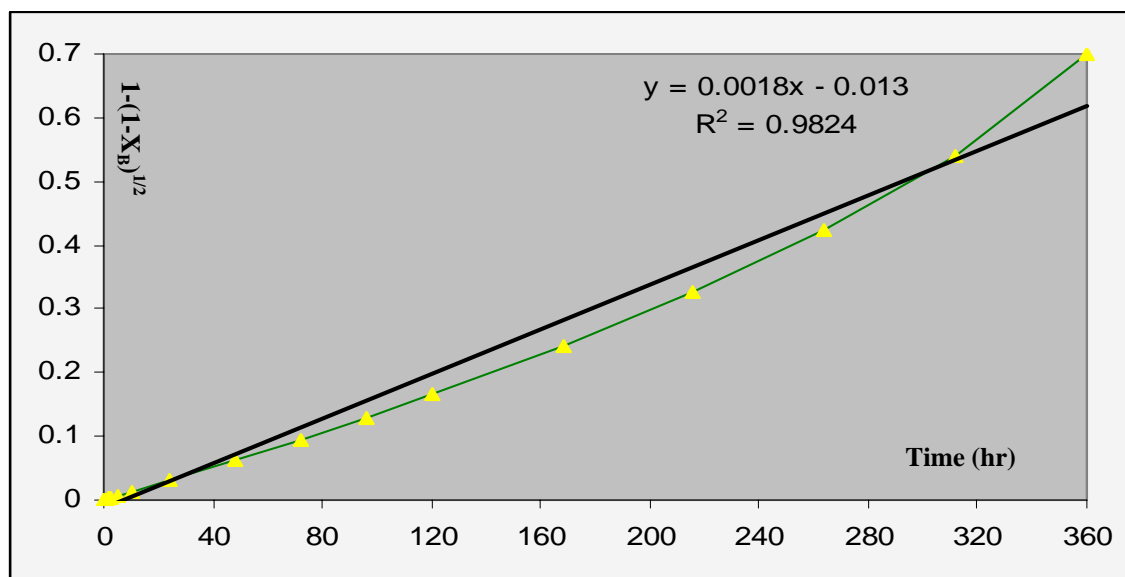


Fig F-7 : Shrinking particle behavior for film diffusion considered as controlling step ($1-(1-X_B)^{1/2}$) on a 75 μm pyrite.

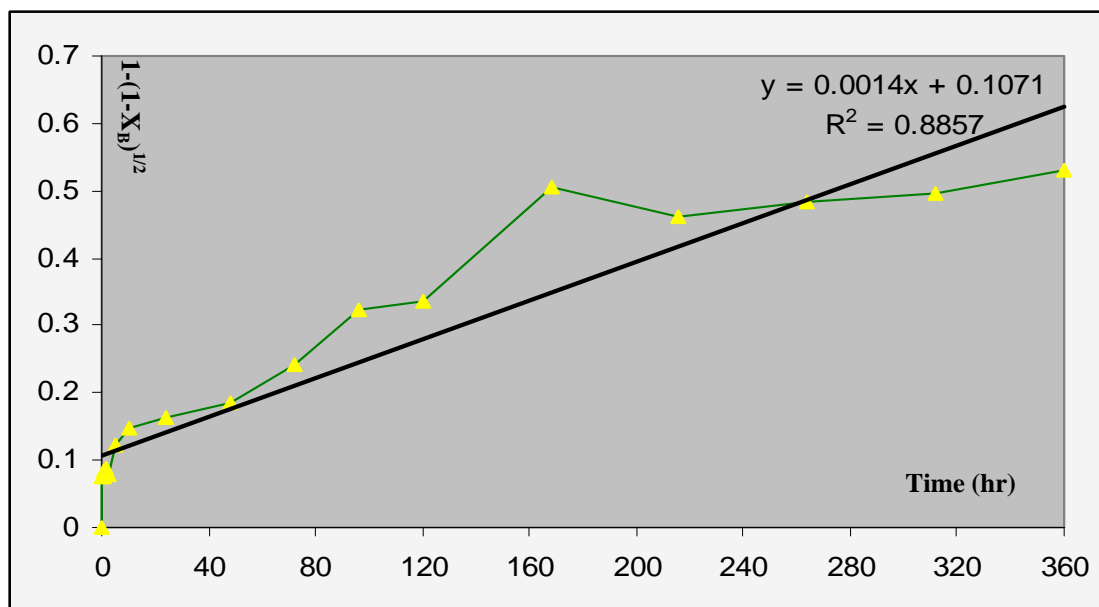


Fig F-8 : Shrinking particle behavior for film diffusion considered as controlling step ($1-(1-X_B)^{1/2}$) on a 125 μm pyrite.

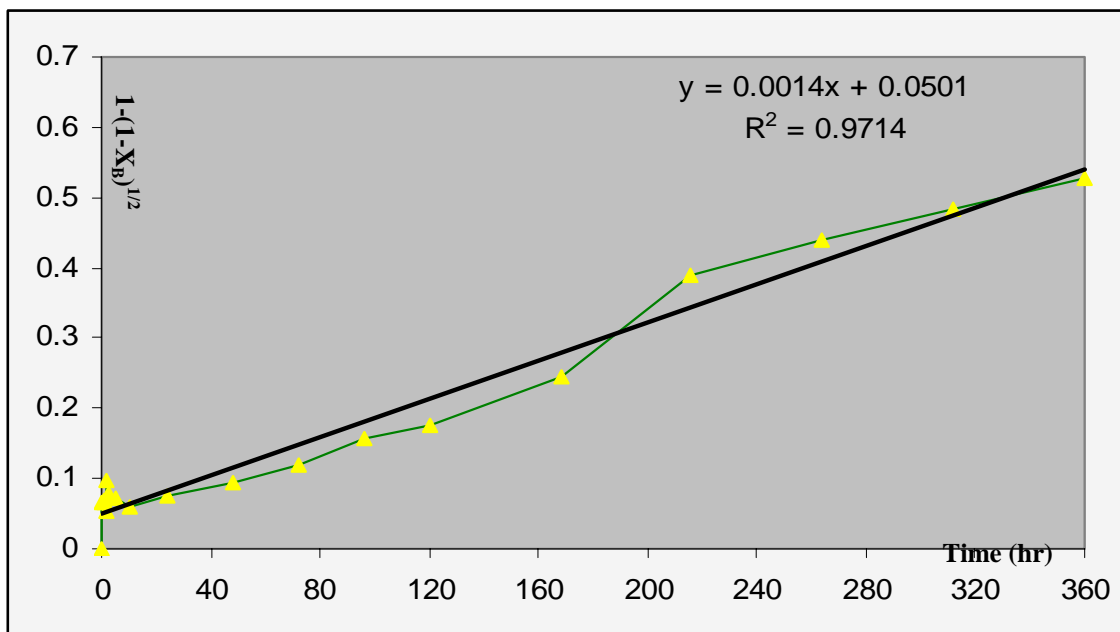


Fig F-9 : Shrinking particle behavior for film diffusion considered as controlling step ($1-(1-X_B)^{1/2}$) on a 180 μm pyrite.

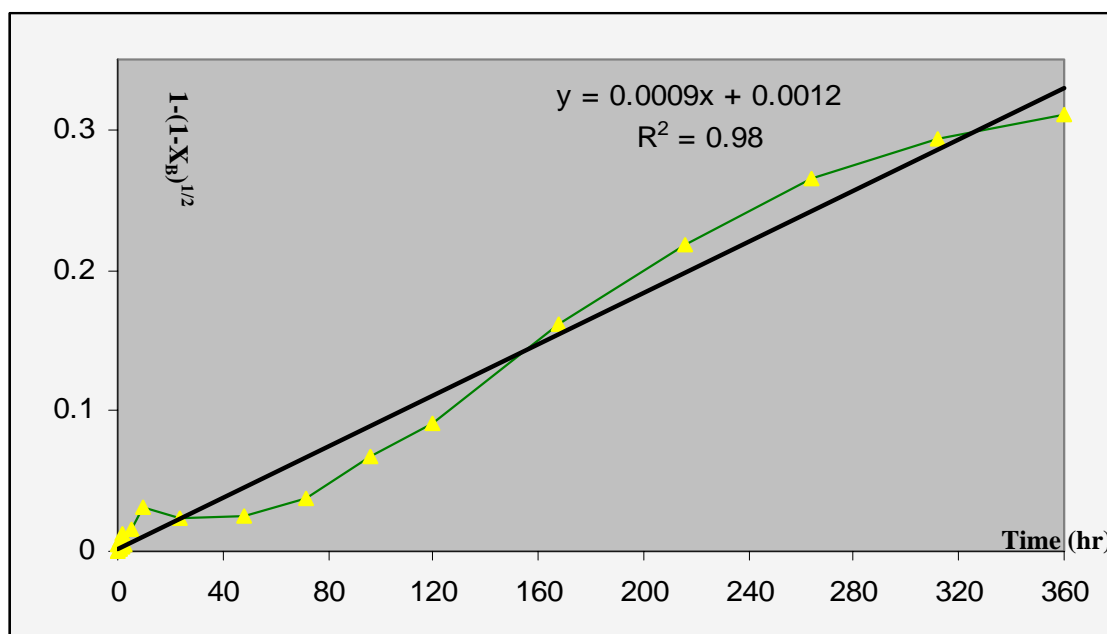


Fig F-10 : Shrinking particle behavior for film diffusion considered as controlling step ($1-(1-X_B)^{1/2}$) on a 250 μm pyrite.

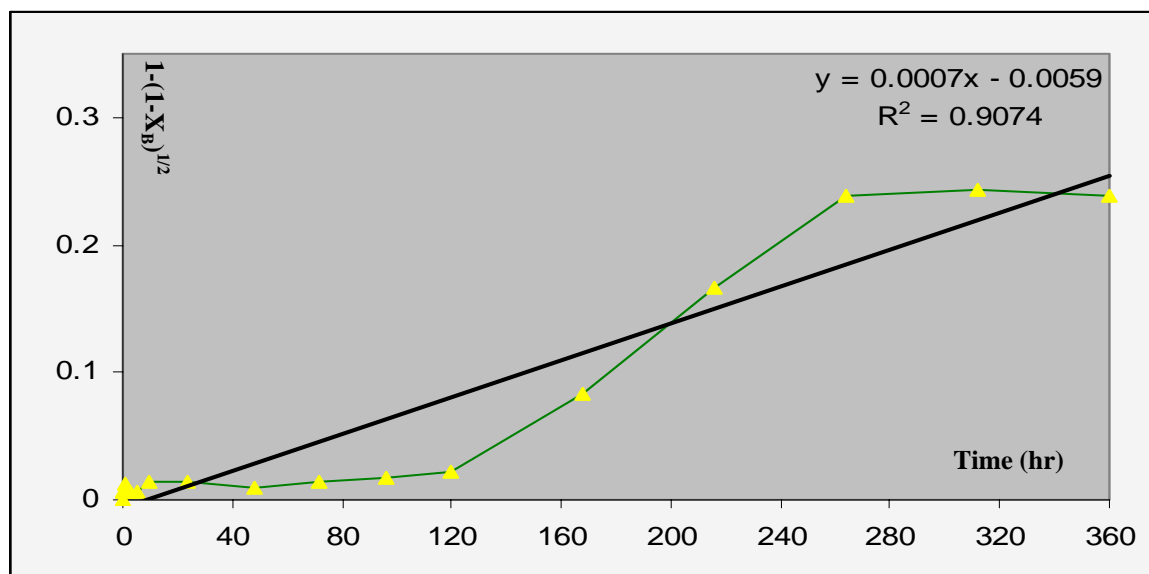


Fig F-11 : Shrinking particle behavior for film diffusion considered as controlling step ($1-(1-X_B)^{1/2}$) on a 500 μm pyrite.

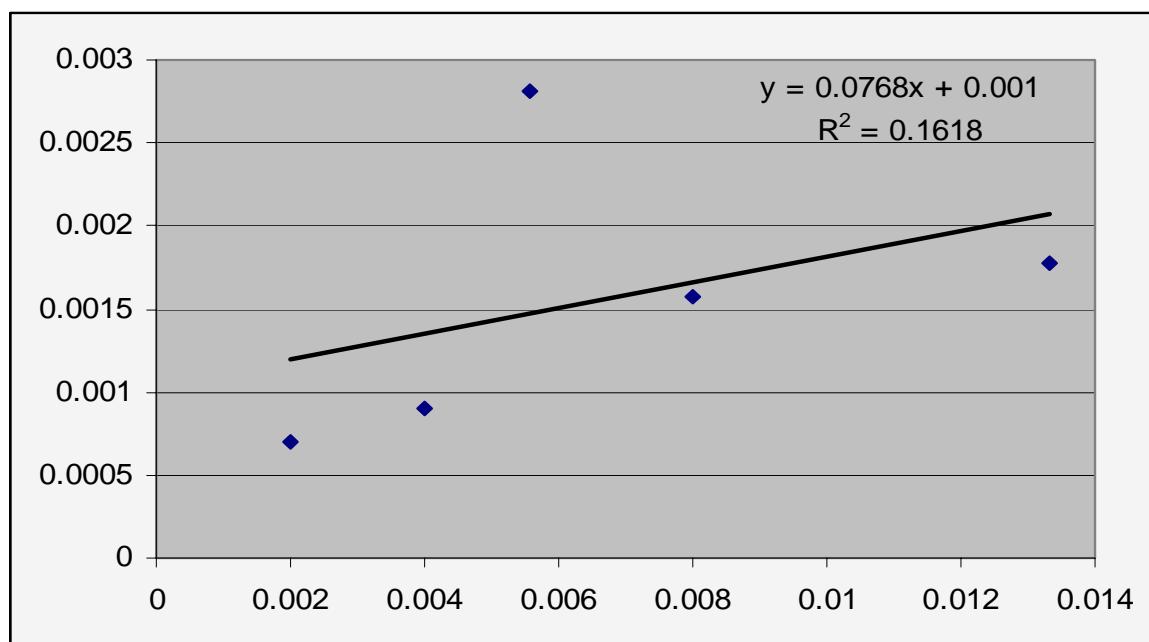


Fig F-12 : relation of required leaching time (t_{total}) and initial particle size for Shrinking particle model for film diffusion considered as controlling step for large particle

Shrinking particle model and shrinking core model of pyrite, with the chemical reaction at a pyrite surface considered as controlling step

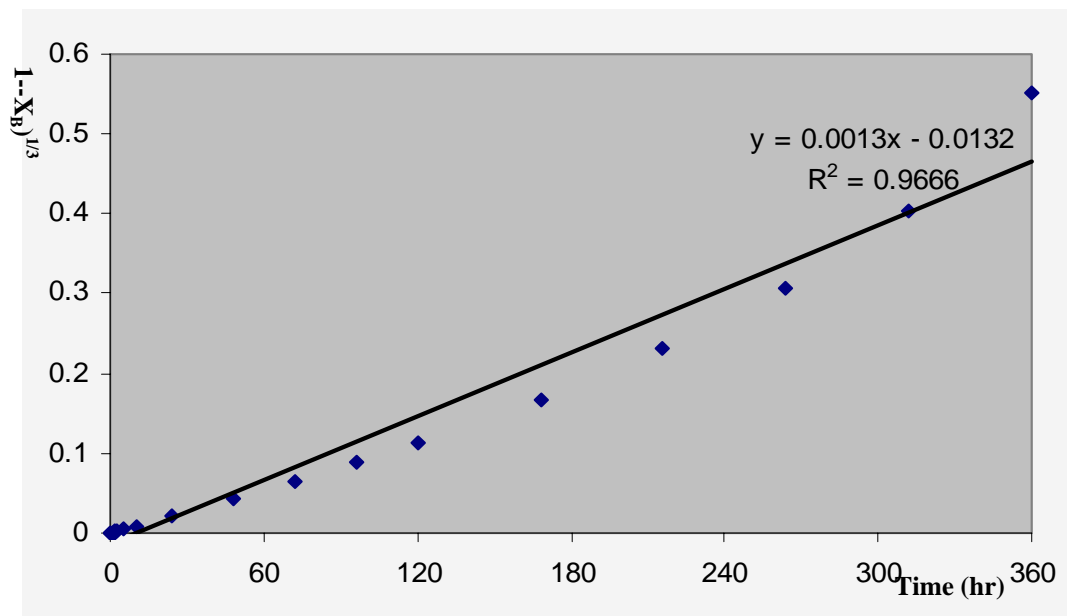


Fig F-13 : Shrinking particle behavior for chemical reaction considered as controlling step ($(1-X_B)^{1/3}$) on a 75 μm pyrite.

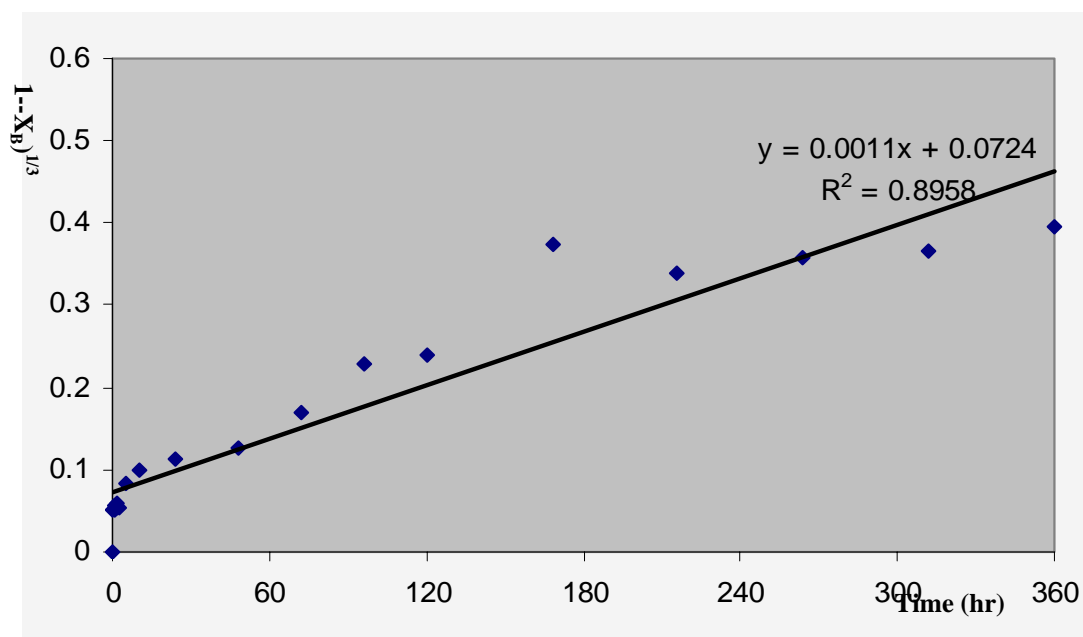


Fig F-14 : Shrinking particle behavior for chemical reaction considered as controlling step ($(1-X_B)^{1/3}$) on a 125 μm pyrite.

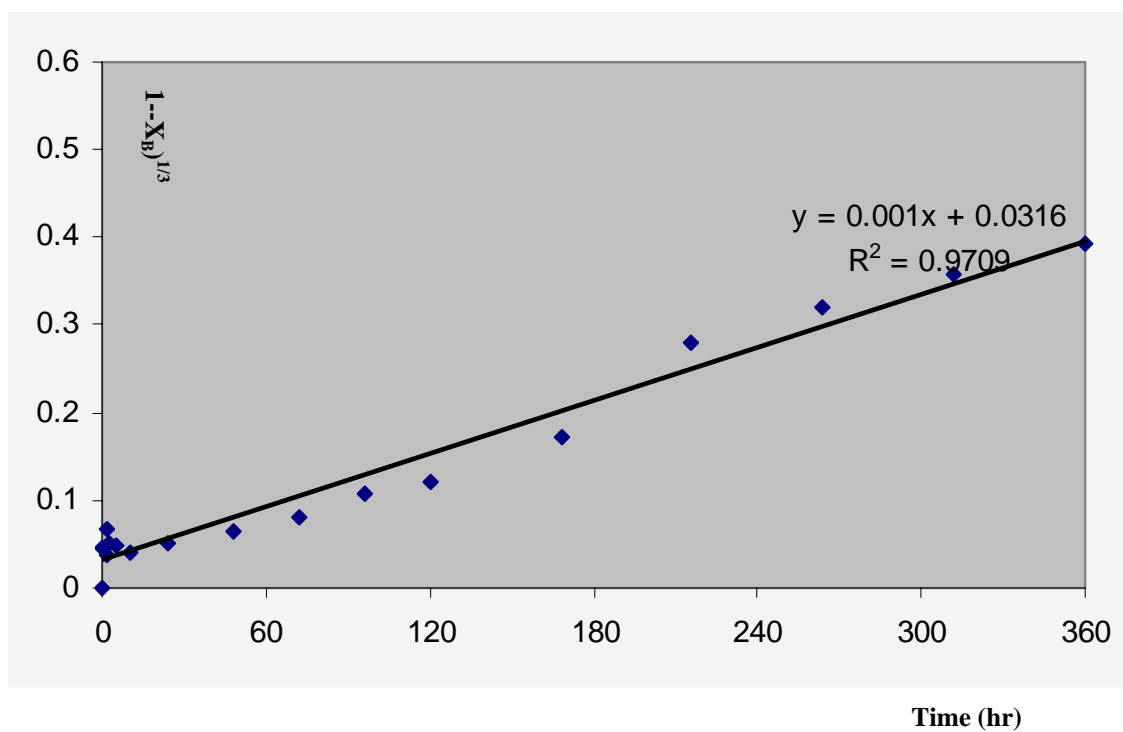


Fig F-15 : Shrinking particle behavior for chemical reaction considered as controlling step ($(1-X_B)^{1/3}$) on a 180 μm pyrite.

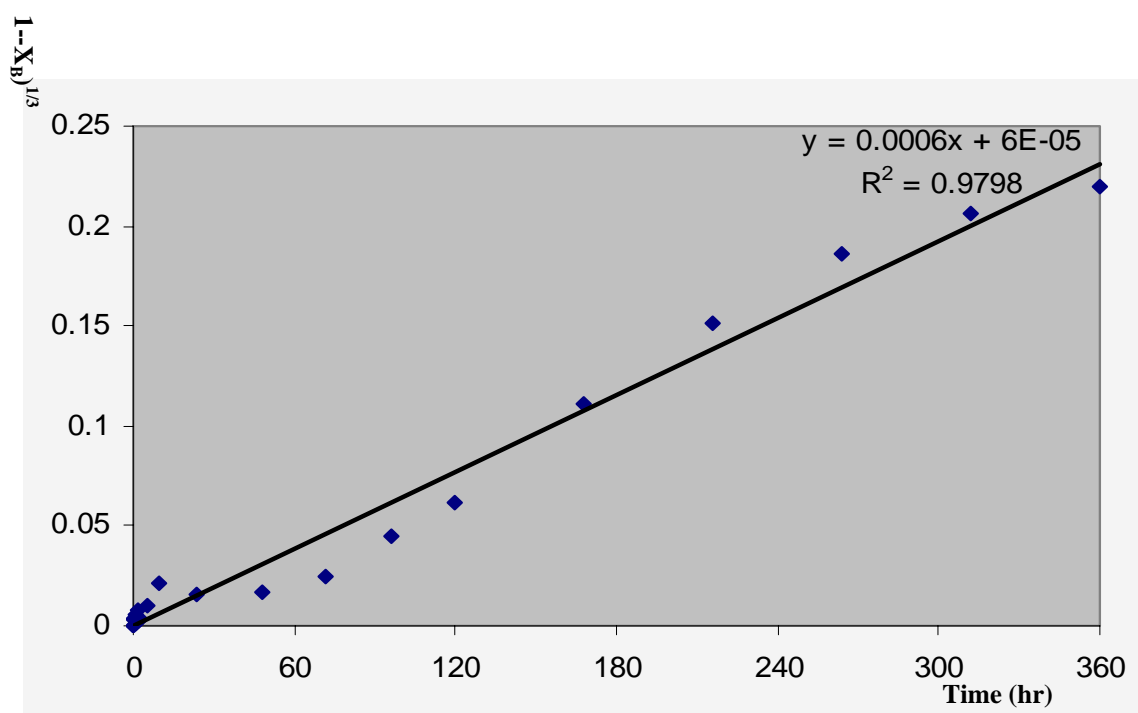


Fig F-16 : Shrinking particle behavior for chemical reaction considered as controlling step ($(1-X_B)^{1/3}$) on a 250 μm pyrite.

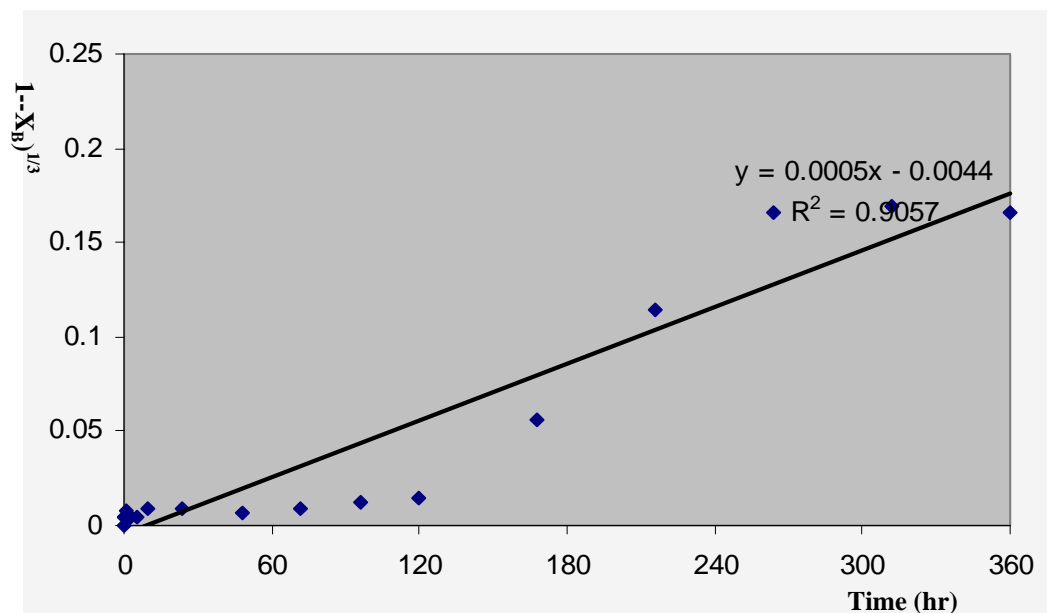


Fig F-17 : Shrinking particle behavior for chemical reaction considered as controlling step ($(1-X_B)^{1/3}$) on a 500 μm pyrite.

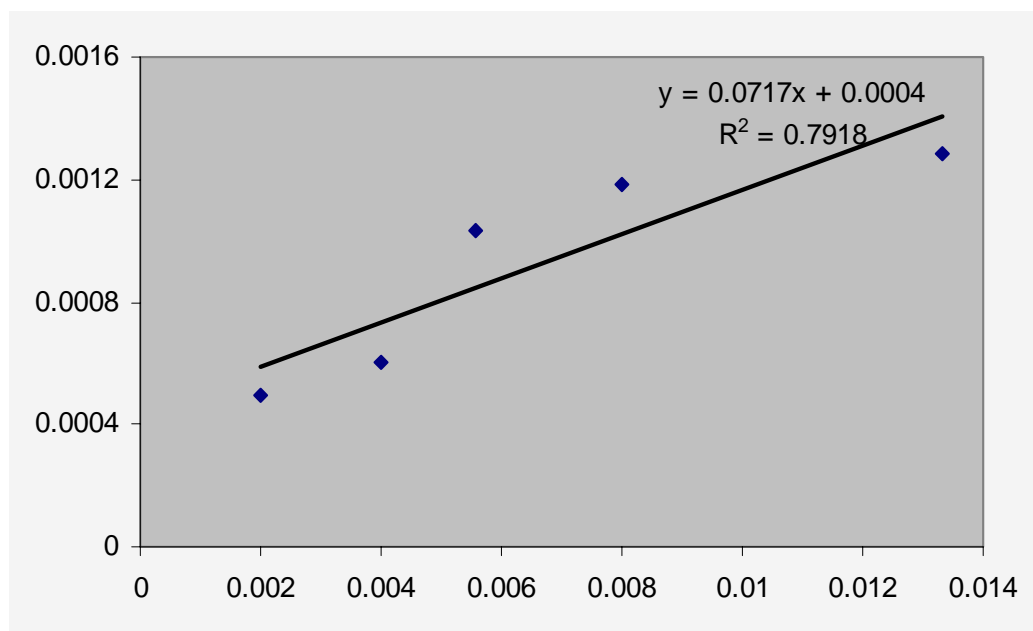


Fig F-18: relation of required leaching time (t_{total}) and initial particle size for Shrinking particle model for chemical reaction considered as controlling step

Shrinking core model

The shrinking core behavior of pyrite with the film diffusion with product layer considered as controlling step.

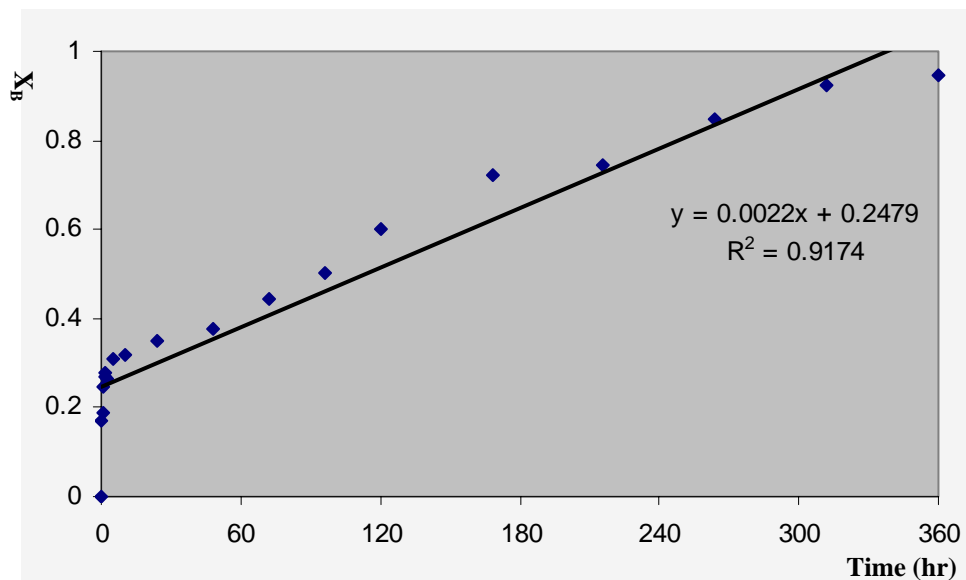


Fig F-19 : Shrinking core behavior for film diffusion considered as controlling step (X_B) on a 250 μm pyrite.

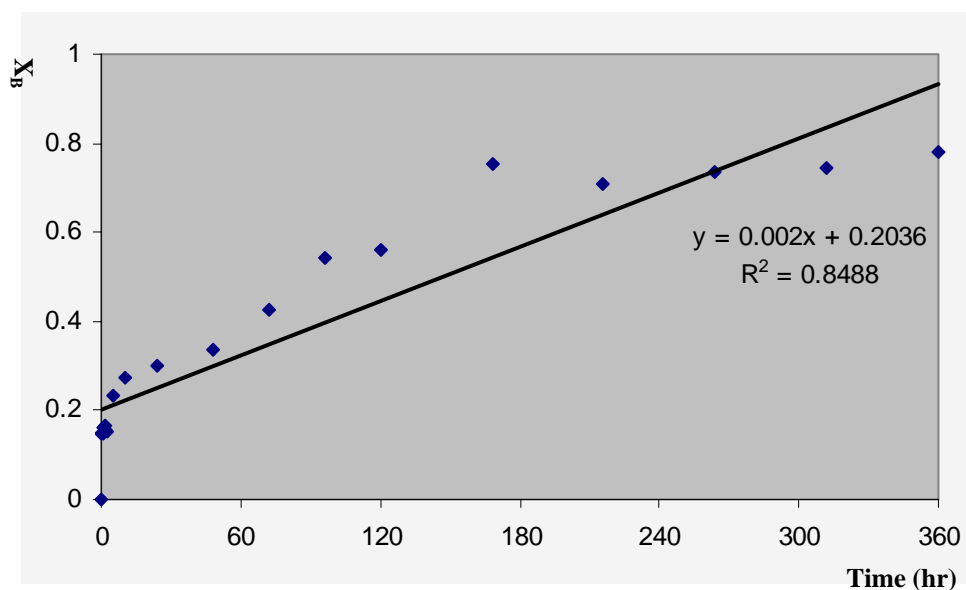


Fig F-20 : Shrinking core behavior for film diffusion considered as controlling step (X_B) on a 250 μm pyrite.

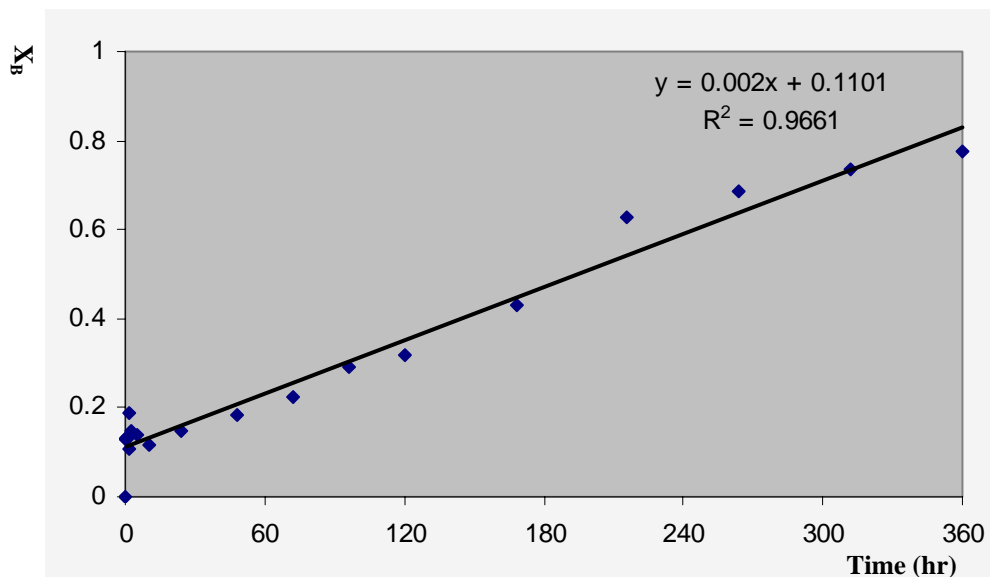


Fig F-21 : Shrinking core behavior for film diffusion considered as controlling step (X_B) on a 250 μm pyrite.

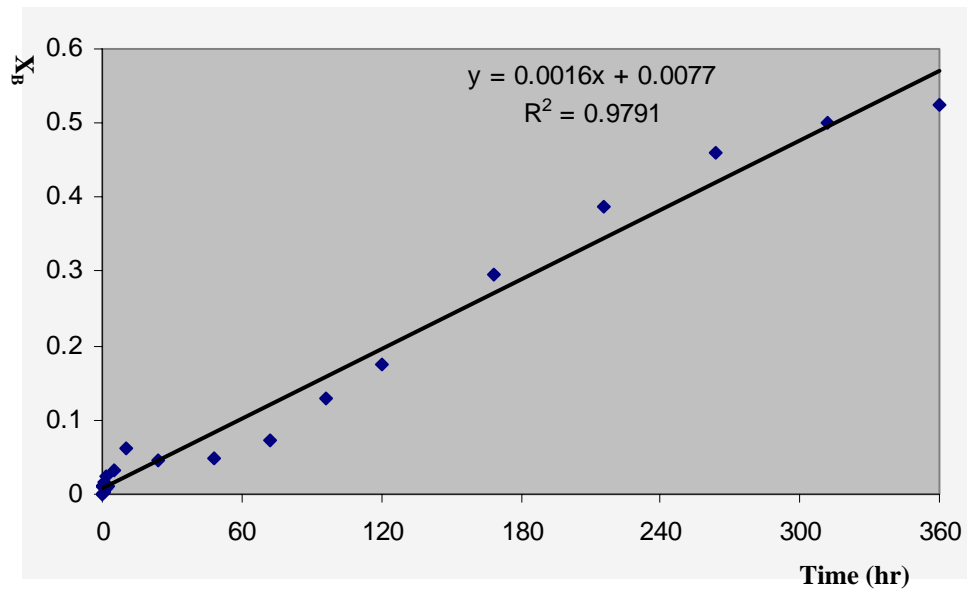


Fig F-22 : Shrinking core behavior for film diffusion considered as controlling step (X_B) on a 250 μm pyrite.

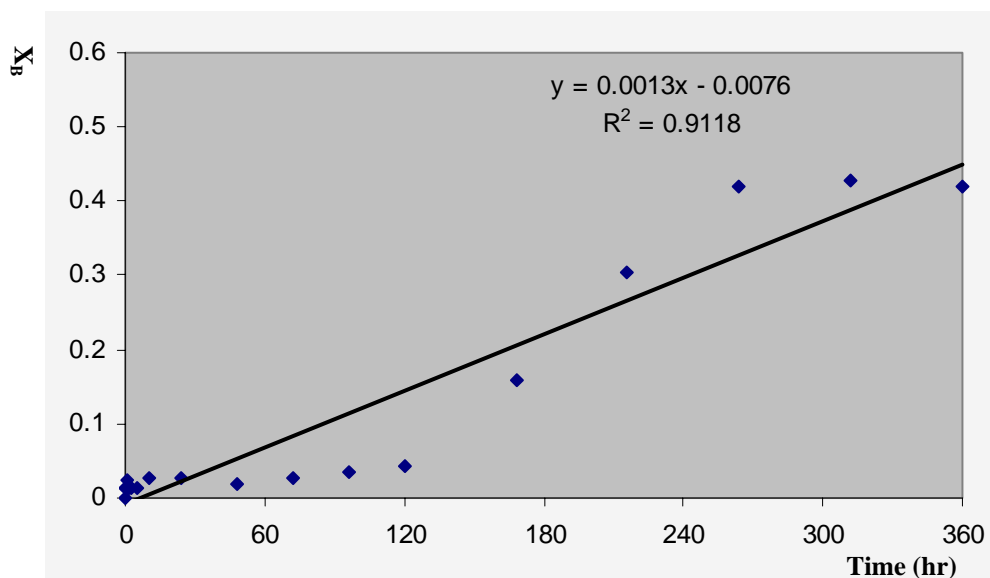


Fig F-23 : Shrinking core behavior for film diffusion considered as controlling step (X_B) on a 250 μm pyrite.

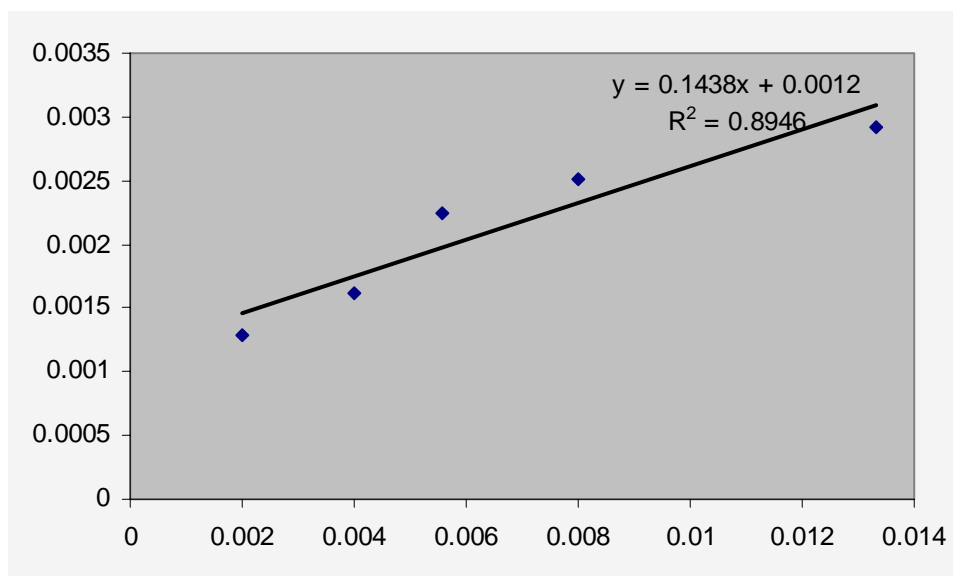


Fig F-24: relation of required leaching time (t_{total}) and initial particle size for shrinking core model for film diffusion considered as controlling step

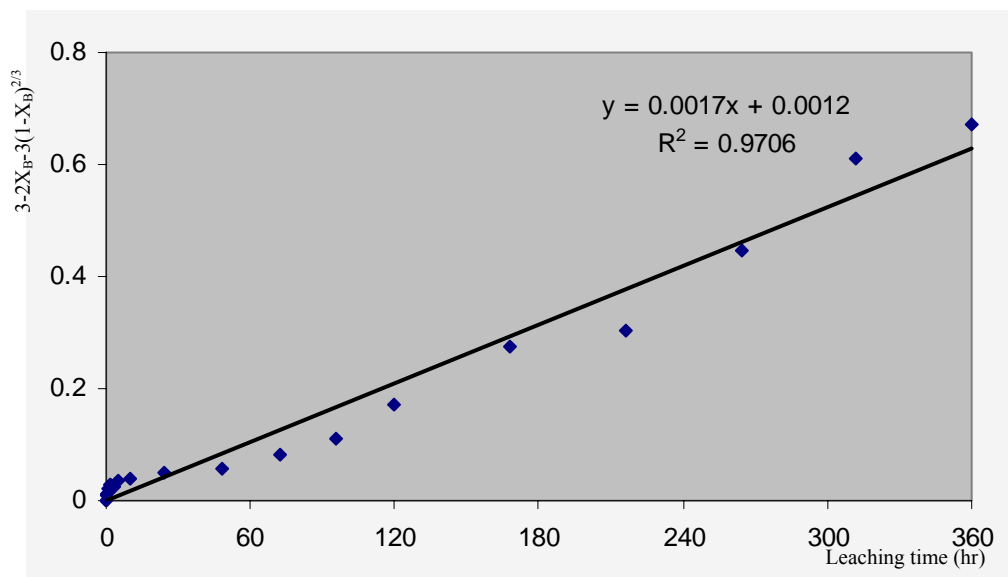


Fig F-25: Behavior of $3-2X_B-3(1-X_B)^{2/3}$ for 75 μm pyrite particle as a function of leaching time (hr)

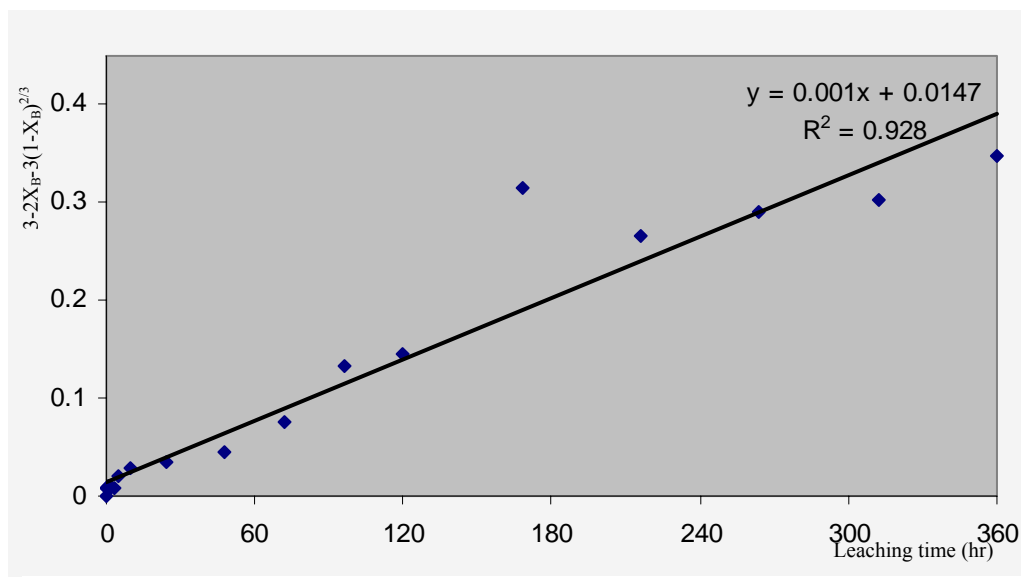


Fig F-26: Behavior of $3-2X_B-3(1-X_B)^{2/3}$ for 125 μm pyrite particle as a function of leaching time (hr)

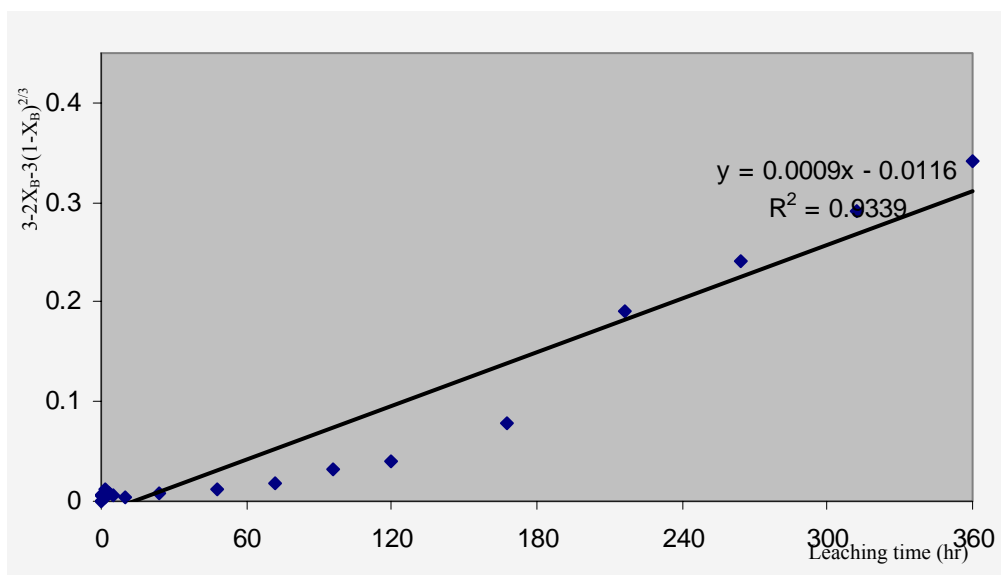


Fig F-27: Behavior of $3-2X_B-3(1-X_B)^{2/3}$ for 180 μm pyrite particle as a function of leaching time (hr)

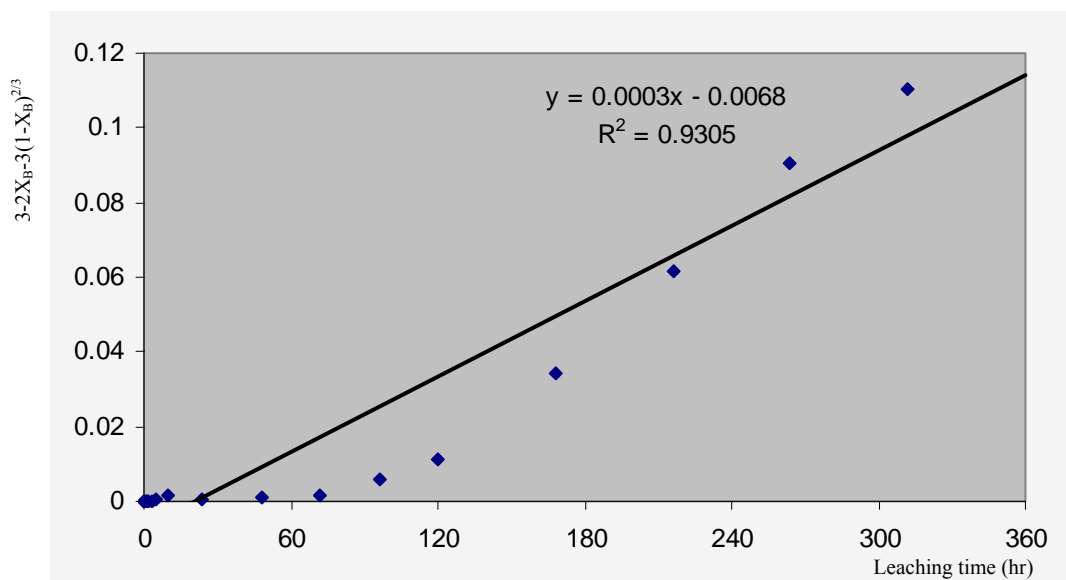


Fig F-28: Behaviour of $3-2X_B-3(1-X_B)^{2/3}$ for 250 μm pyrite particle as a function of leaching time (hr)

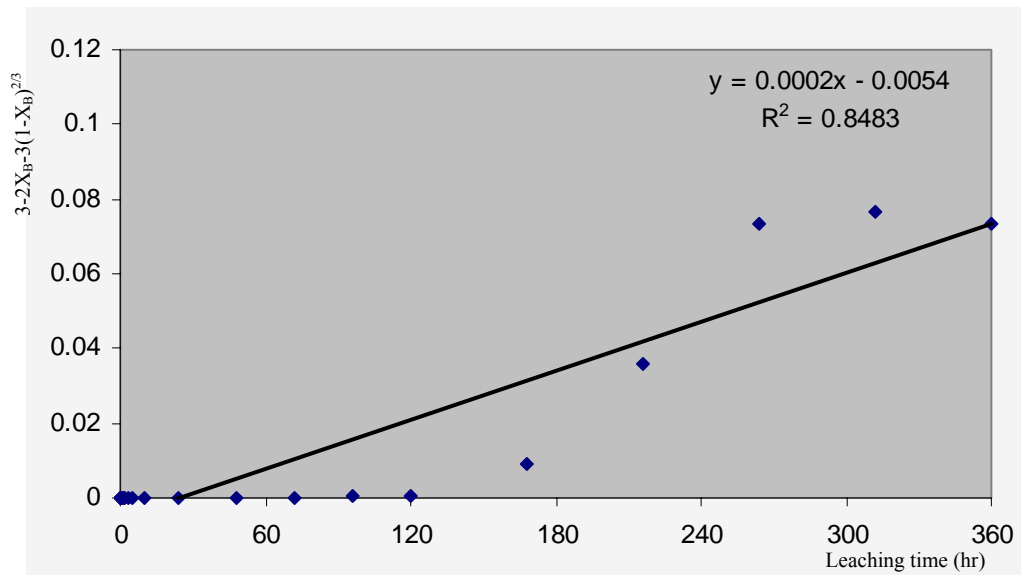


Fig F-29: Behaviour of $3-2X_B-3(1-X_B)^{2/3}$ for 500 μm pyrite particle as a function of leaching time (hr)

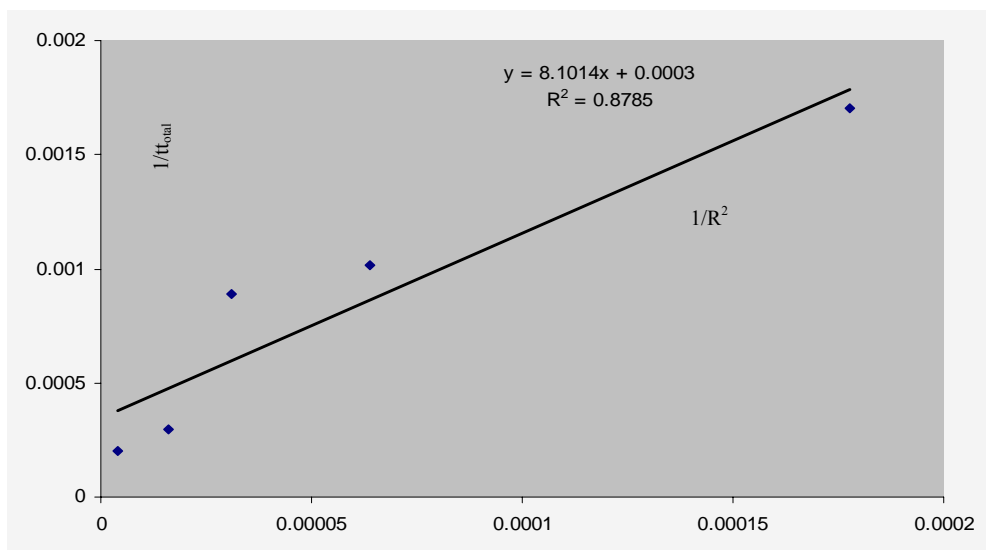


Fig F-30: Relationship of required leaching time $t_{\text{total,hrs}}$ and initial particle size (R) of pyrite

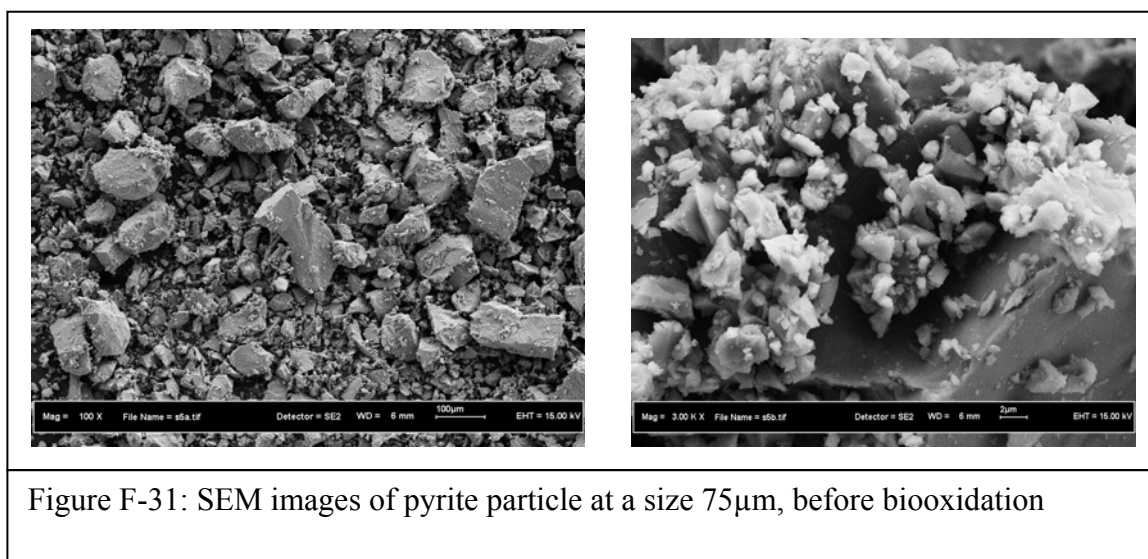


Figure F-31: SEM images of pyrite particle at a size 75µm, before biooxidation

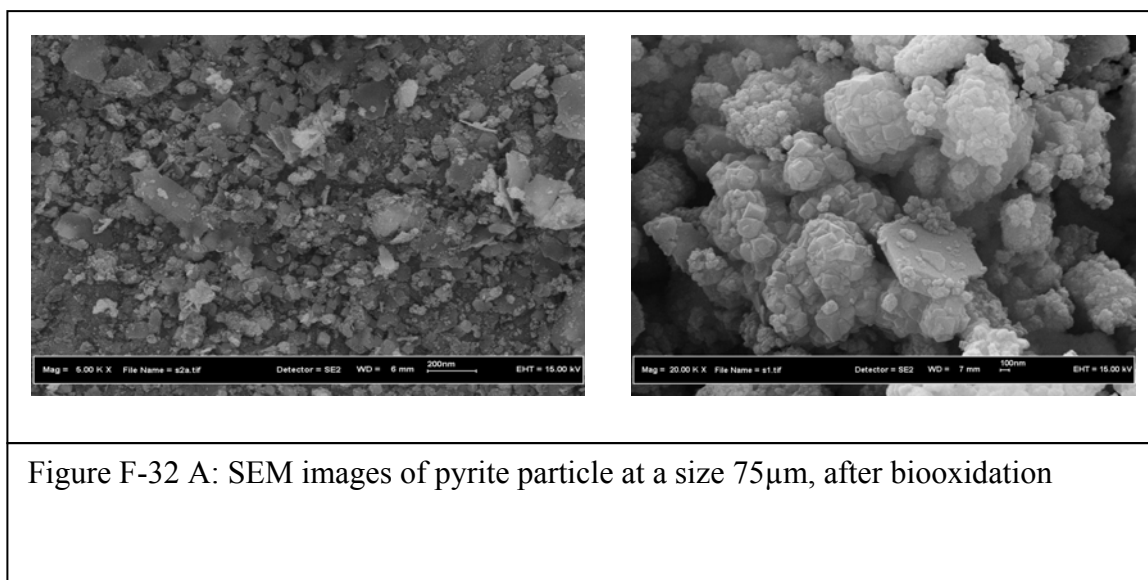


Figure F-32 A: SEM images of pyrite particle at a size 75µm, after biooxidation

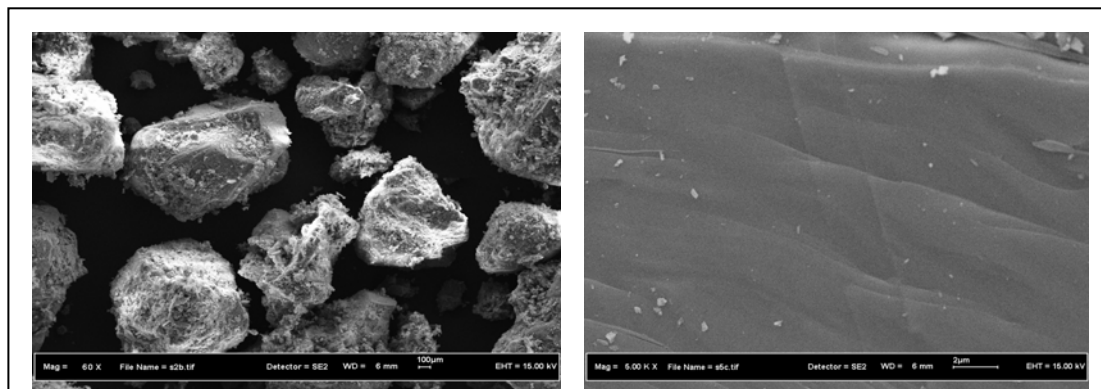


Figure F-33: SEM images of pyrite particle at a size 250µm, before biooxidation

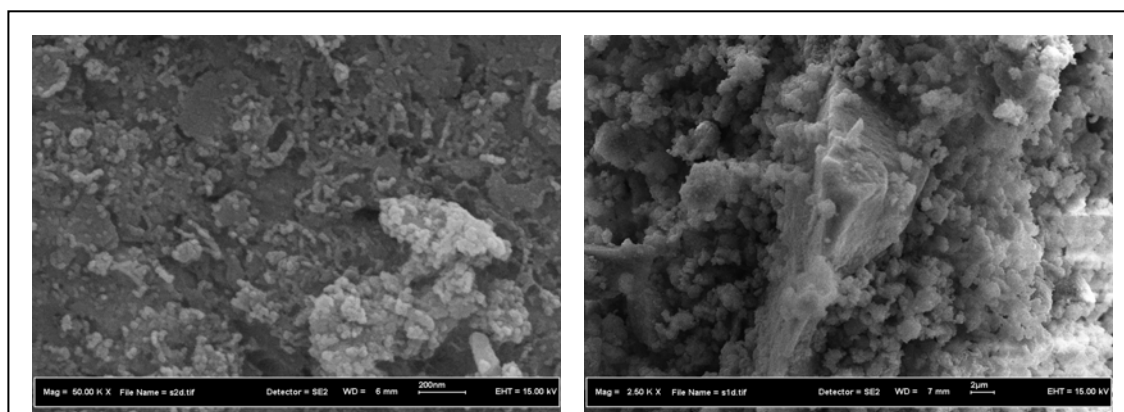


Figure F-34: SEM images of pyrite particle at a size 250µm, after biooxidation

PART 4

IN SITU APPLICATION

TREATMENT AND RECOVERY OF METAL FROM BATTERIES COLLECTED BY DEWAN BANDARAYA KUALA LUMPUR

FOREWORD

Unit Kesihatan Dewan Bandaraya Kuala Lumpur has embarked on a Battery Recycling Campaign which will require the collection and recycling of all used batteries from household and other premises. It aims to prevent spent batteries ending up in incinerators or landfills and at the same time to recover the various metals used in batteries. Due to the metals they contain, batteries pose environmental concerns when they are incinerated or land filled. Since thousands of tones of different metals are used in battery production, their collection and recycling will also contribute substantially to saving natural resources, hence creating a safer and healthier environment.

4.0 Introduction

Recently, a campaign ‘Minggu Alam Sekitar 2002’ has been launched by the Ministry of Science Technology and the Environment in Kuala Lumpur. The Department of Health, Dewan Bandaraya Kuala Lumpur has proactively responded and embarked on batteries recycling program for the elimination of potential health hazard of pollution

due to trace metals in batteries in the environment. The program offers various recycling plans for communities, retailers, businesses, and public agencies.

This paper summarizes the environmental, legislative, technical, and economic factors affecting the use and disposal of batteries. An overview of various battery technologies, their applications and annual production volumes establishes the scope of their impact on the environment. Legislative reaction and technological solutions to the potentially harmful environmental and human health effects resulting from battery disposal are examined. Consideration of reverse logistics issues and future challenges are summarized as part of the analysis.

The document presented here tries to adopt a pragmatic and organized approach toward the environmentally sound management of the recycling of battery wastes. Research work has been carried out by UTM in order to analyze the strengths and weaknesses of leaching technology in the metal recovery processes. In addition, this study provides a critical review of the mechanisms for coordination of program as well as an evaluation of the type of measures being used to integrate environmental considerations into the development process.

4.1 Specific Objectives

- **Protection of improving people and the environment according to the precautionary principle**

- **Optimum use of resources**

(Conservation of non-renewable resources and sustainable use of renewable; adoption of reuse and recycle as means to protect non-renewable natural resources)

- **Solving of disposal problems**

(Disposal without leaving "time bombs" for future generations and without shifting wastes to countries with underdeveloped environmental standards and monitoring systems)

- **Economically acceptable waste management**

(Inter alia, disclosure of the true costs and a favorable cost-benefit ratio of measures taken, existence of incentives for environmentally friendly action)

- **Socially acceptable waste management**

(Inter alia, avoidance of severe exceptional burdens on the population at particular locations, reasonable satisfaction of human needs such as mobility and availability of choice when purchasing products).

4.2 Collection

The volume of batteries made by manufacturers in Malaysia has risen tremendously over the last five years. Locally some 1000 tons of batteries are purchased yearly, in Kuala Lumpur. Approximately 0.5 metric tones of spent batteries are collected since 2003, through about 20 collection points and also upon request spent batteries are fetched from private sector on free of charge basis. The returning rate of spent batteries today is less then 0.1%, much too low a figure. It is astonishing as: such great effort has been done to collect harmless wastes for instance glass, plastic bottles, paper and aluminum cans. Why are batteries, which, after all, are a concentrate of heavy metals and a source of raw material, disposed of in the normal municipal waste? It I high time that we find a solution for the safe disposal of spent batteries. In the meantime spent batteries are disposed off in landfill, which lead to hazardous leachate, not environmental friendly. Certain landfill had to be closed and is now a contaminated site which requires continuous monitoring and remediation.

So far, there has been no recycling process initiated for spent dry batteries in Malaysia apart from the work conducted by Unit Kesihatan, DBKL for the collection of spent batteries during 2002. For this project, some clinics and schools were installed with waste battery collection units to encourage. However, due to negligence, the collection points are perceived as litter cans by people and filled with rubbish.

Specific legislation, based on the polluter–payer principle, has been established in some countries. This means that the manufacturer or the importer of the batteries is also responsible for its destination, after it is used by the consumer. Malaysian legislation does not oblige for the recycling of dry and alkaline batteries, since the concentration of heavy metals is within established limits. Recycling effort has been introduced for example: aluminum cans, old newspaper and car batteries.

When discussing battery recycling, collection is a great problem, since it depends not only on public awareness, but commitment of industries, distributors and the government. For this, DBKL should be commended for taking the first step towards battery recycling and recovery.

The steps that should be taken for recycling of the waste batteries can be summarized as follows:

1. Public awareness should be promoted, with emphasis on effects of batteries on the environment. For example:
 - The waste batteries have hazardous effects on human health and environment.
 - The leakage from the waste batteries damages devices.
 - The recycling of waste batteries contributes to the national economy.
2. All nationwide municipalities should ensure that consumers dispose of their spent batteries safely into the collection containers in their neighborhood.

3. These spent batteries should be collected on regular basis and forwarded to the main collection units.
4. The collected waste batteries should be classified based on their contents and the recovery plant limitation.
5. Valuable metals contained in the waste batteries should be recovered by hydrometallurgical and/or pyrometallurgical methods.

Another measure taken to achieve high collection rates is to install an appropriate and efficient battery collection infrastructure. This infrastructure must be well planned since it involves several different sectors of the society such as scrap dealers, battery dealers, and consumers into an organized scheme which provides a continuous flow of the recycling process. Perhaps the greatest challenge is to encourage end-users to participate. For small batteries, consumers are not willing to return their batteries to the outlet where they have bought them.

1. Some guidelines for batteries container and collection centers:

- Container must be acid-resistant.
- Container should look attractive and contains the batteries recycling logo.
- Container should not be too expensive and bulky.
- Collection point must be fairly distributed and easy to be reached by consumers i.e: in their neighborhood, retailer, garden and pump station.
- The storage place must be sheltered from rain, other water sources and heat sources.
- The storage place must have a ground cover, preferably plastic or any other acid-resistant material that may retain any leakage and direct it to a collecting container from where it can be removed afterwards.
- The storage place must have an exhaust system, in order to avoid hazardous gas accumulation.

- The storage place must have a restricted access and be identified as a hazardous material storing place.
- Collection points must not store large amounts of used batteries and must not be considered as a permanent storage place. Batteries must be cleared frequently.

4.2.1 Suggestion batteries container

The follows is an example of box for batteries recycling (Europe patent FR2766799)

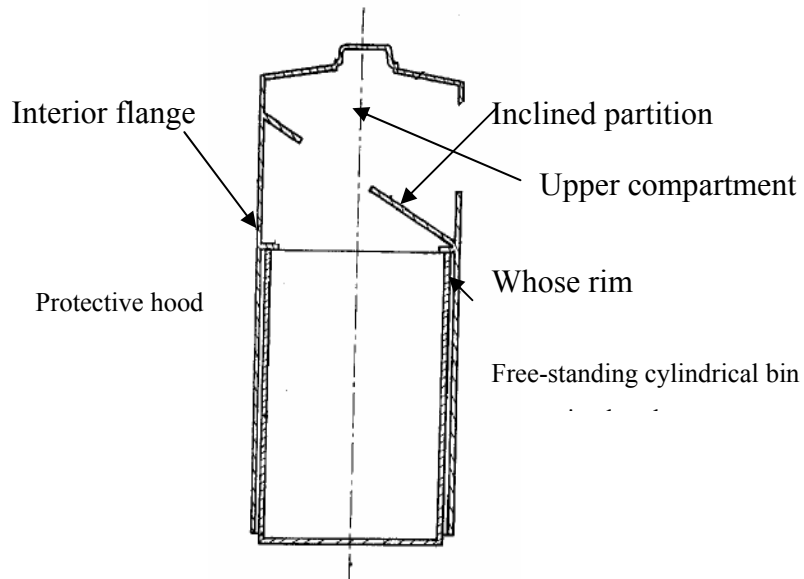


Fig 4.1: Box for batteries recycling

A protective hood has a long skirt close-fitting over the free-standing cylindrical bin, whose rim supports its interior flange leaving the skirt just above ground level. An inclined partition, dividing the hood interior, has an opening above the centre line. Items for collection are passed through a side opening and dropped through the partition. Rubbish, rain, etc. are trapped in the upper compartment. Periodically, the hood is lifted, the bin with contents removed to a recycling centre and the hood slipped down again over a replacement bin. Bin and hood may be of heavy duty plastic.

In Kuala Lumpur, a collecting system has been started by DBKL and it is still difficult to assess its efficiency. There are several established collection methods, mainly implemented in some countries, such as the US, some European countries and Japan.

1) Mail-back

Mail-back procedures are used by product manufacturers to transport spent batteries back to consolidation points. This approach is typically used for custom battery packs which must be ordered from the product manufacturer or custom battery pack manufacturer. In this scheme, the end user orders the replacement battery via mail order and returns the spent battery in the same or special return packaging to a designated consolidation point. Typically, shipping cost and recycling cost are borne by the seller of the replacement battery.

2) Retail collection boxes

Retail collection boxes are most effective for batteries which can be purchased over the counter in retail outlets. In this arrangement, the buyer can conveniently deposit the spent battery in a designated receptacle in the same store or outlet where the new replacement battery is purchased. Some outlets offer the depository service even if the type of battery is not sold at their establishment. Many pharmacies in the USA, for example, voluntarily provide take back boxes for mercuric oxide button cells even though such batteries can no longer be sold. There is no cost to the consumer, the pharmacy contributes shelf space, and pays a fee to local recycling services who operate “milk runs” to collect and consolidate the batteries. Ultimately, mercuric oxide batteries are sent to an authorized mercury reclamation facility.

3) 3rd Party waste hauler

Permitted hazardous waste haulers are another choice to make. The cost of this service is usually high and not a desirable choice for economical handling of waste batteries. This option is the best choice for damaged or leaking batteries.

4) Reverse logistics operations for products

Manufacturers of larger, commercial or industrial type electronic products frequently operate a reverse logistics operation for high value spare parts which can be repaired and reused as spare replacement parts. Take back service for products offers another advantage when the product itself has reached end of life. In this way, the concern about keeping batteries out of municipal waste streams is addressed as part of an ongoing remanufacturing process.

4.2.2 Financial

Dry battery recycling program is much more complex than expected. The technologies used are quite sophisticated. Due to the highly developed technology, small dimensions of treatment plant, storage, campaign and publicity, battery recycling is not a profitable activity. Therefore, a funding scheme with contribute from involved parties, namely producers, importers and retailers should be set up to address the batteries recycling program.

The cost efficiency of recycling spent batteries is perhaps the greatest challenge to managing the environmental burden of batteries. Technological, economic and legislative factors all interact to complicate recycling. Two of the biggest material obstacles to using existing metal reclamation processes are mercury and plastic. Many ferrous and non-ferrous metal recycling processes cannot deal with the control of mercury vapors, electrolyte materials and plastics found in batteries.

4.3 Metal determination

4.3.1 Physical condition of batteries

From 158 kg of batteries received from DBKL, the batteries were mixed well and divided into 4 portions. The batteries were then sorted by their physical condition i.e: size, origin and type. (Fig. 4.2)

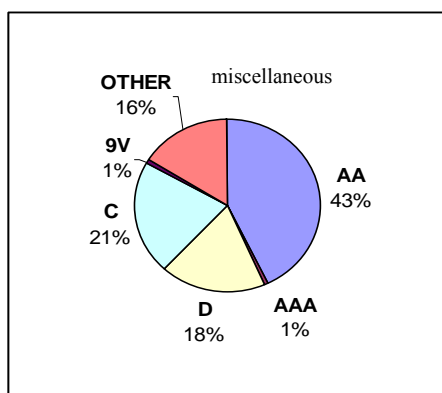


Figure 4.2: Portion of batteries segregation by size

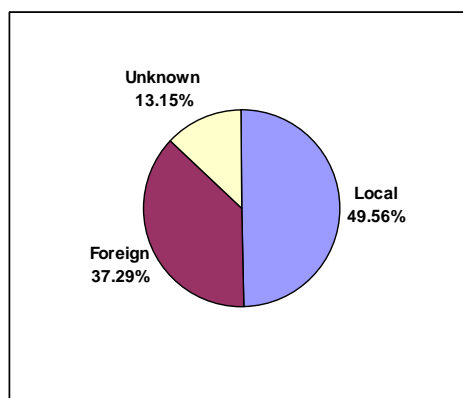


Figure 4.3: Portion of batteries segregation by origin of producer

The largest portion of collected batteries were those of AA size (27.76 kg), followed by D (11.96kg) and C (13.76kg). Most portable devices require AA, C or D batteries, which accounts for the largest percentage of batteries used for general household purposes. i.e: AA (Clock, toys and walkman), D (Radio and torchlight) and C (torchlight). Button cell, mobile phone batteries and 6V type batteries (16.14%) constitute those group under miscellaneous

It is interesting to note that 37.29% of the total batteries collected was imported (mostly from China), compared to 49.56% which was produced locally. Large portion of imported batteries found inside our waste stream is due to its cheap prices, short life time and is usually sold together with equipment, especially toys. The cheap imported type batteries has a high tendency to leak and might have a high Hg and Pb content

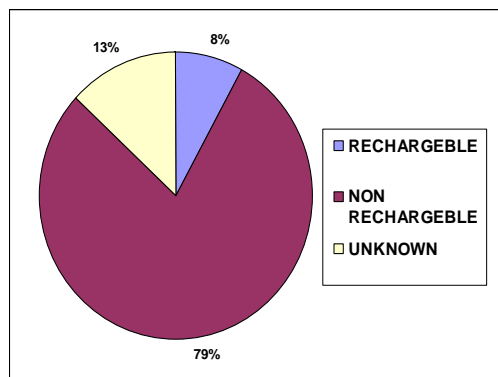


Figure 4.4: Portion of batteries, segregation by recharge ability

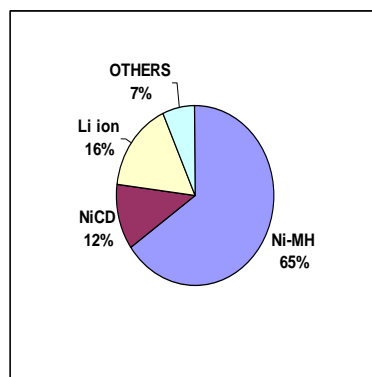


Figure 4.5: Portion of rechargeable batteries

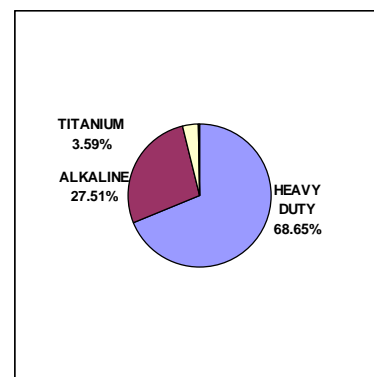


Figure 4.6: Portion of non-rechargeable batteries

From the batteries collected, 79% was the non rechargeable type, 13% rechargeable and 8% of unknown type. More non rechargeable batteries have been collected compared to the rechargeable batteries. Low prices and short lifetime contribute to the large consumption of non rechargeable batteries.

The metal composition differs considerably depending on the battery type, thus some batteries are potentially more hazardous than others. Changing the trend of batteries consumption will affect the efficiency of metal recovery. As an example, for the Ni–Cd batteries, cadmium, mercury and lead are very toxic metals commonly found in these batteries.

4.3.2 Metal content

Table 4.1: Metal content of non rechargeable dry cell (Zn-C and Alkaline batteries).

Element	Zn-C (entire batteries)	Zn-C (Dry powder)	Alkaline (entire batteries)	Alkaline (dry powder)
Mn (%)	27.065	33.023	29.025	38.596
Zn (%)	5.023	7.0568	12.4862	19.85634
Fe (%)	2.184	0.021245	1.9658	0.001453
As (ppm)	3.425	-	2.159	-
Cd (ppm)	12.47	-	4.253	-
Co (ppm)	26.14	-	84.25	-
Cr (ppm)	23.45	-	29.48	-
Cu (ppm)	5.124	-	2.814	-
Hg (ppm)	-	0.002356	-	0.04598
Ni (ppm)	52.34	69.85	85.23	102.35
Pb (ppm)	23.92	1.5625	49.87	65.68

The metal composition of zinc–carbon and alkaline batteries is quite similar. These batteries contain basically manganese, zinc and iron as main metallic species. The outer layer of batteries comprises mainly of iron (Fe). Steel casing can be separated easily using a magnetic separator. Other heavy metals Cu, Ni, Cr, As, Cd, Co, Hg and Pb are found in trace amounts. Low levels of mercury have been detected at 0.002 ppm and 0.04ppm from the Zn-C and alkaline batteries respectively, even though have been labeled as no mercury added.

After the dismantling of the batteries, the black powder was analyzed and found to contain the following metals (Table 4.2).

Table 4.2: Zn and Mn content of Zn-C and alkaline batteries dust.

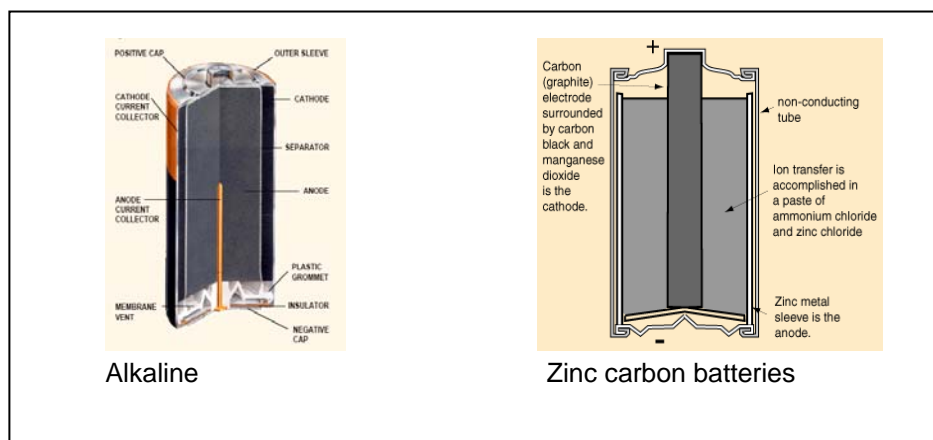
Element	Zn-C	Alkaline
Mn (%)	33.02	38.60
Zn (%)	7.06	19.86

Thus recovery of these metals can be attempted due to their relatively large amounts in this kind of waste. Recycling rates for metals are growing in many developed

countries. In the 1980s, the lead, zinc and tin industries were in a crisis caused by stagnation of the market, and secondary raw materials from lead batteries, zinc plant leach operations and steel plant dusts. The same route can treat residues from zinc–carbon batteries as well as alkaline, because of the similarity in metal composition.

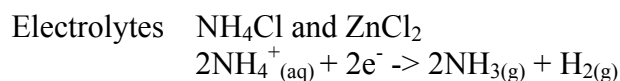
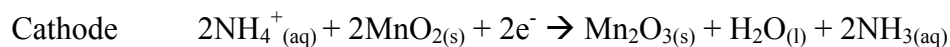
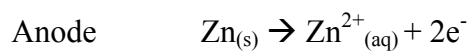
Moisture content of the batteries was found at 4.25% and 3.85% for Zn-C and alkaline batteries respectively. Water acted as batteries electrolyte, consisting of potassium hydroxide for alkaline batteries and ammonium chloride for Zn-C batteries. Instead of metal, the batteries also contain non soluble plastics, paper, carbon and ash. Figure 4.7 shows a cross section diagram of the alkaline and zinc carbon batteries.

Figure 4.7: Cross section of alkaline and zinc carbon batteries

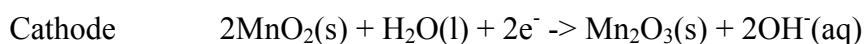


The chemical reaction involved in zinc-carbon and alkaline-manganese batteries is as follows:

Zinc-carbon



Alkaline-manganese



Electrolytes KOH

Alkaline and carbon-zinc "heavy duty" dry cell batteries are the normal "disposable" batteries. They cannot be recharged or recycled. In the past, these contained mercury and were not allowed in household trash. In recent years, however, virtually all of the common disposable batteries have been removed of mercury and government disposal guidelines state that "appropriate disposal" includes "landfill." Some communities collect batteries as part of a recycling program, but the batteries generally end up in a hazardous waste landfill and not recycled.

Both batteries have presented a serious challenge to recycling efforts for several reasons:

Recoverable component materials are of relatively low value and concentration in these battery cells. The average metal composition is approximately 3% steel (case), 10% zinc, carbon, 35% manganese and the balance consists of copper, paper, plastic and electrolyte. The highest valued component of the major components is zinc. It is generally accepted that the zinc portion of any material or product should be greater than 50%, to justify an economically feasible recovery (for the value of the zinc alone). Therefore, previous attempts to recover the zinc from alkaline batteries through recycling were quite expensive, because of the lower zinc content.

Individual component materials are extremely difficult to separate from one another; magnetic separation will only separate the outside steel case as the other components are not magnetic.

The small quantity of electrolyte found in these so-called "dry cell" batteries is highly corrosive and emits ammonia when crushed or pulverized.

The mercury content of batteries collected today is very high; separating it out is not economically viable. Some will probably be stored at hazardous waste sites

Zinc-carbon/air and alkaline-manganese batteries can be reprocessed using a number of different methods, which include smelting and other thermal-metallurgical processes to recover the metal content (particularly zinc).

Table 4.3: Metal content of rechargeable dry cell

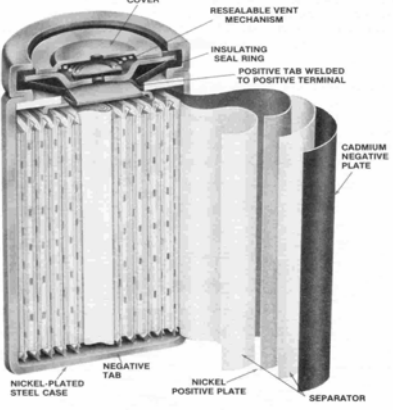
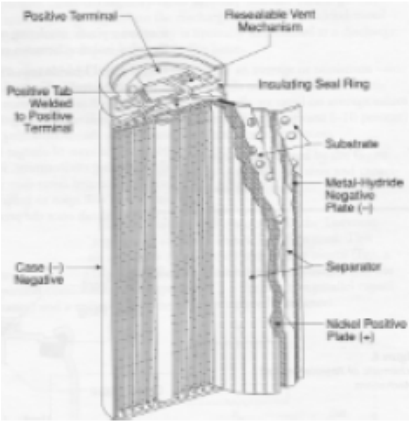
Element	Ni Cd	Ni MH	Li ion
As (ppm)	1.025	1.5234	3.1402
Cd (%)	17.953	-	-
Co (%)	0.617	3.569	15.756
Cr (ppm)	22.018	21.052	37.156
Cu (ppm)	64.248	59.482	6897.42
Hg (ppm)	0.2631	0.01186	0.00952
Mn (%)	0.086	1.482	12.729
Ni (%)	19.127	35.876	9.256
Pb (ppm)	263.5	1.048	0.9235
Fe (%)	29.354	22.485	6.152
Zn (%)	0.04356	0.5725	-
Al (%)	0.053	0.6235	5.689
Li (%)	-	-	4.315
La	-	2.458	-
V	-	-	13.248

Compared to disposable batteries, the metal content of rechargeable batteries is more varied. Metal content of Ni Cd, NiMH and Li ion batteries is slightly higher at 67.3%, 67.1% and 74.0% respectively, compared to 43.5 % for alkaline batteries. Nickel metal hydride (NiMH) batteries represent one of the fastest growing sectors in the battery market. Amongst the many uses include cordless power tools, personal stereos, portable telephones, lap-top computers, shavers, motorised toys with a life of 4-5 years. NiMH batteries are a more environmental friendly alternative to NiCd and tend to have a longer life. Energy storage capacity of Lithium ion (Li-Ion) batteries are reported to be greater than NiCd and NiMH batteries.

The usages of rechargeable batteries offer an advantage i.e. reduction in volume of batteries used; however more metals are used in these batteries, which might pose as carcinogen. Nickel-Cadmium (Ni-Cads) rechargeable batteries contain 18.0% Cd and 263.5ppm Pb. These metals which causes damage to blood and reproductive system, can be toxic to aquatic invertebrates and can bio-accumulate in fish, which makes them unfit for human consumption. These batteries pose no hazard when in use, since the cadmium is in a stable form and contained in the battery, but they can break apart in landfills, allowing the toxic metals to leach into the ground and water supplies. Several countries now prohibit consumers from dumping NiCad batteries as household trash. The warning and recycling logo might prove useful in order to convey this message.

There are various types of lithium batteries in the market today. These batteries are considered the superior performing batteries. They were originally most often used for primary power in such critical devices such as heart pacemakers. Today, their use is rapidly growing and they are commonly used in devices such as cameras because of their high performance, longer life and reliability. The use of lithium batteries in manufactured components is expected to increase drastically, which is a cause for worry due to high content of Li (4.13%). Lithium is reactive and may ignite upon shorting, opening or crushing. In fact, as each cell is crushed in a deactivating process, the cell explodes. The component materials may then be discharged into a solution of potassium hydroxide, where lithium is reduced to lithium salts. Figure 4.8 shows a cross section diagram of the of Ni-Cd and NiMH batteries

Figure 4.8: Cross section of Ni-Cd and NiMH batteries

	
<p>Cross section diagram of Ni-Cd batteries</p>	<p>Cross section diagram of Ni-MH batteries</p>
<p>Positive Electrode: Active material = Nickel oxyhydroxide (NiOOH)</p>	<p>Positive Electrode: Active material = Nickel oxyhydroxide (NiOOH)</p>
<p>Negative Electrode: Active material = Cadmium</p>	<p>Negative Electrode: Active material = Metal hydride</p> <p>Ni-MH technology uses AB₅ alloy composition (e.g. LaNi₅).</p> <p>AB₅ composition offers better corrosion resistance for longer cycle life and better recharging following storage.</p>
<p>Electrolyte Primary electrolyte: dilute solution potassium hydroxide solution with minor constituents as enhancer</p>	<p>Electrolyte Primary electrolyte: aqueous potassium hydroxide solution</p>
<p>Cell Reactions During Discharge: $\text{NiOOH} + \text{H}_2\text{O} + \text{e}^- \rightarrow \text{Ni}(\text{OH})_2 + \text{OH}^-$ and $\text{Cd} + 2\text{OH}^- \rightarrow \text{Cd}(\text{OH})_2 + \text{e}^-$ Overall Reaction: $\text{Cd} + 2\text{NiOOH} + 2\text{H}_2\text{O} \rightarrow \text{Cd}(\text{OH})_2 + 2\text{Ni}(\text{OH})_2$ The process is reversed during charge.</p>	<p>Cell Reactions During Discharge: $\text{NiOOH} + \text{H}_2\text{O} + \text{e}^- \rightarrow \text{Ni}(\text{OH})_2 + \text{OH}^-$ and $\text{MH} + \text{OH}^- \rightarrow \text{M} + \text{H}_2\text{O} + \text{e}^-$ Overall Reaction: $\text{MH} + \text{NiOOH} \rightarrow \text{M} + \text{Ni}(\text{OH})_2$ The process is reversed during charge.</p>

4.3.3 Metal content of batteries collected by DBKL

Table 4.4: Metal content of batteries collected by DBKL (18.36 kg immersed in 50L aqua regia)

Element	Content
As (ppm)	5.0236
Cd (%)	0.3835
Co (%)	2.1356
Cr (ppm)	26.139
Cu (ppm)	242.47
Hg (ppm)	7.0235
Mn (%)	22.842
Ni (%)	5.1454
Pb (ppm)	31.534
Fe (%)	5.2996
Zn (%)	6.0357
Al (%)	0.2777
Li	0.1517
La	0.3020
V	0.4658

The batteries were found to contain 22.84% Mn, 6.04% Zn and 5.3% Fe 5.15 % Ni and 0.38% Al. The quantity of these metals are worthy for recycling.

It is important to note that the concentration of toxic metals i.e: Hg, Pb and As in the collected batteries is much higher compared to the batteries produce locally. A large proportion of these probably come from imported batteries and batteries collected before 1980. High concentration of toxic metals becomes a disturbing problem in recycling process. For example, in the recycling of metals zinc-carbon and alkali manganese batteries must contain less than 5 ppm mercury. In the EU, a new batteries guideline intended to reduce the amount of mercury in domestic batteries from the currently permitted 250 ppm to almost zero has been formulated. With this guideline it is hoped that mercury will not be present in collected batteries from 2003 onwards, and recycling processes will become environmentally and economically viable.

During the last decade, the producers of batteries have been engaged in trying to find substitutes for toxic substances still used in batteries, to match environmental requirements; however, the basic systems of the batteries and its composition(steel, plastic, zinc, manganese dioxide, steel casings, paper, carbon, and brass) still remains the same

4.4 Laboratory test works

4.4.1 Column leaching test work

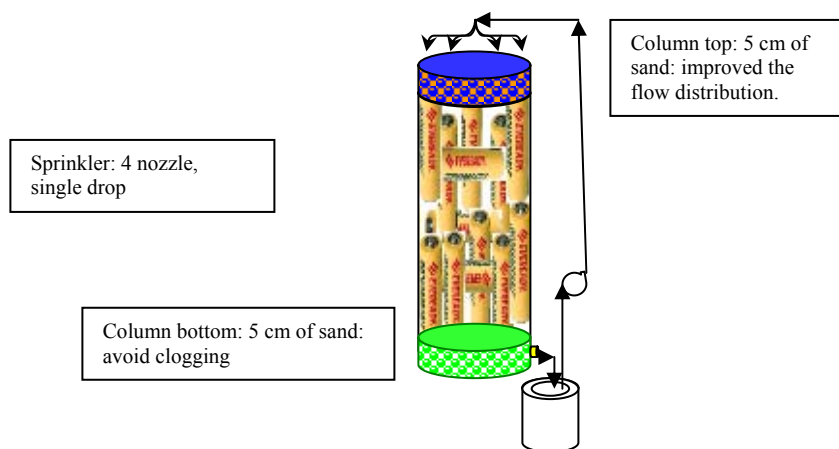


Table 4.5: Column condition

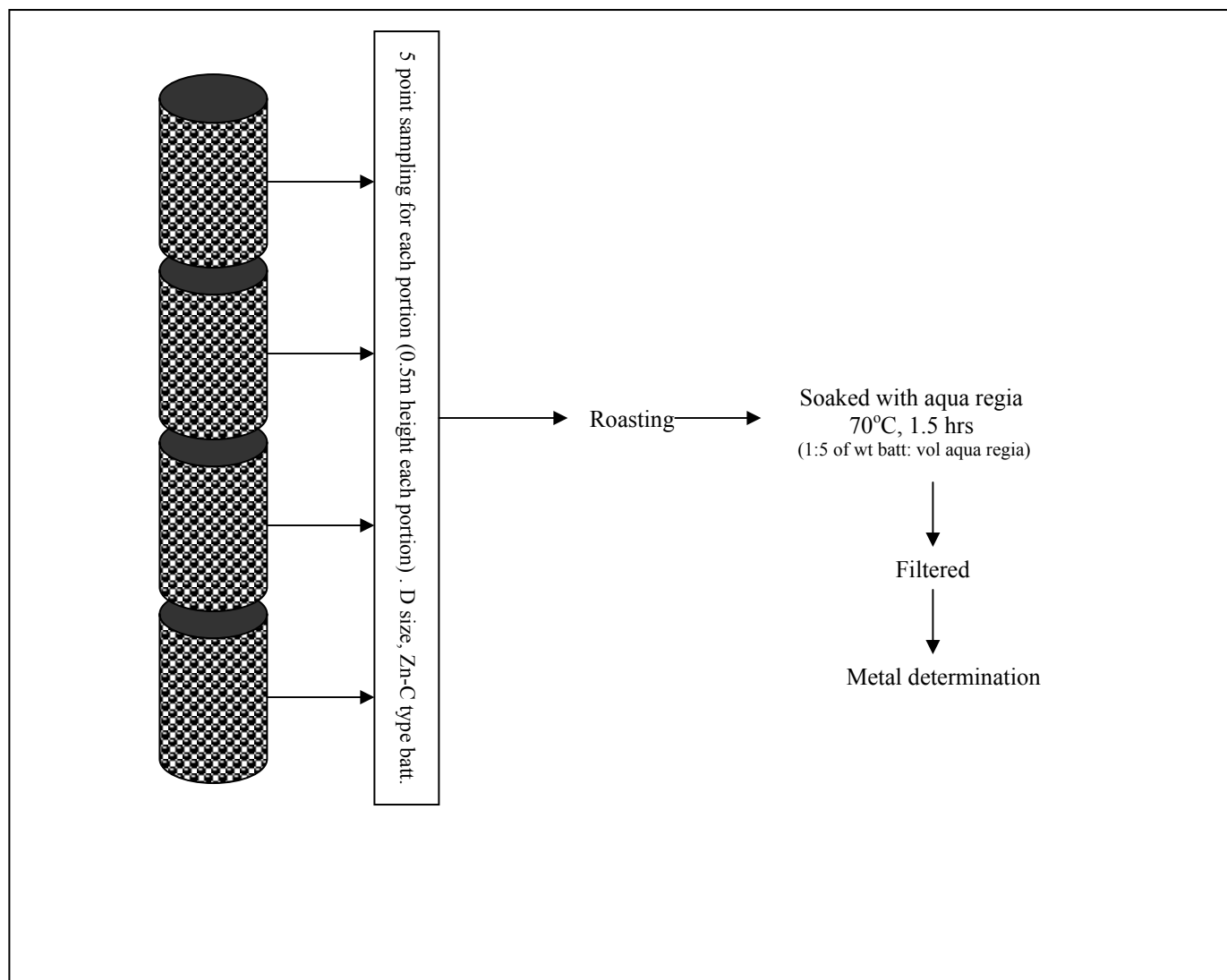
	1	2	3	4
Duration (month)	1 st -2 nd	2 nd -5 th	6 th -8 th	9 th -12 th
volume	60L	60L	200L	200L
content	50kg of mix batt. + 45kg of D size Zn-carbon type batteries.	50kg of mix batt. + 45kg of D size Zn-carbon type batteries.	50kg of mix batt. + 45kg (AA) +150kg (D) size Zn-carbon type batteries.	50kg of mix batt. + 90kg (AA) +190kg (D) size Zn-carbon type batteries.
	Column bottom: 5 cm of sand Column top: 5 cm of sand	Column bottom: 5 cm of sand Column top: 5 cm of sand 20% sand mix with batteries	Column bottom: 5 cm of sand Column top: 5 cm of sand 20% sand mix with batteries	Column bottom: 5 cm of sand Column top: 5 cm of sand 50% sand mix with batteries
Leachate solution	5L. sprayed at 17ml/mnt, solution top up daily, single drop	5L. sprayed at 17ml/mnt, solution top up daily, 4 nozzle Air supply from the bottom of column	10L. sprayed at 25ml/mnt, solution top up daily, 4 nozzle	10L. sprayed at 25ml/mnt, solution top up daily, 4 nozzle



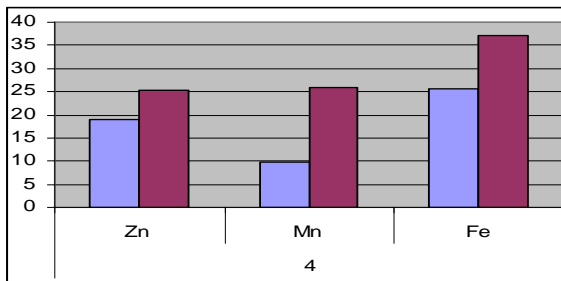
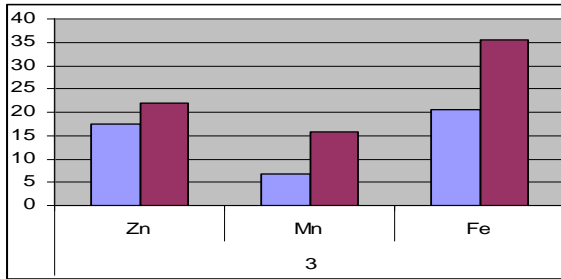
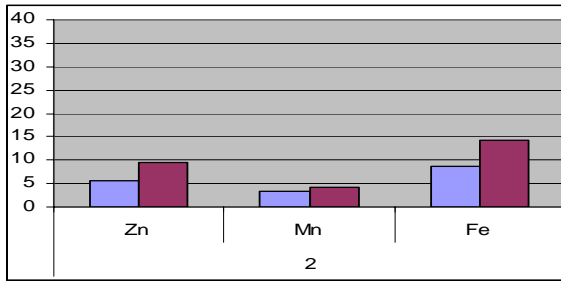
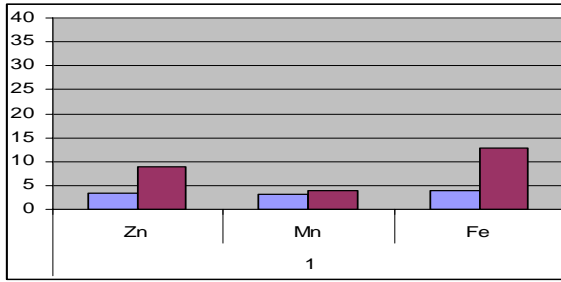
Table 4.6: Leaching condition

	Column A	Column B
1 1 st -2 nd month	<p>Part 1: Chemical leaching</p> <p>Solution used: Portion 1A . Hydrochloric acid (1M)</p> <p>Duration 10 days.</p> <p>Portion 1B . Ferric chloride added to achieve 0.5M hydrochloric acid (1M) test</p> <p>Duration 50 days</p>	<p>Part 1: Chemical leaching</p> <p>Solution used: Portion 1A . Sulfuric acid (1M)</p> <p>Duration 10 days.</p> <p>Portion 1B . Ferric sulphate added to achieve 0.5M into sulfuric acid (1M) test</p> <p>Duration 50 days</p>
2 2 nd -5 th month	<p>Part 2: Bioleaching</p> <p>Culture used: Part 2A: . Mixture of <i>Thiobacillus ferrooxidans</i> and <i>Leptospirillum ferrooxidans</i> Continuing test for another 15 days, sample</p> <p>Off spraying: days 15th -20th</p> <p>Part 2B: Culture SL5B Continuing test for another 60 days, Off spraying: days 15th -20th, 35th -40th</p>	<p>Part 2: Bioleaching</p> <p>Culture used: Part 2A: . Mixture of <i>Thiobacillus ferrooxidans</i> and <i>Leptospirillum ferrooxidans</i> Continuing test for another 15 days</p> <p>Off spraying: days 15th -20th</p> <p>Part 2B: Culture SL5B Continuing test for another 60 days, Off spraying: days 15th -20th, 35th -40th</p>
3 6 th -8 th month	<p>Part 3: Acid leaching (200L column)</p> <p>Portion 3A Solution used: . Hydrochloric acid (0.5M)</p> <p>Duration 10 days. Solution changed every 5 days for metal recovery</p>	<p>Part 3: Acid leaching (200L column)</p> <p>Portion 3A Solution used: . Sulfuric acid (0.5M)</p> <p>Duration 10 days. Solution changed every 5 days for metal recovery</p>

	<p>Portion 3B Bioleaching Culture used: H₂SO₄ producer . Mixture of <i>Thiobacillus thiooxidans</i> and <i>Acidianus Brierleyi</i> Grown in hydrochloric acid (0.5M) test solution (portion 3A) , added with basalt salt</p> <p>Continuing test for another 40 days Solution changed every 10 days for metal recovery Off spraying: days 15th -20th , 40th -50th</p>	<p>Portion 3B Bioleaching Culture used: H₂SO₄ producer . Mixture of <i>Thiobacillus thiooxidans</i> and <i>Acidianus Brierleyi</i> Grown in sulfuric acid (0.5M) test solution (portion 3A) , added with basalt salt</p> <p>Continuing test for another 40 days Solution changed every 10 days for metal recovery Off spraying: days 15th -20th , 40th -50th</p>
4 9 th -12 th month	<p>Part 4: Ferric leaching (200L column)</p> <p>Portion 4A Ferric chloride 0.3M added to <i>TT</i> and <i>AB</i> (3B) solution</p> <p>Duration 10 days. Solution changed every 5 days for metal recovery</p> <p>Portion 4B Bioleaching Culture used: ferric ion producer . Mixture of <i>Thiobacillus ferrooxidans</i> and <i>Leptospirillum ferrooxidans</i> Grown in Ferric chloride (0.3M) test solution (portion 4A) , added with basalt salt</p> <p>Continuing test for another 30 days Solution changed every 10 days for metal recovery Off spraying: days 15th -20th</p> <p>Part 4C: Bioleaching (200L column) Culture SL5B Inoculated in a 4B solution (containing <i>TF</i> and <i>LF</i>) Continuing test for 50 days, Off spraying: days 20th -30th</p>	<p>Part 4: Ferric leaching (200L column)</p> <p>Portion 4A Ferric sulphate 0.3M added to <i>TT</i> and <i>AB</i> (3B) solution</p> <p>Duration 10 days. Solution changed every 5 days for metal recovery</p> <p>Portion 4B Bioleaching Culture used: ferric ion producer . Mixture of <i>Thiobacillus ferrooxidans</i> and <i>Leptospirillum ferrooxidans</i> Grown in Ferric sulphate (0.3M) test solution (portion 4A) , added with basalt salt</p> <p>Continuing test for another 30 days Solution changed every 10 days for metal recovery Off spraying: days 15th -20th</p> <p>Part 4C: Bioleaching (200L column) Culture SL5B Inoculated in a 4B solution (containing <i>TF</i> and <i>LF</i>) Continuing test for 50 days, Off spraying: days 20th -30th</p>

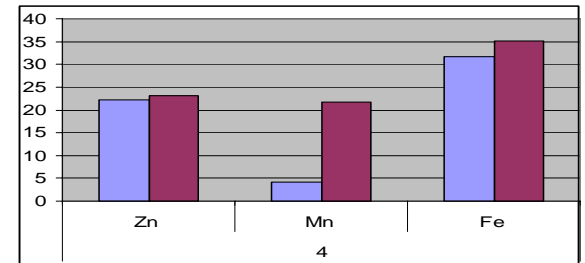
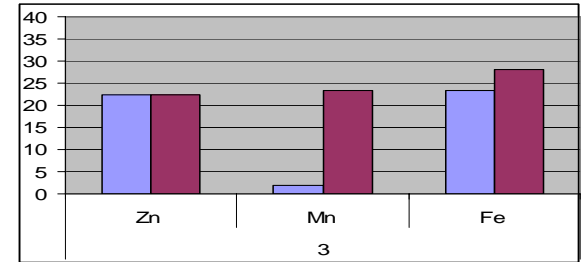
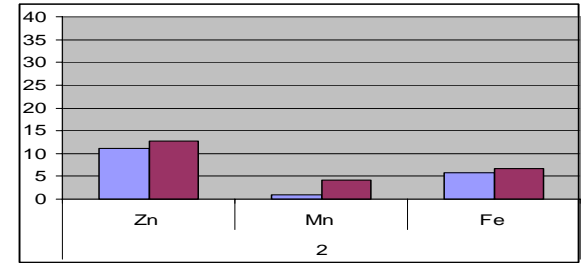
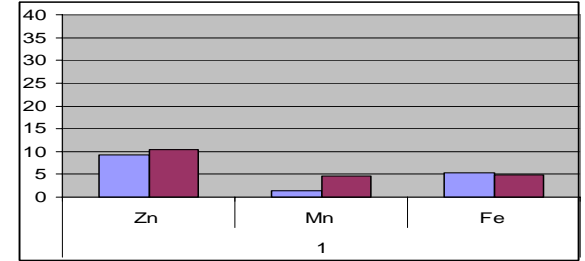
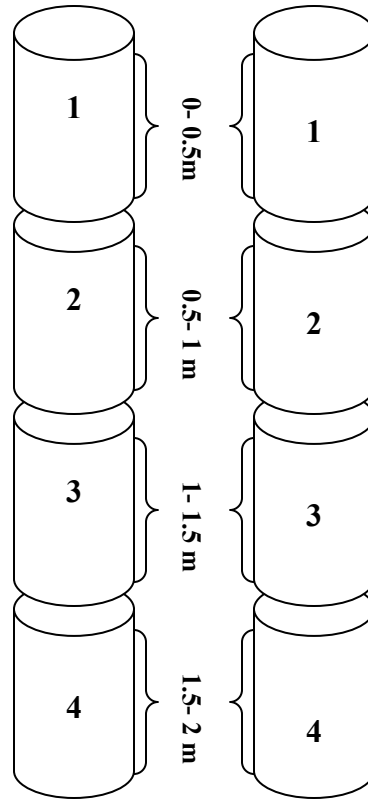


60L Column



Column 1
60L

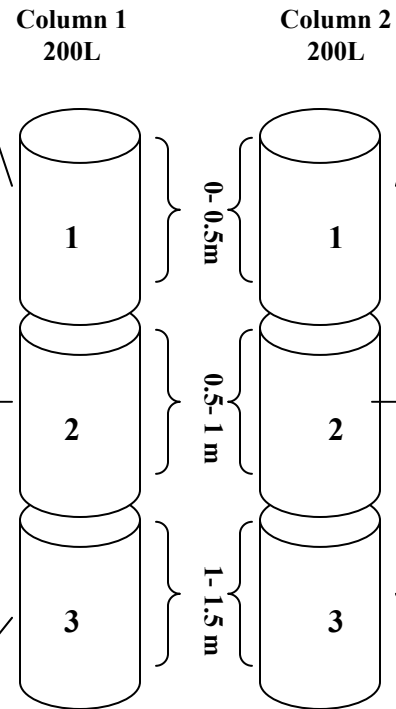
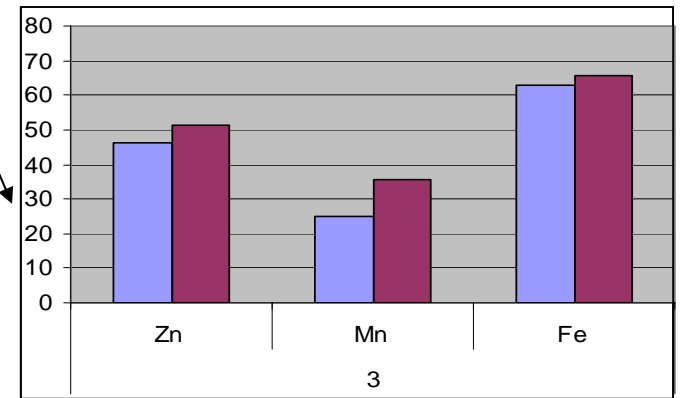
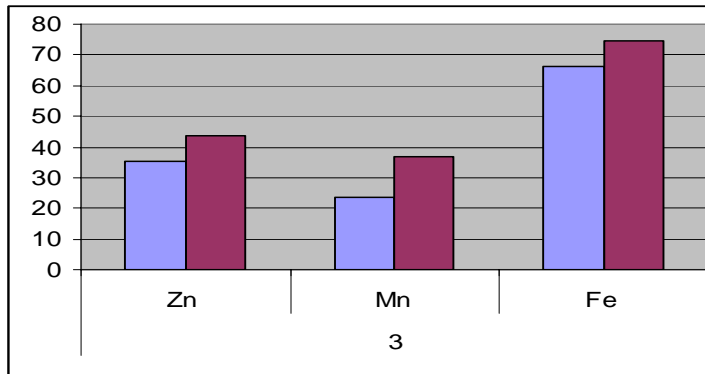
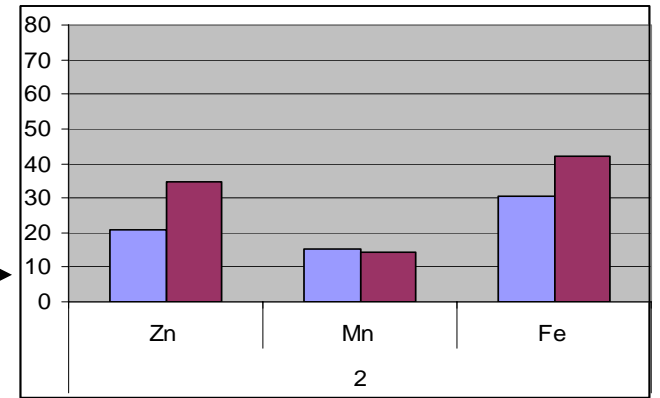
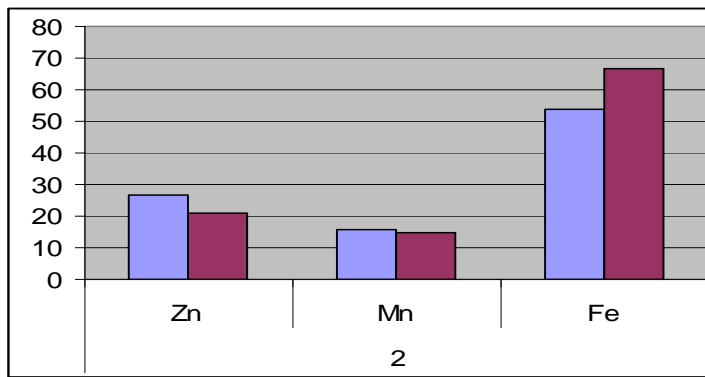
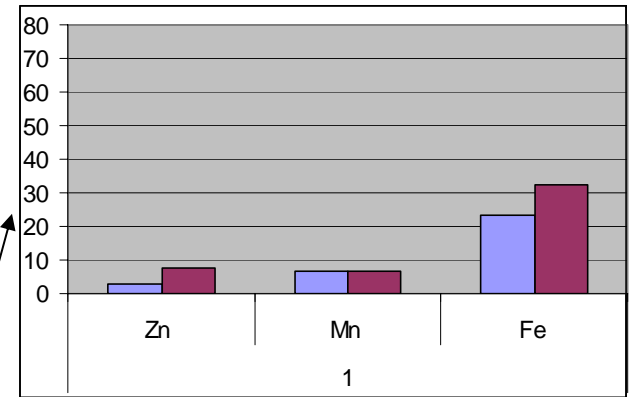
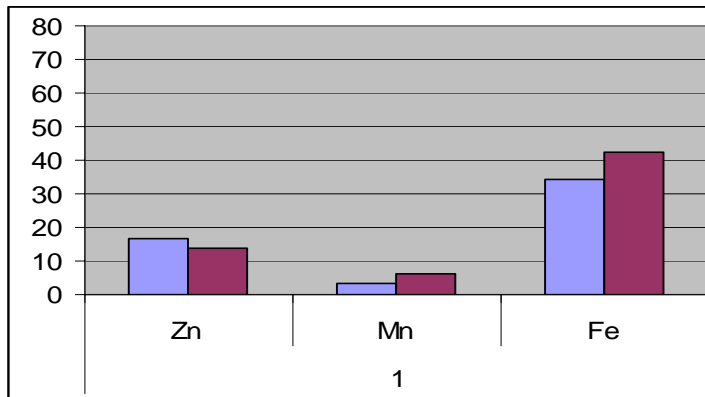
Column 2
60L



200L Column

■ 1st-2nd month and
 ■ 2nd-5th month.

Recovery of metal at different height of column:
 Y-axis - % of metal recovered
 X-axis: Position of metal recovered from column

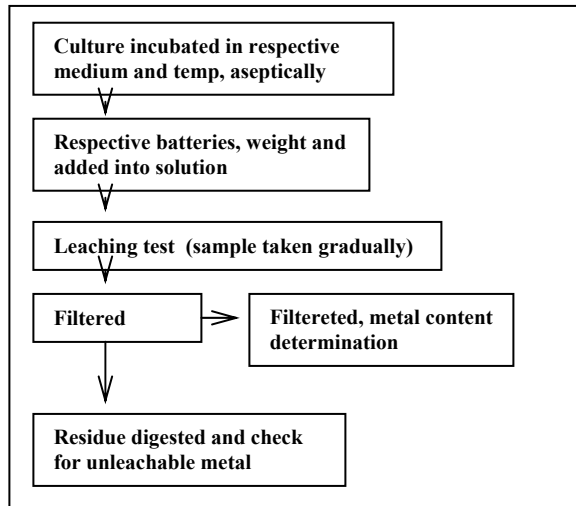


Recovery of metal at different height of column: ■ 6st-8nd month and ■ 9nd-12th month.
 Y-axis - % of metal recovered
 X-axis: Position of metal recovered from column

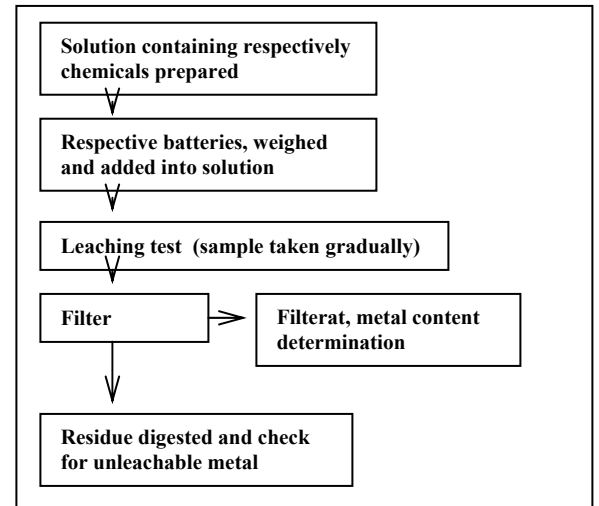
4.5 Laboratory test

4.5.1 Shake flask test

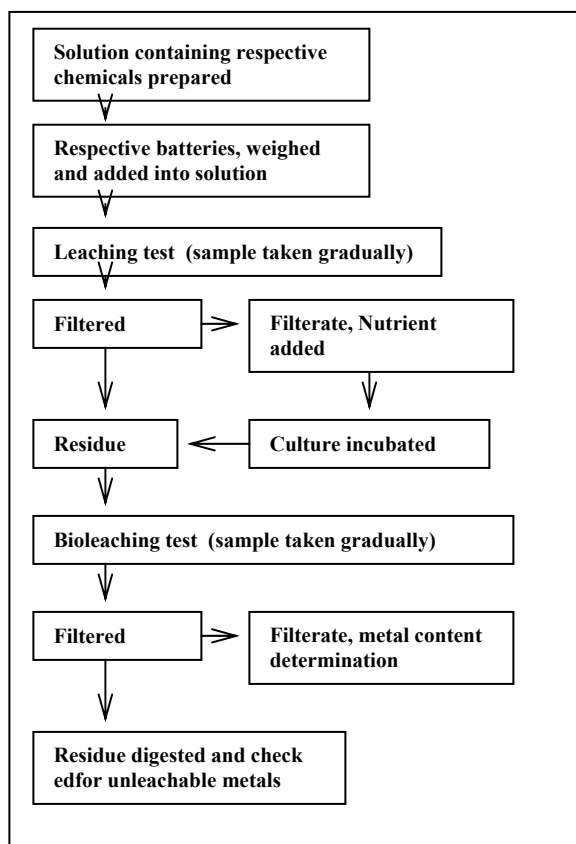
Bioleaching test



Chemical leaching test



Combination of chemical leaching and bioleaching test

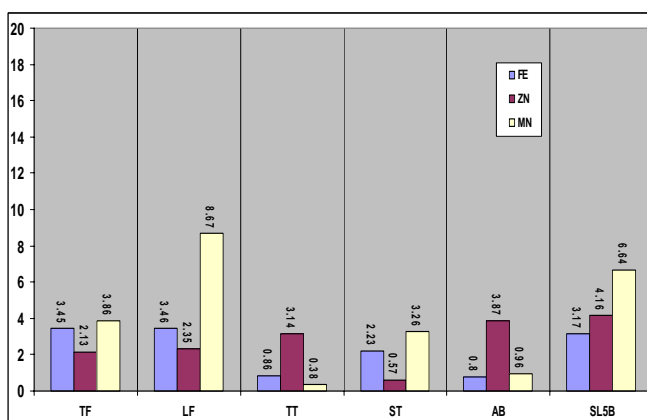


Shake flask test: Set 1

Set 1: Shaken, not broken	Flask 250mL, Leaching solution 100mL, shaken at 200 rpm using orbital shaker, 5 pc. of AA type batteries unbroken.
	<p>Culture used: <i>Thiobacillus ferrooxidans</i> (30⁰C), <i>Leptospirillum ferrooxidans</i> (30⁰C) <i>Thiobacillus thiooxidans</i> (30⁰C). <i>SulfobacillusThermosulfodioxidans</i> (45⁰C), <i>Acidianus Brierleyi</i>(70⁰C), <i>SL5B</i>(70⁰C),</p> <p>Chemical used: Hydrochloric acid (1M) Sulfuric acid (1M) Ferric chloride (1M) Ferric sulphate (1M) Sodium thiosulphate (0.250 M Na₂ 0.15 M NH₄OH, 0.02 M CuSO₄, pH;9.0) Sodium hypochlorite (75 mL/L NaOCl, 25 g/L NaCl and 0.35 M HCl)</p> <p>Duration 90 days</p>

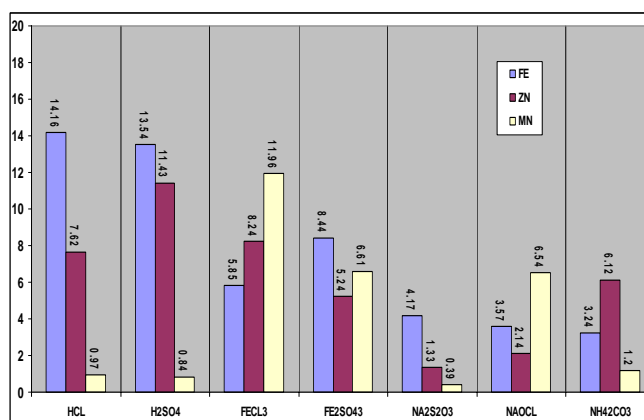
Set 1A: Metal extraction from Zn-C batteries. Not broken but shaken at 200 rpm for 90 days

Bacterial leaching



Percentages of Fe, Zn and Mn solubilization from Zn-C dry cell, 90 days of leaching using different types of culture. Batteries are unbroken but shaken at 200 rpm.

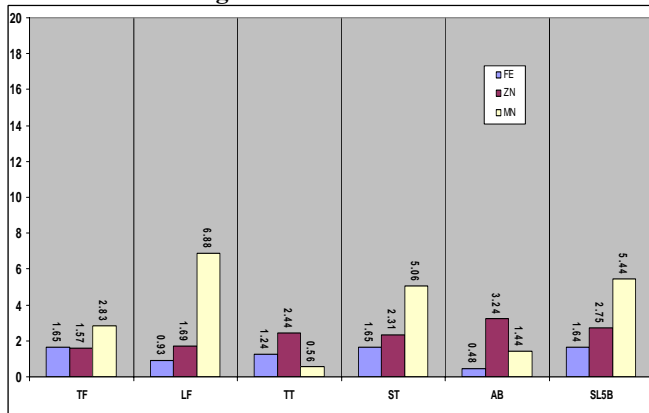
Chemical lixiviant



Percentages of Fe, Zn and Mn solubilization from Zn-C dry cell, 90 days of leaching using different types of chemical as lixiviant solution . Batteries are unbroken but shaken at 200 rpm.

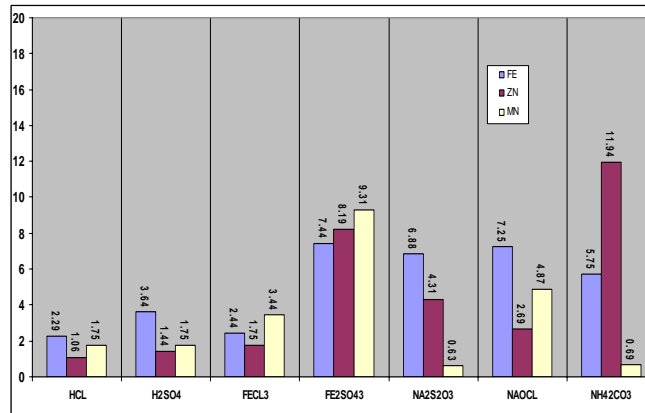
Set 1B: Metal extraction from alkaline batteries. Not broken but shaken at 200 rpm for 90 days

Bacterial leaching



Percentages of Fe, Zn and Mn solubilization from alkaline dry cell, 90 days of leaching using different types of culture. Batteries are unbroken but shaken at 200 rpm.

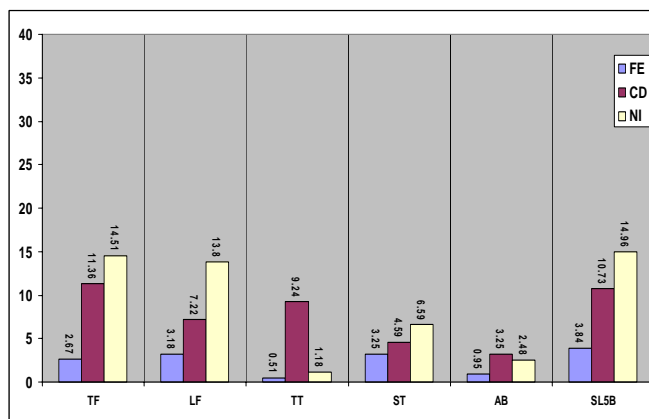
Chemical lixiviant



Percentages of Fe, Zn and Mn solubilization from alkaline dry cell, 90 days of leaching using different types of chemical as lixiviant solution. Batteries are unbroken but shaken at 200 rpm.

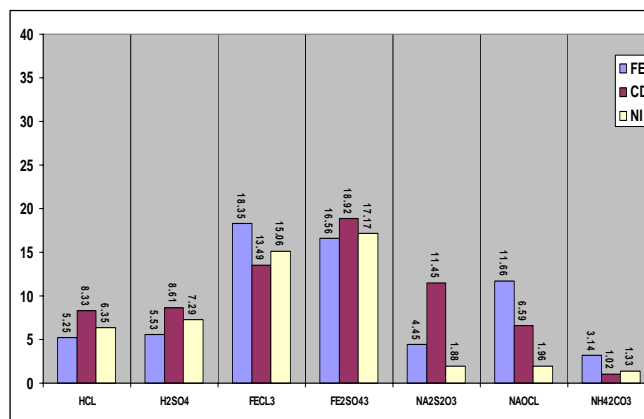
Set 1C: Metal extraction from Ni-Cd rechargeable batteries. Not broken but shaken at 200 rpm for 90 days

Bacterial leaching



Percentages of Fe, Cd and Ni solubilization from Ni-Cd dry cell, 90 days of leaching using different types of culture. Batteries are unbroken but shaken at 200 rpm.

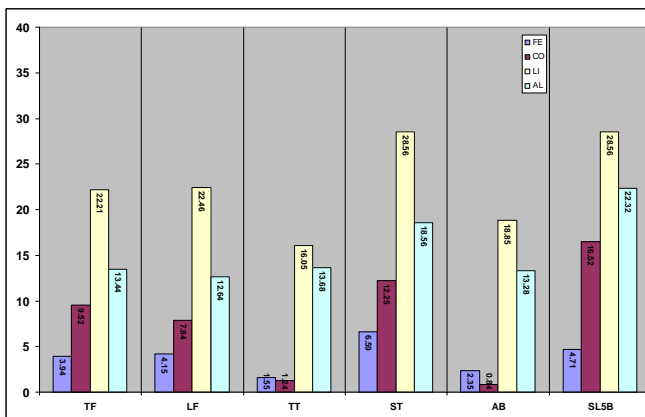
Chemical lixiviant



Percentages of Fe, Cd and Ni solubilization from Ni-Cd dry cell, 90 days of leaching using different types of chemical as lixiviant solution. Batteries are unbroken but shaken at 200 rpm.

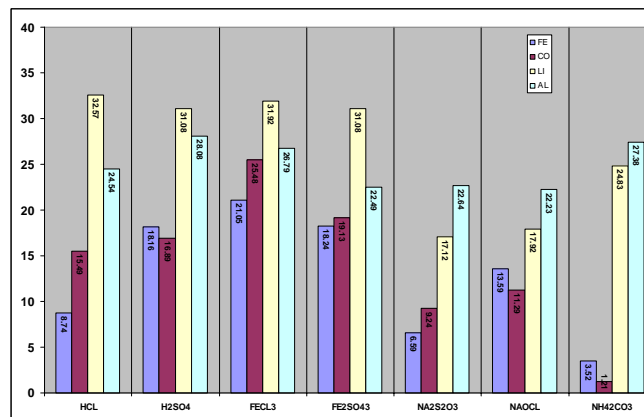
Set 1D: Metal extraction from Li-rechargeable batteries. Not broken but shaken at 200 rpm for 90 days

Bacterial leaching



Percentages of Fe, Cd, Li and Al solubilization from Li-ion dry cell, 90 days of leaching using different types of culture. Batteries are unbroken but shaken at 200 rpm.

Chemical lixiviant



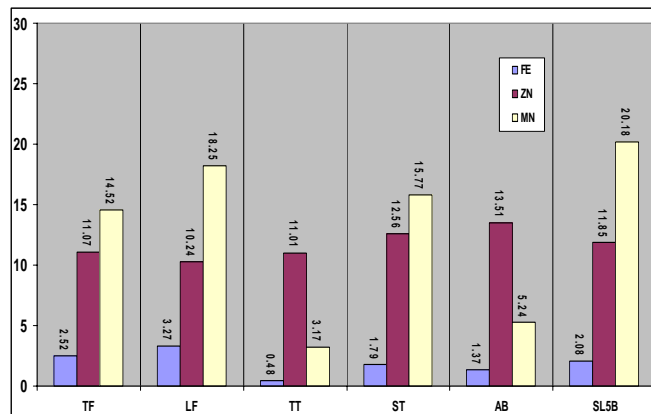
Percentages of Fe, Cd, Li and Al solubilization from Li-ion dry cell, 90 days of leaching using different types of chemical as lixiviant solution. Batteries are unbroken but shaken at 200 rpm.

Shake flask test: Set 2

Unshaken, broken Set 2:	<p>Flask 250mL, not shaken, Leaching solution 100mL, 5 pc. of AA type batteries were broken and shredded.</p> <p>Culture used: <i>Thiobacillus ferrooxidans</i> (30⁰C), <i>Leptospirillum ferrooxidans</i> (30⁰C) <i>Thiobacillus thiooxidans</i> (30⁰C). <i>SulfobacillusThermosulfodioxidans</i> (45⁰C), <i>Acidianus Brierleyi</i>(70⁰C), <i>SL5B</i>(70⁰C),</p> <p>Chemicals used: Hydrochloric acid (1M) Sulfuric acid (1M) Ferric chloride (1M) Ferric sulphate (1M) Sodium thiosulphate (0.250 M Na₂ 0.15 M NH₄OH, 0.02 M CuSO₄, pH;9.0) Sodium hypochlorite (75 mL/L NaOCl, 25 g/L NaCl and 0.35 M HCl)</p> <p>Duration 90 days</p>
----------------------------	---

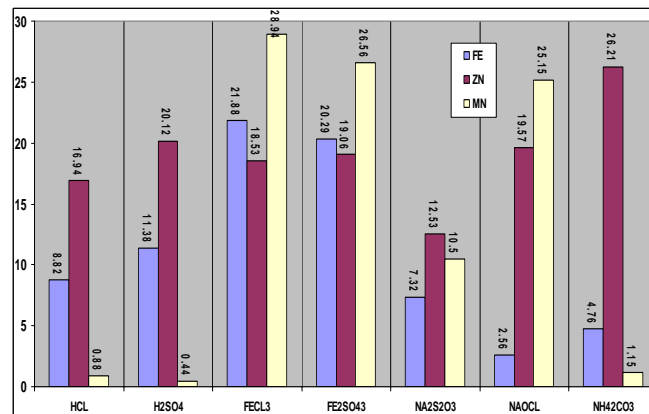
Set 2A: Metal extraction from Zn-C batteries for 90 days. Batteries were not shaken but broken

Bacterial leaching



Percentages of Fe, Zn and Mn solubilization from Zn-C dry cell, 90 days of leaching using different types of culture. Batteries are broken but not shaken.

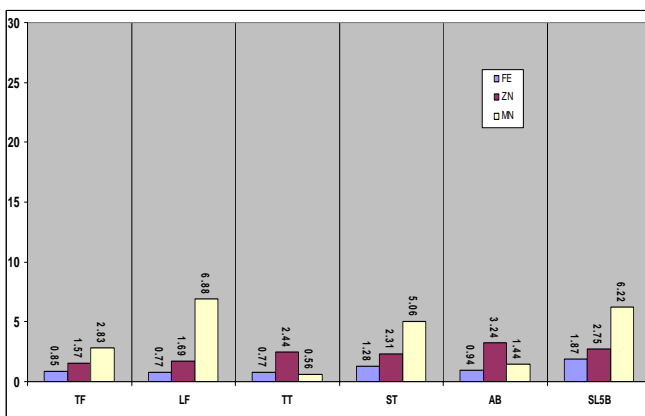
Chemical lixiviant



Percentages of Fe, Zn and Mn solubilization from Zn-C dry cell, 90 days of leaching using different types of chemical as lixiviant solution. Batteries are broken but not shaken.

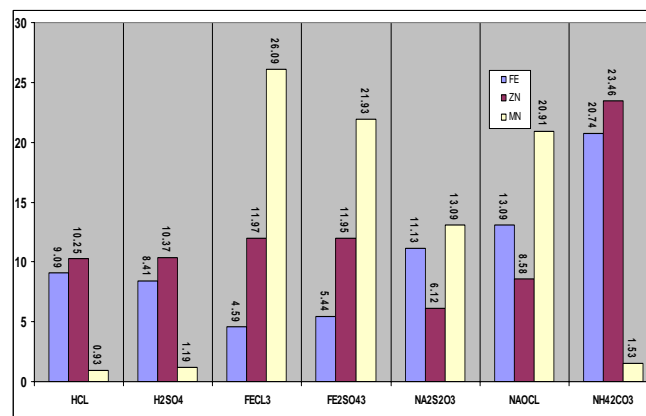
Set 2B: Metal extraction from alkaline batteries for 90 days. Batteries were not shaken but broken

Bacterial leaching



Percentages of Fe, Zn and Mn solubilization from alkaline dry cell, 90 days of leaching using different types of culture. Batteries are broken but not shaken.

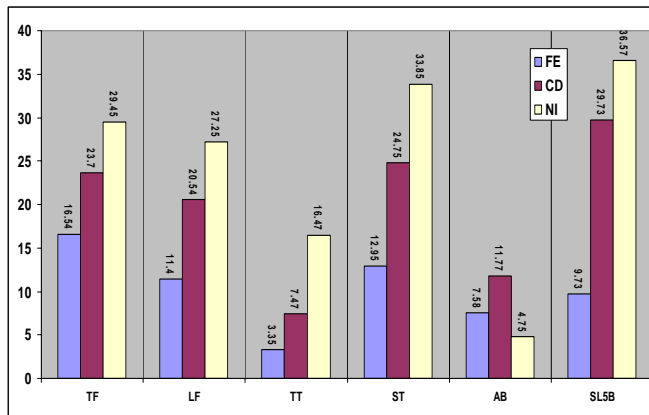
Chemical lixiviant



Percentages of Fe, Zn and Mn solubilization from alkaline dry cell, 90 days of leaching using different types of chemical as lixiviant solution. Batteries are broken but not shaken.

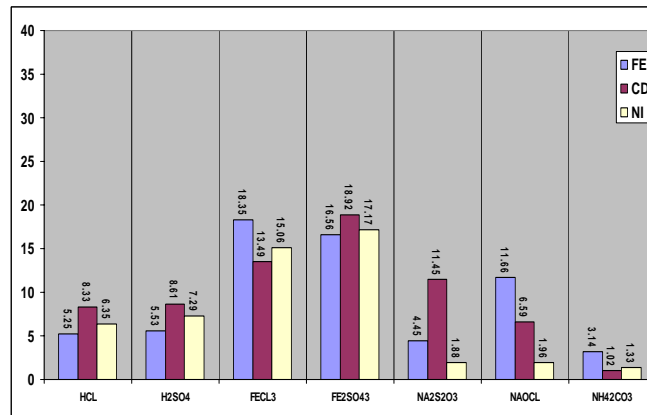
Set 2C: Metal extraction from Ni-Cd rechargeable batteries for 90 days. Batteries were not shaken but broken

Bacterial leaching



Percentages of Fe, Cd and Ni solubilization from Ni-Cd dry cell, 90 days of leaching using different types of culture. Batteries are broken but not shaken

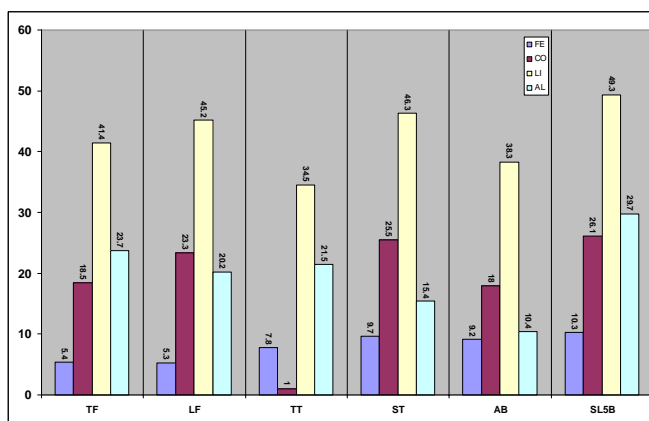
Chemical lixiviant



Percentages of Fe, Cd and Ni solubilization from Ni-Cd dry cell, 90 days of leaching using different types of chemical as lixiviant solution. Batteries are broken but not shaken.

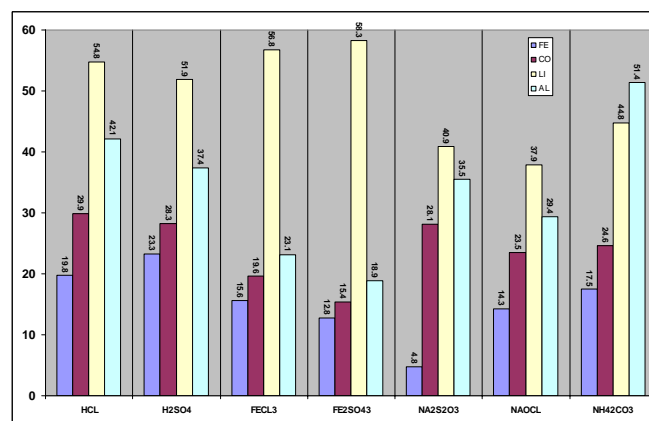
Set 2D: Metal extraction from Li-rechargeable batteries for 90 days. Batteries were not shaken but broken

Bacterial leaching



Percentages of Fe, Cd, Li and Al solubilization from Li-ion dry cell, 90 days of leaching using different types of culture. Batteries are broken but not shaken

Chemical lixiviant

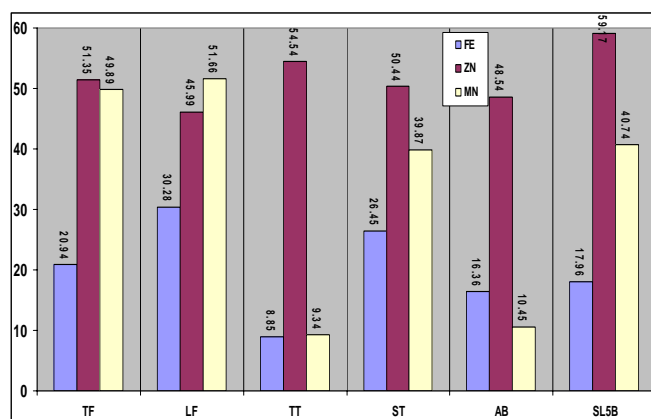


Percentages of Fe, Cd, Li and Al solubilization from Li-ion dry cell, 90 days of leaching using different types of chemical as lixiviant solution. Batteries are broken but not shaken.

Set 3: Shaken, broken	<p>Flask 250mL, Leaching solution 50mL, shaken at 200 rpm using orbital shaker, A pieces of AA type batteries were broken and shredded.</p> <p>Culture used: <i>Thiobacillus ferrooxidans</i> (30⁰C), <i>Leptospirillum ferrooxidans</i> (30⁰C) <i>Thiobacillus thiooxidans</i> (30⁰C). <i>SulfobacillusThermosulfodioxidans</i> (45⁰C), <i>Acidianus Brierleyi</i>(70⁰C), <i>SL5B</i>(70⁰C),</p> <p>Chemical used: Hydrochloric acid (1M) Sulfuric acid (1M) Ferric chloride (1M) Ferric sulphate (1M) Sodium thiosulphate (0.250 M Na₂S₂O₃, 0.15 M NH₄OH, 0.02 M CuSO₄, pH;9.0) Sodium hypochlorite (75 mL/L NaOCl, 25 g/L NaCl and 0.35 M HCl)</p> <p>Duration 30 days</p>
--------------------------	---

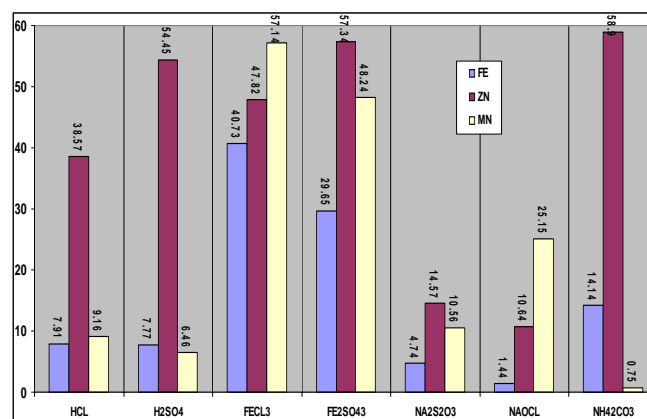
Set 3A: Metal extraction from Zn-C batteries for 30 days. Batteries were broken and shaken at 200 rpm

Bacterial leaching



Percentages of Fe, Zn and Mn solubilization from Zn-C dry cell, 30 days of leaching using different types of culture. Batteries are broken and shaken at 200rpm.

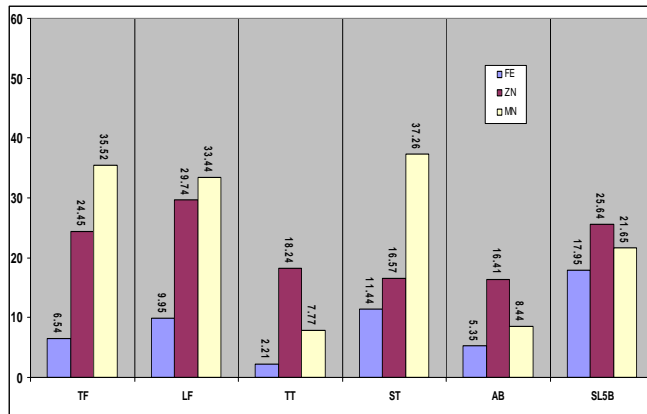
Chemical lixiviant



Percentages of Fe, Zn and Mn solubilization from Zn-C dry cell, 30 days of leaching using different types of chemical as lixiviant solution . Batteries are broken and shaken at 200rpm.

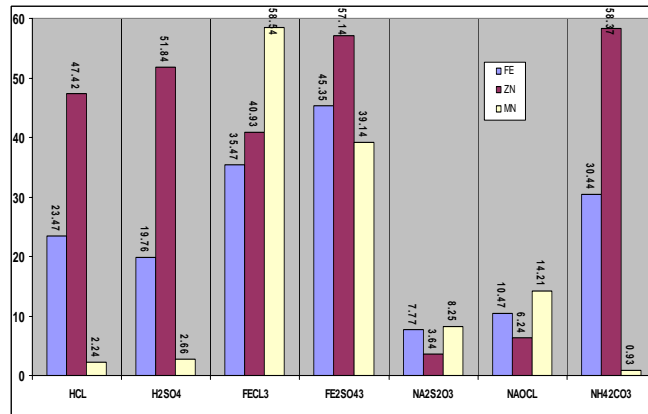
Set 3B: Metal extraction from alkaline batteries for 30 days. Batteries were broken and shaken at 200 rpm

Bacterial leaching



Percentages of Fe, Zn and Mn solubilization from Zn-C dry cell, 30 days of leaching using different types of culture. Batteries are broken and shaken at 200rpm.

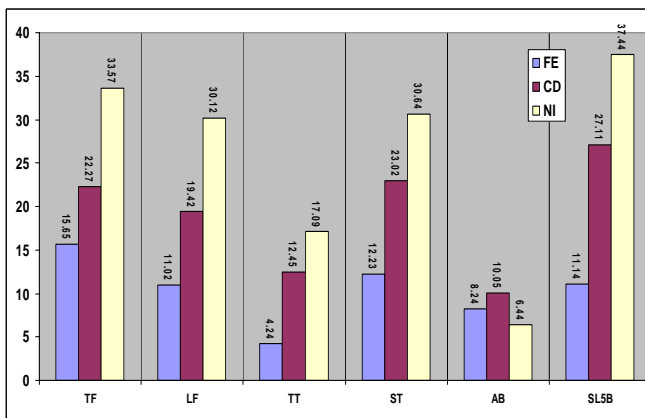
Chemical lixiviant



Percentages of Fe, Zn and Mn solubilization from alkaline dry cell, 30 days of leaching using different types of chemical as lixiviant solution. Batteries are broken and shaken at 200rpm.

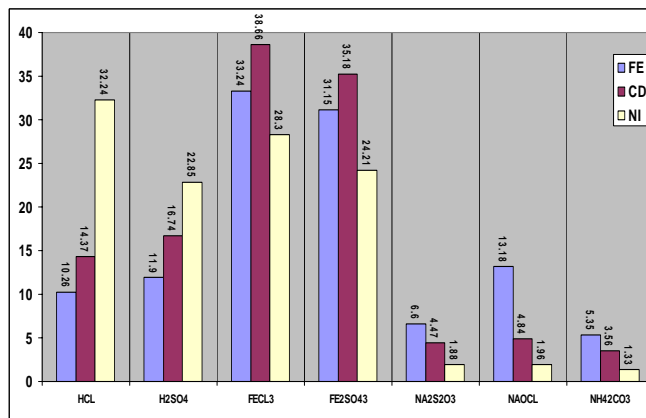
Set 2C: Metal extraction from Ni-Cd rechargeable batteries for 30 days. Batteries were broken and shaken at 200 rpm

Bacterial leaching



Percentages of Fe, Cd and Ni solubilization from Ni-Cd dry cell, 30 days of leaching using different types of culture. Batteries are broken and shaken at 200rpm.

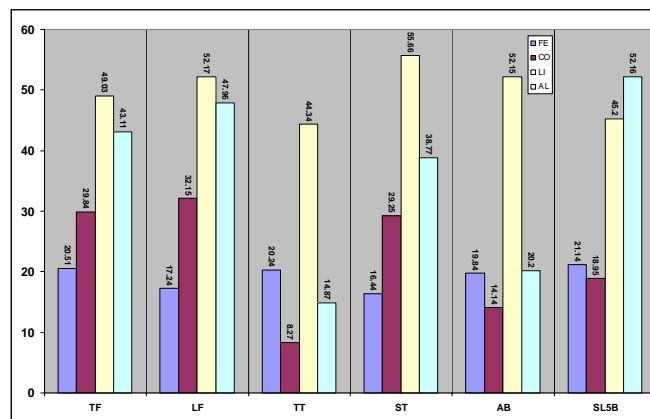
Chemical lixiviant



Percentages of Fe, Cd and Ni solubilization from Ni-Cd dry cell, 30 days of leaching using different types of chemical as lixiviant solution. Batteries are broken and shaken at 200rpm.

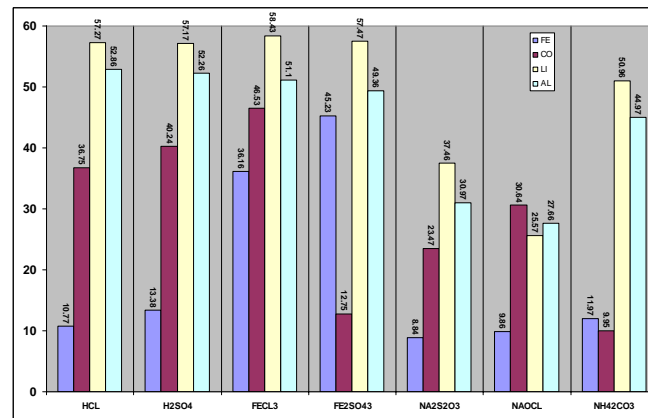
Set 3D: Metal extraction from Li-rechargeable batteries for 30 days. Batteries were not shaken but broken

Bacterial leaching



Percentages of Fe, Cd, Li and Al solubilization from Li-ion dry cell, 30 days of leaching using different types of culture. Batteries was broken and shaken at 200rpm.

Chemical lixiviant



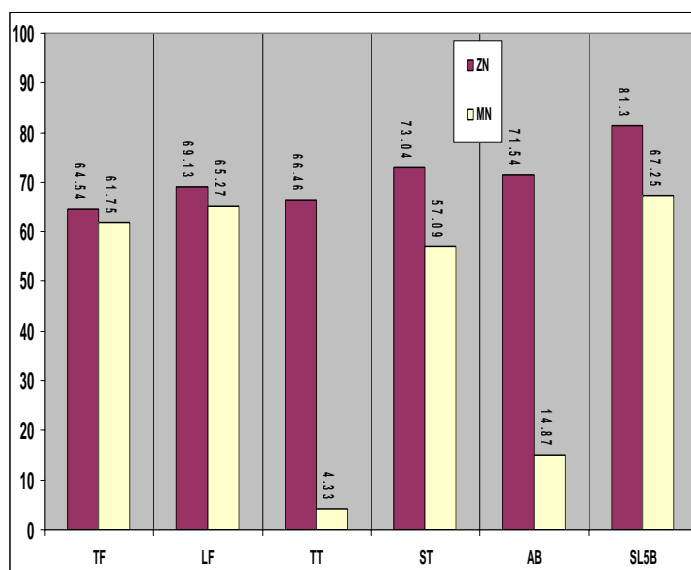
Percentages of Fe, Cd, Li and Al solubilization from Li-ion dry cell, 30 days of leaching using different types of chemical as lixiviant solution . Batteries are broken and shaken at 200rpm.

Shake flask test: Set 4

Shaken, broken and inner part dismantling Set 4	Flask 250mL, Shaken at 200rpm, Leaching solution 100mL, D type batteries Zn-carbon batteries, internal portion manually exposed (inner part: ground, sieved, washed and dried), weight: 25g
	<p>Culture used:</p> <p><i>Thiobacillus ferrooxidans</i> (30⁰C), <i>Leptospirillum ferrooxidans</i> (30⁰C) <i>Thiobacillus thiooxidans</i> (30⁰C). <i>SulfobacillusThermosulfodioxidans</i> (45⁰C), <i>Acidianus Brierleyi</i>(70⁰C), <i>SL5B</i>(70⁰C),</p> <p>Chemical used:</p> <p>Hydrochloric acid (1M) Sulfuric acid (1M) Ferric chloride (1M) Ferric sulphate (1M) Sodium thiosulphate (0.250 M Na₂, 0.15 M NH₄OH, 0.02 M CuSO₄ , pH:9.0) Sodium hypochlorite (75 mL/L NaOCl, 25 g/L NaCl and 0.35 M HCl) Ammonium carbonate (1M)</p> <p>Duration 30 days.</p>

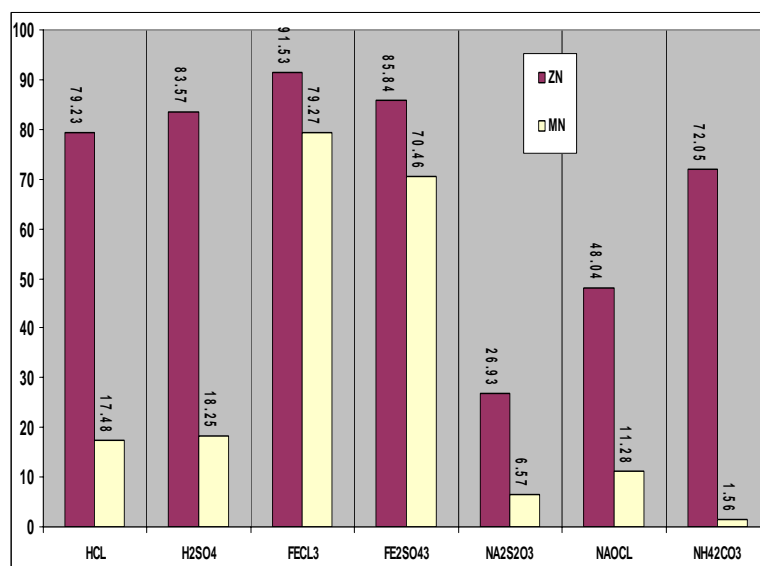
Set 4: Metal extraction from Zn-C batteries dust (inner part) for 30 days. Batteries dust were ground, wash and dried

Bacterial leaching



Percentages of Zn and Mn solubilization from the dust of Zn-C dry cell, 30 days of leaching using different types of culture. Batteries are broken and inner part of batteries were dismantled, ground, wash and dried. Slurry was shaken at 200rpm.

Chemical lixiviant

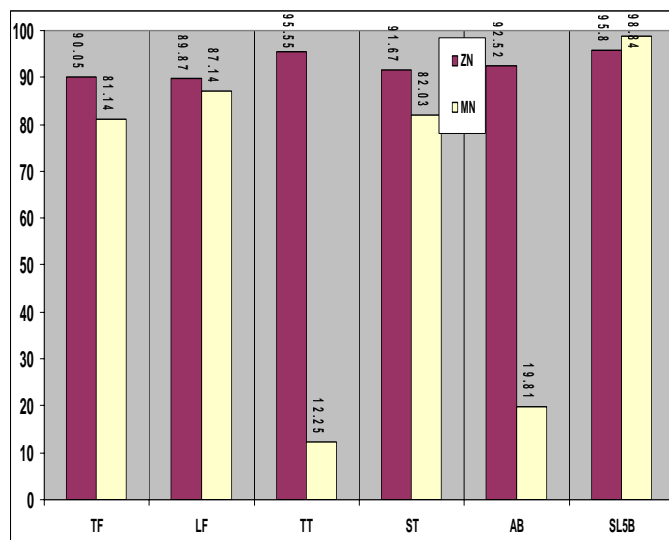


Percentages of Zn and Mn solubilization from Zn-C dry cell, 30 days of leaching using different types of chemical as lixiviant solution Batteries are broken and inner part of batteries were dismantled, ground, wash and dried. Slurry was shaken at 200rpm..

Shaken, broken, inner part dismantling and roasted Set 5:	<p>Flask 250mL, Shaken at 200rpm, Leaching solution 100mL, D type batteries Zn-carbon batteries, internal portion manually exposed (inner part: ground, sieve and dried), weight: 25g , sample then roasted on the hot plate (8 hrs, max current)</p> <p>Culture used: <i>Thiobacillus ferrooxidans</i> (30⁰C), <i>Leptospirillum ferrooxidans</i> (30⁰C) <i>Thiobacillus thiooxidans</i> (30⁰C). <i>SulfobacillusThermosulfodioxidans</i> (45⁰C), <i>Acidianus Brierleyi</i>(70⁰C), <i>SL5B</i>(70⁰C),</p> <p>Chemical used: Hydrochloric acid (1M) Sulfuric acid (1M) Ferric chloride (1M) Ferric sulphate (1M) Sodium thiosulphate (0.250 M Na₂, 0.15 M NH₄OH, 0.02 M CuSO₄, pH;9.0) Sodium hypochlorite (75 mL/L NaOCl, 25 g/L NaCl and 0.35 M HCl) Ammonium carbonate (1M)</p> <p>Duration 10 days.</p>
--	---

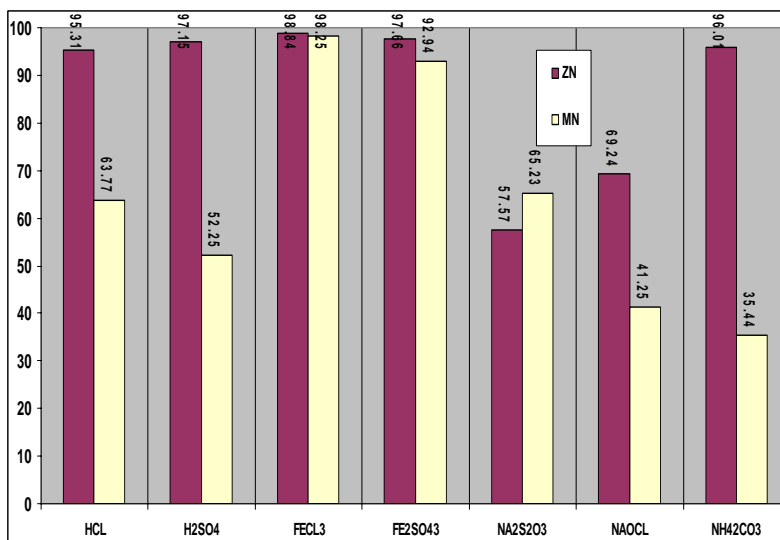
Set 4: Metal extraction from Zn-C batteries dust (inner part) for 10 days. Batteries dust were ground, dismantled, wash and dried. Sample then roasted on the hot plate (8 hrs, max current)

Bacterial leaching



Percentages of Zn and Mn solubilization from the dust of Zn-C dry cell, 10 days of leaching using different types of culture. Batteries are broken and inner part of batteries were dismantled, ground, wash and dried. Sample then roasted on the hot plate (8 hrs, max current). Slurry was shaken at 200rpm.

Chemical lixiviant



Percentages of Zn and Mn solubilization from Zn-C dry cell, 10 days of leaching using different types of chemical as lixiviant solution Batteries are broken and inner part of batteries were dismantled, ground, wash and dried. Sample then roasted on the hot plate (8 hrs, max current) Slurry was shaken at 200rpm..

Combination of chemical leaching and bioleaching test

Table 4A: Combination of chemical leaching and bioleaching (Chloride system)

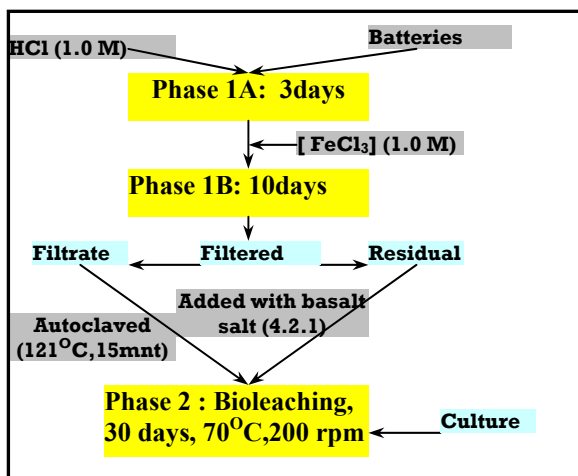
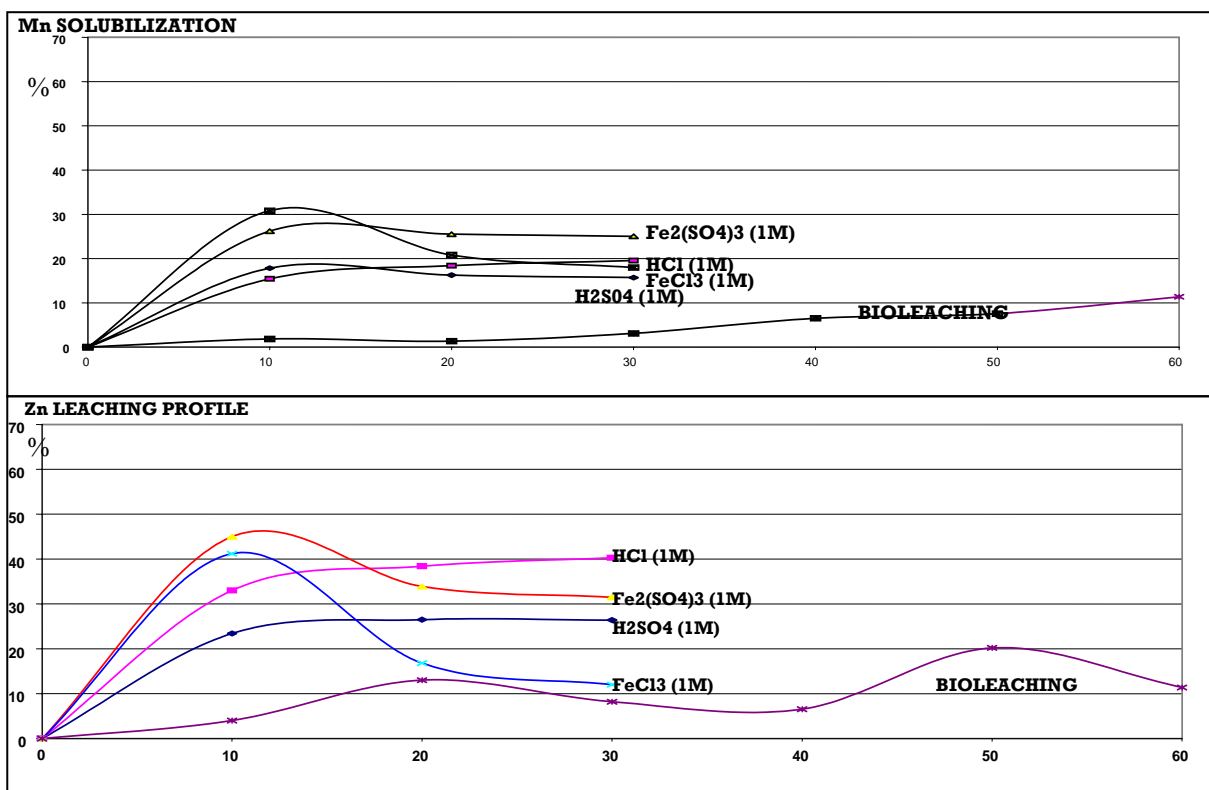
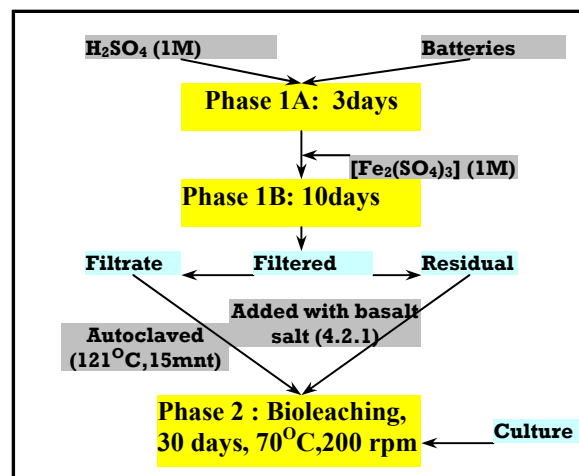
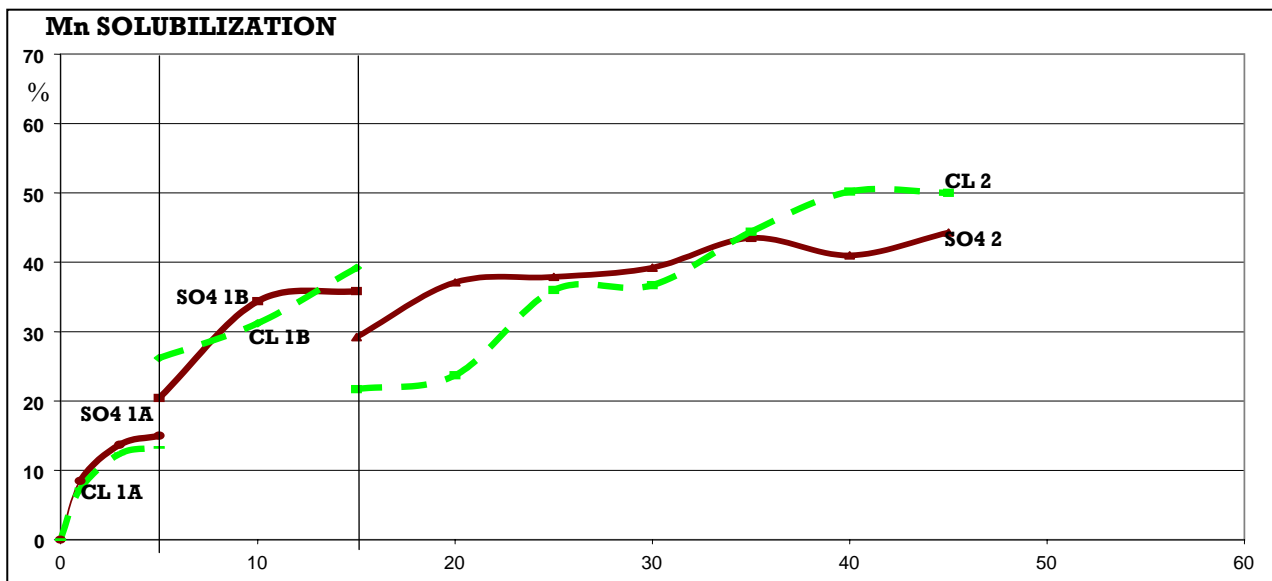


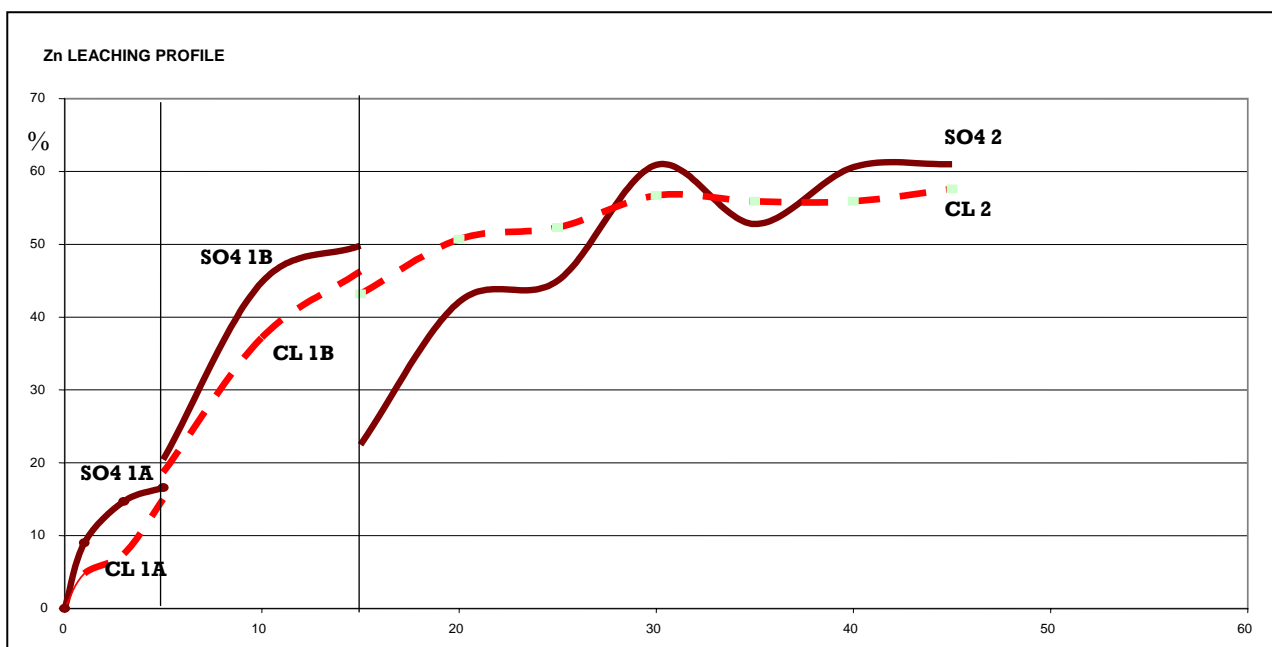
Table 4A: Combination of chemical leaching and bioleaching (Sulfate system)



Manganese and Zinc solubilisation profiles for chemical leaching and bioleaching



Manganese leached by sequential leaching test using combination of acid, ferric and bioleaching



Zinc leached by sequential leaching test using combination of acid, ferric and bioleaching

4.6 Laboratory test

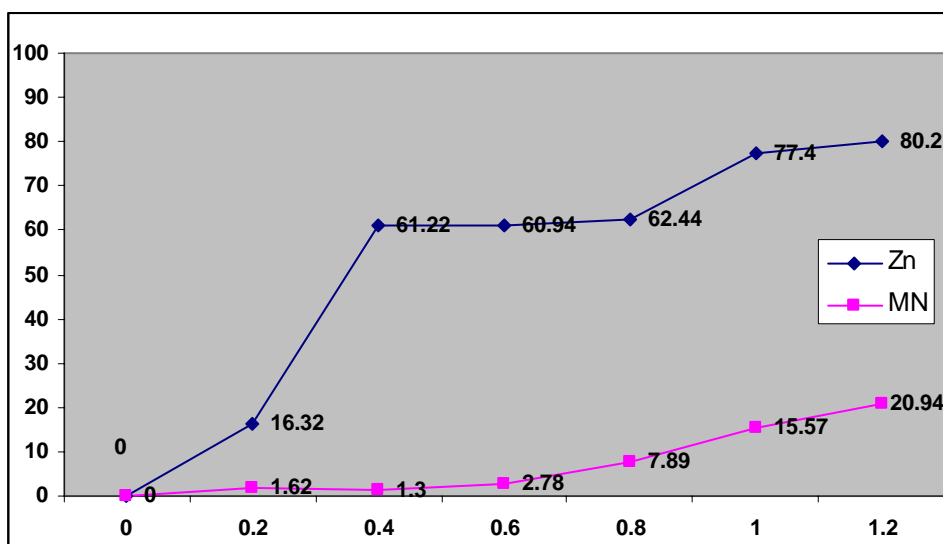
4.6.1 Stirred tank reactor (STR) test

STR: SET 1

STR Set 1 : H_2SO_4 leaching	<p>2L reactor, Agitated at 400 rpm, D type batteries Zn-carbon batteries, internal portion manually exposed. Inner part of batteries were ground, sieved, washed and dried. Lixiviant solution leaching using H_2SO_4:</p> <p>Condition of leaching</p> <p>1: Constant parameters: Pulp densities: 10%, Temperatures: 20°C, Duration 3 days Variable : H_2SO_4 concentration: 0.2M, 0.4M, 0.6M, 0.8M, 1.0M and 1.5M</p> <p>2: Constant parameters: Pulp densities: 10%, H_2SO_4 concentration 0.5M, Duration 3 days Variable : Temperatures: 20°C, 40°C, 50°C, 60°C, 70°C, 80°C</p> <p>3: Constant parameters: H_2SO_4 concentration 0.5M, Temperatures: 50°C, Duration 3 days Variable : Pulp densities: 5%, 10%, 15%, 20%, 50%, 100%</p> <p>4: Constant parameters: H_2SO_4 concentration 0.5M, Temperatures: 50°C, Pulp densities: 15%, Variable : Duration: 4hrs, 8 hrs, 12 hrs, 24hrs, 48hrs and 36hrs.</p>
-----------------------------------	---

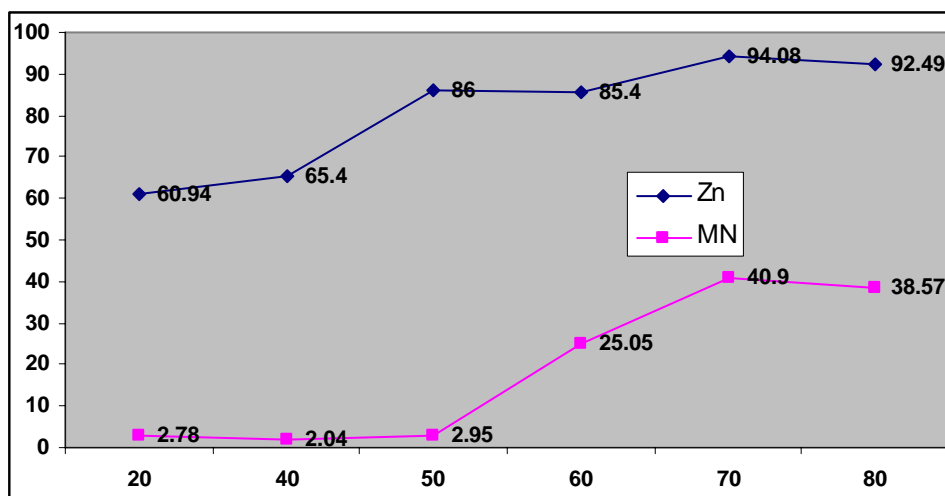
Set 1: Lixiviant solution leaching using H_2SO_4

Set 1A: Metal extraction from Zn-C batteries dust (inner part) for 3 days. Batteries dust were ground, dismantled, washed and dried. Lixiviant solution leaching using different concentrations of H_2SO_4



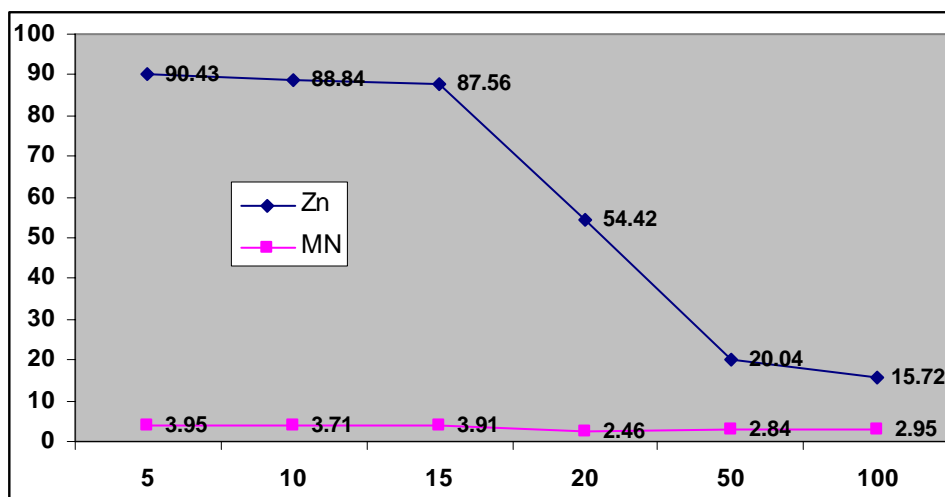
Percentages of \blacklozenge Zn and \blacksquare Mn solubilization from the dust of Zn-C dry cell, 3 days of leaching using different concentrations of H_2SO_4 . Batteries are broken and inner part of batteries were dismantled, ground, washed and dried. Slurry was stirred at 400rpm.

Set 1B: Metal extraction from Zn-C batteries dust (inner part) for 3 days. Batteries dust were ground, dismantled, washed and dried. Lixiviant solution leaching at different temperatures



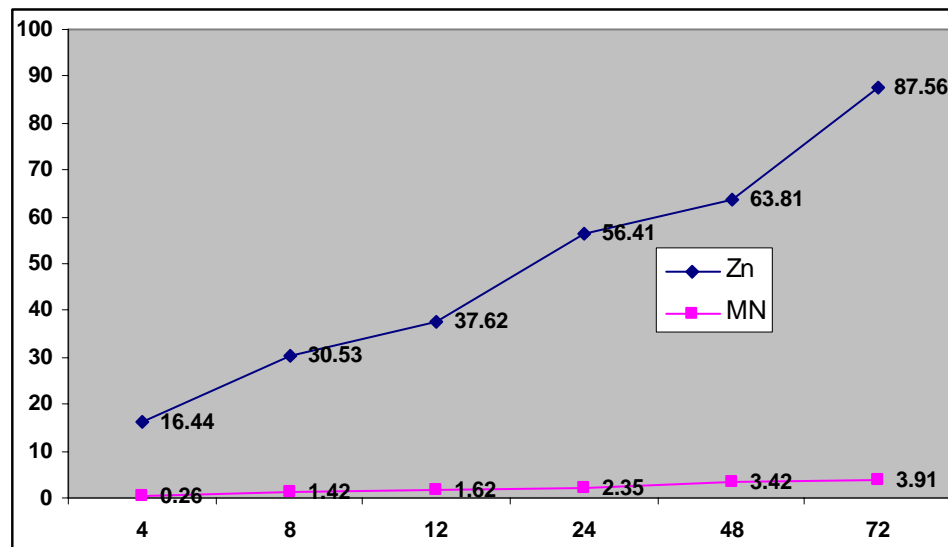
Percentages of \blacklozenge Zn and \blacksquare Mn solubilization from the dust of Zn-C dry cell, 3 days of leaching at different temperatures. Batteries are broken and inner part of batteries were dismantled, ground, washed and dried. Slurry was stirred at 400rpm.

Set 1C: Metal extraction from Zn-C batteries dust (inner part) for 3 days. Batteries dust were ground, dismantled, washed and dried. Lixiviant solution leaching at different ratios of solid/solution



Percentages of \blacklozenge Zn and \blacksquare Mn solubilization from the dust of Zn-C dry cell, 3 days of leaching at different ratios of solid/solution. Batteries are broken and inner part of batteries were dismantled, ground, washed and dried. Slurry was stirred at 400rpm.

Set 1D: Metal extraction from Zn-C batteries dust (inner part) for 3 days. Batteries dust were ground, dismantled, washed and dried. Lixiviant solution leaching using H_2SO_4 .



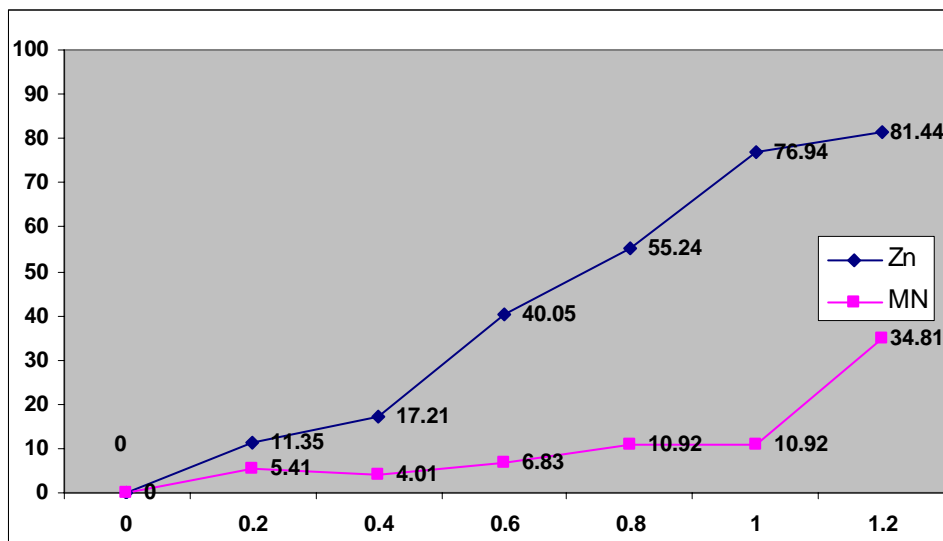
Percentages of \blacklozenge Zn and \blacksquare Mn solubilization from the dust of Zn-C dry cell, 3 days of leaching using H_2SO_4 . Batteries are broken and inner part of batteries were dismantled, ground, washed and dried. Slurry was stirred at 400rpm.

STR: SET 2

STR Set : HCl leaching	<p>2L reactor, Agitated at 400 rpm, D type batteries Zn-carbon batteries, internal portion manually exposed. Inner part of batteries were ground, sieved, washed and dried. Lixiviant solution leaching using HCl:</p> <p>Condition of leaching</p> <p>1: Constant parameters: Pulp densities: 10%, Temperatures: 20°C, Duration 3 days Variable : HCl concentration: 0.2M, 0.4M, 0.6M, 0.8M, 1.0M and 1.5M</p> <p>2: Constant parameters: Pulp densities: 10%, HCl concentration 1M, Duration 3 days Variable : Temperatures: 20°C, 40°C, 50°C, 60°C, 70°C, 80°C</p> <p>3: Constant parameters: HCl concentration 1M, Temperatures: 20°C, Duration 3 days Variable : Pulp densities: 5%, 10%, 15%, 20%, 50%, 100%</p> <p>4: Constant parameters: HCl concentration 1 M, Temperatures: 20°C, Pulp densities: 20%, Variable : Duration: 4hrs, 8 hrs, 12 hrs, 24hrs, 48hrs and 36hrs.</p>
---------------------------	---

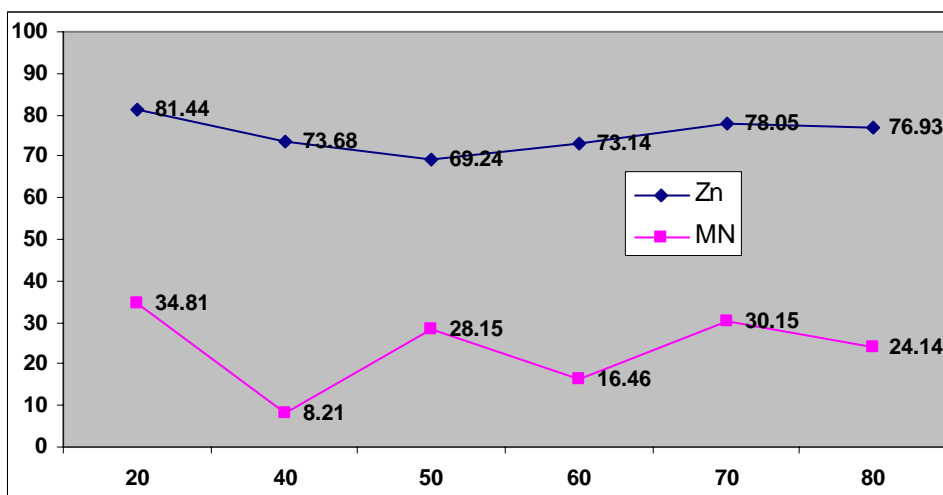
Set 2: Lixiviant solution leaching using HCl

Set 2A: Metal extraction from Zn-C batteries dust (inner part) for 3 days. Batteries dust were ground, dismantled, washed and dried. Lixiviant solution leaching using different concentrations of HCl



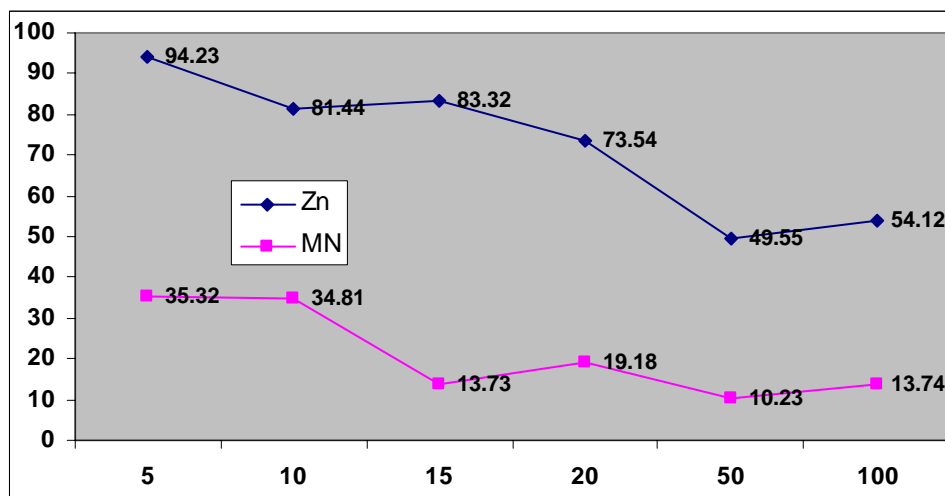
Percentages of \blacklozenge Zn and \blacksquare Mn solubilization from the dust of Zn-C dry cell, 3 days of leaching using different concentration of HCl. Batteries are broken and inner part of batteries were dismantled, ground, washed and dried. Slurry was stirred at 400rpm.

Set 2B: Metal extraction from Zn-C batteries dust (inner part) for 3 days. Batteries dust were ground, dismantled, washed and dried. HCl leaching at different temperatures



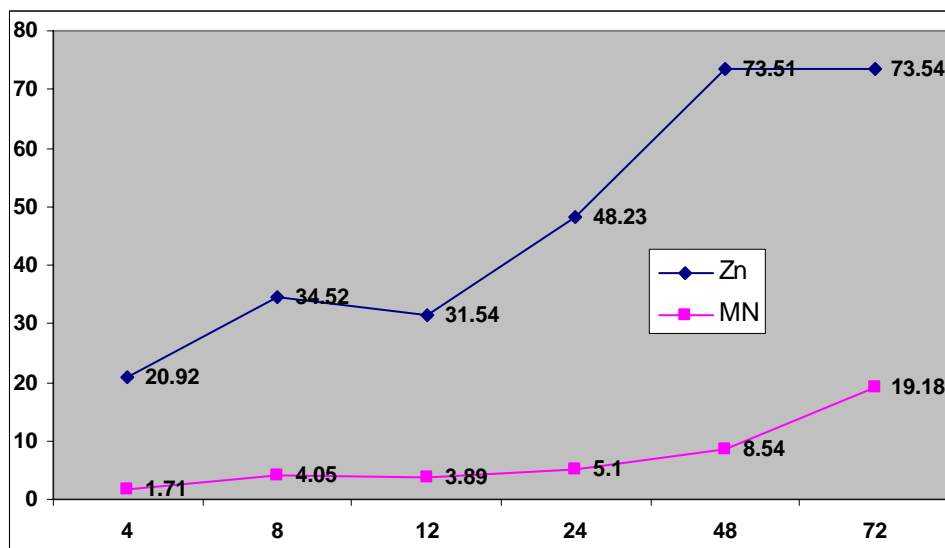
Percentages of \blacklozenge Zn and \blacksquare Mn solubilization from the dust of Zn-C dry cell, 3 days of leaching using HCl at different temperatures. Batteries are broken and inner part of batteries were dismantled, ground, washed and dried. Slurry was stirred at 400rpm.

Set 2C: Metal extraction from Zn-C batteries dust (inner part) for 3 days. Batteries dust were ground, dismantled, washed and dried. Lixiviant solution leaching at different ratios of solid/solution



Percentages of \blacklozenge Zn and \blacksquare Mn solubilization from the dust of Zn-C dry cell, 3 days of leaching at different ratios of solid/solution. Batteries are broken and inner part of batteries were dismantled, ground, washed and dried. Slurry was stirred at 400rpm.

Set 2D: Metal extraction from Zn-C batteries dust (inner part) for 3 days. Batteries dust were ground, dismantled, washed and dried. Lixiviant solution leaching using HCl



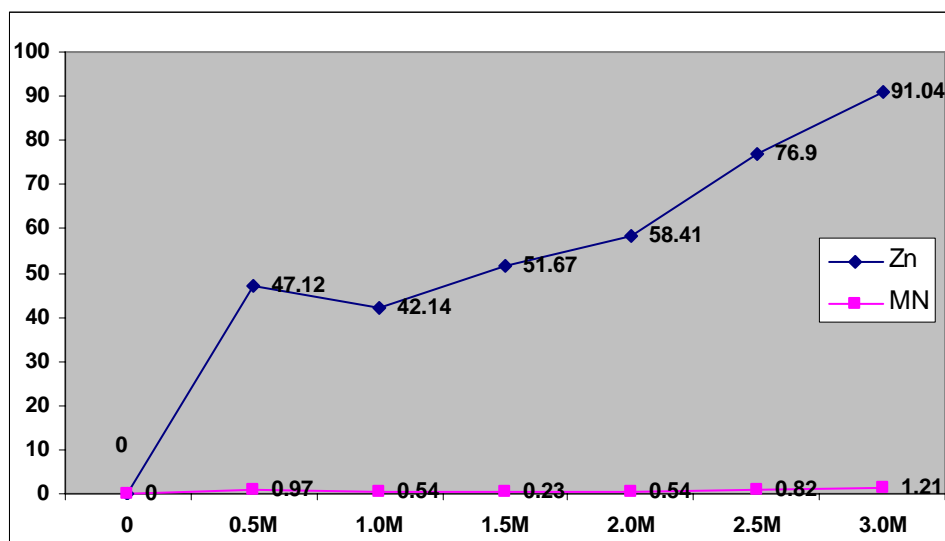
Percentages of \blacklozenge Zn and \blacksquare Mn solubilization from the dust of Zn-C dry cell, 3 days of leaching using H_2SO_4 . Batteries are broken and inner part of batteries were dismantled, ground, washed and dried. Slurry was stirred at 400rpm.

STR: SET 3

Ammonium carbonate leaching STR Set 2:	<p>2L reactor, Agitated at 400 rpm, D type batteries Zn-carbon batteries, internal portion manually exposed. Inner part of batteries were ground, sieved, washed and dried. Lixiviant solution leaching using $(\text{NH}_4)_2\text{CO}_3$:</p> <p>Condition of leaching</p> <p>1: Constant parameters: Pulp densities: 10%, Temperatures: 20°C, Duration 3 days Variable : $(\text{NH}_4)_2\text{CO}_3$ concentration: 0.5M, 1 M, 1.5 M, 2.0 M, 2.5 M and 3.0 M</p> <p>2: Constant parameters: Pulp densities: 10%, $(\text{NH}_4)_2\text{CO}_3$ concentration 3M, Duration 3 days Variable : Temperatures: 20°C, 40°C, 50°C, 60°C, 70°C, 80°C</p> <p>3: Constant parameters: $(\text{NH}_4)_2\text{CO}_3$ concentration 3 M, Temperatures: 20°C, Duration 3 days Variable : Pulp densities: 5%, 10%, 15%, 20%, 50%, 100%</p> <p>4: Constant parameters: $(\text{NH}_4)_2\text{CO}_3$ concentration 3.0 M, Temperatures: 20°C, Pulp densities: 10%, Variable : Duration: 4hrs, 8 hrs, 12 hrs, 24hrs, 48hrs and 36hrs.</p>
---	---

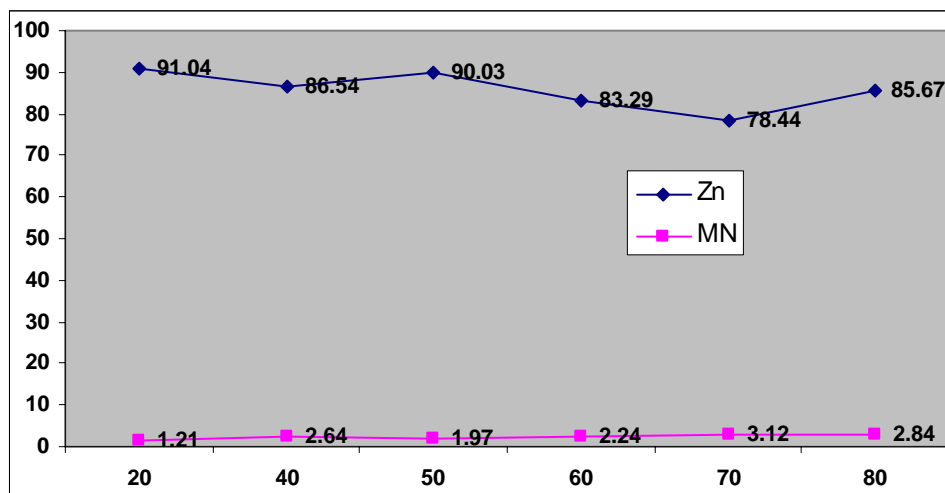
Set 1: Lixiviant solution leaching using $(\text{NH}_4)_2\text{CO}_3$

Set 3A: Metal extraction from Zn-C batteries dust (inner part) for 3 days. Batteries dust were ground, dismantled, washed and dried. Lixiviant solution leaching using different concentration of $(\text{NH}_4)_2\text{CO}_3$



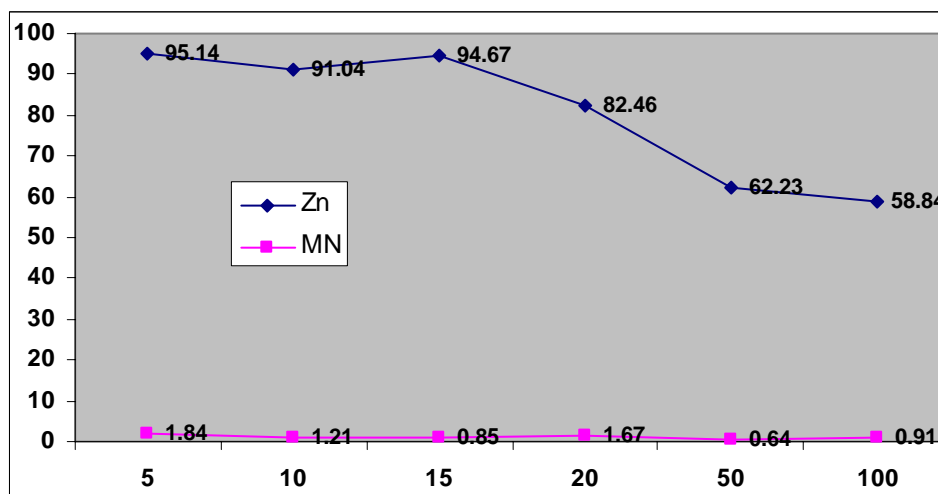
Percentages of \blacklozenge Zn and \blacksquare Mn solubilization from the dust of Zn-C dry cell, 3 days of leaching using different concentrations of $(\text{NH}_4)_2\text{CO}_3$. Batteries are broken and inner part of batteries were dismantled, ground, washed and dried. Slurry was stirred at 400rpm.

Set 3B: Metal extraction from Zn-C batteries dust (inner part) for 3 days. Batteries dust were ground, dismantled, washed and dried. $(\text{NH}_4)_2\text{CO}_3$ leaching at different temperature



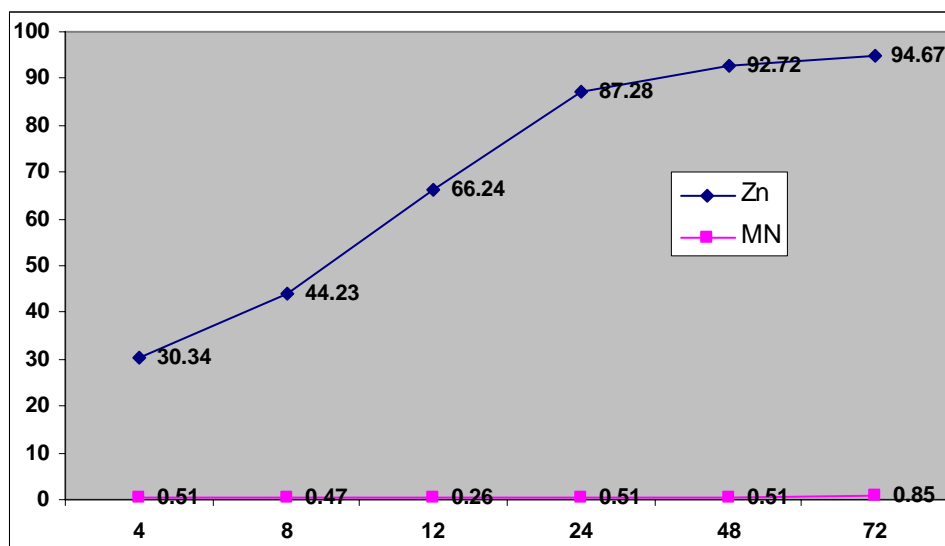
Percentages of \blacklozenge Zn and \blacksquare Mn solubilization from the dust of Zn-C dry cell, 3 days of leaching using HCl at different temperatures. Batteries are broken and inner part of batteries were dismantled, ground, washed and dried. Slurry was stirred at 400rpm.

Set 3C: Metal extraction from Zn-C batteries dust (inner part) for 3 days. Batteries dust were ground, dismantled, washed and dried. Lixiviant solution leaching at different ratios of solid/solution.



Percentages of \blacklozenge Zn and \blacksquare Mn solubilization from the dust of Zn-C dry cell, 3 days of leaching at different ratios of solid/solution. Batteries are broken and inner part of batteries were dismantled, ground, washed and dried. Slurry was stirred at 400rpm.

Set 3D: Metal extraction from Zn-C batteries dust (inner part) for 3 days. Batteries dust were ground, dismantled, washed and dried. Lixiviant solution leaching using $(\text{NH}_4)_2\text{CO}_3$



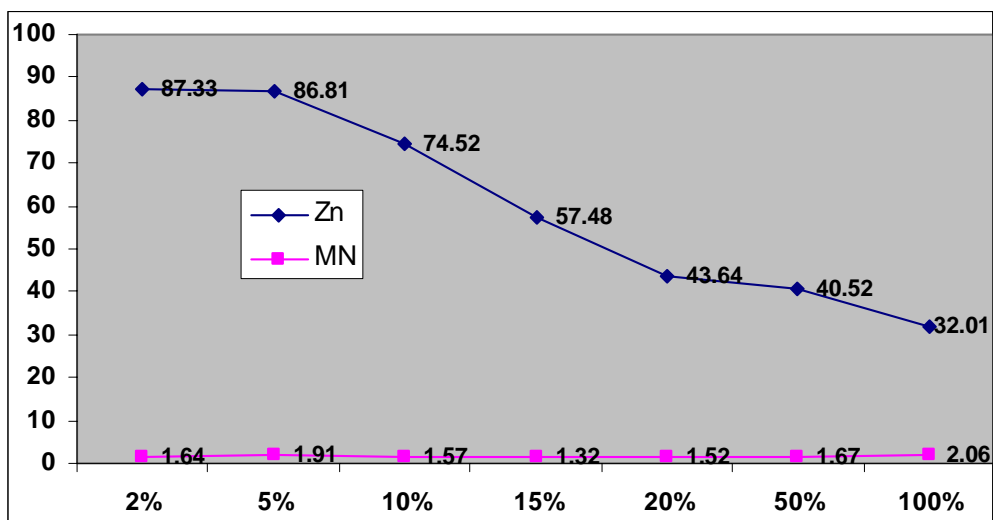
Percentages of \blacklozenge Zn and \blacksquare Mn solubilization from the dust of Zn-C dry cell, 3 days of leaching using $(\text{NH}_4)_2\text{CO}_3$. Batteries are broken and inner part of batteries were dismantled, ground, washed and dried. Slurry was stirred at 400rpm.

STR: SET 4

STR Set 4: <i>Thiobacillus thiooxidans</i> leaching	<p>2L reactor, Agitated at 400 rpm, D type batteries Zn-carbon batteries, internal portion manually exposed. Inner part of batteries were ground, sieved, washed and dried. Lixiviant solution leaching using culture of <i>Thiobacillus thiooxidans</i> :</p> <p>Condition of leaching</p> <p>1: Constant parameters: <i>Thiobacillus thiooxidans</i>, Temperatures: 30°C, Duration 5 days Variable : Pulp densities: 2%, 5%,10%,15%,20%, 50%, 100%</p> <p>2: Constant parameters: <i>Thiobacillus thiooxidans</i> , Temperatures: 30°C, Pulp densities: 15%, Variable : Duration: 4hrs, 8 hrs, 12 hrs, 24hrs, 48hrs, 72hrs, 84hrs and 120hrs.</p>
---	---

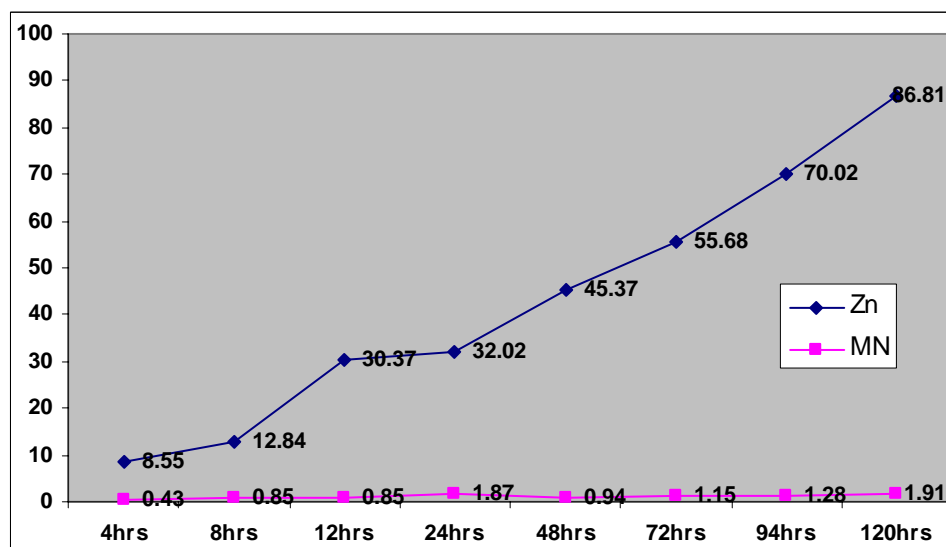
Set 4: Lixiviant solution leaching using *Thiobacillus thiooxidans*

Set 4A: Metal extraction from Zn-C batteries dust (inner part) for 5 days. Batteries dust were ground, dismantled, washed and dried. Lixiviant solution leaching at different ratio of solid/solution.



Percentages of ◆ Zn and ■ Mn solubilization from the dust of Zn-C dry cell, 5 days of leaching at different ratios of solid/solution. Batteries are broken and inner part of batteries were dismantled, ground, washed and dried. Slurry was stirred at 400rpm.

Set 4B: Metal extraction from Zn-C batteries dust (inner part) for 5 days. Batteries dust were ground, dismantled, washed and dried. Lixiviant solution leaching using *TT*.



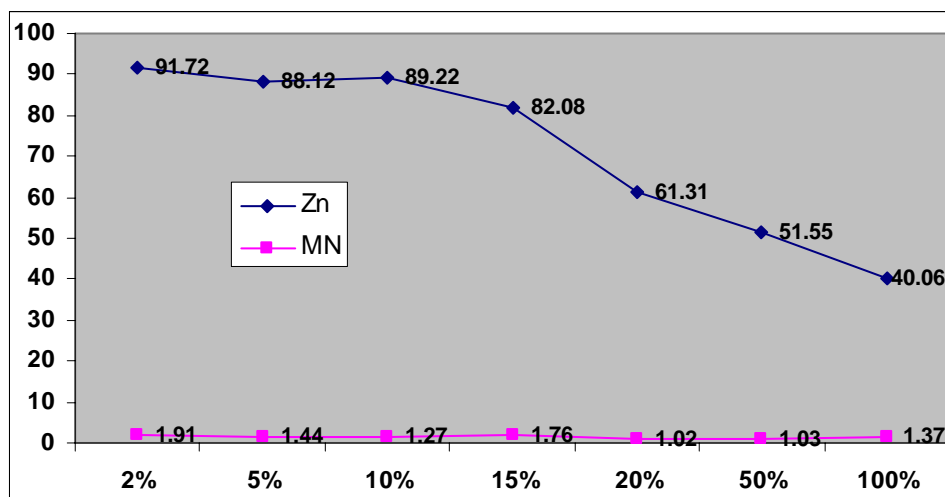
Percentages of ◆ Zn and ■ Mn solubilization from the dust of Zn-C dry cell, 5 days of leaching using *TT*. Batteries are broken and inner part of batteries were dismantled, ground, washed and dried. Slurry was stirred at 400rpm.

STR: SET 5

STR Set 4: <i>Acidianus Brierleyi</i> leaching	2L reactor, Agitated at 400 rpm, D type batteries Zn-carbon batteries, internal portion manually exposed. Inner part of batteries were ground, sieved, washed and dried. Lixiviant solution leaching using culture of <i>Acidianus Brierleyi</i> : Condition of leaching 1: Constant parameters: <i>Acidianus brierleyi</i> , Temperatures: 70°C, Duration 5 days Variable : Pulp densities: 2%, 5%, 10%, 15%, 20%, 50%, 100% 2: Constant parameters: Temperatures: 50°C, Pulp densities: 15%, Variable : Duration: 4hrs, 8 hrs, 12 hrs, 24hrs, 48hrs, 72hrs, 84hrs and 120hrs.
--	--

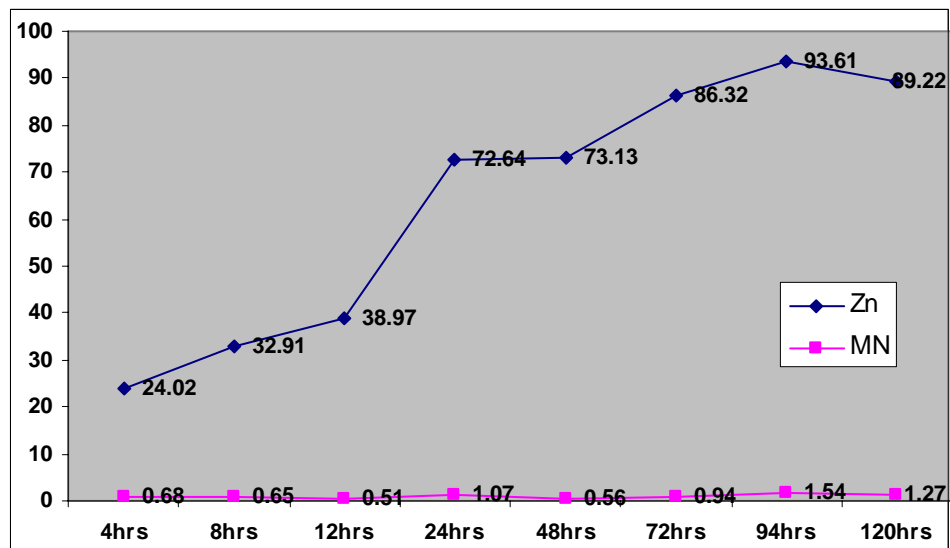
Set 5A: Lixiviant solution leaching using *Acidianus brierleyi*

Set 5A: Metal extraction from Zn-C batteries dust (inner part) for 5 days. Batteries dust were ground, dismantled, washed and dried. Lixiviant solution leaching at different ratios of solid/solution.



Percentages of ◆ Zn and ■ Mn solubilization from the dust of Zn-C dry cell, 5 days of leaching at different ratios of solid/solution. Batteries are broken and inner part of batteries were dismantled, ground, washed and dried. Slurry was stirred at 400rpm.

Set 5B: Metal extraction from Zn-C batteries dust (inner part) for 5 days. Batteries dust were ground, dismantled, washed and dried. Lixiviant solution leaching using AB.



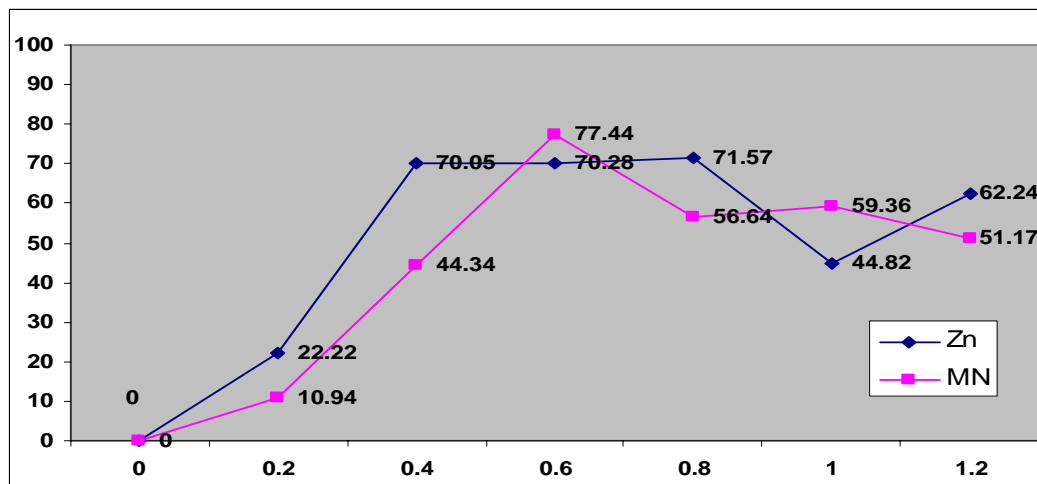
Percentages of \blacklozenge Zn and \blacksquare Mn solubilization from the dust of Zn-C dry cell, 5 days of leaching using AB. Batteries are broken and inner part of batteries were dismantled, ground, washed and dried. Slurry was stirred at 400rpm.

STR: SET 6

STR Set 6: $\text{Fe}_3(\text{SO}_4)_2$ leaching	<p>2L reactor, Agitated at 400 rpm, D type batteries Zn-carbon batteries, internal portion manually exposed. Inner part of batteries were ground, sieved, washed and dried. Lixiviant solution leaching using $\text{Fe}_3(\text{SO}_4)_2$:</p> <p>Condition of leaching</p> <p>1: Constant parameters: Pulp densities: 10%, Temperatures: 20°C, Duration 3 days Variable : $\text{Fe}_3(\text{SO}_4)_2$ concentration: 0.2M, 0.4M, 0.6M, 0.8M, 1.0M and 1.5M</p> <p>2: Constant parameters: Pulp densities: 10%, $\text{Fe}_3(\text{SO}_4)_2$ concentration 0.5M, Duration 3 days Variable : Temperatures: 20°C, 40°C, 50°C, 60°C, 70°C, 80°C</p> <p>3: Constant parameters: $\text{Fe}_3(\text{SO}_4)_2$ concentration 0.5M, Temperatures: 50°C, Duration 3 days Variable : Pulp densities: 5%, 10%, 15%, 20%, 50%, 100%</p> <p>4: Constant parameters: $\text{Fe}_3(\text{SO}_4)_2$ concentration 0.5M, Temperatures: 50°C, Pulp densities: 15%, Variable : Duration: 4hrs, 8 hrs, 12 hrs, 24hrs, 48hrs and 36hrs.</p>
---	--

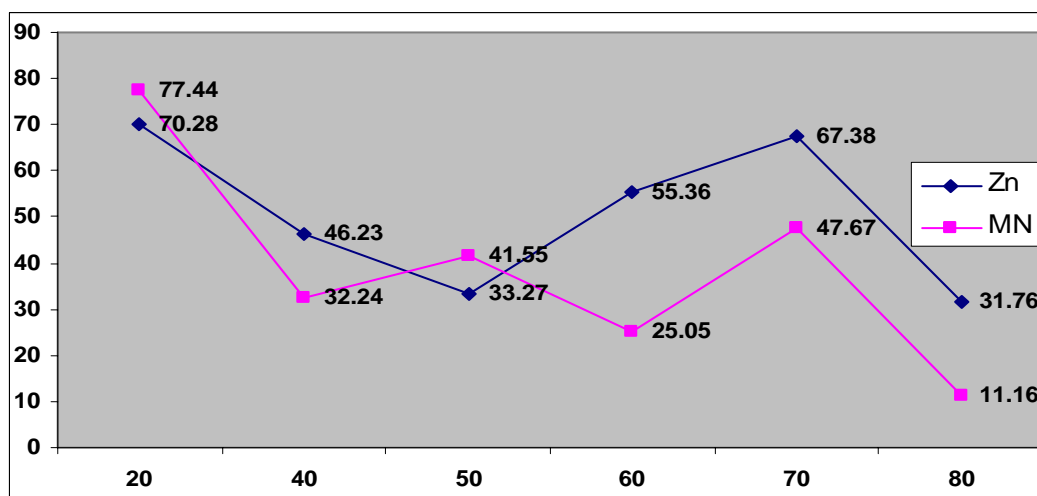
Set 6: Lixiviant solution leaching using $\text{Fe}_3(\text{SO}_4)_2$

Set 6A: Metal extraction from Zn-C batteries dust (inner part) for 3 days. Batteries dust were ground, dismantled, washed and dried. Lixiviant solution leaching using different concentrations of $\text{Fe}_3(\text{SO}_4)_2$.



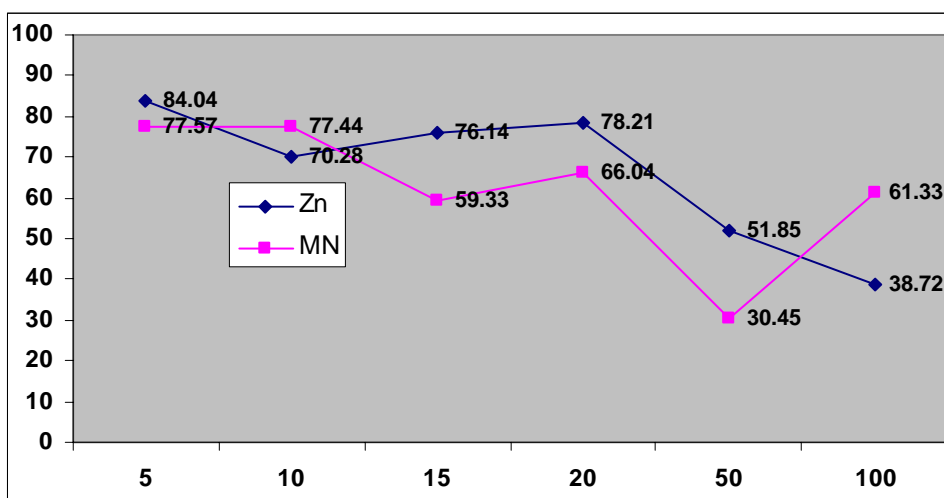
Percentages of \blacklozenge Zn and \blacksquare Mn solubilization from the dust of Zn-C dry cell, 3 days of leaching using different concentrations of $\text{Fe}_3(\text{SO}_4)_2$. Batteries are broken and inner part of batteries were dismantled, ground, washed and dried. Slurry was stirred at 400rpm.

Set 6B: Metal extraction from Zn-C batteries dust (inner part) for 3 days. Batteries dusts were ground, dismantled, washed and dried. Lixiviant solution leaching at different temperatures.



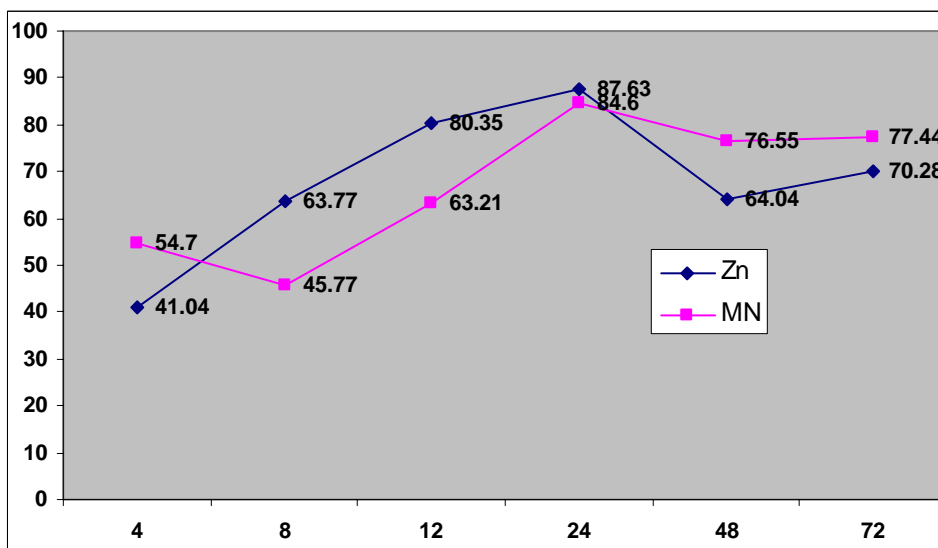
Percentages of \blacklozenge Zn and \blacksquare Mn solubilization from the dust of Zn-C dry cell, 3 days of leaching at different temperatures. Batteries are broken and inner part of batteries were dismantled, ground, washed and dried. Slurry was stirred at 400rpm.

Set 6C: Metal extraction from Zn-C batteries dust (inner part) for 3 days. Batteries dust were ground, dismantled, washed and dried. Lixiviant solution leaching at different ratios of solid/solution.



Percentages of \blacklozenge Zn and \blacksquare Mn solubilization from the dust of Zn-C dry cell, 3 days of leaching at different ratios of solid/solution. Batteries are broken and inner part of batteries were dismantled, ground, washed and dried. Slurry was stirred at 400rpm.

Set 7D: Metal extraction from Zn-C batteries dust (inner part) for 3 days. Batteries dust were ground, dismantled, washed and dried. Lixiviant solution leaching using $\text{Fe}_3(\text{SO}_4)_2$.



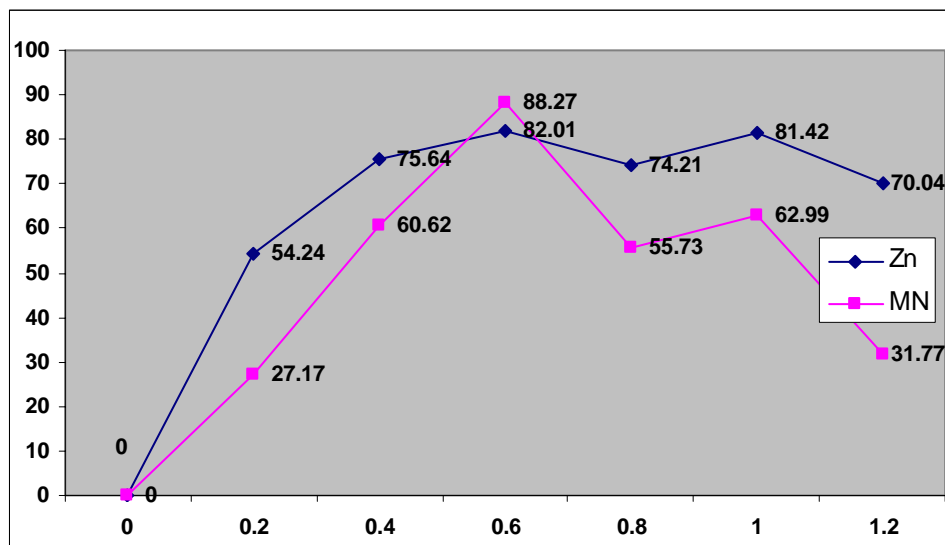
Percentages of \blacklozenge Zn and \blacksquare Mn solubilization from the dust of Zn-C dry cell, 3 days of leaching using $\text{Fe}_3(\text{SO}_4)_2$. Batteries are broken and inner part of batteries were dismantled, ground, washed and dried. Slurry were stirred at 400rpm.

STR: SET 7

STR Set 6: Fe ₃ Cl leaching	<p>2L reactor, Agitated at 400 rpm, D type batteries Zn-carbon batteries, internal portion manually exposed. Inner part of batteries were ground, sieved, washed and dried. Lixiviant solution leaching using Fe₃Cl:</p> <p>Condition of leaching</p> <p>1: Constant parameters: Pulp densities: 10%, Temperatures: 20°C, Duration 3 days Variable : Fe₃Cl concentration: 0.2M, 0.4M, 0.6M, 0.8M, 1.0M and 1.5M</p> <p>2: Constant parameters: Pulp densities: 10%, Fe₃Cl concentration 0.5M, Duration 3 days Variable : Temperatures: 20°C,40°C, 50°C, 60°C, 70°C, 80°C</p> <p>3: Constant parameters: Fe₃Cl concentration 0.5M ,Temperatures: 50°C, Duration 3 days Variable : Pulp densities: 5%,10%,15%,20%, 50%, 100%</p> <p>4: Constant parameters: Fe₃Cl concentration 0.5M ,Temperatures: 50°C, Pulp densities: 15%, Variable : Duration: 4hrs, 8 hrs, 12 hrs, 24hrs, 48hrs and 36hrs.</p>
---	---

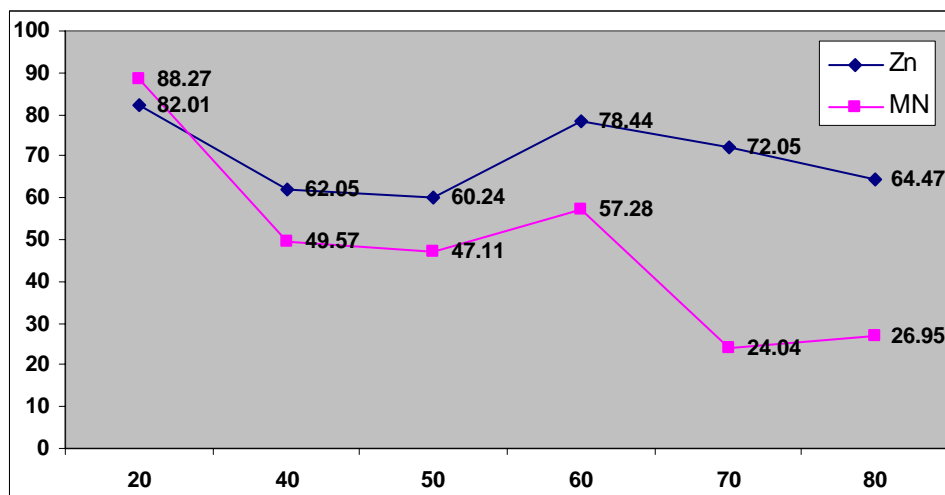
Set 7: Lixiviant solution leaching using FeCl₃

Set 7A: Metal extraction from Zn-C batteries dust (inner part) for 3 days. Batteries dust were ground, dismantled, washed and dried. Lixiviant solution leaching using different concentration of FeCl₃.



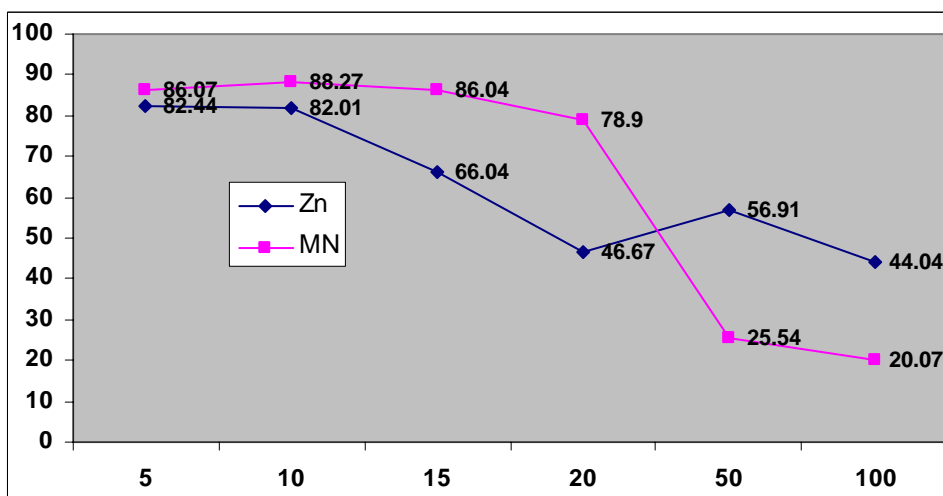
Percentages of ◆ Zn and ■ Mn solubilization from the dust of Zn-C dry cell, 3 days of leaching using different concentration of FeCl₃. Batteries are broken and inner part of batteries were dismantled, ground, washed and dried. Slurry was stirred at 400rpm.

Set 7B: Metal extraction from Zn-C batteries dust (inner part) for 3 days. Batteries dusts were ground, dismantled, washed and dried. Lixiviant solution leaching at different temperatures.



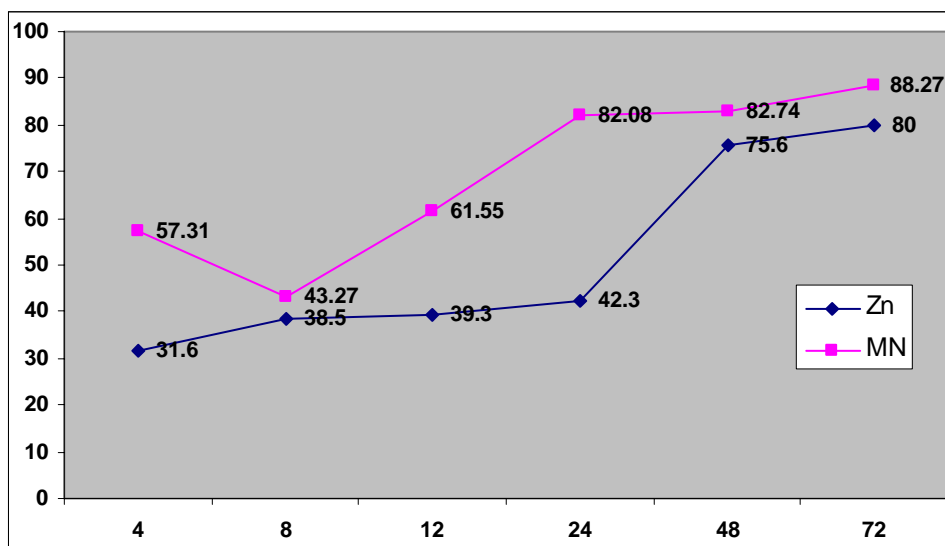
Percentages of \blacklozenge Zn and \blacksquare Mn solubilization from the dust of Zn-C dry cell, 3 days of leaching at different temperatures. Batteries are broken and inner part of batteries were dismantled, ground, washed and dried. Slurry was stirred at 400rpm.

Set 7C: Metal extraction from Zn-C batteries dust (inner part) for 3 days. Batteries dust were ground, dismantled, washed and dried. Lixiviant solution leaching at different ratio of solid/solution.



Percentages of \blacklozenge Zn and \blacksquare Mn solubilization from the dust of Zn-C dry cell, 3 days of leaching at different ratios of solid/solution. Batteries are broken and inner part of batteries were dismantled, ground, washed and dried. Slurry was stirred at 400rpm.

Set 7D: Metal extraction from Zn-C batteries dust (inner part) for 3 days. Batteries dust were ground, dismantled, washed and dried. Lixiviant solution leaching using Fe_3Cl .



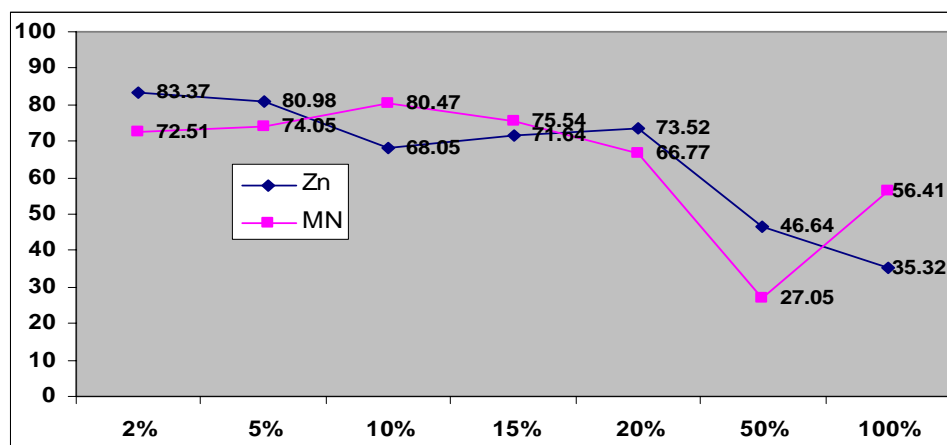
Percentages of \blacklozenge Zn and \blacksquare Mn solubilization from the dust of Zn-C dry cell, 3 days of leaching using $\text{Fe}_3(\text{SO}_4)_2$. Batteries are broken and inner part of batteries were dismantled, ground, washed and dried. Slurry was stirred at 400rpm.

STR: SET 8

STR Set 8: Mix culture of <i>Thiobacillus ferrooxidans</i> (TF) and <i>Leptospirillum ferrooxidans</i> (LF) at ratio: 1:1 leaching	<p>2L reactor, Agitated at 400 rpm, D type batteries Zn-carbon batteries, internal portion manually exposed. Inner part of batteries were ground, sieved, washed and dried. Lixiviant solution leaching using mix culture of <i>Thiobacillus ferrooxidans</i> (TF) and <i>Leptospirillum ferrooxidans</i>(LF) at ratio: 1:1:</p> <p>Condition of leaching</p> <p>1: Constant parameters: TF:LF; 1;1 ,Temperatures: 30°C, Duration 5 days Variable : Pulp densities: 2%, 5%,10%,15%,20%, 50%, 100%</p> <p>2: Constant parameters:Temperatures: 30°C, Pulp densities: 10%, Variable : Duration: 4hrs, 8 hrs, 12 hrs, 24hrs, 48hrs, 72hrs, 84hrs and 120hrs.</p>
--	--

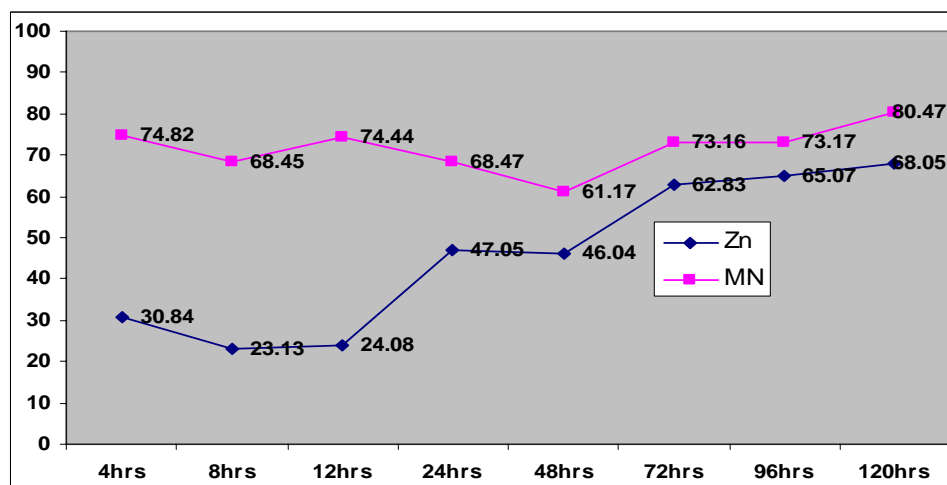
Set 8: Lixiviant solution leaching using mix culture of *Thiobacillus Ferroxidans* (TF) and *Leptospirillum Ferroxidans*(LF) at ratio: 1:1

Set 8A: Metal extraction from Zn-C batteries dust (inner part) for 5 days. Batteries dust were ground, dismantled, washed and dried. Lixiviant solution leaching at different ratios of solid/solution.



Percentages of \blacklozenge Zn and \blacksquare Mn solubilization from the dust of Zn-C dry cell, 5 days of leaching at different ratios of solid/solution. Batteries are broken and inner part of batteries were dismantled, ground, washed and dried. Slurry was stirred at 400rpm.

Set 8B: Metal extraction from Zn-C batteries dust (inner part) for 5 days. Batteries dust were ground, dismantled, washed and dried. Lixiviant solution leaching using $TF:LF; 1;1$



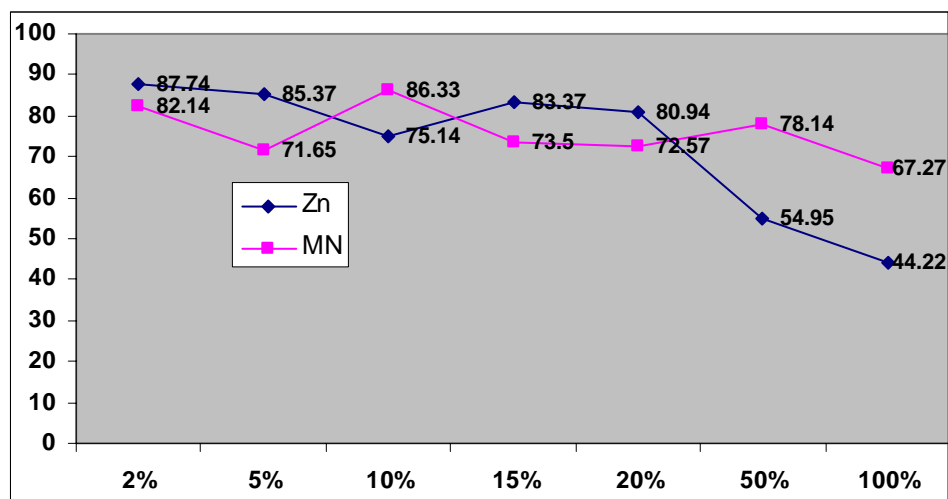
Percentages of \blacklozenge Zn and \blacksquare Mn solubilization from the dust of Zn-C dry cell, 5 days of leaching using TF . Batteries are broken and inner part of batteries were dismantled, ground, washed and dried. Slurry was stirred at 400rpm.

STR: SET 9

STR Set 9: <i>SL5B</i> leaching	<p>2L reactor, Agitated at 400 rpm, D type batteries Zn-carbon batteries, internal portion manually exposed. Inner part of batteries were ground, sieved, washed and dried. Lixiviant solution leaching using culture of <i>SL5B</i>:</p> <p>Condition of leaching</p> <p>1: Constant parameters: <i>SL5B</i>, Temperatures: 70°C, Duration 5 days Variable : Pulp densities: 2%, 5%, 10%, 15%, 20%, 50%, 100%</p> <p>2: Constant parameters: Temperatures: 70°C, Pulp densities: 15%, Variable : Duration: 4hrs, 8 hrs, 12 hrs, 24hrs, 48hrs, 72hrs, 84hrs and 120hrs.</p>
---------------------------------------	---

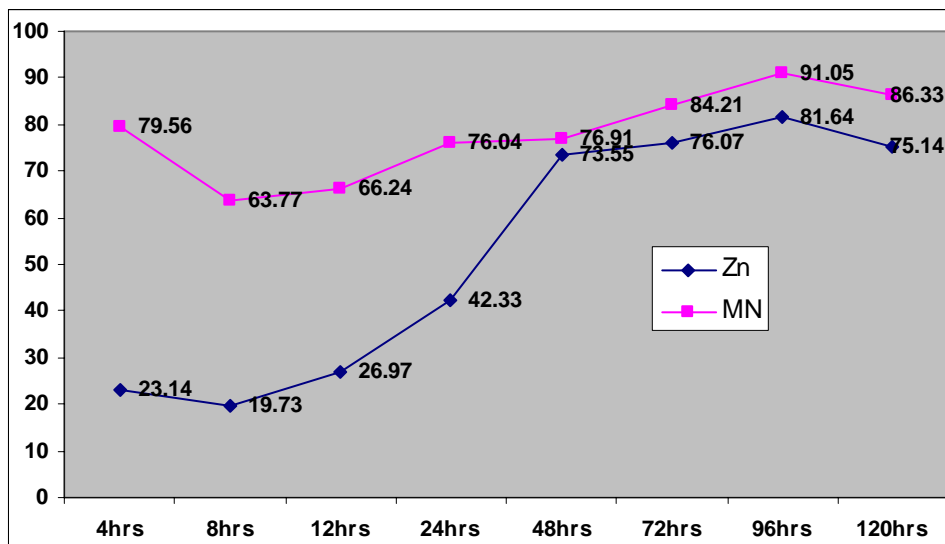
Set 9: Lixiviant solution leaching using culture *SL5B*

Set 9A: Metal extraction from Zn-C batteries dust (inner part) for 5 days. Batteries dust were ground, dismantled, washed and dried. Lixiviant solution leaching at different ratios of solid/solution.



Percentages of ◆ Zn and ■ Mn solubilization from the dust of Zn-C dry cell, 5 days of leaching at different ratios of solid/solution. Batteries are broken and inner part of batteries were dismantled, ground, washed and dried. Slurry was stirred at 400rpm.

Set 9B: Metal extraction from Zn-C batteries dust (inner part) for 5 days. Batteries dust were ground, dismantled, washed and dried. Lixiviant solution leaching using *SL5B*.



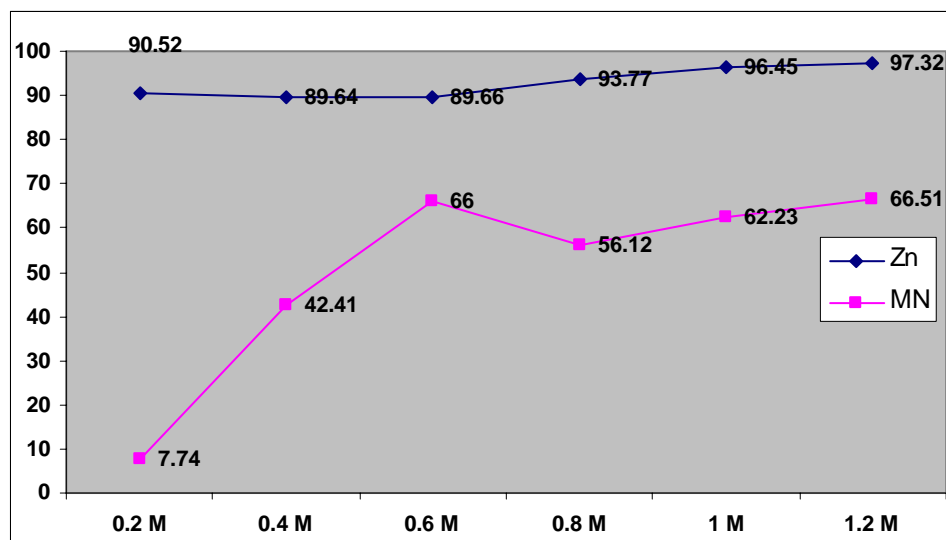
Percentages of \blacklozenge Zn and \blacksquare Mn solubilization from the dust of Zn-C dry cell, 5 days of leaching using *SL5B*. Batteries are broken and inner part of batteries were dismantled, ground, washed and dried. Slurry was stirred at 400rpm.

STR: SET 10

Roasted, H_2SO_4 leaching STR Set 10:	<p>2L reactor, Agitated at 400 rpm, D type batteries Zn-carbon batteries, internal portion manually exposed. Inner part of batteries were ground, sieved, washed and dried. Sample then roasted on the hot plate (max current) Lixiviant solution leaching using H_2SO_4:</p> <p>Condition of leaching</p> <p>1: Constant parameters: Pulp densities: 10%, Temperatures: 20°C, Duration 3 days, Sample roasted, 24hrs. Variable : H_2SO_4 concentration: 0.2M, 0.4M, 0.6M, 0.8M, 1.0M and 1.2M</p> <p>2: Constant parameters: Pulp densities: 10%, H_2SO_4 concentration 0.2M, Duration 3 days Variable : Roasting duration: 2hrs, 4hrs, 6hrs, 8hrs, 12hrs and 24hrs</p> <p>3: Constant parameters: H_2SO_4 conc: 0.2M ,Temperatures: 20°C, Duration 3 days, Sample roasted 4hrs Variable : Pulp densities: 5%,10%,15%,20%, 50%, 100%</p> <p>4: Constant parameters: H_2SO_4 conc: 0.2M ,Temperatures: 20°C, Pulp densities 10%, Sample roasted 4hrs Variable : Duration: 4hrs, 8 hrs, 12 hrs, 24hrs, 48hrs and 36hrs.</p>
--	--

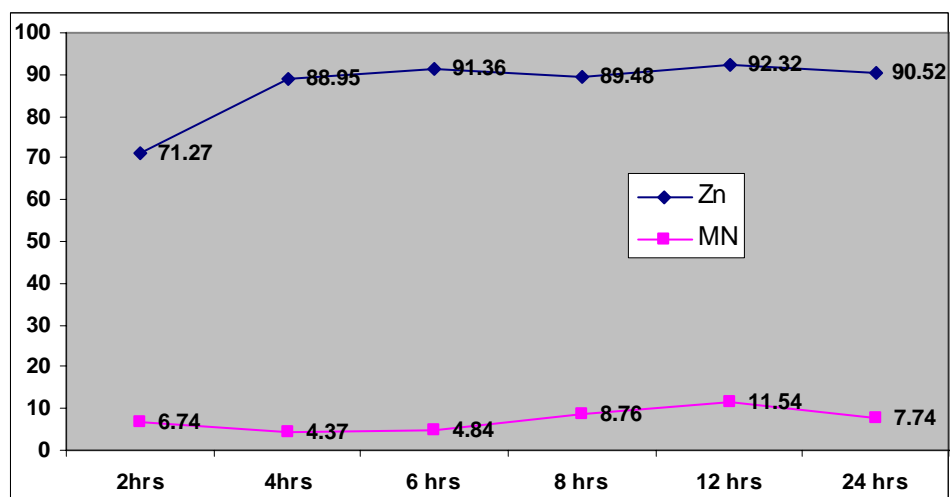
Set 10: Roasted batteries, Lixiviant solution leaching using H_2SO_4 .

Set 10A: Metal extraction from Zn-C batteries dust (inner part) for 3 days. Batteries dust were ground, dismantled, washed and dried. Sample then roasted on the hot plate (max current). Lixiviant solution leaching using different concentrations of H_2SO_4 .



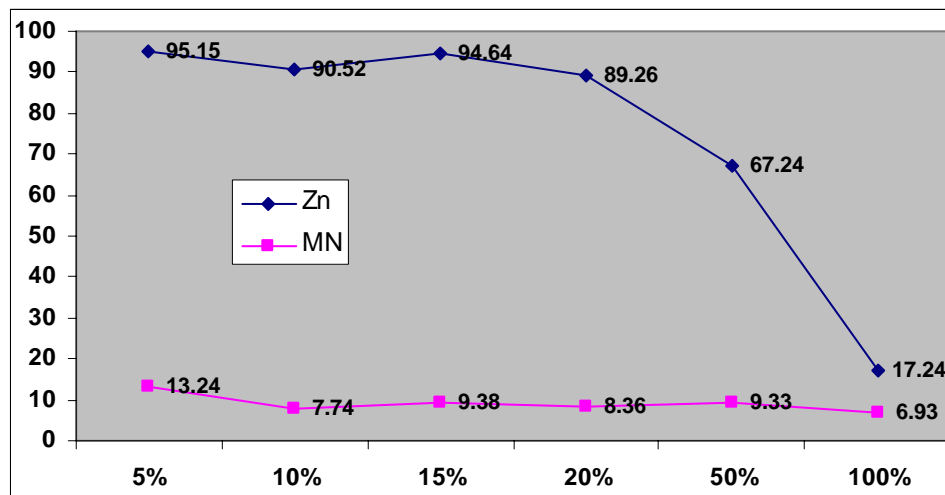
Percentages of \blacklozenge Zn and \blacksquare Mn solubilization from the dust of Zn-C dry cell, 3 days of leaching using different concentrations of H_2SO_4 . Batteries are broken and inner part of batteries were dismantled, ground, washed and dried. Sample then roasted on the hot plate (max current) Slurry was stirred at 400rpm.

Set 10B: Metal extraction from Zn-C batteries dust (inner part) for 3 days. Batteries dusts were ground, dismantled, washed and dried. Sample then roasted on the hot plate (max current). Leaching using different roasting duration of sample.



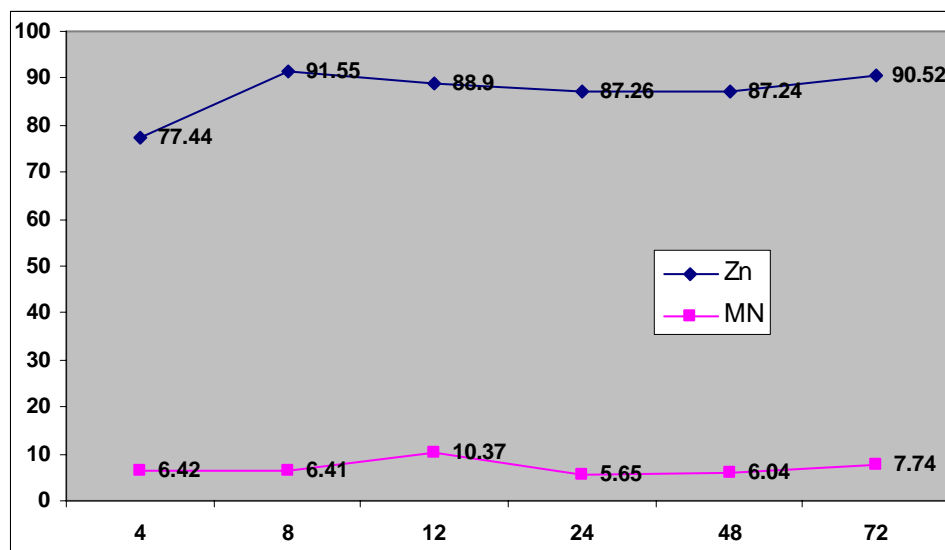
Percentages of \blacklozenge Zn and \blacksquare Mn solubilization from the dust of Zn-C dry cell, 3 days of leaching using different roasting durations of sample. Batteries are broken and inner part of batteries were dismantled, ground, washed and dried. Sample then roasted on the hot plate (max current) Slurry was stirred at 400rpm.

Set 10C: Metal extraction from Zn-C batteries dust (inner part) for 3 days. Batteries dust were ground, dismantled, washed and dried. Sample then roasted on the hot plate (max current). Lixiviant solution leaching at different ratios of solid/solution.



Percentages of \blacklozenge Zn and \blacksquare Mn solubilization from the dust of Zn-C dry cell, 3 days of leaching at different ratios of solid/solution. Batteries are broken and inner part of batteries were dismantled, ground, washed and dried. Sample then roasted on the hot plate (max current). Slurry was stirred at 400rpm.

Set 10D: Metal extraction from Zn-C batteries dust (inner part) for 3 days. Batteries dust were ground, dismantled, washed and dried. Sample then roasted on the hot plate (max current). Lixiviant solution leaching using H_2SO_4 .



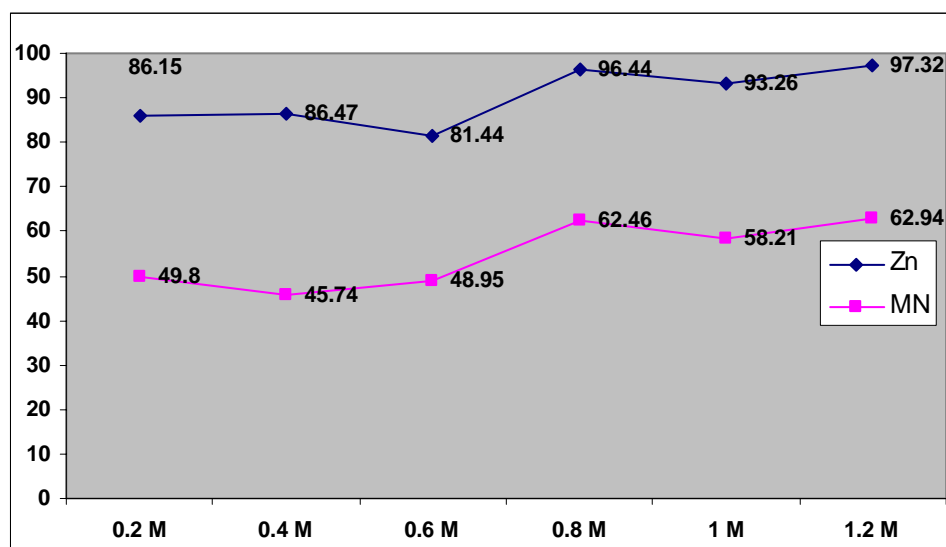
Percentages of \blacklozenge Zn and \blacksquare Mn solubilization from the dust of Zn-C dry cell, 3 days of leaching using H_2SO_4 . Batteries are broken and inner part of batteries was dismantled ground, washed and dried. Sample then roasted on the hot plate (max current). Slurry was stirred at 400rpm.

STR: SET 11

Roasted, HCl leaching	<p>2L reactor, Agitated at 400 rpm, D type batteries Zn-carbon batteries, internal portion manually exposed. Inner part of batteries were ground, sieved, washed and dried. Sample then roasted on the hot plate (max current) Lixiviant solution leaching using HCl:</p> <p>Condition of leaching</p> <p>1: Constant parameters: Pulp densities: 10%, Temperatures: 20°C, Duration 3 days, Sample roasted, 24hrs. Variable : HCl concentration: 0.2M, 0.4M, 0.6M, 0.8M, 1.0M and 1.2M</p> <p>2: Constant parameters: Pulp densities: 10%, HCl concentration 0.4M, Duration 3 days Variable : Roasting duration: 2hrs, 4hrs, 6hrs, 8hrs, 12hrs and 24hrs</p> <p>3: Constant parameters: HCl conc: 0.4M ,Temperatures: 20°C, Duration 3 days, Sample roasted 24hrs Variable : Pulp densities: 5%,10%,15%,20%, 50%, 100%</p> <p>4: Constant parameters: HCl conc: 0.4M ,Temperatures: 10°C, Pulp densities 10%, Sample roasted 24hrs Variable : Duration: 4hrs, 8 hrs, 12 hrs, 24hrs, 48hrs and 36hrs.</p>
-----------------------	---

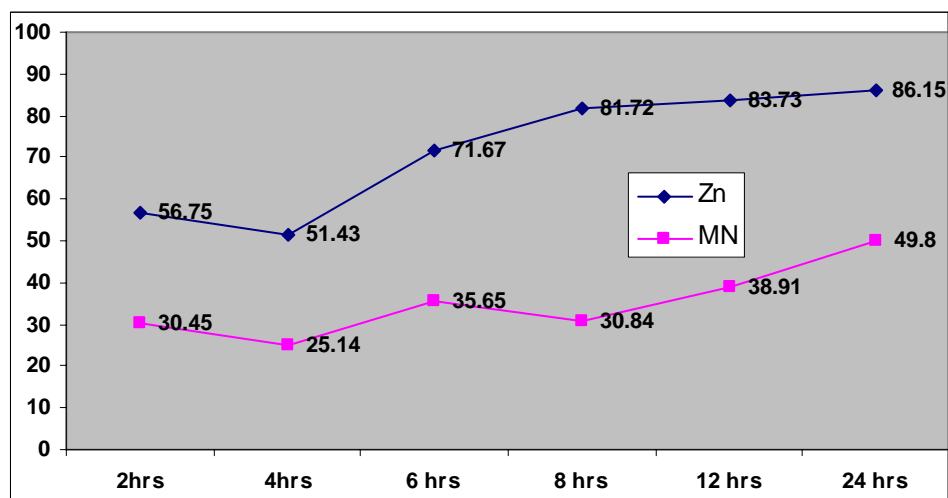
Set 11: Roasted batteries, Lixiviant solution leaching using HCl

Set 11A: Metal extraction from Zn-C batteries dust (inner part) for 3 days. Batteries dust were ground, dismantled, washed and dried. Sample then roasted on the hot plate (max current). Lixiviant solution leaching using different concentrations of HCl.



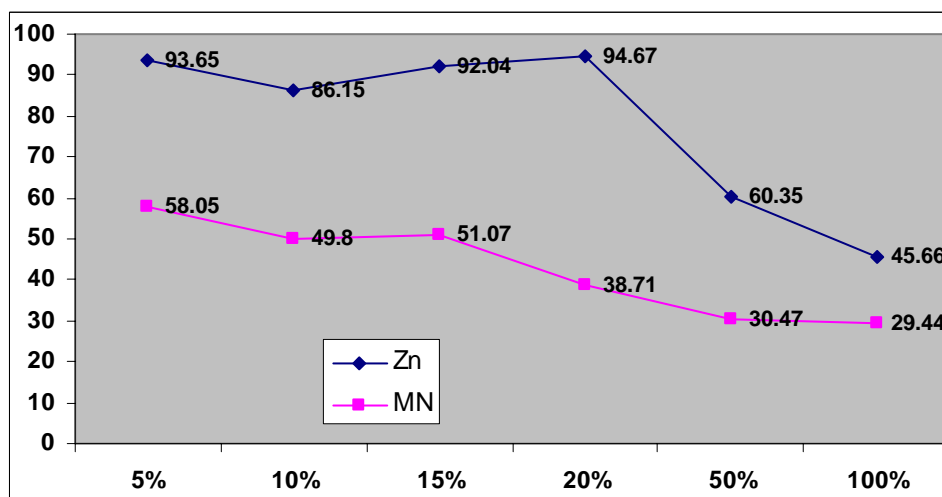
Percentages of ◆ Zn and ■ Mn solubilization from the dust of Zn-C dry cell, 3 days of leaching using different concentrations of HCl. Batteries are broken and inner part of batteries were dismantled, ground, washed and dried. Sample then roasted on the hot plate (max current) Slurry was stirred at 400rpm.

Set 11B: Metal extraction from Zn-C batteries dust (inner part) for 3 days. Batteries dusts were ground, dismantled, washed and dried. Sample then roasted on the hot plate (max current). Leaching using different roasting durations of sample.



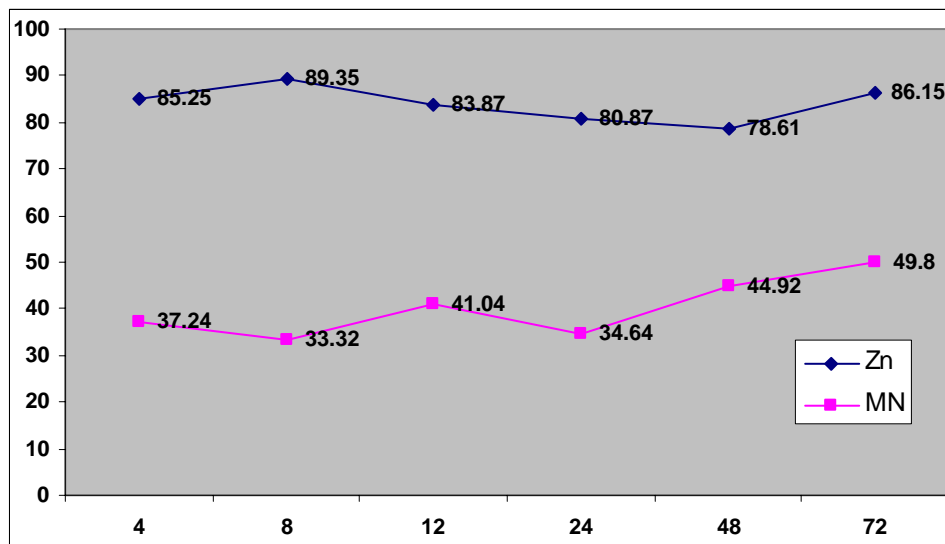
Percentages of \blacklozenge Zn and \blacksquare Mn solubilization from the dust of Zn-C dry cell, 3 days of leaching using different roasting durations of sample. Batteries are broken and inner part of batteries were dismantled, ground, washed and dried. Sample then roasted on the hot plate (max current) Slurry was stirred at 400rpm.

Set 11C: Metal extraction from Zn-C batteries dust (inner part) for 3 days. Batteries dust were ground, dismantled, washed and dried. Sample then roasted on the hot plate (max current). Lixiviant solution leaching at different ratios of solid/solution.



Percentages of \blacklozenge Zn and \blacksquare Mn solubilization from the dust of Zn-C dry cell, 3 days of leaching at different ratios of solid/solution. Batteries are broken and inner part of batteries were dismantled, ground, washed and dried. Sample then roasted on the hot plate (max current). Slurry was stirred at 400rpm.

Set 11D: Metal extraction from Zn-C batteries dust (inner part) for 3 days. Batteries dust were ground, dismantled, washed and dried. Sample then roasted on the hot plate (max current). Lixiviant solution leaching using $\text{Fe}_2(\text{SO}_4)_3$.



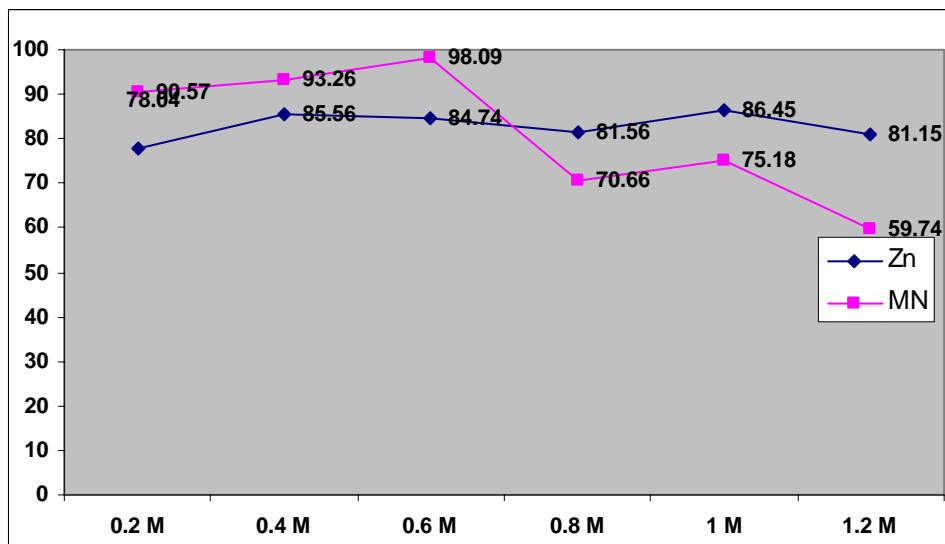
Percentages of \blacklozenge Zn and \blacksquare Mn solubilization from the dust of Zn-C dry cell, 3 days of leaching using HCl. Batteries are broken and inner part of batteries were dismantled, ground, washed and dried. Sample then roasted on the hot plate (max current). Slurry was stirred at 400rpm.

STR: SET 12

Roasted, $\text{Fe}_2(\text{SO}_4)_3$ leaching STR Set 12:	<p>2L reactor, Agitated at 400 rpm, D type batteries Zn-carbon batteries, internal portion manually exposed. Inner part of batteries were ground, sieved, washed and dried. Sample then roasted on the hot plate (max current) Lixiviant solution leaching using $\text{Fe}_2(\text{SO}_4)_3$:</p> <p>Condition of leaching</p> <p>1: Constant parameters: Pulp densities: 10%, Temperatures: 20°C, Duration 3 days, Sample roasted, 24hrs. Variable : H_2SO_4 concentration: 0.2M, 0.4M, 0.6M, 0.8M, 1.0M and 1.2M</p> <p>2: Constant parameters: Pulp densities: 10%, $\text{Fe}_2(\text{SO}_4)_3$ concentration 0.6M, Duration 3 days Variable : Roasting duration: 2hrs, 4hrs, 6hrs, 8hrs, 12hrs and 24hrs</p> <p>3: Constant parameters: $\text{Fe}_2(\text{SO}_4)_3$ conc: 0.6M ,Temperatures: 20°C, Duration 3 days, Sample roasted 24hrs Variable : Pulp densities: 5%,10%,15%,20%, 50%, 100%</p> <p>4: Constant parameters: $\text{Fe}_2(\text{SO}_4)_3$ conc: 0.6M ,Temperatures: 20°C, Pulp densities 10%, Sample roasted 24hrs Variable : Duration: 4hrs, 8 hrs, 12 hrs, 24hrs, 48hrs and 36hrs.</p>
---	--

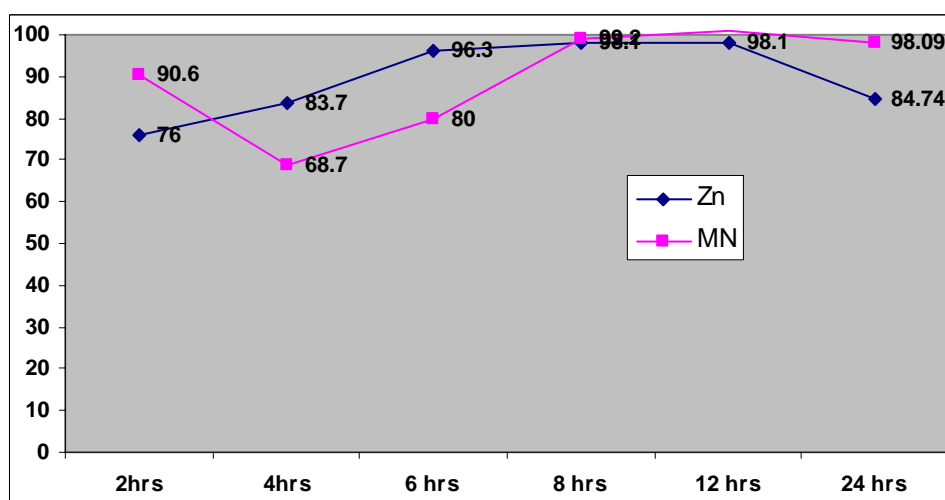
Set 12: Roasted batteries, Lixiviant solution leaching using $\text{Fe}_2(\text{SO}_4)_3$

Set 12A: Metal extraction from Zn-C batteries dust (inner part) for 3 days. Batteries dust were ground, dismantled, washed and dried. Sample then roasted on the hot plate (max current). Lixiviant solution leaching using different concentrations of $\text{Fe}_2(\text{SO}_4)_3$.



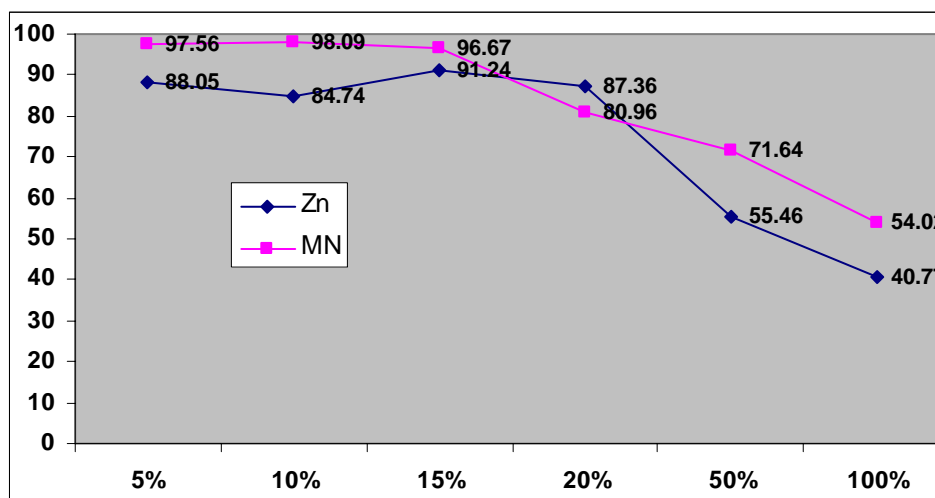
Percentages of \blacklozenge Zn and \blacksquare Mn solubilization from the dust of Zn-C dry cell, 3 days of leaching using different concentration of $\text{Fe}_2(\text{SO}_4)_3$. Batteries are broken and inner part of batteries were dismantled, ground, washed and dried. Sample then roasted on the hot plate (max current) Slurry was stirred at 400rpm.

Set 12B: Metal extraction from Zn-C batteries dust (inner part) for 3 days. Batteries dusts were ground, dismantled, washed and dried. Sample then roasted on the hot plate (max current). Leaching using different roasting durations of sample.



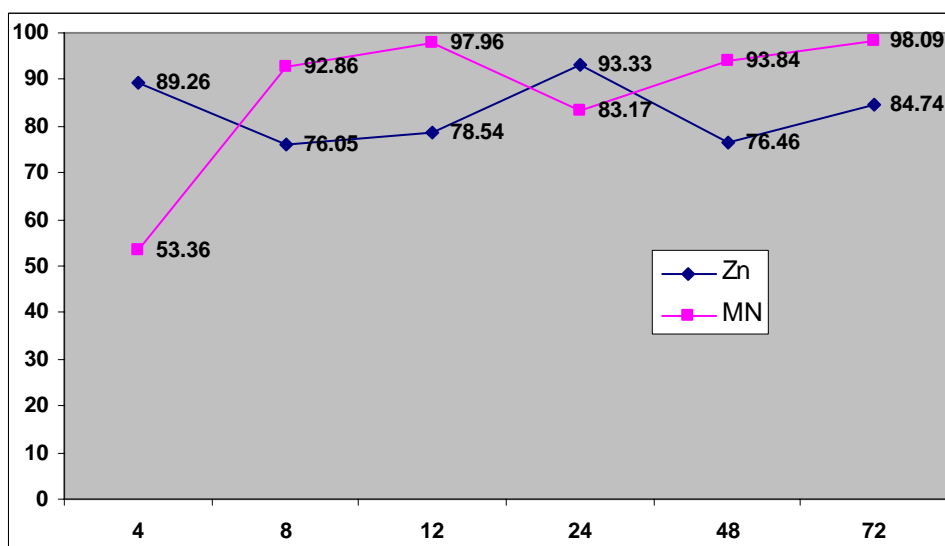
Percentages of \blacklozenge Zn and \blacksquare Mn solubilization from the dust of Zn-C dry cell, 3 days of leaching using different roasting duration of sample. Batteries are broken and inner part of batteries were dismantled, ground, washed and dried. Sample then roasted on the hot plate (max current) Slurry was stirred at 400rpm.

Set 12C: Metal extraction from Zn-C batteries dust (inner part) for 3 days. Batteries dust were ground, dismantled, washed and dried. Sample then roasted on the hot plate (max current). Lixiviant solution leaching at different ratios of solid/solution.



Percentages of \blacklozenge Zn and \blacksquare Mn solubilization from the dust of Zn-C dry cell, 3 days of leaching at different ratio of solid/solution. Batteries are broken and inner part of batteries were dismantled, ground, washed and dried. Sample then roasted on the hot plate (max current). Slurry was stirred at 400rpm.

Set 12D: Metal extraction from Zn-C batteries dust (inner part) for 3 days. Batteries dust were ground, dismantled, washed and dried. Sample then roasted on the hot plate (max current). Lixiviant solution leaching using $\text{Fe}_2(\text{SO}_4)_3$.



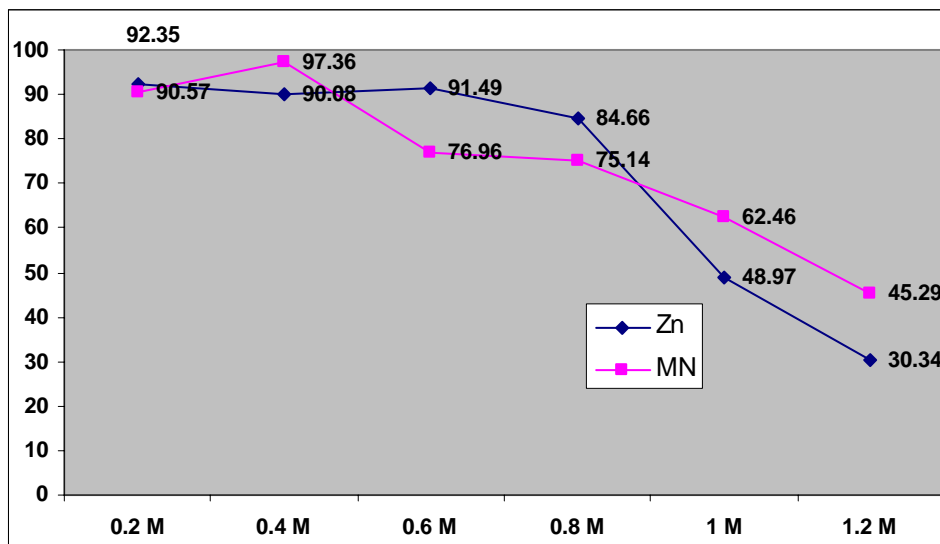
Percentages of \blacklozenge Zn and \blacksquare Mn solubilization from the dust of Zn-C dry cell, 3 days of leaching using $\text{Fe}_2(\text{SO}_4)_3$. Batteries are broken and inner part of batteries were dismantled, ground, washed and dried. Sample then roasted on the hot plate (max current). Slurry was stirred at 400rpm.

STR: SET 13

STR Set 13: Roasted, FeCl ₃ leaching	<p>2L reactor, Agitated at 400 rpm, D type batteries Zn-carbon batteries, internal portion manually exposed. Inner part of batteries were ground, sieved, washed and dried. Sample then roasted on the hot plate (max current) Lixiviant solution leaching using FeCl₃:</p> <p>Condition of leaching</p> <p>1: Constant parameters: Pulp densities: 10%, Temperatures: 20°C, Duration 3 days, Sample roasted, 24hrs. Variable : FeCl₃ concentration: 0.2M, 0.4M, 0.6M, 0.8M, 1.0M and 1.2M</p> <p>2: Constant parameters: Pulp densities: 10%, FeCl₃ concentration 0.4M, Duration 3 days Variable : Roasting duration: 2hrs, 4hrs, 6hrs, 8hrs, 12hrs and 24hrs</p> <p>3: Constant parameters: FeCl₃conc: 0.4M ,Temperatures: 20°C, Duration 3 days, Sample roasted 24hrs Variable : Pulp densities: 5%,10%,15%,20%, 50%, 100%</p> <p>4: Constant parameters: FeCl₃ conc: 0.2M ,Temperatures: 20°C, Pulp densities 10%, Sample roasted 24hrs Variable : Duration: 4hrs, 8 hrs, 12 hrs, 24hrs, 48hrs and 36hrs.</p>
--	---

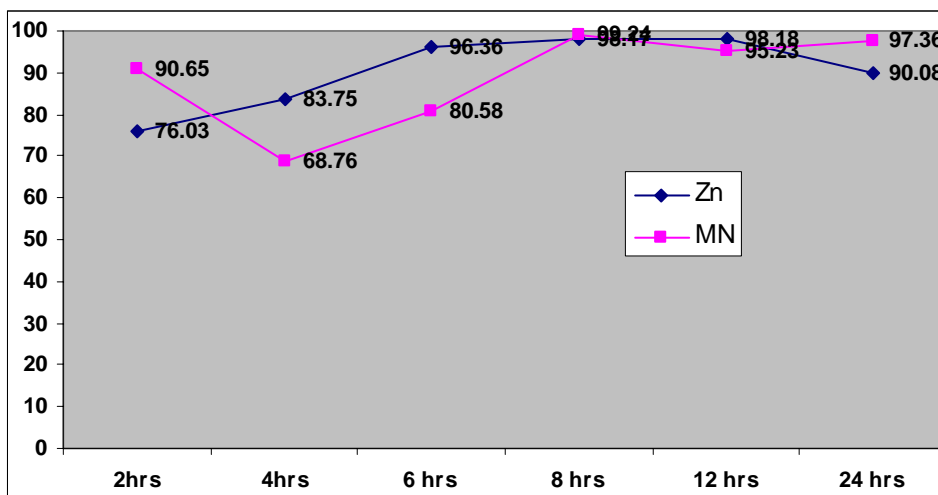
Set 13: Roasted batteries, Lixiviant solution leaching using FeCl₃

Set 13A: Metal extraction from Zn-C batteries dust (inner part) for 3 days. Batteries dust were ground, dismantled, washed and dried. Sample then roasted on the hot plate (max current). Lixiviant solution leaching using different concentrations of FeCl₃.



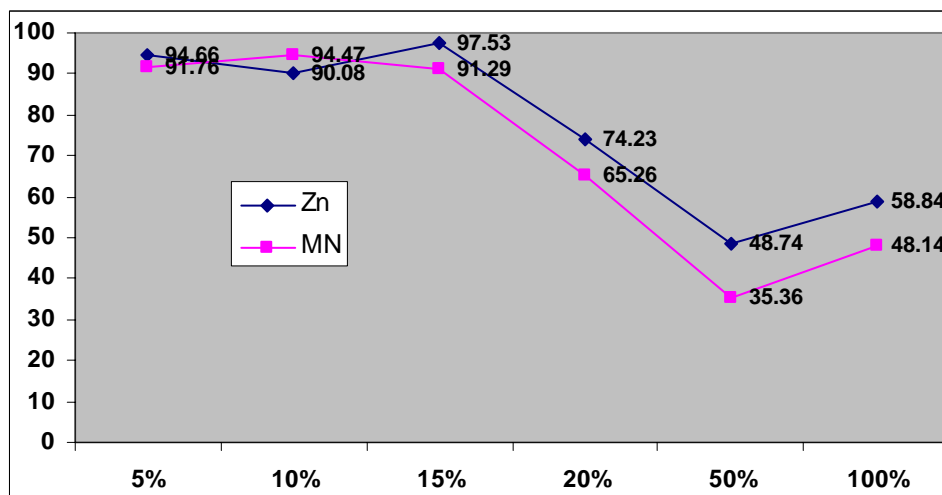
Percentages of \blacklozenge Zn and \blacksquare Mn solubilization from the dust of Zn-C dry cell, 3 days of leaching using different concentrations of FeCl₃. Batteries are broken and inner part of batteries were dismantled, ground, washed and dried. Sample then roasted on the hot plate (max current). Slurry was stirred at 400rpm.

Set 13B: Metal extraction from Zn-C batteries dust (inner part) for 3 days. Batteries dusts were ground, dismantled, washed and dried. Sample then roasted on the hot plate (max current). Leaching using different roasting durations of sample.



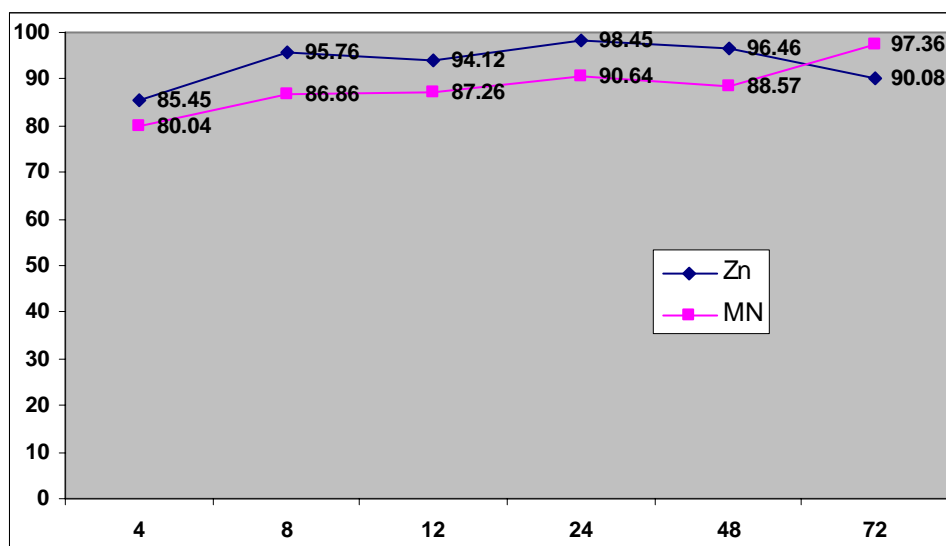
Percentages of \blacklozenge Zn and \blacksquare Mn solubilization from the dust of Zn-C dry cell, 3 days of leaching using different roasting durations of sample. Batteries are broken and inner part of batteries were dismantled, ground, washed and dried. Sample then roasted on the hot plate (max current) Slurry was stirred at 400rpm.

Set 13C: Metal extraction from Zn-C batteries dust (inner part) for 3 days. Batteries dust were ground, dismantled, washed and dried. Sample then roasted on the hot plate (max current). Lixiviant solution leaching at different ratio of solid/solution.



Percentages of \blacklozenge Zn and \blacksquare Mn solubilization from the dust of Zn-C dry cell, 3 days of leaching at different ratios of solid/solution. Batteries are broken and inner part of batteries were dismantled, ground, washed and dried. Sample then roasted on the hot plate (max current). Slurry was stirred at 400rpm.

Set 13D: Metal extraction from Zn-C batteries dust (inner part) for 3 days. Batteries dust was ground, dismantled, washed and dried. Sample then roasted on the hot plate (max current). Lixiviant solution leaching using FeCl_3



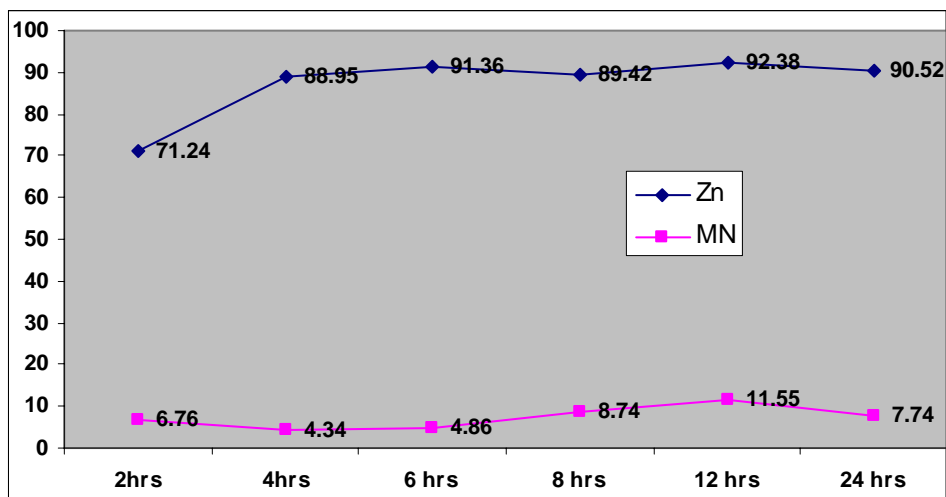
Percentages of \blacklozenge Zn and \blacksquare Mn solubilization from the dust of Zn-C dry cell, 3 days of leaching using FeCl_3 . Batteries are broken and inner part of batteries were dismantled, ground, washed and dried. Sample then roasted on the hot plate (max current). Slurry was stirred at 400rpm.

STR: SET 14

Roasted, <i>Thiobacillus thiooxidans</i> leaching STR Set 14:	<p>2L reactor, Agitated at 400 rpm, D type batteries Zn-carbon batteries, internal portion manually exposed. Inner part of batteries were ground, sieved, washed and dried. Sample then roasted on the hot plate (max current) Lixiviant solution leaching using culture of <i>Thiobacillus thiooxidans</i>:</p> <p>Condition of leaching</p> <p>1: Constant parameters: Pulp densities: 10%, <i>Thiobacillus thiooxidans</i>, Duration 3 days Variable : Roasting duration: 2hrs, 4hrs, 6hrs, 8hrs, 12hrs and 24hrs</p> <p>2: Constant parameters: <i>Thiobacillus thiooxidans</i>, Temp: 30°C, Duration 3 days, Sample roasted 24hrs Variable : Pulp densities: 5%,10%,15%,20%, 50%, 100%</p> <p>3: Constant parameters: <i>Thiobacillus thiooxidans</i>, Temp: 30°C, Pulp densities 10%, Sample roasted 24hrs Variable : Duration: 4hrs, 8 hrs, 12 hrs, 24hrs, 48hrs and 36hrs.</p>
--	---

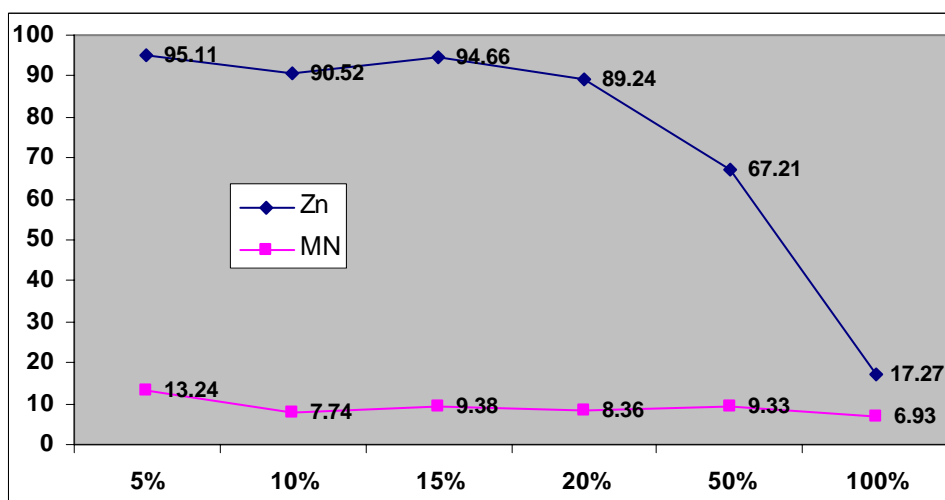
Set 14: Roasted batteries, Leaching using *Thiobacillus thiooxidans*(TT)

Set 14A: Metal extraction from Zn-C batteries dust (inner part) for 3 days. Batteries dusts were ground, dismantled, washed and dried. Sample then roasted on the hot plate (max current). Leaching using different roasting durations of sample



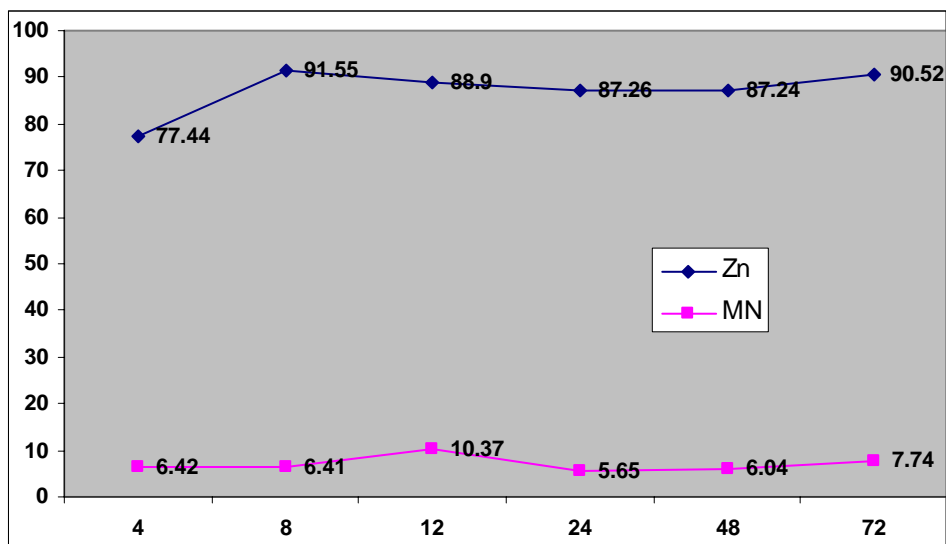
Percentages of \blacklozenge Zn and \blacksquare Mn solubilization from the dust of Zn-C dry cell, 3 days of leaching using different roasting duration of sample. Batteries are broken and inner part of batteries were dismantled, ground, washed and dried. Sample then roasted on the hot plate (max current) Slurry was stirred at 400rpm.

Set 14B: Metal extraction from Zn-C batteries dust (inner part) for 3 days. Batteries dust was ground, dismantled, washed and dried. Sample then roasted on the hot plate (max current). Lixiviant solution leaching at different ratios of solid/solution



Percentages of \blacklozenge Zn and \blacksquare Mn solubilization from the dust of Zn-C dry cell, 3 days of leaching at different ratio of solid/solution. Batteries are broken and inner part of batteries were dismantled, ground, washed and dried. Sample then roasted on the hot plate (max current). Slurry was stirred at 400rpm.

Set 14C: Metal extraction from Zn-C batteries dust (inner part) for 3 days. Batteries dust was ground, dismantled, washed and dried. Sample then roasted on the hot plate (max current). Lixiviant solution leaching using *Thiobacillus Thiooxidans*



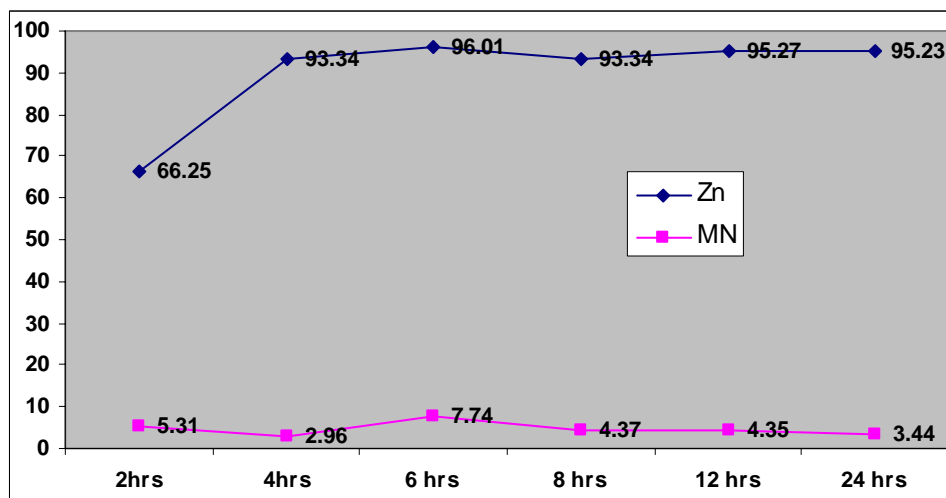
Percentages of ◆ Zn and ■ Mn solubilization from the dust of Zn-C dry cell, 3 days of leaching using *Thiobacillus Thiooxidans*. Batteries are broken and inner part of batteries were dismantled, ground, washed and dried. Sample then roasted on the hot plate (max current). Slurry was stirred at 400rpm.

STR: SET 15

Roasted, leaching <i>Acidianus Brierleyi</i> STR Set 15:	<p>2L reactor, Agitated at 400 rpm, D type batteries Zn-carbon batteries, internal portion manually exposed. Inner part of batteries were ground, sieved, washed and dried. Sample then roasted on the hot plate (max current) Lixiviant solution leaching using culture of <i>Acidianus Brierleyi</i>(AB):</p> <p>Condition of leaching</p> <p>1: Constant parameters: Pulp densities: 10%, <i>Acidianus Beierleyi</i>, Duration 3 days Variable : Roasting duration: 2hrs, 4hrs, 6hrs, 8hrs, 12hrs and 24hrs</p> <p>2: Constant parameters: <i>Acidianus Brierleyi</i>, Temp: 70°C, Duration 3 days, Sample roasted 24hrs Variable : Pulp densities: 5%,10%,15%,20%, 50%, 100%</p> <p>3: Constant parameters: <i>Acidianus Brierleyi</i>, Temp: 70°C, Pulp densities 10%, Sample roasted 24hrs Variable : Duration: 4hrs, 8 hrs, 12 hrs, 24hrs, 48hrs and 36hrs.</p>
---	---

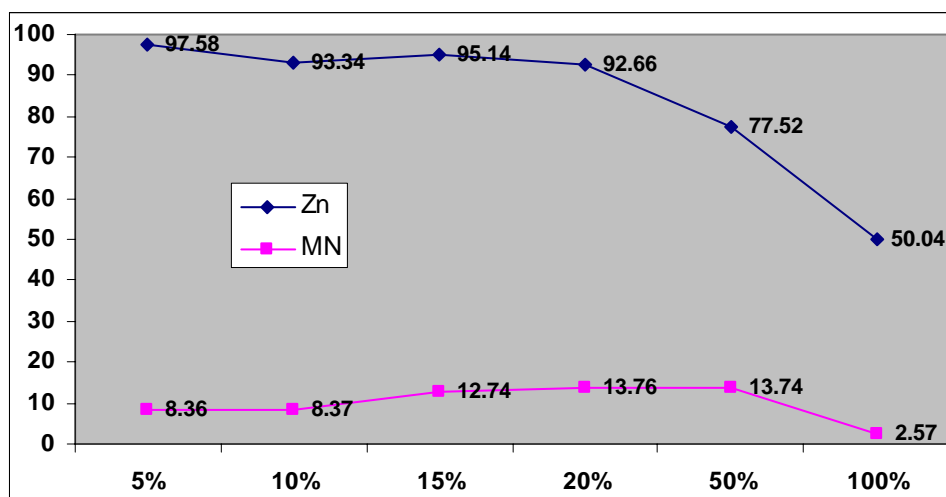
Set 15: Roasted batteries, Leaching using *Acidianus Brierleyi*(AB)

Set 15A: Metal extraction from Zn-C batteries dust (inner part) for 3 days. Batteries dusts were ground, dismantled, washed and dried. Sample then roasted on the hot plate (max current). Leaching using different roasting durations of sample



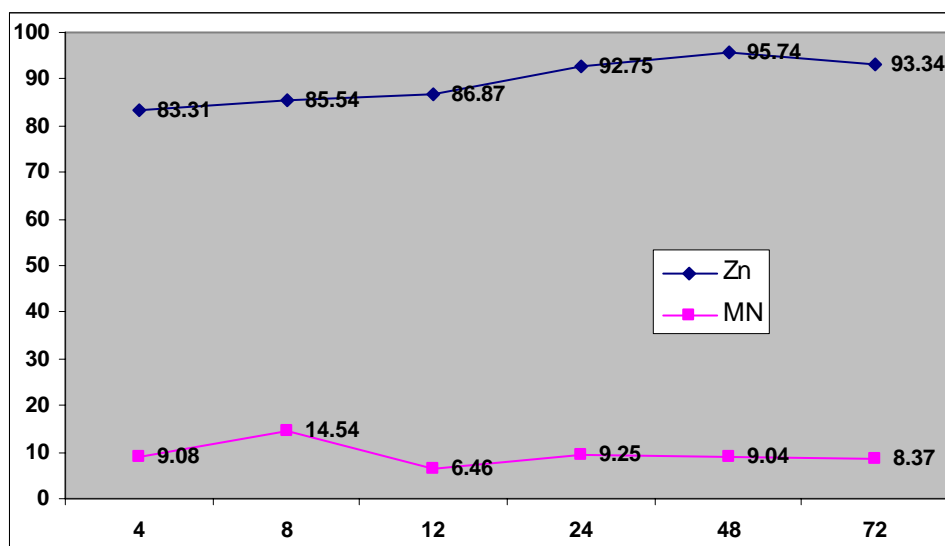
Percentages of \blacklozenge Zn and \blacksquare Mn solubilization from the dust of Zn-C dry cell, 3 days of leaching using different roasting duration of sample. Batteries are broken and inner part of batteries were dismantled, ground, washed and dried. Sample then roasted on the hot plate (max current) Slurry was stirred at 400rpm.

Set 15B: Metal extraction from Zn-C batteries dust (inner part) for 3 days. Batteries dust was ground, dismantled, washed and dried. Sample then roasted on the hot plate (max current)Lixiviant solution leaching at different ratio of solid/solution



Percentages of \blacklozenge Zn and \blacksquare Mn solubilization from the dust of Zn-C dry cell, 3 days of leaching at different ratios of solid/solution. Batteries are broken and inner part of batteries were dismantled, ground, washed and dried. Sample then roasted on the hot plate (max current). Slurry was stirred at 400rpm.

Set 15C: Metal extraction from Zn-C batteries dust (inner part) for 3 days. Batteries dust was ground, dismantled, washed and dried. Sample then roasted on the hot plate (max current). Lixiviant solution leaching using *Acidianus Brierleyi*



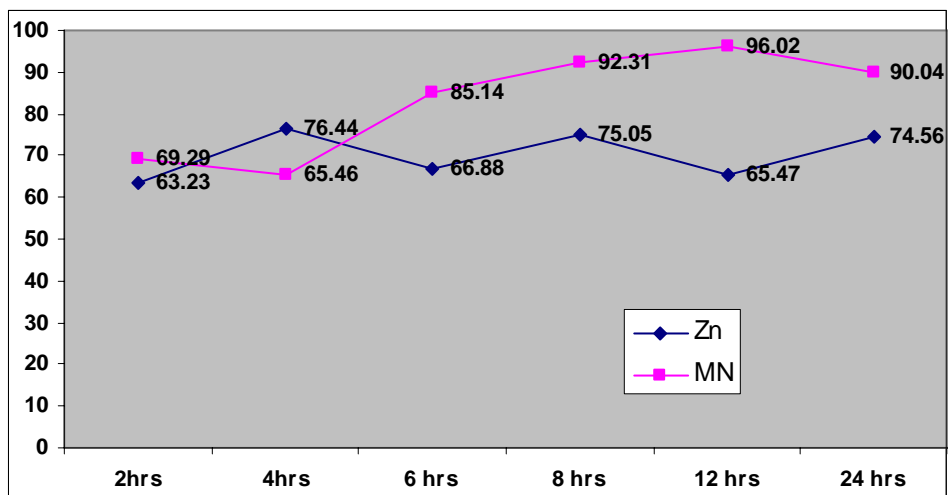
Percentages of \blacklozenge Zn and \blacksquare Mn solubilization from the dust of Zn-C dry cell, 3 days of leaching using *Acidianus Brierleyi*. Batteries are broken and inner part of batteries were dismantled, ground, washed and dried. Sample then roasted on the hot plate (max current). Slurry was stirred at 400rpm.

STR: SET 16

Roasted, Mix culture of <i>Thiobacillus ferroxidans (TF)</i> and <i>Leptospirillum ferroxidans(LF)</i> at ratio: 1:1 leaching STR Set 16:	<p>2L reactor, Agitated at 400 rpm, D type batteries Zn-carbon batteries, internal portion manually exposed. Inner part of batteries were ground, sieved, washed and dried. Sample then roasted on the hot plate (max current) Lixiviant solution leaching using mix culture of <i>Thiobacillus ferroxidans (TF)</i> and <i>Leptospirillum ferroxidans(LF)</i> at ratio: 1:1:</p> <p>Condition of leaching</p> <p>1: Constant parameters: Pulp densities: 10%, <i>TF:LF</i>; 1:1, Duration 3 days Variable : Roasting duration: 2hrs, 4hrs, 6hrs, 8hrs, 12hrs and 24hrs</p> <p>2: Constant parameters: <i>TF:LF</i>; 1:1, Temp: 30°C, Duration 3 days, Sample roasted 24hrs Variable : Pulp densities: 5%,10%,15%,20%, 50%, 100%</p> <p>3: Constant parameters: <i>TF:LF</i>; 1:1, Temp: 30°C, Pulp densities 10%, Sample roasted 24hrs Variable : Duration: 4hrs, 8 hrs, 12 hrs, 24hrs, 48hrs and 36hrs.</p>
---	--

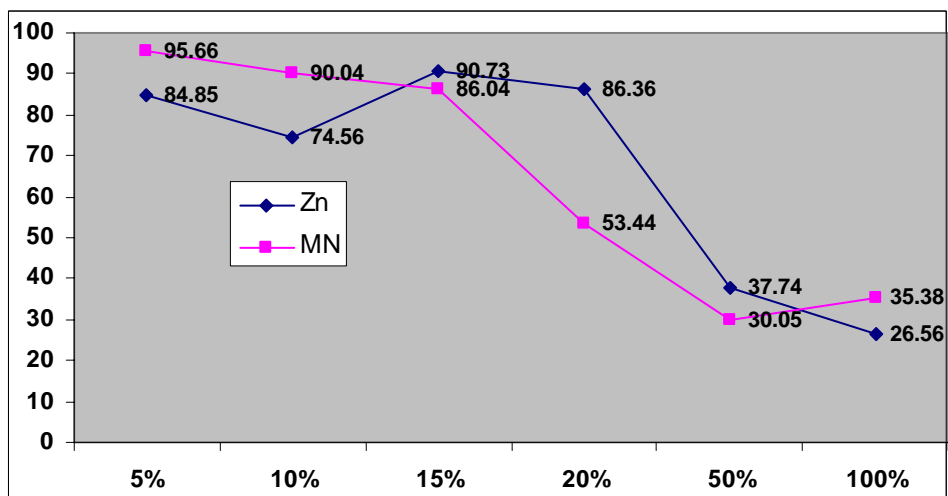
Set 16: Roasted batteries, Leaching using mix culture of *Thiobacillus Ferroxidans (TF)* and *Leptospirillum Ferroxidans(LF)* at ratio: 1:1

Set 16A: Metal extraction from Zn-C batteries dust (inner part) for 3 days. Batteries dusts were ground, dismantled, washed and dried. Sample then roasted on the hot plate (max current). Leaching using different roasting duration of sample



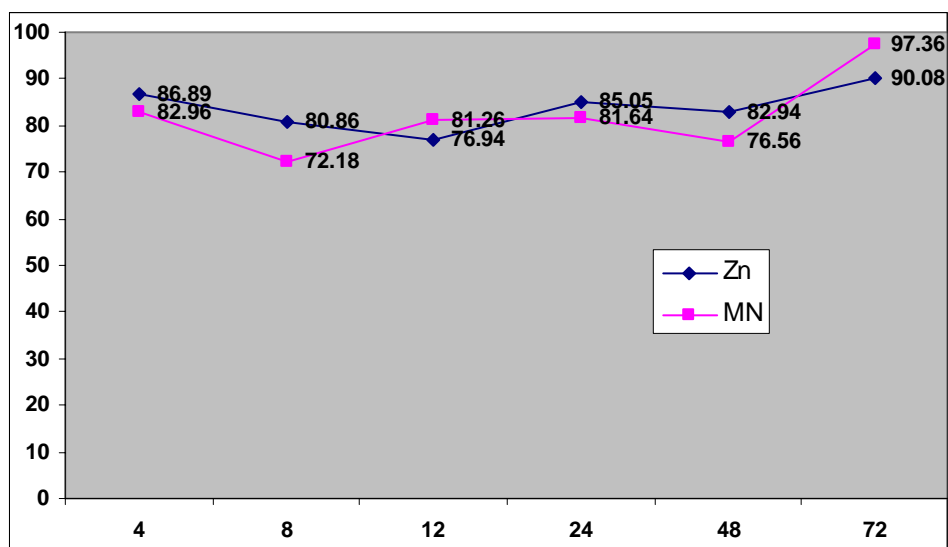
Percentages of \blacklozenge Zn and \blacksquare Mn solubilization from the dust of Zn-C dry cell, 3 days of leaching using different roasting time. Batteries are broken and inner part of batteries were dismantled, ground, washed and dried. Sample then roasted on the hot plate (max current) Slurry was stirred at 400rpm.

Set 16B: Metal extraction from Zn-C batteries dust (inner part) for 3 days. Batteries dust was ground, dismantled, washed and dried. Sample then roasted on the hot plate (max current) Lixiviant solution leaching at different ratios of solid/solution



Percentages of \blacklozenge Zn and \blacksquare Mn solubilization from the dust of Zn-C dry cell, 3 days of leaching at different ratios of solid/solution. Batteries are broken and inner part of batteries were dismantled, ground, washed and dried. Sample then roasted on the hot plate (max current). Slurry was stirred at 400rpm.

Set 16C: Metal extraction from Zn-C batteries dust (inner part) for 3 days. Batteries dust was ground, dismantled, washed and dried. Sample then roasted on the hot plate (max current). Lixiviant solution leaching using $TF:LF; 1;1$



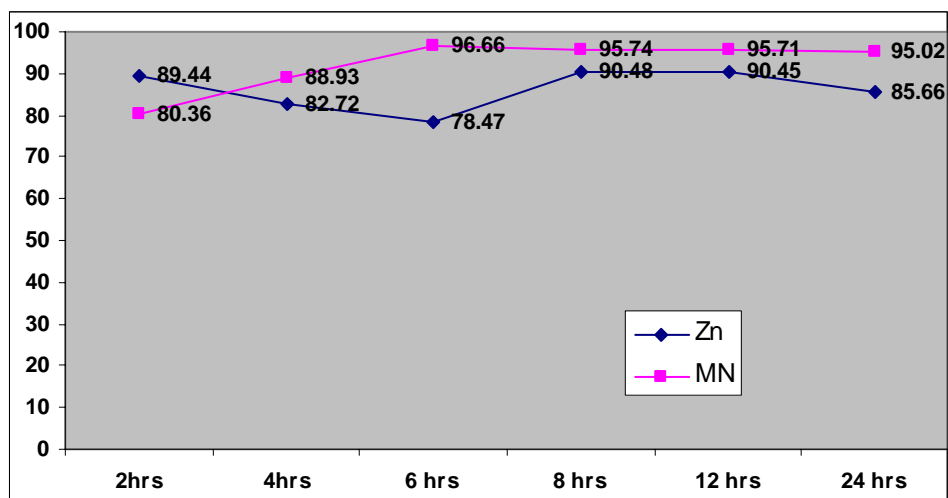
Percentages of \blacklozenge Zn and \blacksquare Mn solubilization from the dust of Zn-C dry cell, 3 days of leaching using $TF:LF; 1;1$. Batteries are broken and inner part of batteries were dismantled, ground, wash and dried. Sample then roasted on the hot plate (max current). Slurry was stirred at 400rpm.

STR: SET 17

STR Set 14: Roasted, <i>SL5B</i> leaching	<p>2L reactor, Agitated at 400 rpm, D type batteries Zn-carbon batteries, internal portion manually exposed. Inner part of batteries were ground, sieved, washed and dried. Sample then roasted on the hot plate (max current) Lixiviant solution leaching using culture of <i>SL5B</i>:</p> <p>Condition of leaching</p> <p>1: Constant parameters: Pulp densities: 10%, <i>SL5B</i>, Duration 3 days Variable : Roasting duration: 2hrs, 4hrs, 6hrs, 8hrs, 12hrs and 24hrs</p> <p>2: Constant parameters: <i>SL5B</i>, Temp: 70°C, Duration 3 days, Sample roasted 24hrs Variable : Pulp densities: 5%,10%,15%,20%, 50%, 100%</p> <p>3: Constant parameters: <i>SL5B</i>, Temp: 70°C, Pulp densities 10%, Sample roasted 24hrs Variable : Duration: 4hrs, 8 hrs, 12 hrs, 24hrs, 48hrs and 36hrs.</p>
---	---

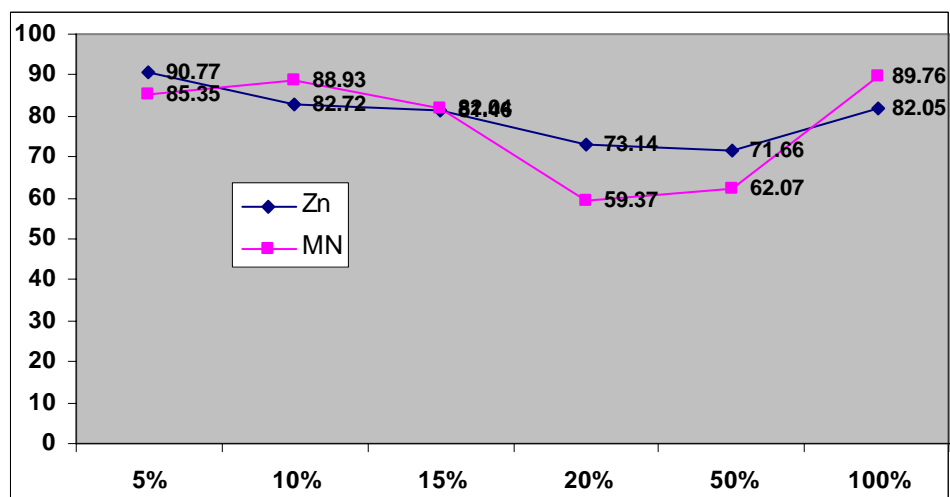
Set 17: Roasted batteries, Leaching using culture *SL5B*

Set 17A: Metal extraction from Zn-C batteries dust (inner part) for 3 days. Batteries dusts were ground, dismantled, washed and dried. Sample then roasted on the hot plate (max current). Leaching using different roasting time



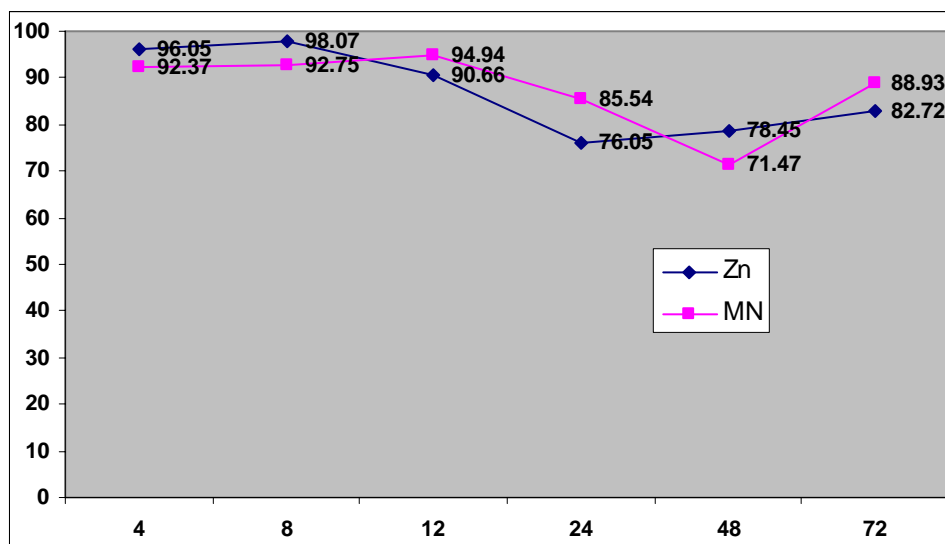
Percentages of \blacklozenge Zn and \blacksquare Mn solubilization from the dust of Zn-C dry cell, 3 days of leaching using different roasting time. Batteries are broken and inner part of batteries were dismantled, ground, washed and dried. Sample then roasted on the hot plate (max current) Slurry was stirred at 400rpm.

Set 17B: Metal extraction from Zn-C batteries dust (inner part) for 3 days. Batteries dust was ground, dismantled, washed and dried. Sample then roasted on the hot plate (max current). Lixiviant solution leaching at different ratios of solid/solution



Percentages of \blacklozenge Zn and \blacksquare Mn solubilization from the dust of Zn-C dry cell, 3 days of leaching at different ratio of solid/solution. Batteries are broken and inner part of batteries were dismantled, ground, washed and dried. Sample then roasted on the hot plate (max current). Slurry was stirred at 400rpm.

Set 17C: Metal extraction from Zn-C batteries dust (inner part) for 3 days. Batteries dust was ground, dismantled, washed and dried. Sample then roasted on the hot plate (max current). Lixiviant solution leaching using *SL5B*

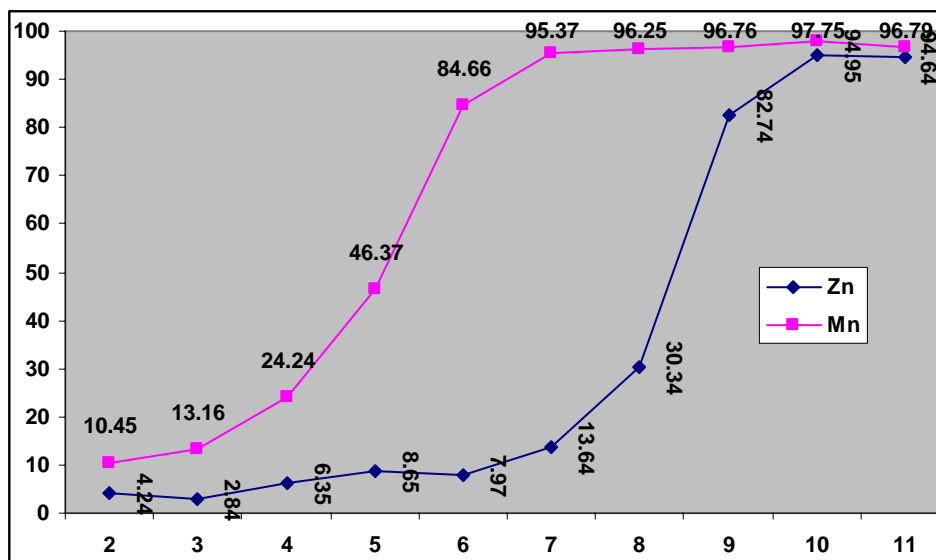


Percentages of \blacklozenge Zn and \blacksquare Mn solubilization from the dust of Zn-C dry cell, 3 days of leaching using *SL5B*. Batteries are broken and inner part of batteries were dismantled, ground, washed and dried. Sample then roasted on the hot plate (max current). Slurry was stirred at 400rpm.

pH adjustment

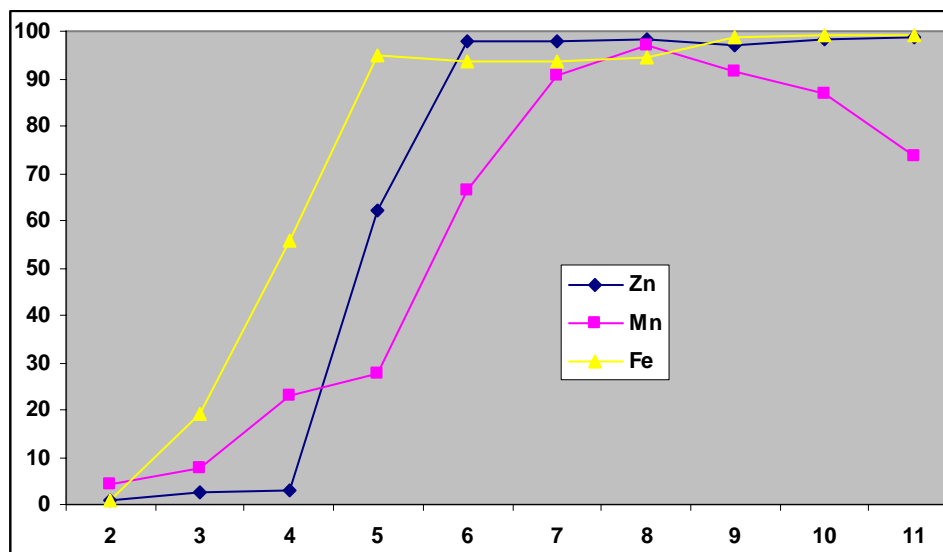
Set 18: Precipitation, pH adjustment	<p>pH of solution adjusted to 2,3,4,5,6,7,8,9,10,11 by gradually adding KOH: Sample of solution taken for metal determination at respective pH</p> <p>Raw sample</p> <ul style="list-style-type: none"> • Solution from column test H_2SO_4 • Solution from column test $\text{Fe}_2(\text{SO}_4)_3$ • Solution from column test HCl • Solution from column test FeCl_3
--	---

Set 18A: Metal precipitate from H_2SO_4 column test solution. pH of solution adjusted to 2,3,4,5,6,7,8,9,10,11 using KOH



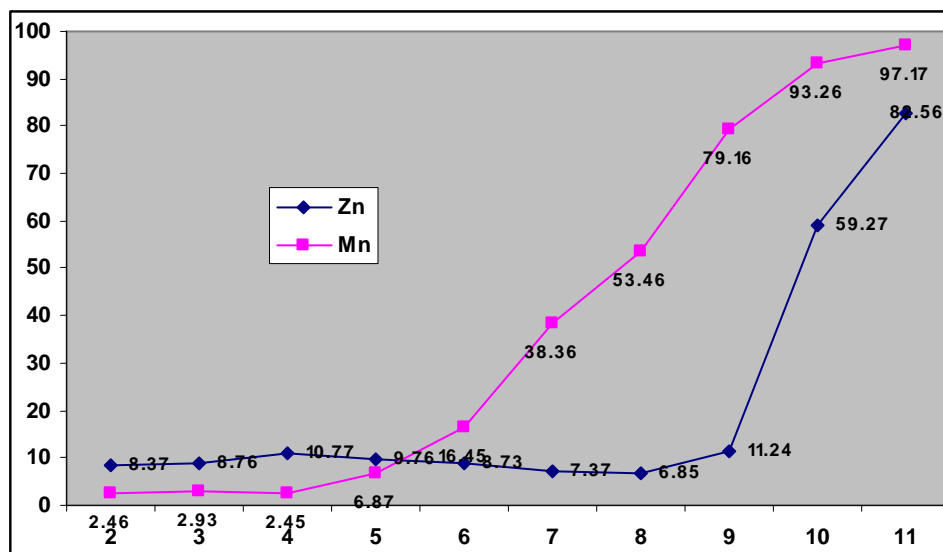
Percentages of \blacklozenge Zn and \blacksquare Mn precipitate from H_2SO_4 column test solution. pH of solution adjusted to 2,3,4,5,6,7,8,9,10,11 using KOH. Sample was stirred for 2 hrs at respective pH.

Set 18B: Metal precipitate from $\text{Fe}_2(\text{SO}_4)_3$ column test solution. pH of solution adjusted to 2,3,4,5,6,7,8,9,10,11 using KOH



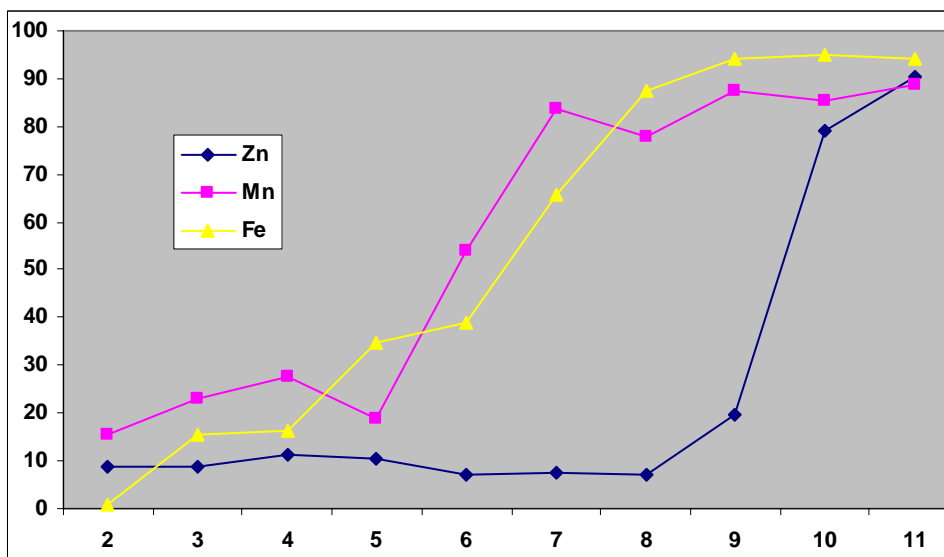
Percentages of \blacklozenge Zn and \blacksquare Mn precipitate from $\text{Fe}_2(\text{SO}_4)_3$ column test solution. pH of solution adjusted to 2,3,4,5,6,7,8,9,10,11 using KOH. Sample was stirred for 2 hrs at respective pH.

Set 18C: Metal precipitate from HCl column test solution. pH of solution adjusted to 2,3,4,5,6,7,8,9,10,11 using KOH



Percentages of \blacklozenge Zn and \blacksquare Mn precipitate from HCl column test solution. pH of solution adjusted to 2,3,4,5,6,7,8,9,10,11 using KOH. Sample was stirred for 2 hrs at respective pH.

Set 18D: Metal precipitate from FeCl_3 column test solution. pH of solution adjusted to 2,3,4,5,6,7,8,9,10,11 using KOH

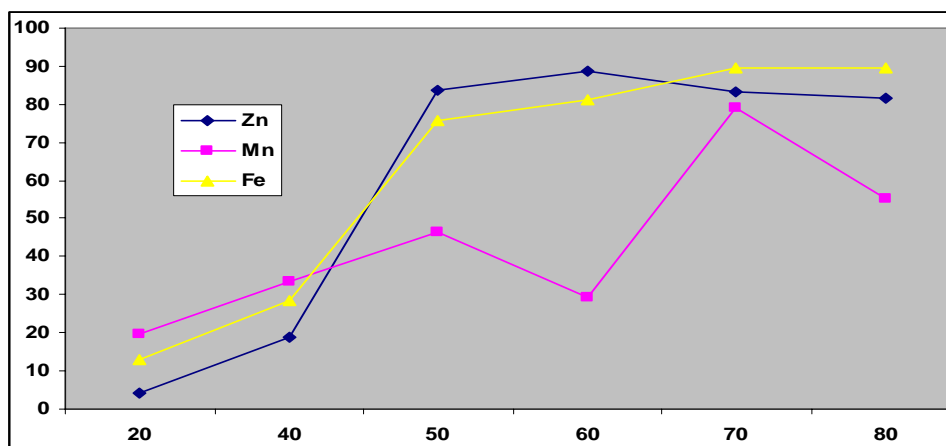


Percentages of \blacklozenge Zn and \blacksquare Mn precipitate from FeCl_3 column test solution. pH of solution adjusted to 2,3,4,5,6,7,8,9,10,11 using KOH. Sample was stirred for 2 hrs at respective pH.

Set 19: Precipitation, Different temperature

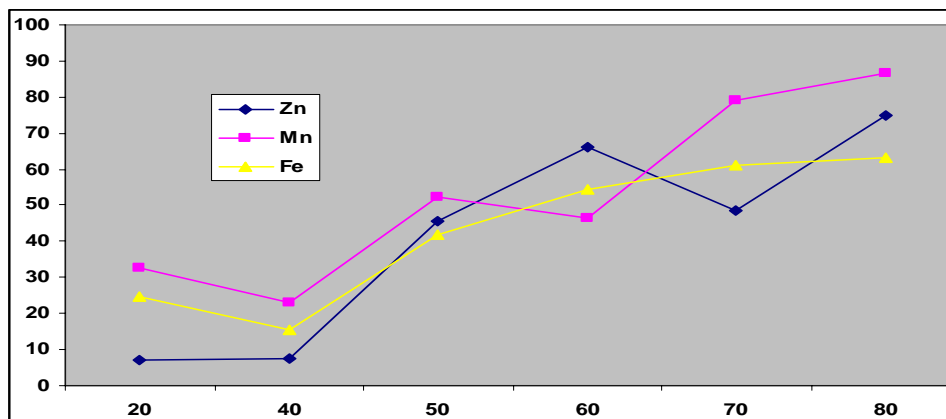
Set 19: Precipitation, Different temperature	Temperature of solution adjusted to 40,50,60,70,80 and shaken for 3 days, Sample of solution taken for metal determination at respective temperature Raw sample <ul style="list-style-type: none"> • Solution from column test $\text{Fe}_2(\text{SO}_4)_3$ • Solution from column test FeCl_3
--	---

Set 19A: Metal precipitate from $\text{Fe}_2(\text{SO}_4)_3$ column test solution. Temperature of solution adjusted to 40,50,60,70,80 and shaken for 3 days



Percentages of \blacklozenge Zn \blacktriangle Fe and \blacksquare Mn precipitate from $\text{Fe}_2(\text{SO}_4)_3$ column test solution. Temperature of solution adjusted to 40,50,60,70,80 and shaken for 3 days

Set 19B: Metal precipitate from FeCl_3 column test solution. Temperature of solution adjusted to 40,50,60,70,80 and shaken for 3 days



Percentages of \blacklozenge Zn \blacktriangle Fe and \blacksquare Mn precipitate from FeCl_3 column test solution. Temperature of solution adjusted to 40,50,60,70,80 and shaken for 3 days

Set 20:

Solvent extraction

Solution and respective organic solvent blend well overnight at ratio 1:1:

a) Solvent used

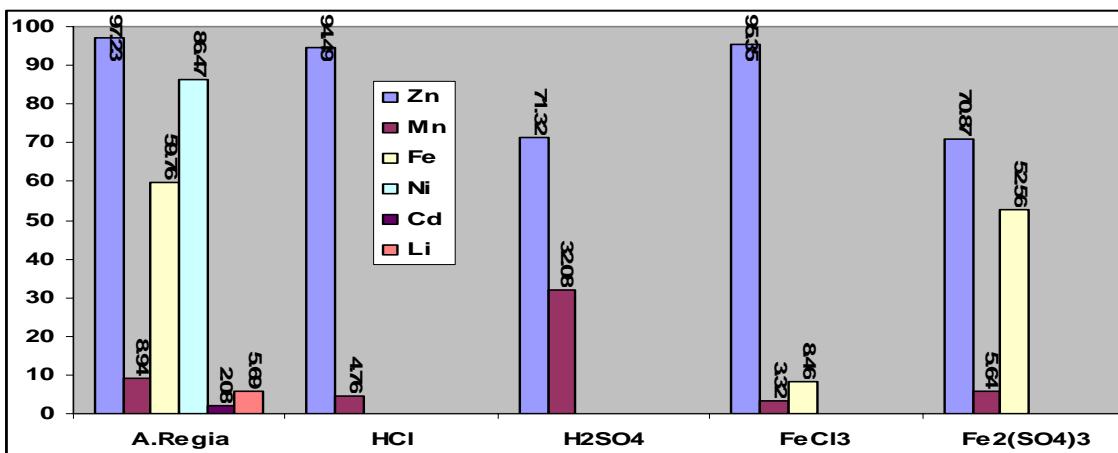
- mixture of 5-dodecylsalicylaloxime and tridecanol in a high flash-point hydrocarbon diluents

Solvent then stripped using:

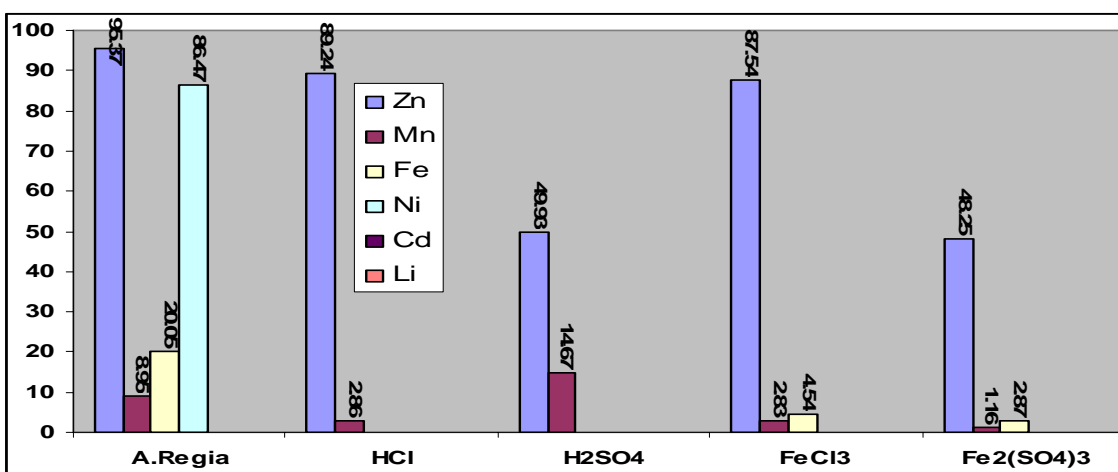
- 1M Sulfuric acid

Raw sample

- Solution from batteries digestion
- Solution from column test HCl
- Solution from column test FeCl_3
- Solution from column test H_2SO_4
- Solution from column test $\text{Fe}_2(\text{SO}_4)_3$



20A: Percentages of metal extraction using mixture of 5-dodecylsalicylaldoxime and tridecanol in a high flash-point hydro-carbon diluent. Sample from column test solution.



20B: Percentages of metal stripped using 1M H₂SO₄. Solvent containing a mixture of 5-dodecylsalicylaldoxime and tridecanol in a high flash-point hydro-carbon diluent. Ratio solvent/stripping solution 1:1.

b) Solvent used

- mixture of 5-dodecylsalicylaldoxime and 2-hydroxy-5-nonyl-acetophenone oxime in a high flash point kerosene

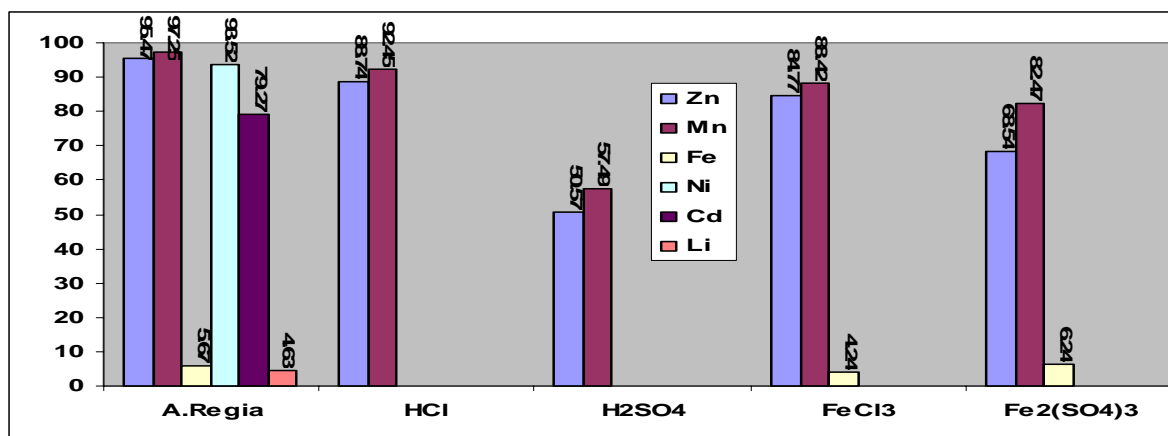
Solvent then stripped using:

- 1M Sulfuric acid

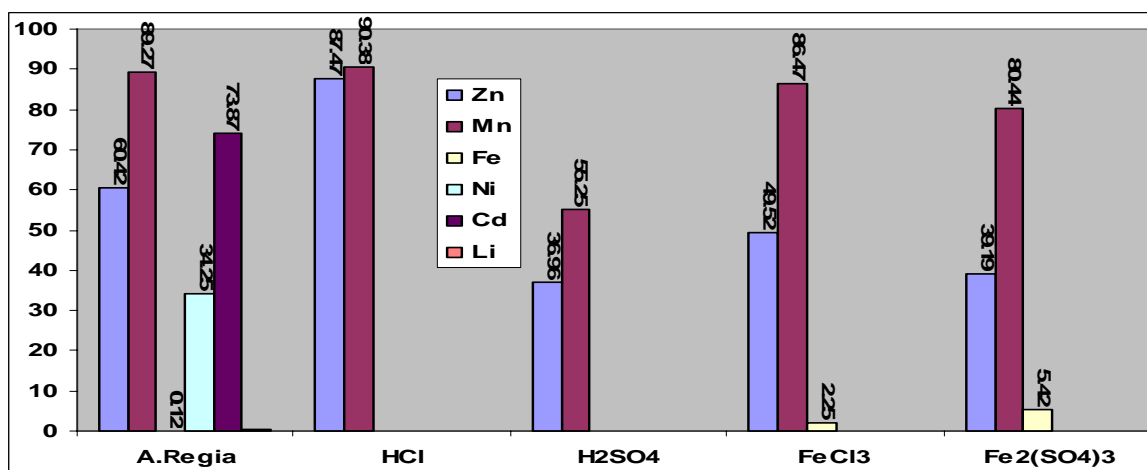
Raw sample

- Solution from batteries digestion
- Solution from column test HCl
- Solution from column test FeCl₃
- Solution from column test H₂SO₄

Solution from column test Fe₂(SO₄)₃



20A: Percentages of metal extraction using mixture of 5-dodecylsalicylaldoxime and 2-hydroxy-5-nonyl-acetophenone oxime in a high flash point kerosene. Sample from column test solution.



20B: Percentages of metal stripped using 1M H₂SO₄. Solvent containing a mixture of 5-dodecylsalicylaldoxime and 2-hydroxy-5-nonyl-acetophenone oxime in a high flash point kerosene. Ratio of solvent/stripping solution at 1:1.

Solution and respective organic solvent, blend well overnight:

c) Solvent used

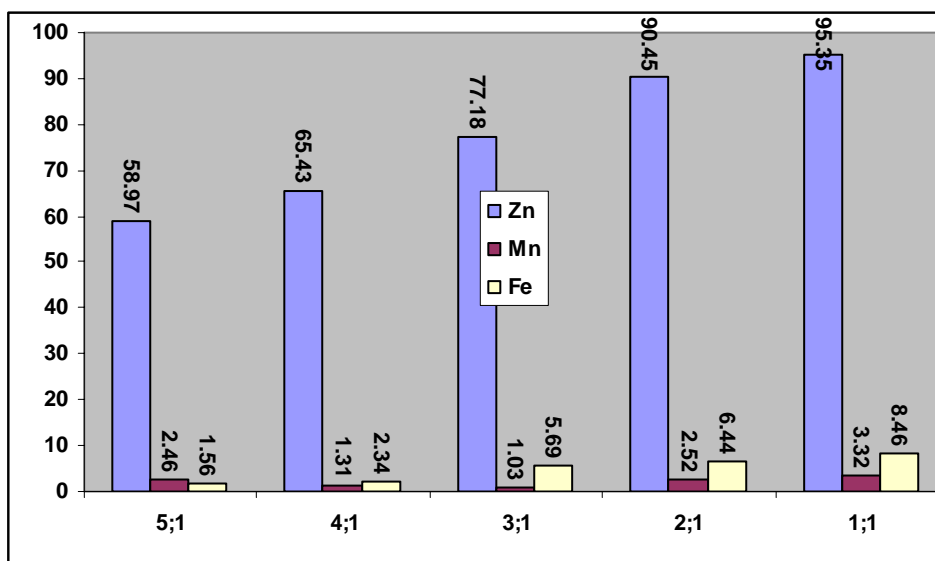
- mixture of 5-dodecylsalicylaldoxime and tridecanol in a high flash-point hydro-carbon diluent

Variable: Solution/Solvent ratio

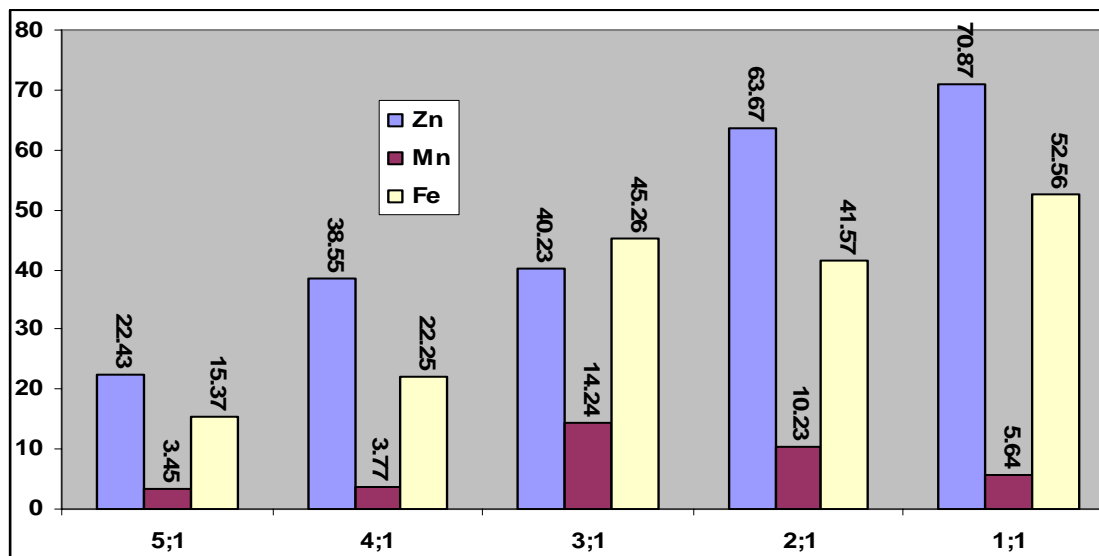
- 1/1, 2/1, 3/1, 4/1, 5/1

Raw sample

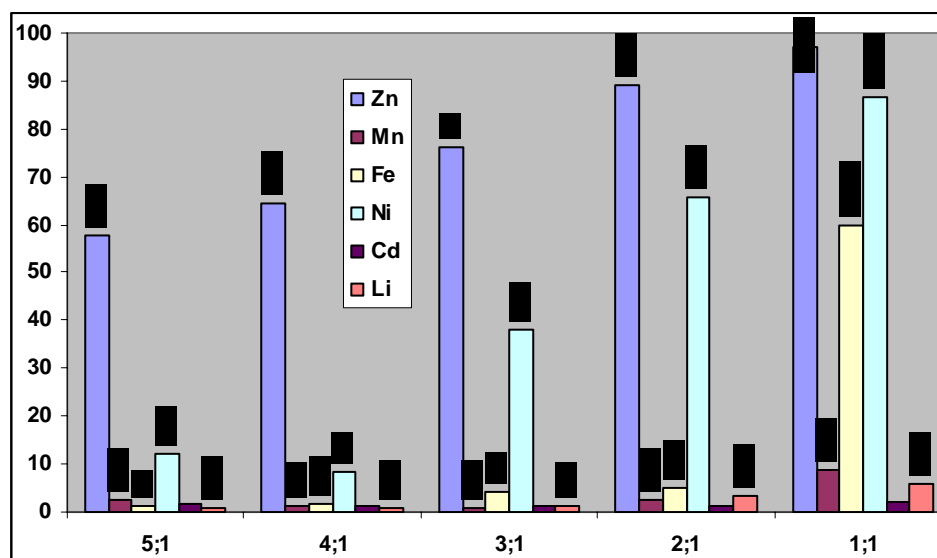
- Solution from column test FeCl_3
- Solution from column test $\text{Fe}_2(\text{SO}_4)_3$
- Solution from batteries digestion



21A: Percentages of metal extraction using mixture of 5-dodecylsalicylaldoxime and tridecanol in a high flash-point hydro-carbon diluent. Sample from FeCl_3 column test solution. Solution/Solvent ratio set at 1/1, 2/1, 3/1, 4/1 and 5/1



21B: Percentages of metal extraction using mixture of 5-dodecylsalicylaldoxime and tridecanol in a high flash-point hydro-carbon diluent. Sample from $\text{Fe}_2(\text{SO}_4)_3$ column test solution. Solution/Solvent ratio set at - 1/1, 2/1, 3/1, 4/1 and 5/1



21C: Percentages of metal extraction using mixture of 5-dodecylsalicylaldoxime and tridecanol in a high flash-point hydro-carbon diluent. Sample from aqua regia batteries digestion. Solution/Solvent ratio set at - 1/1, 2/1, 3/1, 4/1 and 5/1

Solvent extraction

Solution and respective organic solvent blend well overnight.

d) Solvent used

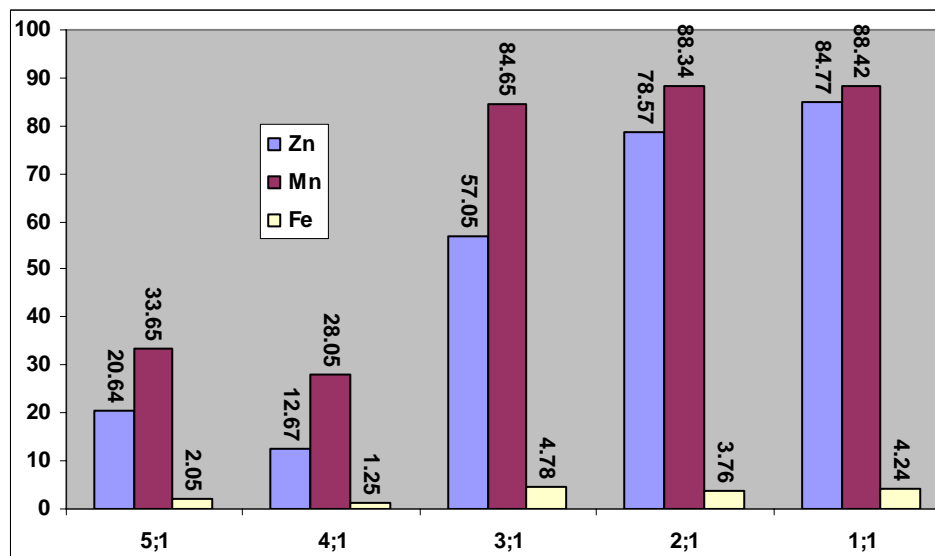
- mixture of 5-dodecylsalicylaldoxime and 2-hydroxy-5-nonyl-acetophenone oxime in a high flash hydro-carbon diluent

Variable: Solution/Solvent ratio

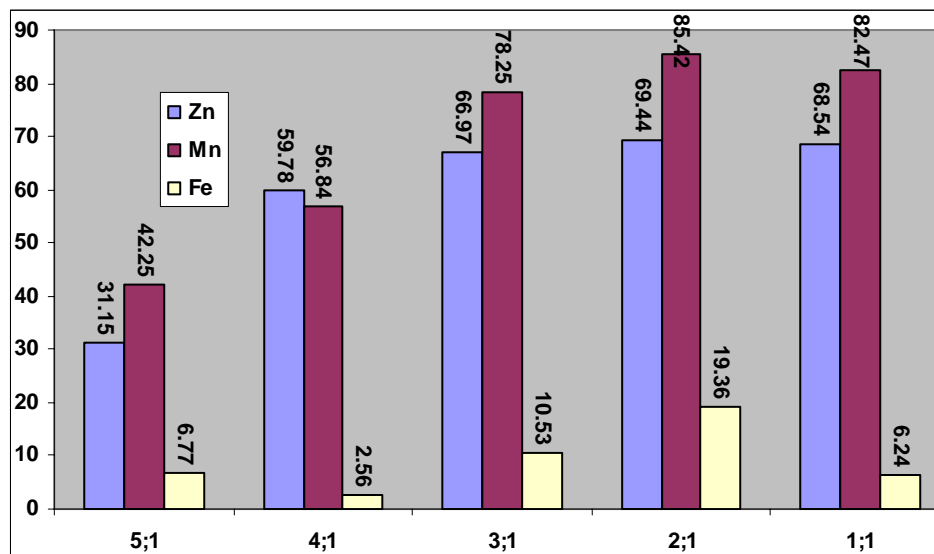
- 1/1, 2/1, 3/1, 4/1, 5/1

Raw sample

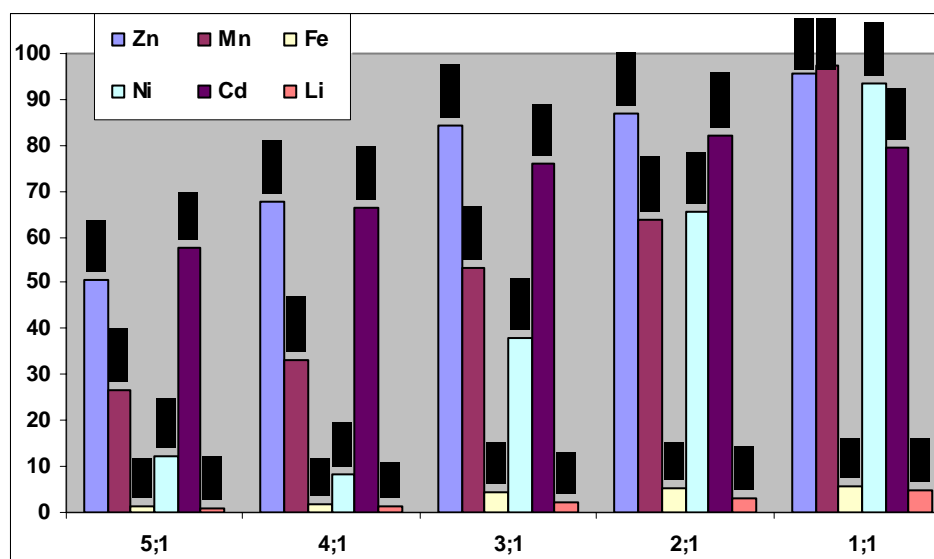
- Solution from column test FeCl_3
- Solution from column test $\text{Fe}_2(\text{SO}_4)_3$
- Solution from batteries digestion



21A: Percentages of metal extraction using mixture of 5-dodecylsalicylaldoxime and 2-hydroxy-5-nonyl-acetophenone oxime in a high flash hydro-carbon diluent. Sample from FeCl_3 column test solution. Solution/Solvent ratio set at - 1/1, 2/1, 3/1, 4/1 and 5/1



21B: Percentages of metal extraction using mixture of 5-dodecylsalicylaldoxime and 2-hydroxy-5-nonyl-acetophenone oxime in a high flash hydro-carbon diluent. Sample from $\text{Fe}_2(\text{SO}_4)_3$ column test solution. Solution/Solvent ratio set at - 1/1, 2/1, 3/1, 4/1 and 5/1



21C: Percentages of metal extraction using mixture of mixture of 5-dodecylsalicylaldoxime and 2-hydroxy-5-nonyl-acetophenone oxime in a high flash hydro-carbon diluent. Sample from aqua regia batteries digestion. Solution/Solvent ratio set at - 1/1, 2/1, 3/1, 4/1 and 5/1

4.7 Case 1: Treatment process conducted by Kualiti Alam Sdn Bhd.

Cementation and secured landfill

Cementation is prescribed for the treatment of dry cell batteries and other miscellaneous wastes which could not be properly and safely treated by existing treatment facilities. Cement and sand are the main materials used to encapsulate and cement hazardous and toxic contaminants in the wastes and prevent them from leaching into the environment. The cost for cementation and disposal at a secured landfill is RM 900 per tonne of dry cell batteries.

Waste Group Z	Packaged Waste RM per tonne
Dry Cell batteries	900

A number of companies have been sending their wastes for these two treatment methods since 1997. Dry cell type C onwards and button cell have been classified as scheduled waste for batteries manufacturers, while AA and AAA batteries is permitted to landfill.

In the cementation plant, metal containing wastes, which do not fulfill the criteria for disposal directly into the Secure Landfill, are treated. Such wastes are typically metal hydroxide sludge containing heavy metals such as lead, arsenic, nickel, zinc and chromium. During the cementation process the heavy metals become insoluble and the wastes therefore can safely be disposed off in the Secure Landfill. Fly ash from the Incinerator Plant and sludge from the PCT Plant are also treated at the cementation plant.

At the cementation plant, waste is loaded into waste bunkers, where it will be mixed with other similar waste. It is then loaded into the waste hopper before being transferred to the mixer by screw conveyors. In the mixer, waste is carefully mixed with consumables such as cement, lime and water. The system is able to handle waste that

contains foreign materials such as stones, wood and scrap iron. A typical cementation recipe is as follows:-

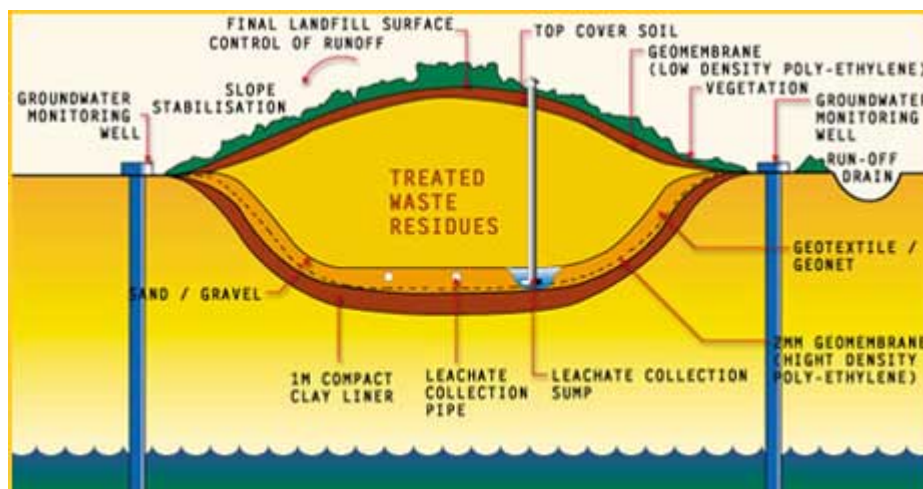
Waste (kg)	Fly Ash (kg)	Cement (kg)	Lime (kg)	Sand (kg)	Water (kg)
100	20	35	7	100	30

After treatment, the waste will appear as a concrete mixture. The mixture is disposed off to the secure landfill for the final curing over a few days. The objective of the whole process is to fix all the heavy metals in the inorganic solid waste into a concrete/silica matrix for long-term disposal in the secure landfill. As a result, hazardous heavy metals will not leach out to the environment.

The Secure Landfill is the final destination for the cemented batteries. The landfill site is some 80 acres in area to accommodate the construction of 8 secure landfill cells with a total volume of 2.5 million cubic meters. As it is a permanent waste disposal facility, all waste materials have to meet the strict Landfill Acceptance Criteria as provided for under the Department of Environment Secure Landfill Licensing Conditions. Only inorganic solid waste that meets all parameters of the Landfill Acceptance Criteria is eligible for direct landfill disposal. Otherwise, the waste will have to be treated at either the solidification or incineration plant.

The secure landfill is designed to prevent seepage of leachate into ground water with a double membrane comprising a one-meter thick compacted clay liner and a 2 mm thick High Density Poly-Ethylene geo-membrane. Above the HDPE membrane is a drainage system made up of a 0.4-meter thick layer of crushed rocks. Rainwater, which percolates from the top of the landfill, is called leachate and it is channeled to the leachate collection sump found within each landfill cell.

SCHEMATIC CROSS-SECTION OF A SECURE LANDFILL



Waste can be disposed off in the landfill in drums, polypropylene bags, in bulk or in cemented form. Radioactive, infectious and explosive wastes are not treated or disposed off at this Waste Management Centre. The records, including the consignment note numbers, amount and location are kept at the landfill office. Internal waste, such as slag from the incineration plant and solidified materials from the solidification plant are sent to the landfill for final disposal. Other internal waste such as incineration ash and physical/chemical treatment plant slurry, are treated at the solidification plant prior to disposal.

The Leachate Treatment Plant (LTP) is capable of treating leachate from secure and rubber sludge landfills, internal wastewater generated from plant operations as well as the first ten-minute flush of rainwater run-off. The Leachate Treatment Plant is a requirement under Kualiti Alam's Environmental Management Programme.

- Cementation is a simple method to treat batteries, preventing it from natural leaching.
- Low cost, low explosion and leakage risk during process.
- No metals can be recovered

4.7.1 Case 2: The BATENUS process

The BATENUS process has been operated by Batterierecycling Schtnebeck GmbH at Schönebeck/ Sachsen-Anhalt. The process was developed by Pira GmbH, a research institute in Stihlingen, Germany, during a period of five years. The development included process design, laboratory experiments, pilot-plant experiments, testing each individual operation under realistic conditions, and fine tuning of the modular units towards each other. This new process combines hydrometallurgical operations in a nearly closed reagent cycle that involves electrochemical and membrane techniques. It utilizes a combination of proven hydrometallurgical operations like solid-liquid extraction, selective ion exchange and solvent extraction with state-of-the-art membrane technology, i.e. reverse osmosis and electro dialysis with bipolar membranes.

Most municipalities and bigger companies in Germany collect all kinds of consumer batteries. This mixture must then be handled as hazardous waste and is subjected to special treatment. BATENUS offers the possibility of a nearly complete metal recovery from mixtures of spent batteries. This plant has a capacity of 7000 tons batteries per annum. The average specific energy consumption in a plant processing is about 2500 kWh / t of batteries.

The plant operator claims that their process as:

- in a flexible, modular construction, which can easily be modified
- with a very low sensitivity towards variations of the composition of the input
- forming a nearly closed cycle, thus avoiding effluent emissions
- producing metals of high purity and easily marketable basic materials and chemicals

The schematic diagram of the BATENUS recycling process is as follows:

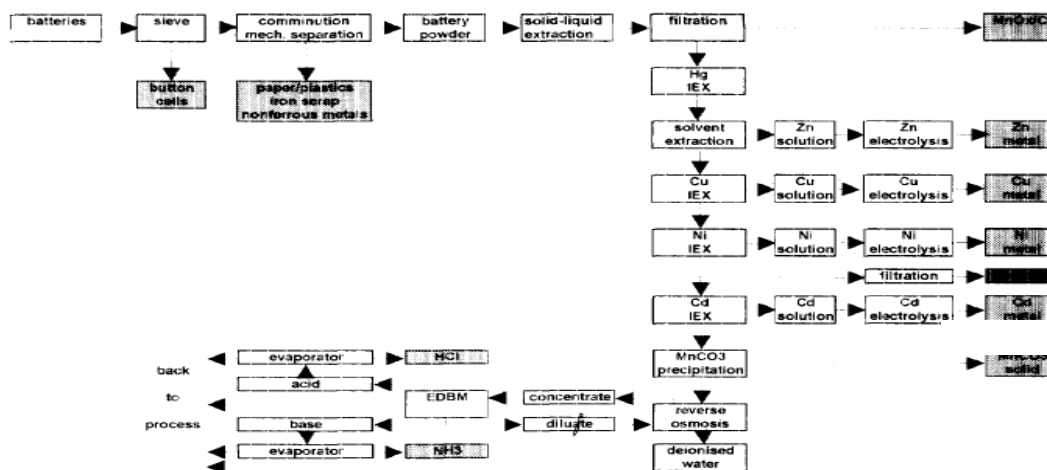


Fig. 3. Flow chart of the BATENUS recycling process.

A mixture of batteries that are delivered to the BETANUS plant is first shredded. A magnet removes scrap iron from the shredded material. Paper, plastics and nonferrous metals are separated from the battery contents with the sieves. The battery contents are then pulverized in order to get a very fine powder which is then passed to the hydrometallurgical unit. The fine particles are leached out using acidic leaching media. The leaching suspension is filtered and the filter cake (consisting mainly of manganese oxide and carbon black) is washed and dried.

The filtrate is cleaned of mercury traces by a ion exchanger. Zinc is extracted from the mercury-free process solution in a multistep solvent extraction. Stripping of the organic phase with sulfuric acid yields a pure zinc sulfate solution from which zinc metal is generated electrolytically.

Copper, nickel and cadmium are successively separated from the solution by selective ion-exchangers. The resins are eluted by sulfuric acid yielding the corresponding sulfate solutions. The pure metals are recovered by electrolysis. The iron concentration has to be controlled in the nickel eluate.

At this stage the main process solution contains only manganese and alkaline metal sulfate. Addition of sodium carbonate yields a manganese carbonate precipitate. This precipitate is filtered out and washed with water. After drying, this product can be marketed as a raw material for manganese or manganese dioxide production.

The remaining alkaline metal sulfate solution is concentrated by reverse osmosis. Subsequently the concentrate is split into acid and base by electro dialysis with bipolar membranes (EDBM).

The diluted salt solution from the EDBM is again concentrated by reverse osmosis. The resulting concentrate is led back to EDBM and demineralized water is recovered for washing purposes

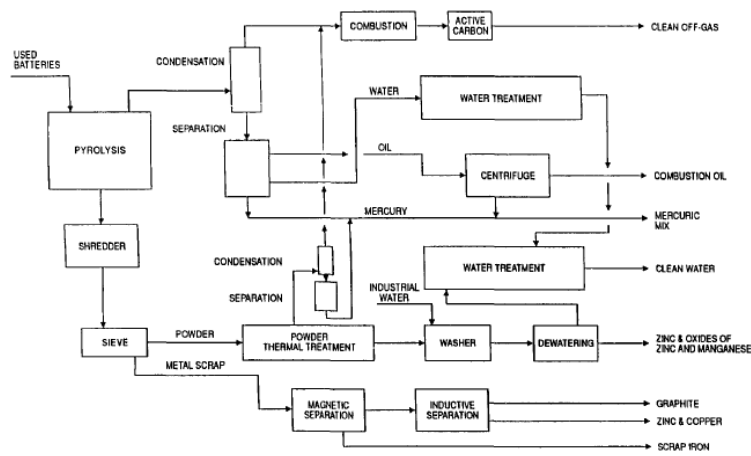
4.7.2 Case 3: Recytec process

Industrial batch pilot plant of Recytec was started in 1991 with a capacity of 500 t/year. Continuous industrial base plant is successfully operated in 1994 with 800 tons of waste batteries. Recytec is considered by the battery producers as highly expensive due to the high temperatures used and is feed batteries selective.

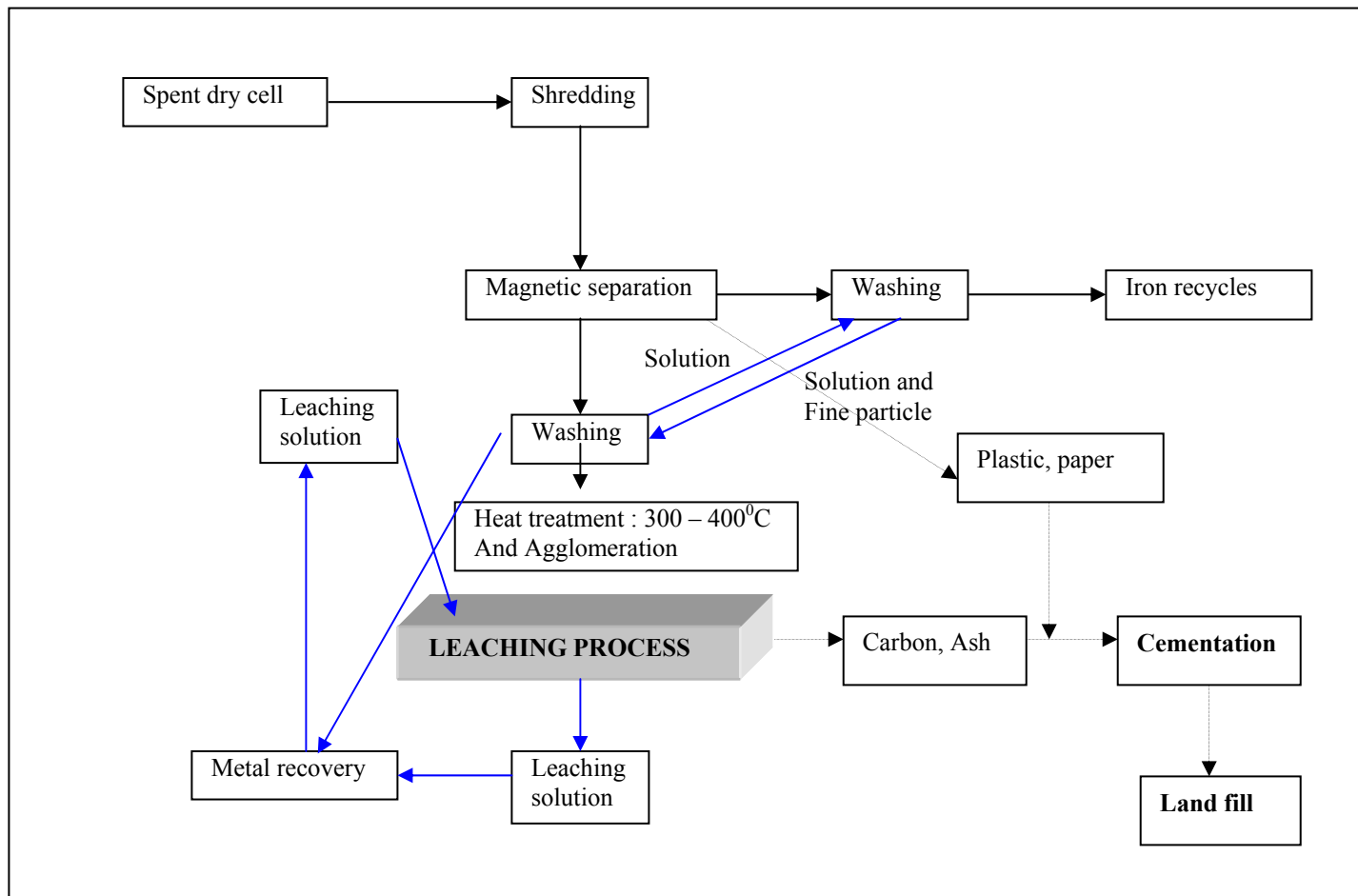
The built-in process steps consist of:

- one-step thermal treatment (650 °C, inert atmosphere, 1 ton/batch)
- shredding (maximum 10 ram)
- washing and sieving (< 2 ram)
- magnetic and inductive separation of washed scraps (ferrous, non-ferrous, inerts)
- anodic dissolution and electrolytic deposition of nonferrous scraps
- chemical dissolution of active mass and electrolytic deposition of zinc, cadmium, copper and nickel

A schematic diagram of the Recytec process is as follows:

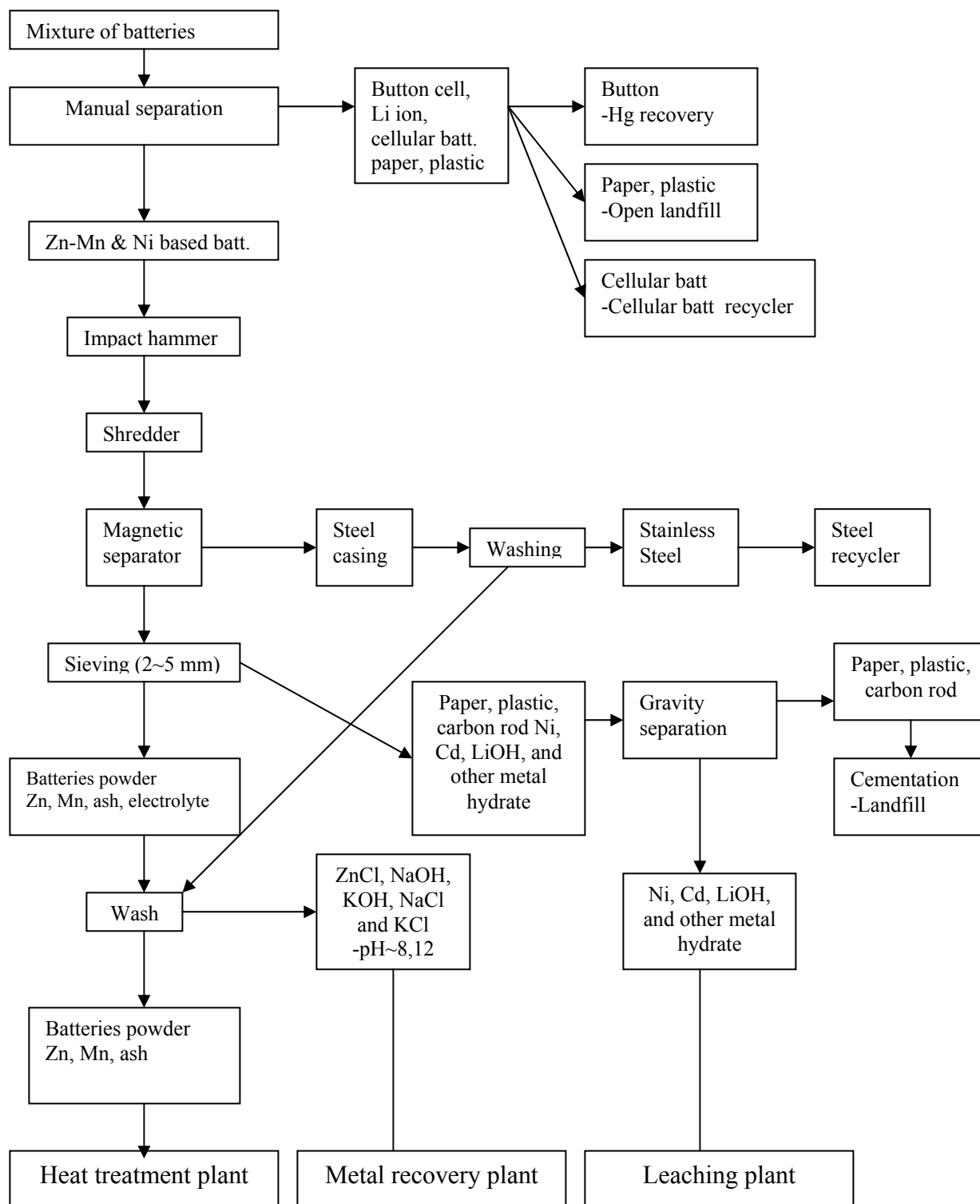


4.7.3 Our proposed batteries recycling process



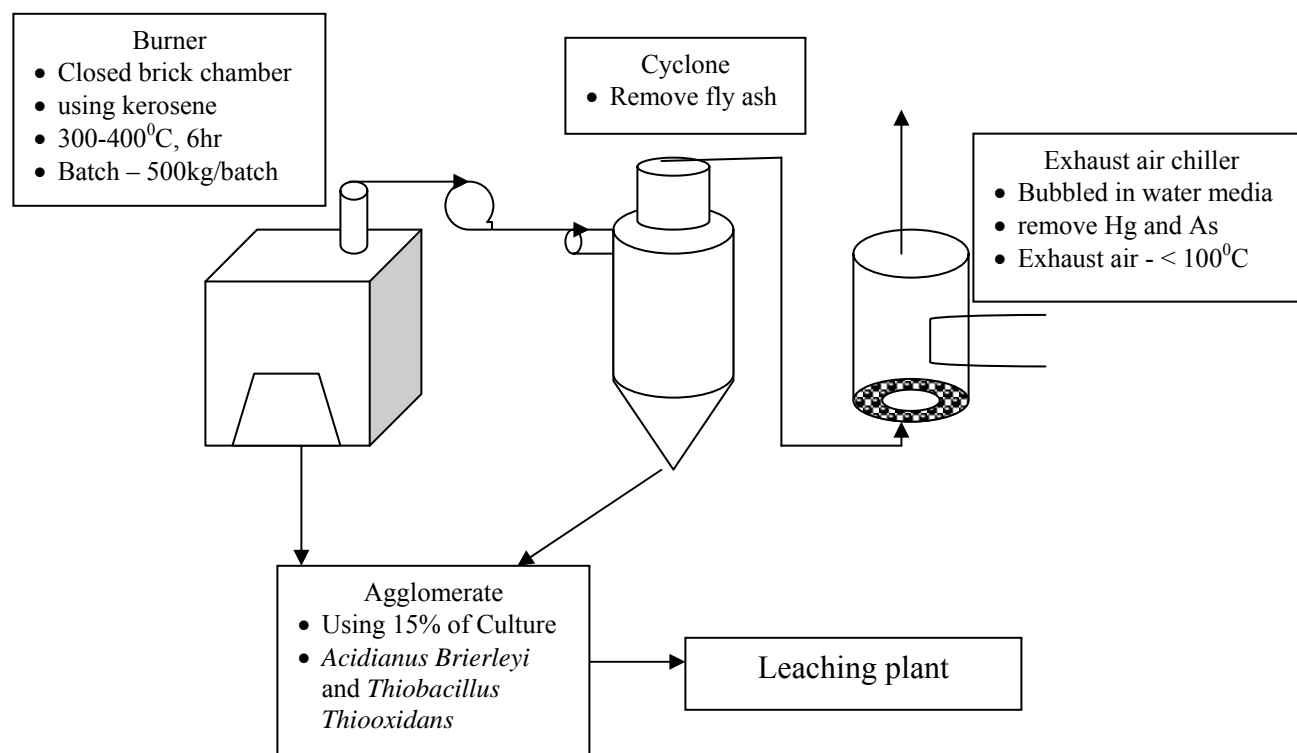
The components of the process are magnetic separation, washing using water, heat pre-treatment, bioleaching process, metal recovery, regeneration of leaching solution and cementation.

Mechanical separation



The first mechanical operation is sieving out the button cells, paper and plastic. Those cells are sent to a mercury recovery company. The batteries are shredded. At the shredder exit, a magnet removes scrap iron. After washing, this scrap is sold to a scrap dealer. Paper, plastics and nonferrous metals are separated from the battery contents with the aid of sieves. A further separation yields a paper/plastics portion and a nonferrous scrap portion using gravity separator. The battery powder is then subjected to the heat treatment plant and hydrometallurgical unit.

4.7.4 Heat treatment plant



4.7.4.1 Leaching plant

Option 1: Heap Leaching








Based on our experience in setting up a pilot scale heap leaching plant at Lubuk Mandi gold mine, we would propose heap leaching of batteries to Dewan Bandaraya Kuala Lumpur.

Some advantages of heap leaching are:

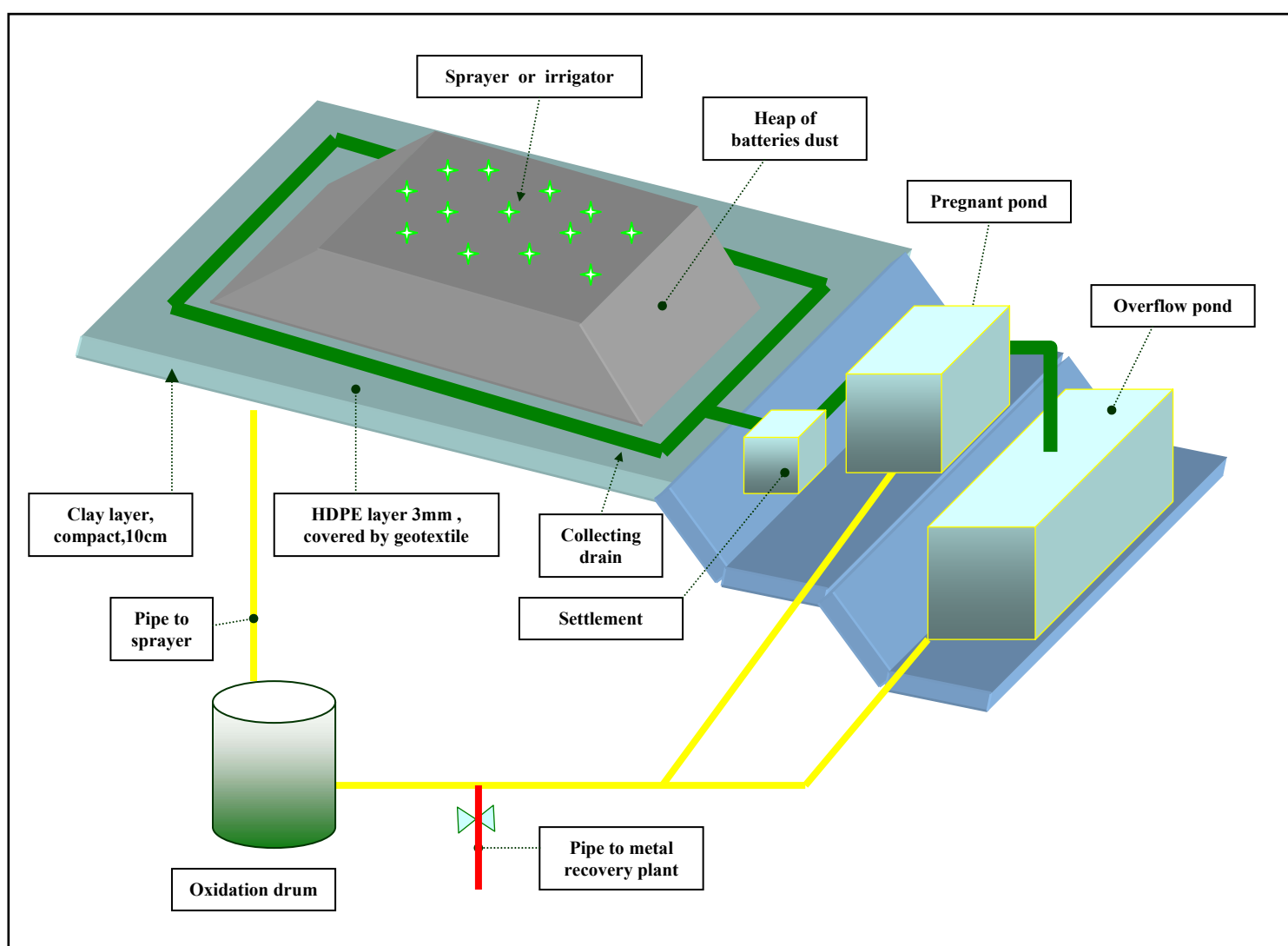
1. capability to processing a huge amount of waste.
2. Less power and capital required
3. Easy to handle

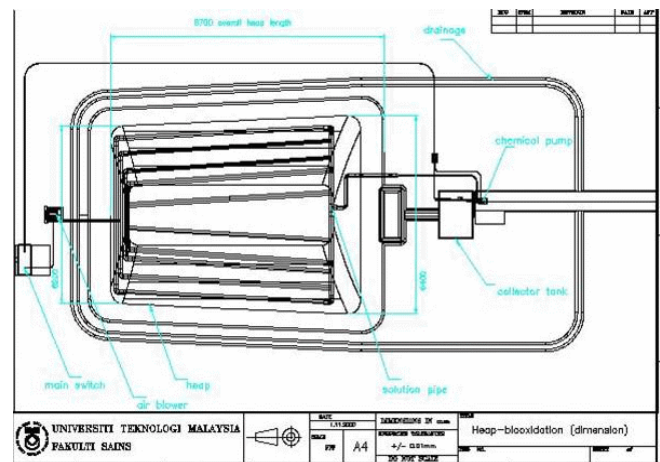
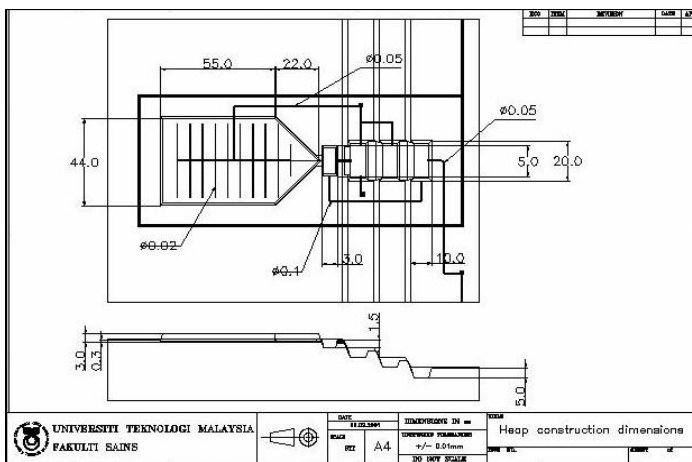
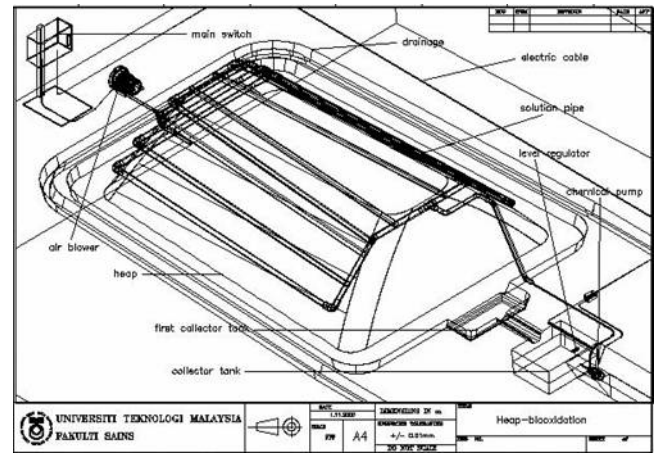
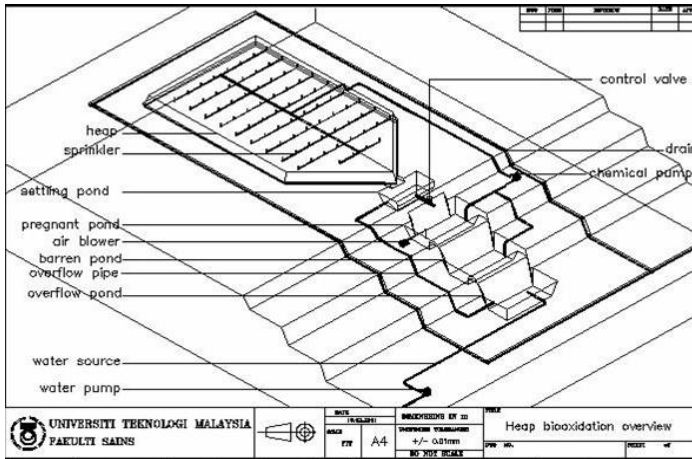
Summary of Pilot Plant Description

Material and equipment	Description
Heap content	<ul style="list-style-type: none"> - 100 tonnes of roasted-non rechargeable batteries powder - Agglomerate with 15% culture - Fully covered with roof - Safety leakage protection system
Pad and liner	<ul style="list-style-type: none"> - Area: 10m x 5m at 2m height - Pad slope: 0.5⁰-1.0⁰ - Liner type: 0.2mm HDPE pad / layering with sand - Pond: Pregnant pond Overflow pond Settlement pond Biooxidation tank Chemical storage tank
Spraying irrigation	<ul style="list-style-type: none"> - Sprayer: Rain bird garden spray with radius of spraying 1m - Rate of irrigation – 36.3 m³/hour - Drainage: total leakage system with a improved drainage system -
Leaching media	<ul style="list-style-type: none"> - Biological leaching Mixed culture of mesophilic and thermophilic

Project Activities (Project Milestone)	
	Permit and enforcement: 1st - 2nd month
	Earth work: 2nd month
	Stacking the batteries: 4th - 5th month
	Prepare the culture: 3rd - 4th month
	Piping, water and electricity: 5th month
	Biooxidation: 6th - 10th month
	Metal purification: 8 th and 10th month

Milestone of pilot process of batteries bioheap leaching





4.7.4.2 Conditions for heap leaching

Option 1: Heap containing a Zn-Mn dust

Step 1:

Solution containing 2% H_2SO_4 sprayed for heap acidification. The heap is already agglomerated with TT and AB.

Solution mostly loaded with Zn.

Zn recovered using LIX 612 or precipitation at pH 4~5 at high concentration

Step 2:

Reconditioning of leaching solution. Adding of $\text{FeSO}_4 \cdot 7\text{H}_2\text{O}$ and basalt salt to grow TF and SL5. Heap is schedule for off-irrigation every 15 days for metal recovery and accelerates biological reaction inside heap. Metal recovery using ferro-manganese jarosite precipitation at pH 5~8.

Option 2: Heap containing a Zn-Mn dust

Leaching medium contain $\text{FeSO}_4 \cdot 7\text{H}_2\text{O}$ and basalt salt. TF and SL5 have been grown before spraying. The heap is already agglomerated with TT and AB.

Solution mostly loaded with Zn and Mn.

Metal recovery using ferro-jarosite precipitation at pH 3~5.

Option 3: Heap containing a Zn-Mn dust and Ni, Cd, LiOH, and other metal hydrate

Step 1:

Solution containing 2% H_2SO_4 sprayed for heap acidification. The heap is already agglomerated with TT and AB.

Solution mostly loaded with Zn, Li and some Cd.

Zn recovered using LIX 612 and precipitation at pH 4~5 at high concentration

Step 2:

Reconditioning of leaching solution. Adding of $\text{FeSO}_4 \cdot 7\text{H}_2\text{O}$ and basalt salt to grow TF and SL5. Heap is schedule for off-irrigation every 15 days for metal recovery and accelerate biological reaction inside heap.

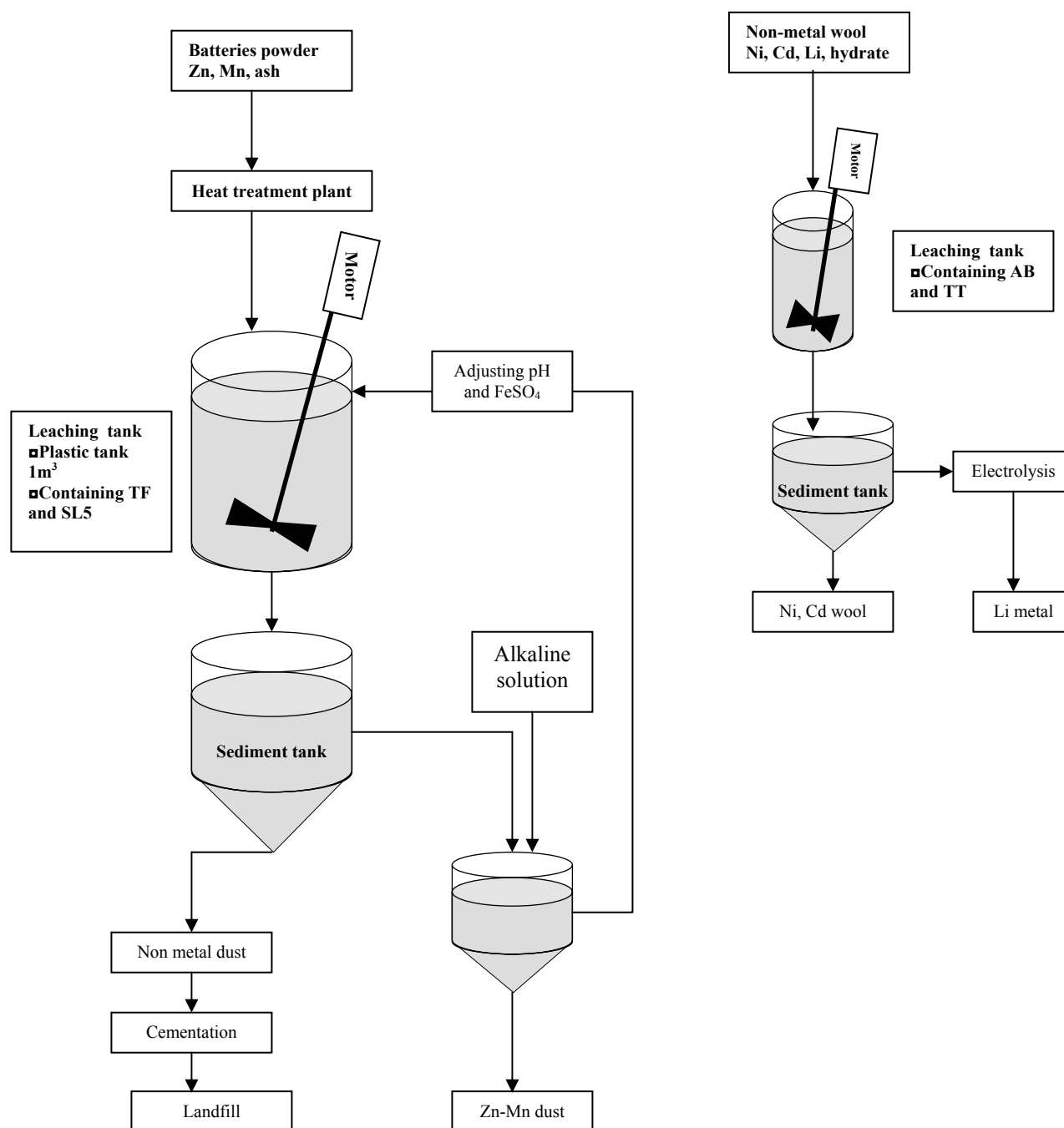
Mn, Ni and Cd extracted using LIX984 and Mn recovered using ferro-manganese jarosite precipitation at pH 3~4

Li and other metal recovered using activated carbon or other water treatment.

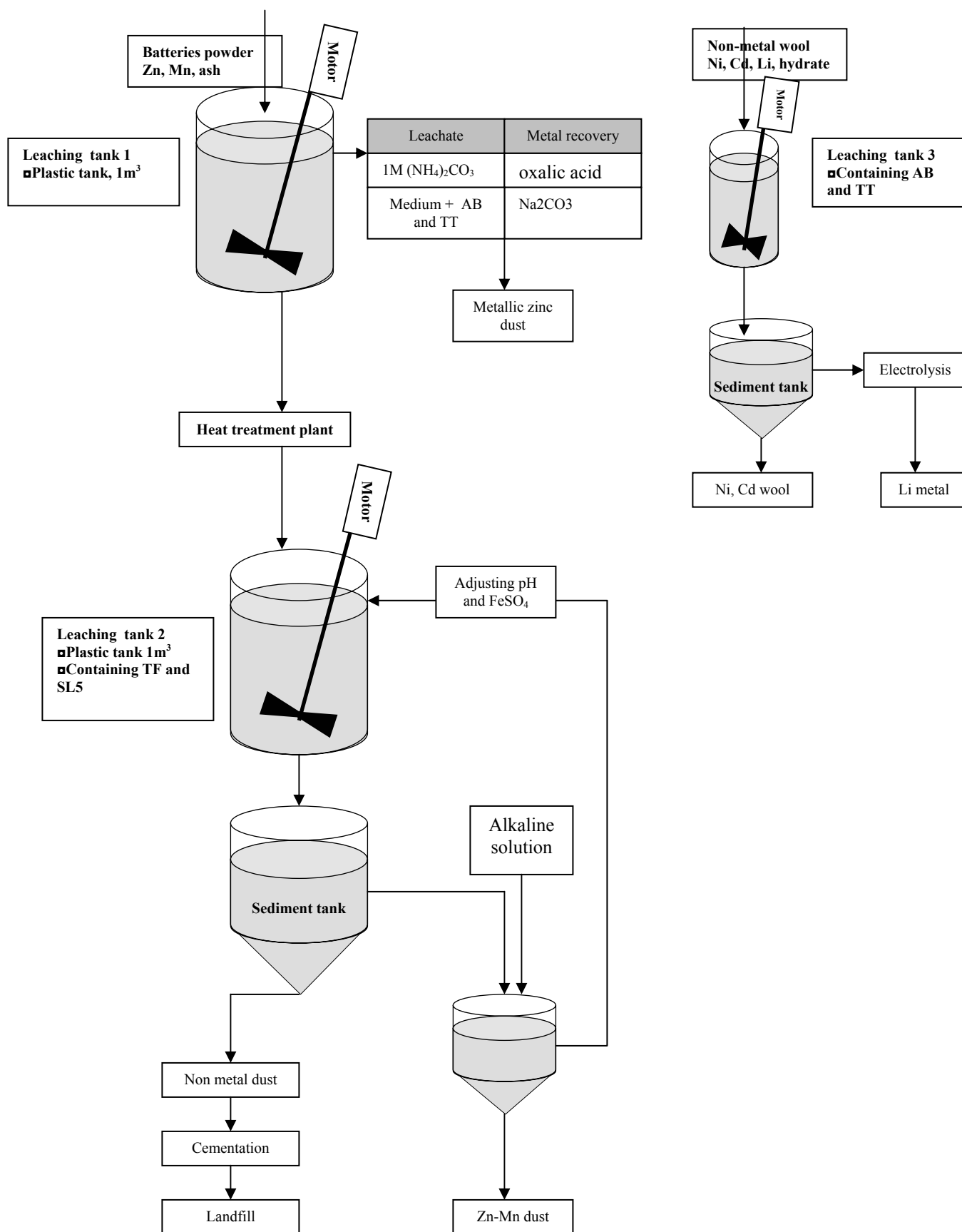
Option 4: Leaching using stirred reactor

Rate of metal leaching using stirred reactor is much higher than heap. It does not require a large space for processing. However, this process is complicated, power and water consuming. A series of parallel stirred tanks have been proposed to treating batteries dust and other metal hydrate separately.

STR 2A:



STR 2B:



4.7.4.3 Battery Breaking

Many of these batteries have steel cases which require removal by cutting the case open with a cutting torch, a hand-held gas powered saw, or other equipment that can separate the case from its contents.

Consideration factor during breaking:

- For manual cutting or breaking operations, acid or alkaline mist containing metal may be emitted which may dry and release dust if disturbed.
- Automated operations using crushers may release metal containing mist that may dry and release dust if disturbed.
- Vibrating equipment with metal dust contaminated surfaces may cause re entrainment of metal dust.
- Cutting industrial battery cases open with a torch may result in exposures to airborne metal dust.

4.7.4.4 Battery shredder

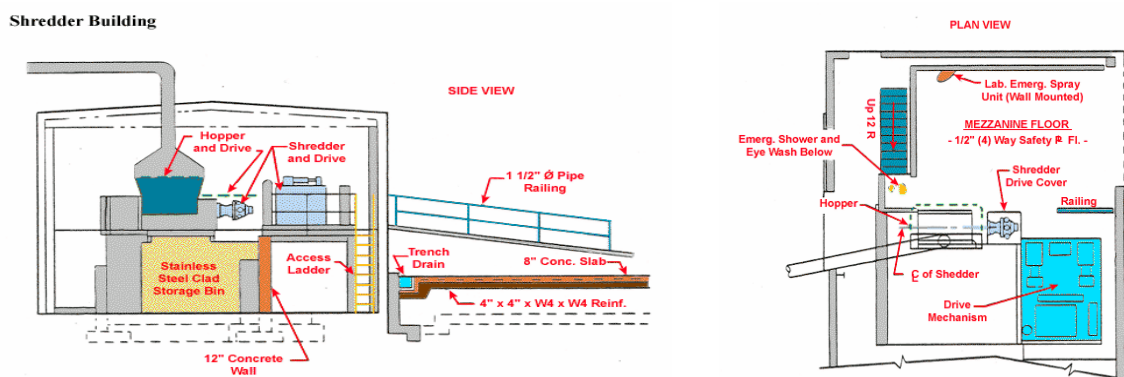
The most common raw material at a batteries recycling process consist of mixture of dry cell. Batteries are typically unloaded by hand from trailers, conveyors, or from pallets. The batteries are then prepared for smelting by draining the electrolyte and separating the plates, rubber, plastic containers, and iron.

The four most common processes for breaking of batteries are:

- High speed saw
- Slow speed saw
- Shear
- Whole battery crushing

The use of saws and shears involves cutting the tops off of the batteries, then dumping the contents of the battery. The whole battery crushing process involves crushing the entire battery in a crusher, shredder or hammer mill, and separating the components by gravity separation.

4.8 Battery Shredding and Emission Control Unit



Possible Work Control Practices during shredding and breaking

- Provide properly designed local exhaust hoods with local exhaust ventilation for saws, shears, shredders, and crushers (hammer mills) to control emissions.
- Automate the process with slow speed saws to cut off the tops of batteries. Slow speed saws emit less metal dust and acid mist than high speed saws.
- Provide curtains or shields on battery- breaking equipment to contain mists and liquid droplets containing particulate.
- Use wet suppression techniques to control exposure levels during cutting and sawing operations.
- Provide adequate make-up air.
- If it is determined through source identification sampling that lead dust is coming from mobile equipment or is coming from adjacent areas, reevaluate material handling patterns and work practices and isolate the area through barriers and provide ventilation as needed.

4.8.1 Battery Separating

After the batteries have been "broken", the non ferrous metal must be separated from the steel casing, plastic and paper. The three most widely used techniques for accomplishing this task are:

- Tumbler
- Sink/Float Process

1. Tumbler

A "tumbler" is a device in which batteries are placed after the batteries have been sawed or sheared off to separate the battery plates from the cases. Ribs inside the tumbler dump the groups as it slowly rotates. The batteries dust fall through the slots in the tumbler while the steel cases, plastics and rechargeable batteries are conveyed to the far end and are collected as they exit. Steel cases are being collected via magnetic separation. Plastic and rubber are separated from the non-ferrous metal via gravity separation.

2. Sink/Float Process

The "sink/float process" is typically combined with the hammer mill or crushing process for battery breaking. Battery pieces, both batteries dust and cases, are placed in a series of tanks filled with water. Batteries dust material sinks to the bottom of the tanks and is removed by screw conveyor or drag chain while the case material floats and is skimmed off the tank's surface.



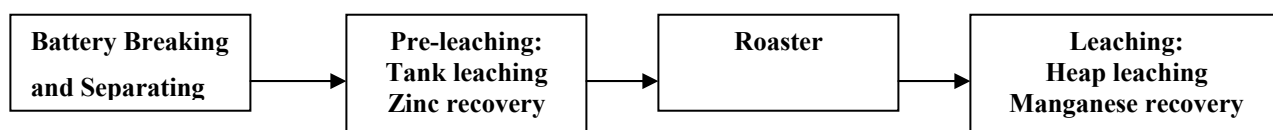
View of sink/float

4.9 Cost estimation

The estimation cost to setting up the pilot scale test of metal recovery from spent dry cell. The cost is not inclusive the manpower, chemical analysis, permitted and enforcement.

Pilot scale test to process 150tonne of batteries.

The proposed recovery plant consists of following major compartment:



1. Batteries Breaker and Separation

A) Breaker

Batteries can be crush using steamroll - to exposed the inner part

Machine	Quantity	Cost/unit/day	Estimation cost
Excavator	1	Facilities can be provided by DBKL	RM 3000.00
Lorry	1		RM 2500.00
Steamroll	1		RM 3000.00

Batteries shredded

Machine	Quantity	Capacity	Estimation cost
Shredder	1	20 tonne /days	RM 25000.00

B) Separation

Machine	Quantity	Capacity	Estimation cost
Agitation tank - Motor with controller - Stirrer - Water pump - Water tank - Piping	1	5m ³	RM 16000
Sieving - Sedimentation tank - Water collection tank	1		RM 2600
Magnet separator			RM 10000
Gravity separation	1	20 tonne /days	RM 2600

2. Pre-leaching: Agitation tank leaching, Zinc recovery

Machine	Quantity	Capacity	Estimation cost
Agitation tank - Motor with controller - Stainless steel Stirrer - Water pump - Water tank - Piping	1	5m ³	RM 15000
Zn recovery plant : SX-EW - Solvent Extraction - Stripping plant - Electro winning	1		RM 10000
Chemical - Leaching - Solvent			RM 8500
Sedimentation tank and dryer	1		RM 2500

3. Roasting

Machine	Quantity	Capacity	Estimation cost
Furnace	1	500kg/batch	RM 13000
Fly ash remover			RM 2500
Exhaust air chiller			RM 7000
Fuel			RM 500

4. Leaching: Heap leaching Manganese recovery

Instrument	Quantity	Cost/unit	Total Cost
Heap construction Based: HDPE pad Compact Clay Geomembrane Building structure Pond Drain			RM 40 000
Piping Chemical pump Water tank Sprinkler Culture tank			RM 15 000
Zn recovery plant : - Precipitation	1		RM 12 700
Chemical and others			RM 3900

Total estimation cost: RM 195 000

PART 3

LIST OF PUBLICATIONS AND AWARDS

Publications

1. “Applications of Bioremediation in Recycling of Spent Batteries”, Wan Azlina Ahmad and Jefri Jaapar. *Jurnal Natur Indonesia*. Lembaga Penelitian Universitas Riau, Pekanbaru, Indonesia Pg 1-4, Vol 7 (1) (2004)
2. “Bacteria as Bioindicators for Metal Contamination”, Wan Azlina Ahmad, Zainul Akmar Zakaria and Jefri Jaapar “Biomonitoring in Tropical Coastal Ecosystems” University of Malaya Maritime Research Centre pg 131-135 (2004). ISBN 983-9576-29-1
3. Two chapters in “Concise Encyclopedia of Bioresource Technology” Haworth Press Inc, New York (2004). ISBN 1-56022-980-2
Title:
 - a) Bioremediation (pg 63 – 69)
 - b) The removal of heavy metals from industrial wastewater (pg 152 – 157)

Papers Presented at Seminars

1. “Recovery of Valuable Metals from Dry Cell Batteries” Jefri Jaapar and Wan Azlina Ahmad. Proceedings of the *International Conference on Environment*. USM. Penang, 12-15th November 2006. ISBN 983-3391-54-0

2. “Bioleaching of Cu and Ni from Sungai Lembing Tin Mine By-Product Using Adapted Strains of *Acidithiobacillus ferrooxidans*”, Lai Huat Choi and Wan Azlina Ahmad. *International Conference For Young Chemists*, USM Penang 24th -27th May 2006.

3. “Biorecovery of Sungai Lembing Tin Mine By Product Using Adapted Strains of *Acidithiobacillus ferrooxidans*”, Wan Azlina Ahmad, Shahrul Halim Sohor and Lai Huat Choi. ARRPET National Workshop III. Palm Garden Hotel, Putra Jaya 7th October 2004.

Awards Received

1. “A Novel Biological Method to Recycle Valuable Metals from Non-Rechargeable Batteries”, Wan Azlina Ahmad, Jefri Jaapar and Ruzaini Razak.

Award: **Gold Medal**

British Invention Show, Alexandra Palace, London 18-21 Oktober 2006

2. “Biorecovery of Metals from Spent Dry Cell”

Wan Azlina Ahmad, Jefri Jaapar and Ruzaini Razak

Award: **Bronze Medal**

8th Industrial Art And Technology Exhibition 2006 (29th Aug – 4th Sept 2006)

3. “A Novel Biological Method to Recycle Valuable Metals from Non-Rechargeable Batteries”, Wan Azlina Ahmad, Jefri Jaapar and Ruzaini Razak.

Award: **Gold Medal**

British Invention Show, Alexandra Palace, London 18-21 Oktober 2006

Keratan Akbar

1. Skudai Post Bil 7/2006
“Perawatan Kromium Heksavalen Menggunakan Teknik Bakteria Dua Peringkat INATEX 2006 mampu lahirkan lebih ramai penyelidik”.
2. Utusan Malaysia 1 Nov 2006
“4 Produk penyelidikan UTM bolot 3 anugerah di London”.
3. Kosmo 1 Nov 2006
“UTM menang empat anugerah di Britain Berjaya kesan pengawet mayat”.
4. Berita Harian 1 Nov 2006
“Pensyarah UTM temui kaedah warna tekstil”.

PART 8

PUBLICATIONS AND AWARDS

1. PUBLICATION

A) JOURNAL

No.	Title of article	Title of Journal	Author	Publisher	Page, Volume	Year	Level/ refereed
1	Applications of Biobleaching in Recycling of Spent Batteries	Jurnal Natur Indonesia	Wan Azlina Ahmad and Jefri Jaapar	Lembaga Penelitian Universitas Riau, Pekanbaru, Indonesia	Pg 1-4, Vol 7 (1)	2004	International/ refereed

B) PROCEEDING

No.	Title of article	Author	Proceeding/Symposium	Date	
1.	Biooxidation of Mine Tailings Using A Mixed Bacterial Population	Wan Azlina Ahmad, Jefri Jaafar, Azri Bunyok, Shahrul Halim Sohor and Mior Ahmad	15th International Biohydrometallurgy Symposium (IBS 2003), Athens, Helias.	14th – 19th September 2003	

		Khushairi Zahari			
2.	Biorecovery of Sg Lembing Tin Mine By Product Using Adapted Strains of <i>Acidithiobacillus ferrooxidans</i>	Wan Azlina Ahmad, Shahrul Halim Sohor and Lai Huat Choi	ARRPET National Workshop III Palm Garden Hotel, Putra Jaya	7 th October 2004	
3.	Biobleaching of Cu and Ni from Sungai Lembing Tin Mine By-Product Using Adapted Strains of <i>Acidithiobacillus ferrooxidans</i>	Lai Huat Choi and Wan Azlina Ahmad	International Conference For Young Chemists, USM Penang	24 th -27 th May 2006	
4.	Recovery of Valuable Metals from Dry Cell Batteries	Wan Azlina Ahmad and Jefri Jaapar	International Conference on Environment. USM. Penang	12-15 th November 2006	ISBN 983-3391-54-0

C) BOOKS

No.	Title	Author	Publisher	Page, Volume	Year
1.	Chapter in "Biomonitoring in Tropical Coastal Ecosystems" Title: Bacteria as Bioindicators for Metal Contamination	Wan Azlina Ahmad, Zainul Akmar Zakaria and Jefri Jaapar	University of Malaya Maritime Research Centre ISBN 983-9576-29-1	Page -135	2004

2.	Two chapters in “Concise Encyclopedia of Bioresource Technology”		Haworth Press Inc, New York		
	Title: 1) Bioremediation	Wan Azlina Ahmad and Zainul Akmar Zakaria	ISBN 1- 56022-980-2	Page 63 -69	
	2) The removal of heavy metals from industrial wastewater	Wan Azlina Ahmad, Jefri Jaapar and Mior Ahmad Khushairi Ahmad Zahari		Page 152 - 157	

2. AWARDS

No.	Research Title	Research Team Members	Competition	Date	Award
1.	A Novel Biological Method to Recycle Valuable Metals from Non – Rechargeable Batteries	Wan Azlina Ahmad, Jefri Jaapar and Ruzaini Razak	British Invention Show, Alexandra Palace, London	18 th – 21 st October 2006	Gold
2.	Biorecovery of Metals from Spent Dry Cell	Wan Azlina Ahmad, Jefri Jaapar and Ruzaini Razak	8 th Industrial Art And Technology Exhibition 2006, UTM	29 th Aug – 4 th Sept 2006	Bronze

3. NEWSPAPERS

No.	Newspaper/Post	News Articles/Headlines	Date
1.	Skudai Post Bil 7/2006	“Perawatan Kromium Heksavalen Menggunakan Teknik Bakteria Dua Peringkat” “INATEX 2006 mampu lahirkan lebih ramai penyelidik”	July 2006
2.	Utusan Malaysia	“4 Produk penyelidikan UTM bolot 3 anugerah di London”	1 Nov 2006
3.	Berita Harian	“Pensyarah UTM temui kaedah warna tekstil”	1 Nov 2006
4.	Kosmo	“UTM menang empat anugerah di Britain Berjaya kesan pengawet mayat”	1 Nov 2006

APPENDIX